Biosynthesis of Monoterpene Indole Alkaloids in *Tabernanthe iboga*

Mohamed Omar Kamileen

PhD

University of York

Biology

September 2024

Abstract

Plants have evolved to produce specialised metabolites that enhance their ecological fitness. *Tabernanthe iboga* (iboga) produces monoterpene indole alkaloids (MIAs), valued for their chemical complexity and therapeutic potential. Native to West Africa, iboga holds cultural significance for its use in spiritual practices due to the psychoactive effects of ibogaine, its most well-known MIA. In addition to ibogaine, iboga produces other MIAs with intricate chemical structures, underexplored biological properties, and unknown biosynthetic pathways. This thesis elaborates on the discovery and characterization of enzymes involved in the biosynthesis of these rare MIA scaffolds in *T. iboga*. Through state-of-the-art plant pathway elucidation techniques combined with classical biochemical methods, this work reveals the pathway discovery of elusive MIAs and presents mechanistic proposals for their biosynthesis for the first time. Key discoveries include the elucidation of pseudo-tabersonine and pseudo-vincadifformine biosynthesis, along with a revised mechanism for the biosynthesis of coronaridine. These studies also demonstrate how biosynthetic enzymes are reused in different sequences to generate alternative scaffolds through intricate redox reactions. Additionally, the development of a streamlined screening platform using *Nicotiana benthamiana* leaf disks and *Catharanthus roseus* flowers led to the discovery of the oxidative tailoring enzymes pachysiphine synthase (TiPS) and tabersonine-16-hydroxylase (TiT16H), discoveries that illuminated plant strategies for structural diversification. Finally, the divergent biosynthesis of four MIA scaffolds from geissoschizine is explored. Oxidative rearrangements, catalyzed by P450 enzymes, drive new bond formations, including a unique C-N bond leading to *mavacurane-type* alkaloids in the related plant species *Catharanthus roseus*. The versatility of geissoschizine is investigated through functional characterization and gene silencing, revealing how neo-functionalized P450s drive scaffold divergence earlier on in MIA biosynthesis. Overall, this thesis advances our understanding of MIA biosynthesis in plants, particularly in *T. iboga*, and introduces new approaches to addressing challenges in plant pathway discovery, especially in non-model species.

Declaration

I, Mohamed Omar Kamileen, declare that this thesis is a presentation of original work, and I am the sole author. This work has not previously been presented for a degree or other qualification at this University or elsewhere. All sources are acknowledged as references. This thesis is presented in a "journal-style" format, where Chapter 2 and Chapter 3 have been published in peer-reviewed journals, and Chapter 4 is written in a format for publication with the intention of submission. The format of the published manuscripts has been slightly modified to accommodate the formatting requirements of this "journal-style" thesis.

Chapter 2

Status of publication: published

Title: Recycling Upstream Redox Enzymes Expands the Regioselectivity of Cycloaddition in Pseudo-Aspidosperma Alkaloid Biosynthesis

Authors: Mohamed O. Kamileen[1,2], Matthew D. DeMars II[1], Benke Hong[1], Yoko Nakamura[1,3], Christian Paetz[3], Benjamin R. Lichman[2], Prashant D. Sonawane[1], Lorenzo Caputi[1*] and Sarah E. O'Connor[1*]

Affiliations:

[1] Department of Natural Product Biosynthesis, Max Planck Institute for Chemical Ecology, Hans-Knöll-Straße 8, Jena 07745 Germany.

[2] Centre for Novel Agricultural Products, Department of Biology, University of York, York, YO10 5DD, UK.

[3] Research Group Biosynthesis and NMR, Max Planck Institute for Chemical Ecology, Hans-Knöll-Straße 8, Jena 07745 Germany.

Journal: Journal of the American Chemical Society (JACS)

Date of submission: August 1st, 2022

Date of publication: October 14th, 2022

DOI: 10.1021/jacs.2c08107

Link: https://doi.org/10.1021/jacs.2c08107

Author contributions: Chapter 2

M.O.K: Designed and planned all experiments and coordination of the project. Designed constructs and performed cloning for in vitro and in vivo experiments. Purified angryline and stemmadenine acetate from crude workup required as substrates for experiments. Expressed and purified all enzymes for in vitro assays. Performed all in vitro and in vivo experiments, including pathway reconstitution in *N. bentamiana*. Analyzed and interpreted data from labelled and non-labelled experiments in vitro and in vivo. Performed preparative scale reactions for the isolation of labelled and non-labelled compounds described in the manuscript other than compounds worked on by **M.D.DII** and **B.H**. Performed LC-MS data acquisition and analysis. Writing the first draft and subsequent versions of the manuscript for submission. Performed revisions after review and final publication proofreading. Prepared all figures and graphs for the main text and supporting information of the manuscript. Prepared figure for graphical abstract.

M.D.D II: Isolation of deuterium labelled (−)-16-carbomethoxycleavamine from chemical workup. Assisted with the mechanistic proposal. Assisted with revisons of the final draft of the manuscript.

B.H: Synthesized crude substrate angryline for in vitro assays. Synthesized racemic standards pseudo-tabersonine and pseudo-vincadifformine and characterised by NMR. Writing synthesis methods and assisting with writing the initial draft of the manuscript.

Y.N: Performed NMR data acquisition and analysis. Structure elucidation of deuterium labelled and non-labelled compounds purified. Acquired ECD spectra from compounds isolated. Writing up methods and providing data for supporting information.

C.P: Performed calculations of ECD spectra.

B.R.L: Formal supervision of the project. Advised on the mechanism. Corrections and proofreading of the final draft of the manuscript.

P.D.S: Advised on plasmid design for *N. benthamiana* transient expression.

L.C: Formal supervision of the project. Corrections and proofreading of the final draft of the manuscript.

S.E.O: Principle investigator and formal supervison of the project. Proposal of the reaction mechanism and data analysis. Funding, resources, administration, editing and writing of the manuscript for submission and final publication.

Chapter 3

Status of publication: published

Title: Streamlined screening platforms lead to the discovery of pachysiphine synthase from *Tabernanthe iboga*

Authors: Mohamed O. Kamileen[1,2], Yoko Nakamura[1,3], Katrin Luck[1], Sarah Heinicke[1], Benke Hong[4], Maite Colinas[1], Benjamin R. Lichman[2], Sarah E. O'Connor[1*]

Affiliations:

[1] Department of Natural Product Biosynthesis, Max Planck Institute for Chemical Ecology, D-07745 Jena, Germany.

[2] Centre for Novel Agricultural Products, Department of Biology, University of York, York YO10 5DD, UK.

[3] NMR and Natural Product Biosynthesis Group, Max Planck Institute for Chemical Ecology, D-07745 Jena, Germany.

[4] Department of Chemistry, Westlake University, 18 Shilongshan Road, 310024, Hangzhou, China.

Journal: New Phytologist

Date of submission: July 1st, 2024

Date of publication: September 16th, 2024

DOI: 10.1111/nph.20133

Link: https://doi.org/10.1111/nph.20133

Author contributions: Chapter 3

M.O.K: Designed and planned all experiments and coordination of the project. Designed all constructs and performed cloning for in vitro and in vivo experiments. Purified stemmadenine acetate from crude workup required as substrates for experiments. Expressed and purified all yeast microsomes for in vitro assays. Performed all in vitro and in vivo experiments, including pathway reconstitution in *N. benthamiana* and *C. roseus*. Analyzed and interpreted data from labelled and non-labelled experiments in vitro and in vivo. Performed preparative scale reactions for the isolation of compounds described in the manuscript. Isolation of products from *N. benthamiana.* Performed LCMS data acquisition and analysis. Prepared all

figures and graphs for the main text and supporting information of the manuscript. Writing the manuscript for publication and subsequent corrections and proofreading.

Y.N: Performed NMR data acquisition and analysis. Structure elucidation of compounds purified. Acquired ECD spectra from compounds isolated. Writing up methods and providing data for supporting information.

K.L: RNA isolation from *T. iboga* tissues for gene amplification.

S.H: Method development for chiral LC-MS analysis.

B.H: Synthesis of (−)-[^{13}C]-tabersonine.

M.C: Assisted with *C. roseus* flower petal transformation.

B.R.L: Formal supervision of the project. Data analysis. Corrections and proofreading of the final draft of the manuscript.

S.E.O: Principle investigator and formal supervison of the project. Data interpretation. Funding, resources, administration, editing and writing of the manuscript for publication.

Chapter 4

Status of publication: written as for publication with the intention of submission

Title: Divergent biosynthesis of monoterpene indole alkaloids from geissoschizine in *Catharanthus roseus*.

Authors: Mohamed O. Kamileen[1,2**], Benke Hong[1,3**], Klause Gasse[1], Maritta Kunert[1], Lorenzo Caputi[1], Benjamin R. Lichman[2], Sarah E. O'Connor[1*]

Affiliations:

[1] Department of Natural Product Biosynthesis, Max Planck Institute for Chemical Ecology, D-07745 Jena, Germany.

[2] Centre for Novel Agricultural Products, Department of Biology, University of York, York YO10 5DD, UK.

[3] Department of Chemistry, Westlake University, 18 Shilongshan Road, 310024, Hangzhou, China.

Author contributions: Chapter 4

M.O.K: Conceptualization of the project. Performed cloning for yeast and *N. benthamiana* expression. Performed cloning for yeast expression and microsomal preparation. Designed VIGS experiments. Harvest and qPCR analysis of VIGS tissue. LCMS data acquisition and analysis. expression. Generation of figures for the draft of the manuscript and supporting information. Writing of daft manuscript.

B.H: Conceptualization of the project. Synthesis of the substrate and isolation of enzyme products. NMR and structural characterization. Cloning of constructs for *N. benthamiana* expression. LC-MS data acquisition. Assistance with yeast expression and microsomal preparation.

K.G: Designed VIGS construct and performed VIGS experiments in *C. roseus*.

M.K: Assisted with LC-MS method development and data acquisition.

L.C: Coordination of VIGS experiments. Assistance with VIGS experiments.

B.R.L: Formal supervision of the project and assistance with proof reading the first draft.

S.E.O: Principle investigator, conceptualization and formal supervison of the project. Proposal of the reaction mechanism and data analysis. Writing the draft of the manucript. Funding, resources, administration for the the proejct.

Acknowledgements

This thesis represents the culmination of years of dedication and perseverance. It would not have been possible without the incredible support and encouragement I have received from so many people along the way.

First and foremost, I owe my deepest gratitude to my supervisors, Prof. Sarah E. O'Connor and Dr. Benjamin R. Lichman. Your guidance, encouragement, and unwavering support, even during challenging times, have been invaluable throughout my PhD journey. Your mentorship has been deeply inspiring, guiding both my personal and scientific development and reshaping my perspective on what it truly means to be a good scientist. I aspire to follow your example, particularly in your scientific vision and the clarity with which you approach and communicate complex ideas. I would also like to extend a special thank you to Prof. Sarah E. O'Connor for offering me the opportunity to be part of the SOC lab in various capacities over the past 10 years and for facilitating this PhD in partnership with The University of York. I am forever grateful to you for your enduring support and trust.

I would also like to express my gratitude to my secondary supervisor, Prof. Neil C. Bruce, for your valuable insights and for being a supportive and encouraging presence throughout my PhD progression. Additionally, I extend my sincere appreciation to Dr. Lorenzo Caputi for sharing your experience and knowledge, and for being a constant and familiar face throughout my scientific journey.

I express my sincere appreciation to everyone who has supported me throughout my PhD journey, contributing to the quality and standard of this thesis. A special thank you to Dr. Yoko Nakamura, Dr. Benke Hong, Dr. Maritta Kunert, Sarah Heinick, Katrin Luck, Dr. Viet Grabe, and Dr. Prashant Sonawanne for always being available and generously sharing your knowledge and expertise. Your support made both the challenging and rewarding moments far more enjoyable. I would also like to extend my thanks to the greenhouse team, especially Dr. Danny Kessler and Eva Rothe, for your invaluable help.

I feel truly fortunate to have worked with both past and present members of the SOC and Lichman labs. Thank you all for contributing to my growth as a scientist and for being a consistent source of inspiration and support. A special thanks goes to Matilde Florian, Dr. Ryan Alam, Dr. Moonyoung Kang, Dr. Carsten Schotte, Dr. Gabriel Titchiner, Dr. Kaouthar ElJounaidi, Dr. Samuel J. Smit, and Dr. Sandesh Swamidatta—your friendship and kindness made my time in research both

personally enriching and truly enjoyable. Last but not least, I would like to extend a special thank you to my steadfast colleague in the SOC lab, Dr. Chloe Langley. Thank you for making the tough days in the lab more manageable with your interlect, energy and humor.

A heartfelt thank you to Grit Winnefeld for all the administrative work and to Dr. Stefan Bartram for your support since I moved to Germany. I am also grateful to all the staff of the SOC lab—every bit of assistance has been truly appreciated.

I would like to express my deep gratitude to Dr. Colwyn Thomas, Dr. Hajo Kries, Dr. Scott Farrow, Dr. Quentin Dudley, Dr. Thu-Thuy Dang, Prof. Jakob Franke, Dr. Evangelos C. Tatsis, Dr. Néstor J. Hernández Lozada, and Dr. Carlos Rodríguez-López. Your kindness, generosity with your time, and mentorship in the past were instrumental in inspiring me to undertake this PhD. I truly cherish the support and guidance you've provided along my journey.

Thank you, Janine Francesca Marie Otto, Marlen Siegmund, Radhika Keshan, and Adiya Tauassarova, for your hard work and for giving me the opportunity to mentor you during your studentships. Working with you has helped me reflect on my journey, both as a person and as a scientist.

To my friends in Jena, thank you for nourishing both my soul and body with your company, meaningful conversations, and quality time together. Giovanni De Angelis, Pamela Medina van Berkum, Raihan Raffii, (Dr.) Marine Vallet, (Dr.) Andrew O'Donnell, and most especially Kelly Chiapolino—I cherish each of you deeply.

Lastly, thank you to my family—Mazeena, Basheer, and Zara. Everything I have and all that I am able to do is because of you. This thesis is dedicated to the three of you.

Al-Ḥamdu lillāh (praise be to God), it has been a fulfilling journey.

Table of Contents

Abstract 2

Declaration 3

Acknowledgements 8

List of Figures 13

List of Tables 21

Abbreviations 22

Chapter 1 Introduction 25

1.1 Plant Specialised Metabolites 25

1.2 Plant Monoterpene Indole Alkaloids (MIAs): Nature's Treasure Trove of Chemistry. 27

1.3 Chemistry of Plant MIAs 28

1.3.1 Occurrence of Plant MIAs 30

1.4 *Tabernanthe iboga* 32

1.4.1 The Discovery, Habitat, and Botany of T. iboga 33

1.4.2 Ethnobotany of *Tabernanthe iboga*. 36

1.4.3 Medicinal Relevance of *Tabernanthe iboga* 36

1.5 Monoterpene Indole Alkaloids (MIAs) of *Tabernanthe iboga* 40

1.5.1 Iboga-type MIAs 41

1.5.2 Aspidosperma-type MIAs 43

1.5.3 Pseudo-aspidosperma-type MIAs 44

1.6 Biosynthesis of Monoterpene Indole Alkaloids (MIAs) 48

1.6.1 Biosynthesis of Strictosidine 49

1.6.2 Biosynthesis of Strictosidine Aglycones 51

1.6.3 Biosynthesis of Geissoschizine 53

1.6.4 Biosynthesis of Stemmadenine 56

1.6.5 Biosynthesis of Dehydrosecodine 62

1.6.6 Biosynthesis of Tabersonine and Catharanthine 65

1.6.7 Biosynthesis of Ibogaine 67

1.7 Modern Approaches to Plant Gene Discovery and Pathway Elucidation. 69

1.7.1 Chemical Hypothesis and Pathway Logic 70
1.7.2 Gene Identification and Candidate Gene Prioritisation 71
1.7.3 Functional Characterization. 73
1.8 The aims and scope of this thesis 75
1.9 References 76
Chapter 2 Recycling Upstream Redox Enzymes Expands the Regioselectivity of Cycloaddition in Pseudo-Aspidosperma Alkaloid Biosynthesis 90
2.1 Graphical Abstract submitted to JACS 91
2.2 Abstract 92
2.3 Manuscript 93
2.4 References 103
2.5 Supporting Information 105
2.7 Supporting References 176
Chapter 3 Streamlined screening platforms lead to the discovery of pachysiphine synthase from Tabernanthe iboga 178
3.1 Summary 179
3.2 Manuscript 180
3.4 References 203
3.5 Supporting Information 209
3.6 Supporting References 272
Chapter 4 Divergent biosynthesis of monoterpene indole alkaloids from geissoschizine in Catharanthus roseus 274
4.1 Abstract 275
4.2 Manuscript (draft) 276
4.3 References 286
4.4 Supporting Information 288
4.5 Supporting references 310
Chapter 5 Conclusions, Future Perspective and Outlook 312
5.1 Conclusions 312

5.1.1 Pseudo-aspidosperma Alkaloid Biosynthesis 312
5.1.2 Pachysiphine Synthase Discovery 313
5.1.3 Divergent Biosynthesis of MIAs from Geissoschizine 313
5.2 Future perspective 314
5.2.1 Integrative Omics Technologies 315
5.2.2 Protein-Protein Interactions 317
5.2.3 Biosynthesis, Chemical Logic and Alternative Routes 317
5.2.4 Pathway Reconstitution and Metabolic Engineering 323
5.2.5 Functional Characterization 323
5.3 Outlook 324
5.4 References 325

List of Figures

Figure 1.1. Classes of the most common plant specialised metabolites. 26

Figure 1.2. Structural diversity of plant monoterpene indole alkaloids (MIAs). 27

Figure 1.3. Strictosidine is the central precursor for MIAs. 29

Figure 1.4. MIA scaffolds and the biogenetic numbering system proposed by Le Men and Taylor[16] 30

Figure 1.5. Distribution of MIAs across angiosperms. 31

Figure 1.6. Native distribution of *Tabernanthe iboga* plant. 32

Figure 1.7. Phylogenetic relationship of genus Tabernanthe in the family Apocynaceae. 34

Figure 1.8. Botany of *Tabernanthe iboga*. 35

Figure 1.9. Ibogaine-inspired synthetic iboga analogues. 38

Figure 1.10. Bioactivity of ibogaine and noribogaine. 39

Figure 1.11. MIA scaffolds found in *T. iboga*. 40

Figure 1.12. Structure of ibogaine. 41

Figure 1.13. Root-specific MIAs found in *Tabernanthe iboga*. 43

Figure 1.14. Shoot-specific aspidosperma-type MIAs found in *Tabernanthe iboga*. 44

Figure 1.15. Shoot-specific pseudo-aspidosperma-type MIAs found in *T. iboga*. 45

Figure 1.16. Tissue-specific distribution of MIAs found in *Tabernanthe iboga*. 47

Figure 1.17. Biosynthesis of (–)-(*S*)-strictosidine. 49

Figure 1.18. Stepwise mechanism of strictosidine synthase (STR). 50

Figure 1.19. Catalytic mechanism of strictosidine β-D-glucosidase (SGD). 52

Figure 1.20. ADH directed reductions of strictosidine aglycones. 54

Figure 1.21. The central role of 19*E*-geissoschizine in MIA scaffold formations. 55

Figure 1.22. Oxidative rearrangement catalyzed by geissoschizine oxidase (GO). 57

Figure 1.23. Stepwise mechanism of the GO-catalyzed oxidative rearrangement of 19*E*-geissoschizine. 58

Figure 1.24. Cytochrome P450 (CYP) catalyzed oxidations of 19*E*-geissoschizine. 59

Figure 1.25. Biosynthesis of stemmadenine from 19*E*-geissoschizine. 61

Figure 1.26. Biosynthesis of dehydrosecodine from stemmadenine. 63

Figure 1.26. Dehydrosecodine-derived MIA scaffolds. 65

Figure 1.27. Biosynthesis of (–)-tabersonine, (+)-catharanthine and (–)-coronaridine. 66

Figure 1.28. Biosynthesis of (–)-ibogaine in *Tabernanthe iboga*. 68

Figure 1.29. Proposed alternative pathway to (–)-ibogaine via (–)-ibogamine in *Tabernanthe iboga*. 69

Figure 1.30. Overview of gene discovery pipeline used in plant pathway elucidation. 70

Figure 1. Dehydrosecodine (1)-derived alkaloids produced by the Apocynaceae family of plants. 94

Figure 2. Biosynthesis of Ψ-tabersonine (5). 95

Figure 3. Formation of 16-carbomethoxycleavamine (10). 98

Figure 4. Proposed mechanism for the formation of (–)-iboga and (+)-Ψ-aspidosperma alkaloids. 99

Figure S1. Amino-acid alignments of cyclases. 125

Figure S2. SDS-PAGE gel image of proteins used for in vitro enzymatic assays. 126

Figure S3. Amino-acid alignments of reductases. 127

Figure S4. Amino-acid alignments of oxidases. 128

Figure S5. Systematic optimization of conditions that lead to production of (+)-Ψ-tabersonine (5), (+)-Ψ-vincadifformine (9) and (–)-coronaridine (4) from stemmadenine acetate (6), TiCorS and TiDPAS1. 129

Figure S6. Systematic optimization of conditions that lead to production of (+)-Ψ-tabersonine (5) and (–)-coronaridine (4) from stemmadenine acetate (6), TiCorS and TiDPAS2. 130

Figure S7. In vitro production of the over-reduced product (+)-Ψ-vincadifformine (9). 131

Figure S8. In vitro coupled enzymatic assays showing optimized production of (+)-Ψ-tabersonine (5), ii. (+)-Ψ-vincadifformine (9), iii. (–)-tabersonine (2) and iv. (–)-coronaridine (4) from angryline (1a). 132

Figure S9. Systematic optimization of conditions that lead to production of (–)-coronaridine (4) from angryline (1a), with TiCorS and TiDPAS homologues. 133

Figure S10. Systematic optimization of pH conditions that lead to production of (–)-coronaridine (4) from angryline, TiCorS and TiDPAS2. 134

Figure S11. Generation of (–)-16(*R*)-carbomethoxycleavamine (10) from angryline (1a), by TiCorS and TiDPAS1. 135

Figure S12. Generation of 16-carbomethoxycleavamine (10a) from acid-catalyzed opening and reduction of (+)-catharanthine (3). 136

Figure S13. Stereochemistry of (–)-16(*R*)-carbomethoxycleavamine (10). 137

Figure S14. In vitro deuterium labelled enzyme assays using stemmadenine acetate (6) as starting material. 138

Figure S15. In vitro deuterium labelled enzyme assays from angryline (1a).. 139

Figure S16. CD spectra of biosynthetic products. 140

Figure S17. Production of (–)-Ψ-tabersonine (5a) and (+)-Ψ-tabersonine (5) from 16-carbomethoxycleavine enantiomers. 141

Figure S18. Production of precondylocarpine acetate (7) from stemmadenine acetate (6). 142

Figure S19. Authentic standards of chemicals used in this study. 144

NMR data for synthesized (–)-Ψ-tabersonine (5a) (pseudo-tabersonine) 147

(–)-Ψ-tabersonine (5a): Phase sensitive HSQC, full range in MeOH-d_3 148

Red: CH_2, black: CH, CH_3 148

(–)-Ψ-tabersonine (5a): Phase sensitive HSQC, aliphatic range in MeOH-d_3 .. 148

Shaded areas mark impurities and solvent, red: CH_2, black: CH, CH_3 148

Structure of (–)-Ψ-tabersonine (5a). Structure optimized using Gaussian 16W (PM6, solvent MeOH). Important ROESY correlations in green. 149

NMR data for (+)-Ψ-tabersonine-d_2 (5-d2) (Enzymatic product, formic acid salt). 150

(+)-Ψ-tabersonine-d_2 (5-d2): Phase sensitive HSQC, full range in MeOH-d_3 ... 151

red: CH_2, black: CH, CH_3 151

(+)-Ψ-tabersonine-d_2 (5-d2): Phase sensitive HSQC, aliphatic range in MeOH-d_3 151

Shaded areas mark impurities and solvent, red: CH_2, black: CH, CH_3 151

NMR data for synthesized (–)-Ψ-vincadifformine (9a) (pseudo-vincadifformine) 152

(–)-Ψ-vincadifformine (9a): Phase sensitive HSQC, full range in MeOH-d_3 153

Shaded areas mark impurities and solvent, red: CH_2, black: CH, CH_3 153

(–)-Ψ-vincadifformine (9a): Phase sensitive HSQC, aliphatic range in MeOH-d_3 153

Shaded areas mark impurities and solvent, red: CH_2, black: CH, CH_3 153

Structure of (–)-Ψ-vincadifformine (9a). Structure optimized using Gaussian 16W (PM6, solvent MeOH). Important ROESY correlations in green..... 154

NMR data for (+)-Ψ-vincadifformine-d_3 (9-*d3*) (pseudo-vincadifformine-d_3) ... 155

(Enzymatic product, formic acid salt). 155

(+)-Ψ-vincadifformine-d_3 (9-*d3*): Phase sensitive HSQC, full range in MeOH-d_3 156

Shaded areas mark impurities and solvent, red: CH_2, black: CH, CH_3 156

(+)-Ψ-vincadifformine-d_3 (9-d3): Phase sensitive HSQC, aliphatic range in MeOH-d_3 Shaded areas mark impurities and solvent, red: CH_2, black: CH, CH_3 156

NMR data for (–)-tabersonine-*d* (2-d) 157

(–)-tabersonine-d (2-*d*): Phase sensitive HSQC, full range in MeOH-d_3 158

Shaded areas mark impurities and solvent, red: CH_2, black: CH, CH_3 158

(–)-tabersonine-d (2-*d*): Phase sensitive HSQC, aliphatic range in MeOH-d_3 . 158

Shaded areas mark impurities and solvent, red: CH_2, black: CH, CH_3 158

NMR data for (–)-16(*R*)-carbomethoxycleavamine (10). 160

(–)-16(*R*)-carbomethoxycleavamine (10): 161

^{1}H NMR with water suppression (zgpr) full range in MeOH-d_3 161

(–)-16(*R*)-carbomethoxycleavamine (10): 161

^{1}H NMR with water suppression (zgpr) aromatic range in MeOH-d_3 161

(–)-16(*R*)-carbomethoxycleavamine (10): 162

^{1}H NMR with water suppression (zgpr) 5.0-5.5 ppm in MeOH-d_3 162

(–)-16(*R*)-carbomethoxycleavamine (10): 162

^{1}H NMR with water suppression (zgpr) aliphatic range in MeOH-d_3 162

(–)-16(*R*)-carbomethoxycleavamine (10): 163

Phase sensitive HSQC, full range in MeOH-d_3 163

(–)-16(*R*)-carbomethoxycleavamine (10): 163

Phase sensitive HSQC, aliphatic range in MeOH-d_3 163

(–)-16(*R*)-carbomethoxycleavamine (10): Phase sensitive HSQC. 164

(–)-16(*R*)-carbomethoxycleavamine (10): HMBC, full range in MeOH-d_3 164

Shaded areas mark impurities and solvent 164

(–)-16(*R*)-carbomethoxycleavamine (10): HMBC. aromatic 165

(–)-16(*R*)-carbomethoxycleavamine (10): HMBC. 165

(–)-16(*R*)-carbomethoxycleavamine (10): HMBC. aliphatic 166

(–)-16(*R*)-carbomethoxycleavamine (10) 1H-1H DQF COSY full 166

(–)-16(*R*)-carbomethoxycleavamine (10) ^{1}H-^{1}H DQF COSY aromatic 167

(–)-16(*R*)-carbomethoxycleavamine (10): ^{1}H-^{1}H ROESY full 168

(–)-16(*R*)-carbomethoxycleavamine (10): ^{1}H-^{1}H ROESY aromatic 168

(–)-16(*R*)-carbomethoxycleavamine (10): ^{1}H-^{1}H ROESY 169

(–)-16(*R*)-carbomethoxycleavamine (10): ^{1}H-^{1}H ROESY aliphatic 169

(–)-16(*R*)-carbomethoxycleavamine (10): ^{1}H-^{1}H ROESY 170

Structure of (–)-16(*R*)-carbomethoxycleavamine (10). Structure optimized Gaussian 16W (DFT, B3LYP-6-311G+(d,p), solvent MeOH). 170

NMR data for (–)-16(*R*)-carbomethoxycleavamine-d (10-*d*). 171

^{1}H NMR with water suppression (zgpr) 2.5 – 3.5 ppm in MeOH-d_3 172

^{1}H NMR with water suppression (zgpr) 2.5 – 3.5 ppm in MeOH-d_3 173

(–)-16(*R*)-carbomethoxycleavamine-d (10-d): Phase sensitive HSQC. Full range 174

(–)-16(*R*)-carbomethoxycleavamine-d (10-d): Phase sensitive HSQC, aliphatic range in MeOH-d_3 174

Comparison of the NMR spectra of (–)-16(*R*)-carbomethoxycleavamine (10) and (+)-16(*S*)-carbomethoxycleavamine (10a) (synthesized from (+)-catharanthine (3)). 175

Fig. 1 The enzymatic reactions involved in aspidosperma and pseudo-aspidosperma alkaloid biosynthesis. 181

Fig. 2 Multigene constructs for (–)-tabersonine and (+)-pseudo-tabersonine production via transient expression in *Nicotiana benthamiana*. 190

Fig. 3 Hydroxylations of aspidosperma alkaloid (–)-tabersonine catalyzed by *Catharanthus roseus* CYP71 enzymes. 192

Fig. 4 Screening of *Tabernanthe iboga* CYP71 for enzymatic activity in *N. benthamiana*. 193

Fig. 5 Characterization of *Tabernanthe iboga* CYP450s in yeast. 195

Fig. 6 Transient overexpression of *Tabernanthe iboga* enzymes in *Catharanthus roseus* var. LBE flowers. 198

Fig. S1 Design of multi-transcriptional unit constructs. 211

Fig. S2 *N. benthamiana* leaf disk assay workflow. 212

Fig. S3 Testing multi-gene constructs in *N. benthamiana*. 213

Fig. S4 Chiral LC-MS analysis of pseudo-tabersonine. 214

Fig. S5 Phylogenetic tree of *Tabernanthe iboga* (Ti) cytochrome P450s. 215

Fig. S6 Iboga CYP71s assayed with (+)-pseudo-tabersonine in *N. benthamiana*. 216

Fig. S7 HPLC isolation of hydroxylated tabersonine products from yeast workup. 217

Fig. S8 Structure elucidation of (–)-16-OH-tabersonine by NMR. 218

Structure elucidation of (–)-16-OH-tabersonine by NMR. (Continued to next page) 218

Fig. S9 MS^2 spectral comparison of lochnericine and CL9160.contig1 product. 223

Fig. S10 Structure elucidation of (–)-pachysiphine by NMR. 224

Fig. S11 Electronic circular dichroism (ECD) spectra of (–)-pachysiphine. ... 230

Fig. S12 Structure elucidation of (–)-16-OH-pachysiphine by NMR. 231

Fig. S13 LC-MS metabolite profiles of *T. iboga* tissues. 237

Fig. S14 MIA precursors present in *C. roseus* var. LBE flower petals. 238

Fig. S15 Derivatization of tabersonine by endogenous enzymes present in *C. roseus flowers*. 239

Fig. S16 Structure confirmation of (–)-[^{13}C]-tabersonine by NMR 240

Fig. S16 Structure confirmation of (–)-[^{13}C]-tabersonine. 241

Fig. S17 Incubation of *C. roseus* flowers with ^{13}C-labelled tabersonine. 242

Fig. S18 Overexpression of TiPS and TiT16H in *C. roseus* flowers. 243

Fig. S19 Overexpression of TiPS and TiT16H in *C. roseus* flowers with ^{13}C-labeled tabersonine 244

Fig. S20 Percentage of identity shared by TiPS and TiT16H with *C. roseus* P450s. 245

Fig. S21 Sequence alignment of TiPS and TiT16H. 246

Fig. S22 Molecular docking of (–)-tabersonine into AlphaFold models of TiPS and TiT16H. 247

Fig. S23 Transcriptomics and metabolomics related to (–)-16-OH-pachysiphine biosynthesis in *T. iboga*. 248

Methods S1 Fig. 1 LC-MS profiles and MS^2 spectra of authentic standards based on $[M+H]^+$ parent ion. 271

Figure 1. Divergent scaffold formations of 19*E*-geissoschizine. 277

Figure 2. Oxidative rearrangements of geissoschizine in *C. roseus*. 279

Figure 3. Biosynthesis of Mavacurane-type alkaloids. 282

Figure S1. Phylogenetic tree of *Catharanthus roseus* (CRO) cytochrome P450s of the family CYP71. 301

Figure S2. Sequence similarity of CrRS and CrSBE to known CYP71AY proteins. 302

Figure S3. Multiple sequence alignments of CrRS and CrSBE. 303

Figure S4. Metabolite analysis of akuammiline in *C. roseus* tissues. 304

Figure S5. In vitro reactions of CrSBE (CRO_T029838). 305

Figure S6. In planta VIGS of CrSBE (CRO_T029838) in *C. roseus*. 306

Figure S7. Metabolite analysis of pleiocarpamine and 16-*epi*-pleiocarpamine in *C. roseus* tissues. 307

Figure S8. In planta VIGS of CrGO in *C. roseus*. 308

Figure 5.1. Proposed biosynthesis of (+)-ibophyllidine and (+)-iboxyphylline. 319

Figure 5.2. Hydroxylations of the iboga-type alkaloid scaffold observed in *T. iboga*. 321

List of Tables

Table S1. Nucleotide sequences for genes cloned and described in this study. 117

Table S2. Primers used in this study. Primer sequences. Primer sequences with homology to the destination plasmid for DNA assembly are in bold. 121

Table S3. Reaction components for the production of final products using stemmadenine acetate (6) as substrate. 123

Table S4. Reaction components for the production of final products using angryline (1a) as substrate. 124

Table S1 Nucleotide sequences of genes transcriptional elements described in this study. 249

Table S2 Primers used in this study. 259

Table S1. Nucleotide sequences for genes cloned and described in this study. 297

Table S2. Primers used in this study. Primer sequences. Primer sequences with homology to the destination plasmid for DNA assembly are in bold. 299

Table S3. VIGS fragment (300 bp) used for silencing. 300

Table S4. Primers used for qPCR analysis. 300

Abbreviations

18-MAC	18-methylaminocoronaridine
18-MC	18-methoxycoronaridine
2-ODD	2-Oxoglutarate/Fe(II)-Dependent Dioxygenases
ADH	Alcohol dehydrogenases
AKR	Aldo-keto reductase
AS	Alstonine synthase
BBL	Berberine bridge-like
BDNF	Brain-derived neurotrophic factor
BGCs	Biosynthetic gene clusters
CD	Circular Dichroism
cDNA	Complementary DNA
CoA	Coenzyme A
CorS	Coronaridine synthase
Cr	*Catharanthus roseus*
CS	Catharanthine synthase
CYP450	Cytochrome P450
DA	Dopamine
DAT	Dopamine transporter
DCS	Dihydrocorynantheine synthase
DFT	Density functional theory
DNA	Deoxyribonucleic acid
DPAS	Dihydroprecondylocarpine acetate synthase
ECD	Electronic Circular Dichroism
EDTA	Ethylenediaminetetraacetic acid
EIC	Extracted ion chromatogram
ER	Endoplasmic reticulum
FAD	Flavin adenine dinucleotide
G6P	Glucose-6-phosphate
G6PDH	Glucose-6-phosphate dehydrogenase
GDND	Glial cell line-derived neurotrophic factor
GO	Geissoschizine oxidase
GS	Geissoschizine synthase
GWAS	Genome-wide association studies
HMBC	Heteronuclear multiple-bond correlation spectroscopy
HPLC	High-performance liquid chromatography
HSQC	Heteronuclear single quantum correlation spectroscopy
HYS	Heteroyohimbine Synthase
I10H	Ibogamine-10-hydroxylase
IPTG	Isopropyl β-D-1-thiogalactopyranoside
KOR	Kappa opioid receptor
LC	Liquid chromatography

LC-MS	Liquid chromatography–mass spectrometry
m/z	Mass-to-charge ratio
MATE	Multidrug and toxic compound extrusion
MEP	Methylerythritol phosphate
MIA	Monoterpene indole alkaloid biosynthesis
MOR	Mu opioid receptor
MS	Mass spectrometry
MTU	Multi-transcriptional unit constructs
N10OMT	Noribogaine-10-O-methyltransferase
$NaBD_4$	Sodium borodeuteride
$NaBH_4$	Sodium borohydride
nAChRs	Nicotinic acetylcholine receptors
NADPD	Deuterated nicotinamide adenine dinucleotide phosphate
NADPH	Nicotinamide adenine dinucleotide phosphate
NMDA	*N*-methyl-D-aspartate
NMDAR	*N*-methyl-D-aspartate receptor
NMR	Nuclear magnetic resonance
NPF	Nitrate/peptide family
PAS	Precondylocarpine acetate synthase
PCR	Polymerase chain reaction
pH	Potential of hydrogen
PIP-seq	Particle-templated Instant Partition sequencing
PMSF	Phenylmethylsulfonyl fluoride
PNAE	Polyneuridine aldehyde esterase
PPI	Protein-protein interactions
PS	Pachysiphine synthase
PTO	Please turn over
PTSD	Post-traumatic stress disorder
PVPP	Oolyvinylpolypyrrolidone
qPCR	Quantitative polymerase chain reaction
QToF	Quadrupole time-of-flight
Redox 1	Redox-enzyme 1
Redox 2	Redox-enzyme 2
RS	Rhazimal synthase
SAT	Stemmadenine acetyltransferase
SBE	Sarpagan bridge enzyme
scMet	Single-cell metabolomics
scRNA-seq	Single-cell RNA sequencing
SD	Standard deviation
SE	Standard error
SERT	Serotonin transporter
SGD	Strictosidine glucosidase
SOM	Self-Organizing Maps

SS	Serpentine synthase
STR	Strictosidine synthase
STU	Single transcriptional unit
SUDs	Substance use disorders
T16H	Tabersonine-16-hydroxylase
T16H	Tabersonine-3-oxidase
T19H	Tabersonine-19-hydroxylase
TBG	Tabernanthalog
TBSV	Tomato bushy stunt virus
TDC	Tryptophan decarboxylase
TEX	Tabersonine 6,7-epoxidase
THAS	Tetrahydroalstonine Synthase
Ti	*Tabernanthe iboga*
TIC	Total ion chromatogram
TLC	Thin-layer chromatography
TS	Tabersonine synthase
VAS	Vitrosamine synthase
VIGS	Virus-induced gene silencing

Chapter 1
Introduction

1.1 Plant Specialised Metabolites

Plant specialised metabolites, also known as secondary metabolites, are organic compounds produced by plants that are not directly involved in primary processes such as growth, development, or reproduction. These compounds are often unique to specific plant species or families and provide various ecological and adaptive functions[1,2]. Although poorly understood, specialised metabolites are essential in plant defence against herbivores, pathogens, and environmental stresses[2,3]. Additionally, they can function as signalling molecules, attractants for pollinators, and mediators of plant-microbe interactions. Recent developments in plant natural product biosynthesis shift the rigid distinction between primary and specialised metabolism[4]. Instead, metabolism is now viewed more dynamically, with primary and specialised pathways seen as interconnected and integrated rather than segregated processes[5]. Broadly speaking, specialised metabolites can be considered the language through which plants communicate and interact with each other and their surrounding environment. These metabolites possess an evolutionary history shaped by natural selection over time.

Humans have used plants for millennia because of for their medicinal properties. It was not known until recently however, that the benefits of these plant preparations, known as paleomedicines[6], were derived from specialised metabolites that were not yet understood or identified. Recent studies also have shown that great apes, such as gorillas and chimpanzees, seek out medicinal plants for self-medication, revealing evolutionary links between specialised metabolites and animals[7,8]. Apart from pharmacological use[9,10], plant specialised metabolites have shaped society and culture by forging relations with empires through the trade of exotic spices with flavour and fragrance, stimulating the age of discovery, seeking the lands in which these plants are sourced, and even serving as catalysts for the Opium wars.

Plant specialised metabolites are typically organized into three classes[11]: terpenoids, phenylpropanoids, and alkaloids (**Figure 1.1**). These compounds are derived from primary metabolic pathways, including isoprenoid metabolism, phenylpropanoid metabolism, and amino acid metabolism. Studying plant specialised metabolites has significantly advanced our understanding of plant biology, evolution, and ecology while paving the way for the development of numerous pharmaceuticals, flavours, fragrances, and other commercially valuable products.

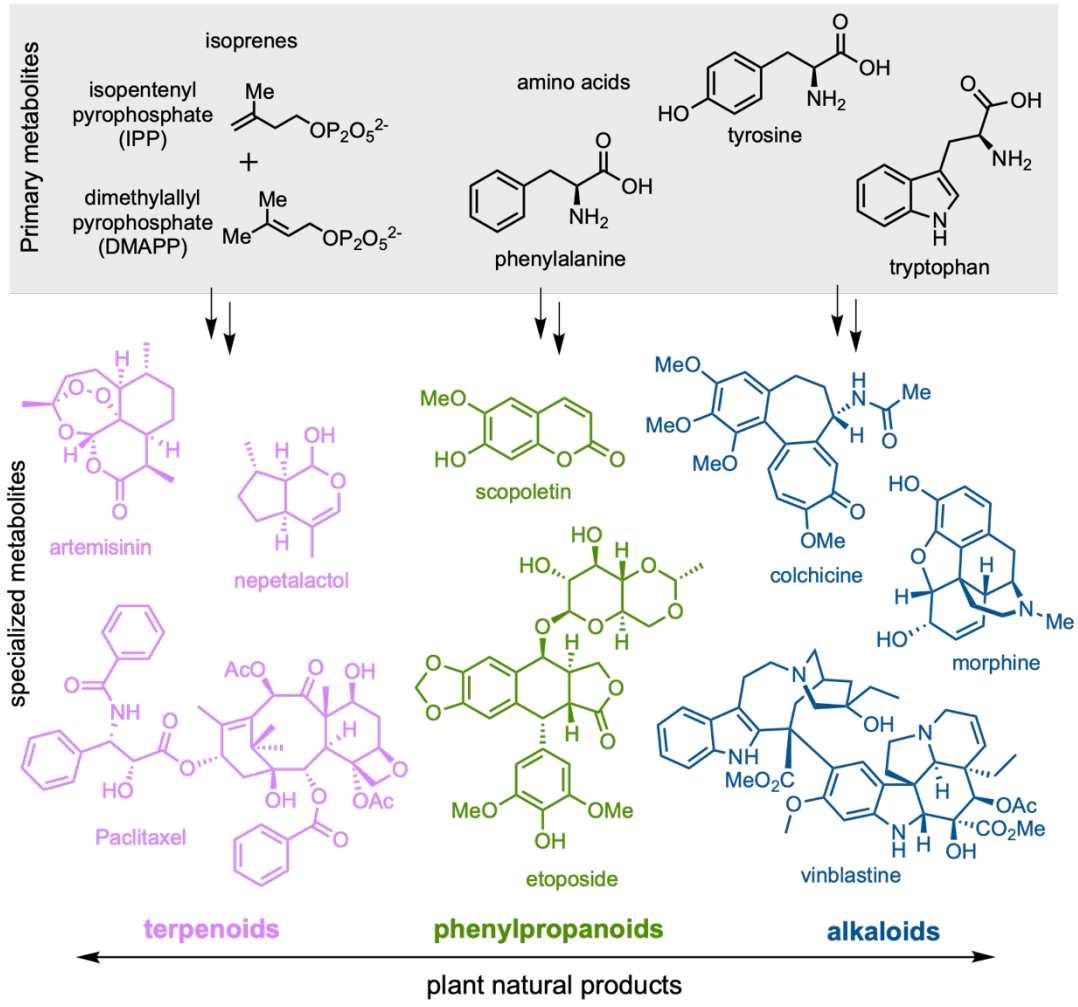


Figure 1.1. Classes of the most common plant specialised metabolites.

Representative chemical structures are highlighted for alkaloids (blue), phenylpropanoids (green), and terpenoids (purple). Specialised metabolites are derived from primary metabolism, including isoprenyl metabolism for terpene biosynthesis and amino acid metabolism for alkaloid and phenylpropanoid biosynthesis.

1.2 Plant Monoterpene Indole Alkaloids (MIAs): Nature's Treasure Trove of Chemistry.

Monoterpene indole alkaloids (MIAs) constitute one of the largest groups of plant-derived alkaloids[12,13]. These structurally diverse molecules exist as both monomeric and dimeric units (**Figure 1.2**). The structural diversity of MIAs is believed to allow plants to adapt to a range of environmental conditions, including defence against predators and pathogens. However, the ecological role of these alkaloids remains to be rigorously investigated. For centuries, humans have utilized plants containing MIAs for their perceived medicinal benefits as treatments for various ailments and as stimulants (**Figure 1.2**).

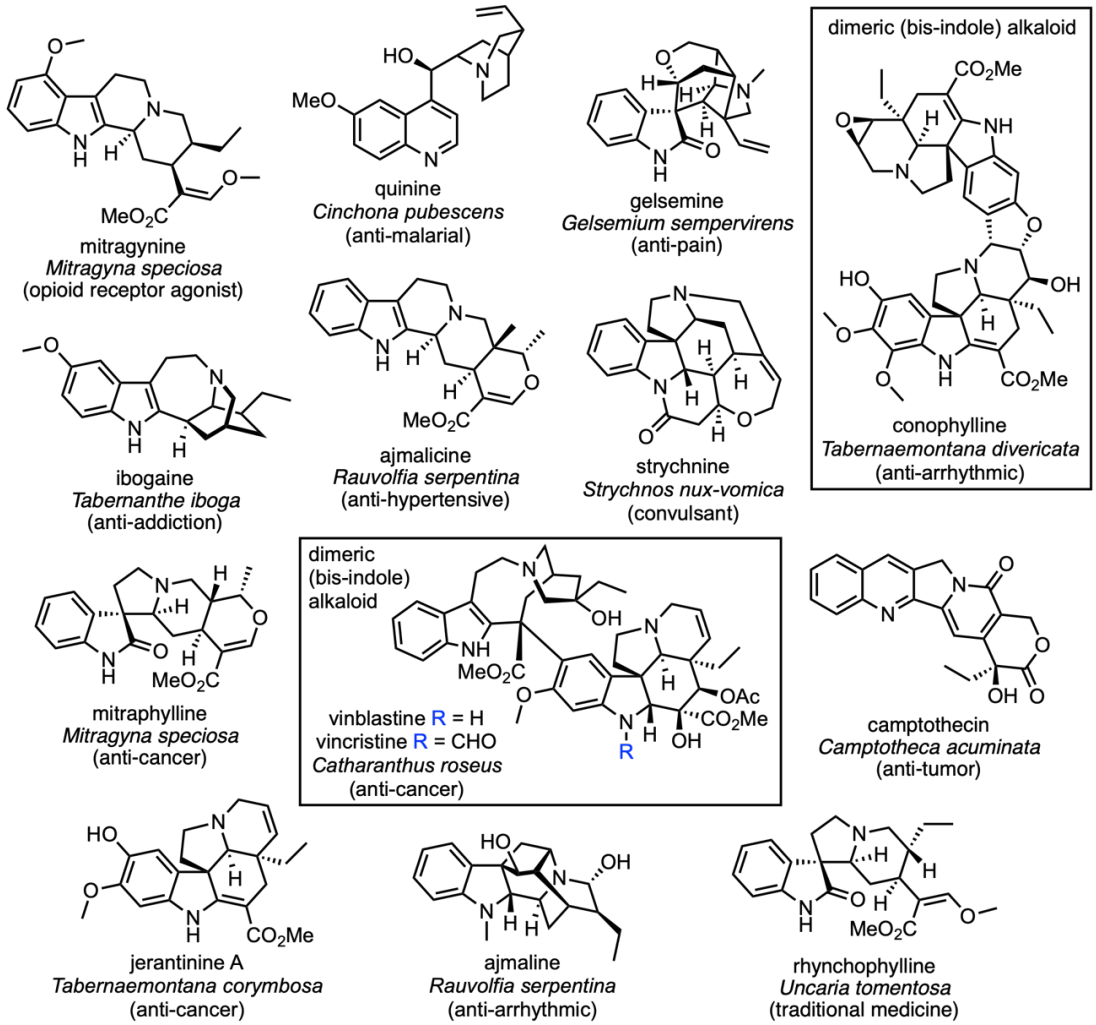


Figure 1.2. Structural diversity of plant monoterpene indole alkaloids (MIAs).

Figure 1.2. Structural diversity of plant monoterpene indole alkaloids (MIAs). MIAs, in nature, form very intricate skeletal arrangements as monomers and dimers (bis-indole alkaloids). Medicinally relevant plant-derived MIAs are presented with biological sources and activity.

The advent of modern chromatography and spectroscopy in the 1960s ushered in new heights of discovery and comparative analysis for phytochemicals, including MIAs. These advancements significantly accelerated the discovery rate of MIAs from groups of plant species with remarkable chemical diversities, a period often referred to as the "grind and find" era of natural products. Although the exact number is difficult to determine, it is estimated that over 3000 MIAs with more than 42 different structural scaffolds[13] have been isolated and structurally characterised from various plants. Recently, there has been a resurgence in the systematic exploration of plants used in traditional medicine, such as Chinese medicine and Ayurveda, to discover rare chemical structures with potential bioactivity[14]. This renewed interest, driven by advances in plant systematics, continues to fuel the discovery of MIAs across the plant kingdom.

Owing to their unique chemistry, coupled with potent biological activities (**Figure 1.2**), MIAs have also gained significant attention in the fields of biotechnology and medicinal chemistry. The versatility of MIA scaffolds has inspired a movement in metabolic engineering to design and build synthetic biology platforms to overproduce MIAs, analogues of MIAs and their precursors in heterologous systems. The structural complexities of MIAs have captured the imagination of synthetic organic chemists, inspiring them to develop pioneering bio-inspired synthetic routes that will contribute to new avenues in drug development.

1.3 Chemistry of Plant MIAs

MIAs are chemically described as aromatic heterocyclic molecules containing a bicyclic structure of a six-membered benzene ring fused to a five-membered nitrogen-containing pyrrole ring[12]. These are true alkaloids formed by two primary building blocks: secologanin (C10 monoterpene unit) and tryptamine (indole unit) (**Figure 1.3**). The monoterpene is derived from the non-mevalonate,

methylerythritol phosphate (MEP) pathway, and the nitrogen-containing indole unit is derived from the amino acid tryptophan, which in turn is from the shikimate pathway. An enzyme-mediated condensation of these two building blocks gives rise to strictosidine, the central precursor molecule for MIA biosynthesis[12,15] (**Figure 1.3**). The biosynthesis of MIAs, including strictosidine, will be discussed in section 1.6.1 of this Chapter.

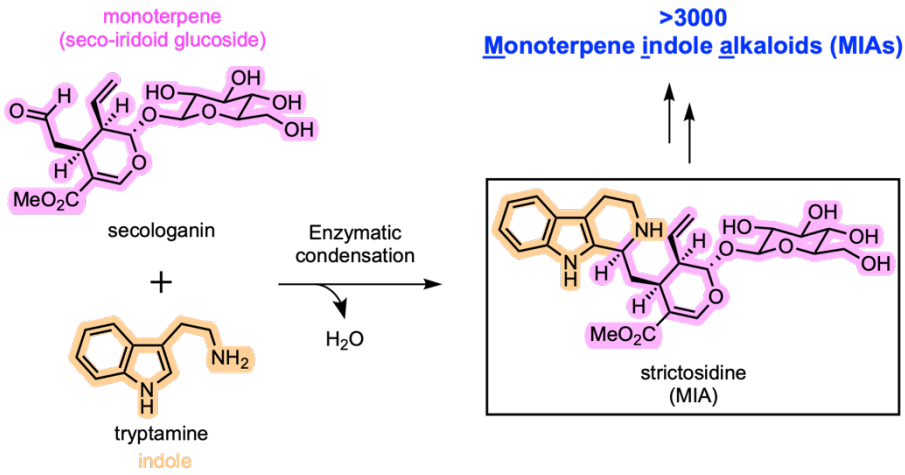


Figure 1.3. Strictosidine is the central precursor for MIAs.
Strictosidine is derived from tryptamine and secologanin.

In 1965, Le Men and Taylor[16] proposed a unified numbering system for MIAs to describe their chemical scaffolds. This system classified MIAs into three types based on their chemical diversity at the time: type I (yohimbinoid class), type II (iboga class), and type III (aspidosperma class) (**Figure 1.4**). While additional scaffolds have been discovered[13] and the nomenclature has expanded significantly, the original numbering system remains a valuable model for tracking atom transformations catalyzed by MIA biosynthetic enzymes.

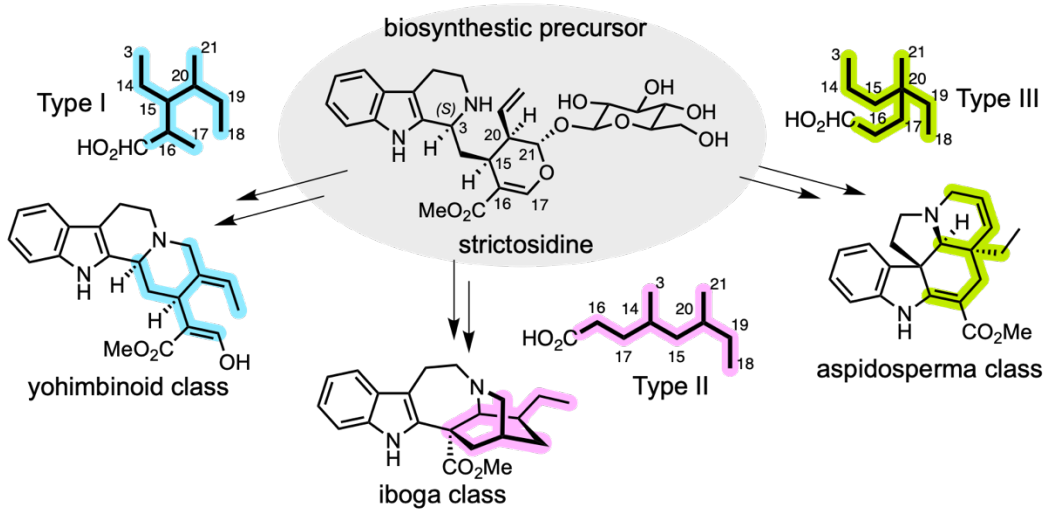


Figure 1.4. MIA scaffolds and the biogenetic numbering system proposed by Le Men and Taylor[16].

1.3.1 Occurrence of Plant MIAs

MIAs are predominantly found in three plant families in Angiosperms, namely Apocynaceae, Loganiaceae, and Rubiaceae, within the order Gentianales (**Figure 1.5**)[12,17,18]. Additionally, MIAs have been identified in the family Nyssaceae and Icacinaceae within the orders of Cornales and Icacinales (**Figure 1.5**). These plant families are globally distributed across regions with rich biodiversity, facilitating adequate pollination and species dispersal[19]. Their presence spans temperate, subtropical, and warm tropical areas, providing the ecological niches necessary to drive the evolution and support the diversity of MIAs produced by these plants.

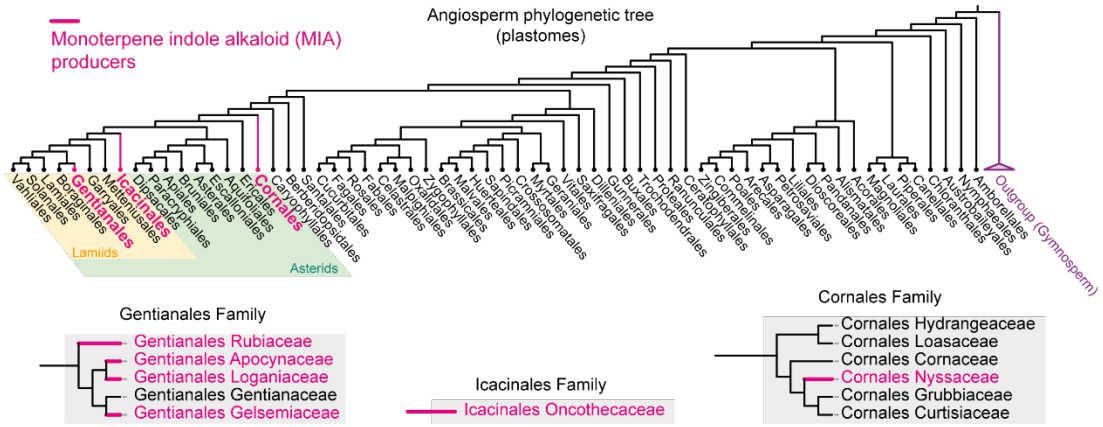


Figure 1.5. Distribution of MIAs across angiosperms.
MIAs are found in the plant orders of Gentianales, Cornales and Icacinales. Plant families associated with the order are shown in grey boxes. Angiosperm phylogenetic tree adapted from most recent phylogenetic inference by Baker[18,20].

Strychnine (**Figure 1.2**), the first MIA to be isolated, was extracted from the seeds of *Strychnos nux-vomica*, a plant from the Loganiaceae family, by Pelletier and Caventou in 1819[21]. The Apocynaceae family, commonly referred to as the dogbane family, accounts for the most extensive distribution and diversity of MIAs reported to date[22–24]. Some well-known plants within this family include *Tabernanthe iboga*[25–27], *Voacanga thouarsii*[28], *Rauvolfia tetraphylla*[29], *Rauvolfia serpentina*[30], *Alstonia scholaris*[31], and the model plant *Catharanthus roseus*[32].

Catharanthus roseus, commonly known as Madagascar periwinkle, is a medicinal plant renowned for producing the anti-cancer alkaloids vinblastine and vincristine[32] (**Figure 1.2**). This plant is known to make over 150 MIAs across various tissues and has been extensively studied for its ability to biosynthesize some of the most complex alkaloids found in nature[32,33]. With one of the most complex plant biosynthetic pathways, *C. roseus* has become a model system for investigating MIA biosynthesis. Much of what is known about MIAs today was either discovered in or functionally characterised using this plant. Research on MIA alkaloids in *C. roseus* spans over 60 years, beginning with the discovery of vinblastine and continuing to this day.

1.4 *Tabernanthe iboga*

Tabernanthe iboga, commonly known as iboga, is a medicinal plant in the Apocynaceae family[34]. This perennial understory shrub is native to the tropical forests of West and Central Africa, specifically in regions such as Gabon, Cameroon, Congo, the Democratic Republic of the Congo, the Central African Republic, and Angola[35] (**Figure 1.6**). *T. iboga* holds significant cultural value in West Central Africa, particularly within Bwiti communities in Gabon, where it is used as a sacrament in rites of passage and healing ceremonies[35]. The roots and bark of the iboga plant are highly valued for their psychoactive effects[36,37], primarily due to the presence of MIAs, with ibogaine being the most prominent[34]. In the 1960s, the plant extracts potential for treating substance use disorders sparked the emergence of a medical subculture and initiated research into its clinical applications. This section will address the botany, ethnobotany, MIA diversity and the medicinal relevance of this plant.

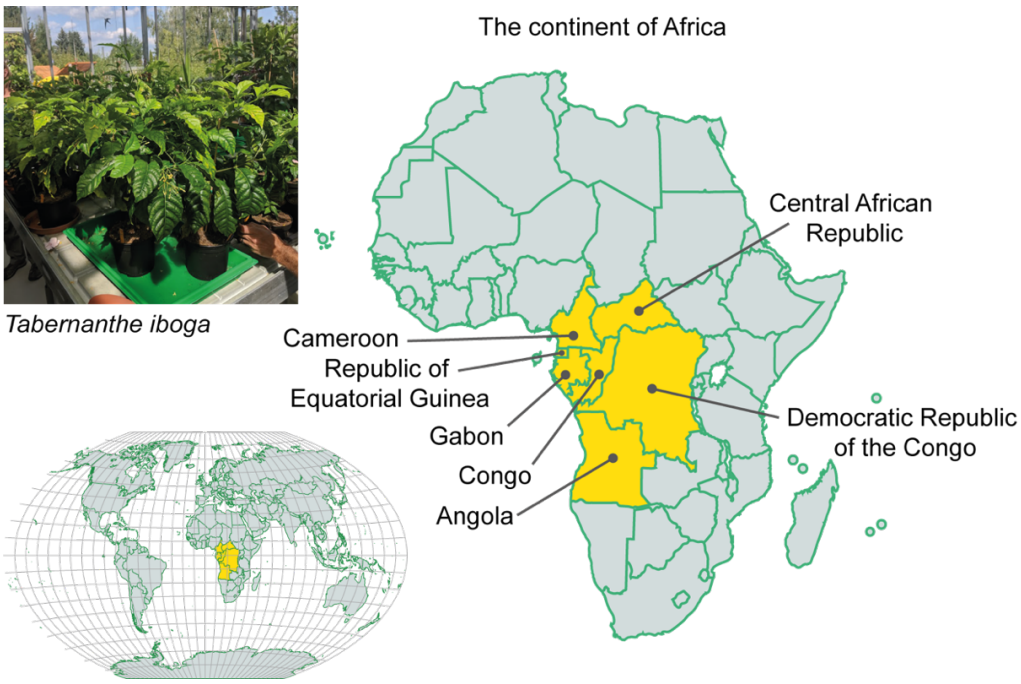


Figure 1.6. Native distribution of *Tabernanthe iboga* plant.
Iboga is native to the tropical forests of West and Central Africa. Image shows *T. iboga* plants grown at the greenhouse of Max-Planck Institute for Chemical Ecology, Jena, Germany. Photo credits, Mohamed Omar Kamileen.

1.4.1 The Discovery, Habitat, and Botany of *T. iboga*

In the 19th century, Belgian and French colonists made the earliest known Western references to the plant *Tabernanthe iboga*. These initial observations were part of the broader colonial exploration and documentation efforts in West Africa and the Congo basin[35]. In 1864, Griffon du Bellay recorded the use of iboga near Cape Lopez, Gabon[34]. He noted that the indigenous people consumed iboga root in small quantities, describing its effects as a nervous system stimulant. This use was particularly prevalent among warriors and hunters, who ingested iboga roots and bark powder to combat fatigue and maintain alertness during their activities. In 1889, a French botanist, Henri Baillon, presented the first formal botanical description of *Tabernanthe iboga* at the Linnaen Society in Paris, officially naming the plant[34,35]. The genus *Tabernanthe* derives from Tabernae-anthos (similar to *Tabernaemontana* flowers), whereas the species name iboga derives from the Tsogho word “to heal”[34].

Botanist Stapf reported seven species within the genus *Tabernanthe* from the West African region, stabilizing the genus in the early 1900s. Later, in 1988, Leeuwenberg[38] (Wageningen, Netherlands) revised the taxonomy of the genus *Tabernanthe* and recognized only two of the species, *Tabernanthe iboga* (Baillon) and *Tabernanthe elliptica* (Stapf) Leeuwenb[38]. This led to consolidating the genus *Tabernanthe* into two species, aligning with most herbarium specimens documented. Additionally, these records suggest that hybridization between the two species, *T. iboga* and *T. elliptica,* could result in progeny that may not be botanically distinct, indicating the possibility of genetic exchange between the two species. The ethnobotanical significance of *T. iboga* has overshadowed the study and curation of the other species in this genus, which are indigenous to West Africa’s geography. This focus has contributed to the poorly resolved taxonomic relationship between the genus *Tabernanthe* and the closely related genera *Tabernaemontana* and *Voacanga* within the Apocynaceae family[39] (**Figure 1.7**). These genera also produce psychoactive compounds[37].

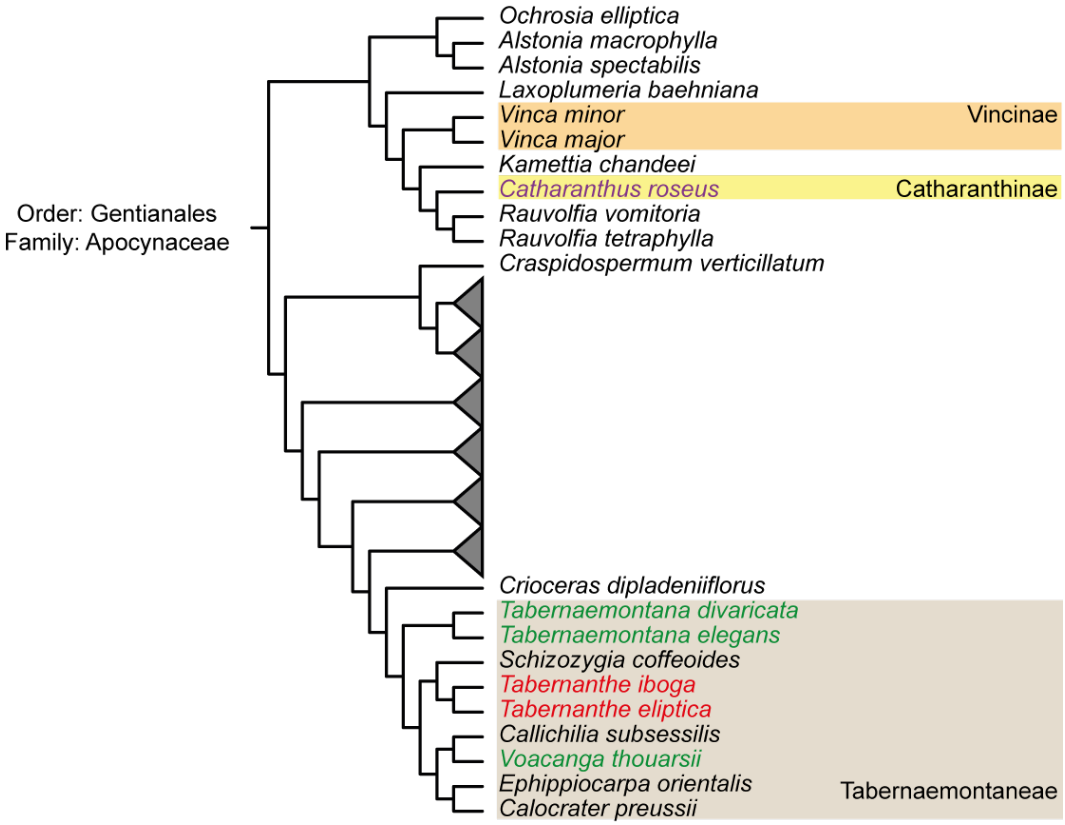


Figure 1.7. Phylogenetic relationship of genus *Tabernanthe* in the family Apocynaceae.

The genus *Tabernanthe* (red) is phylogenetically related to the *Tabernaemontana* (green) and *Voacanga* (green) genus. The tribe Tabernaemontaneae (brown) is known to produce psychoactive MIAs[37]. The phylogenetic relationship between the well-studied Catharanthinae and Vincinae tribes are highlighted in yellow and orange, respectively. The phylogenetic tree was adopted from the Tree of Life[40].

The botanical aspects of *T. iboga* are well-documented, with detailed descriptions of its morphology, habitat, and growth characteristics available in various studies[34,35,38,41,42]. In the wild, *T. iboga* thrives in well-drained soils around riverine forests, preferring the shade of forested canopies. This evergreen shrub can range from a 1 m shrub to a 10 m tree. It features opposing pairs of oval-shaped glossy leaves, each measuring about 5-20 cm in length and 3-5 cm in width. The flowers of iboga are small, approximately 1 cm in diameter, blossoms with white and pink colours, and consist of five petals. The stem diameter varies from 0.2 cm to 3 cm, and it is woody and thick. It contains a significant amount of latex and emits a noxious smell. The fruits of iboga come in pairs, are inedible, and range in colour from sunshine yellow to orange. They are oblong, measuring about 5 cm in length

and 3 cm in diameter. Inside, the pericarp is smooth, and the mesocarp is pulpy and white, containing 15-20 wrinkled seeds, each approximately 0.5 cm in diameter. Interestingly, the fruits are used as a classification system by the Indigenous community in Gabon. The male iboga is distinguished by its lengthened fruits, while the female iboga is characterised by its globular fruit. Despite its distinct morphology, the pollination and breeding systems of *T. iboga* remain poorly understood. Images of the *T. iboga* plants grown at the greenhouses of the Max-Planck Institute for Chemical Ecology, Jena, Germany, are presented in **Figure 1.8**.

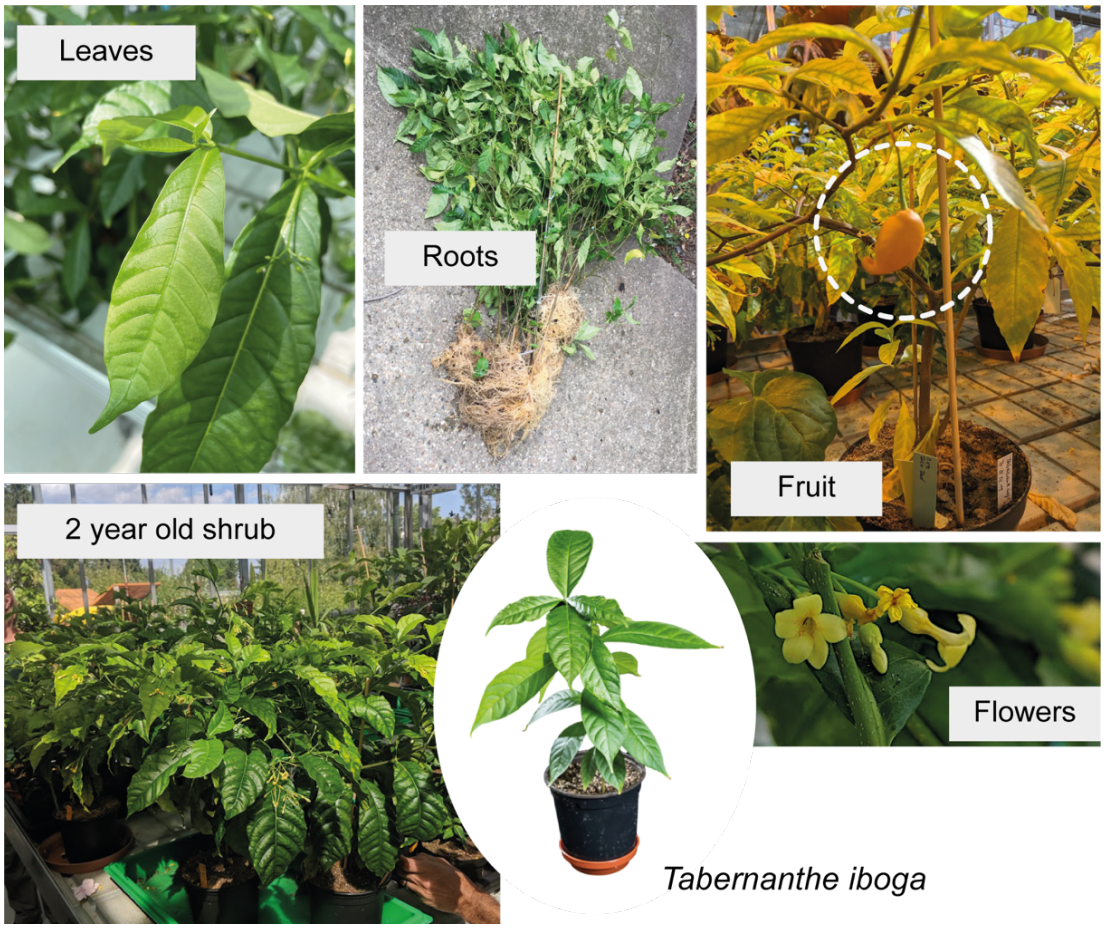


Figure 1.8. Botany of *Tabernanthe iboga*.
Images of plant leaf, roots, fruit, and flowers of *T. iboga* grown in the greenhouses of the Max-Planck Institute for Chemical Ecology, Jena, Germany. Photo credits, Mohamed Omar Kamileen.

1.4.2 Ethnobotany of *Tabernanthe iboga*.

Ethnobotany, the study of how people of a particular community or region use native plants, has been well-documented for iboga in West Africa thanks to the efforts of Fernandez J. W. and Fernandez R. L[41]. It is believed that the Pygmies of the Congo Basin first encountered the iboga plant by observing wild animals such as boars, gorillas, and elephants dig up and consume its roots, after which the animals would enter a state of wild frenzy[35,41].

Iboga is widely adopted as a medicinal plant, and communities often cultivate it near their villages. Traditional healers have employed different parts of the plant administered alone or as in mixture with other herbal extracts to address ailments such as fever, stomachaches, mental disorders, depression, and addiction to local narcotics and alcohol. Extracts from the plant are ordinarily used as neuro-stimulants to combat fatigue and maintain alertness or an aphrodisiac. This initial documentation was instrumental in paving the way for further exploration of the plant's pharmacological and therapeutic potential.

In Gabon, the iboga plant, commonly referred to as "eboka," is considered sacred[34,41]. For centuries, it has been an integral part of the rituals practiced by the Bwiti and Mbiri communities, and it continues to be used in their ceremonies to the present day. It is used in rituals that mark important life transitions and is believed to facilitate communication with ancestors, reflecting its deep spiritual significance. This is achieved by consuming iboga roots, which induce powerful visions and experiences in waking-dream hallucinations, allowing initiates to connect with ancestors and the spiritual world. *T. iboga* commemorates life and death within Bwiti society in West Africa.

1.4.3 Medicinal Relevance of *Tabernanthe iboga*

The medical use of ibogaine began in France in 1939 when the root extracts of *Tabernanthe manii* containing ibogaine were sold under the product name Lambarène[36,43]. It was marketed to relieve fatigue, treat depression, and aid in recovery from infectious diseases. Later, the drug was discontinued in the late 1960s. Howard Lotsof is credited for discovering ibogaine’s anti-addiction properties to treat

substance use disorders (SUDs). In 1962, Lotsof, a heroin user, reported overcoming his addiction after using ibogaine[36]. He later pioneered the development of ibogaine for anti-addiction treatment in the form of Endabuse®[44,45], a procedure describing the formulation and administration of ibogaine for use in human SUD treatment and secured four patents related to its use. Despite Ibogaine's legal status change in the United States of America (USA) in the late 1960s, through international coalition, several clinical studies provided support for ibogaine's efficacy in anti-addiction and as a promising target for SUD treatment[46]. The US National Institute on Drug Abuse funded clinical trials on ibogaine, but these were hampered due to its safety, legal challenges and industry opposition. Despite its therapeutic promise, ibogaine use is associated with adverse effects, including cardiotoxicity, hallucinations, neurotoxicity, and fatalities, raising concerns about safety[47,48]. Nevertheless, a subculture within the medical community emerged, advocating for ibogaine's use in addiction treatment[36]. Several excellent reviews have been published, outlining the history, development, early clinical studies, and the medical subculture of ibogaine[34,36,43,49,50].

Recently, there has been a renewed interest in ibogaine research to develop commercially viable treatments and create the next generation of therapeutics[51,52] for SUDs and psychological conditions such as depression and post-traumatic stress disorder (PTSD). Clinical trials featuring appropriate double-blind and placebo-controlled methods have advanced in demonstrating the efficacy of ibogaine across various model systems, including mice and zebrafish[52–54]. Synthesis of ibogaine or *iboga-type* analogues, known as ibogalogs, has improved to enhance bioactivity as psychedelics and, in turn, develop safer, non-hallucinogenic lead compounds for clinical testing. Naturally occurring alkaloids from *T. iboga,* such as ibogaine, noribogaine, coronaridine, and tabernanthine, have inspired the development of potential therapeutic ibogalogs[52], including 18-methoxycoronaridine (18-MC), 18-methylaminocoronaridine (18-MAC), and tabernanthalog (TBG) (**Figure 1.9**).

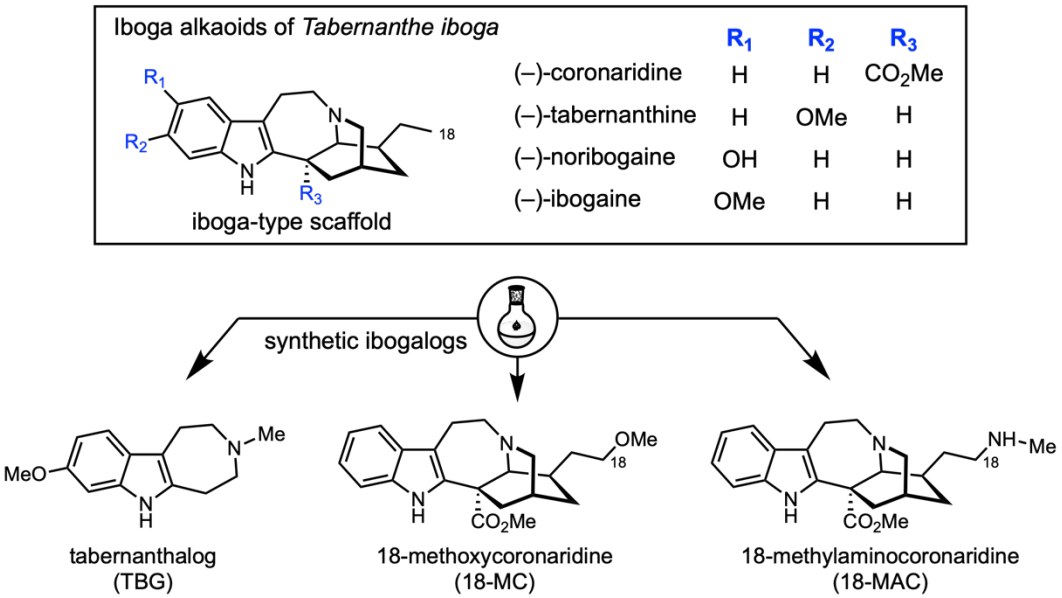


Figure 1.9. Ibogaine-inspired synthetic iboga analogues.
Ibogalogs are inspired by naturally occurring alkaloids with core *iboga-type* scaffold.

Ibogaine exhibits both psychedelic and anti-addictive effects in humans and animals[55–57]. It is highly lipophilic and is metabolized to noribogaine through the function of cytochrome P450 (CYP450) 2D6 enzyme[58]. It has a half-life of 2-5 hours[59], after which it is cleared from the bloodstream. The molecular mechanisms by which ibogaine exerts its psychoactive and anti-addictive effects used to treat substance use disorders (SUDs) remain cryptic and not fully elucidated. It is known to engage with weak affinity across multiple receptors in the brain, including *N*-methyl-D-aspartate (NMDA), serotonin (5HT2, 5HT3), acetylcholine, nicotinic kappa-opioid, and mu-opioid receptors, affecting neurotransmitter release and transport[55,57,60] (**Figure 1.10**). Although poorly understood, ibogaine impacts brain-derived neurotrophic factor (BDNF) and glial cell line-derived neurotrophic factor (GDNF) release, activating a link for neuroplastic changes beneficial in treating neurological and psychiatric disorders[57].

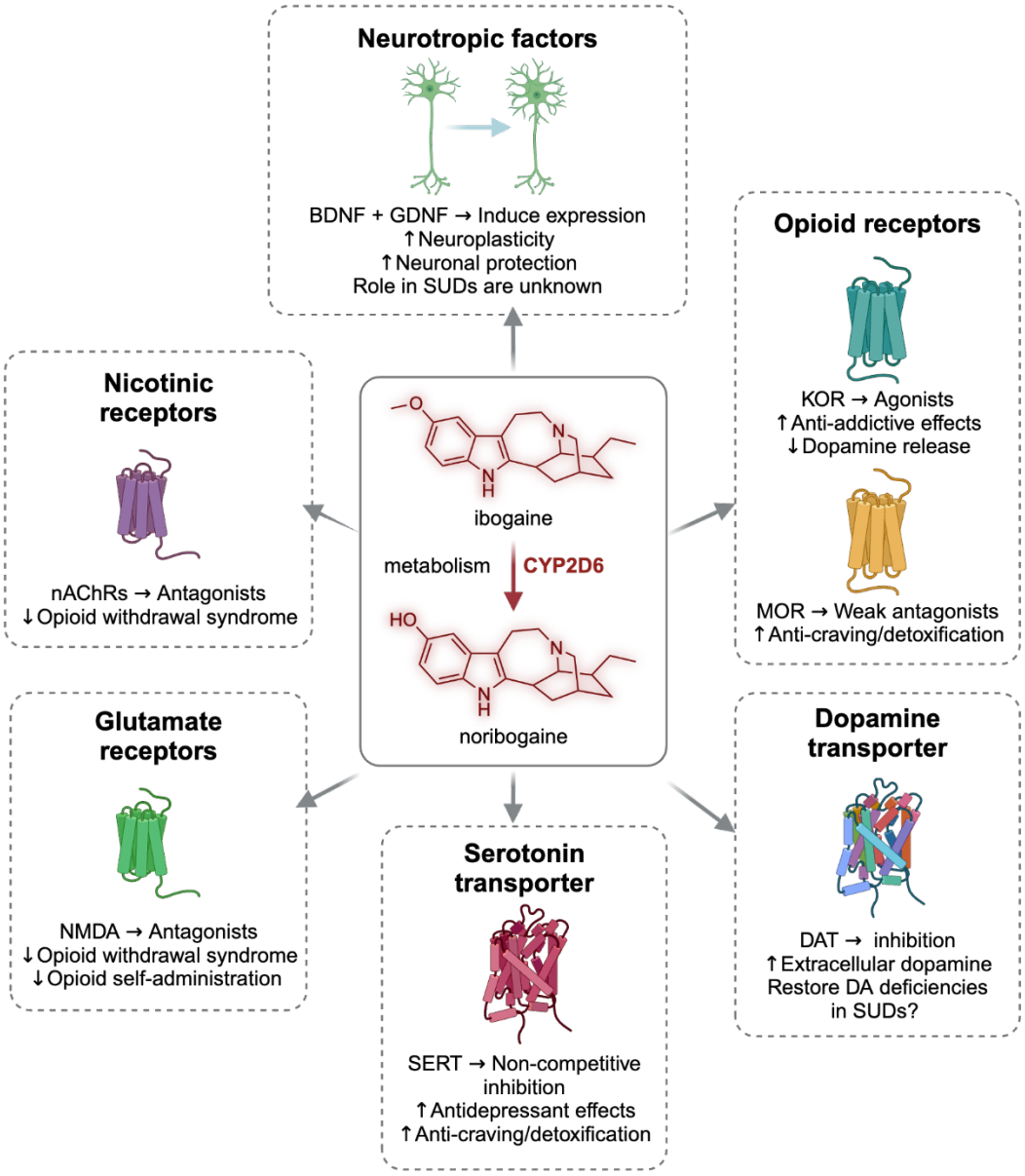


Figure 1.10. Bioactivity of ibogaine and noribogaine.

Ibogaine is metabolized to noribogaine by the CYP2D6 enzyme. Iboga alkaloids bind to many neural receptors. BDNF: brain-derived neurotrophic factor; GDNF: glial cell-derived neurotrophic factor; DA: dopamine; DAT: dopamine transporter; KOR: kappa opioid receptor; MOR: mu opioid receptor; nAChRs: nicotinic acetylcholine receptors; NMDAR: *N*-methyl-D-aspartate receptor; SERT: serotonin transporter; SUDs: substance use disorders. Figure adapted from Ona[59] review on ibogaine's mode of action. Figure created using BioRender (https://www.biorender.com).

1.5 Monoterpene Indole Alkaloids (MIAs) of *Tabernanthe iboga*

Iboga contains a variety of MIAs that are distributed across the plant at various concentrations in a tissue-specific manner. Natural product isolation studies have led to the successful isolation and characterization of some of the most abundant MIAs produced by *T. iboga*[61–65].

Based on the isolation studies, the three major MIA structural scaffolds, *iboga-type*, *aspidosperma-type*, and *pseudo-aspidosperma-type* alkaloids found in iboga, can be classified according to their tissue-specific distribution (**Figure 1.11**). These alkaloid scaffolds are accumulated within the plant in a shoot-specific or root-specific manner. *Iboga-type* alkaloids are primarily, and in some cases exclusively, found in the root-specific tissues. In contrast, *aspidosperma-type* and *pseudo-aspidosperma-type* alkaloids are mainly observed in shoot-specific tissues. This section will describe these structural scaffolds and their representative MIAs in *T. iboga*.

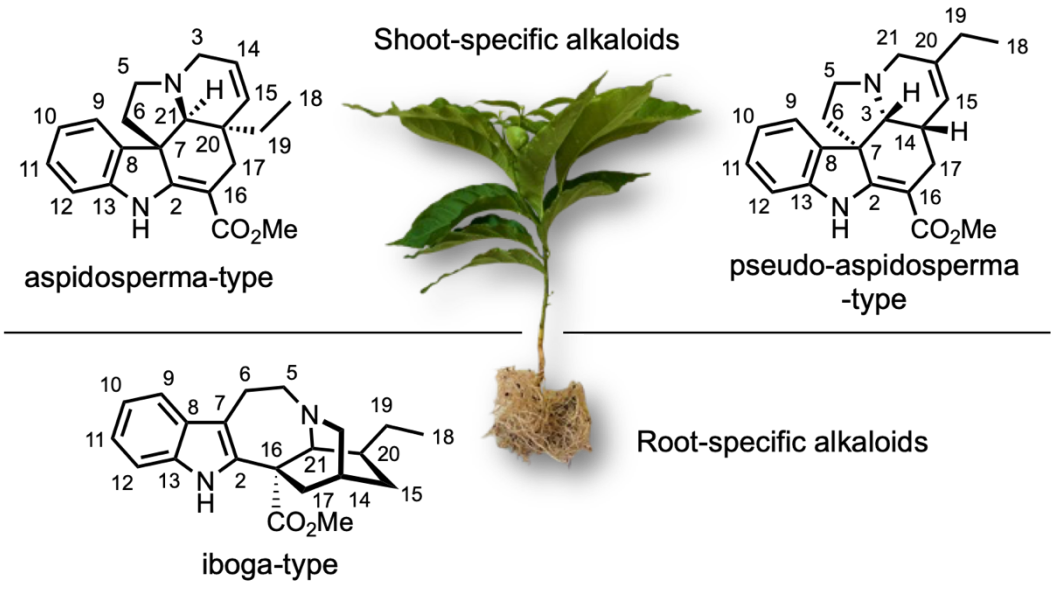


Figure 1.11. MIA scaffolds found in *T. iboga*.
Root-specific MIAs are predominantly of the *Iboga-type* scaffold. The shoot-specific MIAs found in iboga are of both *aspidosperma-type* and *pseudo-aspidosperma-type* scaffolds. Roots-specific describes tissues containing roots and the main stem of the plant, while shoot-specific describes tissues containing flowers, young leaves, and

mature leaves. Le Men and Taylor numbering convention[16] is indicated for the respective MIA scaffolds.

1.5.1 *Iboga-type* MIAs

The root-specific alkaloids of *T. iboga* are predominantly of the iboga scaffold (*iboga-type*) (**Figure 1.11**). This scaffold is defined by the unique 6-5-7-6-6 ring system, which comprises an indole and 7-membered tertrahydroazepine fused to an isoquinuclidine ring to form a pentacyclic skeleton with a tertiary amine serving as the bridgehead (**Figure 1.12a**). The roots contain up to 17 different *iboga-type* MIAs in various amounts[42,65]. The root bark is particularly valued because of its high accumulation of the psychoactive compound ibogaine (**Figure 1.12a**). Interestingly, the *iboga-type* alkaloids produced by *T. iboga* and, at large, the Tabernaemontaneae tribe are structurally different to catharanthine, a well-known *iboga-type* alkaloid exclusively produced in the related vinblastine-producing species, *Catharanthus roseus*[66]. Catharanthine, although it resembles the *iboga-type* scaffold, belongs to the opposite optical series to other known iboga alkaloids[26,27] (**Figure 1.12b**).

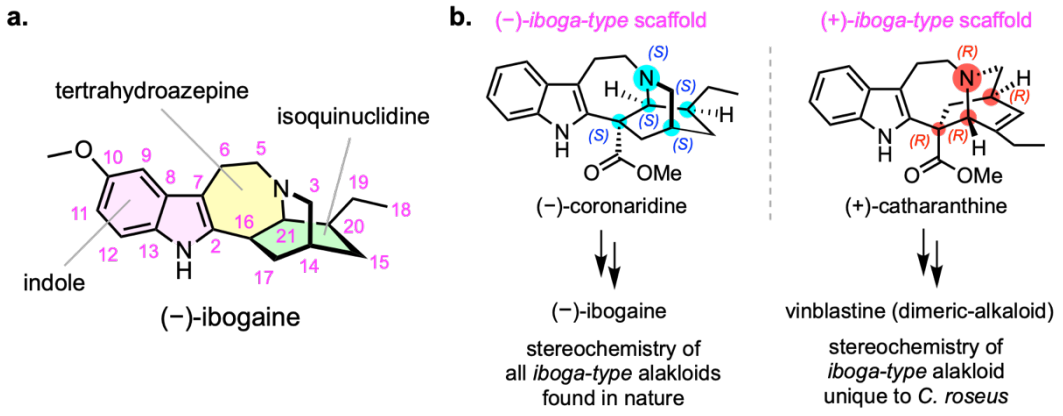


Figure 1.12. Structure of ibogaine.

(**a**) Ibogaine is an *iboga-type* MIA with a carbon ring system comprising an indole, a seven-membered tetrahydroazepine, and a bicyclic isoquinuclidine core[51]. (**b**) Catharanthine is an *iboga-type* alkaloid found with opposite stereochemistry to *iboga-type* alkaloids found in *T. iboga*. (–)-Coronaridine is a precursor to (–)-ibogaine, and the stereocenters of (–)-coronaridine and (+)-catharanthine are highlighted in blue and red, respectively.

Ibogaine is prized for its action on the central nervous system as a hallucination-inducing psychoactive MIA[51]. The biology and chemistry of *T. iboga* have primarily focused on the plant's accumulation of ibogaine, and its structure-activity relationship has drawn scientific attention for many decades. French chemists Dybowski and Landrin isolated ibogaine as a hydrochloride salt from the plant in 1901[34]. The chemical configuration of ibogaine was determined by Bartlett, Dickel, and Taylor in 1958[67]. Arai, Coppola, and Jeffrey confirmed the absolute stereochemistry of ibogaine by X-ray crystallography in 1960[68]. The first total synthesis of ibogaine as a racemate was achieved by Büchi in 1966[69] through a 15-step process, resulting in an overall yield of 0.2%[69]. The complexity of this scaffold, with its unique 6-5-7-6-6 ring system, presents a challenging target for total synthesis with enantiomeric purity. Several significant syntheses of ibogaine have been developed to increase the yield up to 4.6%[70] from its pioneering route. On the other hand, iboga produces enantiomerically pure (–)-ibogaine up to 6 mg/g of its dry weight [63].

In addition to ibogaine, the plant accumulates other related *iboga-type* MIAs in the root[42,61,67]. These include (–)-coronaridine, (–)-voacangine, (–)-tabernanthine, (–)-ibogamine, (–)-nortabernanthine, (–)-noribogaine, and (–)-ibogaline (**Figure 1.13a**). Also, other MIAs in the roots have been identified as chemical oxidation products[63] of ibogaine and noribogaine due to light exposure and solvent effects (**Figure 1.13b**).

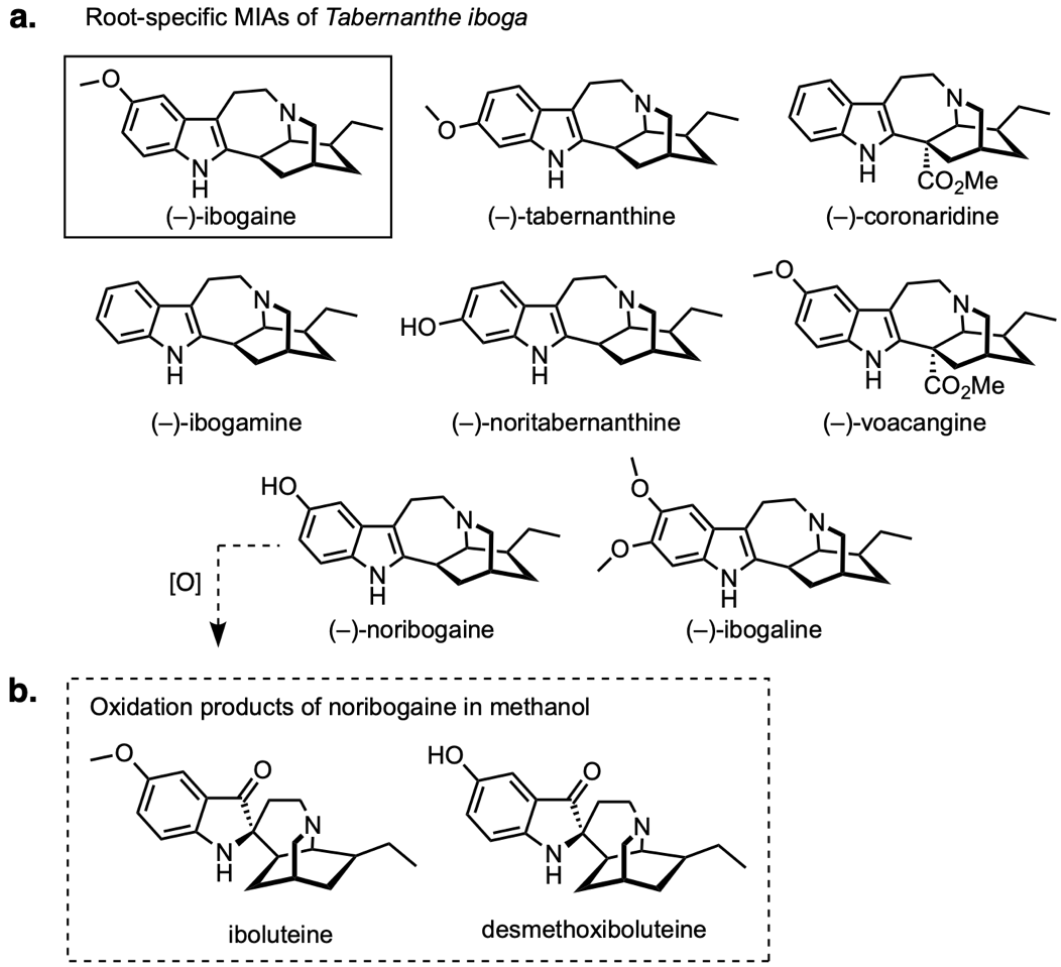


Figure 1.13. Root-specific MIAs found in *Tabernanthe iboga*.
(**a**) *Iboga-type* (*iboga-type* scaffold) alkaloids found in the roots of *T. iboga* with the principal alkaloid, ibogaine. (**b**) Oxidation products of noribogaine.

1.5.2 *Aspidosperma-type* MIAs

Aspidosperma-type alkaloids are more abundant than *iboga-type* alkaloids, both in the number of identified compounds and their broader distribution across species within the *Apocynaceae* family. In *T. iboga*, *aspidosperma-type* alkaloids, followed by the rare *pseudo-aspidosperma-type* alkaloids, are shoot-specific (**Figure 1.11**). These alkaloids are predominantly localized in the aerial tissues, with concentrations varying across different parts of these tissues in a tissue-specific manner.

The *aspidosperma-type* alkaloids form a unique structural skeleton which consists of an indole-based pentacyclic core fused to a 6-6-5 ring system named A-

E[71] (**Figure 1.14a**). In iboga, MIAs of this structural scaffold are primarily found in the plant leaves[71–73], as highlighted in **Figure 1.14b**. These alkaloids exhibit a broad range of biological activities, including antimicrobial, antimalarial, and antitumor activities[71].

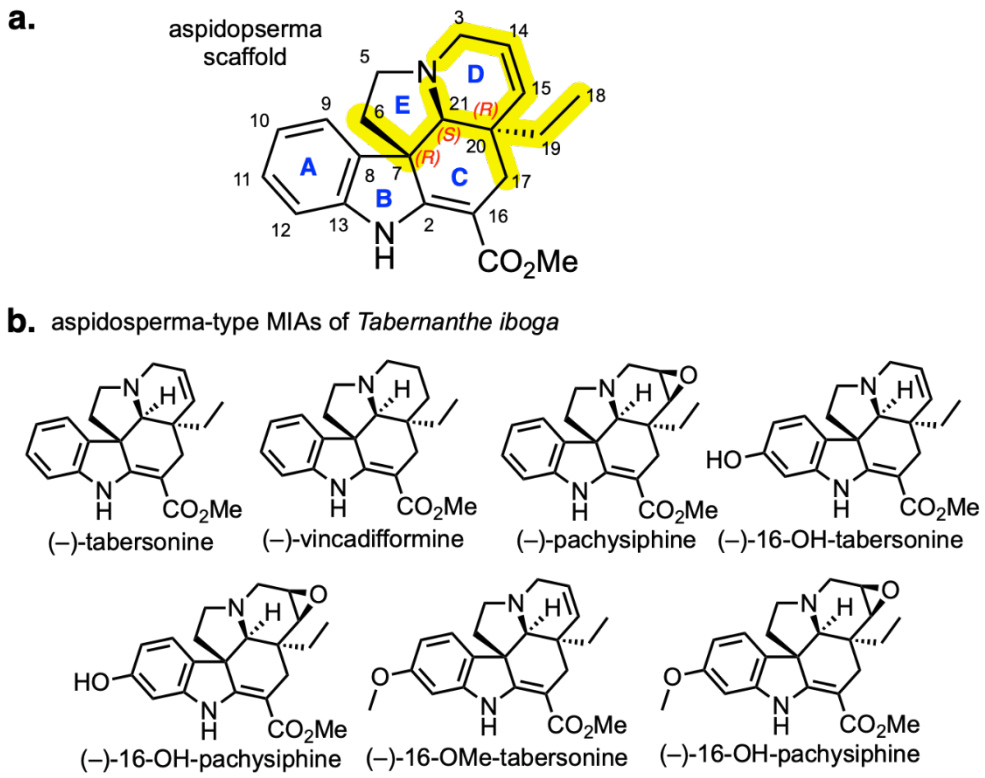


Figure 1.14. Shoot-specific *aspidosperma-type* MIAs found in *Tabernanthe iboga*.

(**a**) Chemical structure of the core aspidosperma-scaffold. The 6-5-6-6-5, A-E ring configuration is shown with bond configuration (yellow) alongside stereocenters (red) with Le Men and Taylor numbering. (**b**) *Aspidosperma-type* MIAs found in the plant leaves of *T. iboga*.

1.5.3 *Pseudo-aspidosperma-type* MIAs

Additionally, the aerial parts of *T. iboga* accumulate *pseudo-aspidosperma-type* (pseudo-aspidosperma scaffold) alkaloids, are rarely found in nature, and their biosynthetic origins remain less understood compared to more widely studied MIA scaffolds. Similar to the aspidosperma scaffold, the pseudo-aspidosperma scaffold

consists of an A-E fused ring structure with an alternative bond configuration compared to the typical aspidosperma skeleton (**Figure 1.15a**). Several of these alkaloids have been characterised from the aerial tissues of *T. iboga*, including (+)-pseudo-tabersonine, (+)-pseudo-vincadifformine, (+)-pandoline, (+)-ibophyllidine, and (+)-iboxyphylline (**Figure 1.15b**). The rarity of this alkaloid scaffold in nature, along with the challenges posed by total synthesis, particularly due to the multiple stereocenters, has left their bioactivity largely unexplored. This thesis describes the biosynthesis of (+)-pseudo-tabersonine and (+)-pseudo-vincadifformine, the biogenetic precursors required for the formation of *pseudo-aspidosperma-type* MIAs in *T. iboga* (**Figure 1.15b**). The detailed findings are presented in Chapter 2.

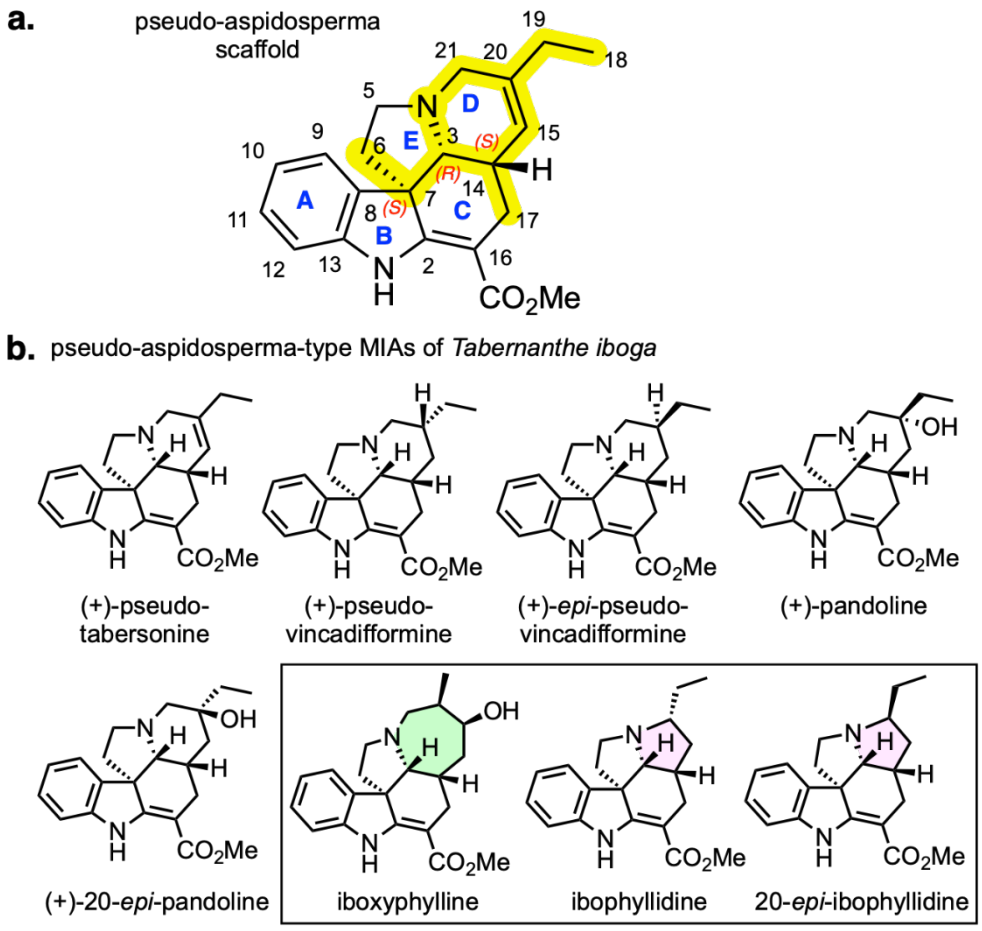


Figure 1.15. Shoot-specific *pseudo-aspidosperma-type* MIAs found in *T. iboga*. (**a**) Chemical structure of the core pseudo-aspidosperma scaffold. The A-E ring configuration is shown (blue) with stereocenters (red) and bond configuration highlighted in yellow. (**b**) *Pseudo-aspidosperma-type* alkaloids are found in the aerial parts of the plant, including leaves, stems, and flowers. D-ring expansion of iboxyphylline (green) and D-ring contraction of ibophyllidine (purple) are highlighted.

Among the *pseudo-aspidosperma-type* MIAs found in *T. iboga*, iboxyphylline and ibophyllidine exhibit distinct structural features (**Figure 1.15b**). Specifically, iboxyphylline and ibophyllidine display modifications in the D-ring, with iboxyphylline undergoing D-ring expansion[74] and ibophyllidine featuring D-ring contraction[74,75] (**Figure 1.15b**). Although the biosynthetic pathways responsible for these novel D-ring modifications remain unknown, several researchers have proposed plausible biogenetic mechanisms by which these compounds may arise from (+)-pandoline[74,76]. Chapter 5, section 5.2.3, **Figure 5.1** of this thesis will discuss the proposed mechanism for iboxyphylline and ibophyllidine biosynthesis and an alternative route arising from (+)-pseudo-tabersonine. A graphical summary of the known *T. iboga* MIAs discussed in this section is provided in **Figure 1.16**.

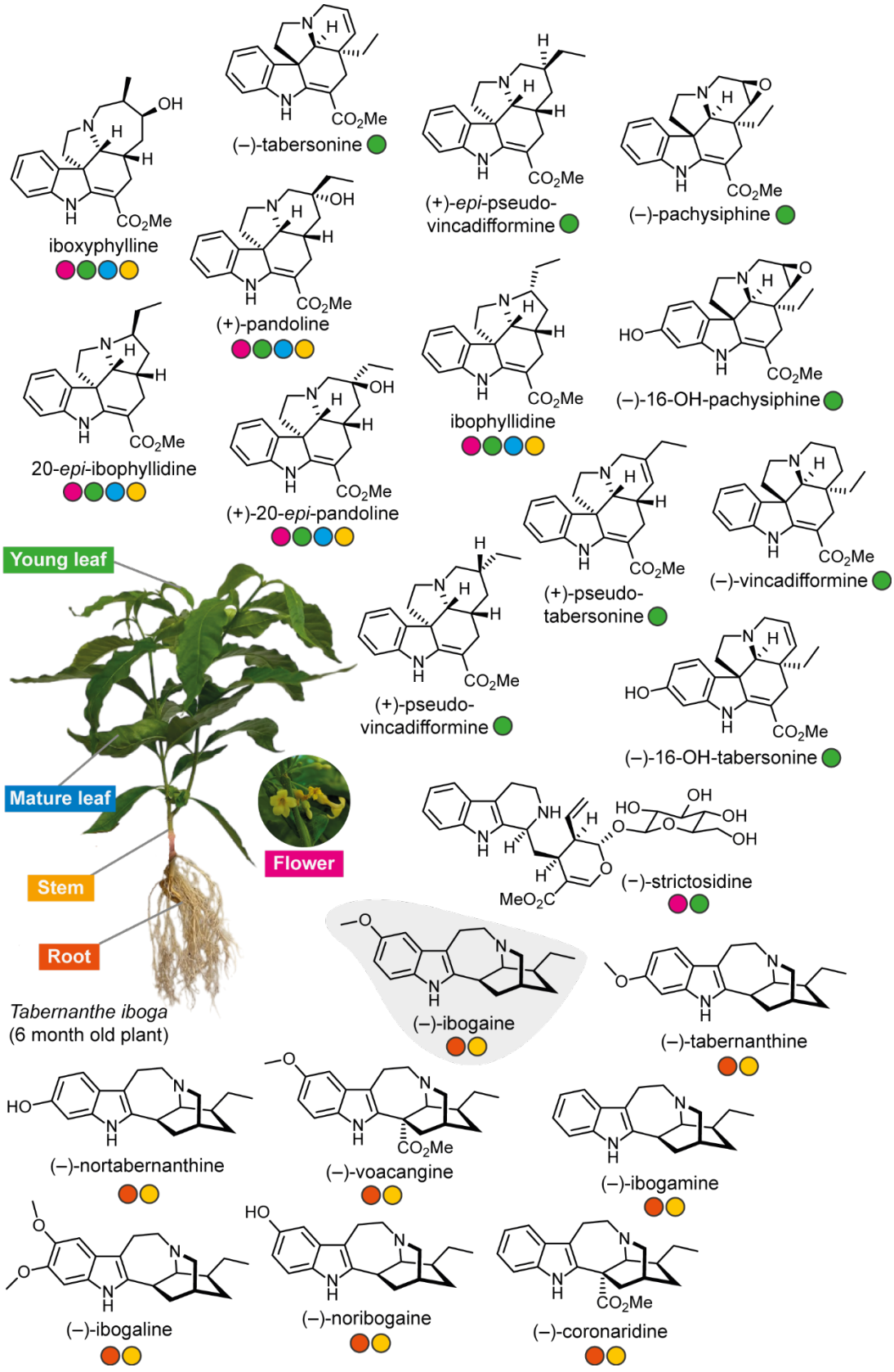


Figure 1.16. Tissue-specific distribution of MIAs found in *Tabernanthe iboga*. Colour-coded dots represent the tissues in which the alkaloids are found. Shaded in grey is ibogaine, the principal MIA, found as a major constituent in the plant's roots.

1.6 Biosynthesis of Monoterpene Indole Alkaloids (MIAs)

The vast structural diversity and associated bioactivities of MIAs prompted chemists to first isolate and envision their biosynthesis in nature through biomimetic synthesis. The pioneering work by Battersby[77,78], Scott[79,80], and Qureshi[81–83] validated the primary building blocks involved in MIA biosynthesis by feeding labelled precursors to *Catharanthus roseus* or *Vinca rosea* plants and seedlings. Their work built upon earlier studies by Robinson[84] and Leete[85], who conducted isotope feeding and biomimetic synthesis to understand plant alkaloid biosynthesis.

Once the foundational building blocks were identified, the challenge was to uncover the enzymatic machinery responsible for MIA assembly. Through *C. roseus* cell cultures and cell-free extracts, the complete enzymatic synthesis of ajmalicine[86,87] was achieved, marking a significant milestone in MIA and plant alkaloid biosynthesis as the first fully elucidated pathway. Over time, with the advent of molecular techniques, the enzymatic basis for MIA biosynthesis in plants such as *C. roseus* and *R. serpentina* was explored with discoveries elucidating the scaffold formation as proposed by early feeding studies.

The pathway elucidation of MIA biosynthesis in plants has evolved significantly, leading to the development of model systems and technologies for investigating plant alkaloid biosynthesis, addressed in Chapter 5 of this thesis. This has led to significant discoveries and breakthroughs in MIA biosynthesis and plant biosynthesis, with pathways such as strictosidine[88,89], strychnine[21] and ajmaline[30] being fully elucidated. However, the vinblastine biosynthetic pathway in *C. roseus* remains partially unresolved[90,91], with the final dimerization step still enigmatic[32], highlighting the challenges that persist despite decades of research.

Despite these challenges, significant progress has been made in understanding the enzymatic basis of MIA biosynthesis. The role of these specialised enzymes in MIA and plant alkaloid biocatalysis has been rigorously explored, with structure and mechanism studies conducted where possible. Maresh[12], Anarat-Cappillino[92], Lichman[93], Walsh[94,95], and Muro-Villanueva[96] provide comprehensive reviews of the biochemical foundations of these specialised enzymes and their families.

This thesis section will describe the biosynthetic steps involved in MIA biosynthesis and introduce the specialised enzymes responsible for the biotransformation and scaffold modifications.

1.6.1 Biosynthesis of Strictosidine

The biosynthesis of almost all known MIAs originates from the common precursor (–)-(*S*)-strictosidine [12,97]. This important reaction is catalyzed by the enzyme strictosidine synthase (STR)[98], which facilitates a Pictet–Spengler reaction by condensing secologanin (an iridoid aldehyde) with tryptamine (an aromatic amine), resulting in the formation of strictosidine[15] (**Figure 1.17**). Tryptamine is introduced into this pathway through the decarboxylation of L-tryptophan, a reaction catalyzed by tryptophan decarboxylase (TDC). The monoterpene precursor, secologanin, is derived from the seco-iridoid biosynthetic pathway, driven by the activity of ten known enzymes[99], starting from the precursor geranyl diphosphate.

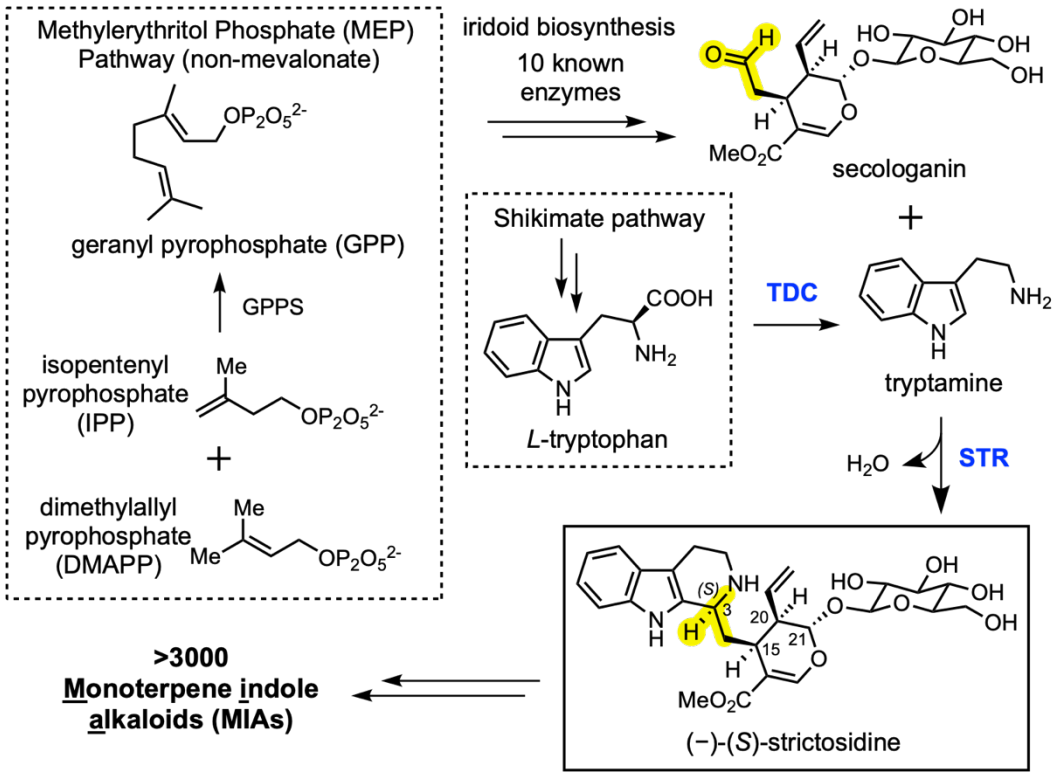


Figure 1.17. Biosynthesis of (–)-(*S*)-strictosidine.

Figure 1.17. Biosynthesis of (–)-(*S*)-strictosidine. The enzyme strictosidine synthase (STR) catalyzes the Pictet–Spengler condensation between tryptamine and secologanin, forming the key biosynthetic precursor (–)-(*S*)-strictosidine.

Given the importance of (–)-(*S*)-strictosidine[100] in MIA biosynthesis, the biochemical significance of STR cannot be overstated. STR was first identified in 1979 from *C. roseus* cell suspension cultures[101], and the crystal structure bound with (–)-(S)-strictosidine was determined from *Rauvolfia serpentina* STR[102,103]. Interestingly, STR was the first gene to be cloned and heterologously expressed in MIA biosynthesis research[104]. The reaction mechanism of STR has been shown to proceed stepwise, following a pathway similar to the classical Pictet–Spengler mechanism[15] (**Figure 1.18**).

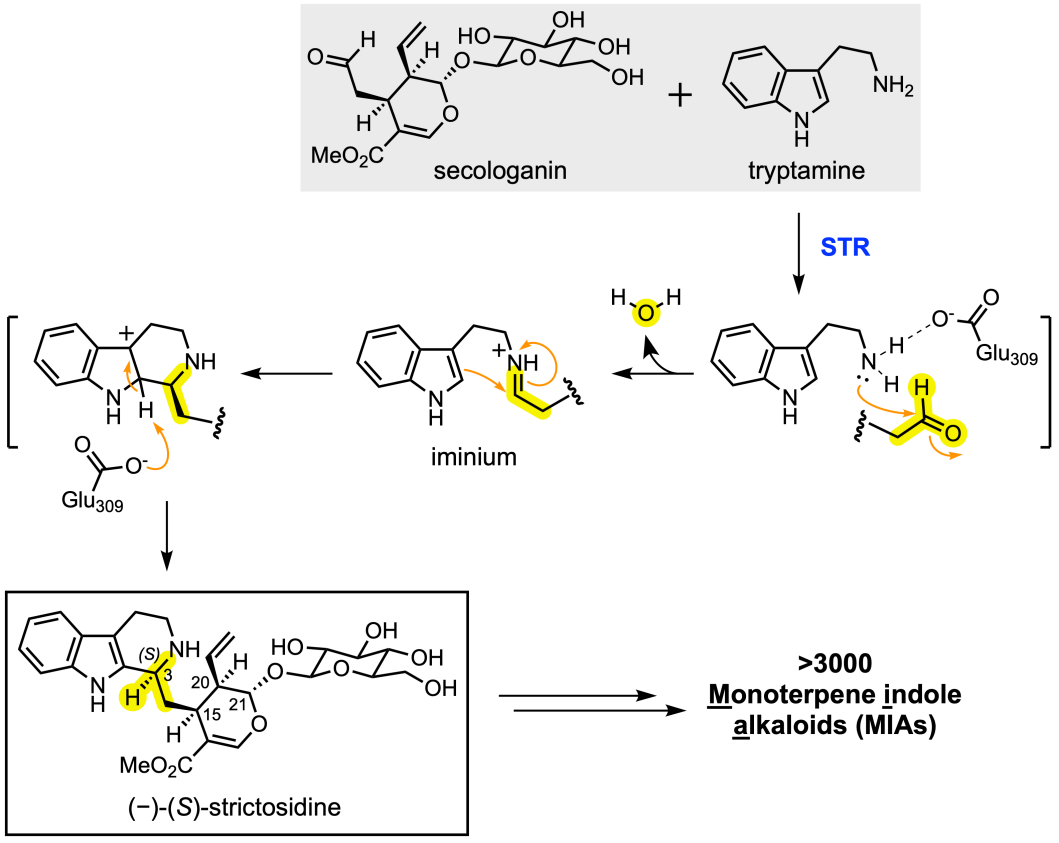


Figure 1.18. Stepwise mechanism of strictosidine synthase (STR). Analogous to Pictet–Spengler reaction, an iminium intermediate is formed during the condensation of secologanin and tryptamine, catalyzed by the STR enzyme. This intermediate enables the C-C bond formation between secologanin and tryptamine moieties, followed by a deprotonation to produce (–)-(S)-strictosidine. The active-site

residue glutamate 309 in STR is involved in the general acid-base catalysis in multiple steps and ensures the stereospecificity of the product.

The STR-mediated reaction begins with the binding and precise orientation of tryptamine facilitated by an "indole sandwich" formed by the catalytic residues Tyr-151 and Phe-226[105], ensuring stereoselectivity during the cyclization step. Tryptamine and secologanin[106] undergo a condensation reaction to form an iminium intermediate, which is subsequently cyclized via an electrophilic aromatic substitution, where the indole ring of tryptamine attacks the iminium carbon. Kinetic isotope effects showed that, surprisingly, rate-limiting step[15] involves the deprotonation and rearomatization of the indole ring, generating the final product, strictosidine. A key catalytic residue, Glu-309[15], acts as a general acid-base catalyst throughout the reaction, likely playing a role in the protonation of the carbinolamine intermediate and the deprotonation of the cyclized product.

STR is localized to the plant vacuole[33,107,108], where it catalyzes the first committed step in MIA biosynthesis. The vacuolar export of (–)-(*S*)-strictosidine across the tonoplast (vacuolar membrane) is facilitated by the nitrate/peptide family (NPF) transporter NPF2.9[109], while the import of secologanin into the vacuole is mediated by the multidrug and toxic compound extrusion (MATE) transporter, SLTr[32,110]. The vacuole, as the reaction site for strictosidine formation, may also play a role in modulating the reaction environment, particularly through its acidic pH, which could influence STR activity. However, the mechanism for the vacuolar import of tryptamine remains unknown, leaving a gap in the understanding of how the STR-catalyzed condensation is orchestrated within the plant cell.

1.6.2 Biosynthesis of Strictosidine Aglycones

Strictosidine is deglycosylated by the enzyme strictosidine β-D-glucosidase (SGD)[111–113] to generate a highly reactive hemiacetal intermediate (**Figure 1.19**). The reactive nature of the strictosidine aglycone allows for the formation of various isomers, contributing to the vast structural diversity observed in MIAs. The hydrolysis of (–)-(*S*)-strictosidine, catalyzed by SGD, results in the release of D-glucose, which opens the six-membered lactol ring of the strictosidine aglycone, forming a reactive dialdehyde intermediate[114]. This intermediate then undergoes an

intramolecular condensation with the secondary amine, leading to the formation of a reactive iminium. The iminium subsequently isomerizes to the more stable 4,21-dehydrogeissoschizine[115,116] (**Figure 1.19**). Although the mechanisms governing the equilibrium among these isomers remain largely unknown, factors including the pH of the cellular environment and downstream enzymes are hypothesized to influence this balance. Strictosidine aglycone can spontaneously rearrange into the thermodynamically favourable *heteroyohimbine-type* alkaloid cathenamine[114] in the absence of downstream enzyme(s). The mechanisms involved in directing the fate of the highly dynamic strictosidine aglycone isomers towards high-value MIA scaffolds are areas of ongoing research in MIA biosynthesis[117].

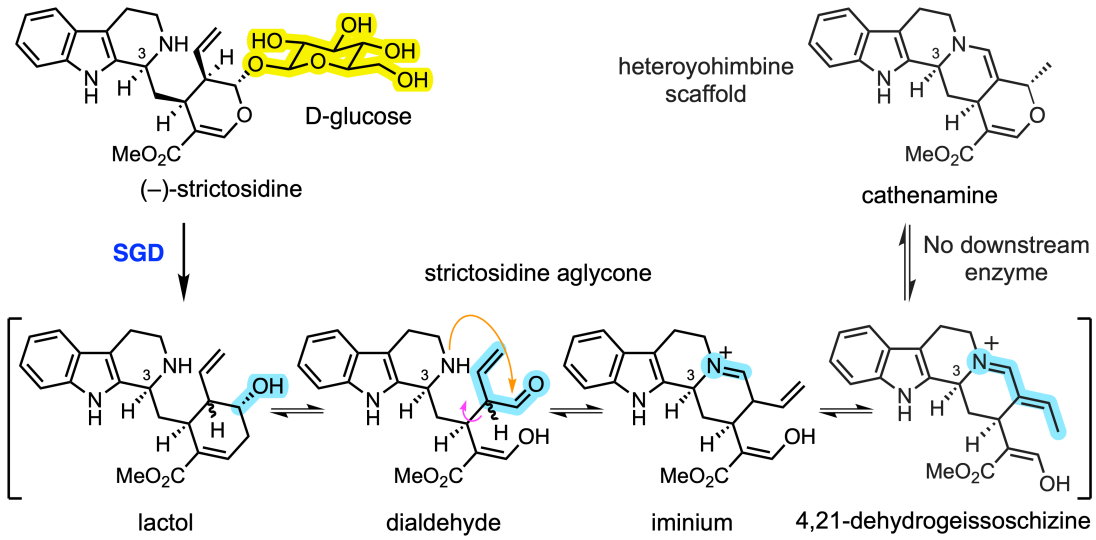


Figure 1.19. Catalytic mechanism of strictosidine β-D-glucosidase (SGD). SGD catalyzes the deglycosylation of (–)-(*S*)-strictosidine, generating the highly reactive strictosidine aglycon, which is believed to exist in spontaneous equilibrium between its lactol, aldehyde, and iminium forms. In the absence of downstream enzyme(s), the SGD product rearranges to form the thermodynamic product, cathenamine, a *heteroyohimbine-type* alkaloid.

SGD belongs to the glycosyl hydrolase family-1 and adopts a (β/α) 8-barrel fold, characteristic of β-D-glucosidase enzymes. The enzyme was first identified in *C. roseus* cell cultures[111,118], and the crystal structure of SGD from *Rauvolfia serpentina*[119] was determined, providing insights into its catalytic mechanism and substrate binding[119]. The enzyme's dual-acid/base mechanism involves Glu-207 as the proton donor and Glu-416 as the nucleophile, which cleaves the glycosidic bond

of strictosidine. His-161 helps position the substrate for hydrolysis, ensuring accurate alignment in the active site. Several conserved residues surrounding the active site interact with the glucose moiety of strictosidine to stabilize the complex during catalysis. A distinctive feature of SGD is the conformation of Trp-388, which forms stacking interactions with the indole ring of strictosidine. This interaction helps create enough space for the large strictosidine substrate, a unique adaptation for processing bulky natural products.

Though uncommon for specialised metabolite enzymes, SGD has been conclusively localized to the nucleus[108,113] in plant cells, where it has been observed to form multimeric aggregates. The substrate, strictosidine, is thought to enter the nucleus through nuclear pores. The biological significance of this nuclear localization remains unclear, but it may suggest a regulatory role for SGD in controlling the highly reactive and potentially toxic strictosidine aglycones[108,120] produced by the reaction, thereby protecting the plant cell from damage.

1.6.3 Biosynthesis of Geissoschizine

The isomers of strictosidine aglycones produced by the SGD reaction play an important role in directing the biosynthesis of various MIA structural classes in the presence of downstream enzymes. The presumed intermediates, which include the dialdehyde and the iminium, 4,21-dehydrogeissoschizine, are selectively reduced by various nicotinamide adenine dinucleotide phosphate (NADPH)-dependent alcohol dehydrogenases (ADH) enzymes (**Figure 1.20a**). These enzymes can reduce the aldehyde or the iminium group, stabilizing the reactive strictosidine aglycone and facilitating early diversification into divergent MIA scaffolds[29,115,121–124] (**Figure 1.20a**).

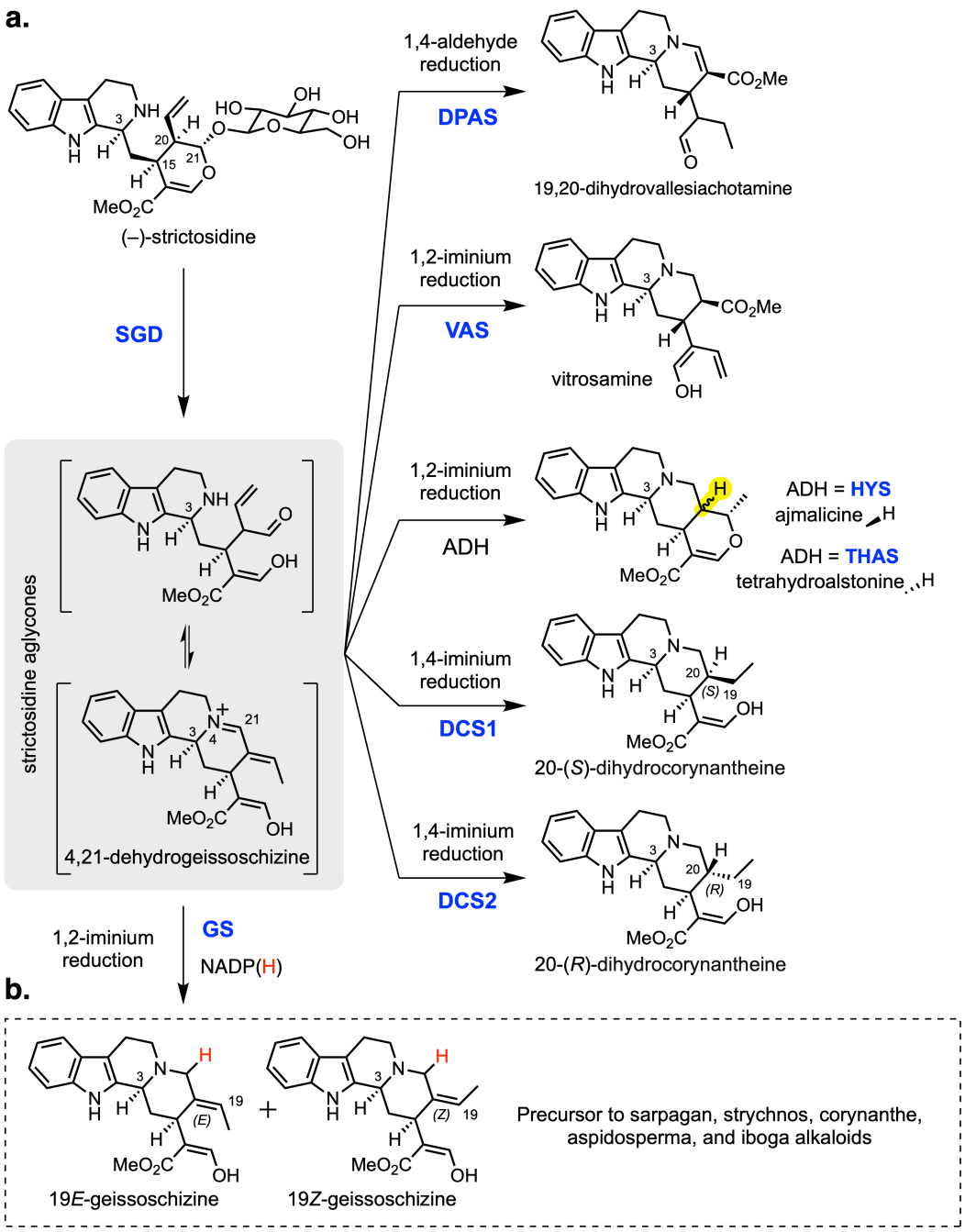


Figure 1.20. ADH directed reductions of strictosidine aglycones.

(**a**) Alcohol dehydrogenase (ADH) enzymes characterised to perform iminium or aldehyde reductions of unstable strictosidine aglycones, leading to the production of stereochemically divergent MIAs and their scaffolds. Abbreviations: strictosidine glucosidase (SGD), geissoschizine synthase (GS), dihydroprecondylocarpine acetate synthase (DPAS), tetrahydroalstonine synthase (THAS), heteroyohimbine synthase (HYS), dihydrocorynantheine synthase (DCS), vitrosamine synthase (VAS). (**b**) The enzyme geissoschizine synthase (GS) catalyzes the formation of 19-*E/Z*-geissoschizine isomers from 4,21-dehydrogeissoschizine. GS reduces the labile

substrate via a 1,2-iminium reduction, generating the stable 19*E*-geissoschizine, which serves as a precursor to major MIA scaffolds.

Geissoschizine synthase (GS)[121,125], a NADPH-dependent ADH enzyme, catalyzes the 1,2-iminium reduction of the strictosidine aglycone, 4,21-dehydrogeissoschizine to form the stable, 19*E/Z*-geissoschizine isomers (**Figure 1.20b**). Functional characterization of GS identified from *C. roseus* revealed that it predominantly produces the 19*E*-geissoschizine isomer, with only trace amounts of the 19*Z* isomer, possibly favoured by pH. The discovery of GS confirmed the biomimetic hypothesis proposed by Battersby[126] and Scott[127], who later demonstrated that the *corynanthe-type* alkaloid, geissoschizine produced by the GS reaction is the bona fide precursor to the *strychnos-type*, *aspidosperma-type*, and *iboga-type* alkaloid scaffolds. The product of geissoschizine synthase (GS), 19*E*-geissoschizine, is a key intermediate in MIA biosynthesis, undergoing enzymatic rearrangement to diversify into major biologically active alkaloid scaffolds (**Figure 1.21**).

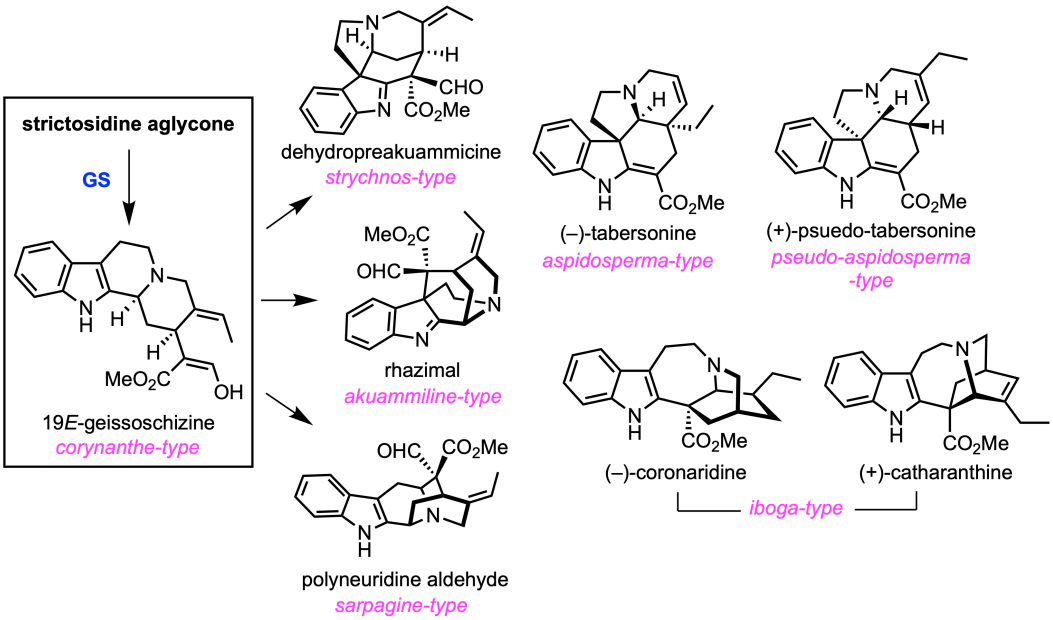


Figure 1.21. The central role of 19*E*-geissoschizine in MIA scaffold formations. The catalytic product of geissoschizine synthase (GS), 19*E*-geissoschizine, serves as a precursor for the biosynthesis of different structural scaffolds. MIAs of *strychnos-type*, *aspidosperma-type*, *iboga-type, sarpagan-type,* and *akuammilan-type* structures share a biogenetic origin from 19*E*-geissoschizine.

The crystal structure of GS[122] from *C. roseus* was recently reported. This revealed that GS is an atypical 1,2-iminium reductase, distinct from canonical aldehyde-reducing ADHs found in nature. Notably, GS retains the catalytic zinc ion but lacks the proton relay system observed in other ADHs. The proposed 1,2-iminium reduction mechanism for GS involves the zinc ion functioning like a Lewis base, with the coordinated water molecule acting as the proton donor to the iminium substrate[122].

GS activity in MIA biosynthesis is part of a highly compartmentalized pathway[33] that involves multiple cell types and subcellular compartments. However, the precise subcellular localization of GS within plant systems is yet to be experimentally validated. Based on signal peptide predictions and the expression systems used for heterologous overexpression, it is assumed that GS is localized in the cytosol of leaf epidermal cells[128]. Interestingly, THAS[115], an ADH like GS that is also involved in MIA biosynthesis (**Figure 1.20a**), is localized to the nuclear cytosol[120], where it is shown to interact with the upstream enzyme SGD[120]. This raises the possibility that GS might also exhibit a nuclear-cytosolic localization and interact with SGD, especially considering that GS has been reported as a rate-limiting step in MIA pathway reconstitutions in yeast[129] and *Nicotiana benthamiana*[130].

1.6.4 Biosynthesis of Stemmadenine

The biosynthesis of stemmadenine from 19*E*-geissoschizine requires a coordinated sequence of enzymatic reactions involving geissoschizine oxidase (GO), Redox-enzyme 1 (Redox 1), and Redox-enzyme 2 (Redox2)[125,128]. This section will explore the specific roles of each enzyme, detailing their contributions to the biosynthesis of stemmadenine and the subsequent production of related MIA alkaloids in plants.

An oxidative rearrangement of 19*E*-geissoschizine is catalysed by the membrane-bound cytochrome P450 (CYP450) enzyme geissoschizine oxidase (GO, CYP71D1V1)[125,128], resulting in the formation of a highly reactive intermediate, dehydropreakuammicine, or akuammicine in the absence of downstream enzymes (**Figure 1.22**). CYP450 enzymes[131–134], like GO, are well known for their role in catalyzing oxidative transformations in plant specialised metabolism, from

monooxygenation and hydroxylation reactions to unusual oxidative rearrangements[135] of carbon skeletons and oxidative C–C bond cleavage. GO's catalytic prowess lies in its ability to orchestrate multiple bond formations and cleavages, resulting in a complex rearrangement that transforms the *cis*-quinolizidine configured beta-carboline structure of 19*E*-geissoschizine[136] into the tetracyclic strychnos scaffold (**Figure 1.22**).

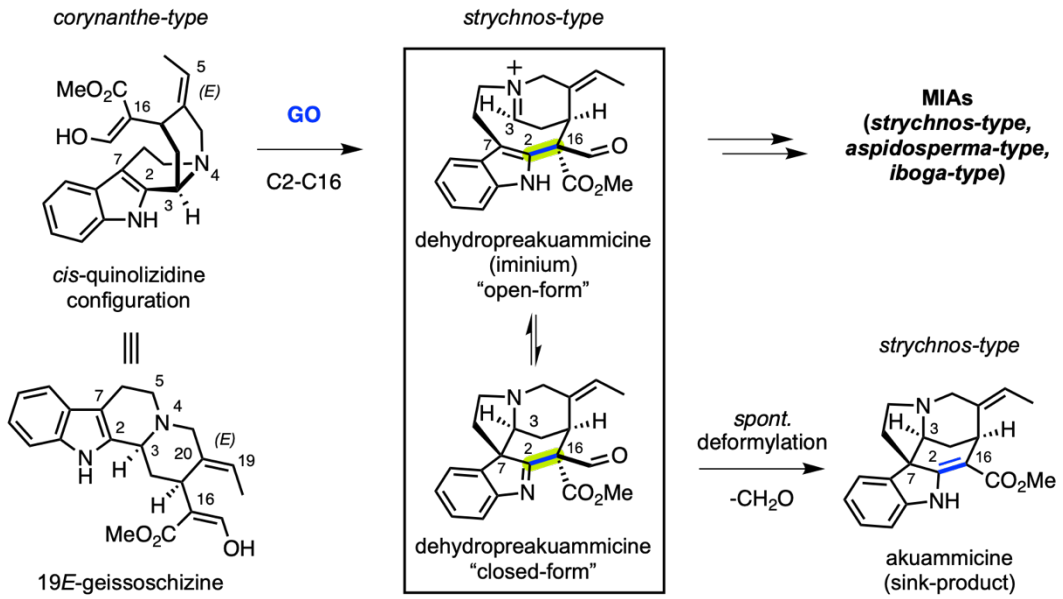


Figure 1.22. Oxidative rearrangement catalyzed by geissoschizine oxidase (GO).

The substrate, 19*E*-geissoschizine undergoes an oxidative rearrangement to forge the C2-C16 bond, leading to the formation of the unstable, yet highly reactive dehydropreakuammicine intermediate. In the absence of downstream enzymes, dehydropreakuammicine undergoes spontaneously deformylation to produce the thermodynamically favoured product, akuammicine.

While not fully understood, the mechanistic intricacies of the GO-catalyzed reaction likely involve a series of well-orchestrated steps. The proposed stepwise mechanism[125,128,137] begins with the site-specific hydroxylation of 19*E*-geissoschizine at the C2 position, generating a short-lived *m/z* 369 hydroxy-indolenine intermediate (**Figure 1.23**). This intermediate would undergo a nucleophilic attack at C16, forming a C2-C16, facilitated by the *cis*-conformation of 19*E*-geissoschizine. Next, cleavage of the C2-C3 bond would occur, accompanied by a 1,2 sigmatropic

rearrangement, which stabilizes the indole by restoring the atomicity and forms a new C3-C7 bond. This process leads to the formation of the unstable but highly reactive intermediate, dehydropreakuammicine, which is believed to exist in equilibrium with its iminium form. In the presence of downstream enzymes, dehydropreakuammicine serves as an on-pathway precursor for stemmadenine biosynthesis. However, in the absence of these enzymes, dehydropreakuammicine is spontaneously deformylated to produce the stable product, akuammicine (**Figure 1.23**).

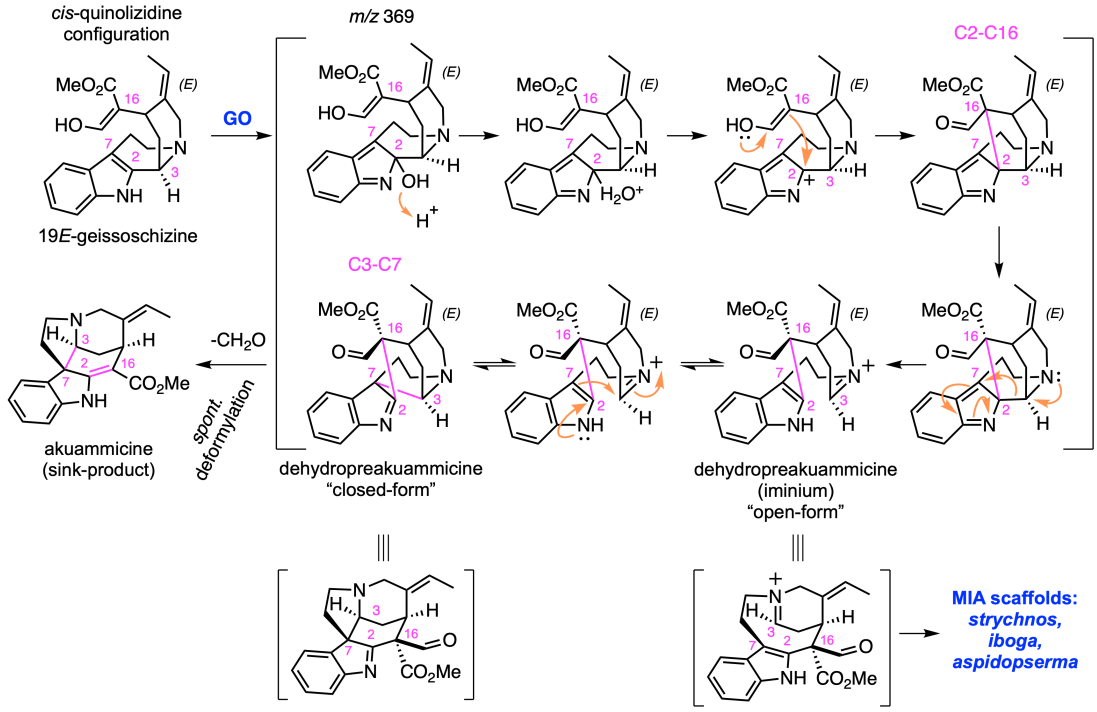


Figure 1.23. Stepwise mechanism of the GO-catalyzed oxidative rearrangement of 19*E*-geissoschizine.

The proposed stepwise mechanism is illustrated, along with hypothetical intermediates, by which geissoschizine oxidase (GO) catalyzes the oxidative rearrangement of 19*E*-geissoschizine to produce dehydropreakuammicine. This product is believed to exist in equilibrium between its iminium form, referred to as the "open form", and its enamine form, referred to as the "closed-form", both sharing the same oxidation state. The open form is considered the kinetic intermediate involved in downstream MIA biosynthesis.

Decades before the discovery of geissoschizine oxidase, Wenkert[138], Scott[79] and Levy[139] proposed mechanisms for the oxidative rearrangement of geissoschizine. Their early hypotheses laid the foundation for understanding the intricate oxidative transformations involved long before the specific enzymatic processes were characterised. Wenkert[138] proposed a mechanism involving a radical-containing intermediate via single electron transfer. Scott[79] proposed a Mannich-reaction hypothesis based on isolating a labile compound, preakuammicine, from *C. roseus* seedlings. Levy[139] later expanded on this by proposing a sigmatropic rearrangement mechanism that connects the *akuammilan-type* alkaloids to Scott's proposed preakuammicine intermediate.

In addition to GO, several other CYP oxidases are known to perform rearrangements of 19*E*-geissoschizine (**Figure 1.24**). These oxidations are remarkable for their ability to dramatically restructure the molecular scaffold of 19*E*-geissoschizine in a single CYP-catalyzed step, forming the basis for divergent biosynthesis. The CYP oxidase enzymes, rhazimal synthase (RS)[137] and sarpagan bridge enzyme (SBE)[140], were discovered to catalyze the oxidative rearrangement of 19*E*-geissoschizine, forging C5-C16 and C7-C16 bonds, respectively (**Figure 1.24**). Chapter 4 of this thesis will explore these transformations, focusing on the discovery of N1-C16 bond-forming *mavacurane-type* scaffolds (**Figure 1.24**).

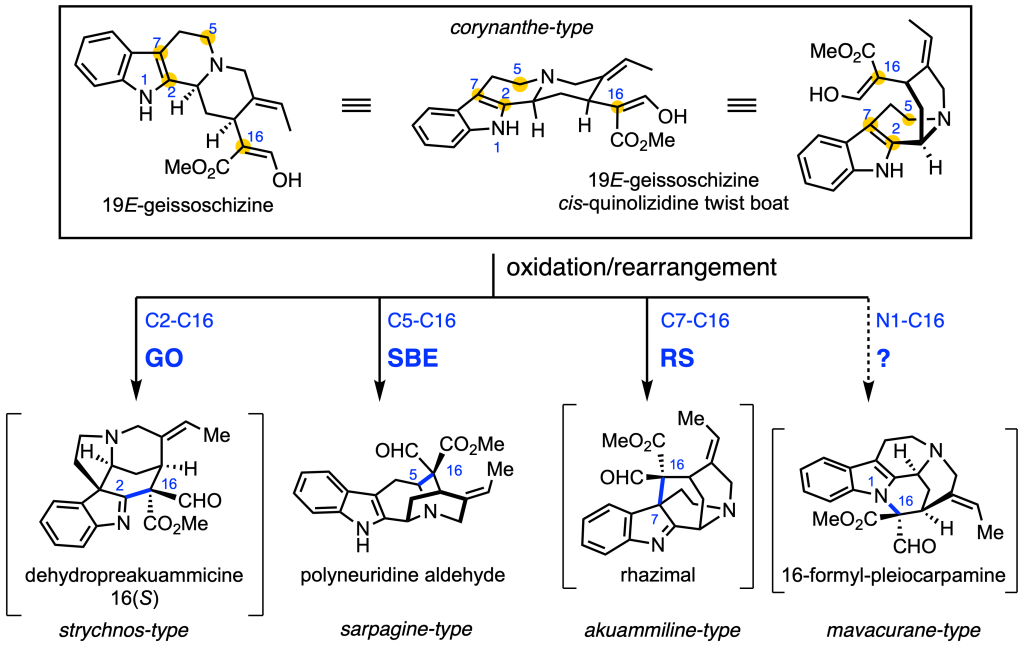


Figure 1.24. Cytochrome P450 (CYP) catalyzed oxidations of 19*E*-geissoschizine.

Figure 1.24. Cytochrome P450 (CYP) catalyzed oxidations of 19*E*-geissoschizine. Oxidative rearrangements of the enzyme-catalyzed reactions are shown with bond formations highlighted in blue. Among others, the *corynanthe-type* alkaloid can be selectively diverted to *strychnos-type*, *sarpagan-type*, *akuammiline-type*, and *mavacurane-type* alkaloid scaffolds.

On the pathway to stemmadenine, dehydroreakuammicine-iminium is reduced by the ADH enzyme redox-enzyme 1 (Redox 1)[128] to generate an unstable aldehyde. Redox 1 facilitates a canonical 1,2-iminium reduction, producing a highly reactive intermediate. In the absence of the downstream enzyme, this intermediate spontaneously deformylate into two isomers of deshydroxymethyl-stemmadenine[128] (**Figure 1.25**). However, in the presence of the downstream enzyme redox-enzyme 2 (Redox 2)[128], the unstable aldehyde is instead reduced to an alcohol, producing the stable intermediate stemmadenine (**Figure 1.25**). Redox 2 is an NADPH-dependent oxidoreductase[141] enzyme belonging to the aldo-keto reductase (AKR)[142] superfamily. AKR enzymes are known for catalyzing reactions that involve the reduction of aldehydes and ketones to their corresponding primary and secondary alcohols.

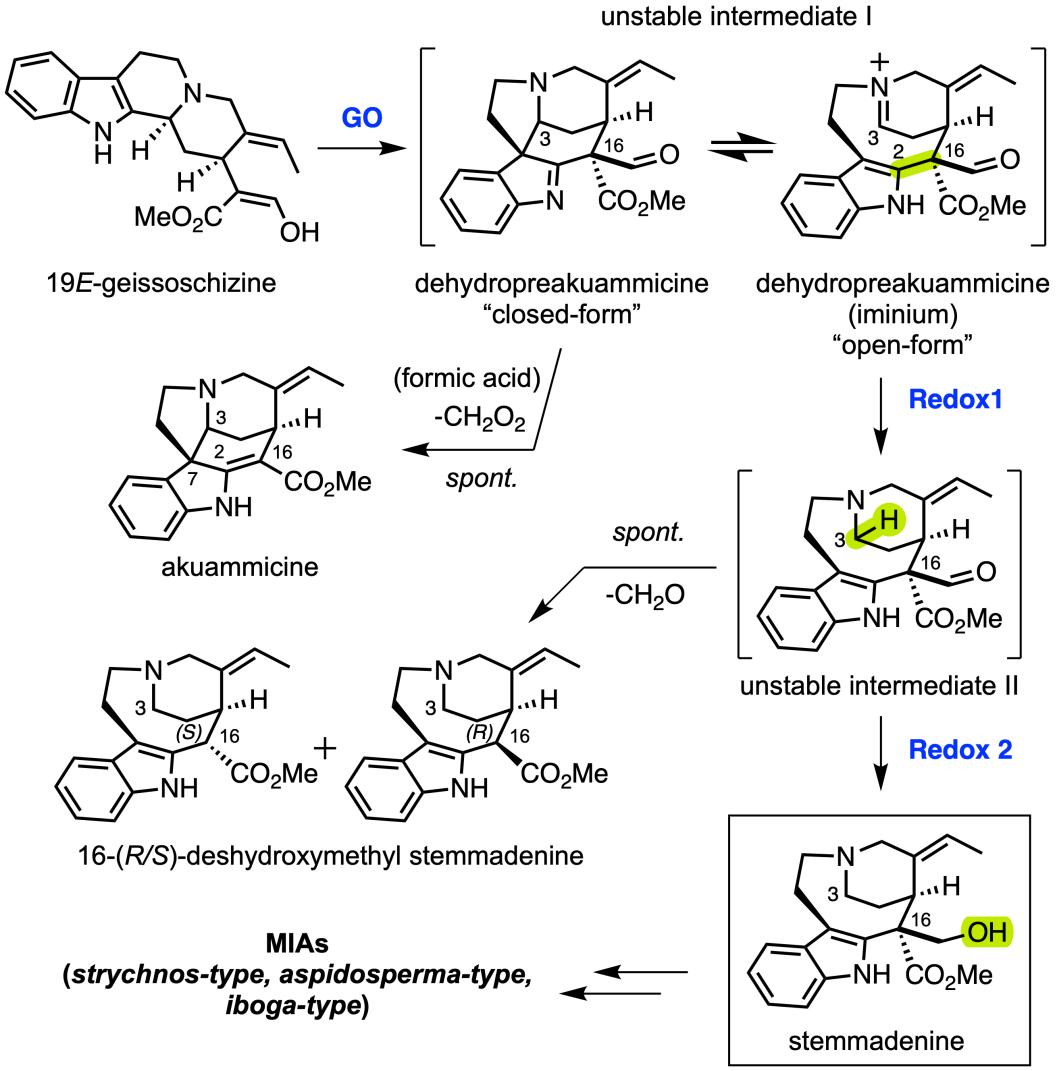


Figure 1.25. Biosynthesis of stemmadenine from 19*E*-geissoschizine.
The concerted biosynthetic pathway involving GO, Redox 1, and Redox 2 enzymes to generate stemmadenine, the stable precursor for aspidosperma, iboga, and strychnos alkaloids. Abbreviations: geissoschizine oxidase (GO), redox-enzyme 1 (Redox 1), and redox-enzyme 2 (Redox 2).

The concerted actions of GO, Redox 1, and Redox 2 are crucial for converting 19*E*-geissoschizine into stemmadenine via two reactive intermediates. This intricate process highlights the synergistic interplay of plant enzymes, working in concert to produce rare complex molecules. The challenging stereoselective rearrangements required for stemmadenine[143] total synthesis have prevented the development of a successful synthetic route. As a result, stemmadenine is primarily sourced from rare tropical plants that yield minimal quantities of the compound. To address these limitations, synthetic biology is being leveraged to biosynthesize

stemmadenine from stable precursors, such as strictosidine[130,144] or 19*E*-geissoschizine[145], in heterologous hosts.

1.6.5 Biosynthesis of Dehydrosecodine

The biosynthesis of dehydrosecodine from stemmadenine involves three enzymatic steps, catalyzed by stemmadenine acetyltransferase (SAT)[90,128], dihydroprecondylocarpine synthase (DPAS)[90], and precondylocarpine acetate synthase (PAS)[90] (**Figure 1.26**). The pathway enzymes were identified and functionally characterised in *C. roseus*[90,128]. First, the primary alcohol of stemmadenine is acetylated by an acetyltransferase[146] enzyme, namely stemmadenine acetyltransferase (SAT), using acetyl-CoA, forming stemmadenine acetate (**Figure 1.26**). This acetylation protects the molecule, slows spontaneous deformylation after oxidation, and creates a leaving group crucial for the subsequent formation of dehydrosecodine.

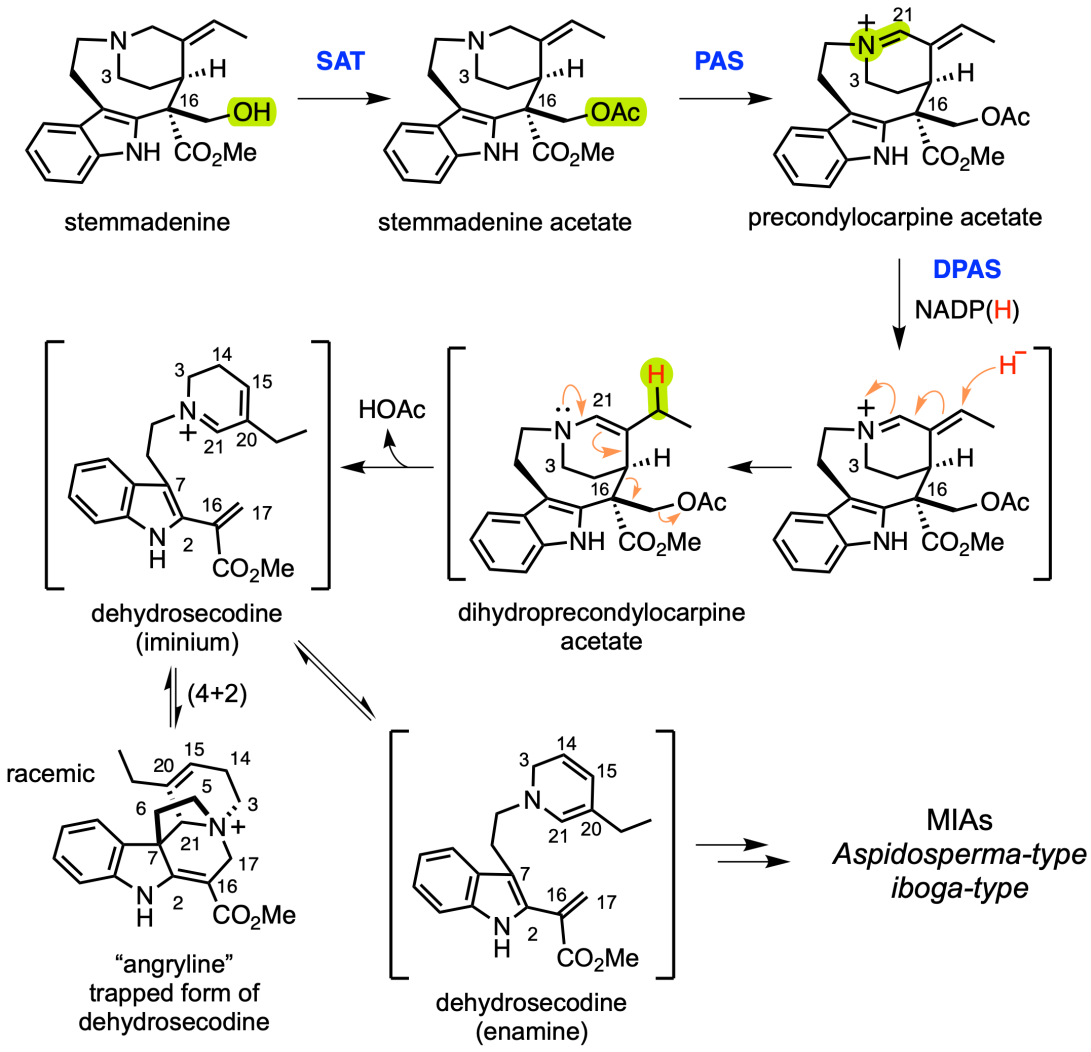


Figure 1.26. Biosynthesis of dehydrosecodine from stemmadenine. Enzymatic transformations are highlighted in green, and the enzymes involved are shown in blue. Abbreviations; stemmadenine acetyltransferase (SAT), precondylocarpine acetate synthase (PAS), dihydroprecondylocarpine synthase (DPAS).

Stemmadenine acetate is converted to dehydrosecodine by two redox enzymes, a flavin-dependent (FAD) berberine bridge-like (BBL)[147] oxidase, PAS[90,128] and an ADH enzyme, DPAS[90]. The PAS enzyme catalyzes the oxidation of the tertiary amine (N4-C21 bond) in stemmadenine acetate, leading to the formation of an iminium intermediate named precondylocarpine acetate (**Figure 1.26**). This intermediate is subsequently reduced by DPAS-catalyzed 1,4-iminium reduction[90,122] to yield the labile intermediate, dihydroprecondylocarpine acetate (**Figure 1.26**). This compound then readily fragments to produce the dehydrosecodine iminium,

which tautomerizes into the enamine form of dehydrosecodine[90,148], the elusive achiral precursor for divergent MIA scaffolds (**Figure 1.26**).

Scott[149] envisioned dehydrosecodine as a labile, highly reactive dihydropyridine-acrylic ester, playing a key role in the biomimetic rearrangements leading to aspidosperma and iboga scaffolds from the precursor, stemmadenine. He proposed pioneering mechanisms for dehydrosecodine involved regiodivergent cycloadditions in generating these complex structures[149,150]. However, due to its achiral dihydropyridine structure and reactivity, dehydrosecodine has never been isolated or fully characterised. Recently, a stabilized intramolecular variant, "angryline"[148], has been successfully isolated and characterised. The reactivity of angryline is pH-dependent, where it is believed to exist in equilibrium with dehydrosecodine iminium (**Figure 1.26**). Under acidic conditions, the equilibrium favours the “closed-form” angryline, in which the iminium is rearranged to stabilize the pyridine ring and protect the reactive intermediate. When the pH is elevated, the equilibrium shifts toward the reactive dehydrosecodine iminium, activating the molecule to participate in downstream biosynthetic reactions. Interestingly, a synthetic analogue[151] inspired by dehydrosecodine was synthesized and structurally determined by X-ray analysis to confer the versatility of this molecule in the divergent synthesis of MIA scaffolds.

The biosynthesis of dehydrosecodine from stemmadenine acetate has been reported from *T. iboga*[26], following a pathway analogous to that found in *C. roseus* (**Figure 1.26**). A suite of redox enzymes orthologous to those in *C. roseus* was characterised, including three PAS enzymes- PAS 1, PAS 2 and PAS 3, along with two DPAS enzymes, DPAS 1 and 2, which were reported to catalyze the biosynthesis of dehydrosecodine in *T. iboga*[26]. Notably, DPAS 1 was crystalized, and a mechanism was proposed for the unusual 1,4-iminium reduction of dihydroprecondylocarpine acetate[122]. The subcellular localization of the enzyme DPAS was confirmed as cytosolic[90]. In contrast, PAS localization was not restricted to a single organelle, as it was observed to be associated with small vesicles budding from the endoplasmic reticulum (ER), with colocalization signals detected in both the vacuole and tonoplast[90].

1.6.6 Biosynthesis of Tabersonine and Catharanthine

Dehydrosecodine is a versatile intermediate capable of undergoing regioselective cycloaddition reactions, as first proposed by Scott[149], to generate biologically active *aspidosperma-type* and *iboga-type* MIA scaffolds (**Figure 1.27**). Dehydrosecodine was proposed as the precursor for naturally occurring *aspidosperma-type*, *iboga-type*, *pseudo-aspidosperma-type*, and *andranginine-type* alkaloid scaffolds (**Figure 1.27**). The biosynthesis of these diverse scaffolds has been progressively discovered through the pioneering work of research groups led by O'Connor[26,27,90,148], Courdavault[90], and DeLuca[128], who have built upon the foundational puzzle that Scott initiated nearly 50 years ago.

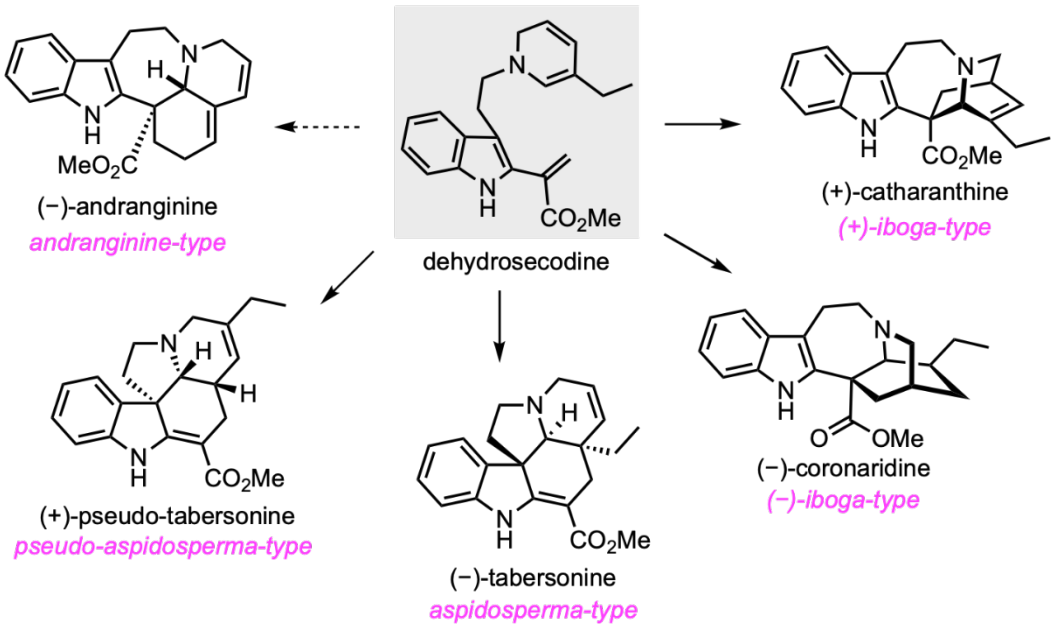


Figure 1.26. Dehydrosecodine-derived MIA scaffolds.

Carboxylesterase-like enzymes of the α/β-hydrolase family from *C. roseus* have been discovered to catalyze crucial scaffold-forming cycloaddition reactions from the reactive intermediate dehydrosecodine[90,128,148]. Tabersonine synthase (TS) and catharanthine synthase (CS) catalyze stepwise [4+2] cycloaddition reactions to produce aspidosperma alkaloid (–)-tabersonine and iboga alkaloid (+)-catharanthine, respectively [90,148](**Figure 1.27**).

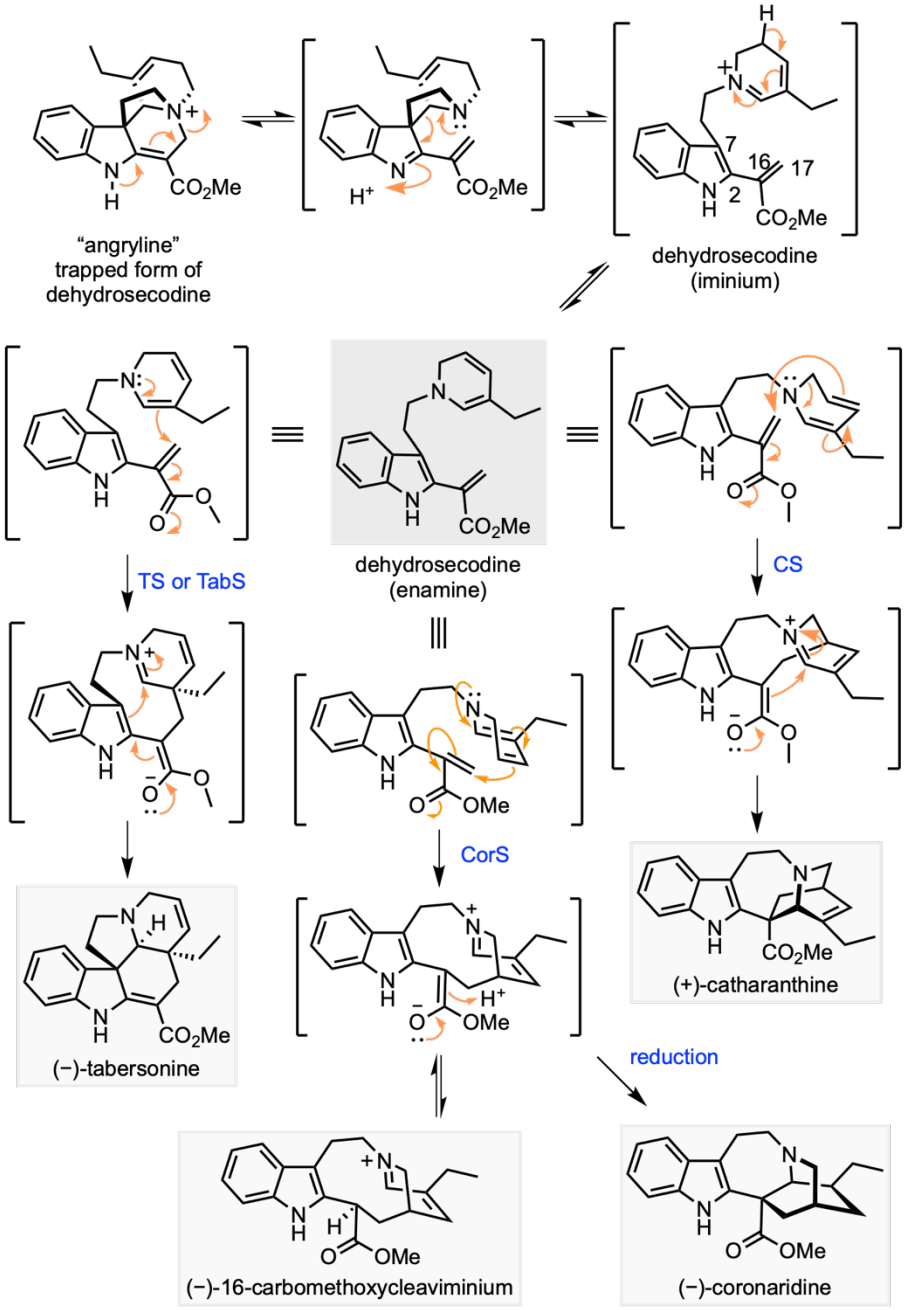


Figure 1.27. Biosynthesis of (–)-tabersonine, (+)-catharanthine and (–)-coronaridine.

Biosynthesis of (–)-tabersonine, (+)-catharanthine and (–)-coronaridine from dehydrosecodine by the action of cyclase enzymes TS, CS and CorS, respectively. The recently discovered CorS mechanism is presented in Chapter 2 of this thesis. Abbreviations: tabersonine synthase (TS), catharanthine synthase (CS), and coronaridine synthase (CorS).

Additionally, orthologous cyclase enzymes, coronaridine synthase (CorS) and tabersonine synthase (TabS)[26], were identified in the ibogaine-producing plant *T. iboga* and shown to be involved in the biosynthesis of (–)-coronaridine and (–)-tabersonine, respectively. The *iboga-type* alkaloid coronaridine, produced via CorS, exhibited stereochemistry opposite to that of (+)-catharanthine[26] (**Figure 1.27**). Mechanistic evidence for the reaction catalysized by CorS from dehydrosecodine will be described in Chapter 2 of this thesis.

Subcellular localization studies revealed that the cyclase enzymes CS, TS, and CorS are targeted to the cytosol[90]. Structural analyses of these three enzymes have provided key mechanistic insights into how the dihydropyridine and methyl acrylate moieties of dehydrosecodine undergo regio- and stereospecific cycloaddition reactions[148]. Additionally, the evolution of these carboxylesterase-like cyclase enzymes has been explored through ancestral sequence reconstitution[66]. The resulting biochemical model suggests that TS activity evolved first, followed by the independent evolution of CorS activity in two separate lineages, leading to the production of *iboga-type* and *pseudo-aspidosperma-type* alkaloids. CS proposed to have arisen later, following the duplication and neofunctionalization of an ancestral CorS enzyme, which occurred exclusively in *C. roseus*.

1.6.7 Biosynthesis of Ibogaine

The biosynthesis of (–)-ibogaine from the intermediate (–)-coronaridine has been elucidated in *T. iboga*[26] (**Figure 1.28**). This involves the conversion of (–)-coronaridine to (–)-10-hydroxy coronaridine by the CYP450 enzyme ibogamine-10-hydroxylase (I10H)[25,26]. Methylation of (–)-10-hydroxy coronaridine by the O-methyl-transferase (OMT) enzyme, noribogaine-10-O-methyltransferase (N10OMT)[26] generates (–)-voacangine. Next, the methyl ester of (–)-voacangine is hydrolyzed to generate (–)-de-ester-voacangine by the action of polyneuridine aldehyde esterase (PNAE)[26], an enzyme known to be involved in the de-esterification and decarboxylation of MIAs in ajmaline biosynthesis[30,152]. The final step involves the decarboxylation of (–)-de-ester-voacangine to produce (–)-ibogaine, which is considered a non-enzymatic reaction aided by heat[26] (**Figure 1.28**). However, the involvement of a decarboxylase-like enzyme to catalyze the reaction cannot be ruled out in the final step leading to (–)-ibogaine biosynthesis.

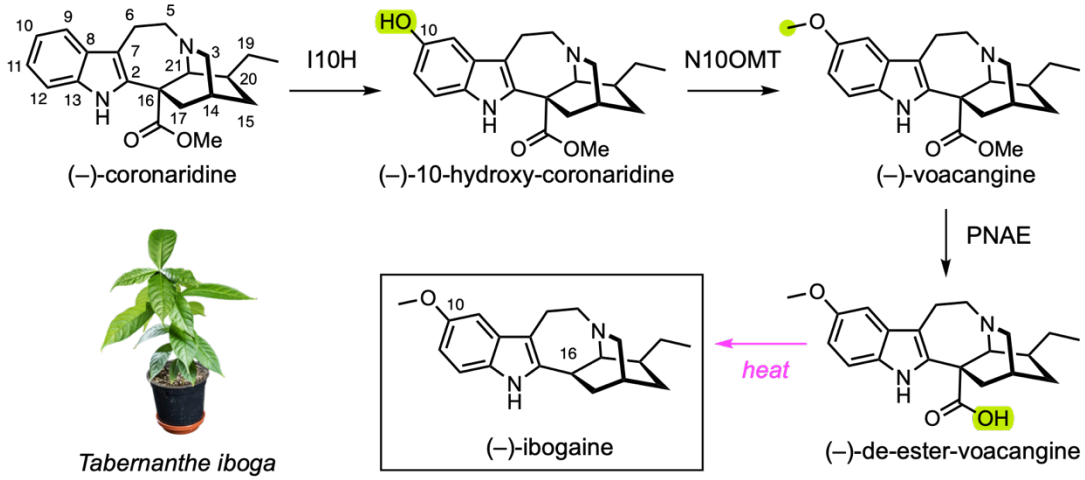


Figure 1.28. Biosynthesis of (–)-ibogaine in *Tabernanthe iboga*.
Biosynthesis of (–)-ibogaine from (–)-coronaridine. Decarboxylation of (–)-de-ester-voacangine occurs spontaneously over time and is accelerated by heat. Transformations catalysed by enzymes are highlighted in green, and non-enzymatic steps are highlighted in purple. Abbreviations: ibogamine-10-hydroxylase (I10H), noribogaine-10-O-methyltransferase (N10OMT).

Additionally, an alternative pathway to (–)-ibogaine might exist via the intermediate (–)-ibogamine, an alkaloid found in the roots of *T. iboga* (**Figure 1.29**). This intermediate can be obtained from (–)-coronaridine through a semi-synthetic process that involves basic saponification to remove the methyl ester, followed by heating to induce decarboxylation. Similarly, the enzyme PNAE catalyzes the formation of (–)-de-ester-coronaridine from (–)-coronaridine by enzymatically hydrolyzing the methyl ester[26]. Although heating alone does not produce (–)-ibogamine, an unknown enzyme, yet to be discovered could potentially decarboxylate (–)-de-ester-coronaridine to generate (–)-ibogamine. It has been demonstrated that I10H can readily hydroxylate (–)-ibogamine to produce the intermediate (–)-noribogaine and that N10OMT can sequentially methylate (–)-noribogaine to produce (–)-ibogaine[25] (**Figure 1.29**). Although N10OMT exhibits poor catalytic efficiency in the methylation of (–)-noribogaine[25], it is possible that a homologous methyltransferase, yet to be identified in *T. iboga*, could catalyze this reaction more effectively.

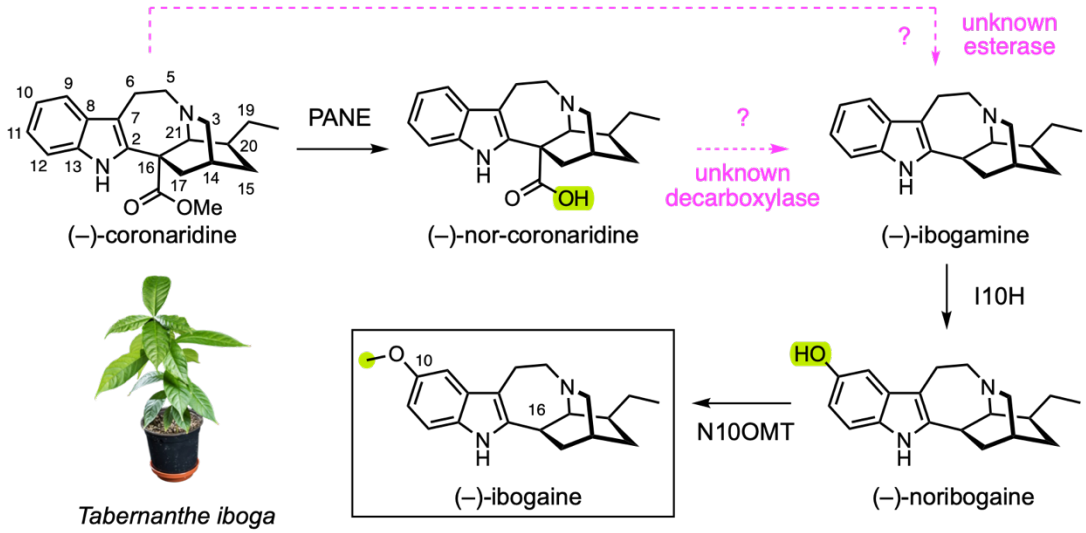


Figure 1.29. Proposed alternative pathway to (–)-ibogaine via (–)-ibogamine in *Tabernanthe iboga*.

Proposed biosynthetic route (–)-ibogaine from (–)-coronaridine via (–)-ibogaine the intermediate. Transformations catalysed by enzymes are highlighted in green, and proposed unknown enzymatic steps are highlighted in purple.

1.7 Modern Approaches to Plant Gene Discovery and Pathway Elucidation.

Modern genomic, biochemical, and synthetic biology tools have revolutionized plant specialised biosynthesis and gene elucidation over the past decade[11,153–155]. Over the last 15 years, the gene discovery and pathway elucidation process has become more streamlined and robust, enabling the study of complex biosynthetic pathways in both model and non-model plant species (**Figure 1.30**). Emerging technologies, such as next-generation sequencing and advanced metabolomics, have enabled the investigation of specialised metabolic pathways in previously inaccessible plants. Advances in sample preparation and robotics have elevated precision tissue sampling, pushing omics technologies beyond the tissue level to single-cell resolution, and creating a new frontier in modern plant pathway elucidation.

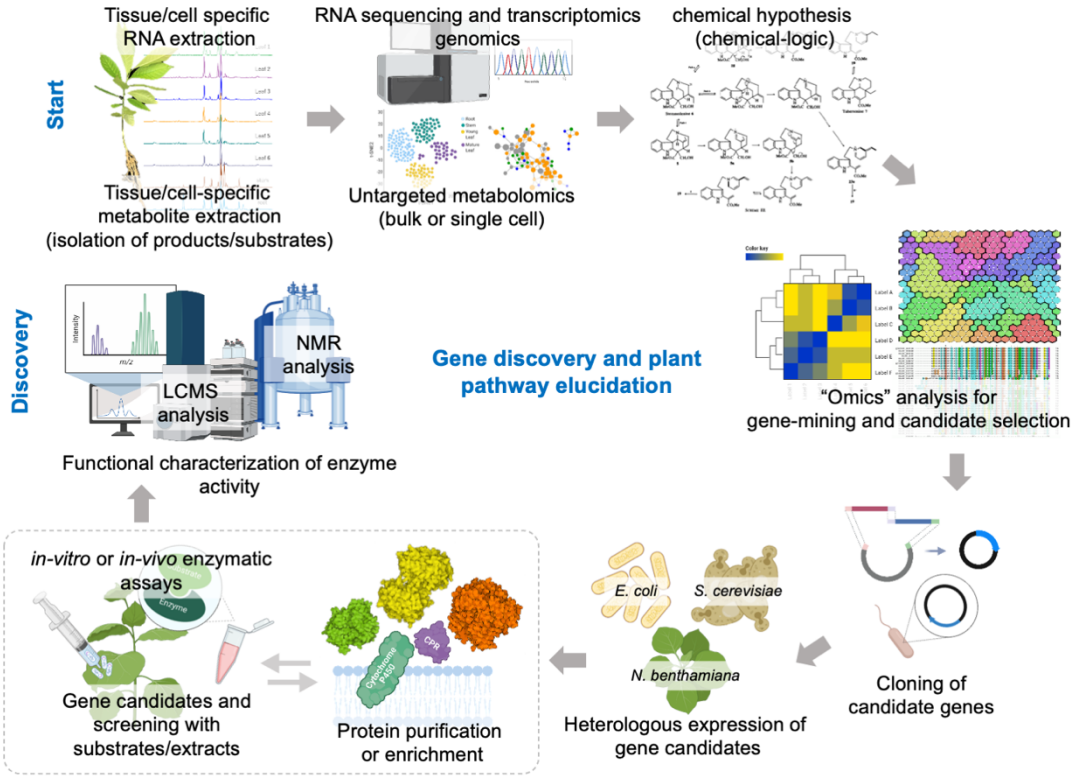


Figure 1.30. Overview of gene discovery pipeline used in plant pathway elucidation.

Figure created using BioRender (https://www.biorender.com).

1.7.1 Chemical Hypothesis and Pathway Logic

Plant gene discovery and pathway elucidation often begins with the proposal of a hypothetical biosynthetic pathway based on chemical logic[12,92,154,156]. This process includes reviewing biomimetic syntheses to provide clues about plausible reaction sequences, isotope labelling studies with the producing plant to identify unknown steps and intermediates and assigning possible enzyme classes to each hypothesized reaction. Stable isotope labelling with isotopes of ^{13}C, ^{15}N, ^{18}O, and deuterium enables researchers to trace specific atoms through biochemical pathways and across plant tissues[157–160]. Isotopes can be introduced into plants through various methods, such as root uptake by dissolving isotopes in water or nutrient solutions and applying them to the soil or growth medium[160], atmospheric exposure for gaseous isotopes, seed imbibition by soaking seeds in isotope-enriched solutions[161], or direct injection into plant tissues[162]. These isotopes are

incorporated into metabolites and used to study metabolic flux[163], offering a non-invasive way to examine tissue-specific physiology and metabolism in vivo. Advances in mass spectrometry and metabolomic analysis have enabled the precise tracing of these isotopes[158,164], even at low incorporation rates, allowing researchers to establish detailed metabolic flux models in plant systems.

1.7.2 Gene Identification and Candidate Gene Prioritisation

Co-expression analysis remains the key approach for gene discovery, as genes involved in specialised metabolite pathways are often, though not always, co-expressed. The spatial organization of specialised metabolism means that pathways are localized to specific tissues, cells, or specialised structures. Co-expression analysis, commonly known as the “guilt-by-association" approach, groups genes based on their expression profiles across different conditions, and correlates gene expression with metabolite accumulation patterns[21,165,166]. Careful assessment of metabolite distribution followed by precision sampling can significantly enhance the power of co-expression analysis[167]. This method can reveal both enzymatic and non-enzymatic genes (e.g., transporters, transcription factors) involved in metabolite biosynthesis[109]. Co-expression analysis is often combined with strategies like phylogenetics and genome mining to efficiently prioritise candidate genes. Recent advancements, including single-cell RNA sequencing and high-quality genome assemblies, have further improved the precision and effectiveness of this technique in identifying genes expressed in specific cell types, as described in Chapter 5 of this thesis.

Unsupervised machine learning approaches like Self-Organizing Maps (SOM)[109,168] are useful for clustering genes based on similar expression profiles without requiring prior knowledge of their role in a pathway. Genes identified by co-expression or differential expression analysis can be integrated into co-expression networks to predict functional relationships. Unsupervised clustering further organizes these genes, helping to reveal potential pathway modules and uncover biosynthetic enzymes leading to pathways.

Phylogenetic analyses are often used to narrow down further and prioritise candidate genes identified through correlation-based approaches. Phylogenetic trees can reveal gene clades that are specific to plant species known to produce

certain metabolites, allowing for targeted investigation[169,170]. Comparing the phylogenies of gene families across multiple species helps identify orthologs that may have conserved roles in biosynthetic pathways[171,172]. This approach is particularly useful for large enzyme families like cytochrome P450s, where sequence similarity alone is often insufficient to predict function. A phylogenetics-based approach is discussed in Chapter 3 of this thesis in the discovery of the P450 enzyme, pachysiphine synthase[162], from *T. iboga*. Phylogenomic context can help prioritise candidate genes by identifying those that have evolved alongside known biosynthetic genes.

Gene identification in plant specialised metabolism extends beyond co-expression analysis through several advanced genomic approaches. One such method is genome mining, which involves searching for biosynthetic gene clusters (BGCs)[173] where physically clustered genes contribute to a shared biosynthetic pathway. Genes responsible for synthesizing various natural products are at times clustered together in plant genomes, forming functional units[93,174,175]. Although BGCs are relatively rare in MIA biosynthesis, advances in chromosome-level genome assemblies have greatly improved the ability to identify these clusters. Another approach is genome-wide association studies (GWAS)[176], which link genetic variants to specific metabolic traits across diverse plant populations, helping to identify genes involved in specialised metabolism. Pangenomic analysis further enhances gene discovery by comparing multiple genomes within a species[177], identifying genes unique to specific subpopulations and revealing variation in biosynthetic gene presence and activity.

Several protein- and proteomics-based methods are employed to identify gene candidates in plant specialised metabolic pathways. One classical approach is sequence homology screening, which uses known enzyme sequences from other plant species to identify orthologous genes[25,26]. Another method, activity-guided fractionation, involves purifying native enzymes from plant crude extracts based on their activity and then identifying proteins in the active fractions using proteomic analysis[178]. Proteomics-based proximity labeling methods[179], such as TurboID[180], are also gaining popularity for identifying protein complexes through protein-protein interactions and protein pulldown. TurboID, an engineered biotin ligase, rapidly biotinylates neighboring proteins, allowing for the identification of proteins in close proximity to a protein of interest.

1.7.3 Functional Characterization.

Functional characterization is essential for elucidating the roles of genes and enzymes in plant specialised metabolic pathways. Molecular biology tools have developed into the next generation, adopting golden-gate cloning methods for seamless integration of single and multiple genes into expression vectors with ease. Heterologous expression systems, including *Escherichia coli* (bacterial), *Saccharomyces cerevisiae* (yeast), insect cell cultures, and *Nicotiana benthamiana*, are commonly used to express target proteins. The expressed proteins are tested for their predicted enzymatic activities using potential substrates and analyzing the products through metabolomic techniques.

N. benthamiana is a crucial and highly sought-after platform for gene discovery and pathway elucidation due to its highly efficient transient expression system[181–183]. This system allows for rapid and straightforward testing of genes and enzymes, excelling in the expression of complex proteins, such as membrane-bound and glycosylated variants[27], without the need for additional optimization. Moreover, *N. benthamiana* supports combinatorial screening of more than 20 gene combinations[184–186] simultaneously, making it invaluable when bioinformatics predictions alone are insufficient. Beyond producing proteins efficiently, the same platform enables functional testing, further reducing the need for external co-factors. Additionally, *N. benthamiana* is capable of producing specialised metabolites at milligram scales[187,188], enhancing its versatility. These advantages make *N. benthamiana* the preferred choice for testing pathway hypotheses in specialised metabolism research. Chapter 3 of this thesis will describe an improved, streamlined method[162] for testing gene candidates for pathway discovery based on the *N. benthamiana* platform.

Virus-induced gene silencing (VIGS)[189] is an efficient reverse genetic approach for validating the functions of candidate genes. Its value in gene discovery comes from its ability to transiently downregulate specific plant genes, allowing the observation of resulting effects on metabolite production[90,128,190]. By silencing a candidate gene and analyzing the accumulation of biosynthetic intermediates, VIGS provides in vivo evidence for a gene's involvement in a particular metabolic pathway. This technique is particularly advantageous when a few candidates need to be

tested. VIGS has been successfully implemented in *C. roseus*[191], with several genes functionally characterised through this approach.

While VIGS offers valuable insights, the molecular tools to perform it remain limited. Not all plant species are equally susceptible to viral infection, which limits its applicability. Nonetheless, VIGS is a functional validation tool for gene discovery in susceptible species. In Chapter 4 of this thesis, VIGS in *C. roseus* enabled the discovery and characterization of the divergent scaffold formation of *mavacurane-type* alkaloids, illustrating its effectiveness in uncovering novel metabolic pathways.

1.8 The aims and scope of this thesis

The primary aim of this thesis was to elucidate the biosynthesis of the rare, *pseudo-aspidosperma-type* and *aspidosperma-type* MIAs found in the shoots of the plant *Tabernanthe iboga*. In pursuit of this goal, an underlying objective was to develop and improve methodologies using modern synthetic biology tools to overcome the limitations inherent in gene discovery and plant pathway elucidation.

Chapter 2 of this thesis describes the discovery of pseudo-aspidosperma alkaloid biosynthesis from the common intermediate stemmadenine acetate through the formation of pseudo-tabersonine and pseudo-vincadifformine. The biochemical roles of the iboga enzymes PAS, DPAS, and CorS are explained using a combination of in vitro enzyme assays, *N. benthamiana* reconstitutions, and deuterium labelling experiments for the biosynthesis of these alkaloids. A stepwise reaction mechanism is proposed for the biosynthesis of pseudo-aspidosperma scaffolds, highlighting how nature recycles existing redox enzymes to generate diverse scaffolds from common precursors.

Chapter 3 describes the development of a streamlined screening platform for biosynthetic gene discovery using *N. benthamiana* leaf disks and *C. roseus* flowers. This method, combined with the findings from Chapter 2, led to the discovery of P450 oxidative tailoring enzymes, TiPS and TiT16H, to produce pachysiphine and 16-OH tabersonine, respectively. This work highlights the effectiveness of using multigene constructs and co-infiltration to efficiently reconstitute pathways in plant chassis from stable intermediates and to screen for downstream enzyme activities, addressing common challenges related to substrate availability and stability in plant pathway elucidation.

In Chapter 4, the divergent biosynthesis of monoterpene indole alkaloids from geissoschizine in *Catharanthus roseus,* closely related to *T. iboga,* is discussed. Two orthologs of cytochrome P450 enzyme GO from *C. roseus* were cloned, characterised and shown to catalyze the formation of alternative alkaloid scaffolds. The presence of a side product formed in the canonical GO reaction gives rise to an oxidative rearrangement of C-N bond formation and is shown to play a physiologically relevant role in the metabolic profile of *C. roseus.*

1.9 References

1. Dixon RA, Dickinson AJ. A century of studying plant secondary metabolism—From “what?” to “where, how, and why?” Plant Physiol. 2024;195(1):48–66.

2. Huang XQ, Dudareva N. Plant specialized metabolism. Curr Biol. 2023;33(11):R473–8.

3. Weng JK, Lynch JH, Matos JO, Dudareva N. Adaptive mechanisms of plant specialized metabolism connecting chemistry to function. Nat Chem Biol. 2021;17(10):1037–45.

4. Colinas M, Fitzpatrick TB. Coenzymes and the primary and specialized metabolism interface. Curr Opin Plant Biol. 2022;66:102170.

5. Maeda HA, Fernie AR. Evolutionary History of Plant Metabolism. Annu Rev Plant Biol. 2021;72(1):1–32.

6. Hardy K. Paleomedicine and the use of plant secondary compounds in the Paleolithic and Early Neolithic. Evol Anthr: Issues, N, Rev. 2019;28(2):60–71.

7. Freymann E, Carvalho S, Garbe LA, Ghazhelia DD, Hobaiter C, Huffman MA, et al. Pharmacological and behavioral investigation of putative self-medicative plants in Budongo chimpanzee diets. PLOS ONE. 2024;19(6):e0305219.

8. Yinda LEDO, Onanga R, Obiang CS, Begouabe H, Akomo-Okoue EF, Obame-Nkoghe J, et al. Antibacterial and antioxidant activities of plants consumed by western lowland gorilla (Gorilla gorilla gorilla) in Gabon. PLOS ONE. 2024;19(9):e0306957.

9. Atanasov AG, Waltenberger B, Pferschy-Wenzig EM, Linder T, Wawrosch C, Uhrin P, et al. Discovery and resupply of pharmacologically active plant-derived natural products: A review. Biotechnol Adv. 2015;33(8):1582–614.

10. Atanasov AG, Zotchev SB, Dirsch VM, Orhan IE, Banach M, Rollinger JM, et al. Natural products in drug discovery: advances and opportunities. Nat Rev Drug Discov. 2021;20(3):200–16.

11. Jacobowitz JR, Weng JK. Exploring Uncharted Territories of Plant Specialized Metabolism in the Postgenomic Era. Annu Rev Plant Biol. 2020;71(1):1–28.

12. O’Connor SE, Maresh JJ. Chemistry and biology of monoterpene indole alkaloid biosynthesis. Nat Prod Rep. 2006;23(4):532–47.

13. Szabó LF. Rigorous Biogenetic Network for a Group of Indole Alkaloids Derived from Strictosidine. Molecules. 2008;13(8):1875–96.

14. Rosales PF, Bordin GS, Gower AE, Moura S. Indole alkaloids: 2012 until now, highlighting the new chemical structures and biological activities. Fitoterapia. 2020;143:104558.

15. Maresh JJ, Giddings LA, Friedrich A, Loris EA, Panjikar S, Trout BL, et al. Strictosidine Synthase: Mechanism of a Pictet−Spengler Catalyzing Enzyme. J Am Chem Soc. 2008;130(2):710–23.

16. Men JL, Taylor WI. A uniform numbering system for indole alkaloids. Experientia. 1965;21(9):508–10.

17. Wink M. Evolution of secondary metabolites from an ecological and molecular phylogenetic perspective. Phytochemistry. 2003;64(1):3–19.

18. Antonelli A, Clarkson JJ, Kainulainen K, Maurin O, Brewer GE, Davis AP, et al. Settling a family feud: a high-level phylogenomic framework for the Gentianales based on 353 nuclear genes and partial plastomes. Am J Bot. 2021;108(7):1143–65.

19. Ollerton J, Liede-Schumann S, Endress ME, Meve U, Rech AR, Shuttleworth A, et al. The diversity and evolution of pollination systems in large plant clades: Apocynaceae as a case study. Ann Bot. 2019;123(2):311–25.

20. Zuntini AR, Carruthers T, Maurin O, Bailey PC, Leempoel K, Brewer GE, et al. Phylogenomics and the rise of the angiosperms. Nature. 2024;629(8013):843–50.

21. Hong B, Grzech D, Caputi L, Sonawane P, López CER, Kamileen MO, et al. Biosynthesis of strychnine. Nature. 2022;607(7919):617–22.

22. Balsevich J. Phytochemicals in Plant Cell Cultures. PART III: Alkaloids. 1988;371–84.

23. Mohammed AE, Abdul-Hameed ZH, Alotaibi MO, Bawakid NO, Sobahi TR, Abdel-Lateff A, et al. Chemical Diversity and Bioactivities of Monoterpene Indole Alkaloids (MIAs) from Six Apocynaceae Genera. Molecules. 2021;26(2):488.

24. Patil RH, Patil MP, Maheshwari VL. Apocynaceae Plants, Ethnobotany, Phytochemistry, Bioactivity and Biotechnological Advances. 2023;1–11.

25. Farrow SC, Kamileen MO, Meades J, Ameyaw B, Xiao Y, O'Connor SE. Cytochrome P450 and O-methyltransferase catalyze the final steps in the biosynthesis of the anti-addictive alkaloid ibogaine from Tabernanthe iboga. J Biol Chem [Internet]. 2018;293(36):13821–33.

26. Farrow SC, Kamileen MO, Caputi L, Bussey K, Mundy JEA, McAtee RC, et al. Biosynthesis of an Anti-Addiction Agent from the Iboga Plant. J Am Chem Soc. 2019;141(33):12979–83.

27. Kamileen MO, DeMars MD, Hong B, Nakamura Y, Paetz C, Lichman BR, et al. Recycling Upstream Redox Enzymes Expands the Regioselectivity of Cycloaddition in Pseudo-Aspidosperma Alkaloid Biosynthesis. J Am Chem Soc. 2022;144(43):19673–9.

28. Cuello C, Stander EA, Jansen HJ, Bernonville TD de, Lanoue A, Giglioli-Guivarc'h N, et al. Genome Assembly of the Medicinal Plant Voacanga thouarsii. Genome Biol Evol. 2022;14(11):evac158.

29. Stander EA, Lehka B, Carqueijeiro I, Cuello C, Hansson FG, Jansen HJ, et al. The Rauvolfia tetraphylla genome suggests multiple distinct biosynthetic routes for yohimbane monoterpene indole alkaloids. Commun Biol. 2023;6(1):1197.

30. Guo J, Gao D, Lian J, Qu Y. De novo biosynthesis of antiarrhythmic alkaloid ajmaline. Nat Commun. 2024;15(1):457.

31. Chen H, Sahu SK, Wang S, Liu J, Yang J, Cheng L, et al. Chromosome-level Alstonia scholaris genome unveils evolutionary insights into biosynthesis of monoterpenoid indole alkaloids. iScience. 2024;27(5):109599.

32. Li C, Wood JC, Vu AH, Hamilton JP, Lopez CER, Payne RME, et al. Single-cell multi-omics in the medicinal plant Catharanthus roseus. Nat Chem Biol. 2023;19(8):1031–41.

33. Kulagina N, Méteignier LV, Papon N, O'Connor SE, Courdavault V. More than a Catharanthus plant: A multicellular and pluri-organelle alkaloid-producing factory. Curr Opin Plant Biol. 2022;67:102200.

34. Popik P, Layer RT, Skolnick P. 100 years of ibogaine: neurochemical and pharmacological actions of a putative anti-addictive drug. Pharmacol Rev. 1995;47(2):235–53.

35. Pope HG. Tabernanthe iboga: an African narcotic plant of social importance. Econ Bot. 1969;23(2):174–84.

36. Alper KR, Lotsof HS, Kaplan CD. The ibogaine medical subculture. J Ethnopharmacol. 2008;115(1):9–24.

37. Alrashedy NA, Molina J. The ethnobotany of psychoactive plant use: a phylogenetic perspective. PeerJ. 2016;4:e2546.

38. Vonk, Leeuwenberg AJM. Vonk, G. J. A., and Anthonius Josephus Maria Leeuwenberg. "A taxonomic revision of the genus Tabernanthe and a study of wood anatomy of T. iboga. Series of revisions of Apocynaceae XXIX. 1989;89(4):1–18.

39. Wang Y, Zhang CF, Odago WO, Jiang H, Yang JX, Hu GW, et al. Evolution of 101 Apocynaceae plastomes and phylogenetic implications. Mol Phylogenetics Evol. 2023;180:107688.

40. Baker WJ, Bailey P, Barber V, Barker A, Bellot S, Bishop D, et al. A Comprehensive Phylogenomic Platform for Exploring the Angiosperm Tree of Life. Syst Biol. 2021;71(2):301–19.

41. Fernandez JW, Fernandez RL. Chapter 13 "Returning to the path": The use of iboga[ine] in an equatorial African ritual context and the binding of time, space, and social relationships. Alkaloids: Chem Biol. 2001;56:235–47.

42. Lavaud C, Massiot G. The Iboga Alkaloids. In Cham: Springer International Publishing; 2017. p. 89–136. (Progress in the Chemistry of Organic Natural Products; vol. 105).

43. Alper KR. Chapter 1 Ibogaine: A review. Alkaloids: Chem Biol. 2001;56:1–38.

44. Alburges ME, Hanson GR. Ibogaine pretreatment dramatically enhances the dynorphin response to cocaine. Brain Res. 1999;847(1):139–42.

45. Lotsof HS, Alexander NE. Chapter 16 Case studies of ibogaine treatment: Implications for patient management strategies. Alkaloids: Chem Biol. 2001;56:293–313.

46. Köck P, Froelich K, Walter M, Lang U, Dürsteler KM. A systematic literature review of clinical trials and therapeutic applications of ibogaine. J Subst Abus Treat. 2022;138:108717.

47. Corkery JM. Ibogaine as a treatment for substance misuse: Potential benefits and practical dangers. Prog Brain Res. 2018;242:217–57.

48. Ona G, Rocha JM, Bouso JC, Hallak JEC, Borràs T, Colomina MT, et al. The adverse events of ibogaine in humans: an updated systematic review of the literature (2015–2020). Psychopharmacology. 2022;239(6):1977–87.

49. Popik P, Skolnick P. Chapter 3 Pharmacology of Ibogaine and Ibogaine-Related Alkaloids. Alkaloids: Chem Biol. 1999;52:197–231.

50. Fernandes-Nascimento MH, Negrão AB, Viana-Ferreira K, Chaves BDR, Wang YP. Three Decades of Research on the Development of Ibogaine Treatment of Substance Use Disorders: A Scientometric Analysis. J Psychoact Drugs. 2023;ahead-of-print(ahead-of-print):1–11.

51. Iyer RN, Favela D, Zhang G, Olson DE. The iboga enigma: the chemistry and neuropharmacology of iboga alkaloids and related analogs. Nat Prod Rep. 2020;38(2):307–29.

52. Cameron LP, Tombari RJ, Lu J, Pell AJ, Hurley ZQ, Ehinger Y, et al. A non-hallucinogenic psychedelic analogue with therapeutic potential. Nature. 2021;589(7842):474–9.

53. Belgers M, Leenaars M, Homberg JR, Ritskes-Hoitinga M, Schellekens AFA, Hooijmans CR. Ibogaine and addiction in the animal model, a systematic review and meta-analysis. Transl Psychiatry. 2016;6(5):e826–e826.

54. Arias HR, Micheli L, Rudin D, Bento O, Borsdorf S, Ciampi C, et al. Non-hallucinogenic compounds derived from iboga alkaloids alleviate neuropathic and visceral pain in mice through a mechanism involving 5-HT2A receptor activation. Biomed Pharmacother. 2024;177:116867.

55. Wasko MJ, Witt-Enderby PA, Surratt CK. DARK Classics in Chemical Neuroscience: Ibogaine. ACS Chem Neurosci. 2018;9(10):2475–83.

56. Mash DC. IUPHAR – invited review - Ibogaine – A legacy within the current renaissance of psychedelic therapy. Pharmacol Res. 2023;190:106620.

57. Michele BMM, Sophie AA. A review of the mechanisms involved in the neuroprotection and neurotoxicity of Iboga alkaloids. Pharmacol Res - Nat Prod. 2023;1:100006.

58. Rodríguez P, Urbanavicius J, Prieto JP, Fabius S, Reyes AL, Havel V, et al. A Single Administration of the Atypical Psychedelic Ibogaine or Its Metabolite Noribogaine Induces an Antidepressant-Like Effect in Rats. ACS Chem Neurosci. 2020;11(11):1661–72.

59. Ona G, Reverte I, Rossi GN, Santos RG dos, Hallak JE, Colomina MT, et al. Main targets of ibogaine and noribogaine associated with its putative anti-addictive effects: A mechanistic overview. J Psychopharmacol. 2023;37(12):1190–200.

60. Straub CJ, Rusali LE, Kremiller KM, Riley AP. What We Have Gained from Ibogaine: α3β4 Nicotinic Acetylcholine Receptor Inhibitors as Treatments for Substance Use Disorders. J Med Chem. 2023;66(1):107–21.

61. Dickel DF, Holden CL, Maxfield RC, Paszek LE, Taylor WI. The Alkaloids of Tabernanthe iboga. Part III. 1 Isolation Studies. J Am Chem Soc. 1958;80(1):123–5.

62. Neuss N. Notes- Alkaloids from Apocynaceae II. Ibogaline, A New Alkaloid From Tabernanthe Iboga Baill. J Org Chem. 1959;24(12):2047–8.

63. Kontrimavičiūtė V, Mathieu O, Balas L, Escale R, Blayac JP, Bressolle FMM. Ibogaine and Noribogaine: Structural Analysis and Stability Studies. Use of LC-MS to Determine Alkaloid Contents of the Root Bark of Tabernanthe Iboga. J Liq Chromatogr Relat Technol. 2007;30(8):1077–92.

64. Khuong-Huu F, Cesario M, Guilhem J, Goutarel R. Alcaloïdes indoliques—CII: Deux nouveaux types d'alcaloïdes indoliques l'ibophyllidine, dérivé du nor-21(+)pandolane et l'iboxyphylline dérivé de l'abeo-21(20→19) (+)pandolane, retirés des feuilles de tabernanthe iboga baillon et de t. subsessilis stapf. Tetrahedron. 1976;32(21):2539–43.

65. Krengel F, Chevalier Q, Dickinson J, Herrera Santoyo J, Reyes Chilpa R. Metabolite Profiling of Anti-Addictive Alkaloids from Four Mexican Tabernaemontana Species and the Entheogenic African Shrub Tabernanthe iboga (Apocynaceae). Chem Biodivers. 2019;16(4):e1800506.

66. DeMars MD, O'Connor SE. Evolution and diversification of carboxylesterase-like [4+2] cyclases in aspidosperma and iboga alkaloid biosynthesis. Proc Natl Acad Sci United States Am. 2024;121(7):e2318586121.

67. Bartlett MF, Dickel DF, Taylor WI. The Alkaloids of Tabernanthe iboga. Part IV. 1 The Structures of Ibogamine, Ibogaine, Tabernanthine and Voacangine. J Am Chem Soc. 1958;80(1):126–36.

68. Arai G, Coppola J, Jeffrey GA. The structure of ibogaine. Acta Crystallogr. 1960;13(7):553–64.

69. Büchi G, Coffen DL, Kocsis K, Sonnet PE, Ziegler FE. The Total Synthesis of Iboga Alkaloids 1. J Am Chem Soc. 1966;88(13):3099–109.

70. Zhao G, Xie X, Sun H, Yuan Z, Zhong Z, Tang S, et al. Bioinspired Collective Syntheses of Iboga-Type Indole Alkaloids. Org Lett. 2016;18(10):2447–50.

71. Lopchuk JM. Chapter 1 Recent Advances in the Synthesis of Aspidosperma-Type Alkaloids. Prog Heterocycl Chem. 2011;23:1–25.

72. Cordell GA. Chapter 3 The Aspidosperma Alkaloids. Alkaloids: Chem Physiol. 1979;17:199–384.

73. Saxton JE. Chapter 1 Alkaloids of the Aspidospermine Group. Alkaloids Chem Biology. 1998;51:1–197.

74. Kuehne ME, Pitner JB. Studies in biomimetic alkaloid syntheses. 17. Syntheses of iboxyphylline and related alkaloids. J Org Chem [Internet]. 1989;54(19):4553–69.

75. Reuß F, Heretsch P. Synthetic strategies for the ibophyllidine alkaloids. Nat Prod Rep. 2020;

76. Reuß F, Heretsch P. Synthesis of Aspidodispermine via Pericyclic Framework Reconstruction. Org Lett. 2020;22(10):3956–9.

77. Battersby AR, Byrne JC, Kapil RS, Martin JA, Payne TG, Arigoni D, et al. The mechanism of indole alkaloid biosynthesis. Chem Commun Lond. 1968;0(16):951–3.

78. Battersby AR, Burnett AR, Parsons PG. Alkaloid biosynthesis. Part XIV. Secologanin: its conversion into ipecoside and its role as biological precursor of the indole alkaloids. J Chem Soc C Org. 1969;0(8):1187–92.

79. Scott AI, Qureshi AA. Biogenesis of Strychnos, Aspidosperma, and Iboga alkaloids. Structure and reactions of preakuammicine. J Am Chem Soc. 1969;91(21):5874–6.

80. Scott AI, Wei CC. Regio- and sterospecific models for the biosynthesis of the indole alkaloids. The Aspidosperma-Iboga relationship. J Am Chem Soc. 1972;94(23):8266–7.

81. Qureshi AA, Scott AI. Biosynthesis of indole alkaloids: sequential precursor formation and biological conversion in Vinca rosea. Chem Commun Lond [Internet]. 1968;0(16):948–50.

82. Qureshi AA, Scott AI. Biogenetic-type synthesis of Iboga alkaloids: (±)-catharanthine. Chem Commun Lond. 1968;0(16):947–8.

83. Qureshi AA, Scott AI. Interconversion of Corynanthe, aspidosperma, and Iboga alkaloids. A model for indole alkaloid biosynthesis. Chem Commun Lond. 1968;0(16):945–6.

84. Robinson R. LXIII.—A synthesis of tropinone. J Chem Soc, Trans. 1917;111(0):762–8.

85. Leete E. Biosynthesis of Alkaloids. Science. 1965;147(3661):1000–6.

86. Stöckigt J, Treimer J, Zenk MH. Synthesis of ajmalicine and related indole alkaloids by cell free extracts of Catharanthus roseus cell suspension cultures. FEBS Lett. 1976;70(1–2):267–70.

87. Zenk MH. Enzymatic Synthesis of Ajmalicine and Related Indole Alkaloids. J Nat Prod. 1980;43(4):438–51.

88. Brown S, Clastre M, Courdavault V, O'Connor SE. De novo production of the plant-derived alkaloid strictosidine in yeast. Proc National Acad Sci [Internet]. 2015;112(11):3205–10.

89. Dudley QM, Jo S, Guerrero DAS, Chhetry M, Smedley MA, Harwood WA, et al. Reconstitution of monoterpene indole alkaloid biosynthesis in genome engineered Nicotiana benthamiana. Commun Biol. 2022;5(1):949.

90. Caputi L, Franke J, Farrow SC, Chung K, Payne RME, Nguyen TD, et al. Missing enzymes in the biosynthesis of the anticancer drug vinblastine in Madagascar periwinkle. Science. 2018;360(6394):1235–9.

91. Zhang J, Hansen LG, Gudich O, Viehrig K, Lassen LMM, Schrübbers L, et al. A microbial supply chain for production of the anti-cancer drug vinblastine. Nature. 2022;609(7926):341–7.

92. Anarat-Cappillino G, Sattely ES. The chemical logic of plant natural product biosynthesis. Curr Opin Plant Biol. 2014;19:51–8.

93. Lichman BR, Godden GT, Hamilton JP, Palmer L, Kamileen MO, Zhao D, et al. The evolutionary origins of the cat attractant nepetalactone in catnip. Sci Adv. 2020;6(20):eaba0721.

94. Walsh CT, Moore BS. Enzymatic Cascade Reactions in Biosynthesis. Angew Chem Int Ed. 2019;58(21):6846–79.

95. Walsh CT. Tailoring enzyme strategies and functional groups in biosynthetic pathways. Nat Prod Rep. 2022;40(2):326–86.

96. Muro-Villanueva F, Nett RS. Emerging functions within the enzyme families of plant alkaloid biosynthesis. Phytochem Rev. 2023;1–22.

97. Rueffer M, Nagakura N, Zenk MH. Strictosidine, the common precursor for monoterpenoid indole alkaloids with 3 α and 3 β configuration. Tetrahedron Lett. 1978;19(18):1593–6.

98. Amann M, Wanner G, Zenk MH. Intracellular compartmentation of two enzymes of berberine biosynthesis in plant cell cultures. Planta. 1986;167(3):310–20.

99. Miettinen K, Dong L, Navrot N, Schneider T, Burlat V, Pollier J, et al. The seco-iridoid pathway from Catharanthus roseus. Nat Commun. 2014;5(1):3606.

100. Kutchan TM. Strictosidine: From alkaloid to enzyme to gene. Phytochemistry. 1993;32(3):493–506.

101. TREIMER JF, ZENK MH. Purification and Properties of Strictosidine Synthase, the Key Enzyme in Indole Alkaloid Formation. Eur J Biochem. 1979;101(1):225–33.

102. Ma X, Panjikar S, Koepke J, Loris E, Stöckigt J. The Structure of Rauvolfia serpentina Strictosidine Synthase Is a Novel Six-Bladed β-Propeller Fold in Plant Proteins. Plant Cell. 2006;18(4):907–20.

103. Stöckigt J, Panjikar S. Structural biology in plant natural product biosynthesis—architecture of enzymes from monoterpenoid indole and tropane alkaloid biosynthesis. Nat Prod Rep. 2007;24(6):1382–400.

104. Kutchan TM, Hampp N, Lottspeich F, Beyreuther K, Zenk MH. The cDNA clone for strictosidine synthase from Rauvolfia serpentina DNA sequence determination and expression in Escherichia coli. FEBS Lett. 1988;237(1–2):40–4.

105. Liu H, Panjikar S, Sheng X, Futamura Y, Zhang C, Shao N, et al. β-Methyltryptamine Provoking the Crucial Role of Strictosidine Synthase Tyr151-OH for Its Stereoselective Pictet−Spengler Reactions to Tryptoline-type Alkaloids. ACS Chem Biol. 2022;17(1):187–97.

106. McCoy E, Galan MC, O'Connor SE. Substrate specificity of strictosidine synthase. Bioorg Med Chem Lett. 2006;16(9):2475–8.

107. Stevens LH, Blom TJM, Verpoorte R. Subcellular localization of tryptophan decarboxylase, strictosidine synthase and strictosidine glucosidase in suspension cultured cells of Catharanthus roseus and Tabernaemontana divaricata. Plant Cell Rep. 1993;12(10):573–6.

108. Guirimand G, Courdavault V, Lanoue A, Mahroug S, Guihur A, Blanc N, et al. Strictosidine activation in Apocynaceae: towards a "nuclear time bomb"? BMC Plant Biol. 2010;10(1):182.

109. Payne RME, Xu D, Foureau E, Carqueijeiro MIST, Oudin A, Bernonville TD de, et al. An NPF transporter exports a central monoterpene indole alkaloid intermediate from the vacuole. Nat Plants. 2017;3(2):16208.

110. Li F, Shahsavarani M, Handy-Hart CJ, Côté A, Brasseur-Trottier X, Montgomery V, et al. Characterization of a vacuolar importer of secologanin in Catharanthus roseus. Commun Biol. 2024;7(1):939.

111. Hemscheidt T, Zenk MH. Glucosidases involved in indole alkaloid biosynthesis of Catharanthus cell cultures. FEBS Lett. 1980;110(2):187–91.

112. Yerkes N, Wu JX, McCoy E, Galan MC, Chen S, O'Connor SE. Substrate specificity and diastereoselectivity of strictosidine glucosidase, a key enzyme in monoterpene indole alkaloid biosynthesis. Bioorg Med Chem Lett. 2008;18(10):3095–8.

113. Carqueijeiro I, Koudounas K, Bernonville TD de, Sepúlveda LJ, Mosquera A, Bomzan DP, et al. Alternative splicing creates a pseudo-strictosidine β-d-glucosidase modulating alkaloid synthesis in Catharanthus roseus. Plant Physiol. 2020;185(3):836–56.

114. Gerasimenko I, Sheludko Y, Ma X, Stöckigt J. Heterologous expression of a Rauvolfia cDNA encoding strictosidine glucosidase, a biosynthetic key to over 2000 monoterpenoid indole alkaloids. Eur J Biochem. 2002;269(8):2204–13.

115. Stavrinides A, Tatsis EC, Caputi L, Foureau E, Stevenson CEM, Lawson DM, et al. Structural investigation of heteroyohimbine alkaloid synthesis reveals active site elements that control stereoselectivity. Nat Commun. 2016;7(1):12116.

116. Stavrinides AK, Tatsis EC, Dang TT, Caputi L, Stevenson CEM, Lawson DM, et al. Discovery of a Short-Chain Dehydrogenase from Catharanthus roseus that Produces a New Monoterpene Indole Alkaloid. ChemBioChem. 2018;19(9):940–8.

117. Bradley SA, Hansson FG, Lehka BJ, Rago D, Pinho P, Peng H, et al. Yeast Platforms for Production and Screening of Bioactive Derivatives of Rauwolscine. ACS Synth Biol. 2024;13(5):1498–512.

118. Geerlings A, Ibañez MML, Memelink J, Heijden R van der, Verpoorte R. Molecular Cloning and Analysis of Strictosidine β-d-Glucosidase, an Enzyme in Terpenoid Indole Alkaloid Biosynthesis in Catharanthus roseus *. J Biol Chem. 2000;275(5):3051–6.

119. Barleben L, Panjikar S, Ruppert M, Koepke J, Stöckigt J. Molecular Architecture of Strictosidine Glucosidase: The Gateway to the Biosynthesis of the Monoterpenoid Indole Alkaloid Family. Plant Cell. 2007;19(9):2886–97.

120. Stavrinides A, Tatsis EC, Foureau E, Caputi L, Kellner F, Courdavault V, et al. Unlocking the Diversity of Alkaloids in Catharanthus roseus: Nuclear Localization Suggests Metabolic Channeling in Secondary Metabolism. Chem Biol. 2015;22(3):336–41.

121. Qu Y, Thamm AMK, Czerwinski M, Masada S, Kim KH, Jones G, et al. Geissoschizine synthase controls flux in the formation of monoterpenoid indole alkaloids in a Catharanthus roseus mutant. Planta. 2018;247(3):625–34.

122. Langley C, Tatsis E, Hong B, Nakamura Y, Paetz C, Stevenson CEM, et al. Expansion of the Catalytic Repertoire of Alcohol Dehydrogenases in Plant Metabolism**. Angew Chem Int Ed. 2022;61(48):e202210934.

123. Kim K, Shahsavarani M, Garza-García JJO, Carlisle JE, Guo J, Luca VD, et al. Biosynthesis of kratom opioids. N Phytol. 2023;240(2):757–69.

124. Schotte C, Jiang Y, Grzech D, Dang TTT, Laforest LC, León F, et al. Directed Biosynthesis of Mitragynine Stereoisomers. J Am Chem Soc. 2023;145(9):4957–63.

125. Tatsis EC, Carqueijeiro I, Bernonville TD de, Franke J, Dang TTT, Oudin A, et al. A three enzyme system to generate the Strychnos alkaloid scaffold from a central biosynthetic intermediate. Nat Commun. 2017;8(1):316.

126. Battersby AR, Hall ES. The intermediacy of geissoschizine in indole alkaloid biosynthesis: rearrangement to the Strychnos skeleton. J Chem Soc D: Chem Commun. 1969;0(14):793–4.

127. Scott AI, Reichardt PB, Slaytor MB, Sweeny JG. Mechanisms of indole alkaloid biosynthesis. Recognition of intermediacy and sequence by short-term incubation. Bioorg Chem. 1971;1(1–2):157–73.

128. Qu Y, Easson MEAM, Simionescu R, Hajicek J, Thamm AMK, Salim V, et al. Solution of the multistep pathway for assembly of corynanthean, strychnos, iboga, and aspidosperma monoterpenoid indole alkaloids from 19E-geissoschizine. Proc Natl Acad Sci United States Am [Internet]. 2018;115(12):3180–5.

129. Gao D, Liu T, Gao J, Xu J, Gou Y, Pan Y, et al. De Novo Biosynthesis of Vindoline and Catharanthine in Saccharomyces cerevisiae. Biodesign Res. 2022;2022:0002.

130. Grzech D, Hong B, Caputi L, Sonawane PD, O'Connor SE. Engineering the Biosynthesis of Late-Stage Vinblastine Precursors Precondylocarpine Acetate, Catharanthine, Tabersonine in Nicotiana benthamiana. ACS Synth Biol. 2023;12(1):27–34.

131. Li Z, Jiang Y, Guengerich FP, Ma L, Li S, Zhang W. Engineering cytochrome P450 enzyme systems for biomedical and biotechnological applications. J Biol Chem. 2020;295(3):833–49.

132. Liu X, Zhu X, Wang H, Liu T, Cheng J, Jiang H. Discovery and modification of cytochrome P450 for plant natural products biosynthesis. Synth Syst Biotechnol. 2020;5(3):187–99.

133. Nguyen TD, Dang TTT. Cytochrome P450 Enzymes as Key Drivers of Alkaloid Chemical Diversification in Plants. Front Plant Sci. 2021;12:682181.

134. Hansen CC, Nelson DR, Møller BL, Werck-Reichhart D. Plant cytochrome P450 plasticity and evolution. Mol Plant. 2021;14(8):1244–65.

135. Mizutani M, Sato F. Unusual P450 reactions in plant secondary metabolism. Arch Biochem Biophys. 2011;507(1):194–203.

136. Sakamoto J, Kitajima M, Ishikawa H. Total Syntheses of (+)-Villocarine A, (−)-Apogeissoschizine, and (+)-Geissoschizine. Chem A Eur J. 2023;29(18):e202300179.

137. Wang Z, Xiao Y, Wu S, Chen J, Li A, Tatsis EC. Deciphering and reprogramming the cyclization regioselectivity in bifurcation of indole alkaloid biosynthesis. Chem Sci. 2022;13(42):12389–95.

138. Wenkert E, Wickberg B. General Methods of Synthesis of Indole Alkaloids. IV. A Synthesis of dl-Eburnamonine 1,2. J Am Chem Soc. 1965;87(7):1580–9.

139. Hugel G, Royer D, Men-Olivier LL, Richard B, Jacquier MJ, Lévy J. Flow Thermolysis Rearrangements in the Indole Alkaloid Series: Strictamine and Akuammicine Derivatives. The Absolute Configurations of Ngouniensine and epi-Ngouniensine. J Org Chem. 1997;62(3):578–83.

140. Dang TTT, Franke J, Carqueijeiro IST, Langley C, Courdavault V, O'Connor SE. Sarpagan bridge enzyme has substrate-controlled cyclization and aromatization modes. Nat Chem Biol. 2018;14(8):760–3.

141. Vidal LS, Kelly CL, Mordaka PM, Heap JT. Review of NAD(P)H-dependent oxidoreductases: Properties, engineering and application. Biochim Biophys Acta (BBA) - Proteins Proteom. 2018;1866(2):327–47.

142. Sengupta D, Naik D, Reddy AR. Plant aldo-keto reductases (AKRs) as multi-tasking soldiers involved in diverse plant metabolic processes and stress defense: A structure-function update. J Plant Physiol. 2015;179:40–55.

143. Fan M, Zou L, Tian K, Chen G, Cheng K, Li Y. Chemistry, bioactivity, biosynthesis, and total synthesis of stemmadenine alkaloids. Nat Prod Rep. 2023;40(5):1022–44.

144. Boccia M, Grzech D, Lopes AA, O'Connor SE, Caputi L. Directed Biosynthesis of New to Nature Alkaloids in a Heterologous Nicotiana benthamiana Expression Host. Front Plant Sci. 2022;13:919443.

145. Shahsavarani M, Utomo JC, Kumar R, Paz-Galeano M, Garza-García JJO, Mai Z, et al. Improved protein glycosylation enabled heterologous biosynthesis of monoterpenoid indole alkaloids and their unnatural derivatives in yeast. Metab Eng Commun. 2023;16:e00215.

146. Moghe G, Kruse LH, Petersen M, Scossa F, Fernie AR, Gaquerel E, et al. BAHD Company: The Ever-Expanding Roles of the BAHD Acyltransferase Gene Family in Plants. Annu Rev Plant Biol. 2022;74(1):165–94.

147. Tjallinks G, Mattevi A, Fraaije MW. Biosynthetic Strategies of Berberine Bridge Enzyme-like Flavoprotein Oxidases toward Structural Diversification in Natural Product Biosynthesis. Biochemistry. 2024;63(17):2089–110.

148. Caputi L, Franke J, Bussey K, Farrow SC, Vieira IJC, Stevenson CEM, et al. Structural basis of cycloaddition in biosynthesis of iboga and aspidosperma alkaloids. Nat Chem Biol. 2020;16(4):383–6.

149. Scott AI, Wei CC. Regio- and stereospecific models for the biosynthesis of the indole alkaloids—II: Biogenetic type synthesis of Aspidosperma and Iboga alkaloids from a corynanthe precursor. Tetrahedron. 1974;30(17):3003–11.

150. Scott AI, Qureshi AA. Regio- and stereospecific models for the biosynthesis of the indole alkaloids—I: Development of strategic approaches and preliminary experiments. Tetrahedron. 1974;30(17):2993–3002.

151. Tay G, Wayama T, Takezawa H, Yoshida S, Sato S, Fujita M, et al. Synthetic Modulation of an Unstable Dehydrosecodine-type Intermediate and Its Encapsulation into a Confined Cavity Enable Its X-ray Crystallographic Observation. Angew Chem Int Ed. 2023;62(32):e202305122.

152. Dogru E, Warzecha H, Seibel F, Haebel S, Lottspeich F, Stöckigt J. The gene encoding polyneuridine aldehyde esterase of monoterpenoid indole alkaloid biosynthesis in plants is an ortholog of theα/β hydrolase super family. Eur J Biochem. 2000;267(5):1397–406.

153. Bernonville TD de, Papon N, Clastre M, O'Connor SE, Courdavault V. Identifying Missing Biosynthesis Enzymes of Plant Natural Products. Trends Pharmacol Sci. 2020;41(3):142–6.

154. Eljounaidi K, Lichman BR. Nature's Chemists: The Discovery and Engineering of Phytochemical Biosynthesis. Front Chem. 2020;8:596479.

155. Swamidatta SH, Lichman BR. Beyond co-expression: pathway discovery for plant pharmaceuticals. Curr Opin Biotechnol. 2024;88:103147.

156. Seligmann B, Liu S, Franke J. Chemical tools for unpicking plant specialised metabolic pathways. Curr Opin Plant Biol. 2024;80:102554.

157. Nett RS, Guan X, Smith K, Faust AM, Sattely ES, Fischer CR. D2O Labeling to measure active biosynthesis of natural products in medicinal plants. AIChE J. 2018;64(12):4319–30.

158. Doppler M, Bueschl C, Kluger B, Koutnik A, Lemmens M, Buerstmayr H, et al. Stable Isotope–Assisted Plant Metabolomics: Combination of Global and Tracer-Based Labeling for Enhanced Untargeted Profiling and Compound Annotation. Front Plant Sci. 2019;10:1366.

159. Nakabayashi R, Saito K. Higher dimensional metabolomics using stable isotope labeling for identifying the missing specialized metabolism in plants. Curr Opin Plant Biol. 2020;55:84–92.

160. Nakabayashi R, Mori T, Takeda N, Toyooka K, Sudo H, Tsugawa H, et al. Metabolomics with 15N Labeling for Characterizing Missing Monoterpene Indole Alkaloids in Plants. Anal Chem. 2020;92(8):5670–5.

161. Ishikawa E, Kanai S, Sue M. Detection of a novel intramolecular rearrangement during gramine biosynthesis in barley using stable isotope-labeled tryptophan. Biochem Biophys Rep. 2023;34:101439.

162. Kamileen MO, Nakamura Y, Luck K, Heinicke S, Hong B, Colinas M, et al. Streamlined screening platforms lead to the discovery of pachysiphine synthase from Tabernanthe iboga. N Phytol. 2024;

163. Arroo RRJ, Bhambra AS, Hano C, Renda G, Ruparelia KC, Wang MF. Analysis of plant secondary metabolism using stable isotope-labelled precursors. Phytochem Anal. 2021;32(1):62–8.

164. Jang C, Chen L, Rabinowitz JD. Metabolomics and Isotope Tracing. Cell. 2018;173(4):822–37.

165. Lau W, Sattely ES. Six enzymes from mayapple that complete the biosynthetic pathway to the etoposide aglycone. Science. 2015;349(6253):1224–8.

166. Nett RS, Lau W, Sattely ES. Discovery and engineering of colchicine alkaloid biosynthesis. Nature. 2020;584(7819):148–53.

167. Mehta N, Meng Y, Zare R, Kamenetsky-Goldstein R, Sattely E. A developmental gradient reveals biosynthetic pathways to eukaryotic toxins in monocot geophytes. Cell. 2024;

168. Chuang L, Liu S, Franke J. Post-Cyclization Skeletal Rearrangements in Plant Triterpenoid Biosynthesis by a Pair of Branchpoint Isomerases. J Am Chem Soc. 2023;145(9):5083–91.

169. Torrens-Spence MP, Pluskal T, Li FS, Carballo V, Weng JK. Complete Pathway Elucidation and Heterologous Reconstitution of Rhodiola Salidroside Biosynthesis. Mol Plant. 2018;11(1):205–17.

170. Pluskal T, Torrens-Spence MP, Fallon TR, Abreu AD, Shi CH, Weng JK. The biosynthetic origin of psychoactive kavalactones in kava. Nat Plants. 2019;5(8):867–78.

171. Christ B, Xu C, Xu M, Li FS, Wada N, Mitchell AJ, et al. Repeated evolution of cytochrome P450-mediated spiroketal steroid biosynthesis in plants. Nat Commun. 2019;10(1):3206.

172. Florean M, Luck K, Hong B, Nakamura Y, O'Connor SE, Köllner TG. Reinventing metabolic pathways: Independent evolution of benzoxazinoids in flowering plants. Proc Natl Acad Sci. 2023;120(42):e2307981120.

173. Smit SJ, Lichman BR. Plant biosynthetic gene clusters in the context of metabolic evolution. Nat Prod Rep. 2022;39(7):1465–82.

174. Liu Z, Duran HGS, Harnvanichvech Y, Stephenson MJ, Schranz ME, Nelson D, et al. Drivers of metabolic diversification: how dynamic genomic neighbourhoods generate new biosynthetic pathways in the Brassicaceae. N Phytol. 2020;227(4):1109–23.

175. Forman V, Luo D, Geu-Flores F, Lemcke R, Nelson DR, Kampranis SC, et al. A gene cluster in Ginkgo biloba encodes unique multifunctional cytochrome P450s that initiate ginkgolide biosynthesis. Nat Commun. 2022;13(1):5143.

176. Fang C, Luo J. Metabolic GWAS-based dissection of genetic bases underlying the diversity of plant metabolism. Plant J. 2019;97(1):91–100.

177. Liu Z, Cheema J, Vigouroux M, Hill L, Reed J, Paajanen P, et al. Formation and diversification of a paradigm biosynthetic gene cluster in plants. Nat Commun. 2020;11(1):5354.

178. Chen X, Hagel JM, Chang L, Tucker JE, Shiigi SA, Yelpaala Y, et al. A pathogenesis-related 10 protein catalyzes the final step in thebaine biosynthesis. Nat Chem Biol. 2018;14(7):738–43.

179. Xu SL, Shrestha R, Karunadasa SS, Xie PQ. Proximity Labeling in Plants. Annu Rev Plant Biol. 2023;74(1):285–312.

180. Feng L, Zhou J, Zhu D, Gao C. TurboID-based proximity labeling accelerates discovery of neighboring proteins in plants. Trends Plant Sci. 2023;29(Nat. Biotechnol. 36 2018):383–4.

181. Bally J, Jung H, Mortimer C, Naim F, Philips JG, Hellens R, et al. The Rise and Rise of Nicotiana benthamiana : A Plant for All Reasons. Annu Rev Phytopathol. 2018;56(1):405–26.

182. Kwan BD, Seligmann B, Nguyen TD, Franke J, Dang TTT. Leveraging synthetic biology and metabolic engineering to overcome obstacles in plant pathway elucidation. Curr Opin Plant Biol. 2023;71:102330.

183. Golubova D, Tansley C, Su H, Patron NJ. Engineering Nicotiana benthamiana as a platform for natural product biosynthesis. Curr Opin Plant Biol. 2024;81:102611.

184. Carlson ED, Rajniak J, Sattely ES. Multiplicity of the Agrobacterium Infection of Nicotiana benthamiana for Transient DNA Delivery. ACS Synth Biol. 2023;12(8):2329–38.

185. Martin LBB, Kikuchi S, Rejzek M, Owen C, Reed J, Orme A, et al. Complete biosynthesis of the potent vaccine adjuvant QS-21. Nat Chem Biol. 2024;20(4):493–502.

186. Jo S, El-Demerdash A, Owen C, Srivastava V, Wu D, Kikuchi S, et al. Unlocking saponin biosynthesis in soapwort. Nat Chem Biol. 2024;1–12.

187. Schultz BJ, Kim SY, Lau W, Sattely ES. Total Biosynthesis for Milligram-Scale Production of Etoposide Intermediates in a Plant Chassis. J Am Chem Soc. 2019;141(49):19231–5.

188. Reed J, Stephenson MJ, Miettinen K, Brouwer B, Leveau A, Brett P, et al. A translational synthetic biology platform for rapid access to gram-scale quantities of novel drug-like molecules. Metab Eng. 2017;42:185–93.

189. Rössner C, Lotz D, Becker A. VIGS Goes Viral: How VIGS Transforms Our Understanding of Plant Science. Annu Rev Plant Biol. 2022;73(1):703–28.

190. Czechowski T, Forestier E, Swamidatta SH, Gilday AD, Cording A, Larson TR, et al. Gene discovery and virus-induced gene silencing reveal branched pathways to major classes of bioactive diterpenoids in Euphorbia peplus. Proc Natl Acad Sci. 2022;119(21):e2203890119.

191. Yamamoto K, Grzech D, Koudounas K, Stander EA, Caputi L, Mimura T, et al. Improved virus-induced gene silencing allows discovery of a serpentine synthase gene in Catharanthus roseus. Plant Physiol. 2021;187(2):846–57.

Chapter 2

Recycling Upstream Redox Enzymes Expands the Regioselectivity of Cycloaddition in Pseudo-Aspidosperma Alkaloid Biosynthesis

This Chapter (Chapter 2) of the thesis is published under the first autourship of Mohamed Omar Kamileen in the Journal of the American Chemical Society (JACS).

Title: Recycling Upstream Redox Enzymes Expands the Regioselectivity of Cycloaddition in Pseudo-Aspidosperma Alkaloid Biosynthesis

Authors: Mohamed O. Kamileen[1,2], Matthew D. DeMars II[1], Benke Hong[1], Yoko Nakamura[1,3], Christian Paetz[3], Benjamin R. Lichman[2], Prashant D. Sonawane[1], Lorenzo Caputi[1*] and Sarah E. O'Connor[1*]

Affiliations:

[1] Department of Natural Product Biosynthesis, Max Planck Institute for Chemical Ecology, Hans-Knöll-Straße 8, Jena 07745 Germany.

[2] Centre for Novel Agricultural Products, Department of Biology, University of York, York, YO10 5DD, UK.

[3] Research Group Biosynthesis and NMR, Max Planck Institute for Chemical Ecology, Hans-Knöll-Straße 8, Jena 07745 Germany.

Journal: Journal of the American Chemical Society (JACS)

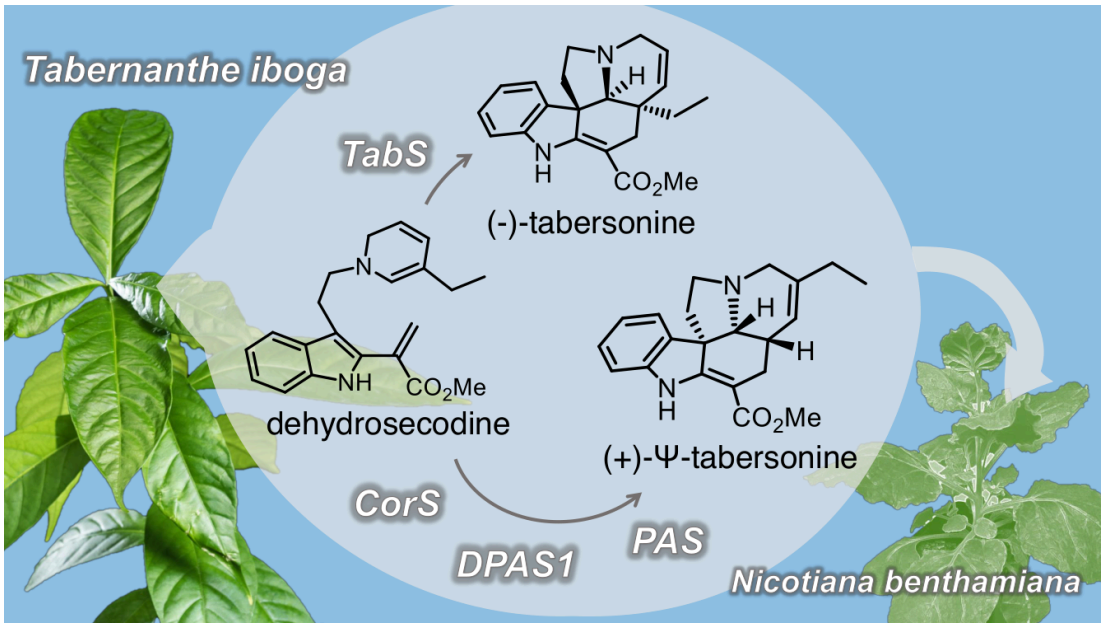
Date of submission: August 1st, 2022

Date of publication: October 14th, 2022

DOI: 10.1021/jacs.2c08107

Link: https://doi.org/10.1021/jacs.2c08107

2.1 Graphical Abstract submitted to JACS



Graphical abstract demonstrating the biosynthesis of monoterpene indole alkaloid alkaloids (MIAs), (−)-tabersonine and (+)-pseudo-tabersonine from the common intermediate dehydrosecodine in the plant *Tabernanthe iboga* and the subsequent pathway reconstitution in *Nicotiana benthamiana*.

Recycling upstream redox enzymes expands the regioselectivity of cycloaddition in pseudo-aspidosperma alkaloid biosynthesis

Mohamed O. Kamileen[1,2], Matthew D. DeMars II[1], Benke Hong[1], Yoko Nakamura[1,3], Christian Paetz[3], Benjamin R. Lichman[2], Prashant D. Sonawane[1], Lorenzo Caputi[1*] and Sarah E. O'Connor[1*]

[1] Department of Natural Product Biosynthesis, Max Planck Institute for Chemical Ecology, Hans-Knöll-Straße 8, Jena 07745 Germany.

[2] Centre for Novel Agricultural Products, Department of Biology, University of York, York, YO10 5DD, UK.

[3] Research Group Biosynthesis and NMR, Max Planck Institute for Chemical Ecology, Hans-Knöll-Straße 8, Jena 07745 Germany.

*Corresponding Authors

2.2 Abstract

Nature uses cycloaddition reactions to generate complex natural product scaffolds. Dehydrosecodine is a highly reactive biosynthetic intermediate that undergoes cycloaddition to generate several alkaloid scaffolds that are the precursors to pharmacologically important compounds such as vinblastine and ibogaine. Here we report how dehydrosecodine can be subjected to redox chemistry, which in turn allows cycloaddition reactions with alternative regioselectivity. By incubating dehydrosecodine with reductase and oxidase biosynthetic enzymes that act upstream in the pathway, we can access the rare pseudo-aspidosperma alkaloids, pseudo-tabersonine and pseudo-vincadifformine, both *in vitro* and by reconstitution in the plant *Nicotiana benthamiana* from an upstream intermediate. We propose a stepwise mechanism to explain the formation of the pseudo-tabersonine scaffold by structurally characterizing enzyme intermediates, and by monitoring the incorporation of deuterium labels. This discovery highlights how plants use redox enzymes to enantioselectively generate new scaffolds from common precursors.

2.3 Manuscript

Alkaloid producing plants in the Apocynaceae family have evolved cyclases that catalyze the cycloaddition of a highly reactive substrate, dehydrosecodine (**1**), into distinct alkaloid scaffolds.[1,2] We and others recently discovered and characterised the only known enzymes that catalyze cycloaddition of **1**: tabersonine synthase (*Ti*TabS and *Cr*TS), which catalyzes the formation of (–)-tabersonine (**2**) (precursor to anti-cancer drugs vinblastine and vincristine), catharanthine synthase (*Cr*CS), which catalyzes formation of (+)-catharanthine (**3**) (precursor to vinblastine and vincristine), and coronaridine synthase (*Ti*CorS), which catalyzes formation of (–)-coronaridine (**4**) (precursor to anti-addiction agent ibogaine) (**Figure 1**).[2–5] *Ti*TabS/*Cr*TS and *Cr*CS directly yield **2** and **3** from **1** by a formal [4+2] cycloaddition,[2,6] while *Ti*CorS initially forms a hitherto uncharacterized unstable intermediate, which is then enzymatically reduced to **4**. The **1** substrate could, in principle, undergo alternative cycloaddition reactions to yield additional scaffolds but extensive mutagenesis of these cyclases did not result in an expansion of the enzymatic product profile.[2] Here we show that the cyclase *Ti*CorS can, in addition to generating **4**, also produce the alternative pseudo-aspidosperma (Ψ-aspidosperma) type alkaloid pseudo-tabersonine (Ψ-tabersonine) (**5**) (**Figure 1**). We show the mechanistic basis behind this transformation by first characterizing the unstable intermediate produced by the cyclase *Ti*CorS. This intermediate can be intercepted by a reductase to generate **4**, or by both a reductase and an oxidase to generate the alternative scaffold **5**. Deuterium labeling provides evidence for the mechanism of these enzymatic transformations. In short, the chemical reactivity of **1** is exploited by both a cyclase, as well as a pair of redox enzymes that can isomerize the alkene moieties, which in turn facilitates new cyclization regioselectivity.

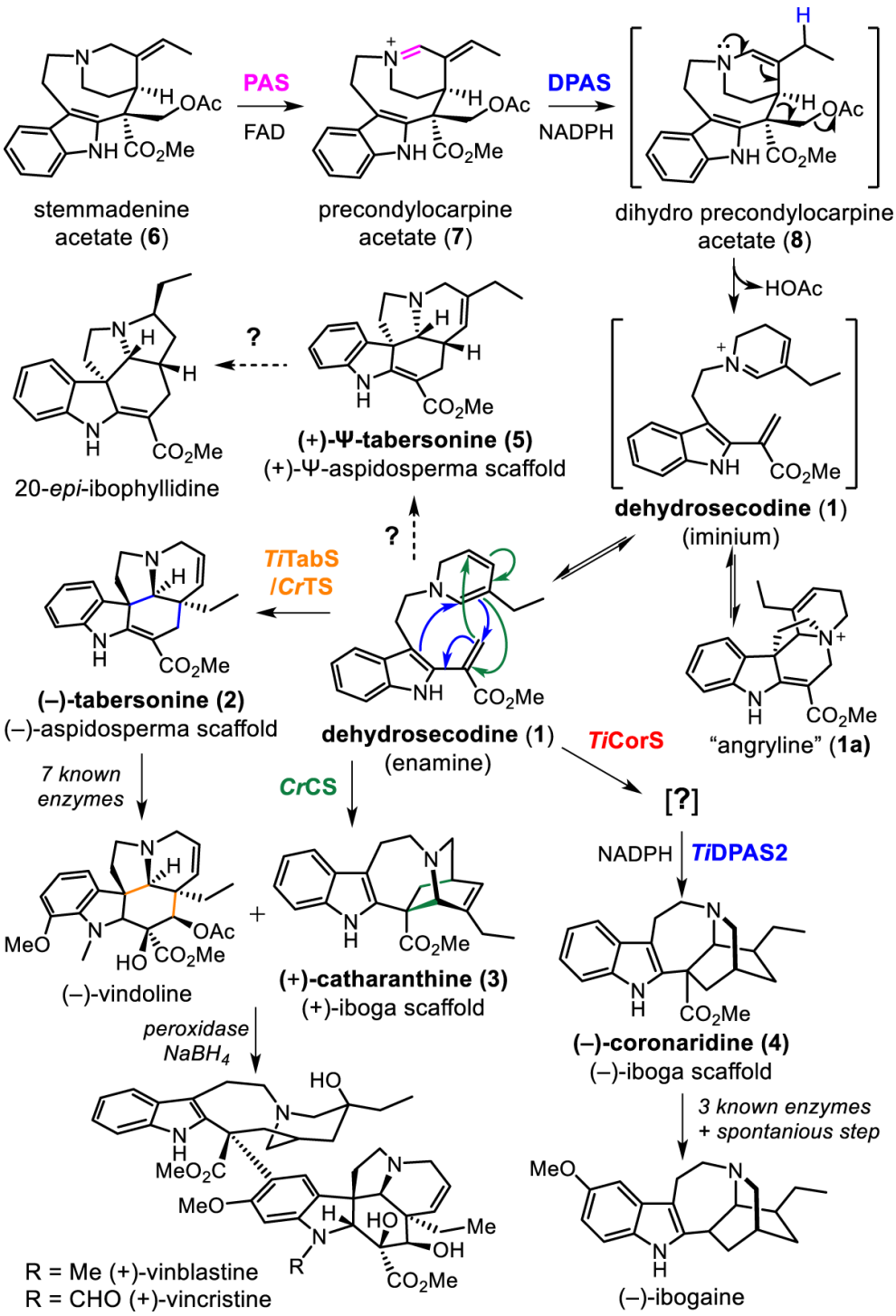


Figure 1. Dehydrosecodine (1)-derived alkaloids produced by the Apocynaceae family of plants.

Tabernanthe iboga, a plant that produces **2** and **4** via enzymes *Ti*TabS and *Ti*CorS, respectively,[3] also produces Ψ-*aspidosperma-type* alkaloid 20-*epi*-ibophyllidine (**Figure 1**).[7–9] We hypothesized that **5** would be the precursor to 20-*epi*-ibophyllidine.[10] The natural product **5**, rarely observed in nature, has only been

isolated from *Tabernaemontana calcarea*, a species closely related to *T. iboga*.[11,12] To identify *T. iboga* enzymes that could form (+)-Ψ-tabersonine **5**, we performed coupled *in vitro* biochemical assays in which the unstable **1** substrate is enzymatically generated from the upstream intermediate stemmadenine acetate (**6**). **6** is first oxidized by the flavin dependent enzyme precondylocarpine acetate synthase (PAS)[5] to generate precondylocarpine acetate (**7**), and then undergoes a 1,4-iminium reduction by the medium chain alcohol dehydrogenase dihydroprecondylocarpine acetate synthase (DPAS) (**Figure 1**).[13] The resulting reduced unstable product, dihydroprecondylocarpine acetate (**8**), undergoes elimination of an acetoxy group to yield **1**, which is then captured by one of the cyclases (**Figure 1**).

Our initial hypothesis was that a dedicated cyclase in *T. iboga* would catalyze isomerization and cyclization of **1** to **5**. The *T. iboga* transcriptome, which contains the two previously identified cyclases *Ti*TabS and *Ti*CorS (81% sequence identity, Figure S1) does not harbor any additional cyclase homologues that might have alternative cyclization specificity. However, to our surprise, we observed that under certain conditions, **5**, rather than **4**, was formed in assays using *Ti*CorS (**Figure 2a**). Therefore, *Ti*CorS appears to be involved in production of both **4** and **5**.

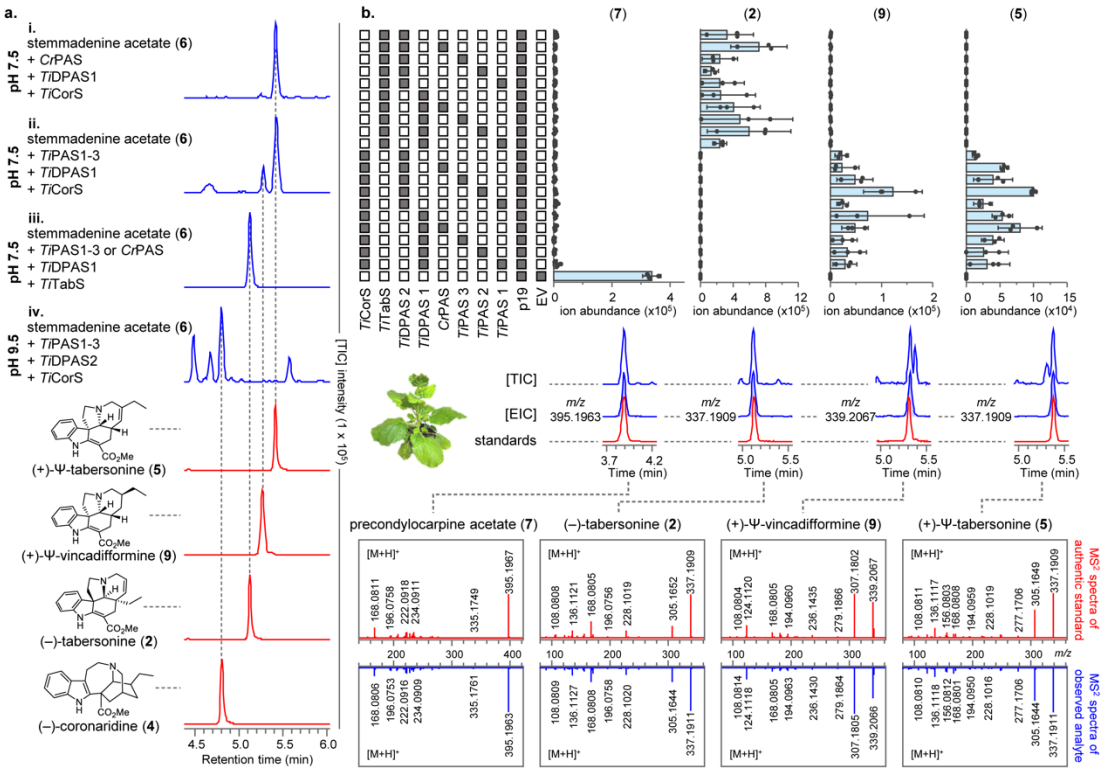


Figure 2. Biosynthesis of Ψ-tabersonine (5).

Figure 2. Biosynthesis of Ψ-tabersonine (**5**). (**a**) *In vitro* production of (**i**) (+)-Ψ-tabersonine (**5**), (**ii**) (+)-Ψ-vincadifformine (**9**), (**iii**) (–)-tabersonine (**2**) and (**iv**) (–)-coronaridine (**4**). (**b**) Reconstitution of Ψ-tabersonine (**5**) biosynthesis in *N. benthamiana* from stemmadenine acetate (**6**). Pathway enzyme combinations (filled grey boxes) transiently expressed in *N. benthamiana,* and harvested leaf disks fed with stemmadenine acetate (**6**) and the resulting levels of precondylocarpine acetate (**7**), (–)-tabersonine (**2**), Ψ-vincadifformine (**9**) and Ψ-tabersonine (**5**) (Bars represent ± S.E.). Representative TIC and EIC for the products observed in *N. benthamiana* reconstitution along with authentic standards and MS^2 fragmentation spectra are shown.

In vitro assays using heterologously produced proteins (Figure S2) were used to probe the conditions that led to a switch in product selectivity. We first noted that the use of specific homologues of reductase DPAS and oxidase PAS with *Ti*CorS led to changes in product profile. *T. iboga* has two homologues of the reductase DPAS (*Ti*DPAS1, *Ti*DPAS2, Figure S3), and three homologues of PAS (*Ti*PAS1, *Ti*PAS2, *Ti*PAS3, Figure S4).[3] Additionally, a PAS homologue (*Cr*PAS)[5] from the taxonomically related plant, *Catharanthus roseus*, which produces vinblastine, is also available and was tested. Most importantly, the pH of the reaction was critical, with **5** formation being observed at pH 7.5, and **4** production observed at pH 9.5 (Figure S5 and S6). Overall, **5** formation was favored at pH 7.5, with *Ti*PAS1-3 or *Cr*PAS, *Ti*DPAS1 and *Ti*CorS, **2** production was favored at pH 7.5, with *Ti*PAS1-3 or *Cr*PAS, *Ti*DPAS1 and *Ti*TabS, and **4** formation was favored at pH 9.5 with *Ti*PAS1-3, *Ti*DPAS2 and *Ti*CorS (**Figure 2a** and Figure S5 and S6). Additionally, we also could produce the over-reduced version of **5**, pseudo-vincadifformine (Ψ-vincadifformine) (**9**), by using *Ti*PAS1-3 (instead of CrPAS), *Ti*DPAS1 and *Ti*CorS (**Figure 2a** and Figure S7).

To further substantiate the results obtained *in vitro*, we reconstituted the biosynthetic enzymes reported here leading to the production of **2**, **5**, and **9** in *Nicotiana benthamiana*. Enzymes were transiently expressed in *N. benthamiana* leaves, disks were excised from the transformed leaf tissue, and these disks were placed in buffer containing **6** (**Figure 2b**). We observed the production of **2**, **5**, and **9** in the extracts of the leaf disks using this expression system (**Figure 2b**). **4** was not detected in any of the enzyme combinations tested in *N. benthamiana*, presumably because of the higher pH conditions required for formation of this product.

Additionally, the selectivity observed for the PAS homologues was not observed *in planta*, because *N. benthamiana* harbors an endogenous enzyme that is able to oxidize substrate **6** (**Figure 2b**).[5]

An acid-stable isomer of dehydrosecodine, angryline (**1a**), can also be isolated and directly used in cyclization assays (**Figure 1**).[2] **1a** must be used at a pH value above 8.5, where it will open to generate the reactive **1**. When **1a** was used in enzymatic assays in place of **6** (pH 9.5), we could observe formation of **5**, **2**, **4** and **9** (Figure S8). Notably, both PAS (*Ti*PAS1-3, *Cr*PAS) and *Ti*DPAS1 were required for the formation of **5** and **9**, indicating that these enzymes are required for the formation of the Ψ-aspidosperma scaffold. PAS was not required for **4** production, which was favored when reductase *Ti*DPAS2 was used (Figure S9 and S10).

To investigate the mechanism by which *Ti*CorS can act, we first set out to characterize the initial, unstable product that is released from *Ti*CorS in the absence of reductase (**Figure 1**). We optimized conditions under which this intermediate could be isolated, and reductively trapped this compound with $NaBH_4$. NMR analysis showed that the compound was 16-carbomethoxycleavamine (**10**), suggesting that the initial cyclization product of *Ti*CorS is 16-carbomethoxycleaviminium (**11**) (**Figure 3** and Figure S11). When the *Ti*CorS product was reduced with $NaBD_4$, the deuterium label was incorporated at carbon 21 **10-d**, which would be expected for 1,2-reduction of **11** (**Figure 3**). Notably, the crystal structure of related cyclase *Cr*CS (70.8% sequence identity, Figure S1) showed that CS initially forms (+)-16-carbomethoxycleaviminium (**11a**),[14] which then subsequently cyclizes to **3**, though unlike *Ti*CorS, the intermediate is not released from the active site.[2] Moreover **3** can open to form **11a** under acidic conditions (Figure S12).[1,2,15] We used CD spectroscopy to show that *Ti*CorS generates (–)-16-carbomethoxycleavamine (**10**), which is the opposite enantiomer that is generated by *Cr*CS (Figure S13).

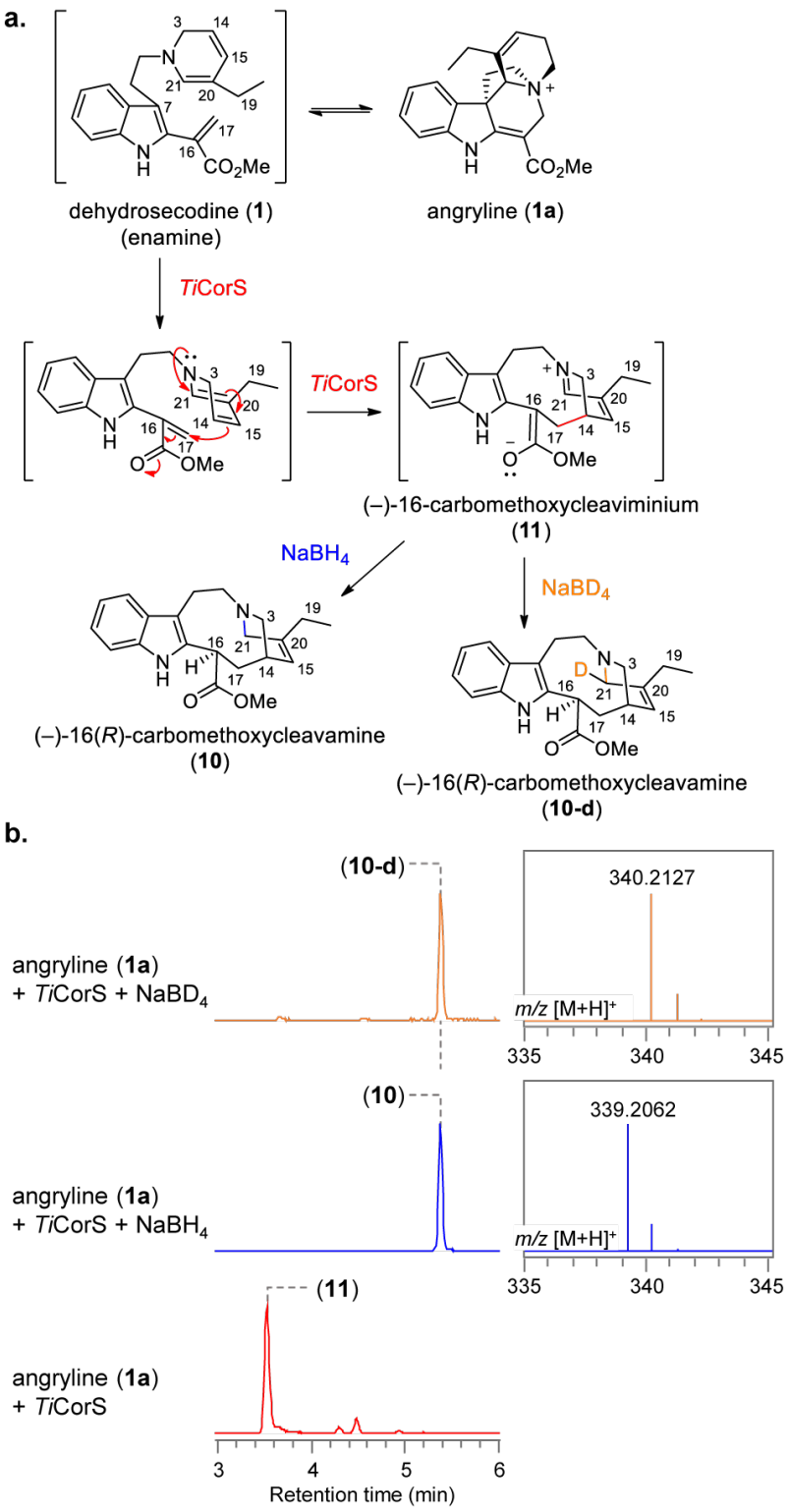


Figure 3. Formation of 16-carbomethoxycleavamine (10).

(**a**) *Ti*CorS generates 16-carbomethoxycleaviminium (**11**) which could be trapped by $NaBH_4$ to generate 16-carbomethoxy-cleavamine (**10**) or $NaBD_4$ to generate 16-carbomethoxy-cleavamine-d (**10-d**). (**b**) TIC and MS spectra representing the formation of 16-carbomethoxycleaviminium (**11**) and 16-carbomethoxycleavamine (**10**) or 16-carbomethoxycleavamine-d (**10-d**).

With knowledge of the cyclization product of *Ti*CorS, we proposed a mechanism for the formation of **4**. After release from the active site of *Ti*CorS, **11** undergoes a 1,4-reduction by *Ti*DPAS2, which in turn would facilitate a second cyclization to form **4** (**Figure 4**). We speculate that at higher pH values, *Ti*DPAS2 favors 1,4-reduction, which when followed by tautomerization,[16] primes the substrate to cyclize to **4**.

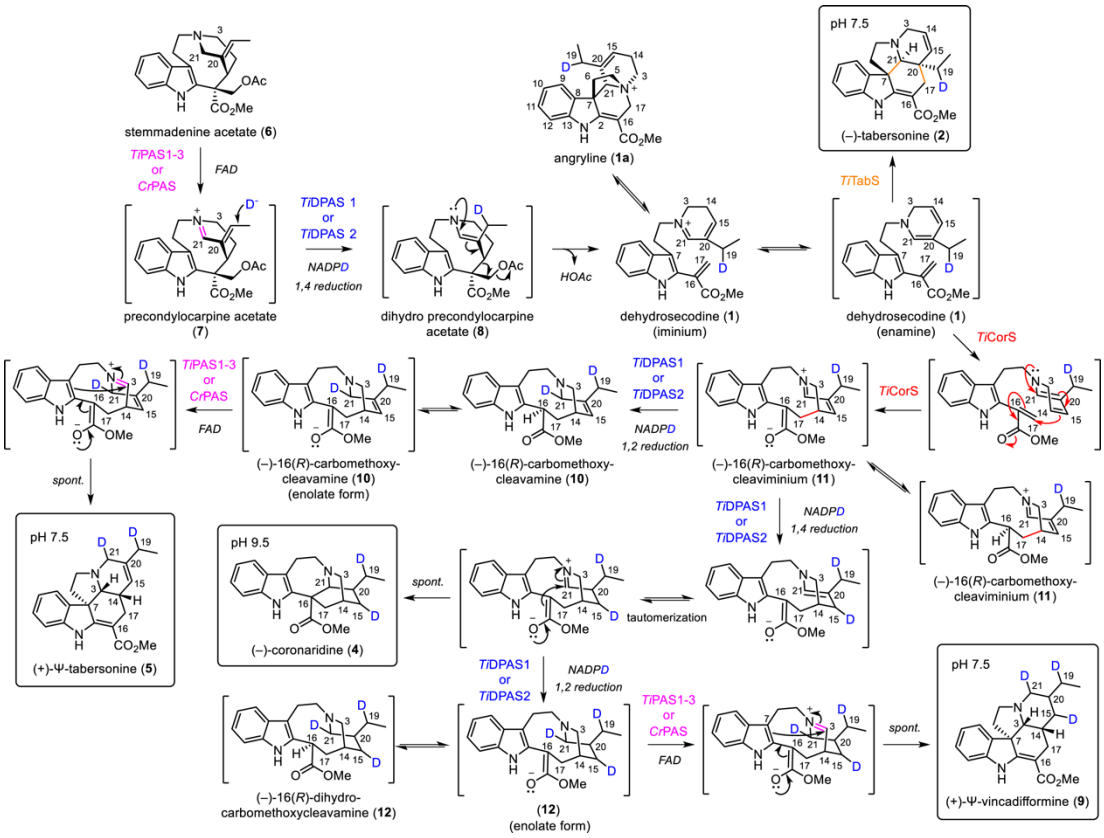


Figure 4. Proposed mechanism for the formation of (–)-iboga and (+)-Ψ-aspidosperma alkaloids.

Biosynthesis of (–)-iboga alkaloid (–)-coronaridine (**4**), and Ψ-aspidosperma alkaloids (+)-Ψ-tabersonine (**5**), and (+)-Ψ-vincadifformine (**9**) with deuterium (blue) tracers using isotopically labelled NADPD.

However, the mechanism by which **11** could be transformed into the **5** scaffold was still not clear. Therefore, we performed the reaction in the presence of isotopically labelled NADPH (pro-(*R*)-NADPD) to determine where the deuteride is incorporated in **5**.[13,17,18] We incubated **6** with *Cr*PAS, *Ti*DPAS1, and *Ti*CorS or *Ti*TabS, along with pro-(*R*)-NADPD, which is required for DPAS reduction (Figure

S14). With *Ti*TabS, we saw formation of the **2** product with a mass consistent with incorporation of one deuterium, as expected from the action of DPAS acting on **7** (**Figure 4**).[13] However, when *Ti*CorS was substituted for *Ti*TabS, the resulting **5** product had a mass consistent with incorporation of two deuterium atoms (**Figure 4** and Figure S14), clearly demonstrating that formation of **5** from **6** requires two reduction steps. Furthermore, the **9** product showed a mass incorporation of three deuterium atoms (**Figure 4** and Figure S14). To corroborate these results, we also incubated the trapped isomer of **1**, **1a** with PAS, *Ti*DPAS1, the labeled NADPD cofactor, and *Ti*TabS or *Ti*CorS. The **2** product produced by *Ti*TabS had no deuterium incorporation, as expected; formation of **5** and **9** from **1a** showed incorporation of one and two deuterium atoms respectively and was strictly dependent upon the presence of both reductase, *Ti*DPAS1, and oxidase, PAS (Figure S15).

We isolated isotopically labeled **2**, **5**, and **9** and showed that the deuterium labels were incorporated at carbon 19 for **2** as expected,[13] carbons 19 and 21 for **5**, carbons 19, 21, and 15 for **9** (**Figure 4)**. We performed CD spectroscopy of these isolated products and assigned the stereochemistry as (+)-Ψ-tabersonine (**5**) and (+)-Ψ-vincadifformine (**9**), which is the expected stereochemistry based on the downstream ibophyllidine products (Figure S16). Finally, we incubated the chemically 1,2-reduced *Ti*CorS product, **10** with the oxidase PAS and observed formation of **5** (**Figure 4** and Figure S17), indicating that cyclization occurs after PAS-catalyzed oxidation.

Together, this evidence strongly supports a mechanism for the formation of **5** (**Figure 4**). *Ti*CorS cyclizes **1** to **11**, and releases it from the active site, where it is reduced to **10** via 1,2-reduction by *Ti*DPAS1 and then re-oxidized by PAS. The resulting intermediate is then primed to spontaneously cyclize to form **5**. **9** forms by PAS oxidation of the doubly reduced (–)-16-dihydrocarbomethoxycleavamine (**12**) (**Figure 4** and Figure S7). The switch between **4** and **5** is ultimately controlled by whether DPAS catalyzes a 1,4-reduction or 1,2-reduction. The changes in the assay pH conditions or protein-protein interactions may be responsible for favoring 1,2-reduction over 1,4-reduction. Alternatively, an as yet undiscovered reductase that generates **4** at physiological pH may be responsible for the biosynthesis of this compound in in *T. iboga*.

We hypothesized that the (+)-16-carbomethoxycleavamine (**10a**) intermediate generated from opening of **3** could serve as a precursor to (–)-Ψ-

tabersonine (**5a**).[19] However, oxidation of (+)-16-carbomethoxycleavamine (**10a**) by PAS yielded only a small amount of product, that, although having a mass and retention time consistent with (+)-Ψ-tabersonine **5**, could not be fully characterised (Figure S17). Thus, PAS may only recognize one 16-carbomethoxycleavamine enantiomer.

Here we show how redox transformations of dehydrosecodine (**1**) enable cycloaddition reactions with alternative regioselectivity to form (–)-coronaridine (**4**), (+)-Ψ-tabersonine (**5**) or (+)-Ψ-vincadifformine (**9**). Notably, these redox enzymes, DPAS and PAS, which transform stemmadenine acetate (**6**) into dehydrosecodine (**1**), are recruited from upstream in the biosynthetic pathway. Therefore, this discovery highlights how plants can recycle enzymes for use in more than one pathway step. Future studies are required to establish how the recruitment of these upstream enzymes is controlled. Nevertheless, the detailed chemical analyses described here provide a compelling hypothesis for the mechanism by which these redox reactions and subsequent cyclizations expand the number of scaffolds produced from the versatile dehydrosecodine (**1**) intermediate.

ASSOCIATED CONTENT

Supporting Information

Supporting Information is available free of charge on the ACS Publications website as a PDF file.

Supplemental information: Additional experimental details, assays, materials, and methods, and NMR spectra described in this study.

Accession Codes

Genbank accession numbers: MH213134 (*Cr*PAS), MK840850 (*Ti*PAS1); MK840851 (TiPAS2); MK840852 (*Ti*PAS3); MK840853 (*Ti*TabS); MK840854 (*Ti*CorS); MK840855 (*Ti*D-PAS1); MK840856 (*Ti*DPAS2).

Abbreviations

Cr, *Catharanthus roseus*; *Ti, Tabernanthe iboga*; *Cr*PAS, Precondylocarpine acetate synthase; *Ti*PAS1, Precondylocarpine acetate synthase 1; *Ti*PAS2, Precondylocarpine acetate synthase 2; *Ti*PAS3, Precondylocarpine acetate synthase 3; *Ti*DPAS1, Dihydro-precondylocarpine acetate synthase 1; *Ti*DPAS2, Dihydroprecondylocarpine acetate synthase 2; *Cr*CS, Catharanthine synthase; *Cr*TS, Tabersonine synthase; *Ti*TabS, Tabersonine synthase; *Ti*CorS, Coronaridine synthase; FAD, flavin adenine dinucleotide; NAD(P)H, nicotinamide adenine dinucleotide (phosphate); TIC, total ion chromatogram; EIC, extracted ion chromatogram; S.E., standard error.

Corresponding Authors

***Sarah E. O'Connor** – Department of Natural Product Biosyn-thesis, Max Planck Institute for Chemical Ecology, Hans-Knöll-Straße 8, Jena 07745 Germany; Email: oconnor@ice.mpg.de

***Lorenzo Caputi** – Department of Natural Product Biosynthesis, Max Planck Institute for Chemical Ecology, Hans-Knöll-Straße 8, Jena 07745 Germany; Email: lcaputi@ice.mpg.de

Notes: The authors declare no competing financial interests.

ACKNOWLEDGMENT

We would like to thank Chloe Langley for useful discussions on this work, Delia Ayled Serna Guerrero, Sarah Heinicke, and Maritta Kunert for assistance with mass spectrometry. Members of the Max Planck Institute for Chemical Ecology Research Green House for providing and taking care of *Nicotiana benthamiana* plants. We gratefully acknowledge the Max Planck Society and the European Research Council (788301) for funding. B.H. acknowledges the Humboldt Foundation.

2.4 References

1. Kutney, J. P., Karton, Y., Kawamura, N. & Worth, B. R. Dihydropyridines in synthesis and biosynthesis. IV. Dehydrosecodine, *in vitro* precursor of indole alkaloids. Can. J. Chem. 60, 1269–1278 (1982).

2. Caputi, L. *et al.* Structural basis of cycloaddition in biosynthesis of iboga and aspidosperma alkaloids. Nat. Chem. Biol. 16, 383–386 (2020).

3. Farrow, S. C. *et al.* Biosynthesis of an Anti-Addiction Agent from the Iboga Plant. J. Am. Chem. So.c 141, 12979–12983 (2019).

4. Qu, Y. *et al.* Solution of the multistep pathway for assembly of corynanthean, strychnos, iboga, and aspidosperma monoterpenoid indole alkaloids from 19E-geissoschizine. Proc. Natl. Acad. Sci. 115, 3180–3185 (2018).

5. Caputi, L. *et al.* Missing enzymes in the biosynthesis of the an-ticancer drug vinblastine in Madagascar periwinkle. Science 360, 1235–1239 (2018).

6. Buonora, P., Olsen, J.-C. & Oh, T. Recent developments in imino Diels–Alder reactions. Tetrahedron 57, 6099–6138 (2001).

7. Khuong-Huu, F., Cesario, M., Guilhem, J. & Goutarel, R. Al-caloïdes indoliques—CII: Deux nou-veaux types d'alcaloïdes in-doliques l'ibophyllidine, dérivé du nor-21(+)pandolane et l'iboxyphylline dé-rivé de l'abeo-21(20→19) (+)pandolane, retirés des feuilles de tabernanthe iboga baillon et de t. subses-silis stapf. Tetrahedron 32, 2539–2543 (1976).

8. Farrow, S. C. *et al.* Cytochrome P450 and O-methyltransferase catalyze the final steps in the biosyn-thesis of the anti-addictive alkaloid ibogaine from Tabernanthe iboga. J. Biol. Chem. 293, 13821–13833 (2018).

9. Lavaud, C. & Massiot, G. The Iboga Alkaloids. in vol. 105 89–136 (Springer International Publishing, 2017).

10. Reuß, F. & Heretsch, P. Synthetic strategies for the ibophyllidine alkaloids. Nat. Prod. Rep. 38(4), 693-701 (2020).

11. Zeches, M., Debray, M. M., Ledouble, G., Men-Olivier, L. L. & Men, J. L. Alcaloïdes du Pandaca caducifolia. Phytochemistry 14, 1122–1124 (1975).

12. Fishbein, M. *et al.* Evolution on the backbone: Apocynaceae phylogenomics and new perspectives on growth forms, flowers, and fruits. Am. J. Bot. 105, 495–513 (2018).

13. Langley, C. *et al.* Expansion of the catalytic repertoire of alcohol dehydrogenases in plant metabolism. bioRxiv 2022.07.24.501124 doi:10.1101/2022.07.24.501124. (accessed 24.07.2022)

14. Cocquet, G., Rool, P. & Ferroud, C. A catalytic versus stoichiometric photoinduced electron transfer promoted selective C_{16}-C_{21} bond cleavage of catharanthine. Tetrahedron Lett. 42, 839–841 (2001).

15. Andriamialisoa, R. Z., Langlois, N. L. and Y. & Langlois, Y. Preparation of 15-oxo-16-methoxycarbonyl-15, 20-dihydro-cleavamine and coupling reaction with vindoline. Heterocycles 1, 245–250 (1981).

16. Stout, D. M. & Meyers, A. I. Recent advances in the chemistry of dihydropyridines. Chem. Rev. 82, 223–243 (1982).

17. Stavrinides, A. *et al.* Structural investigation of heteroyohimbine alkaloid synthesis reveals active site elements that control stereoselectivity. Nat. Commun. 7, 12116 (2016).

18. Pluskal, T. *et al.* The biosynthetic origin of psychoactive kavalactones in kava. Nat. Plants 5, 867–878 (2019).

19. Beatty, J. W. & Stephenson, C. R. J. Synthesis of (−)-Pseudotabersonine, (−)-pseudovincadifformine, and (+)-coronaridine enabled by photoredox catalysis in flow. J. Am. Chem. Soc. 136, 10270–10273 (2014).

2.5 Supporting Information

Recycling upstream redox enzymes expands the regioselectivity of cycloaddition in pseudo-aspidosperma alkaloid biosynthesis

Mohamed O. Kamileen[1,2], Matthew D. DeMars II[1], Benke Hong[1], Yoko Nakamura[1,3], Christian Paetz[3], Benjamin R. Lichman[2], Prashant D. Sonawane[1], Lorenzo Caputi[1*] and Sarah E. O'Connor[1*]

[1] Department of Natural Product Biosynthesis, Max Planck Institute for Chemical Ecology, Hans-Knöll-Straße 8, Jena 07745 Germany.

[2] Centre for Novel Agricultural Products, Department of Biology, University of York, York, YO10 5DD, UK.

[3] Research Group Biosynthesis and NMR, Max Planck Institute for Chemical Ecology, Hans-Knöll-Straße 8, Jena 07745 Germany.

*Corresponding Authors

Table of Contents

Materials and Methods	S02-S08
Supplementary Tables	S09-S13
Supplementary Figures	S14-S33
Synthesis of compounds	S34
NMR spectra	S35-S62
Supplementary References	S63

Materials and Methods

Chemicals and Reagents.

All chemicals, kits and standard molecular biology reagents were purchased from commercial vendors. Stemmadenine was isolated by Professor Ivo J. Curcino Vieira as previously described.[1] Stemmadenine acetate (**6**) was synthesised as previously reported from stemmadenine.[1] Angryline (**1a**) was prepared as previously described from stemmadenine acetate (**6**).[2] Coronaridine (**4**) was synthesized by Professor Corey Stephenson and Rory McAtee (University of Michigan, USA), and obtained as described previously.[3] (+)-16(*S*)-Carbomethoxycleavamine (**10a**) and (+)-16(*R*)-carbomethoxycleavamine (**10a'**) were generated as previously described.[2,4] (+)-Catharanthine (**3**) was purchased from Abcam (cat no. 141419, CAS 2468-21-5). (–)-Tabersonine (cat no. T003900, CAS 4429-63-4) and (–)-vincadifformine (cat no. V314035, CAS 3247-10-7) were purchased from Toronto Research Chemicals. Pseudotabersonine (Ψ-tabersonine) (**5**) and (Ψ-vincadifformine) (**9**) were synthesized as described below (see section Synthesis of compounds).

Plant Growth.

Tabernanthe iboga plants were obtained and maintained as previously described[5], in a controlled environment with periodic watering. Cuttings were used to propagate new plants for RNA isolation and cDNA synthesis. The *Nicotiana benthamiana* plants utilized for transient gene expression were grown in a greenhouse on a standard soil mix under a 16-h-light/8-h-dark photoperiod at 22 °C and 60% relative humidity. Plants were grown for 3-4 weeks before *Agrobacterium* infiltration, with periodic watering as needed.

Cloning methods.

All genes described in this study (**Table S1**) were amplified by PCR from a cDNA library generated from *T. iboga*, as previously described[5] using the primers listed in **Table S2**. P19-TBSV was amplified from clone GB0038 obtained by GB cloning website (https://gbcloning.upv.es)[6]. *Cr*PAS was amplified from a previously reported construct[1]. Overhangs compatible with the appropriate vector were included on the 5' and 3' end of the primers used for PCR amplification (**Table S2**).

High-Fidelity Q5 Hot-Start 2X Master Mix (New England Biolabs) was used for gene amplification according to the manufacturer's instructions. Following PCR amplification, DNA products were analyzed on 1% agarose gel, and the excised gel fragments were purified using Zymoclean Gel DNA Recovery Kit (Zymo Research).

In-Fusion HD cloning kit (Takara Bioscience) was used to ligate all amplified genes into target vectors according to the manufacturer's instructions.

For heterologous expression of proteins in *Escherichia coli*, purified PCR amplicons of *Ti*DPAS1, *Ti*DPAS2, *Ti*CorS, and *Ti*TabS were cloned into pOPINF plasmid ($Carb^R$)[7]. The pOPINF plasmid was linearized using *HindIII* and *KpnI* restriction enzymes (New England Biolabs) to create *N*-terminal His_6-tagged construct suitable for affinity purification. The In-Fusion assembly products were used to transform *E. coli* TOP10 cells (ThermoFisher) by heat-shock. Positive transformants were selected on LB agar (100 µg/mL carbenicillin), and colonies were screened by colony PCR (pOPINF sequencing primers, **Table S2**) using Phire Hot Start II 2X Master Mix (ThermoFisher) according to the manufacturer's instructions. Plasmid DNA was isolated from positive colonies using Wizard Plus SV Minipreps DNA Purification Kit (Promega) and verified by Sanger sequencing. Sequence verified constructs were then used to transform *E. coli* BL21 (DE3) (ThermoFisher) expression cells. Positive transformants were confirmed by colony PCR as described above and were then used to inoculate 10 mL liquid LB medium (100 µg/mL carbenicillin), which were grown overnight at 37 °C, 200 rpm. These cultures were then used to make 25% glycerol stocks to be stored at -80 °C for further use.

For transient expression in *N. benthamiana*, purified PCR amplicons were cloned into a modified 3Ω1[6] binary plasmid ($Spec^R$) and transferred into *Agrobacterium tumefaciens* GV3101 cells by electroporation. The 3Ω1 binary plasmid modification includes a *CCDB* gene cassette between ubiquitin-10 promoter and ubiquitin-10 terminator instead of *LacZ* (present in classical 3Ω1 plasmid). For cloning with In-Fusion HD assembly kit (Takara Bioscience), the modified 3Ω1 was linearized using *BsaI* restriction enzyme (New England Biolabs) and the assembly was carried out with the PCR amplicons as per manufacturer's instructions. The In-Fusion reaction product was transferred into *E. coli* TOP10 (ThermoFisher) cells. Positive transformants were identified by using colony PCR as described above (3Ω1 sequencing primers, **Table S2**) and then grown overnight in liquid LB medium (200 µg/mL spectinomycin) at 37 °C, 200 rpm. Plasmid DNA was isolated and sequence verified as described above. Sequence verified constructs were used to transform electrocompetent *A. tumefaciens* GV3101 cells (Goldbio) by electroporation. Cells were plated on LB agar medium (20 µg/mL rifampicin, 30 µg/mL gentamicin, 200 µg/mL spectinomycin) and grown at 28 °C for 2 days. Positive colonies were identified by colony PCR and a single transformant for each construct was grown in liquid LB medium (20 µg/mL rifampicin, 30 µg/mL gentamicin, 200 µg/mL

spectinomycin) at 28 °C, 250 rpm overnight, after which 25% glycerol stocks were prepared and stored at -80 °C for further use. PAS (FAD-dependent berberine bridge enzyme) enzymes *Cr*PAS, *Ti*PAS1, *Ti*PAS2, and *Ti*PAS3 were overexpressed in *N. benthamiana* and then purified by affinity chromatography. A C-terminal His_6-tag together with a GSGSS linker was introduced into the cloning primers and then cloned into the modified 3Ω1 plasmid as described above (**Table S2**).

Transient expression of candidate genes in *N. benthamiana.*

The *Agrobacterium* strains harboring gene constructs of interest were grown from glycerol stocks in 10 mL liquid LB medium (20 µg/mL rifampicin, 30 µg/mL gentamicin, 200 µg/mL spectinomycin) overnight at 28 °C, 250 rpm. Cells were harvested by centrifugation at 2,000 *g* for 15 min and the depleted media was discarded. The cell pellet for each strain was gently resuspended in *Agrobacterium* infiltration buffer (10 mM MES, pH 5.6, 10 mM $MgCl_2$, 200 µM acetosyringone) and washed to remove residual media and antibiotics. Washed cells were harvested by centrifugation at 2,000 *g* for 15 min and the buffer discarded. Cells were resuspended in 10 mL of *Agrobacterium* induction buffer and incubated in the dark at room temperature with gentle rocking for 2 h. When multiple gene constructs were tested in combinations, strains were pooled in equal cell density so that each strain had an OD_{600} = 0.4 and infiltrated into the abaxial side of 3-week-old *N. benthamiana* leaves covering the entire leaf (approximately 1.5 mL per leaf) using a 1-mL needleless syringe. Each pooled combination consisted of three biological replicates, where an individual leaf (fully expanded) belonging to three different plants was infiltrated to randomize batch effects. Leaves were harvested 3 days post-*Agrobacterium* infiltration for *in vitro N. benthamiana* leaf disk assays (see section *In vitro* assays with *Agrobacterium* infiltrated *N. benthamiana* leaf disks) to test for enzymatic activity.

For the overexpression of PAS enzymes with a *C*-terminal His_6-tag, the corresponding *Agrobacterium* strain was prepared as described above and co-infiltrated with P19-TBSV strain at an equal cell density corresponding to a final OD_{600} = 0.3. Prepared *Agrobacterium* suspension was infiltrated (covering the entirety of the leaves) into the abaxial side of 20 3-week-old *N. benthamiana* plants using a 1-mL needleless syringe and three independent leaves per plant were selected to generate sufficient biomass for protein extraction. Leaves were harvested 3 days post-*Agrobacterium* infiltration; the central vascular tissue was excised using a razor blade and the plant material was snap frozen in liquid N_2 and

stored at -80 °C for protein purification (see section Purification of His_6-tagged proteins from *N. benthamiana*).

Expression and purification of proteins in *E. coli*.

For recombinant protein production in *E. coli*, starter cultures of BL21(DE3) were prepared from glycerol stocks (see section cloning methods) in 10 mL LB medium (100 µg/mL carbenicillin) and grown at 37 °C, 200 rpm for 16 h. The starter cultures (10 mL) were used to inoculate 1 L of 2xYT medium (100 µg/mL carbenicillin) and the resulting large cultures were grown to an optical density at 600 nm (OD_{600}) of 0.7 at 37 °C, 200 rpm. Cultures were then chilled on ice for 20 min, induced with 0.25 mM isopropyl β-D-1-thiogalactopyranoside (IPTG) and incubated overnight (18 h) at 18 °C, 200 rpm for protein production. Cells were harvested by centrifugation at 3,000 *g*, 4 °C, for 10 min and resuspended in 50 ml of pre-cooled buffer A (50 mM Tris-HCl pH 7.4, 50 mM glycine, 500 mM NaCl, 5% glycerol, 20 mM imidazole) with 10 mg/mL lysozyme and an EDTA-free protease inhibitor (Roche Diagnostics). All remaining steps were performed on ice and all buffers were pre-cooled at 4 °C. Cells were lysed by sonication for a total of 5 min (2 sec on, 3 sec off cycle) on ice. The resulting crude protein lysate was clarified by centrifugation at 35,000 *g*, 4 °C, for 20 min and filtered through a 0.45-µm glass filter. His_6-tagged proteins were purified on an ÄKTA Pure 25 fast protein liquid chromatography (FPLC) system (Cytiva) using a 5 mL-HisTrap-HP column (Cytiva) equilibrated with buffer A. Sample was applied at a flow rate of 2 mL/min and step-eluted using buffer B (50 mM Tris-HCl pH 7.4, 50 mM glycine, 500 mM NaCl, 5% glycerol, 500 mM imidazole) and collected in 1 mL fractions. The principal peaks collected were verified by SDS-PAGE with Coomassie Blue staining. Fractions containing the protein of interest were pooled and concentrated using 15 mL-Amicon-Ultra 10 kDa molecular weight cutoff filters (Millipore) by centrifugation at 3,000 *g*, 4 °C, for 10 min intervals with gentle resuspension till the sample was concentrated to 1 mL. Samples were dialyzed in the same filter by the addition of 12 mL buffer C (20 mM HEPES pH 7.4, 150 mM NaCl) and centrifuged as described above. Dialysis was repeated 2 more times and the protein was concentrated to a final volume of 0.5 mL. Protein concentrations were measured using a nano-photometer (Implen) based on the absorbance at 280 nm using the theoretical extinction coefficients. Proteins were aliquoted (50 µL), snap-frozen in liquid N_2 and stored at -80 °C for *in vitro* enzyme assays.

Purification of His_6-tagged proteins from *N. benthamiana*.

To purify *C*-terminal His_6-tag PAS (oxidase) enzymes from *N. benthamiana* leaves, the harvested tissue (see section Transient expression of candidate genes in *N. benthamiana*) was ground to fine powder in liquid N_2 using a mortar and pestle. The powdered tissue (ca. 60 g) was extracted with 360 mL of ice-cold buffer A supplemented with 1 mM PMSF, EDTA-free protease inhibitor (Roche Diagnostics), 2% w/v polyvinylpolypyrrolidone (PVPP). The extract was mixed by inversion and incubated at 4 °C for 30 min with stirring to maximize homogeneity and extraction efficiency. All remaining steps were performed on ice and all buffers were pre-cooled at 4 °C along with consumables. The extract was clarified by centrifugation at 3,000 *g*, 4 °C, for 10 min, and filtered through miracloth (Millipore). The flow through was centrifuged at 35,000 *g*, 4 °C, for 20 min and the cleared protein extract was passed through 0.45-µm glass filters before Ni-affinity purification. His_6-tagged crude protein lysate was purified on an ÄKTA Start protein purification system (Cytiva) using a 5 mL-HisTrap-HP column (Cytiva) conditioned with buffer A. Sample (ca. 300 mL) was applied at a flow rate of 2 mL/min, step-eluted with buffer B, and collected as 1 mL fractions. The fractions were verified for the protein of interest using SDS-PAGE with Coomassie Blue staining. The pooled fractions of interest were dialyzed in buffer C using PD-10 desalting columns (Cytiva) and concentrated to a final volume of 1 mL using 15 mL-Amicon-Ultra 10 kDa molecular weight cutoff filters (Millipore) by centrifugation in 10 min cycles at 3000 *g*, 4 °C with gentle resuspension at the end of each round. Protein concentration was normalized to 8 mg/mL and prepared for storage as described (see section Expression and purification of proteins in *E. coli*).

***In vitro* assays with *Agrobacterium* infiltrated *N. benthamiana* leaf disks.**

At three days post-*Agrobacterium* infiltration (see section Transient expression of candidate genes in *N. benthamiana*), 10 mm leaf disks were cut using a borer and placed into 48-well-plates (10 mm diameter well). For each experiment, disks were collected from three independent plants. The wells contained 250 µL of 50 mM HEPES buffer at pH 7.5 and the leaves were placed (1 leaf disk per well) either on the abaxial or on the adaxial side and submerged in the buffer immediately upon harvest. Stemmadenine acetate (**6**) was used as substrate to a final concentration of 50 µM into the wells containing the leaf disks. Controls of wild-type, empty-vector, and P19-TBSV infiltrated *N. benthamiana* incubated with substrate were also included for each experiment. The plates were closed with the covers provided and sealed with parafilm to avoid excessive evaporation of the buffer. The plates were

incubated in a growth chamber at 22 °C, 60% relative humidity and 16-h-light/8-h-dark photoperiod overnight (16-18h). After overnight incubation, individual leaf disks were collected and placed in a 2 mL safe-lock tube and snap-frozen in liquid nitrogen. The leaf disk was pulverized using a TissueLyser II (Qiagen) homogenizer using 3 mm tungsten beads, with shaking at 25 Hz for 1 min. To extract metabolites, 250 µL of extraction solution (70% methanol in water acidified with 0.1% formic acid) was added to the powdered tissue, mixed well by vortex and sonicated for 10 min at room temperature. The samples were then centrifuged at 20,000 *g* for 10 min to pellet cell debris and the extract was diluted 1:2 with extraction solution. Samples were filtered through 0.22 µm PTFE syringe filters before metabolite analysis by LC-MS.

***In vitro* enzymatic assays.**

The conditions used for analytical scale production of (+)-Ψ-tabersonine (**5**), (+)-Ψ-vincadifformine (**9**), (–)-tabersonine (**2**), and (–)-coronaridine (**4**) from substrates stemmadenine acetate (**6**) and angryline (**1a**) are described below. Substrates were prepared in methanol and added at a final concentration of 40 µM into a 100 µL reaction. For *in vitro* coupled enzyme assays with stemmadenine acetate (**6**) as substrate, reaction mixtures with combinations of purified enzymes were assembled to investigate the production of desired final products as described in **Table S3**. For *in vitro* coupled enzyme assays with angryline (**1a**) as substrate, reaction mixtures with combinations of purified enzymes were assembled to investigate the production of desired final products as described in **Table S4**. In experiments examining the effect of pH for the production of (–)-coronaridine (**4**) from angryline (**1a**) (**Table S4)**, appropriate buffers[8] from pH 7.5 to 9.5 at 50 mM were used in 0.5 pH increments. For all *in vitro* reactions, appropriate control assays omitting enzymes were additionally performed to test the validity of reaction products observed. Optimal pH and enzyme combination for the desired final products of (+)-Ψ-tabersonine (**5**), (+)-Ψ-vincadifformine (**9**), (–)-tabersonine (**2**), and (–)-coronaridine (**4**) from stemmadenine acetate (**6**) (**Table S3)** and angryline (**1a**) (**Table S4**) was established. The same conditions were used for stereo-specific deuterium labelling with pro-(*R*)-NADPD by replacing the NADPH co-factor with the isotopically labelled NADPD analogue. Pro-(*R*)-NADPD was generated *in situ* by the addition of reaction components described below. For 100 µL reactions, 1 mM $NADP^+$, 10 mM isopropanol-d_8 (Sigma-Aldrich, 175897), 1% (v/v) alcohol dehydrogenase (Sigma-Aldrich, 49641) were added, and the optimized reactions were assembled as

described above excluding NADPH. Substrates, angryline (**1a**) and stemmadenine acetate (**6**) were used for deuterium labeling reactions.

*In vitro enzymatic assays for the production of (+)-Ψ-tabersonine (**5**) from (–)-16(R)-carbomethoxycleavamine (**10**).*

For assays initiated with (–)-16(*R*)-carbomethoxycleavamine (**10**) to produce (+)-Ψ-tabersonine (**5**) from PAS (oxidase) enzymes, 100 µL reactions were performed in 50 mM HEPES pH 7.5 buffer with 0.2 mM FAD, 1 µM PAS enzyme, and 40 µM substrate (–)-16(*R*)-carbomethoxycleavamine (**10**). Reactions were incubated at 37 °C, 600 rpm for 60 min and quenched. To attempt to produce (–)-Ψ-tabersonine (**5**), the above conditions were used with 40 µM substrate (+)-16(*S*)-carbomethoxycleavamine (**10a**).

To produce precondylocarpine acetate (**7**) from stemmadenine acetate (**6**), 100 µL reactions were performed. PAS (oxidase) enzymes (1 µM) were incubated in 50 mM HEPES pH 7.5 with 0.2 mM FAD, and 40 µM of substrate stemmadenine acetate (**6**). Reactions were incubated at 37 °C, 600 rpm for 60 min, quenched and subjected to LC-MS analysis (Figure S18).

All analytical scale reactions were quenched by the addition of 100 µL quenching solution (70% methanol in water + 0.1% formic acid). Quenched reactions were vortexed, centrifuged at 20,000 *g* for 10 min and filtered with 0.22 µm PTFE syringe filters for subsequent LC-MS analysis. All reactions were independently replicated 3 times to validate reproducibility.

Preparative scale *in vitro* reaction workup for product isolation.

*Large scale production of deuterium labeled (–)-tabersonine (**2**), (+)-Ψ-tabersonine (**5**), and (+)-Ψ-vincadifformine (**9**)*

Deuterium labeling assays with pro-(*R*)-NADPD analogue (described in the section *In vitro* enzyme assays) were scaled up to 200 µL reaction volumes. Stemmadenine acetate (**6**) at 200 µM was used as the substrate to produce the desired deuterium labeled product, with optimal pH, enzyme combinations, and assay conditions listed in **Table S3**. Multiple reactions were assembled in batches (24 reactions) to yield sufficient product for preparative HPLC isolation. Reactions were quenched with 200 µL of quenching solution, vortexed, and centrifuged at 20,000 *g* for 10 min. Clarified crude mixtures were pooled and filtered into a single vial using 0.22 µm PTFE syringe filters. Dilution (1:1000) of the crude mixture was analyzed by LC-MS and the desired deuterium labeled product was confirmed by *m/z* and retention time. The

pooled mixture was evaporated to dryness using a rotoevaporator and the dried crude product was stored at -20 °C for isolation using preparative HPLC (see section Isolation of products using preparative HPLC).

*Workup for the production of (–)-coronaridine (**4**)*

Production of (–)-coronaridine (**4**) was performed using the optimal pH, enzyme combinations, and assay conditions listed in **Table S3** from stemmadenine acetate (**6**). Reactions were scaled up and performed as described above. The dried crude product was stored at -20 °C for isolation using preparative-HPLC (see section Isolation of products using preparative HPLC).

*Workup for the production of (+)-16(S)-carbomethoxycleavamine (**10a**) and (+)-16(R)-carbomethoxycleavamine (**10a'**)*

(+)-16(*S*)-carbomethoxycleavamine (**10a**) and 16(*R*)-carbomethoxycleavamine (**10a'**) were generated chemically using a modified method previously described[2,4]. Briefly, (+)-catharanthine (**3**) (5 mg) was dissolved in 400 µL of TFA and stirred at room temperature for 3 h. Conversion of (+)-catharanthine (**3**) to (+)-16-carbomethoxycleavamininum (**11a**) intermediate (*m/z* 337.19) was observed. Then, the iminium intermediate (**11a**) was reduced by the addition of an excess $NaBH_4$ in methanol (10 mg in 400 µL). The reaction was stirred at room temperature for 30 min and the 16-carbomethoxycleavamine diastereomers, 16(*S*) (**10a**) and 16(*R*) (**10a'**) were observed by LC-MS. Acetone (500 µL) was added and stirred for 10 min at room temperature. The reaction mixture was evaporated to dryness using a rotoevaporator and the dried product was stored at -20 °C for isolation using preparative HPLC (see section Isolation of products using preparative HPLC).

*Workup for the production of (–)-16(R)-carbomethoxycleavamine (**10**) and deuterium labeled (–)-16(R)-carbomethoxycleavamine (**10-d2**)*

To generate (–)-16(*R*)-carbomethoxycleavamine (**10**), a 4 mL reaction was performed with the substrate angryline (**1a**) at 2 mM final concentration in a reaction mixture consisting of 50 mM CHES buffer at pH 9.5, and 40 µM *Ti*CorS enzyme. The reaction mixture was incubated at 37 °C for 30 min, with shaking at 150 rpm prior to quenching by the addition of 4 mL quench solution to generate the iminium product. Subsequently, the iminium was reduced by the addition of 4 mM $NaBH_4$ sodium borohydride (Sigma Aldrich) (in methanol) to the quenched reaction, and incubation at 37 °C for 30 min, with shaking at150 rpm. Upon completion of the reaction, the precipitated protein was removed by centrifugation at 4000 *g*, for 10

min at room-temperature. Dilution (1:1000) of the crude reaction mixture subjected to LC-MS analysis confirmed the presence of the desired product, (–)-16(*R*)-carbomethoxycleavamine (**10**). The reaction mixture was dried in a rotoevaporator and was stored at -20 °C until purification by preparative HPLC. Generation of deuterium-labeled (–)-16(*R*)-carbomethoxycleavamine-d_2 (**10-d2**) was performed as described for (–)-16(*R*)-carbomethoxycleavamine (**10**). The iminium generated was reduced by the addition of 4 mM $NaBD_4$ (sodium borodeuteride) (Sigma Aldrich) in methanol. All subsequent steps were performed as described above. The crude mixture containing (–)-16(*R*)-carbomethoxycleavamine-d_2 (**10-d2**) was dried using a rotoevaporator and was stored at -20 °C until purified by preparative HPLC (see section Isolation of products using preparative HPLC).

Isolation of products using preparative HPLC.

Preparative-scale *in vitro* reactions (see section Preparative scale *in vitro* reaction workup for product isolation) were subjected to preparative HPLC for compound isolation. A preparative HPLC system (Agilent 1260 Infinity II) coupled to a multiple wavelength detector and fraction collector connected to a Phenomenex Kinetex XB-C18 (250 x 10 mm, 5 µm, 100 A) was used. The mobile phases used for separation were A (water containing 0.1% formic acid) and B (acetonitrile). The flow rate was set at 6.0 mL/min and a gradient of 10-40% B for 15 min, 90% B for 7 min, 10% B for 5 min. Samples prepared for preparative-HPLC analysis (see section Preparative scale *in vitro* reaction workup for product isolation) were resuspended in quenching solution to 1 mg/mL and filtered using a 0.22 µm PTFE syringe filter. Manual injections (200 µL per injection) were performed, and the separation was monitored using specific wavelengths. For (–)-tabersonine-*d* (**2-d**), (+)-Ψ-tabersonine-d_2 (**5-d2**), and (+)-Ψ-vincadifformine-d_3 (**9-d3**), 328 nm was used. For (+)-16(*S*)-carbomethoxycleavamine (**10a**), (+)-16(*R*)-carbomethoxycleavamine (**10a'**), (–)-16(*R*)-carbomethoxycleavamine (**10**), (–)-16(*R*)-carbomethoxycleavamine-d_2 (**10-d2**), and (–)-coronaridine (**4**), detection at 225 nm and 280 nm wavelengths were used. Eluted fractions were analyzed by LC-MS (1:1000 dilution) and desired fractions were pooled and evaporated to dryness. The isolated compounds were then submitted for NMR analysis (see section NMR analysis).

LC-MS data acquisition and analysis of metabolites.

Samples were analyzed using a Thermo Scientific UltiMate 3000 ultra-high performance liquid chromatography (UHPLC) system coupled to an Impact II UHR-Q-ToF (Ultra-High Resolution Quadrupole-Time-of-Flight) mass spectrometer

(Bruker Daltonics). Metabolites were separated by reversed-phase liquid chromatography using a Phenomenex Kinetex XB-C18 (100 x 2.1mm, 2.6 µm; 100 Å) column at 40 °C. The mobile phases for metabolite separation were water with 0.1% formic acid (A) and acetonitrile (B). A flow rate of 0.6 mL/min was used for the chromatography. The injection volume was 2 µL. The chromatographic separation was performed starting at 10% B for 1 min, linear gradient from 10% to 30% B in 6 min, 90% B for 1.5 min, 10% B for 2.5 min. Authentic standards were prepared as 20 µM solutions in methanol and 2 µL was injected under the chromatographic conditions described above. Mass spectrometry acquisition was performed in positive electrospray ionization mode with a capillary voltage of 3500 V and an end plate offset of 500 V; a nebulizer pressure of 2.5 bar was used, with nitrogen at 250 °C and a flow of 11 L/min as the drying gas. Acquisition was done at 12 Hz in the mass range from 80 to 1000 *m/z*, with data dependent MS^2 and an active exclusion window of 0.2 min. For tandem mass spectroscopy (MS^2) fragmentation was triggered on an absolute threshold of 400 and limited to a total cycle time range of 0.5 s. For collision energy, the stepping option model (from 20 to 50 eV) was used. At the beginning of each sample run, a sodium formate-isopropanol calibration solution was directly infused to the source at 0.18 ml/hour using a syringe pump to calibrate MS spectra recorded. To avoid injection peak and salt contamination of the MS, the initial 1 min of the active chromatographic gradient of each run was discarded to waste.

Data analysis was performed using Bruker Compass Data Analysis (Version 5.3) software. For *N. benthamiana* leaf disk experiments, data acquired was analyzed using Bruker Compass MetaboScape 2021b software (version 7.0.1). The non-targeted metabolomics workflow was used to generate an output containing a list of mass signatures with retention times, along with qualitative peak intensities by automated integration of extracted ion chromatograms with 5 ppm tolerance, molecular formula determined by accurate mass of precursors and fragments and statistical test outputs (*P* value and *t*-tests). All metabolites in this study were verified and assigned using authentic standards by validation of retention time and MS^2 spectra (Figure S19). Figures for *N. benthamiana in vitro* leaf disk assays were prepared using the scientific graphing and data analysis program OriginPro 2019 (version 9.6.0) from the processed data obtained by MetaboScape analysis.

NMR analysis.

NMR spectra were measured on a 700 MHz Bruker Advance III HD spectrometer (Bruker Biospin GmbH, Rheinstetten, Germany). For the synthetic (±)-Ψ-tabersonine (**5a**) standard, NMR spectra were measured on a 500 MHz Bruker Advance III HD spectrometer (Bruker Biospin GmbH, Rheinstetten, Germany). For spectrometer control and data processing Bruker TopSpin (version 3.6.1) was used. MeOH-d_3 was used as a solvent and all NMR spectra were referenced to the residual solvent signals at δ_H 3.31 and δ_C 49.0, respectively.

Electronic circular dichroism (ECD) spectra measurements of isolated products.

ECD spectra were measured at 25 °C on a JASCO J-810 spectropolarimeter (JASCO cooperation, Tokyo, Japan) using a 350 µL cell. Spectrometer control and data processing was accomplished using JASCO spectra manager II. All the isolated products were measured in methanol at 0.2 mg/mL concentration.

Electronic circular dichroism (ECD) spectra calculations.

ECD spectra calculations were performed for (+)-Ψ-tabersonine (**5**), (+)-Ψ-vincadifformine (**9**), (–)-tabersonine (**2**), and (–)-16(*R*)-carbomethoxycleavamine (**10**). Based on the structure determined from NMR analysis a molecular model was created in GaussView ver.6 (Semichem Inc., Shawnee, Kansas, USA) and optimized using the semi-empirical method PM6 in Gaussian (Gaussian Inc., Wallingford, Connecticut, USA). The resulting structure was used for conformer variation with the GMMX processor of the Gaussian program package. Resulting structures were DFT-optimized with Gaussian ver.16 (APFD/6-31G(d) level). A cut-off level of 4 kcal/mol was used to select conformers which were subjected to another DFT optimization on a higher level (APFD/6-311G+(2d,p)). The structure of (–)-16(*R*)-carbomethoxycleavamine (**10**) was optimized using the semi-empirical method PM6 and the resulting structure was DFT-optimized (B3LYP/6-311G+(d,p)). All structures up to a deviation of 2.5 kcal/mol from the lowest energy conformer were used to determine the ECD-frequencies in a TD-SCF calculation on the same level as the former DFT optimization. The ECD curve was calculated from the Boltzmann-weighed contributions of all conformers with a cut-off level of two percent. Experimentally measured CD spectra and calculated ECD data were compared using SpecDis[9] (version 1.71).

Supplementary Tables

Table S1. Nucleotide sequences for genes cloned and described in this study.

Gene Name (GenBank Accession))	Nucleotide sequence
*Ti*DPAS 1 (MK840855.1)	**ATG**GCTGTAAAATCACCTGAAGCAGAGCACCCAGTGAAGGCTGTAAAATC ACCTGAAGAAGAGCACCCAGTGAAGGCATACGGATGGGCTATCAAAGAC AGAACATCTGGCATTCTTTCCCCCTTCAAGTTTTCCAGAAGGGCAACAGG AGATGAAGACGTTCGAATAAAGATCCTCTGTTGCGGAGTTTGTCACACGG ATCTCACGTCTACCAAGAATGAATACGAGTTTCTTTCATATCCTCTAGTGC CTGGGTTGGAGACTGTCGGAATAGCGACAGAGGTCGGAAGCAAAGTCAC AAAAGTAAAAGTTGGTGAAAAAGTAGCAGTGGCAGCCTATTTGGGCACTT GTGGCAAATGCCACAATTGTCTAAATGACCAAGAGAATTACTGTCCCGAA GTGATCATTAGCTACGGCACACCATATCACGACGGAACAATCAACTACGG AGGCTTCTCGAATGAGACGGTCGTAAATGAGCGCTTCGTTCTTCATTTTC CTGAAAAGCTTTCACTTTCTGGTGGTGCACCGCTACTCAGCGCAGGAAGC ACCGCTTACAGTGCAATAAGAAATCAAGGCCTTGACAAACCCGGTATCCA CTTGGGAGTCGTCGGCCTTGGTGGACTTGGTCATCTGGCTGTGAAGTTT GCCAAGGCTTTTGGTGTCAAGGTGACAGTGATTAGTTCCACTCCCAGCAA GAAGGATGAAGCCATCAAGAGCCTTGGTGCCGATGCGTTCTTGTTCAGTC GTGATGATGAACAAATGAAGGCCGCTATTGGAACTTTCGATGCAATCATA GATACTATTGCAGTCGCTCATCCTCTTGCGCCATTACTTGATCTACTAAGG AGTCATGGAAAAATTATTTTGGTCGGGGCACCGACCACCCCACTTGAGGT GCCAGTTATTCCTTTAGTAGCAGGTGGGAAATCGATTACTGGATGCGTAG TTGGAAATTTGAAGCAAACTCAAGAAATGCTTGAATTTGCTGCAGAACACA ACATCACTGCAAACGTTGAGGTTATTTCAATGGATTACATAAACACTGCAA TGGAACGTTTAGAAAAAGGTGATGTTAGATATAGATTTGTAATTGATATTG GAAACACACTAACTCCACCGGAA<u>TAG</u>
*Ti*DPAS 2 (MK840856.1)	**ATG**GCAGGAAAATCACCAGAAGAGGAACACCCAGTGAAGGCATATGGAT GGGCTGTCAAGGACAGAACAACTGGGATTCTTTCTCCCTTCAAGTTTTCG AGAAGGGCAACAGGAGACAATGACATCCGAATCAAGATCCTCTATTGTGG AATTTGTCATACAGACCTAACATCTGTCAAGAACGAGTACGAGTTTCTTTC ATATCCTCTTGTGCCTGGGATGGAGATTGTAGGGATAGCGACAGAGGTC GGAAGCAAAGTCACAAAAATAAAAGTTGGTGAAAAAGTAGCAGTAGCAGC CTATTTGGGTACTTGTGGAAAATGCTACAATTGTGTAAATGACCTTGAGAA CTACTGTCCTGAAGTCATCATTGGTTATGGTACGCCATATCACGATGGAA CAATTAACTACGGAGGCCTCTCAAACGAGACGGTCGTAAATGAGCGCTTT GTTCTTCGTTTTCCTGAAAAACTTTCACCTGCTGGTGGTGCCCCGCTACT CAGTGCTGGAATCACCGCGTACAGTGCAATGAGGAATCATGGCCTCGAC AAGCCCGGAATCCAATTGGGAGTCGTCGGTCTTGGTGGACTTGGTCATCT GGCTGTGAAGTTTGCCAAGGCTTTTGGCGTCAGAGTGACTGTGATTAGTA CCACTCCTAGCAAGAAGGATGAAGCTATAAATAATCTTGGTGCTGATGCC TTTTTGTTCAGCCGTGACGATAAGCAAATGAGGGCTGCCATTGGAACGTT TGATGCAATCATCGACACACTAGCGGTTGTTCATCCTATTGCGCCCTTACT CGATCTATTGAGGAGTCATGGAAAACTTGTTTTGGTTGGAGCCCCATCTA AGCCACTTGAGCTACCAACTATTCCTTTATTATCAGGAGGAAAATCATTGA TCGGTAGTGCAGCTGGAAATGTGAAGCAAACTCAGGAAATGCTTGATTTT GCAGCAGAACACGATATTACTGCAAACATTGAGGTTATACCAATAGATTAT ATAAACACTGCAATGGAACGTTTAGATAAAGGTGATATCCGATTTAGGTTT GTGGTTGATATTGAAAATACCTTAACTCCTCCGCCAGAACCG<u>TAA</u>
*Ti*TabS (MK840853.1)	**ATG**GCTTCTTCAACTGAAAGCTCTGATGAGATTATTTTTGATCTTCCTCCA TACATTAGAGTCTTTAAGGATGGAAGAGTAGAGAGACTCCACTCCTCACC ATATGTTCCACCATCACTAGATGATCCCGCAACCGGCGTATCCTGGAAAG ACGTCCCAATTTCATCAGAGGTTTCGGCTAGAATCTACCTCCCAAAGATAA GCCAAAAGGAAAAGGAAAAGCTTCCCATTGTGGTCTATTTCCATGGTGCA

	GGCTTCTGTCTGGAATCCGCCTACAAGTCATTTTTCCACACTTATGTCAAG CACTTTGCAGCCGAGGCCAAAGCAATTGCAGTTTCGGTTGAGTTCAGGCT CTCCCCAGAGCACCACCTGCCTGCAGCTTATGAAGATTGCTGGACTGCC CTTCAGTGGGTGGCTTCACATGTAGATGTTGACAACTCCAGCCTCAAGAA TGCTATAGATAAAGAGCCTTGGATAATCAACCATGGAGACTTTGACAAGAT CTACTTATGGGGTGACAGTACGGGTGCCAATATTGTGCACAACGTACTCA TCAGAGCTGGTAATGAGAGCTTGCATGGCGGAGTGAAAATCGTGGGTGC AATTCTTTATTACCCATATTTCTTGATCAGGACAAGCTCCAGACAGAGCGA TTATATGGAGAACGAGTACAGAGCATACTGGAAGCTGGCTTATCCATCTG CTCCAGGTGGGAACGACAACCCGATGATAAACCCCGTAGCTGAGAACGC TCCTGATTTGGCTGGATATGGATGTTCGAGGCTGCTGGTATCCATGGTGG CAGACGAGGCCAGAGACATAACCCTTCTCTACATCGAGGCAGTGAAGAA GAGTGGGTGGAAAGGTGAATTGGAGGTGGCTGATTTCGAAGGAGATTAC TTTGAAATATTCAGCCCAGAAACTGAGACAGGCAAGAACAAGGTCAAACG TTTAACGTCTTTCATCAACAAGGAGTAA
*Ti*CorS (MK840854.1)	**ATG**GCTAATTCAACTGCAAACTCTGATGAGATTGTTTTCGATCTTCATCCA TACATCAGAGTCTTTAAAAACGGCAAGGTAGAAAGACTTCACGACACCCC ATATGTTCCGCCATCACTTGAAGATCCAGCCACCGGTGTATCCTGGAAAG ACGTCCCAATTTCATCCGACGTTTCAGCTAGAGTCTACCTCCCGAAGATC AGCGAAGCGGAAAAGAAAAAGCTCCCCATTTTCGTCTATTTCCATGGTGC AGGCTTCTGTCTGGAATCAGCCTTCAAATCATTTTTCCATACTTATGTTAA GCACGTTGTTGCCGAAACCAAAGCTGTCGGAGTTTCGGTTGAGTACAGAC TCGCCCCCGAGCACCCTTTACCTGCGGCTTATGAAGATTGCTGGACTGC CCTTCAGTGGGTGGCTTCCCATGTTGGTCTTGACAACTCCAGCCTCAAGA ATGCTATTGATAAAGAGCCTTGGATAATCAACCATGGCGACCTCAATAAG CTTTACTTGGGTGGTGACAGTCCTGGTGGAAATATTGTGCACAACGTACT GATTAGAGCTGGTAAGGAGAGCTTGCATGGCGGAGTGAAAATCCGGGGT GCAATTCTTTATTACCCATATTTCTTGATCAGGACAAGCAAAAGACAGAGT GATTATATGGAGATTGACTATAGAGGCTACTGGAAGTTGGCTTATCCATCT GCTCCTGGCGGCACTGACAACCCAATGATAAACCCTGTAGCTAAGAATGC TCCTGATTTGGCCGGATATGGATGTTCGAGGCTGCTTGTTTCCATGGTTT CGGACGAGACCAGAGATATAACCCTTCTCTACCTTGAGGCATTGAAGAAG AGTGGGTGGAAAGGTGAATTGGAAGTGGGTGACTACGAAGCACATTTCTT TGATTTGTTCAGCCCTGAAAATGAAGTTGGCAAGACTTGGATCAAACGTT CAAGCGATTTCATCAACAAGGAGTAA
*Ti*PAS 1 (MK840850.1)	ATGTATACTACTGAAGTTCGCAAAGTTTTCATATCTTACTGCTTTCTCCTTC TTGTCTCACAATGCCACTGCTTCATTCCTGAATCTTTCATCAGTTGTCTTTC CAAGAAATTTCCAACGGATGAACCCATATTCAGCGTTCTGCATGATCGCC GTAATGCTTCATATCAATCTGTCCTGGAATCTAATCTTCAGAATCTTAGATT TCTCAAATCAGCAAAACCATTGGCTATCATCACTCCTCTCCTTTACTCCCA TGTCCAAGCTGCTGTTGTCTGTTGCAAACGAGCTGGACTACAAATCAGAA TCCGCAGTGGTGGCAATGACTATGAAGGCTTGTCATATCGTTCTGAGGTT CCATATATCATTCTAGACCTTCAAAATCTTAGGTCAATCATGGTTGACATT GAAGACAACAGTGCTTGGGTTGAGTCAGGAGCAACTATTGGTGAACTGTA TTACGAGATAGCTGAGAAGAGTCCTGTTCATGCCTTTCCTGCTGGTGTCC ATCCGACCGTTGGCGTTGGCGGGCACTTAAGTGGTGGTGGGTTTGGTAC TATGCTCAGAAAATATGGACTTGCTGCCGATAACATCCTTGATGCTCATAT TGTTGATGCTGAAGGAAGACTTCTCAATAGGGAATCCATGGGAACAGATT TGTTTTGGGCCATCAGAGGAGGTGGAGGAGCAAGTTTTGGTGTCATAGTT GCCTGGAAAATCAAACTTGTGCATGTTCCTCCAGTAGTCACAGTATTTGAT TTGGCCATGACTTTGGAGGAAGGAGCCATAGATCTTATTCACAAATGGCA AACCGTCGGACCCAATCTCAATGAAGATGCATTTCTTGCCGCTAGTATTAT GGCAGATCCATCAAGTGAAAACATAACACTCCTGGCAGGTTTCTTTTCATT GTTCCTTGGTACAGCTGACCAACTCCTGAAAGAAATGGGGGAAAGCTTCC CCGAGCTCGGCCTACGAAAAGAACATTGTTTGGAGATGAGTTGGATCAAA GCAGCACTGCATTTTTCAGGGTATGAATCTGGTGAAACACTATATGCACTT AAAAATCGAAAGCCTCCTCAACCGAAGCATTGCATCACAGTAAGGTCAGA TTTCATTCAAGAACCTCTATCCCTGCCCGCATTAGACAGGTTGTGGAAGTT TTTATCAGAGGAAGAGAATCCTCCCATAATTGCCATGCTTCCTCATGGCG GAATGATGAGCAAAATATCAGAAACGGAAATTCCATACCCCTACAGAGAA GGTGTGATATATAGCTTTTTGTACGAGTTAATTTGGGATTGTGAGGACGAT TCCTTGTCTGAAAGATACGTTAGTGCATTGACAAGGCTCTATGACCATATG ACTCCTTATGTGCTGAAACATCCAAGAGGTAGTTTTTTGAACATGAGAAGC

	CTCGAAATTGGGAAGAACGATGATTATGGGACAACTTATTCAGAAGCTGA GGAATGGGGATTGAAGTATTTCAAGAATAACTTCAAGAGGTTGGCCATTA CCAAAGGTGTAGTTGATCCAGATAACTTCTTTTACTTCGAGCAGAGCATTC CCCCTCTTGCTTCCAAAGACGAACTTTAA
*Ti*PAS 2 (MK840851.1)	**ATG**GTTGAAGTCTCTAAAGTTCTTTCGTGTTTCTGCTTTCTTCTTCTCCTCT CATTGTCTCATGGCTTGATTCCTGAGGCTTTTATCAGTTGTATTTCCCTGG AATTTGAGTCATATGAATCCATTCTTAGGGTTCTGCATGATCCCGGCAATT CTTCCTACCATTCAGTGCTGCAATCAAGAATTCAAAATCTCAGATTTCTGA AGTCACCCAAACCATTGGCTATTATCACTCCTCTACTTTACTCCCATGTCC AGGCTGCTATTGTTTGTAGCAAACGGGTGGGATTACAAATTAGAATCCGC AGTGGAGGAAGTGACTATGAAGGGTTGTCGTATCGTTCTGAGGTTCCATT TATCCTTCTAGACCTCCATAACCTTAGATCCATTGTGGTTGACATTGAAGA CAACAGCGCATGGGTTGAGTCAGGAGCAACCATTGGCGAACTGTATTATG AGATTGCCCAGAAAAGTCCTATTCATGCCTTTCCTGCGGGGGTGTATGCA ACCGTTGGCGTTGGCGGGCACTTCAGCGGTGGTGGTTTTGGTACGATGC TCAGGAAATATGGACTAGCAGCTGACAATGTGATTGACGCTTATATTGTTG ATGCCAAAGGTAGACTTCTGGATAGGGAATCAATGGGAGAAGATTTGTTT TGGGCCATCAGGGGAGGTGGAGGAGCAAGTTTTGGCGTCATAGTTTCAT GGAAGATCAAACTTGTGCATGTTCCTCCAGTGGTCACTGTTTTTGACATG CCCAAGACTTTAGAGCAAGGAGCCTTGGATCTTCTGAACAAATGGCAATA TATAGGACACAAGCTCAGTGAAGATCTATTCCTTGCTGTAAGTATCATGGC AGATACATCTGGTGGAAATAAAACGCTTATGGCAGGTTTCAACTCGTTGTT TCTCGGCACAGCTGACCAGCTCTTGAAAGAAATGGCAGAAAGCTTCCCC GAGCTAGGGTTGAGAAAAGAACATTGCTCCGAGATGGGTTGGATCAAGG CAGCAATGCATTTTTCTGGATATCCAAGTGTAGAAACCACATCTCCACTTA AAAGTCGAGAACCTCCTCTACCCAAGACTTGCATTGCGACCAAGTCAGAC TTCATTCAAGAACCTCTATCCCTGCCCGCATTAGAGAAGTTGTGGAAGTT GTTATGGGAGGAAGAGAATACTCCCATCATTCTCATGCTTCCTCATGGCG GAATGATGAGCAAAATATCAGAATGGGAACTTCCATTCCCATACAGACAA GATGTGATATACAGCATGATCGATGAAGTAGTATGGGATTGTGAAGACGA TTACTCCTCCGAAGAGCACATTAGTGGACTGAGAAAGCTCTACGATCTTA TGACGCCTTATGTGTCGAAACACCCAAGAGGTACTTTTCTAAACATGAGA AACCTTGACACGGGTAGGAACGGTGATTATTATGGCACAACTTATTCAAA AGCCAAGGAATGGGGATTGAAGTATTTCAAGAACAACTTTCGAAAGTTGG CCATTACCAAGGGTGCAGTTGATCCAGATAACTTCTTTTACTTCGAGCAGA GCATTCCGCCTCTCACTTCACAAGACGAATCATCGTAA
*Ti*PAS 3 (MK840852.1)	**ATG**TTAGCAGAAGTCTCCAAAGTTCTTTCATGTTTCTACTTTCTTGTTCTAC TCTCAACATCGCATGGCTTGATTCCTGAAGCTTTTATTAATTGTGTTTCCC AGAAATTTGTGTCGGATCAATCTATTTTTAGCATTCTGCATGGTCCCGGAA ATTCTTCCTATCATTCTGTGCTGCAATCTAGAATTCAAAATCTTAGATTTCT CAAGTCACCCAAACCACTGGCTATTATCACTCCGCTACTTTACTCTCATGT CCAAGCCGCTGTCGTTTGTAGCAAACAGGTCGGACTACAAATTAGAATCC GCAGTGGAGGGGCCGACTATGAAGGGTTGTCATATCGTTCTGAGGTTCC TTTTGTCCTACTAGACCTCCAAAATCTTAGATCCATTGCGGTTGACATTGA GGACAACAGCGCTTGGGTTGAGTCAGGAGCAACCCTTGGCGAACTGTAT TATGAGATCGCTGAGAAAAGTCCGATTCATGCCTTTCCTGCAGGGGCCTC TGCAACTGTAGGCGTTGGCGGGCACTTCAGTTGTGGTGGTTTTGGTACG ATGCTCAGAAAATATGGACTGGCATCTGACAATGTAATTGATGCTTATATC GTTGATGCCACAGGTAGACTTCTGGATAAGGAATCAATGGGAGAAGATTT GTTTTGGGCCATCAGAGGAGGTGGAGGAGAAAGTTTTGGCGTCATAGTTT CGTGGAAGATCAAACTTGTGTATGTTCCTCCAGTGGTCACTGTTTTTGACT TGCCCAAGACTTTGGAGCAGGGAGCCTTAGATCTTCTTAACAAATGGCAG TATATAGGATACAAGCAAAGTGAAGATCTATTCCTTGCTGTAAGTATCATG GCAGATACATCTGCTGGAAATAAAACACTTATGGCAGGTTTCACCTCGTT GTTTCTGGGTACAGCTGACCAGCTTCTCAAGGAAATGCATGAGAGCTTCC CAGAGCTTGGCTTGAGGAAAGAACATTGCTCCGAGATGAGTTGGATCAAG GCAGCAATGCATTTTTCTGGATATCCAAGTGCAGAAACCATATCTGCACT GAAAAATCAAGATCCTCCTCTACCCAAGACTTGCATTGCGACCAAGTCAG ACTTCATTCAAGAACCTCTACCCCTGGCAGCATTAGAGAAGTTGTGGAAG TTCTCATCGGACGAAGAGAATACTCCCATAATTCTCATGCTTCCTCATGGC GGAATGATGAGCAAAATATCAGATTCTGAAACTCCATTCCCATACAGACAA GGTGTGATCTACAGCATGATCGAAGAAGTAGTTTGGGATTGTCAAGACGA TTACTCCTCCGAAGAGCACGTTAGTGGACTGAGAAGGCTGTATGACCTTA

	TGGCGCCTTATGTGTCGAAACAGCCAAGAGGTACTTTTCGAACCATCAGA AACCTCGATACCGGTAGAAATAATGATTCCGGCACAACTTATTCAGCGGC AAAGGAATGGGGTTTGAAGTATTTCAAGAACAACTTTCGAAAGCTAGCCA TTACCAAGGGTGCAGTTGATCCAGAAAACTTCTTTTATAATGAACAAAGCA TTCCGCCTCTAACTTTACATGATGAATTGTAA
*Cr*PAS (MH213134.1)	**ATG**ATAAAAAAAGTCCCAATAGTTCTTTCAATTTTCTGCTTTCTTCTTCTAC TCTCATCATCCCATGGCTCAATTCCTGAAGCTTTTCTCAATTGTATTTCCAA TAAATTTTCATTAGATGTATCCATTTTAAACATTCTTCATGTTCCCAGCAAT TCTTCCTATGATTCTGTTCTCAAATCTACTATCCAAAATCCAAGATTCCTCA AATCACCCAAGCCCTTAGCTATAATCACCCCAGTACTTCACTCCCATGTCC AATCTGCTGTTATCTGTACCAAACAAGCCGGTTTACAAATTAGAATCCGAA GCGGAGGAGCTGATTACGAGGGCTTATCCTATCGTTCTGAGGTTCCCTTT ATTCTGCTAGATCTCCAGAATCTTCGATCAATTTCCGTTGATATTGAAGAC AACAGCGCTTGGGTCGAATCAGGAGCAACAATTGGTGAATTCTATCATGA GATAGCTCAGAACAGCCCTGTTCATGCGTTTCCAGCTGGGGTCTCTTCCT CTGTTGGAATTGGCGGCCATTTGAGTAGCGGCGGTTTTGGTACATTGCTT CGGAAATATGGATTAGCAGCCGATAATATAATCGATGCAAAAATTGTTGAT GCCAGAGGCAGAATTCTTGATAGGGAATCAATGGGAGAAGATCTATTTTG GGCTATTAGAGGAGGAGGAGGAGCTAGTTTTGGTGTTATAGTTTCTTGGA AGGTTAAACTTGTAAAAGTCCCTCCGATGGTAACTGTTTTCATCTTGTCCA AGACTTATGAAGAAGGAGGTTTAGATCTTCTACACAAATGGCAATATATAG AACACAAACTCCCTGAAGATTTATTCCTTGCTGTAAGCATCATGGATGATT CATCTAGTGGAAATAAAACACTTATGGCAGGTTTTATGTCTCTGTTTCTTG GAAAAACAGAGGACCTTCTGAAAGTAATGGCGGAAAATTTCCCACAACTT GGATTGAAAAAGGAAGATTGCTTAGAAATGAATTGGATTGATGCAGCAAT GTATTTTTCAGGACACCCAATTGGAGAATCCCGATCTGTGCTTAAAAACC GAGAATCTCATCTTCCAAAGACATGCGTTTCGATCAAATCAGACTTTATTC AAGAACCACAATCCATGGATGCATTGGAAAAGTTATGGAAGTTTTGTAGG GAAGAAGAAAATAGTCCCATAATACTGATGCTTCCACTGGGGGGAATGAT GAGTAAAATATCAGAATCAGAAATCCCATTTCCTTACAGAAAAGATGTGAT TTACAGTATGATATACGAAATAGTTTGGAATTGTGAAGACGATGAATCATC GGAAGAATATATCGATGGATTGGGAAGGCTTGAGGAATTAATGACTCCAT ATGTGAAACAACCAAGAGGTTCTTGGTTCAGCACCAGAAACCTTTATACC GGTAAAAATAAAGGTCCAGGAACAACTTATTCCAAAGCTAAAGAATGGGG ATTTCGGTATTTTAATAATAATTTCAAAAAGTTGGCCCTTATCAAAGGACAA GTTGATCCAGAAAACTTCTTCTACTATGAACAAAGCATTCCCCCTCTCCAT TTACAAGTCGAACTTTGA
p19-TBSV (M21958.1)	**ATG**GAACGAGCTATACAAGGAAACGATGCTAGGGAACAAGCTTATGGTGA ACGTTGGAATGGAGGATCAGGAAGTTCCACTTCTCCCTTCAAACTTCCTG ACGAAAGTCCGAGTTGGACTGAGTGGCGGCTACATAACGATGAGACTATT TCGAATCAAGATAATCCCCTTGGTTTCAAGGAAAGCTGGGGTTTCGGGAA AGTTGTATTTAAGAGATATCTCAGATACGACGGGACGGAAACTTCACTGC ACAGAGTCCTTGGATCTTGGACGGGAGATTCGGTTAACTATGCAGCATCT CGATTTCTCGGTTTCGACCAGATCGGATGTACCTATAGTATTCGGTTTCGA GGAGTTAGTGTCACCATTTCTGGAGGGTCGCGAACTCTTCAGCATCTCAG TGAAATGGCAATTCGGTCTAAGCAAGAACTGCTACAGCTTACCCCAGTCA AAGTGGAAAGTGATGTATCAAGAGGATGCCCTGAAGGTGTTGAAACCTTC GAAGAAGAAAGCGAGTAA

Notes

1. Start codon is highlighted in **bold**.
2. Stop codon is underlined.

Table S2. Primers used in this study. Primer sequences. Primer sequences with homology to the destination plasmid for DNA assembly are in bold.

Gene	Plasmid	Primer direction	Sequence (5‘-3‘)
Nicotiana benthamiana transient expression			
*Cr*PAS	3Ω1	Forward	**TTTATGAATTTTGCAGCTCG**ATGATAAAAAAAGTC CCAATAGTTCTTT
		Reverse	**GACAACCACAACAAGCACCG**TCAAAGTTCGACTT GTAAATGGA
*Ti*PAS 1	3Ω1	Forward	**TTTATGAATTTTGCAGCTCG**ATGTATACTACTGAA GTTCGCAAAGTTT
		Reverse	**GACAACCACAACAAGCACCG**TTAAAGTTCGTCTT TGGAAGCAAGA
*Ti*PAS 2	3Ω1	Forward	**TTTATGAATTTTGCAGCTCG**ATGGTTGAAGTCTCT AAAGTTCTTTCG
		Reverse	**GACAACCACAACAAGCACCG**TTACGATGATTCGT CTTGTGAAG
*Ti*PAS 3	3Ω1	Forward	**TTTATGAATTTTGCAGCTCG**ATGTTAGCAGAAGTC TCCAAAGTTC
		Reverse	**GACAACCACAACAAGCACCG**TTACAATTCATCAT GTAAAGTTAGAG
*Ti*DPAS 1	3Ω1	Forward	**TTTATGAATTTTGCAGCTCG**ATGGCTGTAAAATCA CCTGAAGC
		Reverse	**GACAACCACAACAAGCACCG**CTATTCCGGTGGA GTTAGTGTG
*Ti*DPAS 2	3Ω1	Forward	**TTTATGAATTTTGCAGCTCG**ATGGCAGGAAAATCA CCAGAAGA
		Reverse	**GACAACCACAACAAGCACCG**TTACGGTTCTGGC GGAGGAG
*Ti*TabS	3Ω1	Forward	**TTTATGAATTTTGCAGCTCG**ATGGCTTCTTCAACT GAAAGCTCTG
		Reverse	**GACAACCACAACAAGCACCG**TTAGTCCTTGTTGA TGAAAGACGTTAG
*Ti*CorS	3Ω1	Forward	**TTTATGAATTTTGCAGCTCG**ATGGCTAATTCAACT GCGAACTCT
		Reverse	**GACAACCACAACAAGCACCG**TTACTCCTTGTTGA TGAAATCGCTTG
*Cr*PAS-C-6xHis	3Ω1	Forward	**TTTATGAATTTTGCAGCTCG**ATGATAAAAAAAGTC CCAATAGTTCTTT
		Reverse	**GACAACCACAACAAGCACCG**TCA*GTGATGGTGAT GGTGATG*AGAAGAACCAGAACCAAGTTCGACTTG TAAATGGA
*Ti*PAS 1-C-6xHis	3Ω1	Forward	**TTTATGAATTTTGCAGCTCG**ATGTATACTACTGAA GTTCGCAAAGTTT
		Reverse	**GACAACCACAACAAGCACCG**TCA*GTGATGGTGAT GGTGATG*AGAAGAACCAGAACCAAGTTCGTCTTT GGAAGCAAGA
*Ti*PAS 2-C-6xHis	3Ω1	Forward	**TTTATGAATTTTGCAGCTCG**ATGGTTGAAGTCTCT AAAGTTCTTTCG
		Reverse	**GACAACCACAACAAGCACCG**TCA*GTGATGGTGAT GGTGATG*AGAAGAACCAGAACCCGATGATTCGTC TTGTGAAG
*Ti*PAS 3-C-6xHis	3Ω1	Forward	**TTTATGAATTTTGCAGCTCG**ATGTTAGCAGAAGTC TCCAAAGTTC
		Reverse	**GACAACCACAACAAGCACCG**TCA*GTGATGGTGAT GGTGATG*AGAAGAACCAGAACCCAATTCATCATGT AAAGTTAGAG
p19-TBSV	3Ω1	Forward	**TTTATGAATTTTGCAGCTCG**ATGGAACGAGCTATA CAAGGAAA
		Reverse	**GACAACCACAACAAGCACCG**TTACTCGCTTTCTT CTTCGAAGG
Gene	**Plasmid**	**Primer direction**	**Sequence (5‘-3‘)**
Escherichia coli (DE3) expression			
*Ti*DPAS 1	pOPINF	Forward	**AAGTTCTGTTTCAGGGCCCG**GCTGTAAAATCACC TGAAGC

		Reverse	**ATGGTCTAGAAAGCTTTA**TTCCGGTGGAGTTAGTGTG
*Ti*DPAS 2	pOPINF	Forward	**AAGTTCTGTTTCAGGGCCCG**GCAGGAAAATCACCAGAAGA
		Reverse	**ATGGTCTAGAAAGCTTTA**CGGTTCTGGCGGAGGAG
*Ti*TabS	pOPINF	Forward	**AAGTTCTGTTTCAGGGCCCG**GCTTCTTCAACTGAAAGCTCTG
		Reverse	**ATGGTCTAGAAAGCTTTA**GTCCTTGTTGATGAAAGACGTTAG
*Ti*CorS	pOPINF	Forward	**AAGTTCTGTTTCAGGGCCCG**GCTAATTCAACTGCGAACTCT
		Reverse	**ATGGTCTAGAAAGCTTTA**CTCCTTGTTGATGAAATCGCTTG
Gene	**Plasmid**	**Primer direction**	**Sequence (5‘-3‘)**
Primers used for sequencing plasmid constructs			
	3Ω1	Forward	GATGAAAAAGCCCTAAAATTGGAG
		Reverse	ATTATTCACAAATGAGAAACAGAATGG
	pOPINF	Forward	TAATACGACTCACTATAGGG
		Reverse	TAGCCAGAAGTCAGATGCT

Notes:

1. GSGSS(Gly-Ser-Gly-Ser-Ser)-linker: sequence underlined.
2. C-terminal 6 x His (His_6-tag): sequence *italicized.*

Table S3. Reaction components for the production of final products using stemmadenine acetate (6) as substrate.

Desired final product	Buffer used [50 mM]	Oxidase used [1 µM]	Cyclase used [5 µM]	Reductase used [1 µM]	Cofactors used	Incubation method	Optimal pH and enzyme combination
(+)-Ψ-tabersonine (**5**)	HEPES pH 7.5 or CHES pH 9.5	*Cr*PAS or *Ti*PAS 1 or *Ti*PAS 2 or *Ti*PAS 3	*Ti*CorS	*Ti*DPAS 1 or *Ti*DPAS 2	FAD [0.2 mM] and NADPH [1 mM]	Method*	pH 7.5 + *Cr*PAS + *Ti*DPAS1 + *Ti*CorS
(+)-Ψ-vincadifformine (**9**)							pH 7.5 + *Ti*PAS3 + *Ti*DPAS1 + *Ti*CroS
(–)-coronaridine (**4**)							pH 9.5 + *Ti*PAS3 + *Ti*DPAS2 + *Ti*CorS
(–)-tabersonine (**2**)			*Ti*TabS				pH 7.5 + *Cr*PAS + *Ti*DPAS1 + *Ti*TabS

Notes:

Method*: Stepwise reaction, incubate stemmadenine acetate (**6**) (substrate) with oxidase and FAD co-factor in reaction buffer at 37 °C, 600 rpm for 15 min. Then add cyclase, reductase, and co-factor NADPH in sequential order, and further incubate at 37 °C, 600 rpm for 60 min. Reactions were quenched after incubation was complete.

Table S4. Reaction components for the production of final products using angryline (1a) as substrate.

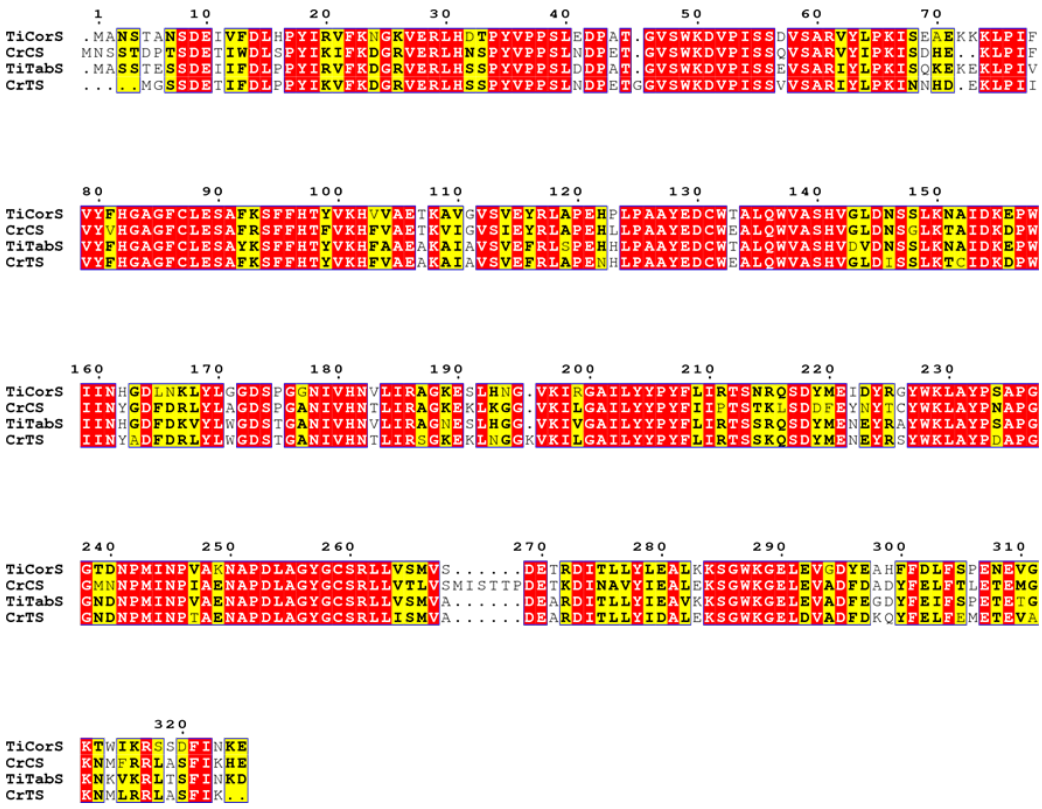
Desired final product	Buffer used [50 mM]	Oxidase used [1 µM]	Cyclase used [5 µM]	Reductase used [1 µM]	Cofactors used	Incubation method	Optimal enzyme combination
(+)-Ψ-tabersonine (**5**)	CHES pH 9.5	*Cr*PAS or *Ti*PAS 1 or *Ti*PAS 2 or *Ti*PAS 3	*Ti*CorS	*Ti*DPAS 1 or *Ti*DPAS 2	FAD [0.2 mM] and NADPH [1 mM]	Method**	+ *Cr*PAS + *Ti*DPAS1 + *Ti*CorS
(+)-Ψ-vincadifformine (**9**)							+ *Ti*PAS 3 + *Ti*DPAS1 + *Ti*CroS
(–)-tabersonine (**2**)			*Ti*TabS				+ *Ti*TabS [no cofactors required]
(–)-coronaridine (**4**)		-	*Ti*CorS		NADPH [1 mM]		+ *Ti*CorS + *Ti*DPAS2

Notes:

Method**: One-pot reaction, assemble reaction mixture in buffer and initiate the reaction by the addition of angryline (**1a**). Incubate at 37 °C, 600 rpm for 90 min and quench reaction.

Supplementary Figures

a.



b.

Enzyme	TiCorS	CrCS	TiTabS	CrTS
TiCorS		70.8	81,0	73.3
CrCS	70.8		71.7	77.4
TiTabS	81,0	71.7		81.7
CrTS	73.3	77.4	81.7	

Figure S1. Amino-acid alignments of cyclases.

a) Protein sequence alignment of α-β hydrolases was generated using Geneious Prime (version 2022.0.1) Muscle v5 algorithm[10]. Aligned sequences were visualized using ESPript V3[11]. Genbank ID of proteins; *Ti*CorS (QED20593.1)[2,3], *Cr*CS (A0A2P1GIW2.1)[2,12], *Ti*TabS (QED20592.1)[3], *Cr*TS (A0A2P1GIW3.1)[2,12]. **b)** Amino-acid similarity matrix of cyclases. Abbreviations: *Cr*CS, *Catharanthus roseus* catharanthine synthase; *Cr*TS, *Catharanthus roseus* tabersonine synthase; *Ti*TabS, *Tabernanthe iboga* tabersonine synthase; *Ti*CorS, *Tabernanthe iboga* coronaridine synthase.

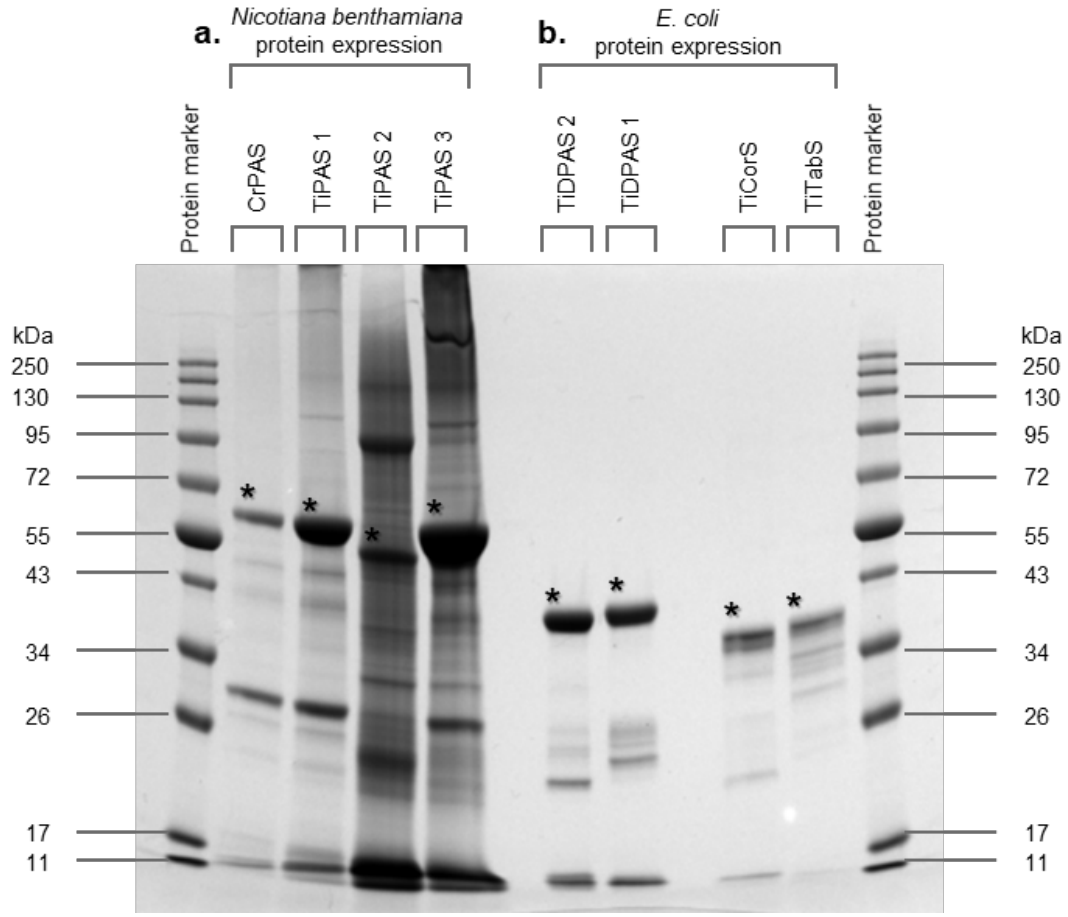
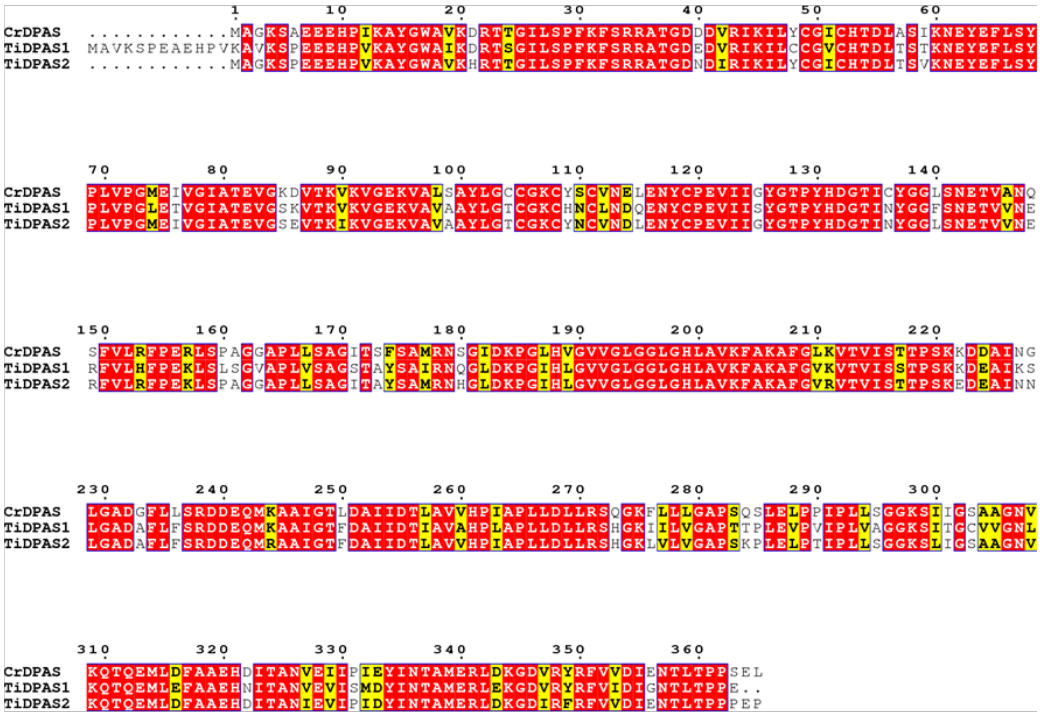


Figure S2. SDS-PAGE gel image of proteins used for *in vitro* enzymatic assays.

a) Proteins with C-terminal His_6-tag expressed heterologously in *N. benthamiana*. **b**) Proteins with N-terminal His_6-tag expressed heterologously in *E. coli*. Size estimates by ProtParam[13] of the target proteins (*) are as follows: *Cr*PAS – 59647 Da; *Ti*PAS 1 – 59410 Da; *Ti*PAS 2 – 56318 Da; *Ti*PAS 3 – 58751 Da; *Ti*DPAS 2 – 39225 Da; *Ti*DPAS 1 – 40151 Da; *Ti*CorS – 36309 Da; *Ti*TabS – 36502 Da. Abbreviations: *Cr*PAS, *Catharanthus roseus* precondylocarpine acetate synthase; *Ti*PAS1, *Tabernanthe iboga* precondylocarpine acetate synthase 1; *Ti*PAS2, *Tabernanthe iboga* precondylocarpine acetate synthase 2; *Ti*PAS3, *Tabernanthe iboga* precondylocarpine acetate synthase 3; *Ti*DPAS1, *Tabernanthe iboga* dihydro-precondylocarpine acetate syn-thase 1; *Ti*DPAS2, *Tabernanthe iboga* dihydroprecondylocarpine acetate synthase 2; *Ti*TabS, *Tabernanthe iboga* tabersonine synthase; *Ti*CorS, *Tabernanthe iboga* coronaridine synthase.

a.



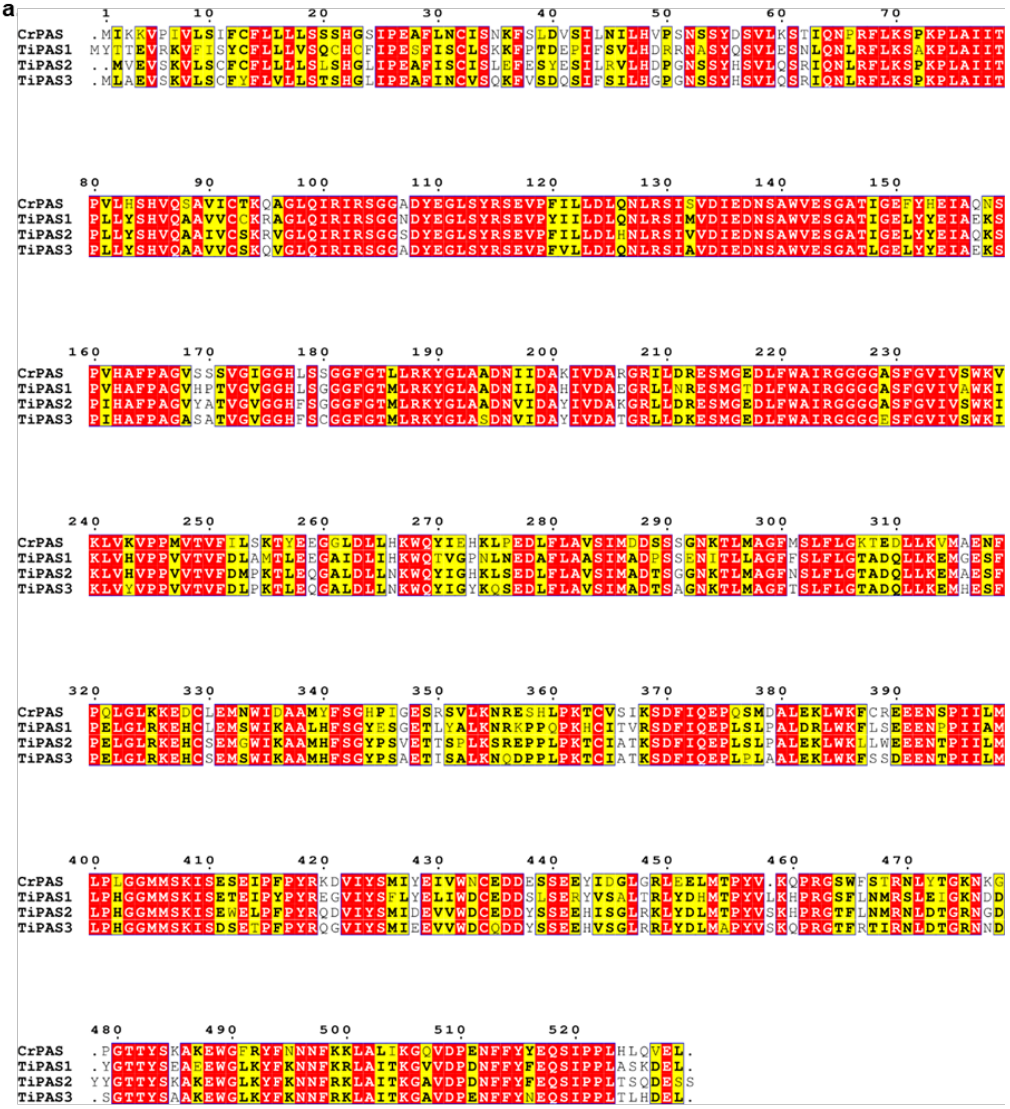
b.

Enzyme	CrDPAS	TiDPAS1	TiDPAS2
CrDPAS		77.7	86.3
TiDPAS1	77.7		83.0
TiDPAS2	86.3	83.0	

Figure S3. Amino-acid alignments of reductases.

a) Protein sequence alignment of medium-chain alcohol dehydrogenase (ADH). Protein sequence alignment was generated using Geneious Prime (version 2022.0.1) Muscle v5 algorithm[10]. Aligned sequences were visualized using ESPript V3[11]. Genbank ID of proteins; *Cr*DPAS (A0A1B1FHP3)[1], *Ti*DPAS1 (A0A5B8XAH0)[3], *Ti*DPAS2 (A0A5B8X8Z0)[3]. **b)** Amino-acid similarity matrix of reductases. Abbreviations: *Cr*DPAS, *Catharanthus roseus* dihydroprecondylocarpine acetate synthase; *Ti*DPAS1, *Tabernanthe iboga* dihydroprecondylocarpine acetate synthase 1; *Ti*DPAS2, *Tabernanthe iboga* dihydroprecondylocarpine acetate synthase 2.

a



b.

Enzyme	CrPAS	TiPAS1	TiPAS2	TiPAS3
CrPAS		67.2	73.8	72.9
TiPAS1	67.2		75.9	73.3
TiPAS2	73.8	75.9		86.1
TiPAS3	72.9	73.3	86.1	

Figure S4. Amino-acid alignments of oxidases.

a) Protein sequence alignment of Flavin-dependent oxidase (PAS). Protein sequence alignment was generated using Geneious Prime (version 2022.0.1) Muscle v5 algorithm[10]. Aligned sequences were visualized using ESPript V3[11]. Genbank ID of proteins; *Cr*PAS (AWJ76616.1)[1], *Ti*PAS1 (QED20589.1)[3], *Ti*PAS2 (QED20590.1)[3], *Ti*PAS3 (QED20591.1)[3]. **b)** Amino-acid similarity matrix of flavin-dependent oxidases. Abbreviations: *Cr*PAS, *Catharanthus roseus* precondylocarpine acetate synthase; *Ti*PAS1, *Tabernanthe iboga* precondylocarpine acetate synthase 1; *Ti*PAS2, *Tabernanthe iboga* precondylocarpine acetate synthase 2; *Ti*PAS3, *Tabernanthe iboga* precondylocarpine acetate synthase 3.

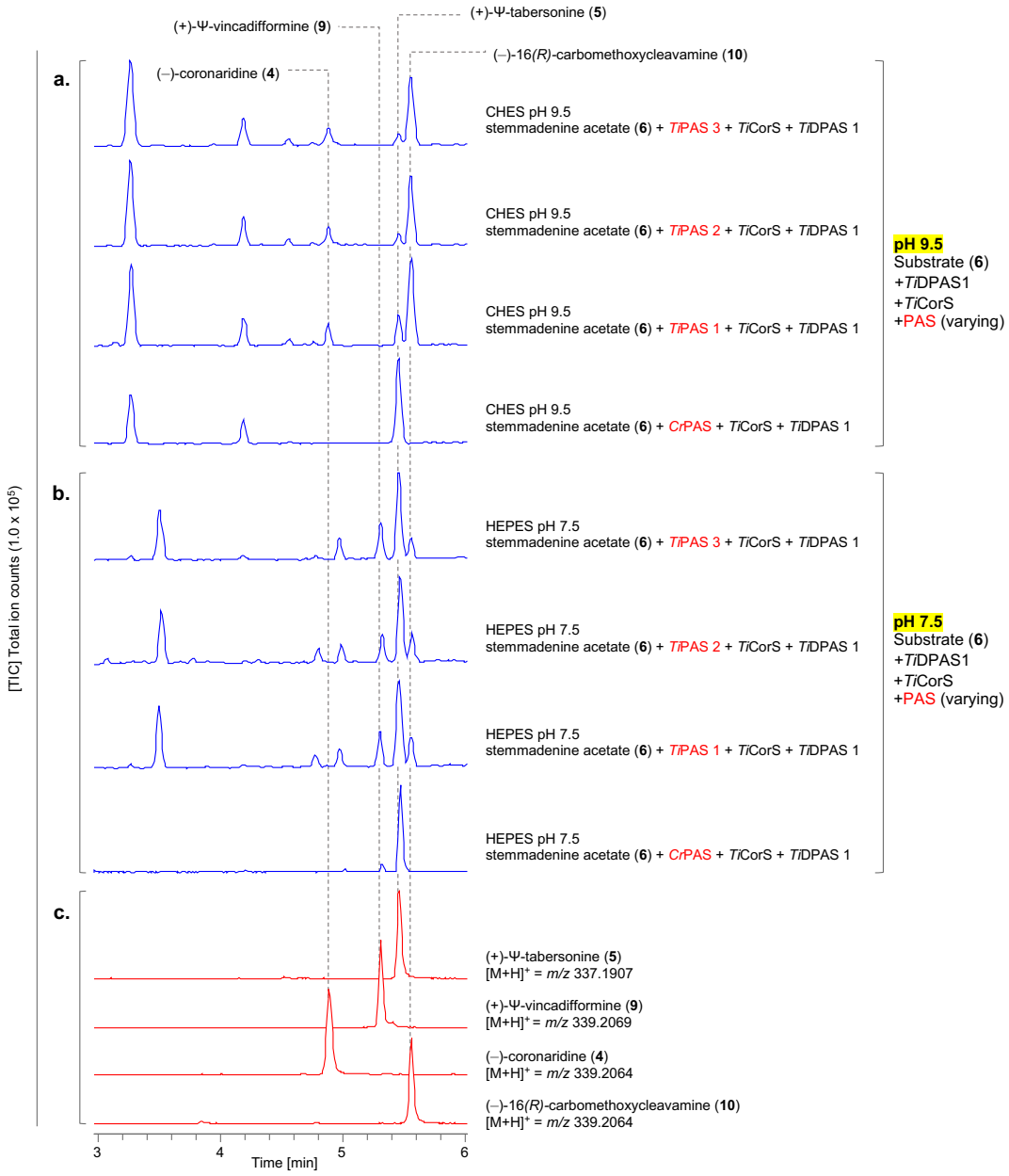


Figure S5. Systematic optimization of conditions that lead to production of (+)-Ψ-tabersonine (5), (+)-Ψ-vincadifformine (9) and (–)-coronaridine (4) from stemmadenine acetate (6), *Ti*CorS and *Ti*DPAS1.

pH conditions and the homologue of PAS that is used in varied. **a)** Conditions at pH 9.5 with *Cr*PAS, *Ti*PAS1, *Ti*PAS2, *Ti*PAS3. **b)** Conditions at pH 7.5 with *Cr*PAS, *Ti*PAS1, *Ti*PAS2, *Ti*PAS3. **c)** Authentic standards of products (TIC).

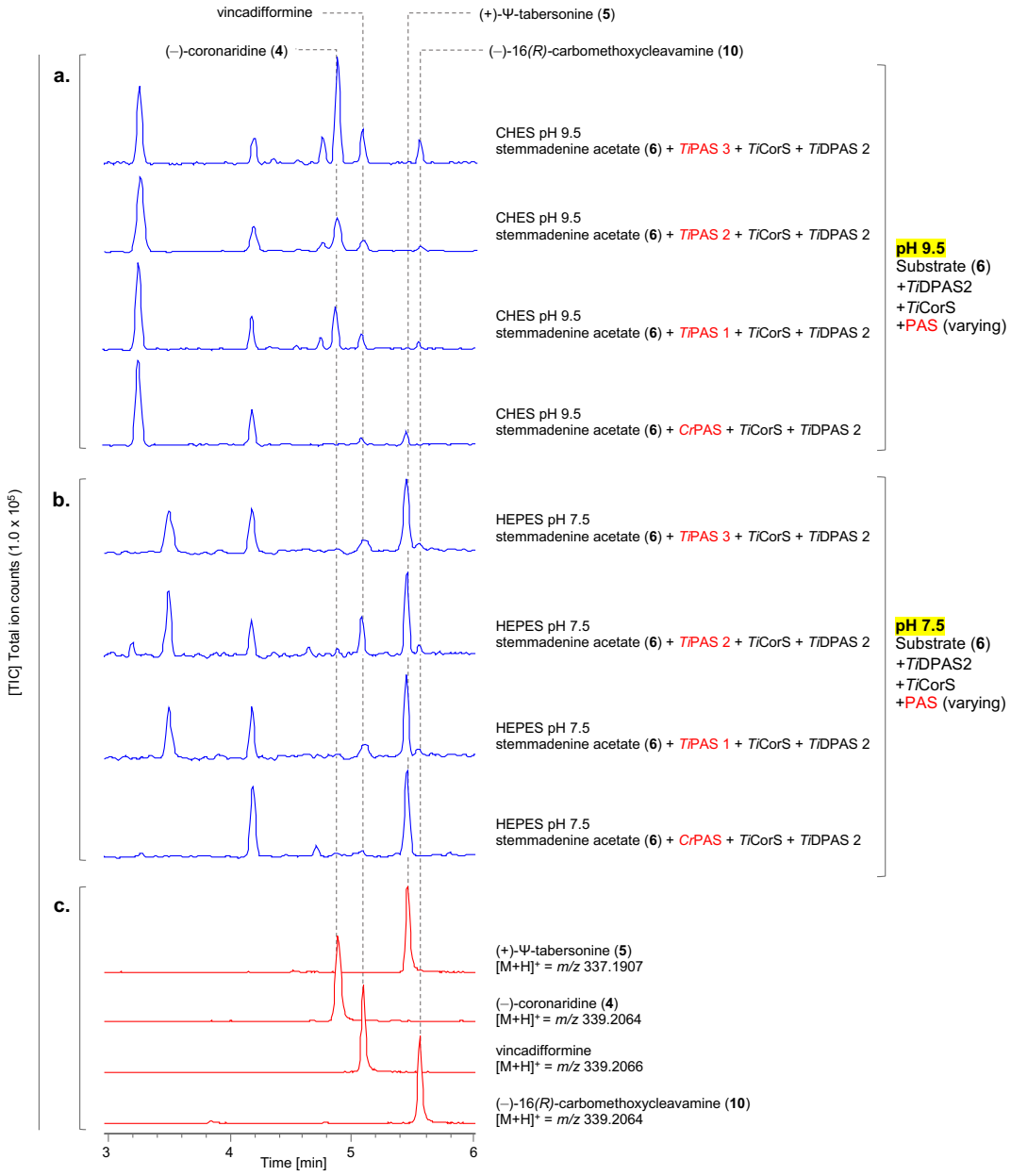


Figure S6. Systematic optimization of conditions that lead to production of (+)-Ψ-tabersonine (5) and (–)-coronaridine (4) from stemmadenine acetate (6), *Ti*CorS and *Ti*DPAS2.

pH conditions and the homologue of PAS that is used is varied. **a)** Conditions at pH 9.5 with *Cr*PAS, *Ti*PAS1, *Ti*PAS2, *Ti*PAS3. **b)** Conditions at pH 7.5 with *Cr*PAS, *Ti*PAS1, *Ti*PAS2, *Ti*PAS3. **c)** Authentic standards of products (TIC).

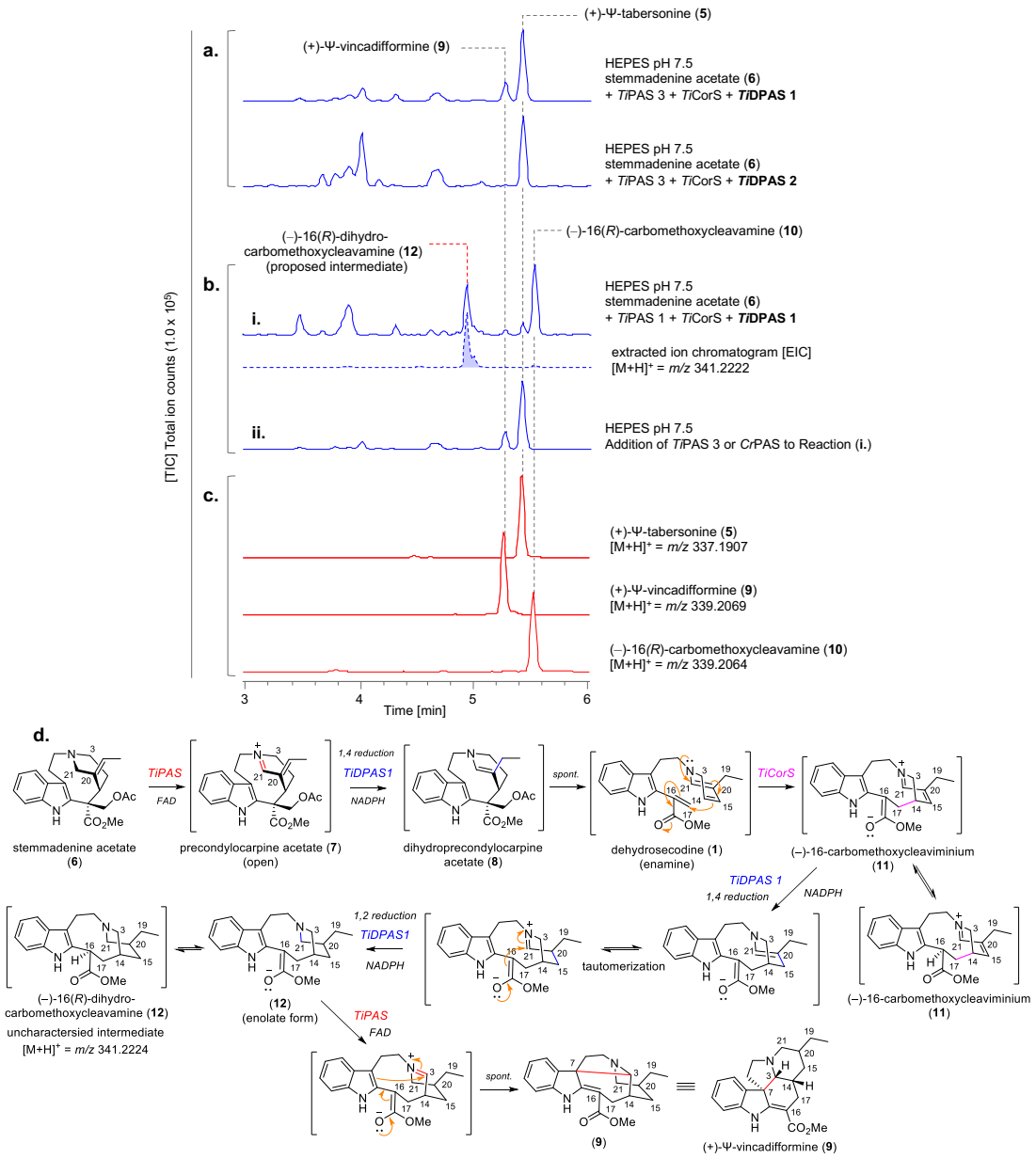


Figure S7. *In vitro* production of the over-reduced product (+)-Ψ-vincadifformine (9).

a) TICs showing the optimized selective production of (+)-Ψ-vincadifformine (**9**) from stemmadenine acetate (**6**) with *Ti*DPAS1 at pH 7.5. **b)** TICs of *in vitro* enzymatic assays showing the uncharacterized over-reduced intermediate, (–)-16(*R*)-dihydrocarbomethoxycleavamine (**12**) (*m/z* = 341.2222) observed (i.) in production of (+)-Ψ-vincadifformine (**9**). Stepwise addition of oxidase (PAS) to reaction (i.) resulted in the formation of desired product (+)-Ψ-vincadifformine (**9**) (ii.) via the proposed intermediate, (–)-16(*R*)-dihydro-carbomethoxycleavamine (**12**) (*m/z* = 341.2224). Production of (+)-Ψ-tabersonine (**5**) was observed in (ii.) because of the oxidation of the intermediate (–)-16(*R*)-carbomethoxycleavamine (**10**) by the same oxidase (PAS). **c)** Authentic standards (TICs) of products. **d)** Proposed mechanism for the production of (+)-Ψ-vincadifformine (**9**) from stemmadenine acetate (**6**) from PAS, *Ti*DPAS1 and *Ti*CorS.

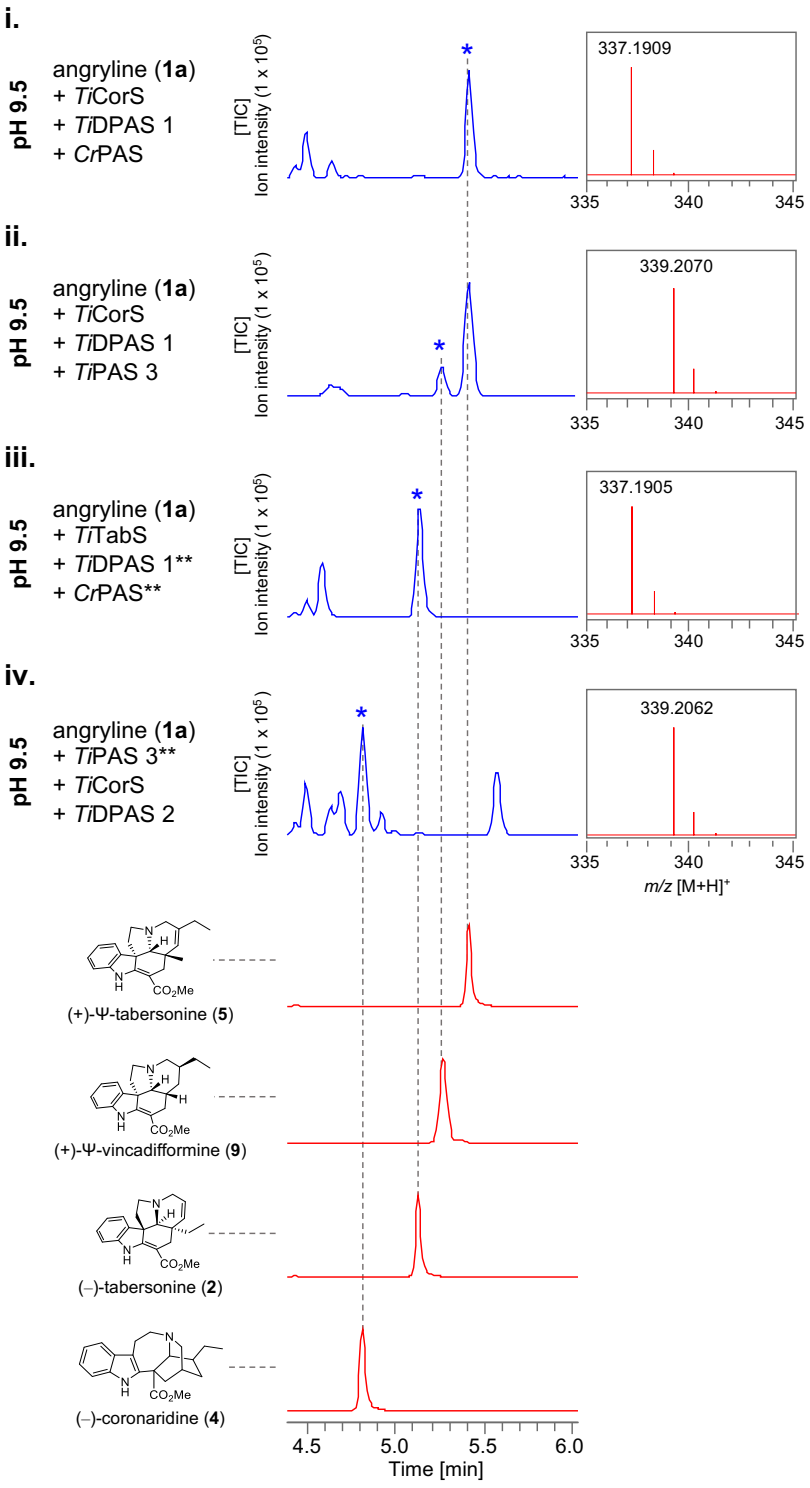


Figure S8. *In vitro* coupled enzymatic assays showing optimized production of (+)-Ψ-tabersonine (5), ii. (+)-Ψ-vincadifformine (9), iii. (–)-tabersonine (2) and iv. (–)-coronaridine (4) from angryline (1a).

The enzyme combination and pH conditions have been optimized for each product. *MS, $[M+H]^+$ spectra of observed product. **Enzymes not required for the biosynthesis of desired product but included to show consistency across all enzyme reactions.

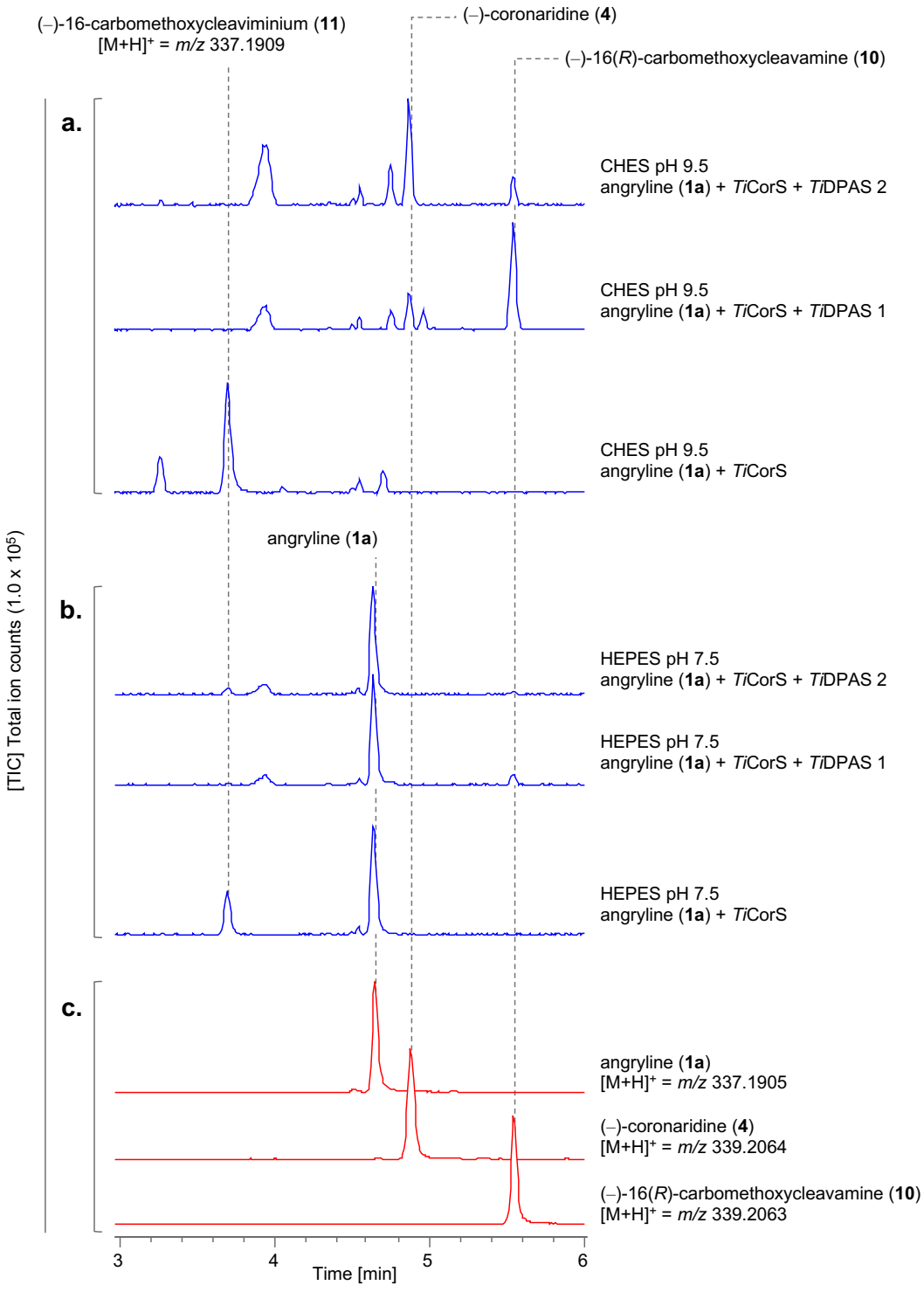


Figure S9. Systematic optimization of conditions that lead to production of (–)-coronaridine (4) from angryline (1a), with *Ti*CorS and *Ti*DPAS homologues.

a) TICs of *in vitro* reactions for the production of (–)-coronaridine (**4**) from angryline (**1a**) at pH 9.5 with stepwise addition of *Ti*CorS, and *Ti*DPAS1, *Ti*DPAS2 homologues. **b)** TICs of *in vitro* reactions using angryline (**1a**) as substrate with stepwise addition of *Ti*CorS, and *Ti*DPAS1, *Ti*DPAS2 homologues at pH 7.5. **c)** Authentic standards (TICs) of products and substrate.

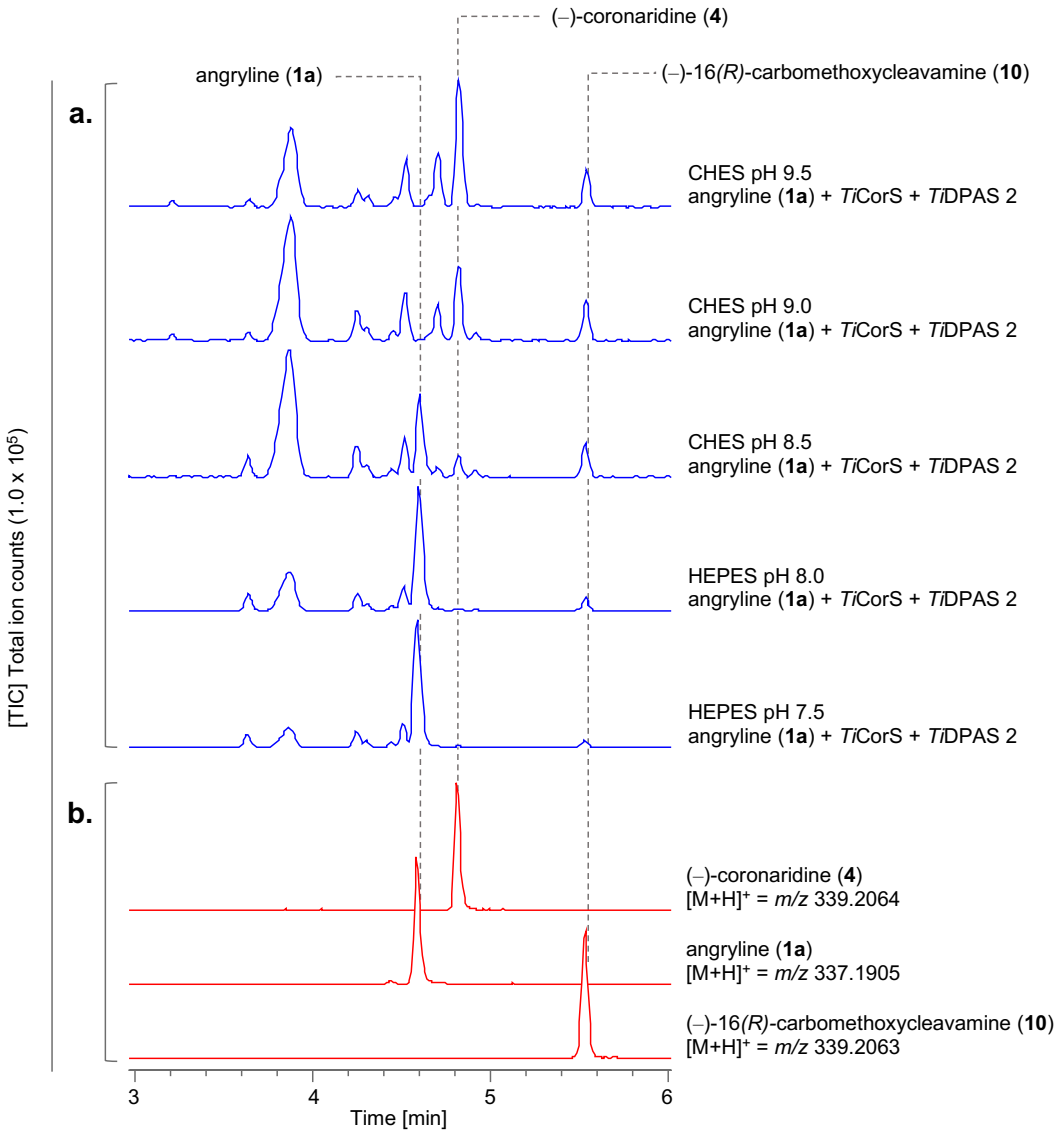


Figure S10. Systematic optimization of pH conditions that lead to production of (–)-coronaridine (4) from angryline, *Ti*CorS and *Ti*DPAS2.

a) TICs of *in vitro* coupled enzymatic assays for the production of (–)-coronaridine (**4**) from angryline (**1a**) using *Ti*CorS and *Ti*DPAS2 enzymes at pH conditions 9.5, 9.0, 8.5, 8.0, and 7.5. **b)** Authentic standards (TICs) of products and substrate.

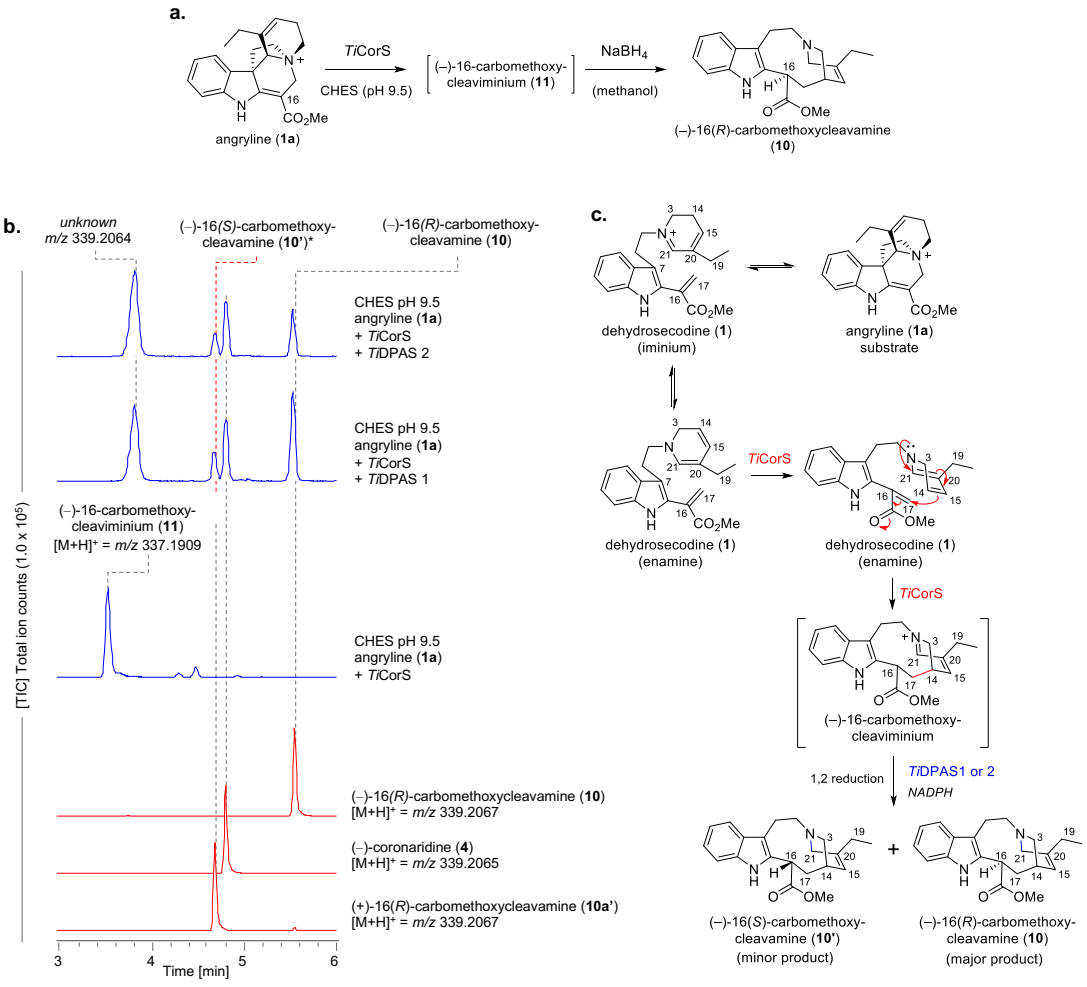


Figure S11. Generation of (–)-16(*R*)-carbomethoxycleavamine (10) from angryline (1a), by *Ti*CorS and *Ti*DPAS1.

a) Reaction scheme showing enzymatic product of *Ti*CorS, (–)-16-carbomethoxycleaviminium (**11**) chemically reduced to (–)-16(*R*)-carbomethoxycleavamine (**10**) with $NaBH_4$ in methanol. **b)** TICs showing the reaction products using angryline, when *Ti*CorS and either *Ti*DPAS1 or *Ti*DPAS2 is added stepwise at pH 9.5. The peak assigned as (–)-16(*S*)-carbomethoxycleavamine (**10'**) is putative and is based on the retention time and fragmentation spectra of (+)-16(*R*)-carbomethoxycleavamine (**10a**), the enantiomer generated from (+)-catharanthine (**3**) (red-dotted line). Authentic standards (TICs) of the products are shown in red. **c)** Proposed mechanism for formation of (–)-16(*R*)-carbomethoxycleavamine (**10**) and (–)-16(*S*)-carbomethoxycleavamine (**10'**) from angryline (**1a**).

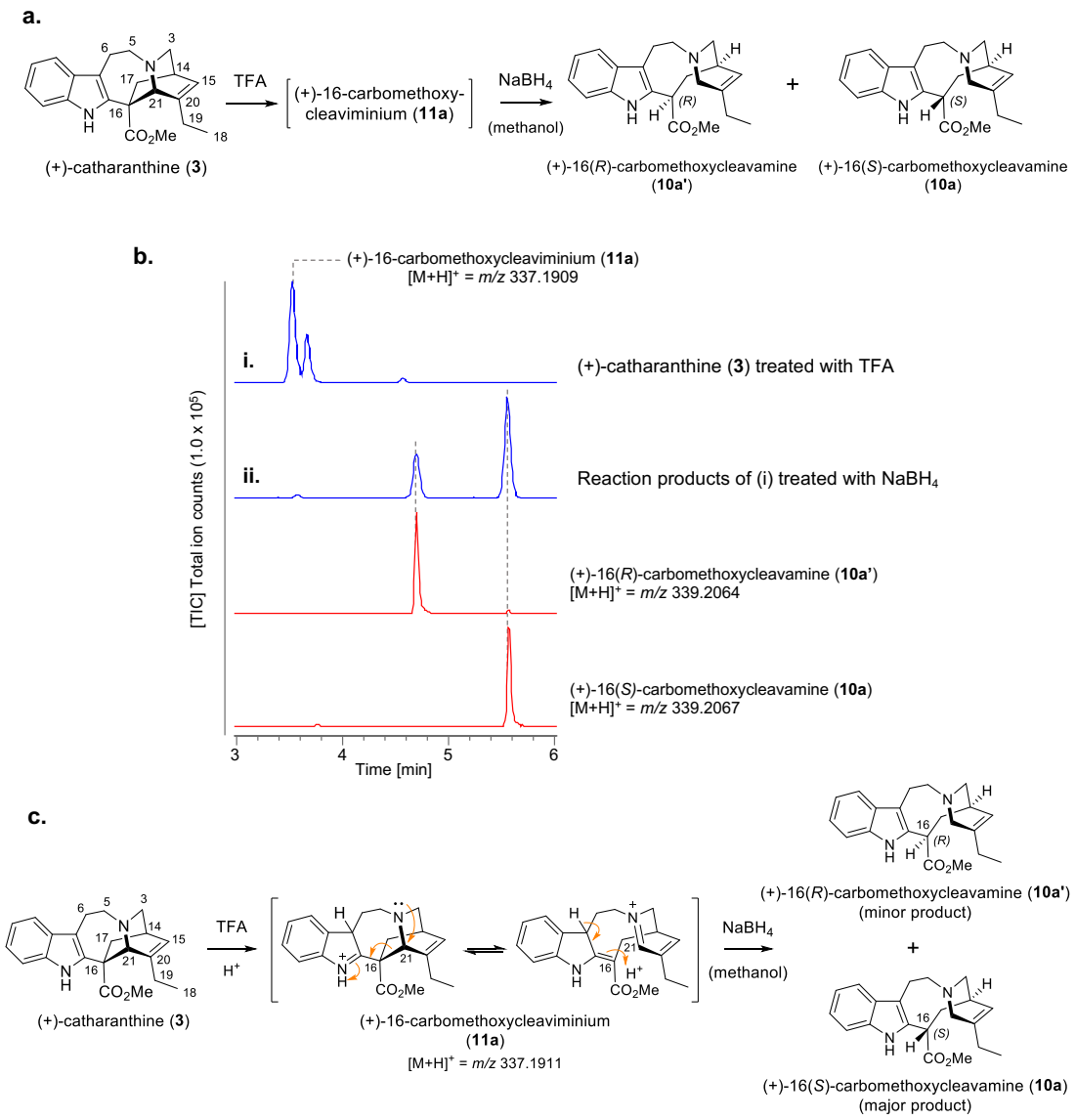


Figure S12. Generation of 16-carbomethoxycleavamine (10a) from acid-catalyzed opening and reduction of (+)-catharanthine (3).

a) Reaction scheme showing conversion of (+)-catharanthine (**3**) to (+)-16(*R*)-carbomethoxycleavamine (**10a'**) and (+)-16(*S*)-carbomethoxycleavamine (**10a**). **b)** TICs showing the reaction products of acid catalyzed opening and reduction of (+)-catharanthine (**3**). Authentic standards (TICs) of products are shown in red. **c)** Proposed reaction mechanism for the production of (+)-16(*R*)-carbomethoxycleavamine (**10a**) and (+)-16(*S*)-carbomethoxycleavamine (**10a'**) from (+)-catharanthine (**3**).

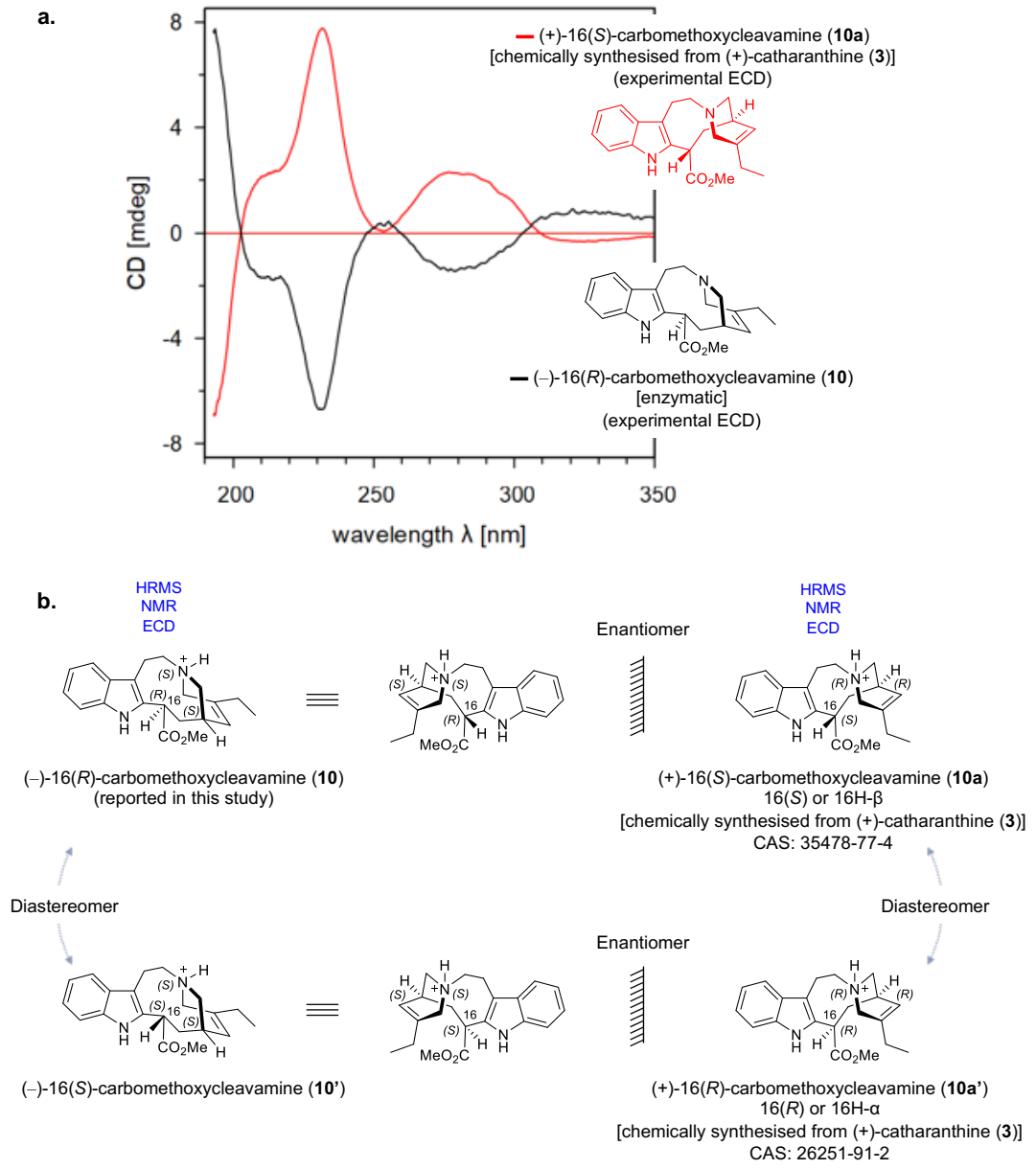


Figure S13. Stereochemistry of (–)-16(*R*)-carbomethoxycleavamine (10).

a) CD spectra of enzymatically prepared and isolated (–)-16(*R*)-carbomethoxycleavamine (**10**) and chemically prepared and isolated (+)-16(*S*)-carbomethoxycleavamine (**10a**).[14] **b)** Stereocenters of 16-carbomethoxycleavamine isomers described in this study.

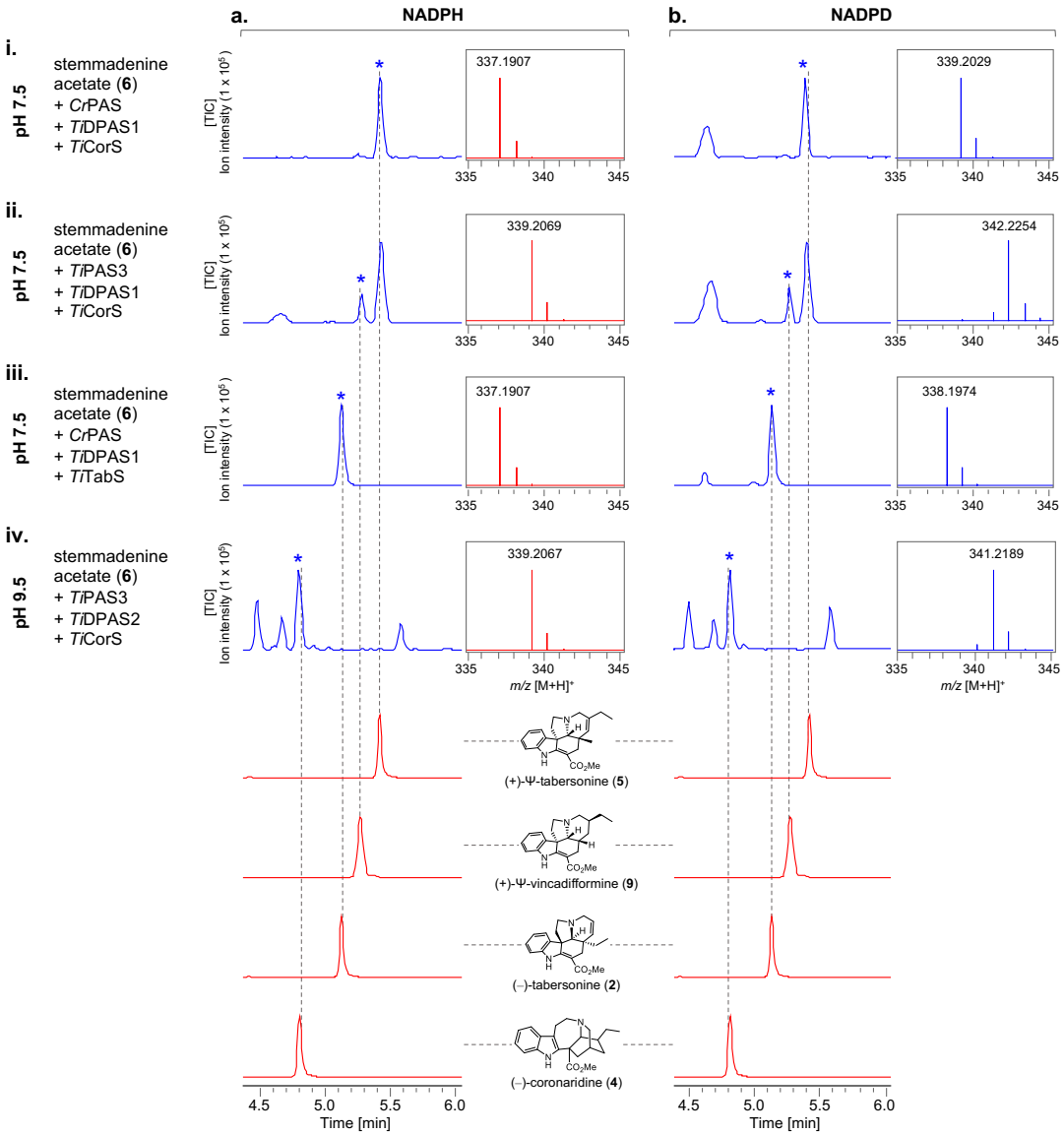


Figure S14*. In vitro* deuterium labelled enzyme assays using stemmadenine acetate (6) as starting material.

TICs of *in vitro* enzymatic assays showing optimized production of **i.** (+)-Ψ-tabersonine (**5**), **ii.** (+)-Ψ-vincadifformine (**9**), **iii.** (–)-tabersonine (**2**), and **iv.** (–)-coronaridine (**4**) from stemmadenine acetate (**6**). The enzyme combination PAS, DPAS, cyclase (CorS or TabS) and pH conditions have been optimized for each of the respective products. TICs of the authentic standards of the final products are shown in red. **a)** Use of NADPH cofactor. **b)** Use of isotopically labeled NADPD cofactor. *MS, $[M+H]^+$ spectra of observed product.

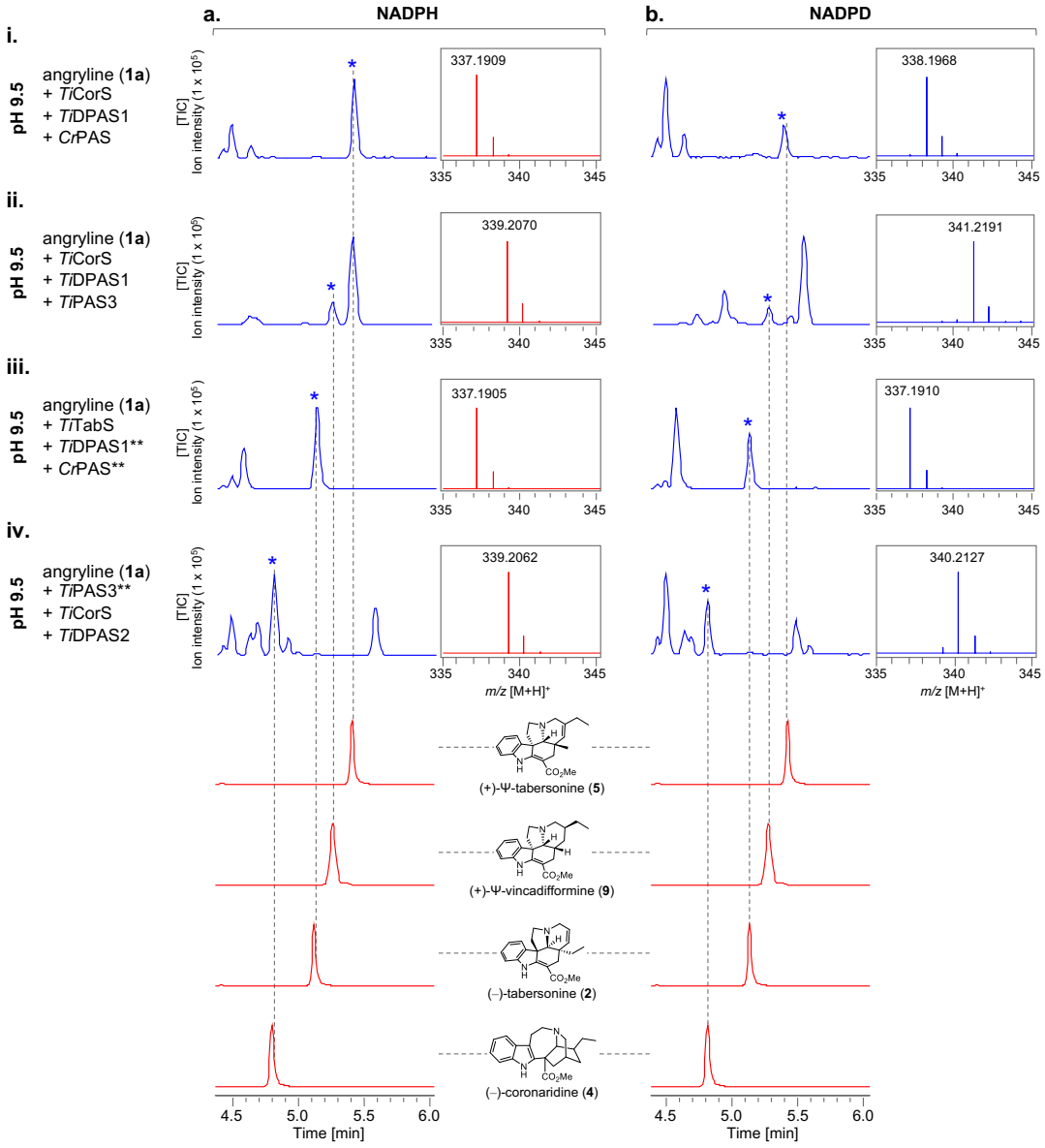


Figure S15*. In vitro* deuterium labelled enzyme assays from angryline (1a).

TICs of *in vitro* enzymatic assays showing optimized production of **i.** (+)-Ψ-tabersonine (**5**), **ii.** (+)-Ψ-vincadifformine (**9**), **iii.** (–)-tabersonine (**2**), and **iv.** (–)-coronaridine (**4**) from angryline (**1a**). The enzyme combination PAS, DPAS, cyclase (CorS or TabS) and pH conditions have been optimized for each of the respective products. Authentic standards (TICs) of the final products are shown in red. **a)** Use of NADPH cofactor. **b)** Use of isotopically labeled NADPD cofactor. *MS $[M+H]^+$ spectra of the observed product. **Enzymes not required for the biosynthesis of desired product but included to show consistency across all enzyme reactions.

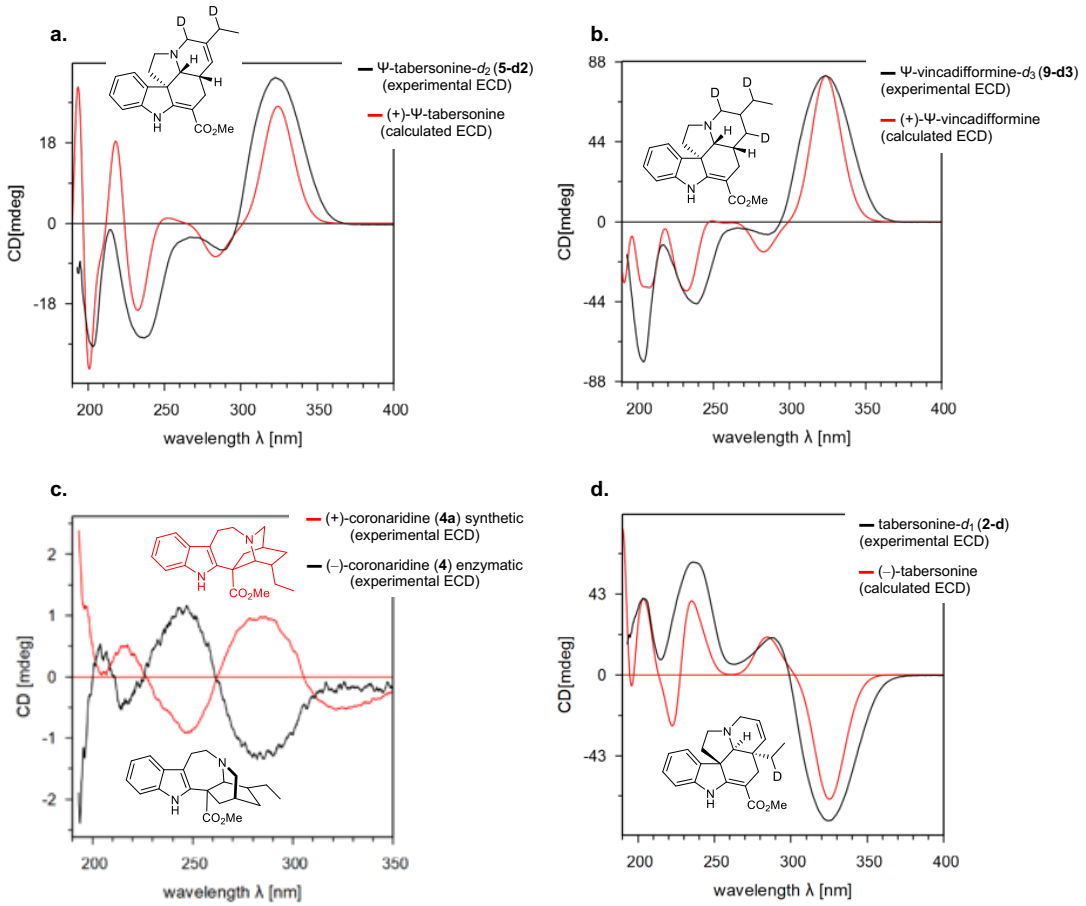


Figure S16. CD spectra of biosynthetic products.

a) CD spectra of enzymatically prepared and isolated (+)-Ψ-tabersonine-d_2 (**5-d2**) (black) alongside computationally calculated spectra (red). **b)** CD spectra of enzymatically prepared and isolated (+)-Ψ-vincadifformine-d_3 (**9-d3**) (black) alongside computationally calculated spectra (red). **c)** CD spectra of enzymatically prepared and isolated (–)-coronaridine (**4**) (black) alongside chemically synthesized (+)-coronaridine (**4a**) (red). **d)** CD spectra of enzymatically prepared and isolated (–)-tabersonine-d_1 (**2-d**) (black) alongside computationally calculated spectra (red).

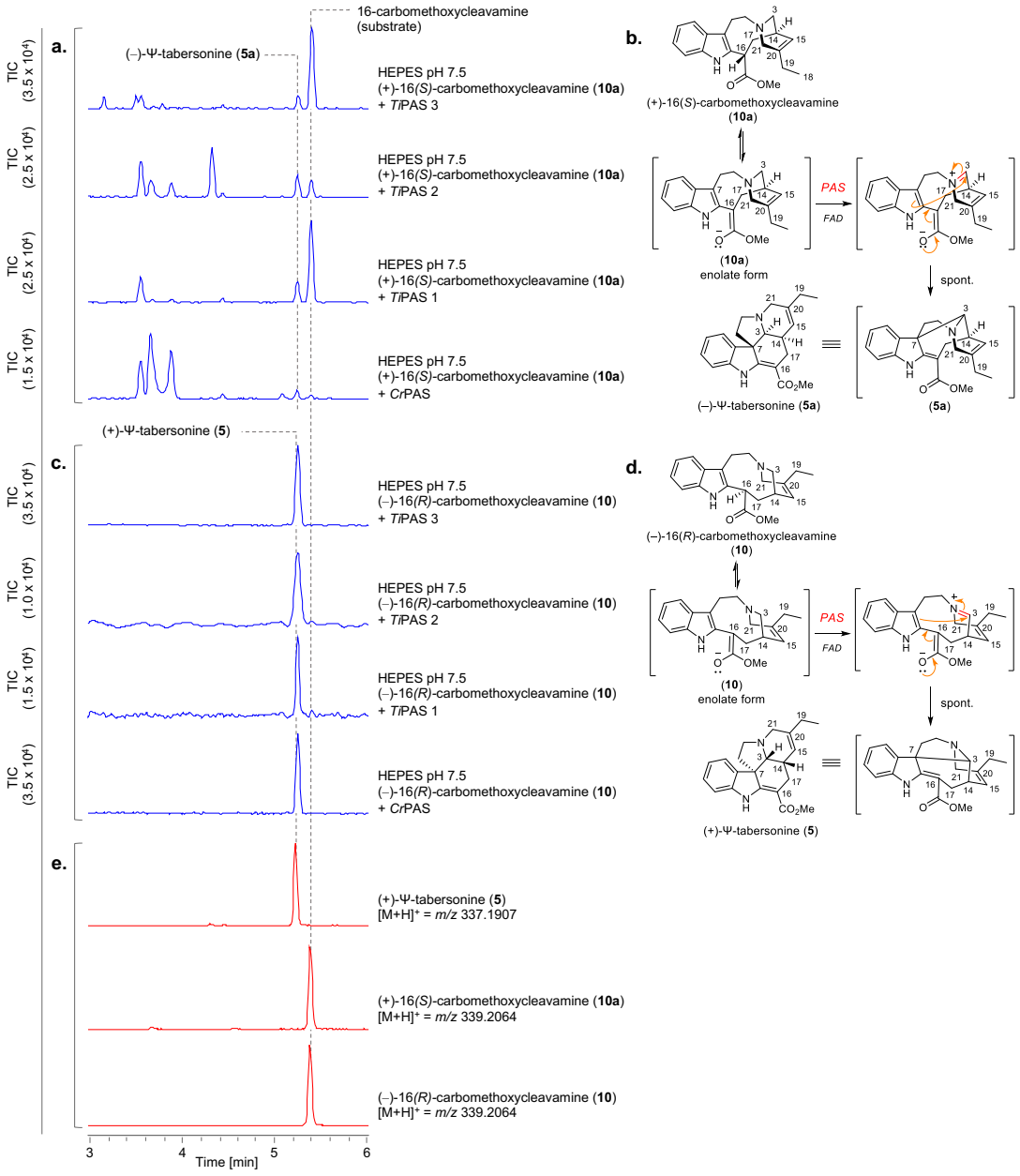


Figure S17. Production of (–)-Ψ-tabersonine (5a) and (+)-Ψ-tabersonine (5) from 16-carbomethoxycleavine enantiomers.

a) TICs showing the production of (–)-Ψ-tabersonine (**5a**) from (+)-16(*S*)-carbomethoxycleavamine (**10a**) using PAS homologues (oxidases) described in the study. (–)-Ψ-tabersonine (**5a**) could not be structurally characterised and is a putative assignment. **b)** Proposed mechanism for the production of (–)-Ψ-tabersonine (**5a**). **c)** TICs showing the production of (+)-Ψ-tabersonine (**5**) from (–)-16(*R*)-carbomethoxycleavamine (**10**) using PAS homologues (oxidases) described in the study. **d)** Proposed mechanism for the production of (+)-Ψ-tabersonine (**5**). **e)** TICs of authentic standards of standards.

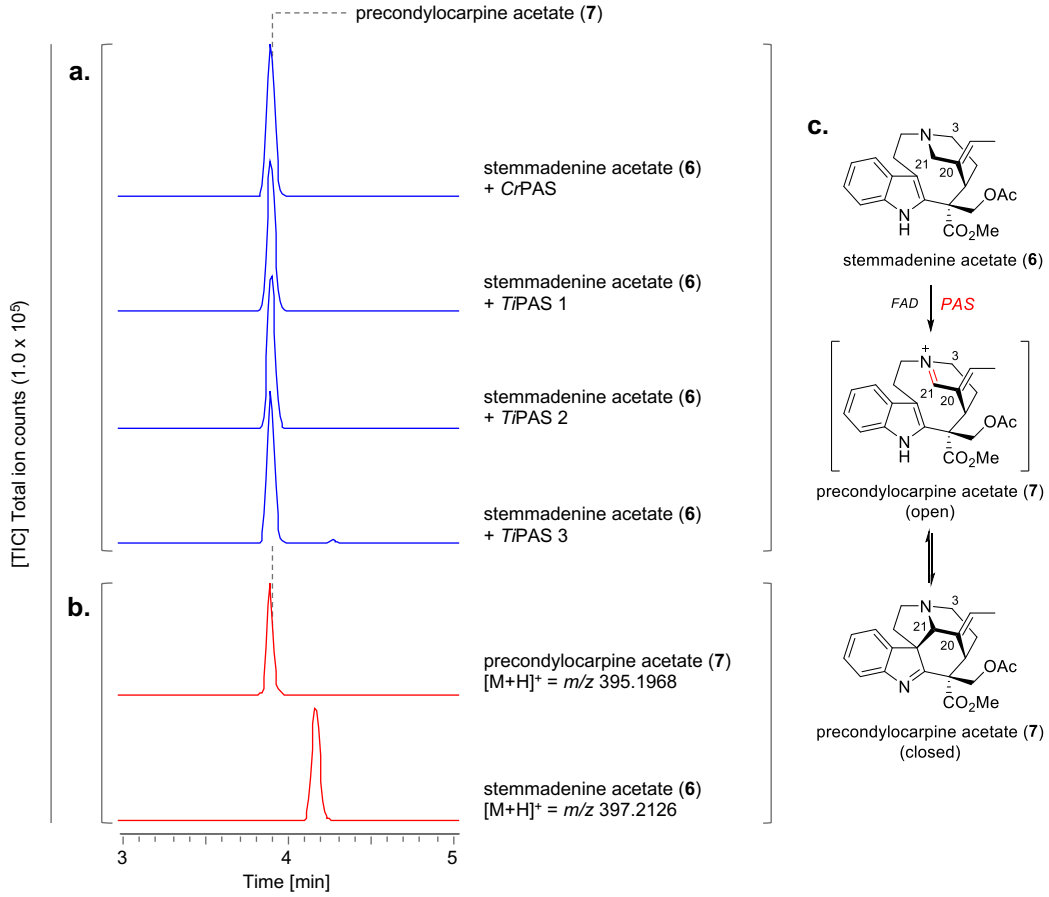
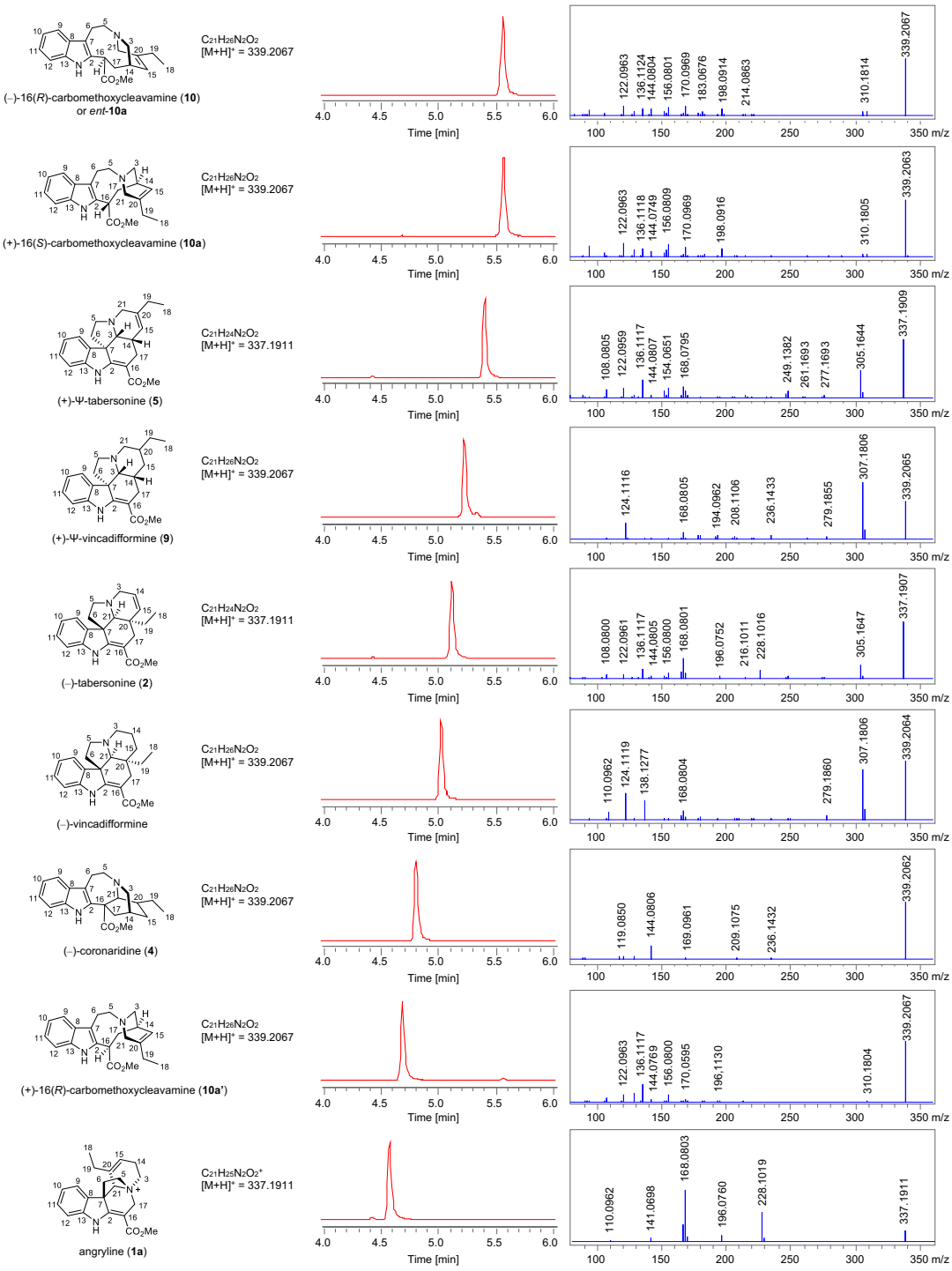


Figure S18. Production of precondylocarpine acetate (7) from stemmadenine acetate (6).

a) TICs of *in vitro* enzyme assays showing the production of precondylocarpine acetate (**7**) from stemmadenine acetate (**6**) by PAS (oxidase) homologues described in this study. **b)** Authentic standards of product (precondylocarpine acetate (**7**)) and substrate stemmadenine acetate (**6**). **c)** Proposed reaction for the formation of precondylocarpine acetate (**7**) by PAS (oxidase).



Continued to next page.

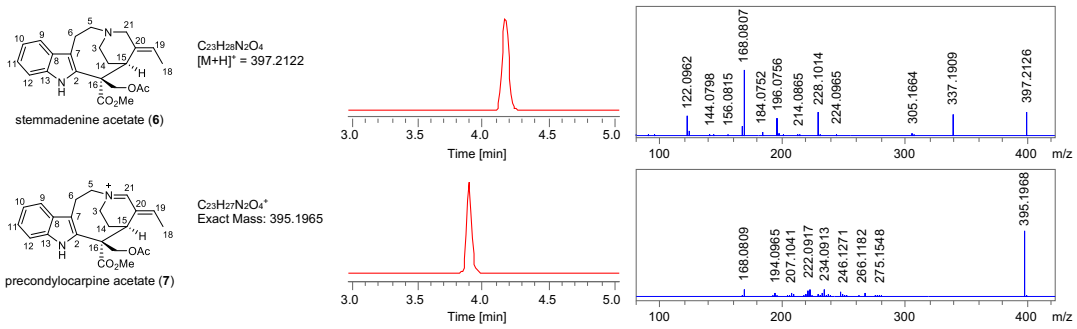
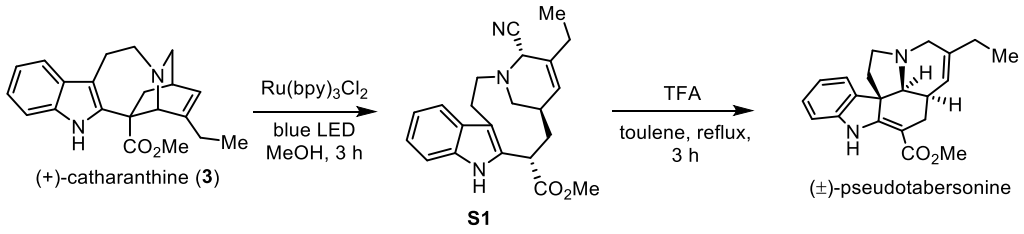


Figure S19. Authentic standards of chemicals used in this study.

Atom numbering of molecules, total ion chromatograms (TICs) and MS^2 fragmentation spectra of authentic standards are shown.

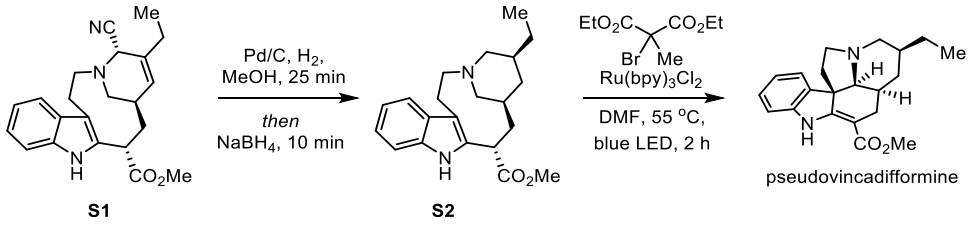
Synthesis of compounds

Synthesis of racemic pseudo-tabersonine [Ψ-tabersonine] (5) and pseudo-vincadifformine [Ψ-vincadifformine] (9).



(±)-Ψ-tabersonine (**5a**) was prepared according to the reported method[15]. The reaction mixture containing (+)- catharanthine (85 mg, 0.253 mmol), $Ru(bpy)_3Cl_2$ (5.7 mg, 0.0076 mmol) and methanol (2.5 mL) was degassed *via* the freeze pump-thaw method (3 cycles) and the flask back-filled with argon. TMSCN (63 µL, 0.506 mmol) was added to the solution. The reaction mixture was irradiated with blue LED and stirred for 3 hours. The reaction was quenched with sat. $NaHCO_3$ (10 mL), extracted with EtOAc (5 mL x 3). The combined organic layers were washed with brine (5 mL) and dried with anhydrous Na_2SO_4. The solvents were evaporated in *vacuo* to afford product **S1** (66 mg, 72%).

The solution of **S1** (36 mg, 0.1 mmol) and toluene (2 mL) was degassed *via* the freeze pump-thaw method (3 cycles) and the flask back-filled with argon. Trifluoroacetic acid (7.4 µL, 0.1 mmol) was added to the solution. The reaction mixture was heated to 120 ^oC and stirred for 3 hours. The reaction was quenched with sat. $NaHCO_3$ (5 mL), extracted with EtOAC (5 mL x 3). The combined organic layers were washed with brine (5 mL) and dried with anhydrous Na_2SO_4, filtered and concentrated in *vacuo.* The residue was purified on silica gel chromatography (petroleum ether/EtOAc = 20/1) to afford (±)-Ψ-tabersonine (12 mg, 36%). The spectroscopic data of (±)-Ψ-tabersonine (**5**) are in accordance with the literature values reported[15]. Full NMR characterization is provided below.

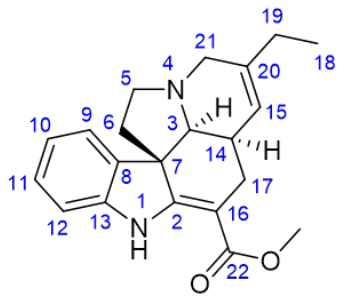


(±)-Ψ-vincadifformine (**9a**) was prepared according to the reported method[15]. The solution of **S1** (9 mg, 0.0248 mmol), 10% Pd/C (5.4 mg) and MeOH (1 mL) was

degassed *via* the freeze pump-thaw method (3 cycles) and the flask back-filled with argon. Hydrogen was bubbled through the reaction from a balloon for 25 minutes. Then the reaction mixture was cooled to 0 °C and $NaBH_4$ (3.8 mg, 0.0992 mmol) was added and stirred at the same temperature for 10 minutes. The reaction was filtered through a column of Celite, washed through with ethyl acetate, and concentrated in *vacuo.* The resulting residue **S2** was used directly in the next step. The above residue was dissolved in anhydrous DMF (1 mL) and $Ru(bpy)_3Cl_2$ (0.2 mg, 0.000267 mmol) was added with stirring. The solution was degassed *via* the freeze pump-thaw method (3 cycles) and the flask back-filled with argon. Diethyl 2-bromo-2-methylmalonate (14 µL, 0.0744 mmol) was added to the solution. The reaction mixture was heated to 55 °C and irradiated with blue LED. After 2 hours, the reaction was diluted with EtOAc (2 mL) and partitioned with water (2 mL). Triethylamine (0.5 mL) was added to the separatory funnel, and the mixture was extracted with ethyl acetate (2 mL, x3). The combined organic layers were washed with brine (5 mL) dried with anhydrous Na_2SO_4, filtered and concentrated in *vacuo.* The residue was purified by silica gel chromatography (petroleum ether/EtOAc = 20/1, argon-sparged) under argon to afford (±)-Ψ-vincadifformine (**9a**) (2 mg, 24%). The spectroscopic data of Ψ-vincadifformine are in accordance with the literature values reported[15]. NMR spectra are shown below.

Supplementary NMR spectra

NMR data for synthesized (–)-Ψ-tabersonine (5a) (pseudo-tabersonine)

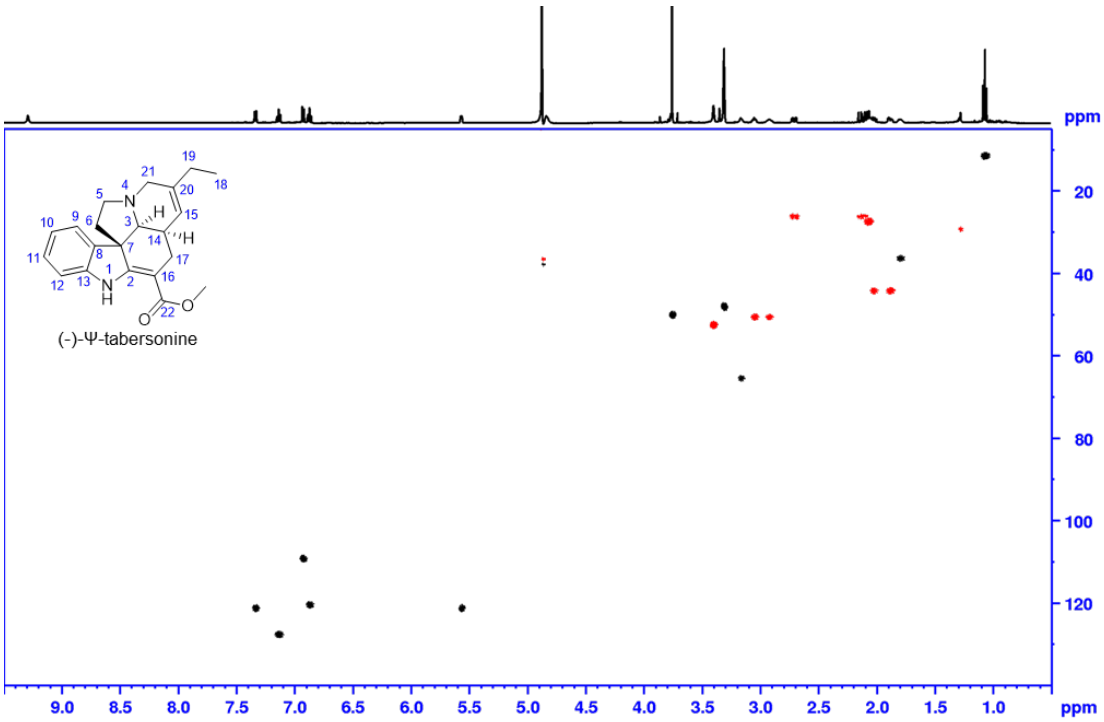


(–)-Ψ-tabersonine (**5a**)
^{1}H-NMR, MeOH-d_3
500 MHz, 25 °C

pos.	δ_H	mult.	J_{HH}	δ_C
1	9.29	*bs*	-	-
2	-	-	-	166.2
3α	3.16	*m*	-	66.4
4	-	-	-	-
5α	2.92	*m*	-	51.6
5β	3.05	*m*	-	51.6
6α	1.88	*ddd*	11.9/5.2/2.0	45.2
6β	2.03	*m*	-	45.2
7	-	-	-	56.8
8	-	-	-	138.1
9	7.34	*bd*	7.4	122.3
10	6.87	*ddd*	7.4/7.3/1.0	121.3
11	7.13	*ddd*	7.7/7.3/1.0	128.5
12	6.92	*bd*	7.7	110.3
13	-	-	-	145.0
14α	1.79	*m*	-	37.3
15	5.57	*m*	-	122.3
16	-	-	-	95.3
17α	2.72	*dd*	15.1/3.3	27.1
17β	2.13	*dd*	15.1/11.6	27.1
18	1.07	*t*	7.5	12.4
19a	2.07	*m*	-	28.4
19b	2.07	*m*	-	28.4
20	-	-	-	139.6
21a	3.40	*m*	-	53.5
21b	3.40	*m*	-	53.5
22	-	-	-	169.3
OMe	3.78	*s*	-	51.0

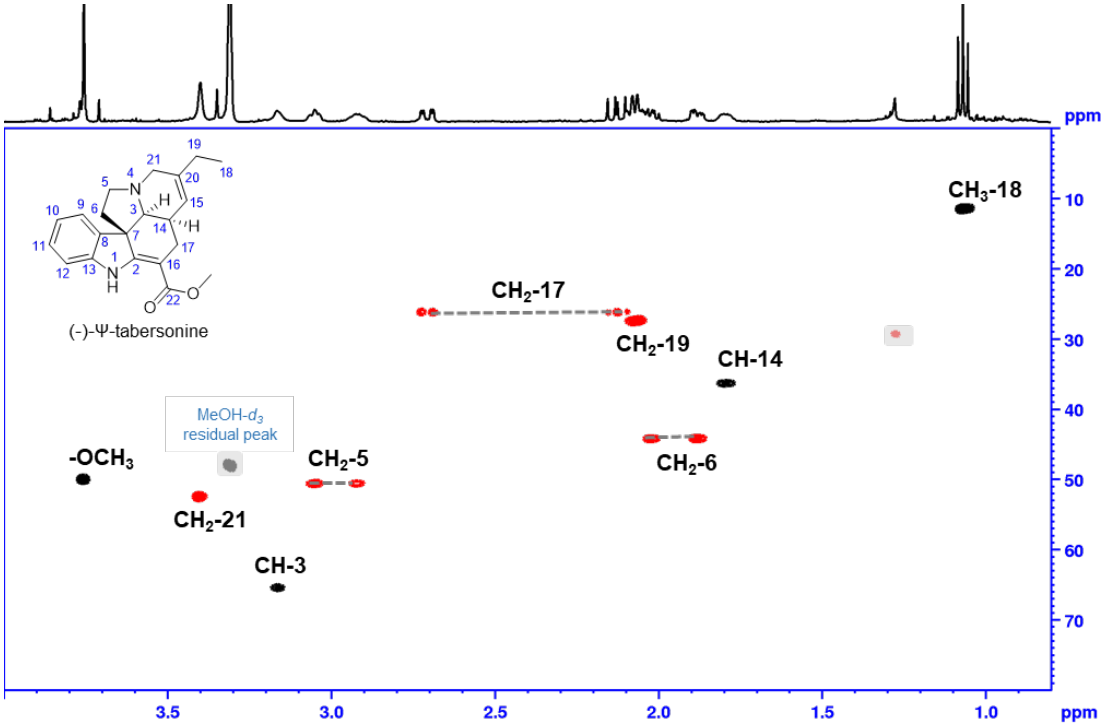
(–)-Ψ-tabersonine (5a): Phase sensitive HSQC, full range in MeOH-d_3

Red: CH_2, black: CH, CH_3

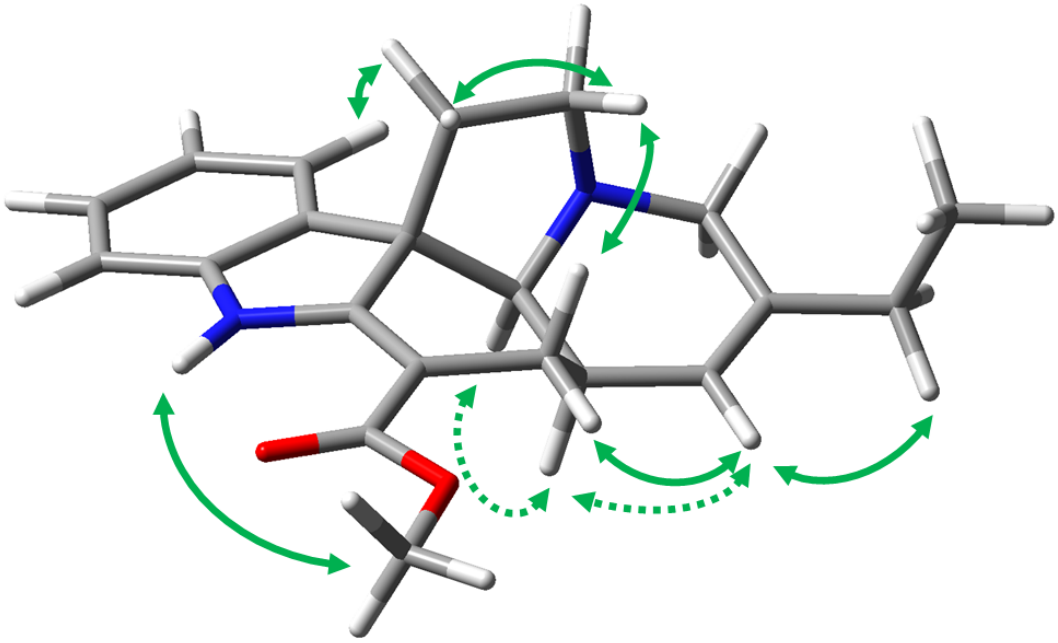


(–)-Ψ-tabersonine (5a): Phase sensitive HSQC, aliphatic range in MeOH-d_3

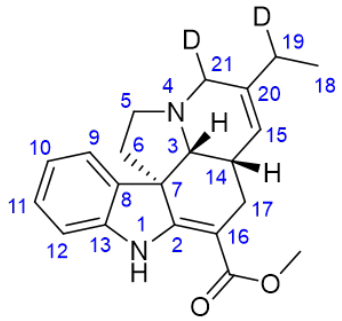
Shaded areas mark impurities and solvent, red: CH_2, black: CH, CH_3



Structure of (–)-Ψ-tabersonine (5a). Structure optimized using Gaussian 16W (PM6, solvent MeOH). Important ROESY correlations in green.



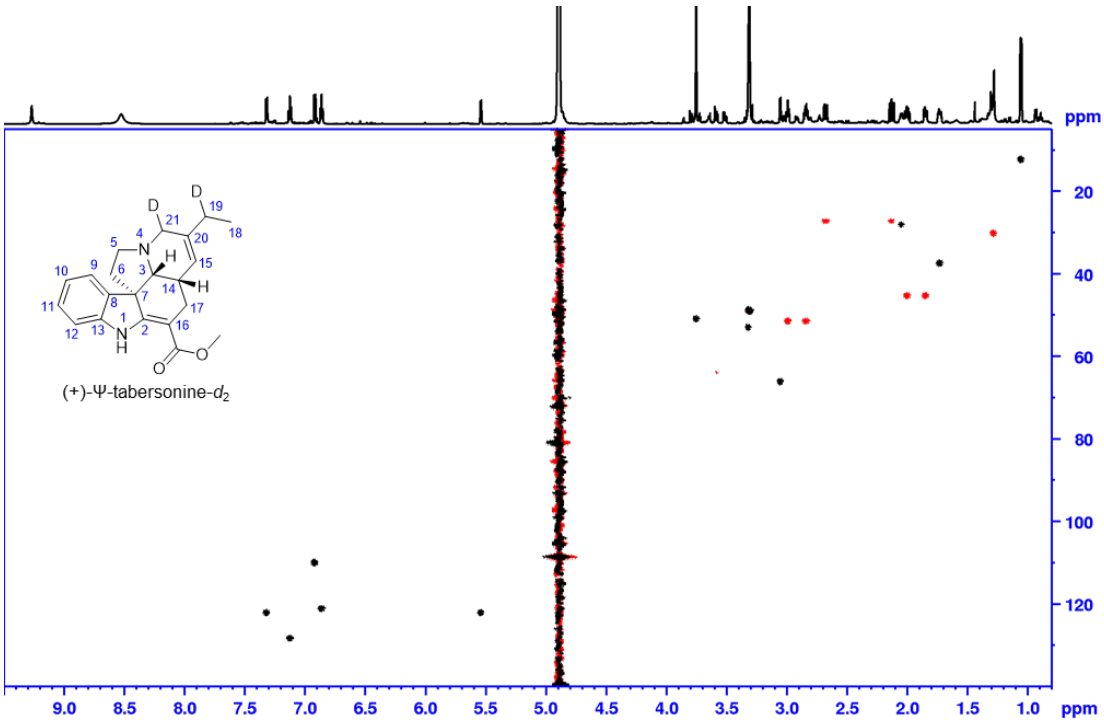
NMR data for (+)-Ψ-tabersonine-d_2 (5-d2) (Enzymatic product, formic acid salt).



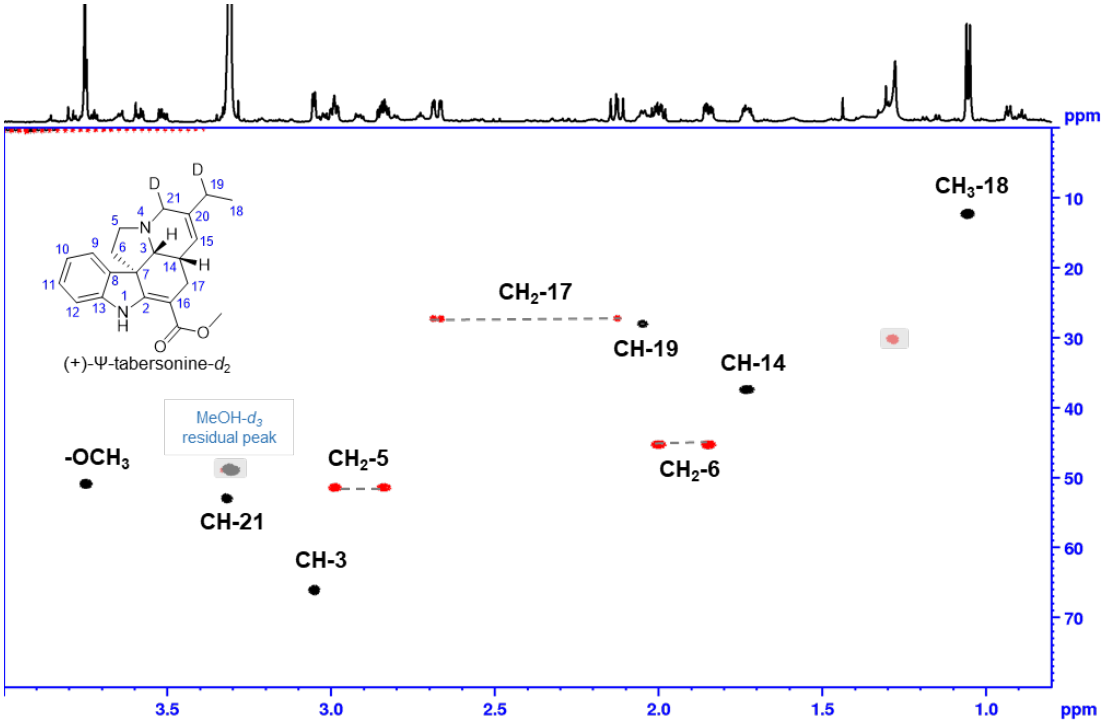
(+)-Ψ-tabersonine-d_2 (**5-d2**)
^{1}H-NMR, MeOH-d_3
700 MHz, 25 °C

pos.	δ_H	mult.	J_{HH}	δ_C
1	9.27	*bs*	-	-
2	-	-	-	166.8
3β	3.05	*m*	-	66.4
4	-	-	-	-
5α	2.99	*ddd*	8.5/6.8/2.0	51.5
5β	2.84	*ddd*	9.8/8.5/5.3	51.5
6α	2.00	*ddd*	11.9/9.8/6.8	45.4
6β	1.85	*ddd*	11.9/5.3/2.0	45.4
7	-	-	-	56.5
8	-	-	-	138.6
9	7.32	*bd*	7.6	122.2
10	6.86	*bdd*	7.6/7.6	121.2
11	7.12	*bdd*	7.8/7.6	128.4
12	6.92	*bd*	7.8	110.1
13	-	-	-	144.8
14α	1.73	*m*	-	37.5
15	5.54	*bd*	4.9	122.2
16	-	-	-	95.3
17α	2.13	*dd*	15.0/11.6	27.3
17β	2.68	*ddd*	15.0/3.6/0.9	27.3
18	1.05	*d*	7.5	12.4
19a*	2.05	*m*	-	28.2
19b	-	-	-	28.2
20	-	-	-	140.0
21a*	3.32	*m***	-	53.1
21b	-	-	-	53.1
22	-	-	-	169.5
OMe	3.75	*s*	-	51.0
*as CH signal				
** overlapped signals J unresolved				

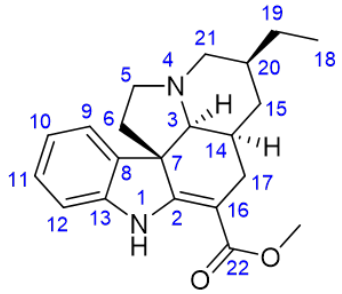
(+)-Ψ-tabersonine-d_2 (5-d2): Phase sensitive HSQC, full range in MeOH-d_3
red: CH_2, black: CH, CH_3



(+)-Ψ-tabersonine-d_2 (5-d2): Phase sensitive HSQC, aliphatic range in MeOH-d_3
Shaded areas mark impurities and solvent, red: CH_2, black: CH, CH_3



NMR data for synthesized (–)-Ψ-vincadifformine (9a) (pseudo-vincadifformine)

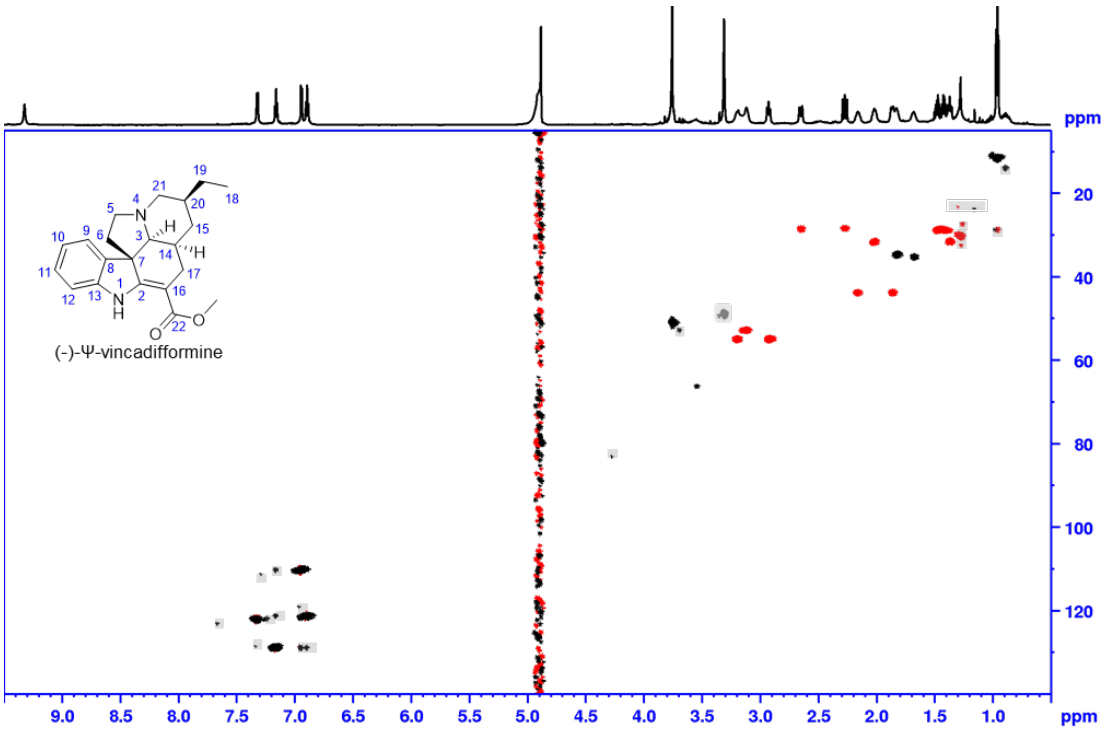


(–)-Ψ-vincadifformine (**9a**)
^{1}H-NMR, MeOH-d_3
700 MHz, 25 °C

pos.	δ_H	mult.	J_{HH}	δ_C
1	9.32	*bs*	-	-
2	-	-	-	164.6
3α	3.55	*m*	-	66.4
4	-	-	-	-
5a	3.13	*m*	-	53.0
5b	3.13	*m*	-	53.0
6α	1.86	*m*	-	44.0
6β	2.16	*m*	-	44.0
7	-	-	-	56.5
8	-	-	-	136.7
9	7.32	*bd*	7.3	122.1
10	6.89	*bdd*	7.7/7.3	121.4
11	7.16	*bdd*	7.8/7.7	129.0
12	6.94	*bd*	7.8	110.4
13	-	-	-	144.7
14α	1.68	*m*	-	35.6
15α	2.02	*m*	-	31.8
15β	1.37	*ddd*	13.8/8.9/4.6	31.8
16	-	-	-	96.2
17α	2.65	*dd*	15.4/3.4	26.9
17β	2.27	*dd*	15.4/12.2	26.9
18	0.96	*t*	7.4	11.8
19a	1.48	*m*	-	29.0
19b	1.42	*m*	-	29.0
20	1.83	*m*	-	35.0
21α	3.20	*m*	-	55.1
21β	2.93	*dd*	9.9/9.4	55.1
22	-	-	-	169.9
OMe	3.78	*s*	-	51.1

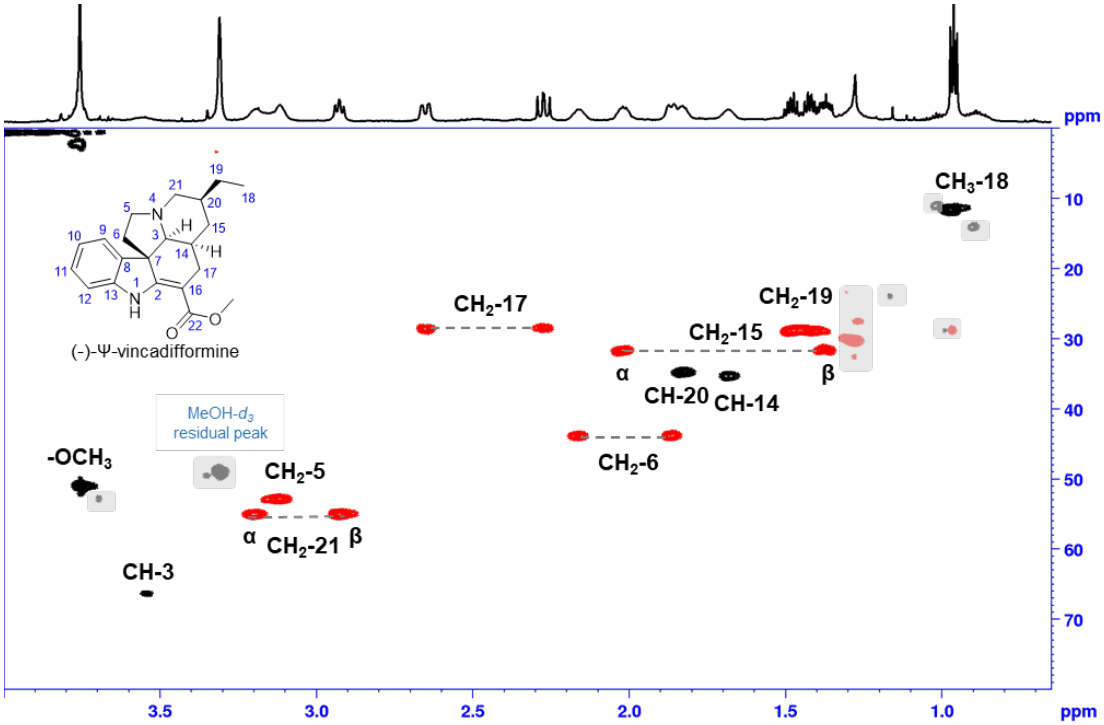
(–)-Ψ-vincadifformine (9a): Phase sensitive HSQC, full range in MeOH-d_3

Shaded areas mark impurities and solvent, red: CH_2, black: CH, CH_3

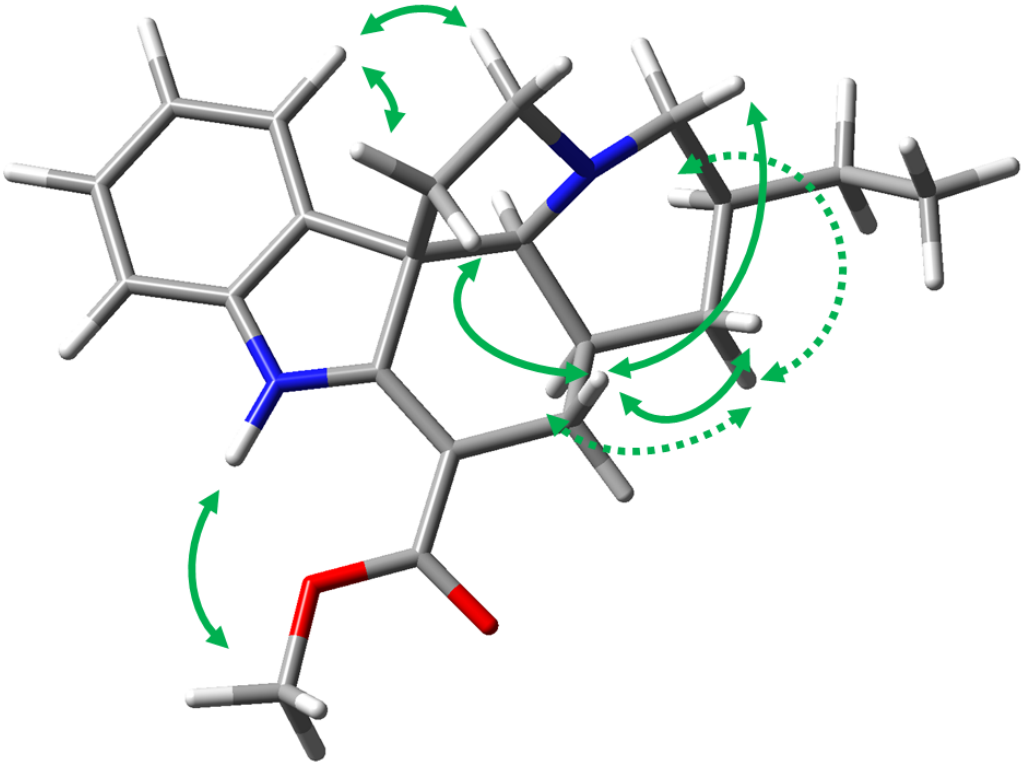


(–)-Ψ-vincadifformine (9a): Phase sensitive HSQC, aliphatic range in MeOH-d_3

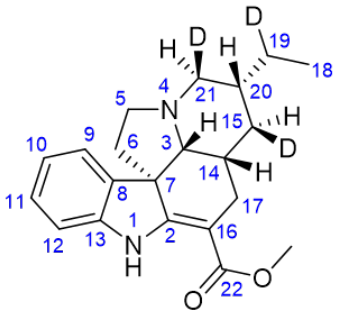
Shaded areas mark impurities and solvent, red: CH_2, black: CH, CH_3



Structure of (–)-Ψ-vincadifformine (9a). Structure optimized using Gaussian 16W (PM6, solvent MeOH). Important ROESY correlations in green.



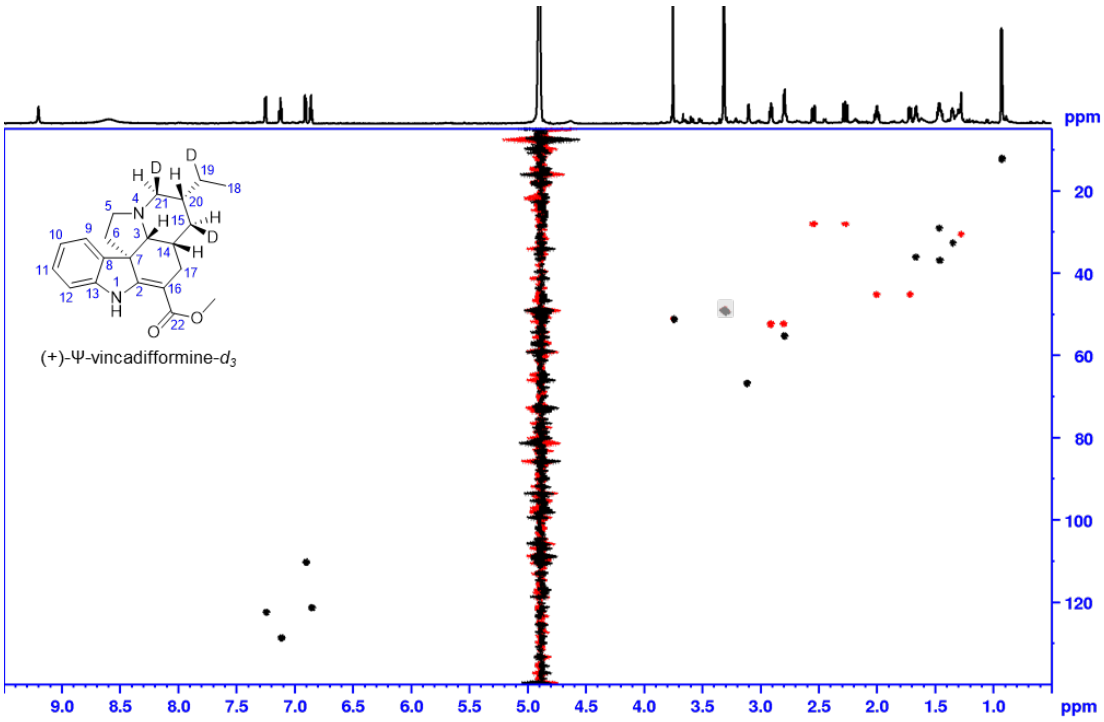
NMR data for (+)-Ψ-vincadifformine-d_3 (9-d3) (pseudo-vincadifformine-d_3) (Enzymatic product, formic acid salt).



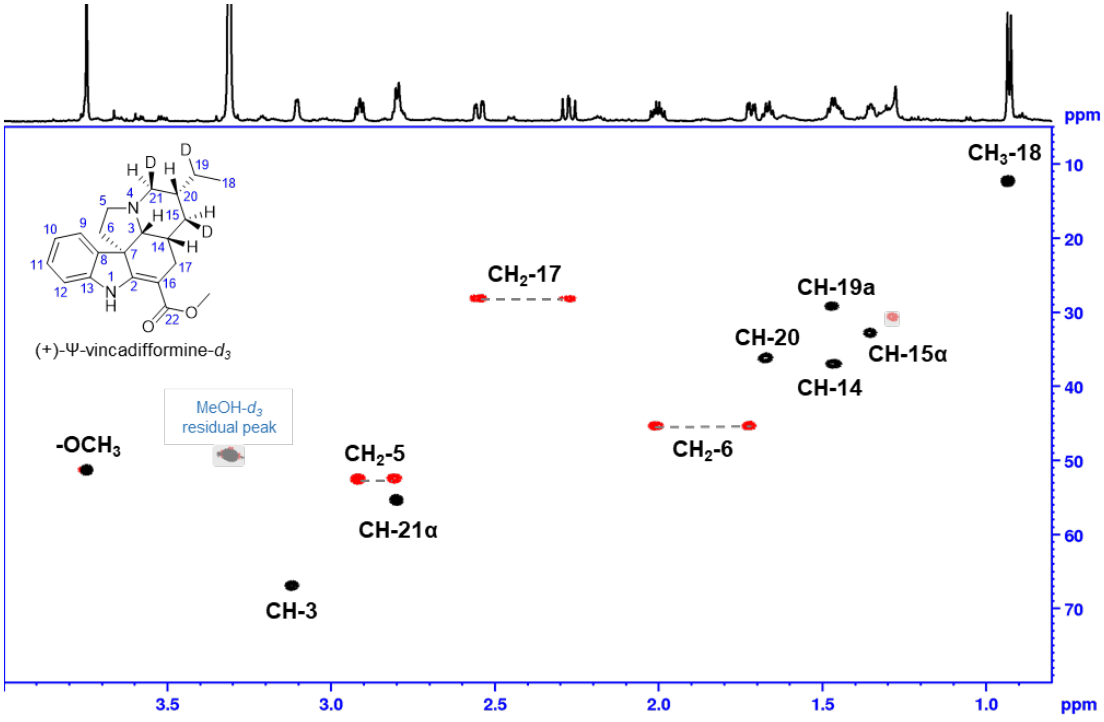
(+)-Ψ-vincadifformine-d_3 (**9-d3**)
^{1}H-NMR, MeOH-d_3
700 MHz, 25 °C

pos.	δ_H	mult.	J_{HH}	δ_C
1	9.20	*bs*	-	-
2	-	-	-	166.7
3β	3.12	*bd*	3.8	66.9
4	-	-	-	-
5a	2.92	*m*	-	52.6
5b	2.81	*m***	-	52.6
6α	2.00	*ddd*	11.2/11.2/6.3	45.4
6β	1.72	*bdd*	11.2/4.6	45.4
7	-	-	-	56.9
8	-	-	-	138.6
9	7.25	*bd*	7.4	122.5
10	6.86	*bdd*	7.5/7.4	121.4
11	7.12	*bdd*	7.8/7.5	128.8
12	6.91	*bd*	7.8	110.4
13	-	-	-	145.1
14β	1.46	*m*	-	37.1
15α*	1.35	*m*	-	32.8
15β	-	-	-	32.8
16	-	-	-	96.3
17α	2.28	*dd*	14.7/11.8	28.2
17β	2.55	*ddd*	14.7/3.5/0.8	28.2
18	0.93	*d*	7.4	12.3
19a*	1.47	*m*	-	29.2
19b	-	-	-	29.2
20	1.67	*ddd*	7.3/7.3/7.3	36.2
21α*	2.80	*m***	-	55.3
21β	-	-	-	55.3
22	-	-	-	169.8
OMe	3.75	*s*	-	51.3
*as CH signal				
** overlapped signals J unresolved				

(+)-Ψ-vincadifformine-d_3 (9-d3): Phase sensitive HSQC, full range in MeOH-d_3 Shaded areas mark impurities and solvent, red: CH_2, black: CH, CH_3

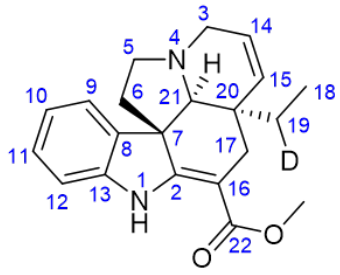


(+)-Ψ-vincadifformine-d_3 (9-d3): Phase sensitive HSQC, aliphatic range in MeOH-d_3 Shaded areas mark impurities and solvent, red: CH_2, black: CH, CH_3



NMR data for (–)-tabersonine-*d* (2-d)

(Enzymatic product, formic acid salt).



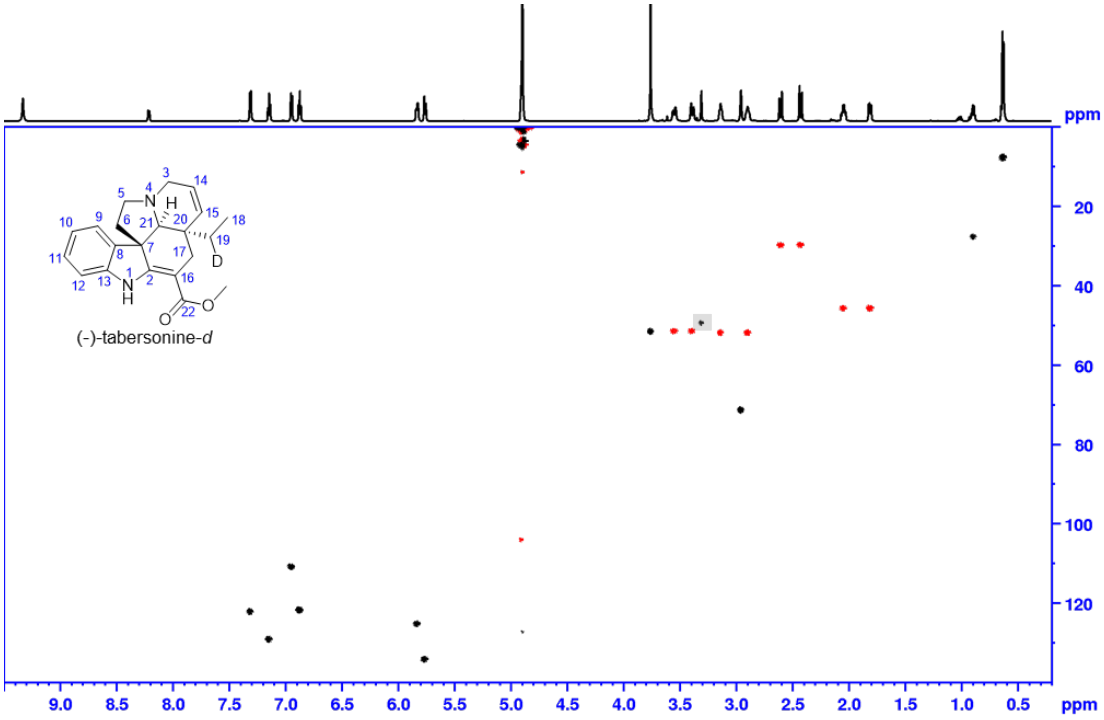
(–)-tabersonine-*d* (**2-d**)

^{1}H-NMR, MeOH-d_3
700 MHz, 25 °C

pos.	δ_H	mult.	J_{HH}	δ_C
1	9.33	*bs*	-	-
2	-	-	-	167.1
3α	3.39	*bd*	15.6	51.2
3β	3.55	*bdd*	15.6/3.8	51.2
4	-	-	-	-
5α	2.90	*m*	-	51.7
5β	3.14	*m*	-	51.7
6α	1.81	*dd*	11.6/4.5	45.5
6β	2.05	*ddd*	11.6/11.6/6.3	45.5
7	-	-	-	56.2
8	-	-	-	138.2
9	7.31	*bd*	7.4	122.1
10	6.87	*bdd*	7.6/7.4	121.7
11	7.15	*bdd*	7.7/7.6	129.1
12	6.95	*bd*	7.7	110.8
13	-	-	-	144.8
14	5.83	*bdd*	9.8/3.8	125.1
15	5.76	*bd*	9.8	134.1
16	-	-	-	92.5
17α	2.61	*bd*	15.4	29.6
17β	2.43	*dd*	15.4	29.6
18	0.63	*d*	7.4	7.6
19a*	0.90	*q*	7.4	27.5
19b	-	-	-	27.5
20	-	-	-	42.2
21α	2.96	*bs*	-	71.3
22	-	-	-	170.0
OMe	3.76	*s*	-	51.4
*as CH signal				

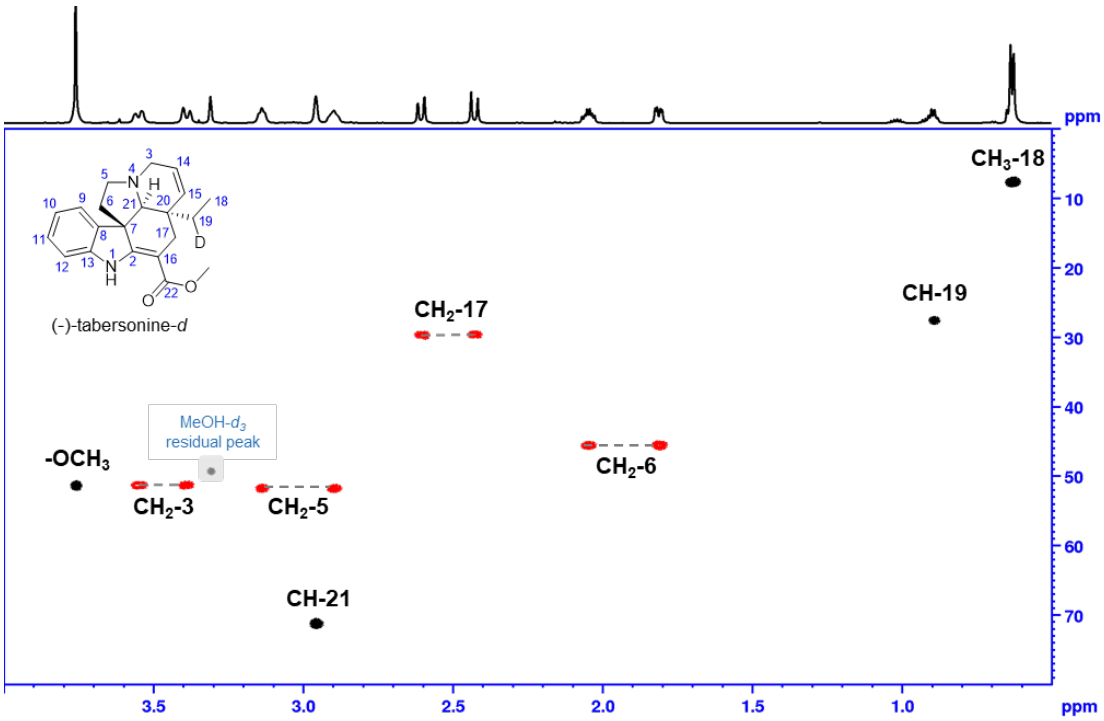
(–)-tabersonine-*d* (2-d): Phase sensitive HSQC, full range in MeOH-d_3

Shaded areas mark impurities and solvent, red: CH_2, black: CH, CH_3



(–)-tabersonine-*d* (2-d): Phase sensitive HSQC, aliphatic range in MeOH-d_3

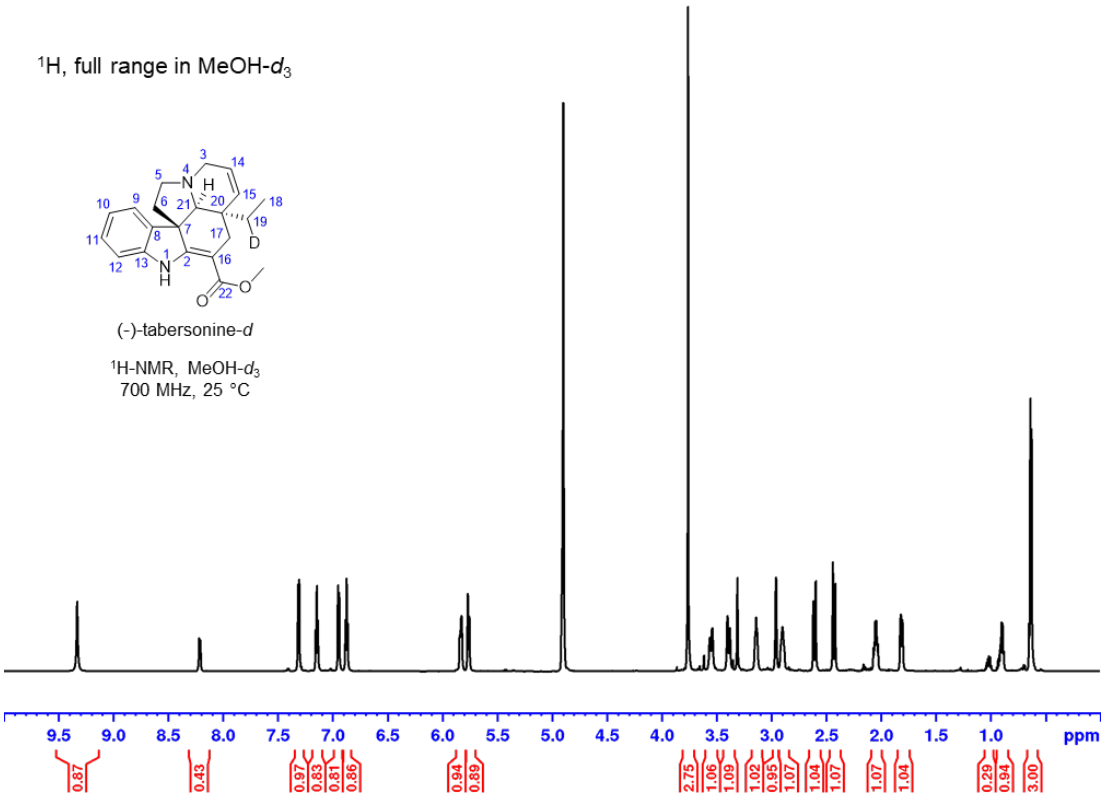
Shaded areas mark impurities and solvent, red: CH_2, black: CH, CH_3



^{1}H, full range in MeOH-d_3

(-)-tabersonine-*d*

^{1}H-NMR, MeOH-d_3
700 MHz, 25 °C

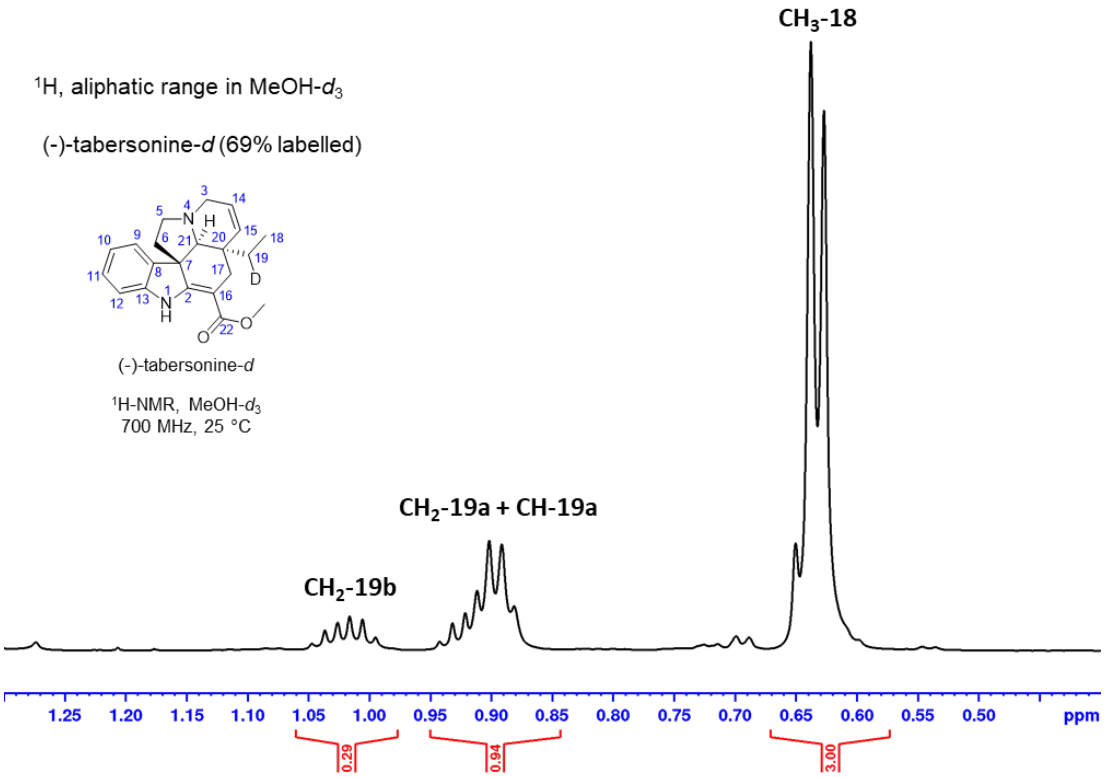


^{1}H, aliphatic range in MeOH-d_3

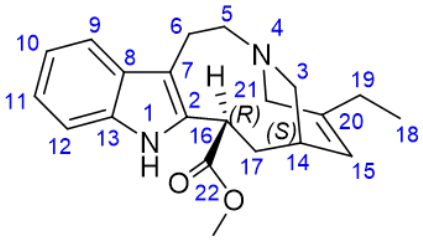
(-)-tabersonine-*d* (69% labelled)

(-)-tabersonine-*d*

^{1}H-NMR, MeOH-d_3
700 MHz, 25 °C



NMR data for (–)-16(*R*)-carbomethoxycleavamine (10).

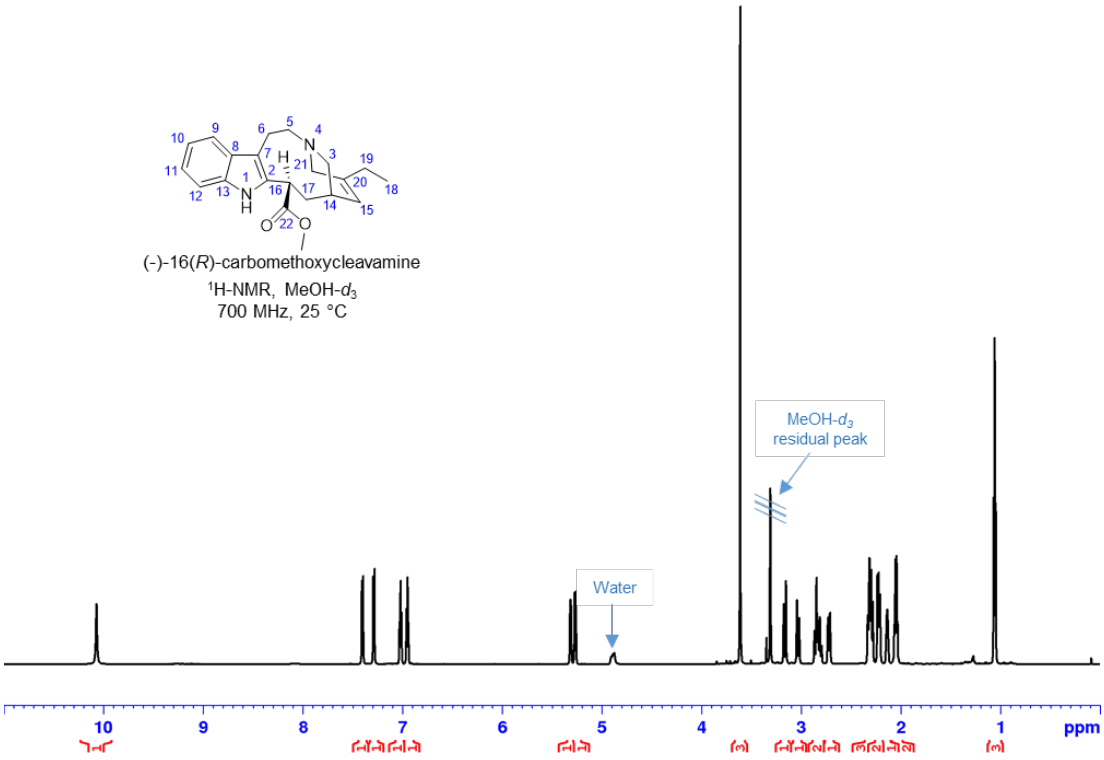


(–)-16(*R*)-carbomethoxycleavamine (**10**)
^{1}H-NMR, MeOH-d_3
700 MHz, 25 °C

pos.	δ_H	mult.	J_{HH}	δ_C
1	10.1	*bs*	-	-
2	-	-	-	135.1
3a	2.33	*m***	-	53.4
3b	2.22	*m***	-	53.4
4	-	-	-	-
5a	2.72	*ddd*	13.3/2.9/2.9	53.1
5b	2.30	*m***	-	53.1
6a	2.85	*m***	-	26.0
6b	2.82	*m***	-	26.0
7	-	-	-	110.5
8	-	-	-	127.6
9	7.4	*bd*	7.8	117.3
10	6.95	*bdd*	7.8/7.6	118.0
11	7.02	*bdd*	7.8/7.6	120.6
12	7.29	*bd*	7.8	110.3
13	-	-	-	136.4
14	2.14	*bs*	-	34.6
15	5.31	*d*	4.1	121.9
16	5.27	*d*	10.1	38.5
17a	2.30	*m***	-	36.5
17b	2.23	*m***	-	36.5
18	1.06	*t*	7.4	11.7
19a	2.05	*q*	7.4	27.3
19b	2.05	*q*	7.4	27.3
20	-	-	-	141.3
21a	3.16	*d*	15.4	54.8
21b	3.03	*d*	15.4	54.8
22	-	-	-	175.1
OMe	3.61	*s*	-	50.8
** overlapped signals J unresolved				

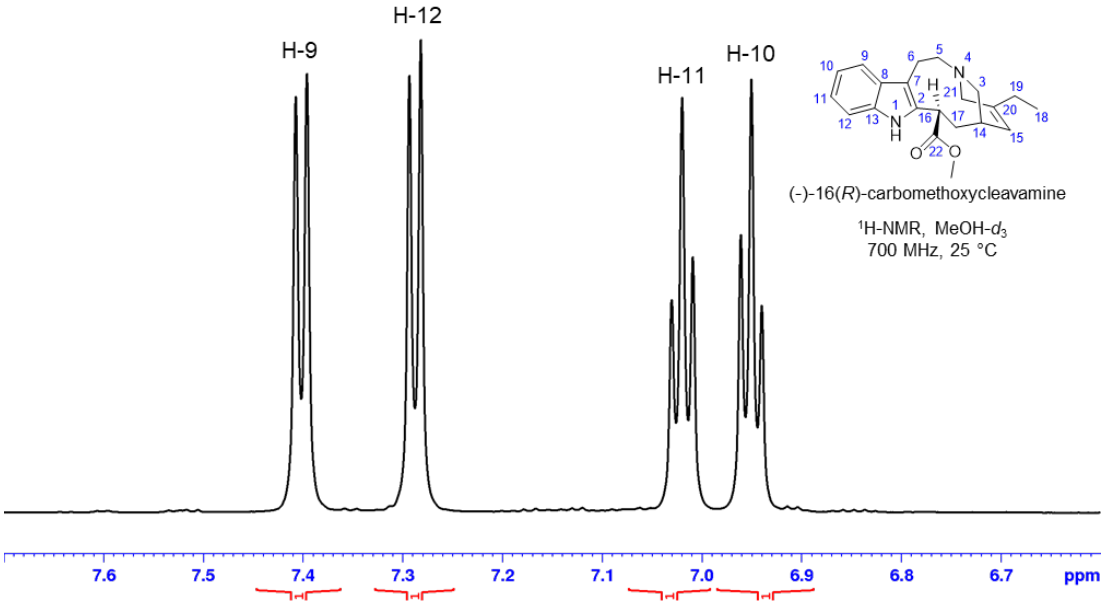
(–)-16(*R*)-carbomethoxycleavamine (10):

^{1}H NMR with water suppression (zgpr) full range in MeOH-d_3



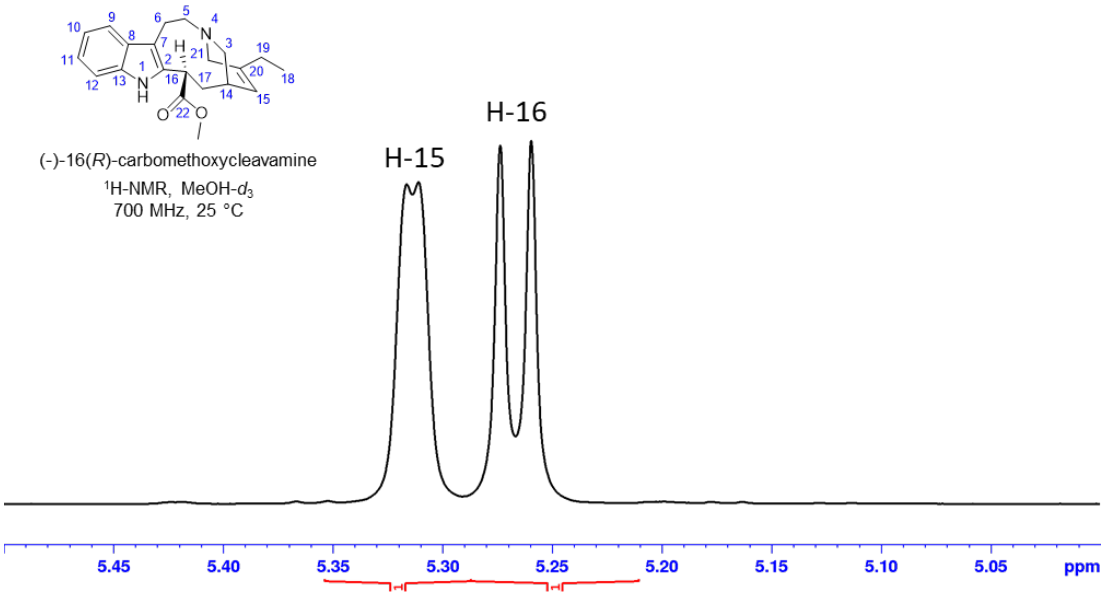
(–)-16(*R*)-carbomethoxycleavamine (10):

^{1}H NMR with water suppression (zgpr) aromatic range in MeOH-d_3



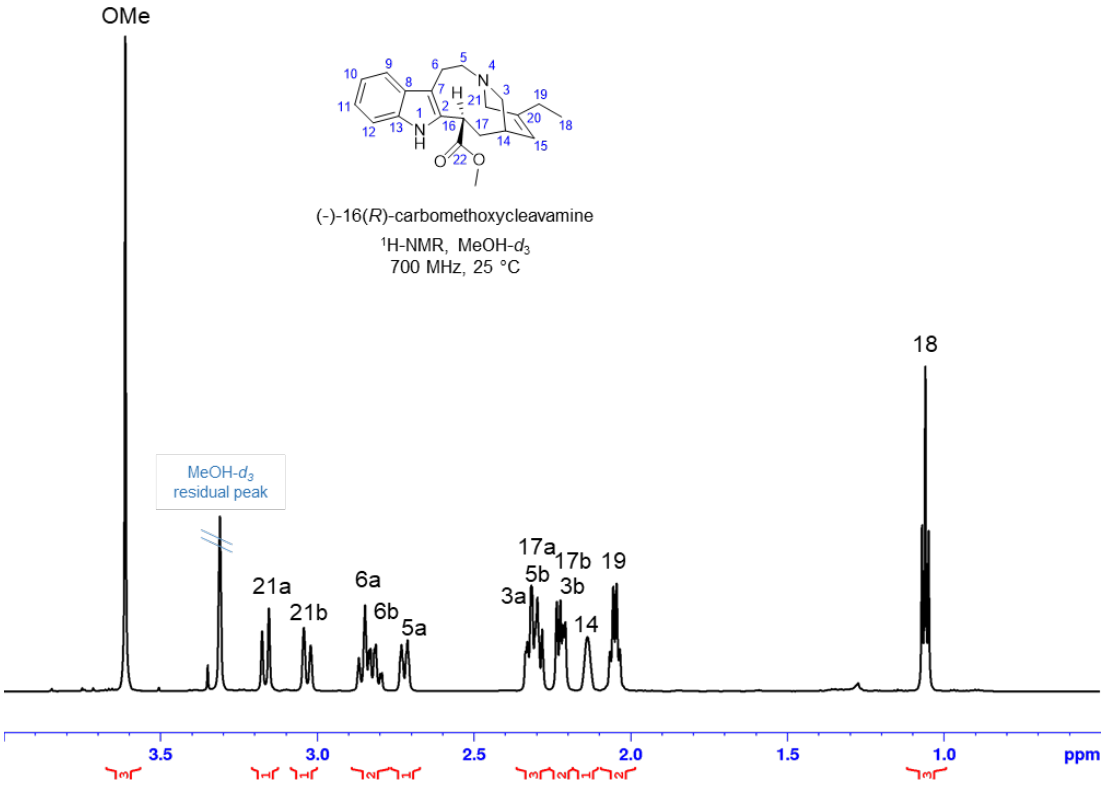
(–)-16(*R*)-carbomethoxycleavamine (10):

^{1}H NMR with water suppression (zgpr) 5.0-5.5 ppm in MeOH-d_3



(–)-16(*R*)-carbomethoxycleavamine (10):

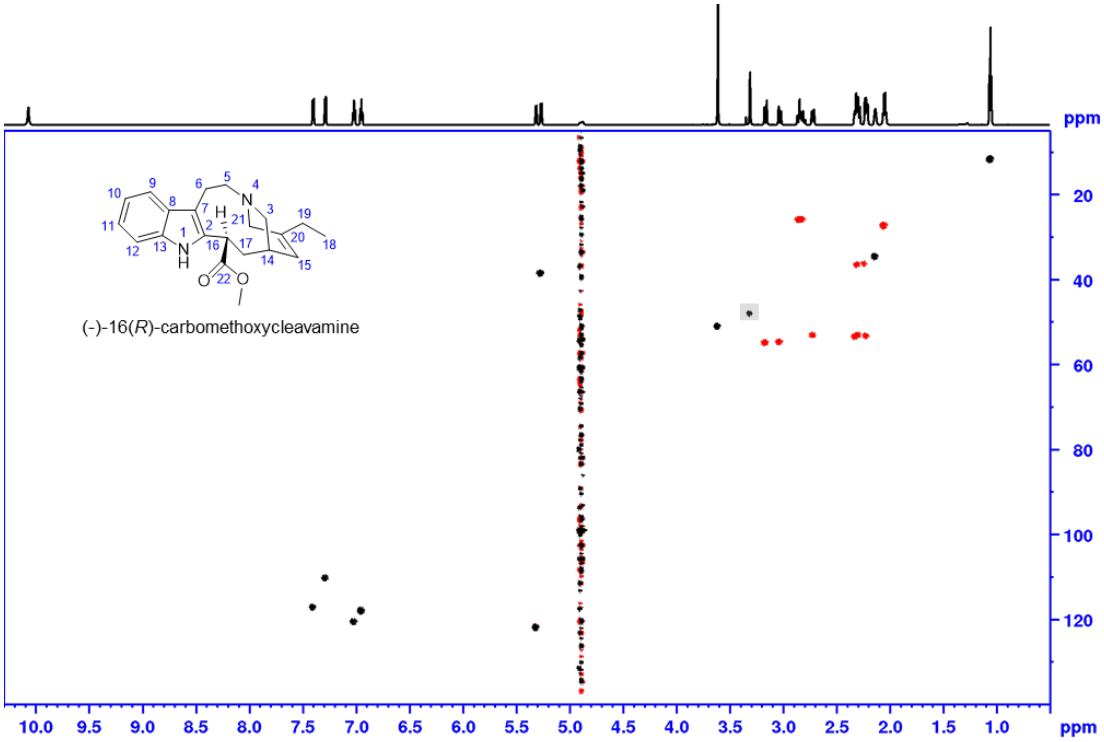
^{1}H NMR with water suppression (zgpr) aliphatic range in MeOH-d_3



(–)-16(*R*)-carbomethoxycleavamine (10):

Phase sensitive HSQC, full range in MeOH-d_3

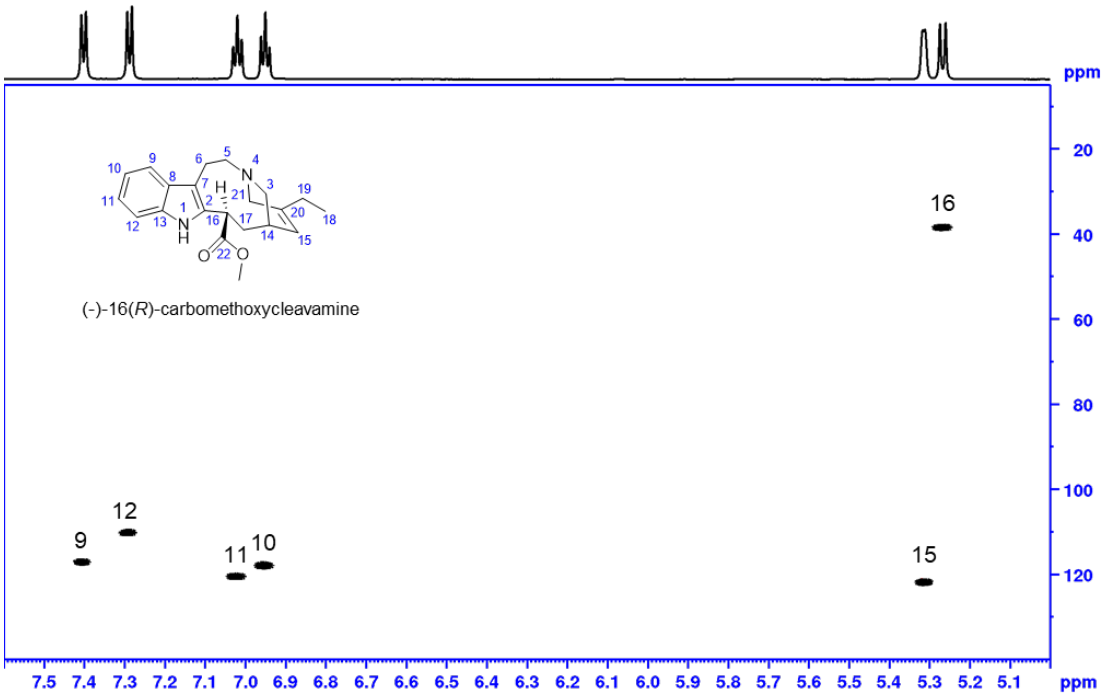
Shaded areas mark impurities and solvent, red: CH_2, black: CH, CH_3



(–)-16(*R*)-carbomethoxycleavamine (10):

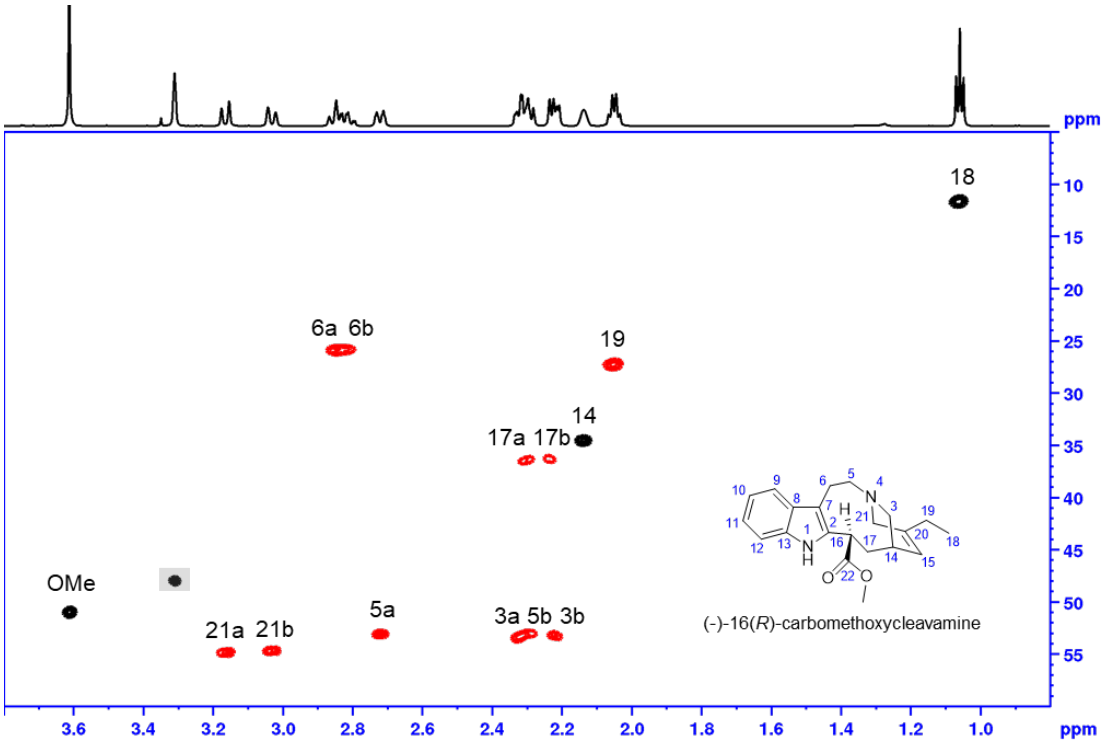
Phase sensitive HSQC, aliphatic range in MeOH-d_3

black: CH, CH_3



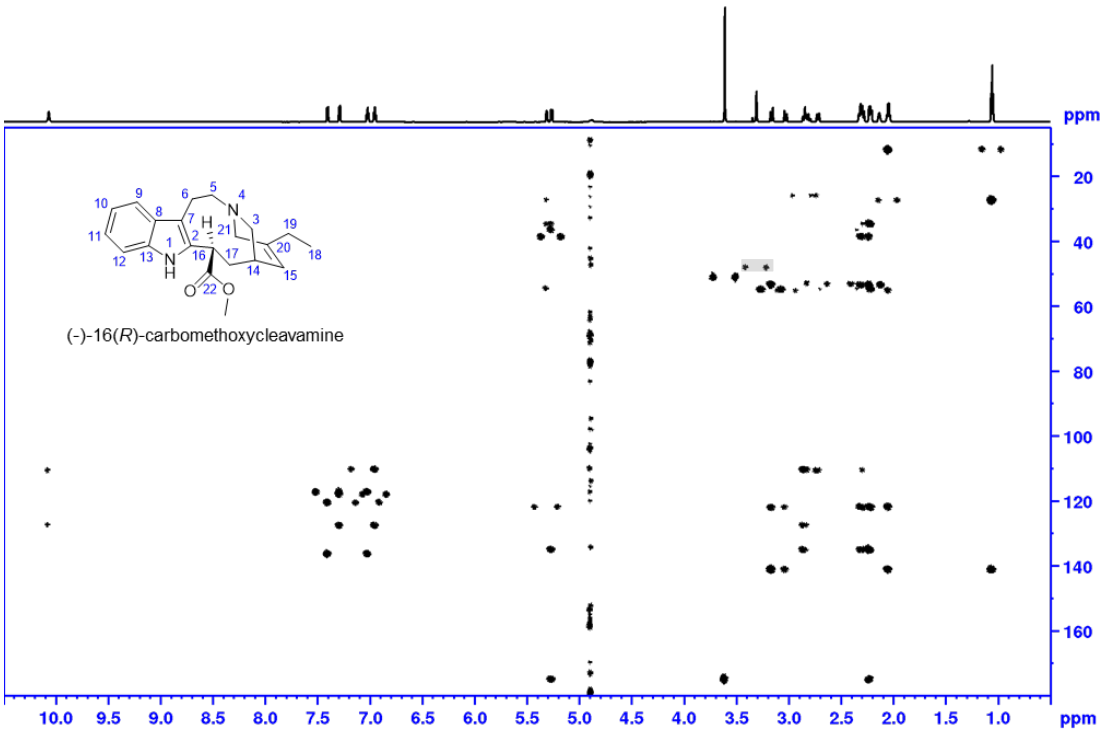
(–)-16(*R*)-carbomethoxycleavamine (10): Phase sensitive HSQC.

Aaliphatic range in MeOH-d_3 Shaded areas mark impurities and solvent, red: CH_2, black: CH, CH_3



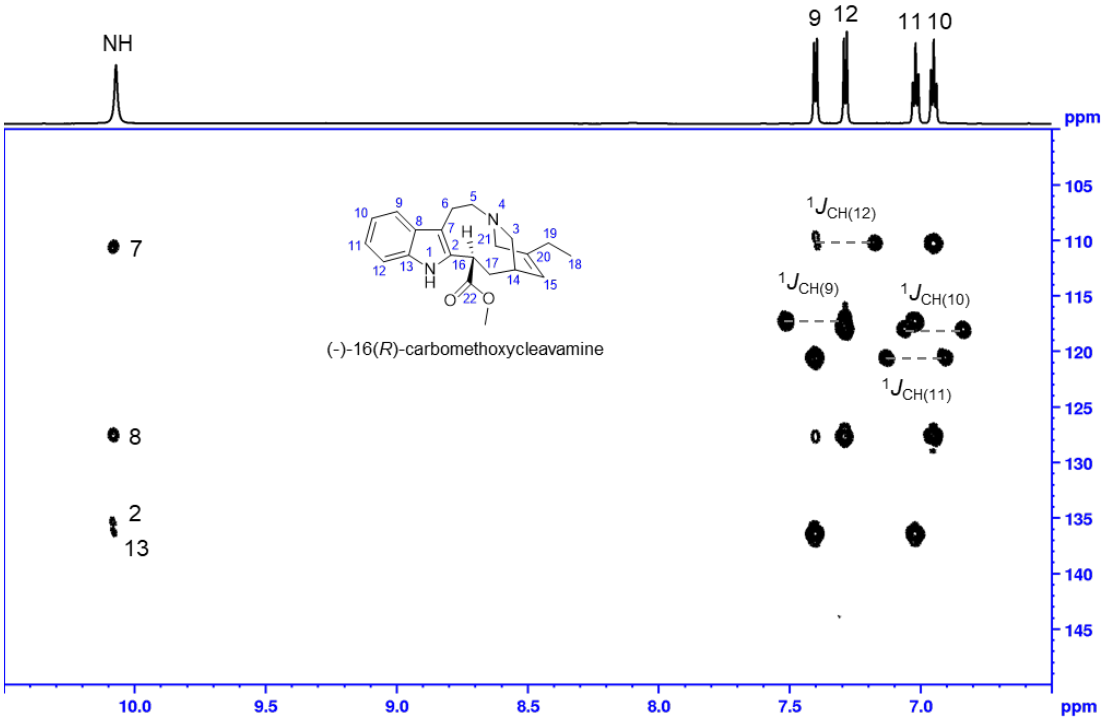
(–)-16(*R*)-carbomethoxycleavamine (10): HMBC, full range in MeOH-d_3

Shaded areas mark impurities and solvent



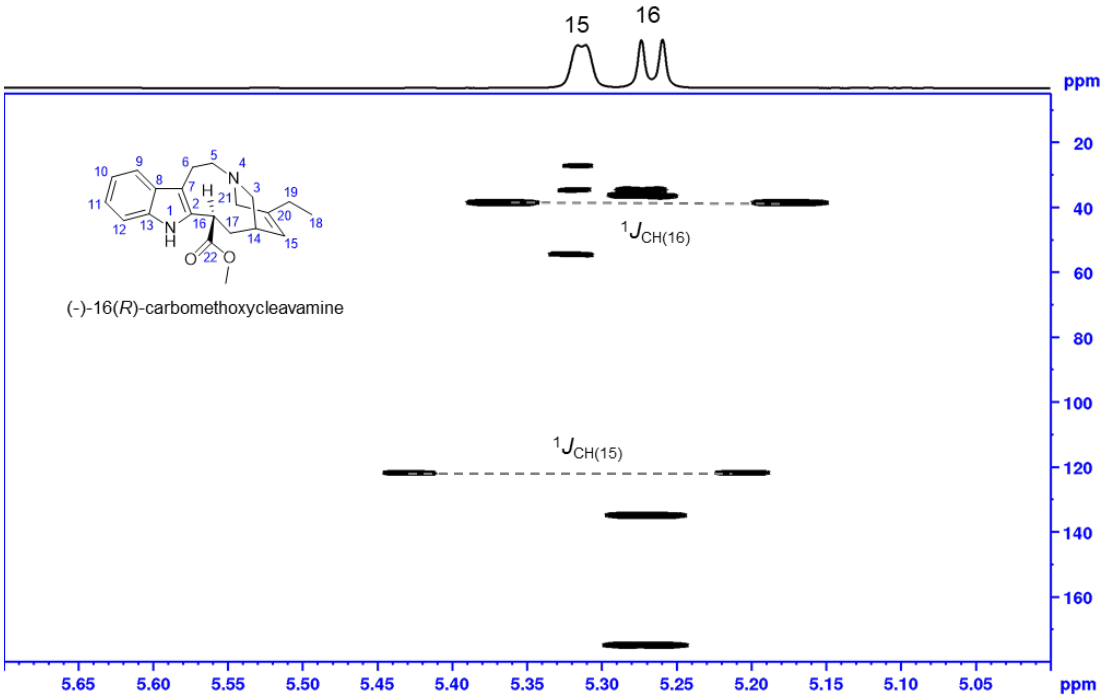
(–)-16(*R*)-carbomethoxycleavamine (10): HMBC. aromatic

Aromatic range in MeOH-d_3 Shaded areas mark impurities and solvent



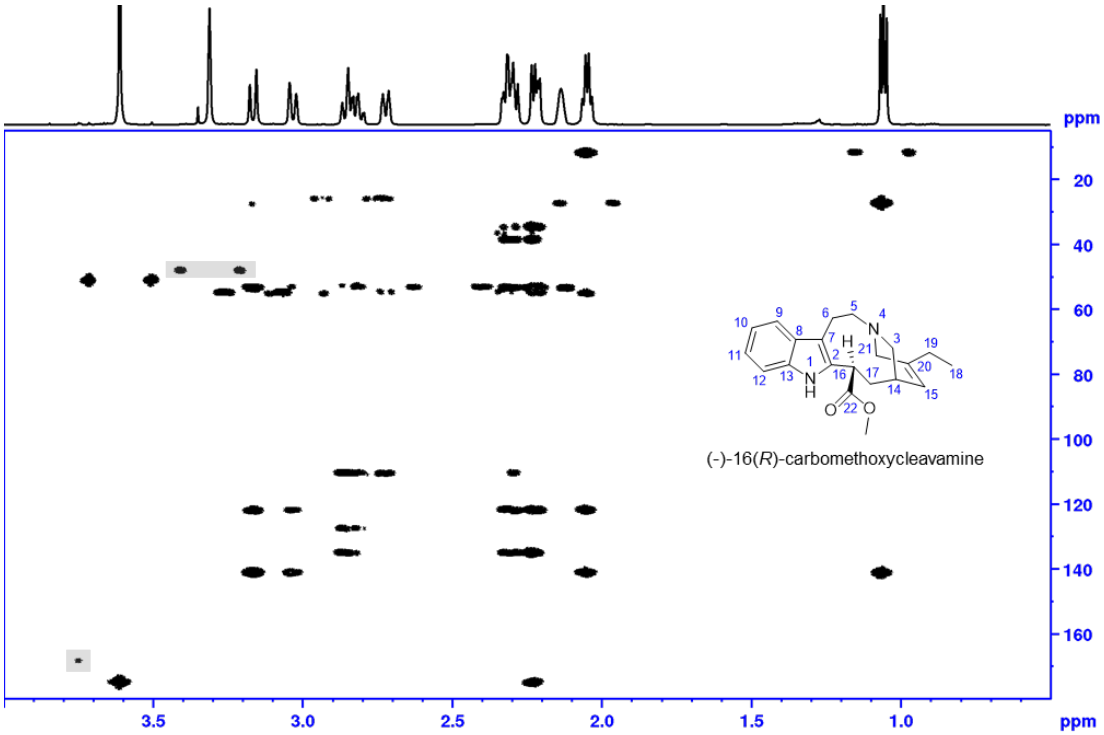
(–)-16(*R*)-carbomethoxycleavamine (10): HMBC.

In MeOH-d_3 5.0-5.7 ppm in MeOH-d_3



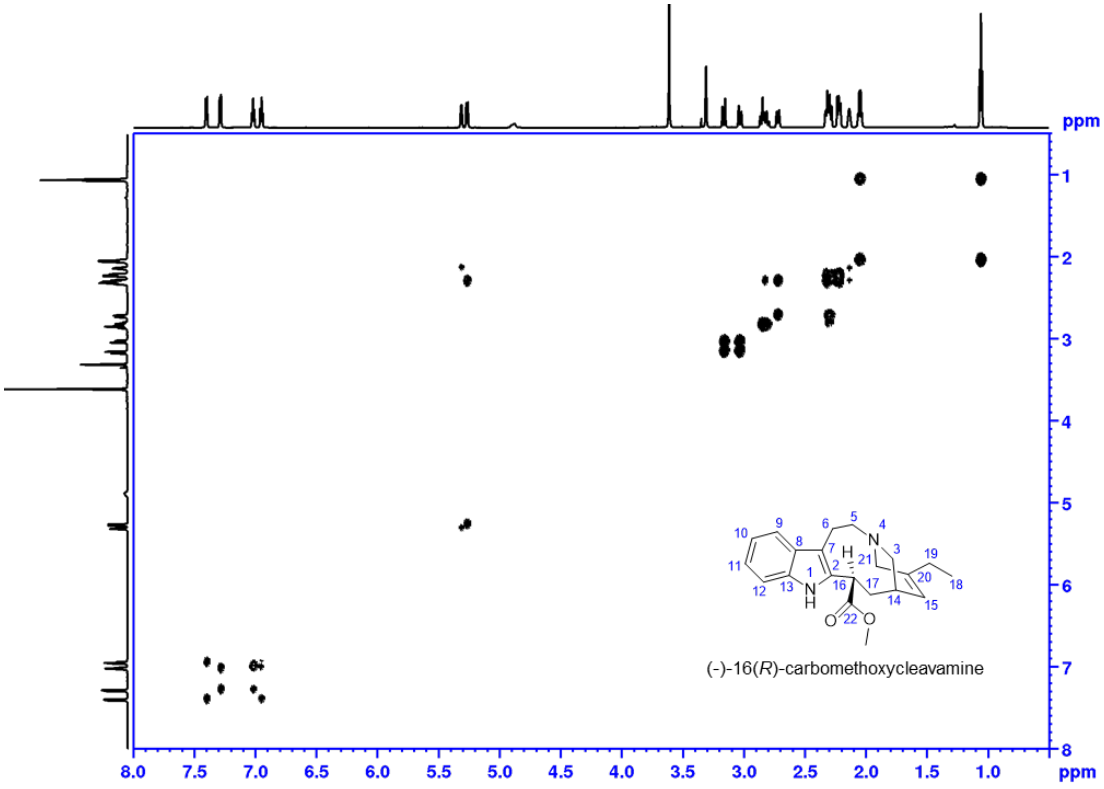
(–)-16(*R*)-carbomethoxycleavamine (10): HMBC. aliphatic

Aliphatic range in MeOH-d_3 Shaded areas mark impurities and solvent



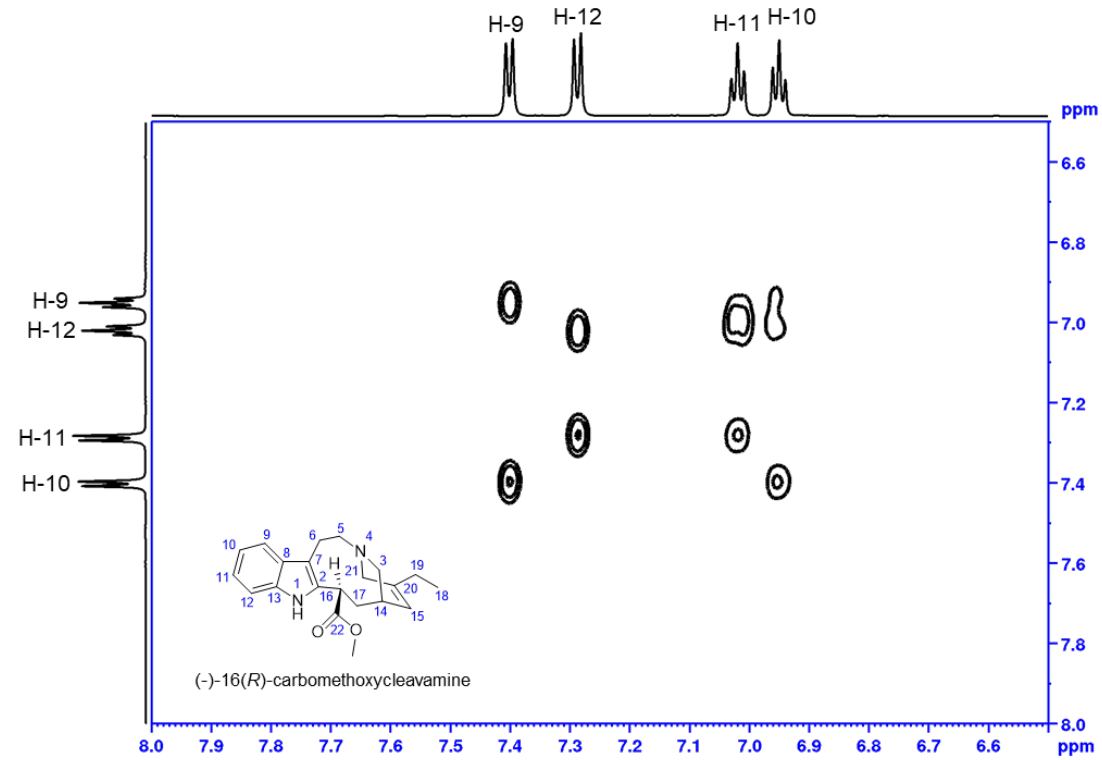
(–)-16(R)-carbomethoxycleavamine (10) 1H-1H DQF COSY full

^{1}H-^{1}H DQF COSY with water suppression, full range in MeOH-d_3

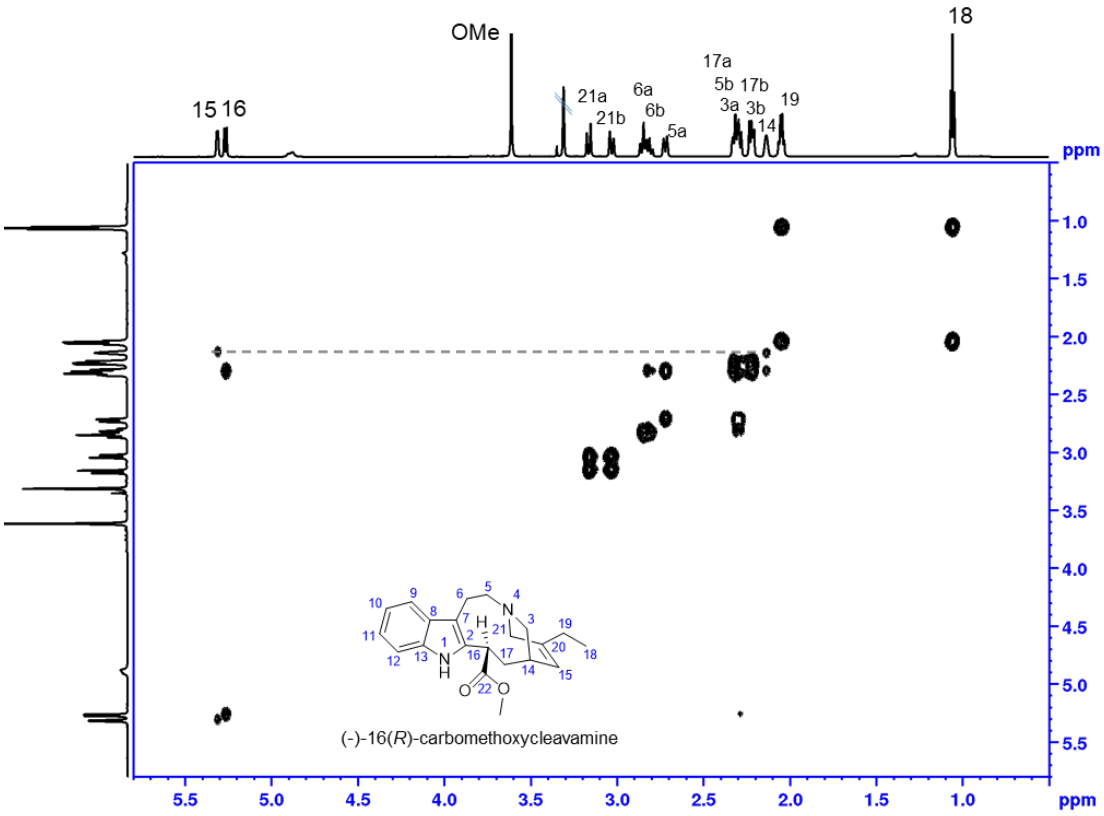


(–)-16(*R*)-carbomethoxycleavamine (10) ^{1}H-^{1}H DQF COSY aromatic

^{1}H-^{1}H DQF COSY with water suppression, aromatic range in MeOH-d_3

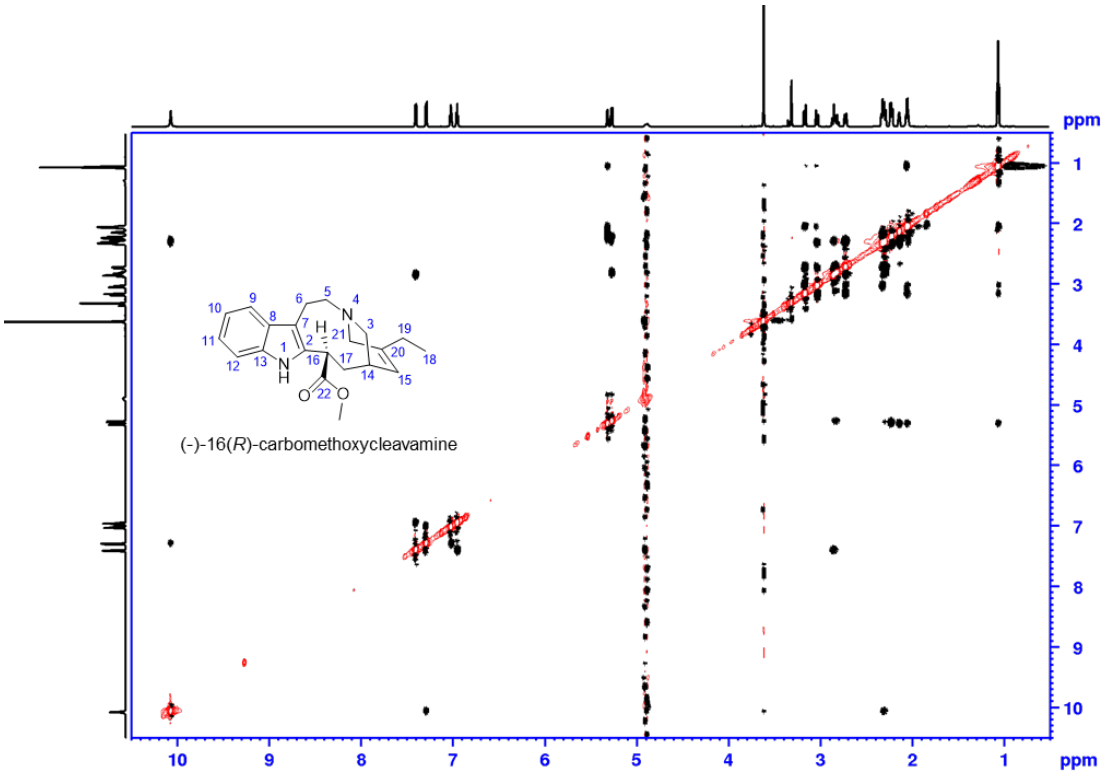


^{1}H-^{1}H DQF COSY with water suppression, aliphatic range in MeOH-d_3



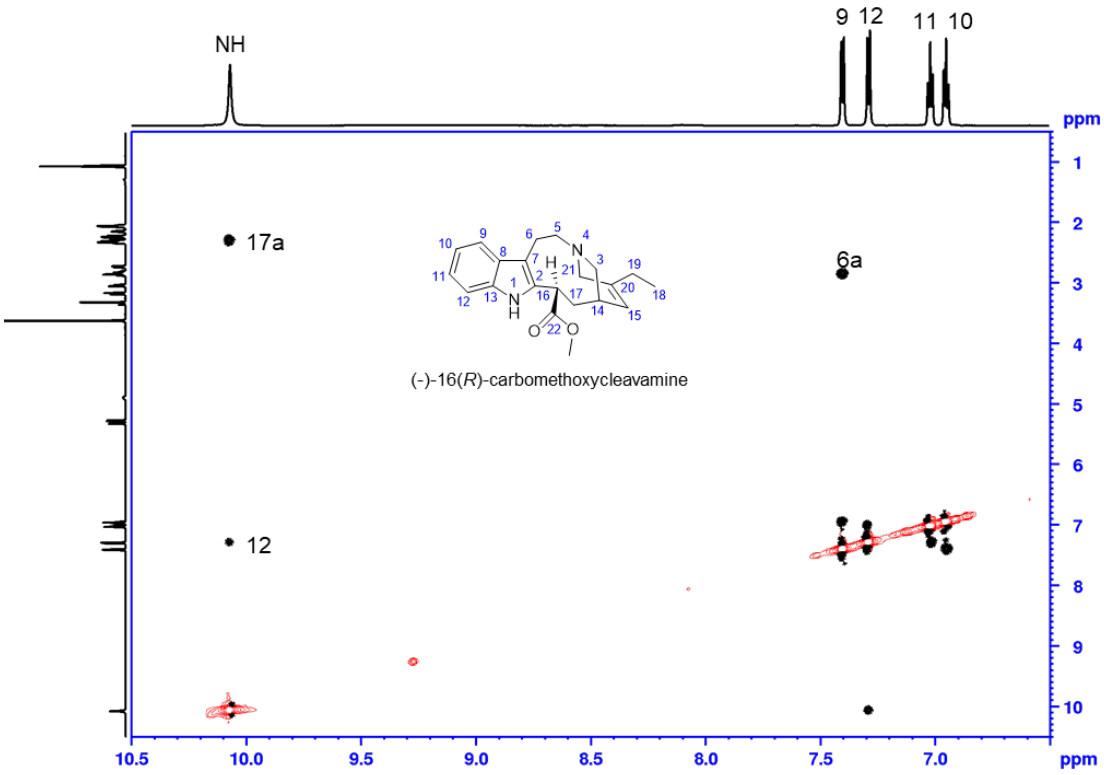
(–)-16(*R*)-carbomethoxycleavamine (10): ^{1}H-^{1}H ROESY full

^{1}H-^{1}H ROESY with water suppression, full range in MeOH-d_3



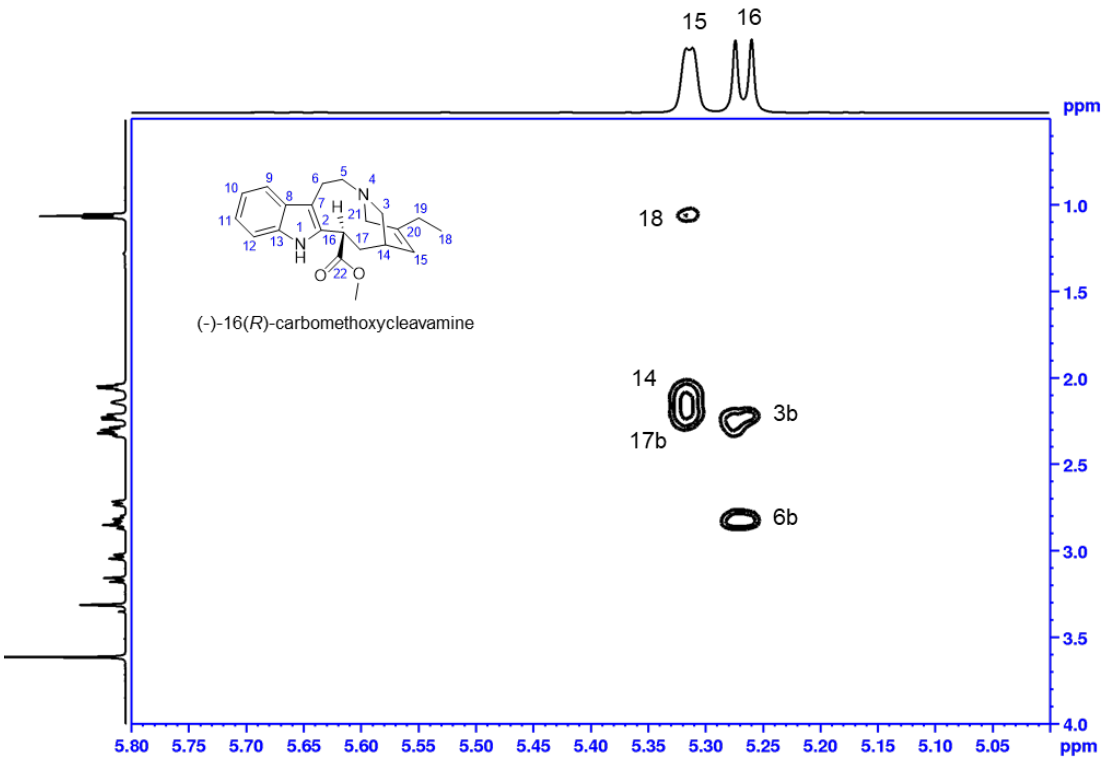
(–)-16(*R*)-carbomethoxycleavamine (10): ^{1}H-^{1}H ROESY aromatic

^{1}H-^{1}H ROESY with water suppression, aromatic range in MeOH-d_3



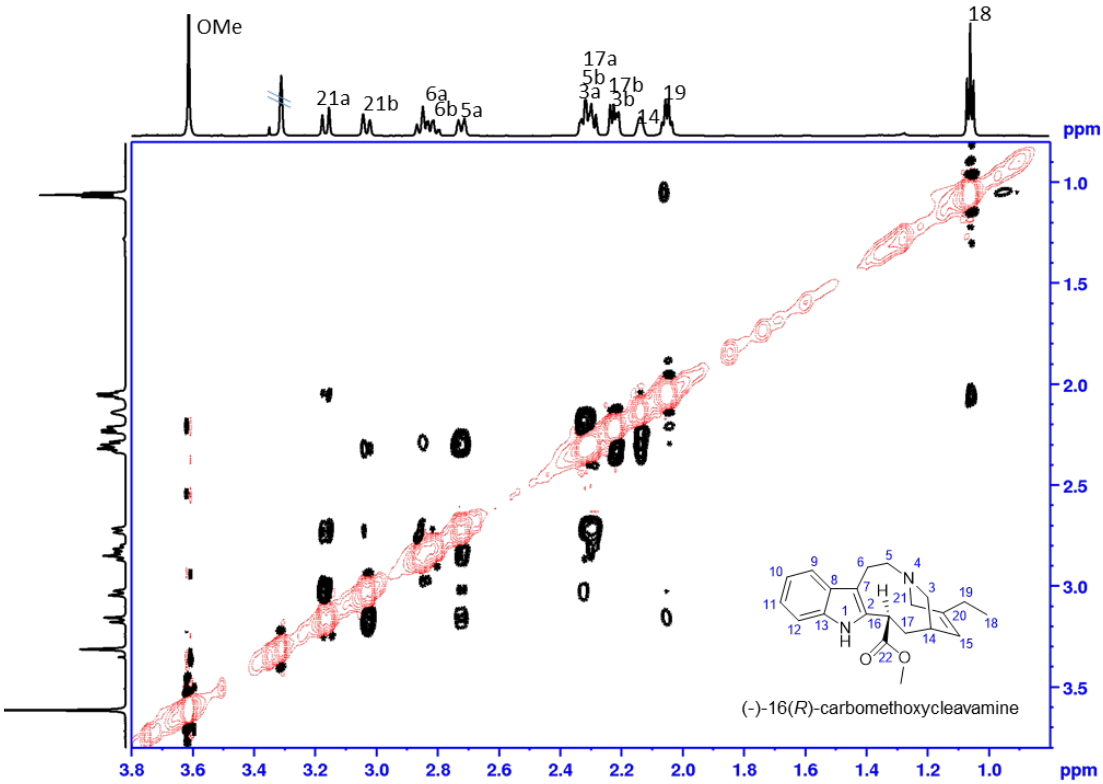
(–)-16(*R*)-carbomethoxycleavamine (10): ^{1}H-^{1}H ROESY

^{1}H-^{1}H ROESY with water suppression, 5.0-5.8 ppm, in MeOH-d_3



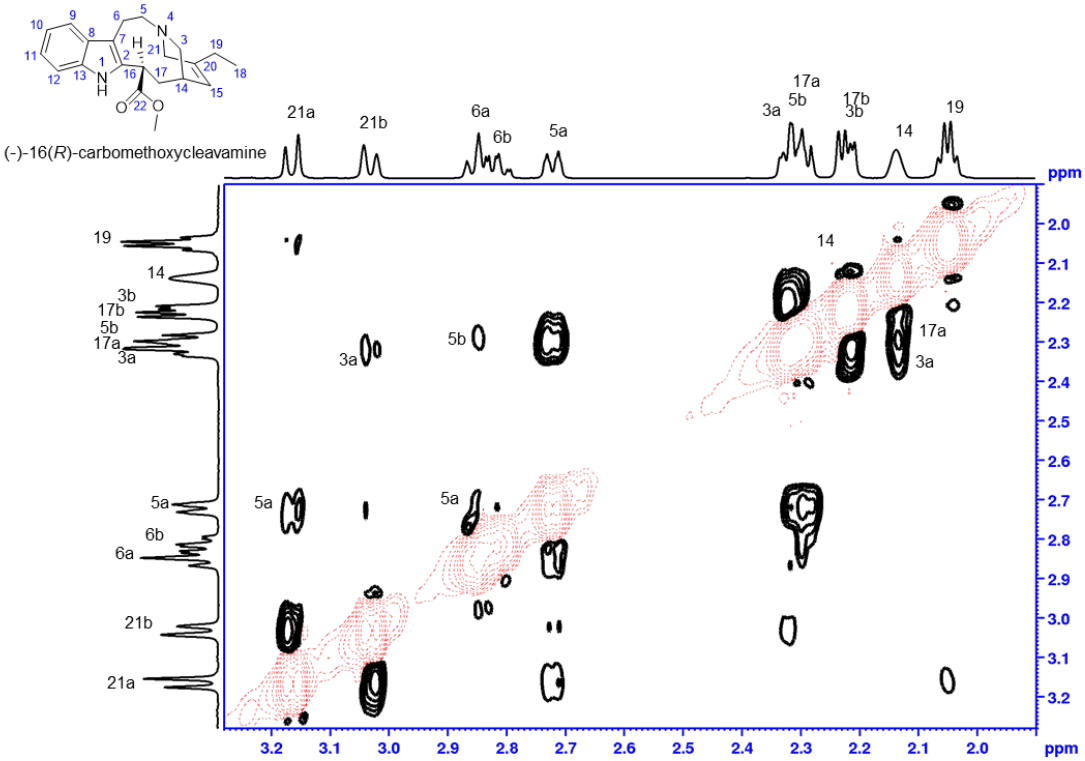
(–)-16(*R*)-carbomethoxycleavamine (10): ^{1}H-^{1}H ROESY aliphatic

^{1}H-^{1}H ROESY with water suppression aliphatic range in MeOH-d_3



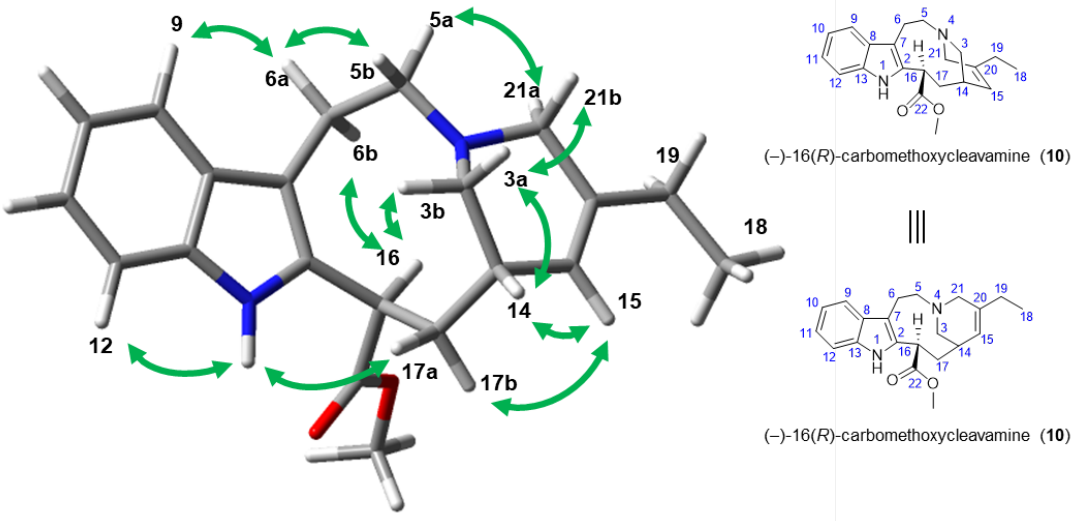
(–)-16(*R*)-carbomethoxycleavamine (10): ^{1}H-^{1}H ROESY

^{1}H-^{1}H ROESY with water suppression aliphatic range in MeOH-d_3



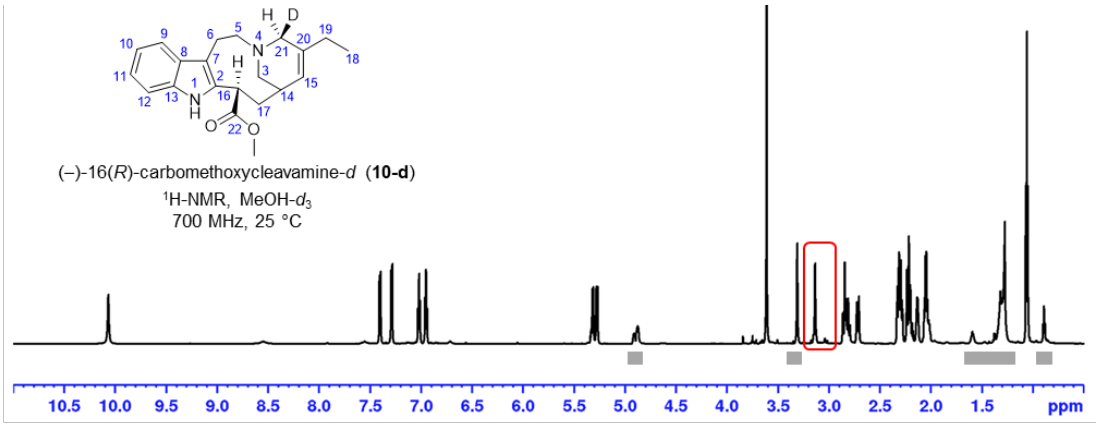
Structure of (–)-16(*R*)-carbomethoxycleavamine (10). Structure optimized Gaussian 16W (DFT, B3LYP-6-311G+(d,p), solvent MeOH).

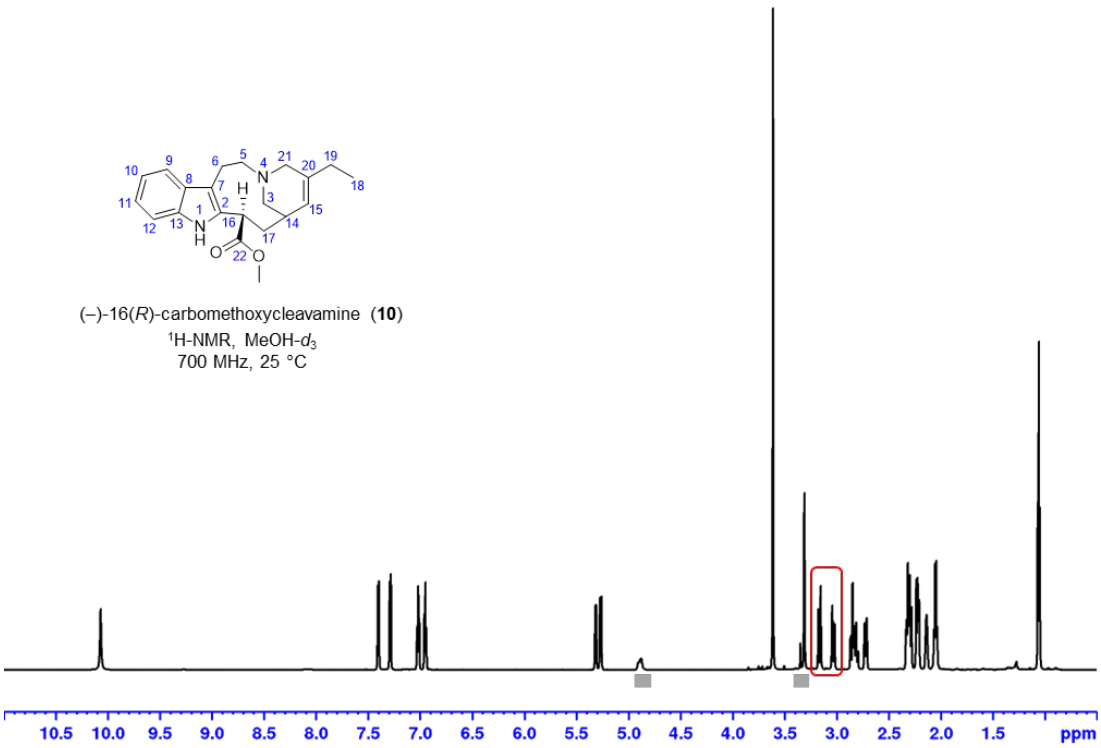
Important ROESY correlations are depicted in green.



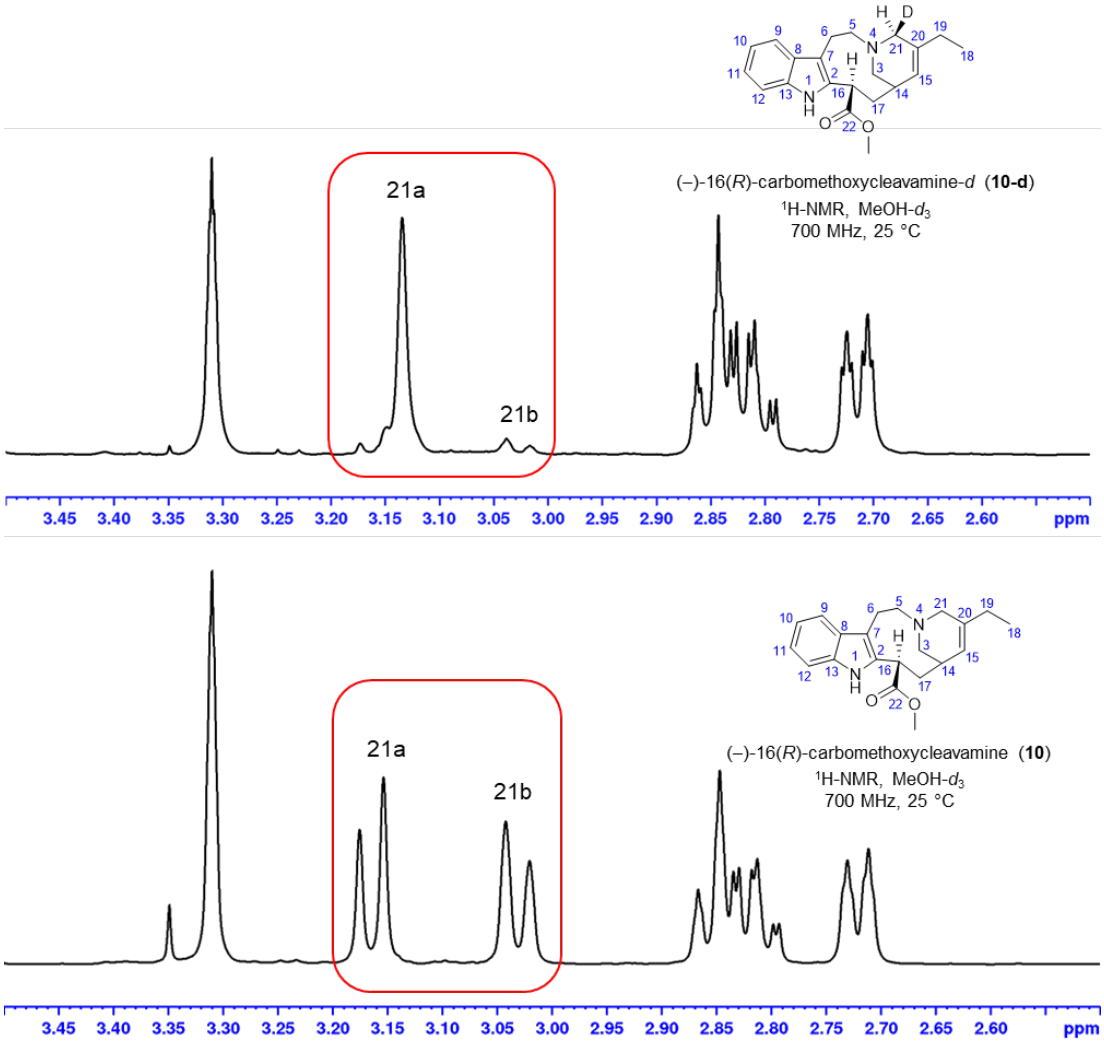
NMR data for (–)-16(*R*)-carbomethoxycleavamine-*d* (10-d).

^{1}H NMR with water suppression (zgpr) full range in MeOH-d_3
Shaded areas (grey bars) mark impurities and solvent

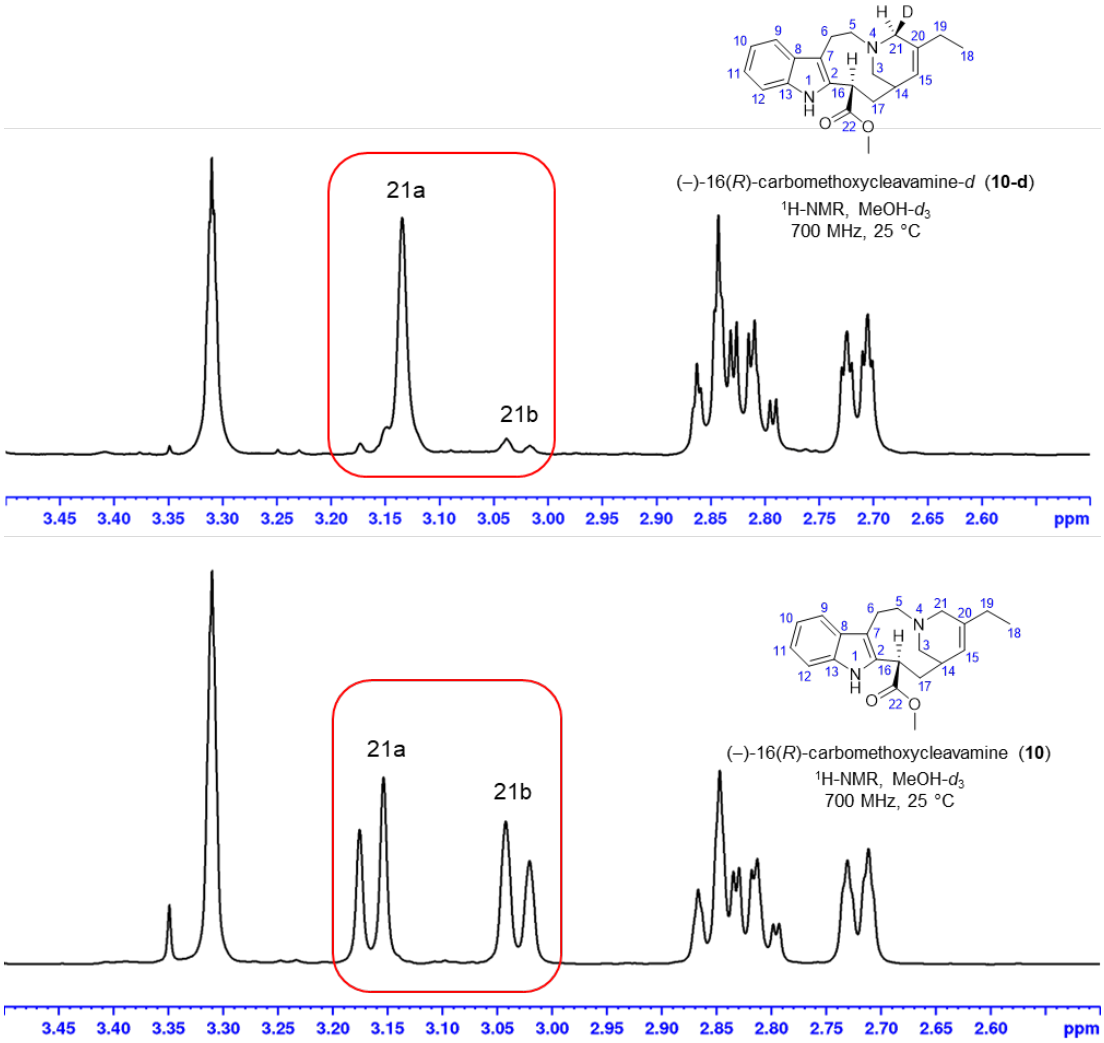




^{1}H NMR with water suppression (zgpr) 2.5 – 3.5 ppm in MeOH-d_3

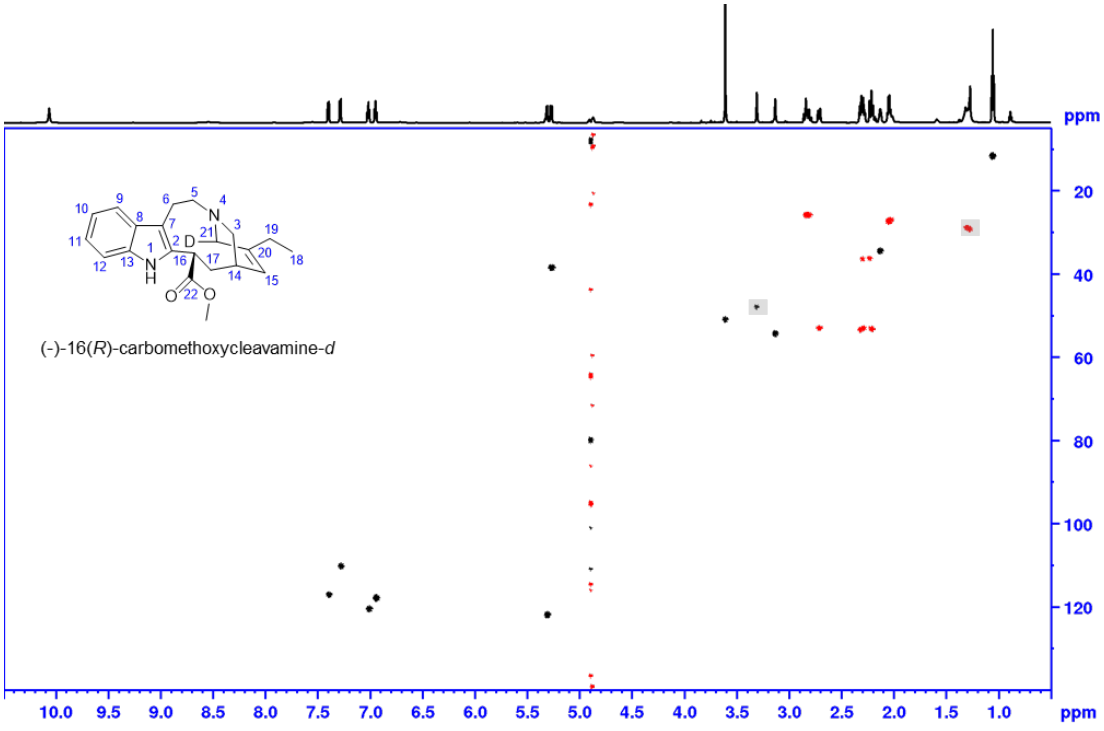


^{1}H NMR with water suppression (zgpr) 2.5 – 3.5 ppm in MeOH-d_3



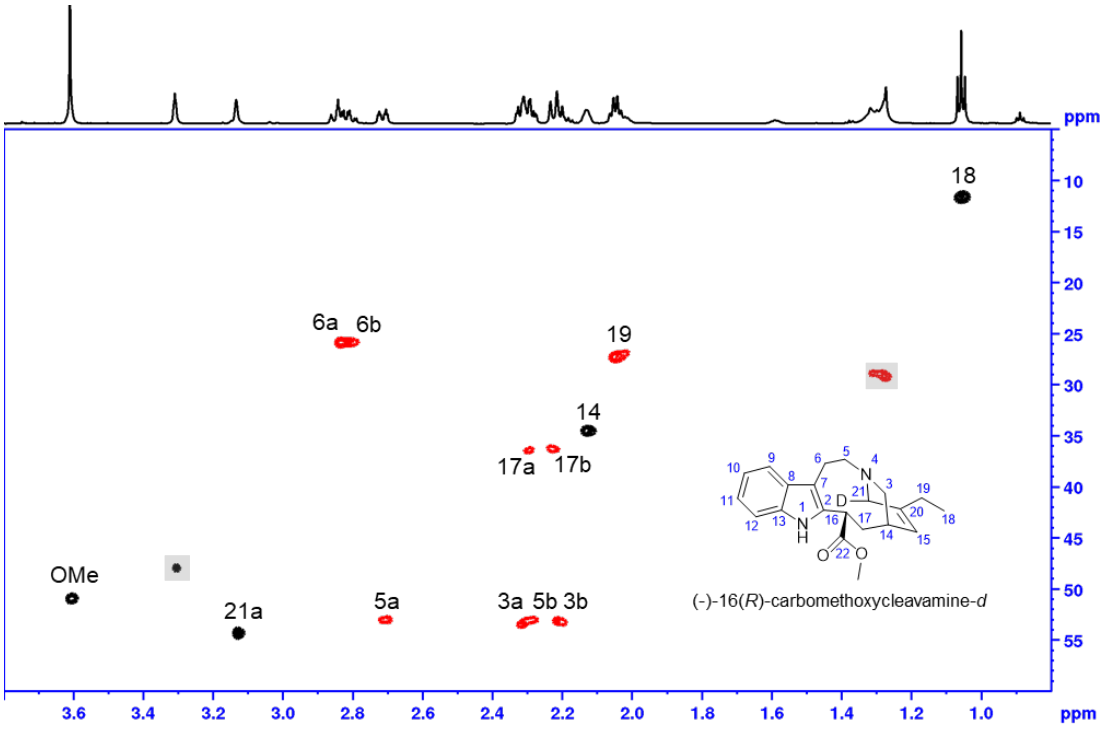
(–)-16(*R*)-carbomethoxycleavamine-*d* (10-d): Phase sensitive HSQC. Full range

Full range in MeOH-d_3 Shaded areas mark impurities and solvent, red: CH_2, black: CH, CH_3



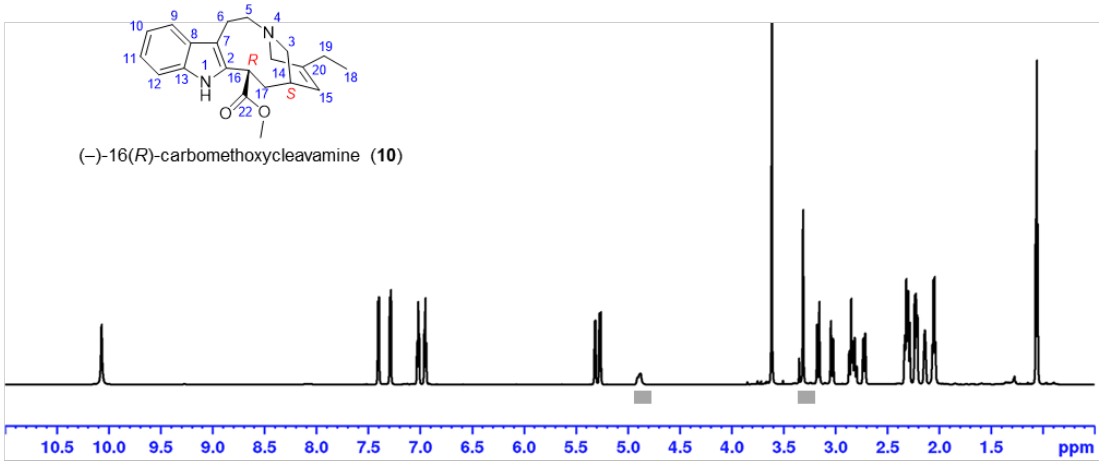
(–)-16(*R*)-carbomethoxycleavamine-*d* (10-d): Phase sensitive HSQC, aliphatic range in MeOH-d_3

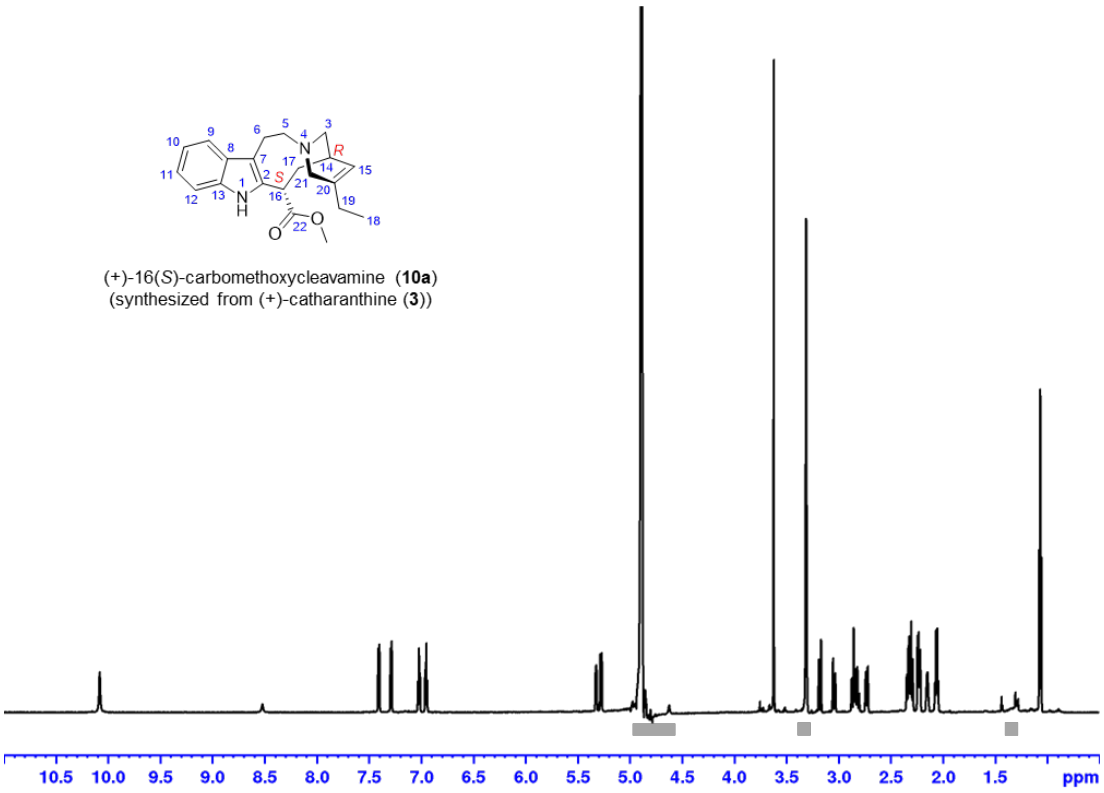
Shaded areas mark impurities and solvent, red: CH_2, black: CH, CH_3



Comparison of the NMR spectra of (–)-16(*R*)-carbomethoxycleavamine (10) and (+)-16(*S*)-carbomethoxycleavamine (10a) (synthesized from (+)-catharanthine (3)).

^{1}H NMR with water suppression (zgpr) full range in MeOH-d_3
Shaded areas (grey bars) mark impurities and solvent





2.7 Supporting References

1. Caputi, L. *et al.* Missing enzymes in the biosynthesis of the anticancer drug vinblastine in Madagascar periwinkle. *Science* 360, 1235–1239 (2018).

2. Caputi, L. *et al.* Structural basis of cycloaddition in biosynthesis of iboga and aspidosperma alkaloids. *Nat Chem Biol* 16, 383–386 (2020).

3. Farrow, S. C. *et al.* Biosynthesis of an Anti-Addiction Agent from the Iboga Plant. *J Am Chem Soc* 141, 12979–12983 (2019).

4. Andriamialisoa, R. Z., Langlois, N. L. and Y. & Langlois, Y. Preparation of 15-oxo-16-methoxycarbonyl-15, 20-dihydro-cleavamine and coupling reaction with vindoline. *Heterocycles* 1, 245–250 (1981).

5. Farrow, S. C. *et al.* Cytochrome P450 and O-methyltransferase catalyze the final steps in the biosynthesis of the anti-addictive alkaloid ibogaine from Tabernanthe iboga. *J. Biol. Chem.* 293, 13821–13833 (2018).

6. Sarrion-Perdigones, A. *et al.* GoldenBraid 2.0: A Comprehensive DNA Assembly Framework for Plant Synthetic Biology. *Plant Physiol* 162, 1618–1631 (2013).

7. Berrow, N. S. *et al.* A versatile ligation-independent cloning method suitable for high-throughput expression screening applications. *Nucleic Acids Res* 35, e45–e45 (2007).

8. Ferreira, C. M. H., Pinto, I. S. S., Soares, E. V. & Soares, H. M. V. M. (Un)suitability of the use of pH buffers in biological, biochemical and environmental studies and their interaction with metal ions – a review. *Rsc Adv* 5, 30989–31003 (2015).

9. Bruhn, T., Schaumlöffel, A., Hemberger, Y. & Bringmann, G. SpecDis: Quantifying the Comparison of Calculated and Experimental Electronic Circular Dichroism Spectra. *Chirality* 25, 243–249 (2013).

10. Edgar, R. C. MUSCLE: multiple sequence alignment with high accuracy and high throughput. *Nucleic Acids Res* 32, 1792–1797 (2004).

11. Gouet, P., Robert, X. & Courcelle, E. ESPript/ENDscript: extracting and rendering sequence and 3D information from atomic structures of proteins. *Nucleic Acids Res* 31, 3320–3323 (2003).

12. Qu, Y. *et al.* Solution of the multistep pathway for assembly of corynanthean, strychnos, iboga, and aspidosperma monoterpenoid indole alkaloids from 19*E*-geissoschizine. *Proc National Acad Sci* 115, 3180–3185 (2018).

13. Gasteiger, E. *et al.* The Proteomics Protocols Handbook. 571–607 (2005) doi:10.1385/1-59259-890-0:571.

14. Cocquet, G., Rool, P. & Ferroud, C. A catalytic versus stoichiometric photoinduced electron transfer promoted selective C16□C21 bond cleavage of catharanthine. *Tetrahedron Lett* 42, 839–841 (2001).

15. Beatty, J. W. & Stephenson, C. R. J. Synthesis of (−)-Pseudotabersonine, (−)-Pseudovincadifformine, and (+)-Coronaridine Enabled by Photoredox Catalysis in Flow. *J Am Chem Soc* 136, 10270–10273 (2014).

Chapter 3
Streamlined screening platforms lead to the discovery of pachysiphine synthase from *Tabernanthe iboga*

This Chapter (Chapter 3) of the thesis is published under the first autourship of Mohamed Omar Kamileen in the Journal of New Phytologist.

Title: Streamlined screening platforms lead to the discovery of pachysiphine synthase from *Tabernanthe iboga*

Authors: Mohamed O. Kamileen[1,2], Yoko Nakamura[1,3], Katrin Luck[1], Sarah Heinicke[1], Benke Hong[4], Maite Colinas[1], Benjamin R. Lichman[2], Sarah E. O'Connor[1*]

Affiliations:

[1] Department of Natural Product Biosynthesis, Max Planck Institute for Chemical Ecology, D-07745 Jena, Germany.

[2] Centre for Novel Agricultural Products, Department of Biology, University of York, York YO10 5DD, UK.

[3] NMR and Natural Product Biosynthesis Group, Max Planck Institute for Chemical Ecology, D-07745 Jena, Germany.

[4] Department of Chemistry, Westlake University, 18 Shilongshan Road, 310024, Hangzhou, China.

Journal: New Phytologist

Date of submission: July 1st, 2024

Date of publication: September 16th, 2024

DOI: 10.1111/nph.20133

Link: https://doi.org/10.1111/nph.20133

Streamlined screening platforms lead to the discovery of pachysiphine synthase from *Tabernanthe iboga*

Mohamed O. Kamileen[1,2], Yoko Nakamura[1,3], Katrin Luck[1], Sarah Heinicke[1], Benke Hong[4], Maite Colinas[1], Benjamin R. Lichman[2], Sarah E. O'Connor[1*]

[1] Department of Natural Product Biosynthesis, Max Planck Institute for Chemical Ecology, D-07745 Jena, Germany.

[2] Centre for Novel Agricultural Products, Department of Biology, University of York, York YO10 5DD, UK.

[3] NMR and Natural Product Biosynthesis Group, Max Planck Institute for Chemical Ecology, D-07745 Jena, Germany.

[4] Department of Chemistry, Westlake University, 18 Shilongshan Road, 310024, Hangzhou, China.

*Corresponding Author

ORCID

MOK 0000-0002-1346-1055

MC 0000-0001-7053-2983

BRL 0000-0002-0033-1120

SEO 0000-0003-0356-6213

3.1 Summary

- Plant-specialized metabolism is largely driven by the oxidative tailoring of key chemical scaffolds catalyzed by cytochrome P450 (CYP450s) enzymes. Monoterpene indole alkaloids (MIAs) tabersonine and pseudo-tabersonine, found in the medicinal plant *Tabernanthe iboga* (commonly known as iboga), are tailored with oxidations, and the enzymes involved remain unknown.
- Here, we developed a streamlined screening strategy to test the activity of *T. iboga* CYP450s in *Nicotiana benthamiana.* Using multigene constructs

encoding the biosynthesis of tabersonine and pseudo-tabersonine scaffolds, we aimed to uncover the CYP450s responsible for oxidative transformations in these scaffolds.

- Our approach identified two *T. iboga* cytochrome P450 enzymes: pachysiphine synthase (PS) and 16-hydroxy-tabersonine synthase (T16H). These enzymes catalyze an epoxidation and site-specific hydroxylation of tabersonine to produce pachysiphine and 16-OH-tabersonine, respectively.
- This work provides new insights into the biosynthetic pathways of MIAs and underscores the utility of *N. benthamiana* and *C. roseus* as platforms for the functional characterization of plant enzymes.

key words

Tabernanthe iboga, cytochrome P450, *Nicotiana benthamiana*, alkaloid, pachysiphine, plant natural product, plant biosynthesis.

3.2 Manuscript

Introduction

Many natural products are derivatized by CYP450 enzymes, which enables extensive chemical diversity to be generated from a small set of starting scaffolds (Bathe & Tissier, 2019; Hansen *et al.*, 2021; Nguyen & Dang, 2021). The medicinal plant *Tabernanthe iboga* Baill. (commonly known as iboga) is most widely known to produce the anti-addiction agent ibogaine, an MIA belonging to an *iboga-type* scaffold. However, in addition to ibogaine, this plant produces dozens of alkaloids derived from aspidosperma and pseudo-aspidosperma type scaffolds (Fig. 1). Many of these derivatives are generated through the action of CYP450s (Fig. 1).

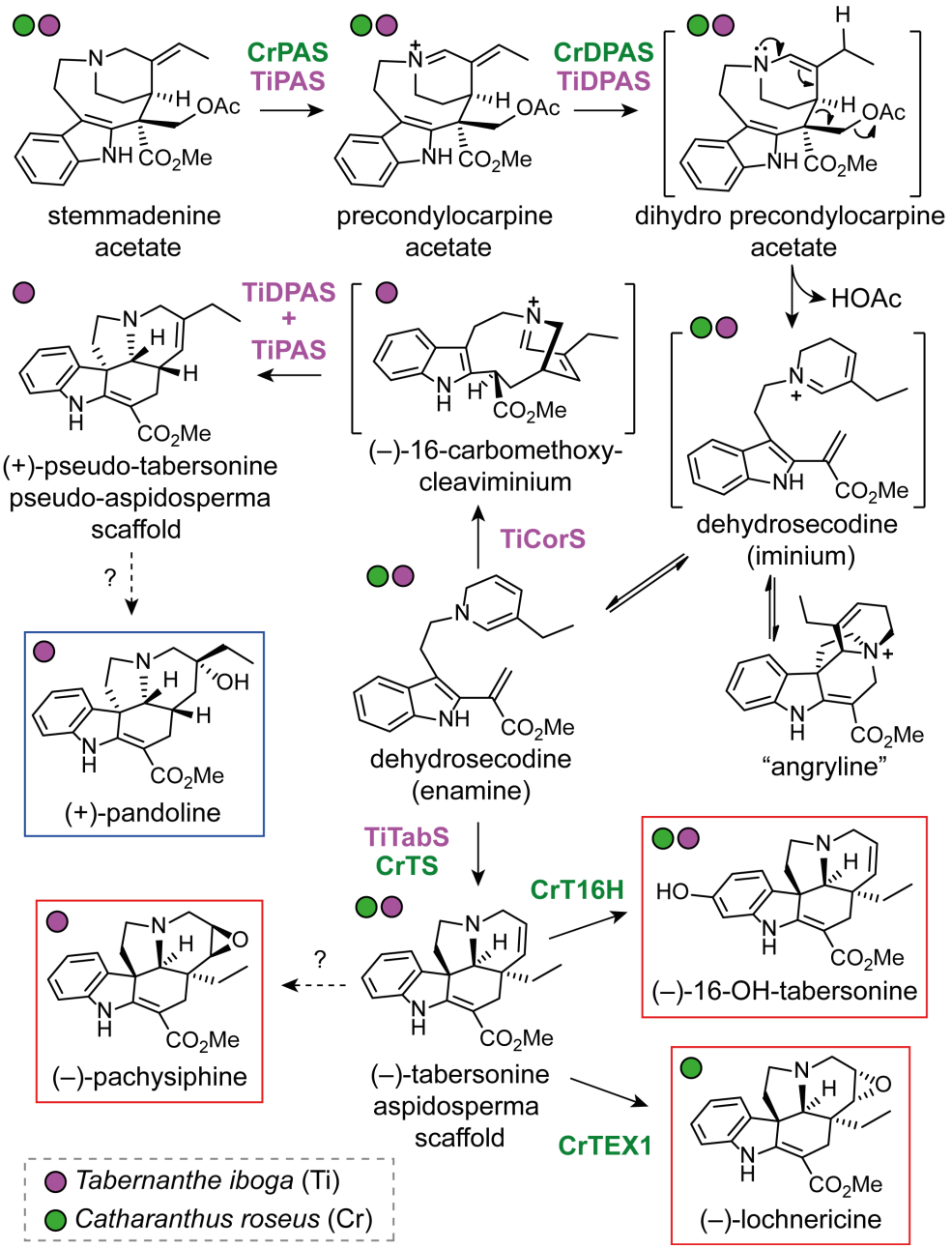


Fig. 1 The enzymatic reactions involved in aspidosperma and pseudo-aspidosperma alkaloid biosynthesis.

Stemmadenine acetate is a precursor to generate (–)-tabersonine (aspidosperma) and (+)-pseudo-tabersonine (pseudo-aspidosperma) alkaloids for further derivatization with known (solid arrows) and unknown (dashed arrows) oxidases (Farrow *et al.*, 2019; Kamileen *et al.*, 2022). Stemmadenine acetate is oxidized and reduced by PAS and DPAS enzymes to generate the highly reactive dehydrosecodine intermediate. This intermediate undergoes cyloaddition by the enzyme TabS to generate the aspidosperma alkaloid tabersonine. Alternatively, dehydrosecodine is cyclized by the enzyme TiCorS to form 16-carbomethoxy cleaviminium, which is subsequently reduced and oxidized by the action of the same

DPAS and PAS enzymes upstream to generate the pseudotabersonine scaffold. The aspidosperma and pseudo-aspidosperma final products are highlighted with red and blue boxes, respectively. Purple dots indicate that the compound is found in *Tabernanthe iboga*, while green dots indicate that the compound is found in *Catharanthus roseus*. Tabersonine derived alkaloids are found in both *T. iboga* and *C. roseus*, while pseudo-tabersonine-derived alkaloids are found only in *T. iboga.*

As part of a larger effort to elucidate the alkaloid pathways of *T. iboga*, we wanted to discover the CYP450s from this plant that catalyze the derivatization of these aspidosperma scaffolds. Discovery of the biosynthetic genes responsible for such derivatization steps requires screening of many candidate genes and the use of large quantities of valuable alkaloid starting substrates. Here we report a streamlined method for combinatorial screening of *T. iboga* CYP450s (308 unique sequences annotated in the transcriptome) from the large CYP71 family (30 unique sequences). We chose to focus on the *T. iboga* CYP71 family, since many members of this enzyme family have been shown to derivatize monoterpene indole alkaloids in other plant species (Giddings *et al.*, 2011; Besseau *et al.*, 2013; Kellner *et al.*, 2015; Tatsis *et al.*, 2017; Carqueijeiro *et al.*, 2018; Dang *et al.*, 2018; Franke *et al.*, 2019; Williams *et al.*, 2019; Hong *et al.*, 2022; Wang *et al.*, 2022). Using this method, we report here the discovery of two new CYP450 genes, pachysiphine synthase and tabersonine 16-hydroxylase, from this plant. The resulting product is a predicted biosynthetic intermediate of several pharmacologically important dimeric alkaloids such as conophylline (anti-diabetic activity) and melodinine K (cytotoxic) (Han-ya *et al.*, 2011; Walia *et al.*, 2020).

Materials and Methods

Chemicals

Stemmadenine acetate was synthesized from stemmadenine as previously described (Caputi *et al.*, 2018). (±)-pseudo-tabersonine was synthesized, and (+)-pseudo-tabersonine was enzymatically generated as previously reported (Kamileen *et al.*, 2022). (–)-tabersonine (cat no. T003900, CAS 4429-63-4) was purchased from Toronto Research Chemicals. Ajmaline (cat no. COMH93D5CE61, CAS 4360-12-7) was purchased from Sigma-Aldrich. (–)-[^{13}C]-tabersonine was synthesized from (–)-tabersonine, as reported (Auriola *et al.*, 1991).

Plant growth conditions

Tabernanthe iboga plants were maintained as previously described (Kamileen *et al.*, 2022). *Catharanthus roseus* (L.) G. Don. (var. Little Bright Eyes, LBE) was germinated in a standard soil mix in a climate chamber under 16 h light/8 h dark photoperiod at 23 °C, and 60% relative humidity. *C. roseus* var. LBE plants aged 6 – 8 months were used for flower petal transformation. *Nicotiana benthamiana* Domin. plants used for transient gene expression were grown in a greenhouse on a low-nutrient F1 compost soil mix under a 16 h light/8 h dark photoperiod at 22 °C, and 55% relative humidity. Plants were grown for 3-4 weeks before *Agrobacterium* infiltration.

Cloning methods

Cytochrome P450 enzymes characterised in this study were amplified by PCR from a cDNA library generated from *T. iboga,* as previously described (Farrow *et al.*, 2019). Known *C. roseus* cytochromes P450 genes (Table S1) were amplified from a cDNA library generated from *C. roseus* var. LBE. RNA. Primers with overhangs (Table S2) compatible with In-Fusion HD cloning kit (Takara Bioscience) were used to clone full-length genes into pESC-HIS (GenBank: AF063850.1, Agilent) vector for yeast expression and 3Ω1 (Sarrion-Perdigones *et al.*, 2013) vector for plant transient expression (*N. benthamiana* or *C. roseus*) in the case of single transcriptional unit (STU) constructs. Multi-transcriptional unit constructs (MTU) for plant transient expression in *N. benthamiana* or *C. roseus* were assembled using the GoldenBraid 2.0 kit (Sarrion-Perdigones *et al.*, 2013) (Addgene kit # 11000000076) (Fig. S1). For yeast expression, pESC-HIS gene constructs were transformed into yeast (*Saccharomyces cerevisiae*) strain WAT11 (*ade2*; contains the *Arabidopsis thaliana* cytochrome P450 reductase I gene, *ATR1*) (Urban *et al.*, 1997) using the Frozen-EZ Yeast Transformation II Kit (Zymo Research). For plant transient expression, all STU and MTU constructs were transformed into *Agrobacterium tumefaciens* GV3101 cells (Goldbio) by electroporation as previously described (Kamileen *et al.*, 2022). Detailed cloning methods are provided in Methods S1.

Transient expression in *N. benthamiana*

The *Agrobacterium* strains harbouring gene constructs of interest were grown overnight at 28 °C, 220 rpm. Cells were harvested by centrifugation at 4,000 × g for 10 min, and the supernatant was discarded. The pellet was gently resuspended in infiltration buffer (10 mM MES, pH 5.6, 10 mM magnesium chloride, 200 µM acetosyringone). Cells were re-harvested by centrifugation, and the supernatant was discarded. Cell pellets were resuspended in 10 ml of infiltration buffer and incubated in the dark at room temperature with gentle rocking for 2 hours. When multiple gene constructs were tested in combinations, strains were pooled in equal cell density. Each strain had an OD_{600} of 0.4 and infiltrated into the abaxial side of a 3-week-old *N. benthamiana* leaf using a 1 ml needleless syringe. When pooling for combinations of ≥ 10 constructs, the OD_{600} was set to 0.15. Each pooled combination consisted of a minimum of three biological replicates, where individual leaves of three different plants were infiltrated to randomize batch effects. Appropriate controls: wild-type, P19, and GFP were included in the experimental setup to be tested with and without substrate. Leaves were harvested four days post-*Agrobacterium* infiltration for plant disk assays.

Transient expression in *C. roseus* flower petals

Transformation of *C. roseus* var. LBE flower petals were performed as previously described (Colinas *et al.*, 2021; Colinas & Goossens, 2022). All open flowers were removed from the plant two days before infiltration. The *Agrobacterium* strains were prepared as outlined for transient expression in *N. benthamiana* to a final OD_{600} of 0.4. For each experiment, a minimum of three biological replicates from different individual plants were selected. Flower petals were pierced once with a sterile needle, and the *Agrobacterium* mixture was infiltrated using a 1 ml needleless syringe. Appropriate controls: wild-type, P19, and GFP were included in the experimental setup to be tested with and without substrate. Petals were harvested three days post-*Agrobacterium* infiltration for plant disk assays.

Plant disk assays of *Agrobacterium* infiltrated *N. benthamiana* leaf and *C. roseus* flower petals

At harvest, 10 mm diameter leaf disks of *N. benthamiana* leaves, or *C. roseus* flower petals were cut using a borer. For each biological replicate, three leaf disks or petal disks were harvested. Each plant disk was then placed in an individual well of a 48-well plate with 300 µl of 50 mM HEPES buffer at pH 7.5. Where necessary, the substrate was added to a final concentration of 25 µM. Plates were closed and sealed with parafilm to avoid evaporation. Plates were incubated at 24 °C overnight (16-18 hours). After incubation, disks were collected, placed in a 2 ml safe-lock tube, and snap-frozen in liquid nitrogen. The disks were homogenized using a Tissue-Lyser II (Qiagen) at 25 Hz for 1 min with 3 mm tungsten beads. Metabolites were extracted from the powdered tissue with 300 µl of extraction solution (70% methanol in water + 0.1% formic acid) and sonicated for 10 min at room temperature. When needed, internal standard ajmaline (final concentration 20 µM) was spiked into the extraction solution before sample extraction. The samples were then centrifuged at 20,000 × g for 10 min to pellet cell debris, and the extract was filtered through 0.22 µm PTFE syringe filters into analytical vials for LC-MS analysis (Fig. S2).

Heterologous expression in yeast and microsome preparation

Yeast cells (WAT11) were cultured in 100 ml of SD-His medium (6.7 g l^{-1} yeast nitrogen base without amino acids, 2 g l^{-1} drop-out mix without histidine, 74 mg l^{-1} adenine hemisulfate) containing 2% glucose (w/v) at 30 °C, 200 rpm for 28-34 hours. Cells were harvested and resuspended in 100 ml of SD-His medium + 1.8% galactose (w/v) + 0.2 % glucose (w/v) for protein production at 30 °C, 200 rpm for 18-24 hours. Yeast cells were harvested, and microsomes were prepared as reported (Pompon *et al.*, 1996). Detailed yeast expression and microsome preparation methods are provided in Methods S1.

Analytical-scale reactions with purified yeast microsomes

All analytical-scale *in vitro* yeast microsome reactions were carried out in 50 mM HEPES buffer (pH 7.5) in a volume of 100 µl. Each reaction consisted of 50 µg of total microsomal protein (0.50 µg $µl^{-1}$ microsomal protein), 25 µM substrate, and 1 mM NADPH. Empty vector (EV) reactions were performed as a negative control. Reactions were initiated by adding microsomes and incubating at 30 °C and 600 rpm for 60 min, after which the reactions were quenched by adding 100 µl of

extraction solution. Quenched reactions were centrifuged at 20,000 × g at room temperature for 10 min and filtered through 0.22-µm PTFE filters into analytical vials for LC-MS analysis.

Semi-preparative-scale reactions with purified yeast microsomes

Reactions scaled to 10 ml volumes were set up to generate (–)-pachysiphine and (–)-16-OH-tabersonine, from (–)-tabersonine and (–)-16-OH-pachysiphine from (–)-pachysiphine. Reactions consisted of 50 mM HEPES pH 7.5 buffer, 2 mg substrate [(–)-tabersonine or (–)-pachysiphine] and, NADPH generation system [1.0 mM $NADP^+$, 2.0 U ml^{-1} glucose-6-phosphate dehydrogenase (G6PDH), and 3.0 mM glucose-6-phosphate (G6P) along with 0.2 mM NADPH]. Reactions were initiated by the addition of 3 mg yeast microsomes (0.3 µg $µl^{-1}$ microsomal protein), TiPS for (–)-pachysiphine or TiT16H for (–)-16-OH-tabersonine and incubated at 30 °C, 200 rpm for 6 hours. To generate (–)-16-OH-pachysiphine, a crude workup of 2 mg of (–)-pachysiphine reconstituted in 5% methanol (aqueous) was used as substrate with 3 mg (0.3 µg $µl^{-1}$) of TiT16H microsomal protein preparation and incubated as described above. The reactions were terminated by the addition of 10 ml ethyl acetate. The aqueous reaction mixture was extracted thrice with ethyl acetate and evaporated to dryness. The dried extract was reconstituted in 5 ml of 10% methanol (aqueous) and subjected to SPE (solid phase extraction) as described in Methods S1.

Semi-preparative HPLC isolation

Semi-preparative-scale product isolation was performed using high-performance liquid chromatography (HPLC). Reaction workups of (–)-pachysiphine, (–)-16-OH-tabersonine, (–)-16-OH-pachysiphine, and *N. benthamiana* extract of pseudo-tabersonine were subjected to HPLC isolation. An Agilent 1260 Infinity II HPLC instrument connected to an autosampler, diode array detector (DAD), and fraction collector for compound detection and isolation. Chromatography was monitored at UV 254 nm and 328 nm (Hisiger & Jolicoeur, 2007). Chromatographic separation was performed using a Phenomenex Kinetex XB-C18 (5.0 µm, 100 Å, 100 × 2.1 mm) column maintained at 40 °C under gradient elution using reversed phase conditions. Detailed HPLC methods are provided in Methods S1.

Extraction of pseudo-tabersonine from *N. benthamiana*

To isolate pseudo-tabersonine, *N. benthamiana* (30 plants) transiently expressing the pS-psTab multigene construct were infiltrated with 400 µM stemmadenine acetate, 4 days post *Agrobacterium* infiltration. After 18 h, the substrate-infiltrated portions of the leaves were harvested for processing. Leaf material 20 g fresh weight was lyophilized using a freeze dryer. Dehydrated leaves were crushed and extracted with 50 ml of extraction solution at room temperature for 1 h with constant stirring. The extract was filtered through a miracloth and filter paper (MN 615, Macherey-Nagel) and evaporated to dryness. The dried extract was reconstituted in 10 ml of 10% methanol (aqueous) and subjected to SPE (solid phase extraction) as described in Methods S1.

LC-MS analysis

LC-MS was performed using an UltiMate 3000 (Thermo Scientific) ultra-high performance liquid chromatography (UHPLC) system coupled to an Impact II UHR-Q-ToF (Ultra-High-Resolution Quadrupole-Time-of-Flight) mass spectrometer (Bruker Daltonics). LC-MS measurements were performed as previously reported (Kamileen *et al.*, 2022). Data analysis was performed using Bruker Compass Data Analysis (Version 5.3) software. Detailed LC-MS methods are described in Methods S1.

Chiral LC-MS analysis

Chiral separation was performed using the LC-MS instrumentation described above with changes to chromatographic conditions. A Phenomenex Lux Amylose-1 (150 x 3 mm, 3 µm particle) chiral LC column set at 30 °C was used to separate (±)-pseudo-tabersonine enantiomers. The column was used in reverse phase with mobile phase A (10 mM ammonium acetate) and B (acetonitrile). An isocratic gradient of 95% B and 0.6 ml min^{-1} flow rate was used.

Structural elucidation by NMR analysis

NMR spectra were measured on a 700 MHz Bruker Advance III HD spectrometer (Bruker Biospin GmbH). Bruker TopSpin (version 3.6.1) was used for spectrometer control and data processing. $CDCl_3$ and MeOH-d_3 were used as *d*-

solvents and referenced to the residual solvent signals at δ_H 7.24 and δ_C 77.0 for $CDCl_3$, and δ_H 3.31 and δ_C 49.0 for MeOH-d_3 respectively. For [^{13}C]-tabersonine, NMR spectra were measured on a 500 MHz Bruker Advance III HD spectrometer (Bruker Biospin GmbH) using MeOH-d_3.

ECD spectra measurements of pachysiphine

The electronic circular dichroism (ECD) spectrum of (–)-pachysiphine was measured at 25 °C on a JASCO J-810 spectropolarimeter (JASCO cooperation) using a 350 µl cell. Spectrometer control and data processing were accomplished using JASCO Spectra Manager II. The spectrum was measured in methanol at 0.35 mg ml^{-1} concentration. Detailed structure optimization and ECD spectral calculation for (–)-pachysiphine are described in Methods S1.

Results

Platform development: Gene expression in *Nicotiana benthamiana* leaf disks

Transient expression of genes in *Nicotiana benthamiana* leaves is a well-established method for screening the biochemical activity of plant enzymes (Christ *et al.*, 2019; Hong *et al.*, 2022; Nett *et al.*, 2023; Jiang *et al.*, 2024; Martin *et al.*, 2024). This process entails infiltrating the *N. benthamiana* leaf with a culture of *Agrobacterium tumefaciens* that harbors an expression plasmid containing the gene of interest. Within 3-5 days after infiltration, the protein is expressed in the leaf, and the resulting tissue can be analyzed by mass spectrometry to monitor what product(s) have formed as a result of the gene expression. If the expected substrate of the gene product is not naturally found in *N. benthamiana*, this substrate can be infiltrated into the leaf after protein expression using a needleless syringe (Fig. S2). However, relatively large amounts of substrate, usually 1 ml of a 0.1-1 mM solution, are required.

To minimize the amount of substrate needed for screening of protein activity, we modified the *N. benthamiana* protocol. The desired protein is transiently expressed in the *N. benthamiana* leaf using standard *Agrobacterium* transformation protocols. The leaf is allowed to remain attached to the plant for four days, allowing protein expression from the infiltrated gene. At this point, a cork borer is used to

punch out disks of leaf tissue in the transfected leaf. These leaf disks are placed in a 24-well microplate, in which each well contains 300 µl of buffer with 25 µM of the substrate of interest. Leaf disks are incubated in this buffer solution for approximately 16 hours, allowing the substrate to diffuse into the disk. Then, the leaf disks are harvested, frozen in liquid nitrogen, ground, and extracted in methanol, and the methanolic extract is analyzed by LC-MS (Fig. S2). This method ensures substrates are effectively delivered into the leaf tissues using minimum substrate quantities, eliminating technical issues associated with substrate wastage and wash-off that commonly occur with traditional *N. benthamiana* syringe-based substrate infiltration. Additionally, the uniform fresh weight of the leaf disks and consistent substrate concentrations streamline the downstream sample preparation process for LC-MS analysis and data normalization.

Platform development: Gene stacked plasmids for expression of (–)-tabersonine and (+)-pseudo-tabersonine in *Nicotiana benthamiana*

Elucidation of multi-step natural product biosynthetic pathways often requires that more than one gene be expressed simultaneously in the *N. benthamiana* leaf. Typically, liquid cultures of individual *Agrobacterium* strains, each harboring a plasmid with a different gene of interest, are cultured separately, and then each culture is diluted to a defined optical density. The individual *Agrobacterium* cultures are then mixed together, and this mixture is then infiltrated into *N. benthamiana* leaves. However, stacking all pathway genes within a single plasmid has been shown in some cases to generate the final product of the enzyme sequence in higher amounts compared to co-infiltration with many *Agrobacterium* strains (Forestier *et al.*, 2021; Kruse *et al.*, 2024). Therefore, to screen for CYP450s that would act on either (–)-tabersonine and (+)-pseudo-tabersonine, we designed and built two multigene constructs to produce these alkaloid scaffolds from the starting substrate stemmadenine acetate using the Goldenbraid 2.0 kit (Sarrion-Perdigones *et al.*, 2013). The three biosynthetic genes that are responsible for producing (–)-tabersonine and (+)-pseudo-tabersonine scaffolds from stemmadenine acetate have been previously reported (Fig. 1) (Farrow *et al.*, 2019; Kamileen *et al.*, 2022).

The first construct, containing the biosynthetic genes TiPAS3, TiDPAS1, and TiTabS, along with silencing suppressor P19, was designed to produce (–)-tabersonine (pS-Tab). The second construct, an analogous multigene construct

containing the biosynthetic genes TiPAS3, TiDPAS1, and TiCorS, along with P19, was designed to produce (+)-pseudo-tabersonine (pS-psTab) (Fig. 2a, Fig. S1). Each transcriptional unit in these multigene constructs was regulated by the ubiquitin10 promoter (pUbq10) and terminator (tUbq10) from tomato (*Solanum lycopersicum*) (Table S1), elements known to be more stable and drive high gene expression (Grefen *et al.*, 2010; Kumar *et al.*, 2022).

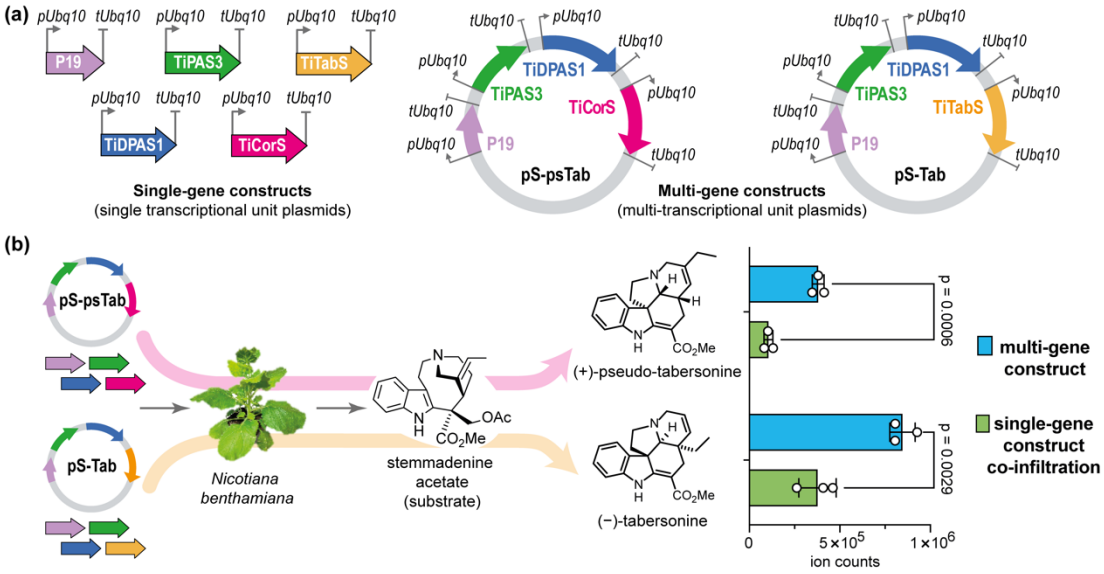


Fig. 2 Multigene constructs for (–)-tabersonine and (+)-pseudo-tabersonine production via transient expression in *Nicotiana benthamiana*.
(a) Multi-transcriptional unit constructs and single transcriptional unit constructs designed to generate (–)-tabersonine and (+)-pseudo-tabersonine in *N. benthamiana* using the exogenous substrate stemmadenine acetate. (b) Comparison of (–)-tabersonine and (+)-pseudo-tabersonine product observed in *N. benthamiana* when single transcriptional unit constructs (green bar) and the multi-transcriptional unit construct (blue bar) are used. The values represent mean ± SD (n = 3), two-tailed Student's *t*-test.

We compared the levels of (–)-tabersonine and (+)-pseudo-tabersonine production that resulted from using these multigene constructs with levels that resulted from the conventional method in which we co-infiltrated four *Agrobacterium* strains harboring the corresponding single gene constructs (Fig 2a). For each experiment, leaf disks were incubated with 25 µM stemmadenine acetate, the starting substrate, in 300 µl buffer (pH 7.5). Notably, we recorded significantly higher

levels of (–)-tabersonine and pseudo-tabersonine when using the multigene constructs (Fig. 2b Fig. S3). Since the stereochemistry of pseudo-tabersonine produced by this enzyme system had only been demonstrated *in vitro* (Kamileen *et al.*, 2022), we isolated the pseudo-tabersonine produced by the pS-psTab multigene construct from *N. benthamiana* by analytical HPLC. We performed chiral HPLC with authentic standards of (+)-pseudo-tabersonine and a racemic (±)-pseudo-tabersonine. This confirmed that the product generated in *N. benthamiana* by the pS-psTab construct is indeed the expected (+)-pseudo-tabersonine isomer (Fig. S4).

Gene functional characterization (*in planta*): Screening of P450 genes using gene-stacked plasmids

These stacked plasmids were used to screen for CYP450 genes that encoded enzymes that oxidizes aspidosperma scaffolds. Each CYP450 gene candidate would be cloned on separate plasmids and then combined with the gene-stacked plasmid to create a flexible screening system. As a positive control to test this approach, we used the pS-TabS multigene construct to test the activity of previously characterised CYP450 genes known to derivatize (–)-tabersonine in *N. benthamiana* leaf disks (Fig. 3a). Using this system, we successfully demonstrated that the expected hydroxylated product (*m/z* 353) of (–)-tabersonine (*m/z* 337) catalyzed by the *C. roseus* CYP450 genes of the CYP71 family, T16H1, T16H2, T19H, TEX1, TEX2, and T3O could be detected (Fig. 3b). Furthermore, we observed that when these CYP71s were combined, the expected double-hydroxylated product (*m/z* 369) could also be detected (Fig. 3c).

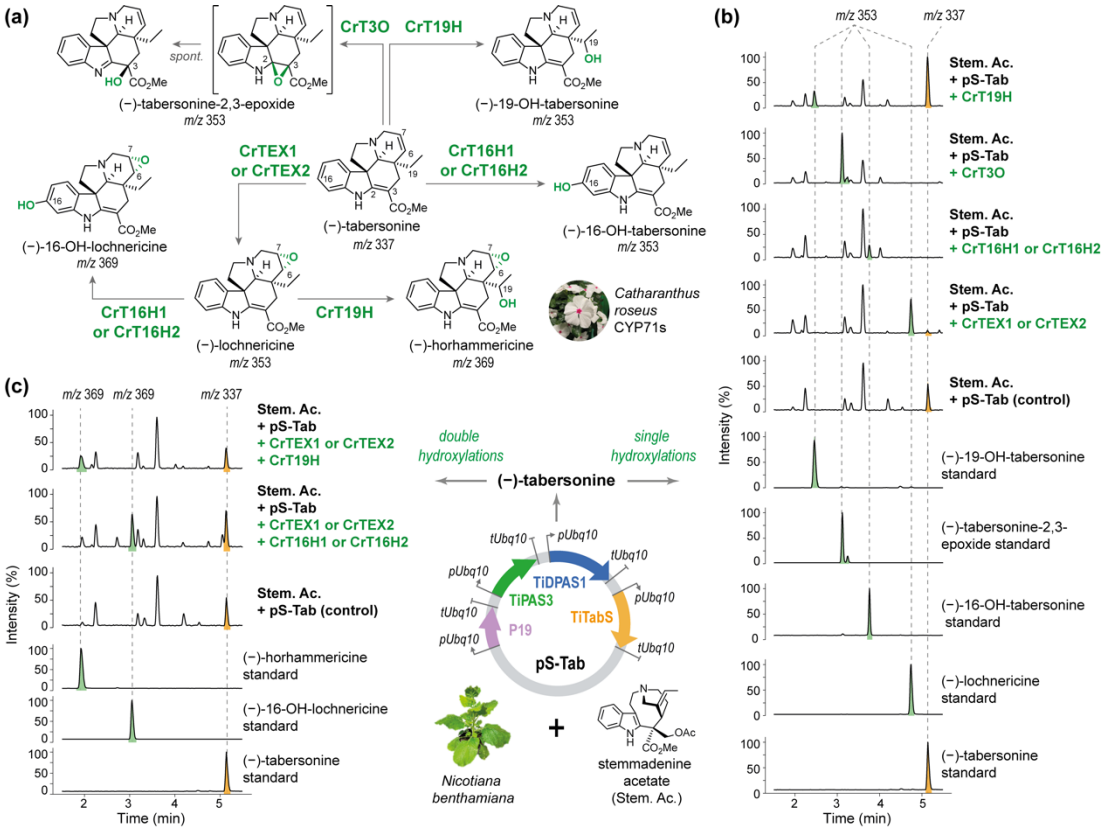


Fig. 3 Hydroxylations of aspidosperma alkaloid (–)-tabersonine catalyzed by *Catharanthus roseus* CYP71 enzymes.

(a) Functionally characterised *C. roseus* CYP71 P450 enzymes involved in (–)-tabersonine hydroxylation(s). (b) LC-MS profiles of the products resulting from a single hydroxylation of (–)-tabersonine in *Nicotiana benthamiana* leaf disk assays. (c) LC-MS profiles of the products resulting from double hydroxylations of tabersonine with combinations of selected *C. roseus* CYP71 genes in *N. benthamiana* leaf disk assays. Single and double hydroxylation products of (–)-tabersonine are confirmed by standards and MS^2 spectra. LC-MS profiles are presented as total ion chromatograms, and *m/z* is presented as $[M+H]^+$ of the parent ion.

Gene functional characterization (*in planta*): Discovery and functional characterization of new P450 genes

With this streamlined assay in hand, we inspected the *T. iboga* transcriptome to identify CYP450-encoding gene sequences (Farrow *et al.*, 2019). Sequences assigned as a CYP450 were curated using transcriptome annotations and phylogenetic analysis (Fig S5). We chose to focus on the *T. iboga* CYP71 family,

since many members of this enzyme family have been shown to derivatize monoterpene indole alkaloids in other plant species (Giddings *et al.*, 2011; Besseau *et al.*, 2013; Kellner *et al.*, 2015; Tatsis *et al.*, 2017; Carqueijeiro *et al.*, 2018; Dang *et al.*, 2018; Franke *et al.*, 2019; Williams *et al.*, 2019; Hong *et al.*, 2022; Wang *et al.*, 2022). A phylogenetic tree of *T. iboga* CYP450 sequences, which included CYP71 genes previously shown to be involved in MIA biosynthesis, was generated (Fig. S5). Using this tree, we curated a list of 30 CYP71 encoding genes from *T. iboga* in a phylogenetically informed manner (Fig. 4a).

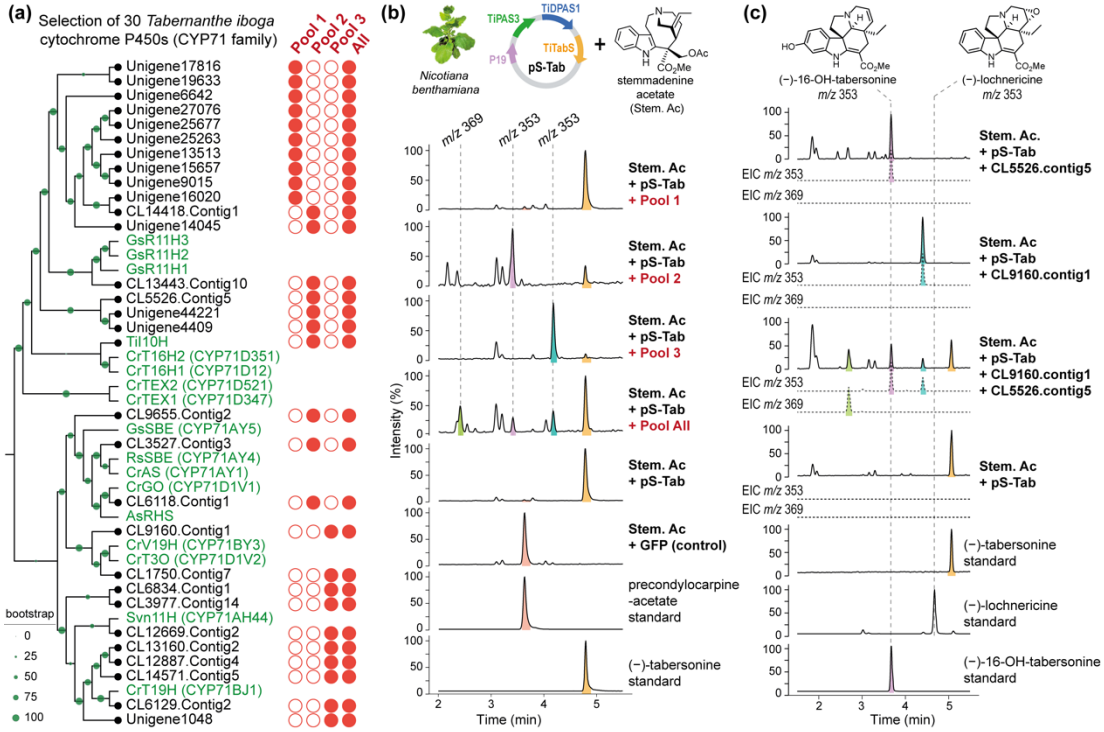


Fig. 4 Screening of *Tabernanthe iboga* CYP71 for enzymatic activity in *N. benthamiana*.

(a) Phylogenetic tree of the 30 *T. iboga* CYP71 candidates (black circles) selected for pooled screening (red shaded circles). (b) LC-MS profiles of *T. iboga* CYP71 pools tested for hydroxylation activity in combination with the tabersonine-producing multigene construct pS-Tab and assayed in leaf disks with the substrate stemmadenine acetate Stemmadenine acetate is oxidized to precondylocarpine acetate by an endogenous *N. benthamiana* enzyme (Caputi *et al*., 2018). (c) Deconvolution of CYP71 pools 2 and 3 to identify gene candidate(s) responsible for the hydroxylation(s) of tabersonine observed in (b). LC-MS profiles in solid lines are presented as total ion chromatograms, and dotted lines as extracted ion chromatograms (EIC) with *m/z* presented as $[M+H]^+$ of the parent ion.

Each CYP71 gene was cloned and transformed into an individual strain of *Agrobacterium*. For the initial screen, we tested the 30 *T. iboga* CYP71 candidates in pools of 10. Each set of *Agrobacterium* strains harboring the 10 genes of the pool were combined and then co-infiltrated into *N. benthamiana* leaves along with an *Agrobacterium* strain harboring either the pS-TabS or pS-psTab multigene construct. Infiltration was followed by leaf disk assays with the substrate stemmadenine acetate. When the *T. iboga* CYP71 pools were tested with the pS-psTab multigene construct, none of the candidates appeared to act on (+)-pseudo-tabersonine (Fig. S6). However, when the pS-TabS multigene construct was used, two of the three CYP71 candidate pools resulted in the production of a new, more hydrophilic product with a *m/z* 353 indicative of hydroxylation (Δ *m/z* 16) of (–)-tabersonine (*m/z* 337) (Fig. 4b). Additionally, when all three CYP71 candidate pools were combined, a third new product with a *m/z* 369 indicative of double hydroxylation (Δ *m/z* 32) of (–)-tabersonine (*m/z* 337) was observed along with the two *m/z* 353 products found in pool 2 and pool 3 (Fig. 4b). To identify the specific *T. iboga* CYP71 candidate(s) responsible for the hydroxylation(s) of (–)-tabersonine, we tested the individual candidates from *T. iboga* CYP71 pool 2 and 3 by co-infiltrating them with the pS-TabS multigene construct in the presence of stemmadenine acetate. We identified the two *T. iboga* CYP71 candidates responsible for the hydroxylation of (–)-tabersonine as CL5526.contig5 and CL9160.contig1 (Fig. 4c). Candidate CL5526.contig5 produced a hydroxylated product (*m/z* 353) that co-eluted and matched with identical MS^2 spectra to the known compound 16-OH-tabersonine and was therefore named *T. iboga* tabersonine-16-hydroxylase (TiT16H, assigned as CYP71BE297) (Fig. 4c). Additionally, we confirmed the structure of 16-OH-tabersonine by NMR, isolated from an *in vitro* enzymatic reaction containing (–)-tabersonine and yeast microsomes containing TiT16H protein (Fig. 5a, Fig. S7a, S8).

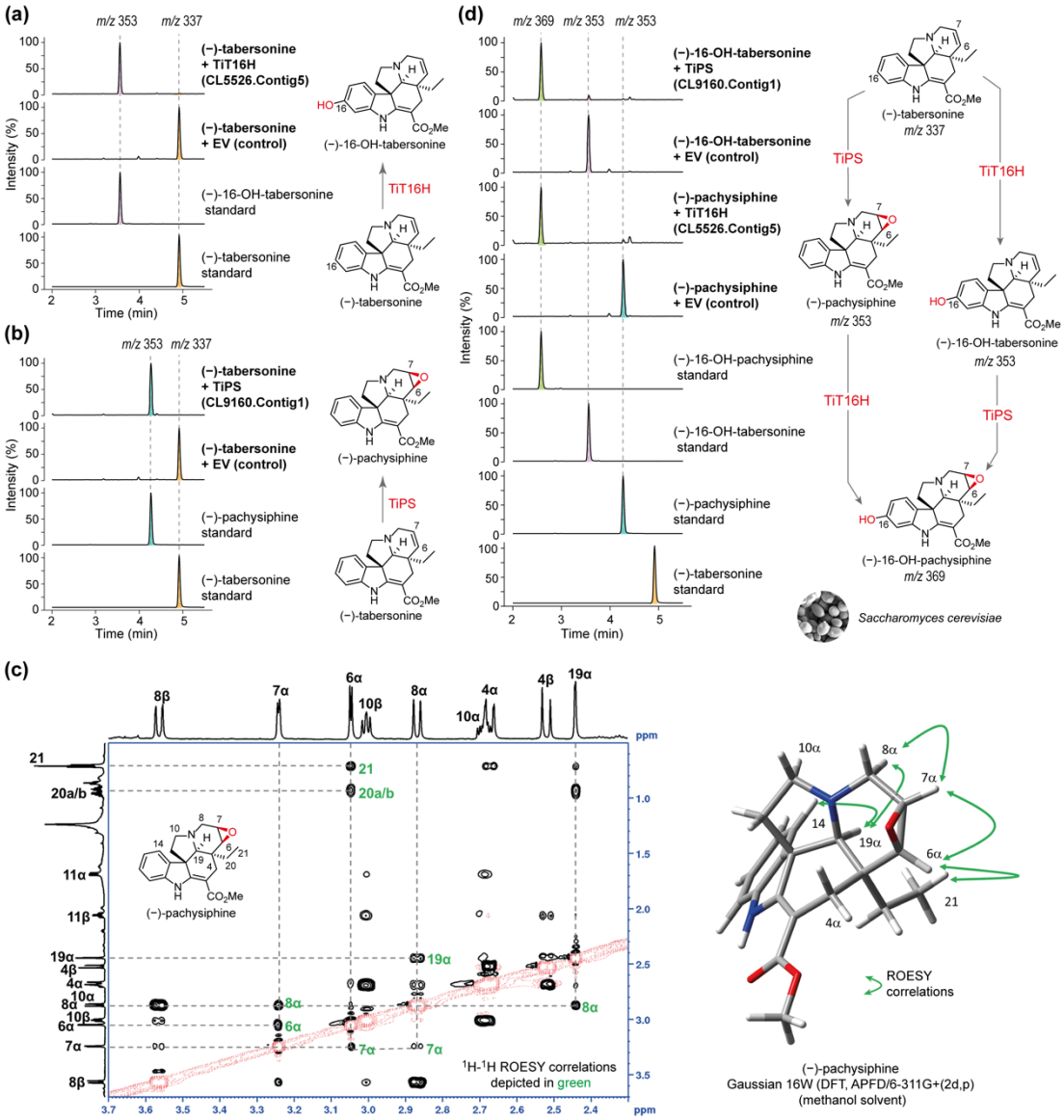


Fig. 5 Characterization of *Tabernanthe iboga* CYP450s in yeast.

(a) Functional characterization of *T. iboga* tabersonine-16-hydroxylase (TiT16H) in yeast for the structure elucidation of 16-hydroxy-tabersonine (16-OH-tabersonine). (b) Functional characterization of *T. iboga* pachysiphine synthase (TiPS) in yeast for the structure elucidation of pachysiphine. (c) ROESY correlation analysis of the β epoxide of pachysiphine alongside a Gaussian model of the compound. (d) Elucidation of 16-hydroxy-pachysiphine (16-OH-pachysiphine) biosynthesis catalyzed by TiT16H and TiPS in yeast for structure validation. LC-MS profiles are presented as total ion chromatograms with *m/z* presented as $[M+H]^+$ of the parent ion.

Interestingly, the MS^2 spectrum of the hydroxylated product (*m/z* 353) of (–)-tabersonine observed from candidate CL9160.contig1 showed a fragmentation pattern similar to that of the epoxide (–)-lochnericine, which is known to be produced by the previously reported CYP71 TEX1 (Carqueijeiro *et al.*, 2018) (Fig. 1, Fig. S9). To determine the product produced by candidate CL9160.contig1, we expressed this gene in yeast, purified yeast microsomes, and incubated the microsomes with (–)-tabersonine to isolate the product. NMR analysis revealed that the product was a tabersonine-6,7-beta (β)-epoxide known as pachysiphine, which is structurally identical to lochnericine except for the stereochemistry of the epoxide (Fig. 5b, Fig. S7b, S10). The stereochemistry of the β-epoxide of pachysiphine was established by ROESY correlation analysis (Fig. 5c, S10). Consequently, CL9160.contig1 was named *T. iboga* pachysiphine synthase (TiPS, assigned as CYP71D821). We performed CD spectroscopy of pachysiphine and assigned the stereochemistry as (–)-pachysiphine (Fig. S11). Surprisingly, (–)-pachysiphine has never been reported in *T. iboga*.

Gene functional characterization (in yeast): Double oxidation of tabersonine by TiT16H and TiPS

Having discovered and functionally characterised TiPS and TiT16H, we combined these two genes with the pS-TabS multigene construct in *N. benthamiana* (Fig. 4c). We observed the formation of a double hydroxylated product corresponding to 16-OH-pachysiphine (*m/z* 369), a compound that has not been reported to be present in *T. iboga*. As described above for (–)-pachysiphine, we expressed both genes in yeast, prepared microsomes that contained TiPS and TiT16H, and then performed *in vitro* reactions with the substrates (–)-pachysiphine and (–)-16-OH-tabersonine. These reactions resulted in the formation of what appeared to be a hydroxylated pachysiphine product, and the yield was unaffected by the order in which the enzymes were added (Fig. 5c). To obtain the compound in sufficient quantities for NMR analysis, we scaled up the reaction containing (–)-pachysiphine with TiT16H protein and isolated the resulting product by HPLC. NMR analysis confirmed that the product was the expected 16-OH-pachysiphine (Fig. S7c, S12). We carefully examined the metabolite profile of *T. iboga* tissue for the presence of pachysiphine and its hydroxylated derivatives. Although neither pachysiphine nor 16-OH-pachysiphine has been reported to be present in *T. iboga,*

we observed the presence of both compounds in methanolic extracts of the young leaf of this plant (Fig. S13).

Platform development: *Catharanthus roseus* flowers as a screening platform

The *N. benthamiana* leaf disk assay minimizes the quantities of exogenous substrate required for testing biosynthetic enzymes and this led to the streamlined identification of TiPS and TiT16H. However, it can be challenging to obtain even small amounts of some chemically complex substrates involved in MIA biosynthesis (*e.g.* stemmadenine acetate) (Caputi *et al.*, 2018). We reasoned that since many MIA-producing plants produce this upstream biosynthetic pathway intermediate if any of these plants could be transformed with these multi-gene constructs, the substrate could be accessed in situ. *T. iboga* is slow to germinate, and efforts to transform this plant have not been successful. However, the MIA-producing plant *Catharanthus roseus* is fast-growing and readily available, and although *C. roseus* leaves are recalcitrant to transient expression, the flowers of *C. roseus* have been successfully transfected to express transcription factors (Schweizer *et al.*, 2018; Colinas *et al.*, 2021). We surveyed the alkaloid profile of the flowers of the *C. roseus* cultivar “Little Bright Eyes” (LBE) using untargeted LC-MS and observed the presence of MIA precursors stemmadenine acetate and precondylocarpine acetate upon *Agrobacterium* infiltration (Fig. S14), suggesting that the substrate utilized by the genes encoded in the pS-Tab and pS-psTab multi-gene constructs is present in this tissue.

To test whether we could access the upstream stemmadenine acetate pools within flower tissue and heterologously produce active enzymes in flower petals, we transfected the petals with multigene constructs designed for tabersonine (pS-Tab) and pseudo-tabersonine (pS-psTab) without the addition of any exogenous substrate. After three days of infection, increased levels of tabersonine were observed in petals transfected with the tabersonine-producing multigene construct (pS-Tab) (Fig 6a). Tabersonine is present as a natural product in *C. roseus* LBE flowers in low abundance, as confirmed by comparison with a standard. However, when the flower was transfected with pS-TabS, the levels of tabersonine were substantially higher. Notably, *C. roseus* does not natively produce and accumulate pseudo-tabersonine (Fig. S14). However, in the case of the pseudo-tabersonine multigene construct (pS-psTab), we observed the formation of this compound in the

flower petals (Fig 6a). The observation of both tabersonine over-production and pseudo-tabersonine accumulation demonstrates that the upstream stemmadenine acetate pools can be utilized within the flower and that multiple active enzymes can be heterologously expressed to catalyze the formation of native and non-native metabolites in the flower petals to explore downstream biosynthesis.

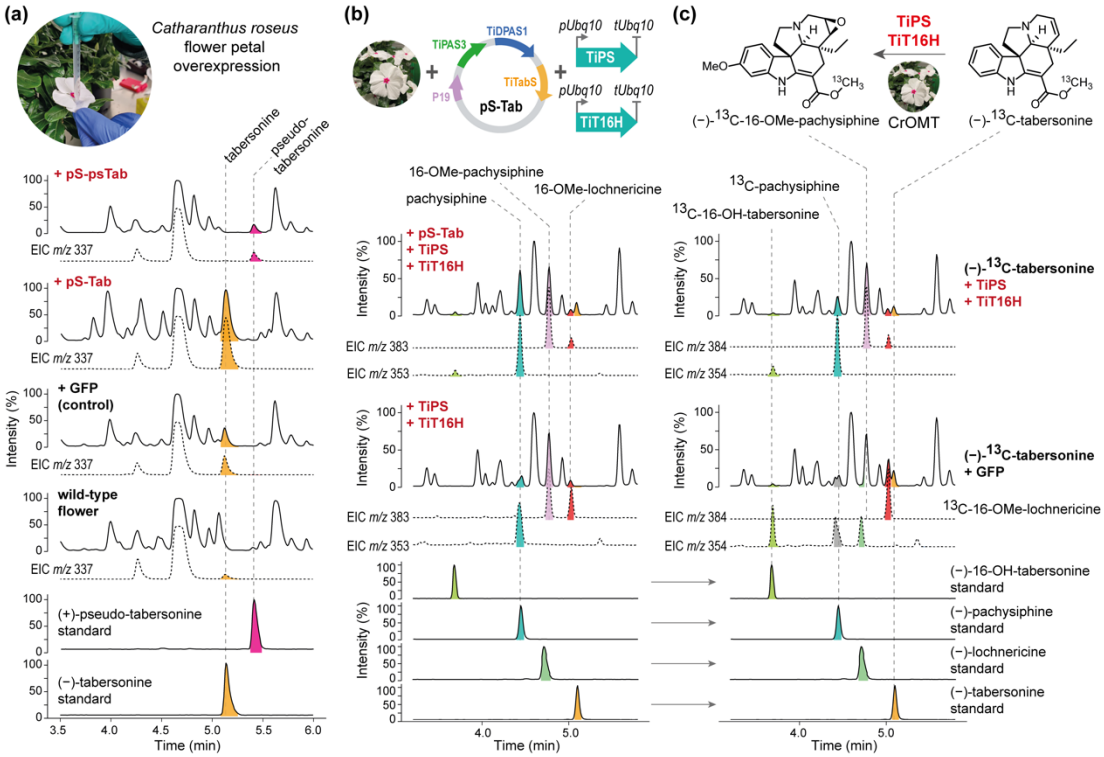


Fig. 6 Transient overexpression of *Tabernanthe iboga* enzymes in *Catharanthus roseus* var. LBE flowers.

(a) LC-MS profiles of the products resulting from the transient expression of multigene constructs pS-Tab (tabersonine-producing) and pS-psTab (pseudo-tabersonine-producing) in *C. roseus* var. LBE flower petals. Expression of pS-Tab and pS-psTab results in the formation of tabersonine and pseudo-tabersonine, respectively in *C. roseus* flowers without the addition of exogenous substrate. (b) LC-MS profiles of the products generated by the co-expression of TiPS and TiT16H in combination with and separately from pS-Tab in *C. roseus* flowers. The expected product pachysiphine is increased when pS-Tab is co-expressed with TiPS and TiT16H alongside putative 16-OMe-pachysiphine catalyzed by endogenous enzyme(s). (c) LC-MS profiles of labeled pachysiphine and 16-OH-tabersonine generated by transient co-expression of TiPS and TiT16H in *C. roseus* flowers assayed with ^{13}C-labeled tabersonine substrate. Consequent labeling of the putative

16-OMe-pachysiphine is also observed due to the endogenous catalytic activity of *C. roseus* enzymes in the flowers. LC-MS profiles in solid lines are presented as total ion chromatograms, dotted lines as extracted ion chromatograms (EIC) with *m/z* presented as $[M+H]^+$ of the parent ion.

When the pS-TabS multigene construct was transfected into the flower petals of *C. roseus*, in addition to the product tabersonine, we unexpectedly observed the formation of its derivatized products 16-OH-tabersonine, lochnericine, and 16-OMe-tabersonine (Fig. S15). These modifications were likely catalyzed by endogenous *C. roseus* enzymes with specificity for tabersonine. To investigate the endogenous enzymatic activity catalyzed by *C. roseus* petals, we incubated wild-type flower petal disks in buffer (300 µl) with 25 µM ^{13}C labeled (Fig. S16) and non-labeled tabersonine, the product of the multigene construct (pS-Tab). The tabersonine substrate was converted into the downstream alkaloids 16-hydroxy-tabersonine (16-OH-tabersonine), lochnericine, 16-methoxy-tabersonine (16-OMe-tabersonine), and 16-O-methoxy-tabersonine (16-OMe-lochnericine) as observed by the formation of equivalent ^{13}C labeled products (Fig. S17). This confirmed the presence of active enzymes in this tissue able to derivatize tabersonine. In contrast, when the pS-psTab multigene construct was expressed, no downstream derivatization products of pseudo-tabersonine were detected. This lack of further modification is not surprising, as *C. roseus* does not naturally produce pseudo-tabersonine, and therefore, this plant would be expected to lack endogenous enzymes with specificity for this substrate.

Having established the native activity of *C. roseus* flower petals on the precursor tabersonine, we transfected flowers simultaneously with the multigene construct pS-Tab and two strains of *Agrobacterium* containing TiPS and TiT16H. After three days, the methanolic extracts of the transformed flower petals were analyzed by LC-MS for metabolic changes. We observed the heterologous production of pachysiphine and a compound with a mass corresponding to 16-O-methoxy pachysiphine (16-OMe-pachysiphine), both natural products not found natively in the *C. roseus* flower (Fig. 6b, Fig. S18). To corroborate this result, we incubated flower disks transfected simultaneously with TiPS and TiT16H in a buffer (300 µl) containing 50 µM ^{13}C-labeled tabersonine. As expected, the transformed

disks showed the formation of ^{13}C-labeled pachysiphine and ^{13}C-labeled 16-OMe-pachysiphine (Fig. 6c Fig. S19).

Discussion

The monoterpene indole alkaloids (–)-tabersonine (aspidosperma) and (+)-pseudo-tabersonine (pseudo-aspidosperma) are alkaloid scaffolds found in many plant species that are modified through various oxidation reactions to generate chemical diversity (Giddings *et al.*, 2011; Besseau *et al.*, 2013; Kellner *et al.*, 2015; Carqueijeiro *et al.*, 2018). Here, we report the discovery of two tabersonine derivatizing enzymes from *T. iboga*, TiPS, and TiT16H. We used a miniaturized assay that uses *N. benthamiana* leaf disks to screen for enzyme activity, allowing the use of only small quantities of precious starting substrate. There was complete conversion of the starting material to pachysiphine or 16-OH-tabersonine (Fig 4c). Despite the *N. benthamiana* leaf disk assay being developed for screening purposes at an analytical scale, we could approximate the amount of product derived from the starting material stemmadenine acetate inferred from the internal standard (ajmaline) used for metabolite extraction (ca. 1.4 μM mg^{-1} (fresh weight) for 16-OH-tabersonine and ca. 2.4 μM mg^{-1} (fresh weight) for pachysiphine). Furthermore, we also demonstrate that flower petals of the MIA-producing plant *C. roseus* can be transformed with the desired genes and that after gene expression, the resulting enzymes can access the biosynthetic intermediates present in this tissue as a source of in situ substrates. For monoterpene indole alkaloid biosynthetic enzymes that utilize rare or difficult-to-access substrates, this is a convenient and efficient expression platform for biosynthetic gene candidate screening.

The activity of TiT16H, which catalyzes the hydroxylation of the 16 position of tabersonine, has been previously identified in the closely related plant *C. roseus* (CrT16H). Surprisingly, while both of these enzymes belong to the CYP71 family, these genes are found in different clades in the phylogenetic tree (Figure 4a). TiT16H and CrT16H share only 56% amino acid identity (Fig. S20, S21), suggesting that the enzymatic activity in these two closely related plants may have evolved independently. We also discovered the enzyme that catalyzes the formation of the β epoxide moiety on tabersonine to form pachysiphine (TiPS). Although pachysiphine is not found in *C. roseus*, this compound is structurally similar to lochnericine, a natural product that is found in *C. roseus* roots (Carqueijeiro *et al.*, 2018). The only

difference between lochnericine and pachysiphine is the stereochemistry of the epoxide. In *C. roseus*, the formation of this alpha (α) epoxide moiety on the (–)-tabersonine substrate is catalyzed by CrTEX1 or CrTEX2 in the presence of tabersonine (Carqueijeiro *et al.*, 2018). However, TiPS, which catalyzes the formation of the β epoxide on (–)-tabersonine to yield pachysiphine, has only 46% amino acid identity to CrTEX1 (45% identity with CrTEX2). Therefore, it would appear that the stereoselectivity of this epoxidation reaction also may have evolved independently. Docking of the tabersonine substrate into the active sites of TiPS and CrTEX1 using AlphaFold shows how the active sites of these two enzymes each orient the substrate to generate the respective α and β stereoisomers (Fig. S22). However, given the lack of sequence similarity between TiPS and CrTEX1, it is difficult to attribute this stereoselectivity to specific residues in the enzyme active sites. Finally, we show that these two enzymes can act together to generate 16-OH-pachysiphine from tabersonine. Although pachysiphine has not been reported to be found in *T. iboga*, after the discovery of these enzyme activities, we carefully inspected the metabolite profile of *T. iboga* tissues and saw the presence of both pachysiphine and 16-OH-pachysiphine in young leaves (Fig. S13). We also examined the gene expression profile of TiPS and TiT16H from the transcriptomic data and observed TiPS to be expressed in the roots, flowers, and young leaves, whereas TiT16H was expressed in the leaves of the plant (Fig. S23). Although 16-OH-tabersonine is synthesized and stored in the leaves of the plant, the same cannot be said for pachysiphine. It seems that pachysiphine might be transported across the areal parts of the plant for storage, or it may be metabolized more readily in the roots and flowers. This could explain why pachysiphine is not detected in the roots or flowers despite being expressed there.

Pachysiphine and 16-OH-pachysiphine have no known biological function but are well known to serve as precursors for a variety of dimeric alkaloids, including melodinine K (Walia *et al.*, 2020), conophylline (Han-ya *et al.*, 2011), conolodinines A–D (Sim *et al.*, 2019), and scandomelidine (Mehri & Plat, 1992) which display a variety of pharmacological activities. Therefore, the discovery of these biosynthetic genes from *T. iboga* provides the foundation for assay and discovery of the biosynthetic genes that make this structurally complex family of dimeric alkaloids. Overall, *T. iboga* is a rich source of oxidative derivatization enzymes, and the miniaturized screening platforms described here can streamline the identification of these enzymes.

Acknowledgements

We thank Prashant D. Sonawanne for advice on Goldenbraid cloning and design, Maritta Kunert for assistance with mass spectrometry, Eva Rothe, Franz Kaltofen, and the members of the Max Planck Institute for Chemical Ecology Research Green House for providing and tending to the *Catharanthus roseus*, *Tabernanthe iboga*, and *Nicotiana benthamiana* plants. We thank David Nelson for his assistance in assigning the CYP family of TiPS and TiT16H. We gratefully acknowledge the Max Planck Society and the Leibniz Prize (DfG, 505457618) for funding.

Competing interests

None declared.

Data availability

The data supporting this study's findings are available within the article and in the Supporting Information file. Sequences for TiPS (PQ178877) and TiT16H (PQ178876) have been deposited in GenBank.

3.4 References

Auriola S, Naaranlahti T, Lapinjoki SP. **1991**. Synthesis of [methyl-^{2}H]-labelled ajmalicine, yohimbine, tabersonine and catharanthine. *Journal of Labelled Compounds and Radiopharmaceuticals* **29**: 117–121.

Bathe U, Tissier A. **2019**. Cytochrome P450 enzymes: A driving force of plant diterpene diversity. *Phytochemistry* **161**: 149–162.

Besseau S, Kellner F, Lanoue A, Thamm AMK, Salim V, Schneider B, Geu-Flores F, Höfer R, Guirimand G, Guihur A, *et al.* 2013. A Pair of Tabersonine 16-Hydroxylases Initiates the Synthesis of Vindoline in an Organ-Dependent Manner in *Catharanthus roseus*. *Plant Physiology* **163**: 1792–1803.

Caputi L, Franke J, Farrow SC, Chung K, Payne RME, Nguyen T-D, Dang T-TT, Carqueijeiro IST, Koudounas K, Bernonville TD de, *et al.* 2018. Missing enzymes in the biosynthesis of the anticancer drug vinblastine in Madagascar periwinkle. *Science* **360**: 1235–1239.

Carqueijeiro I, Brown S, Chung K, Dang T-T, Walia M, Besseau S, Bernonville TD de, Oudin A, Lanoue A, Billet K, *et al.* 2018. Two Tabersonine 6,7-Epoxidases Initiate Lochnericine-Derived Alkaloid Biosynthesis in *Catharanthus roseus*. *Plant Physiology* **177**: 1473–1486.

Christ B, Xu C, Xu M, Li F-S, Wada N, Mitchell AJ, Han X-L, Wen M-L, Fujita M, Weng J-K. **2019**. Repeated evolution of cytochrome P450-mediated spiroketal steroid biosynthesis in plants. *Nature Communications* **10**: 3206.

Colinas M, Goossens A. **2022**. *Catharanthus roseus*, Methods and Protocols. *Methods in Molecular Biology* **2505**: 281–291.

Colinas M, Pollier J, Vaneechoutte D, Malat DG, Schweizer F, Milde LD, Clercq RD, Guedes JG, Martínez-Cortés T, Molina-Hidalgo FJ, *et al.* 2021. Subfunctionalization of Paralog Transcription Factors Contributes to Regulation of Alkaloid Pathway Branch Choice in *Catharanthus roseus*. *Frontiers in Plant Science* **12**: 687406.

Dang T-TT, Franke J, Carqueijeiro IST, Langley C, Courdavault V, O'Connor SE. **2018**. Sarpagan bridge enzyme has substrate-controlled cyclization and aromatization modes. *Nature chemical biology* **14**: 760–763.

Farrow SC, Kamileen MO, Caputi L, Bussey K, Mundy JEA, McAtee RC, Stephenson CRJ, O'Connor SE. **2019**. Biosynthesis of an Anti-Addiction Agent from the Iboga Plant. *Journal of the American Chemical Society* **141**: 12979–12983.

Forestier ECF, Czechowski T, Cording AC, Gilday AD, King AJ, Brown GD, Graham IA. **2021**. Developing a Nicotiana benthamiana transgenic platform for high-value diterpene production and candidate gene evaluation. *Plant Biotechnology Journal* **19**: 1614–1623.

Franke J, Kim J, Hamilton JP, Zhao D, Pham GM, Wiegert-Rininger K, Crisovan E, Newton L, Vaillancourt B, Tatsis E, *et al.* 2019. Gene Discovery in Gelsemium Highlights Conserved Gene Clusters in Monoterpene Indole Alkaloid Biosynthesis. *ChemBioChem* **20**: 83–87.

Giddings L-A, Liscombe DK, Hamilton JP, Childs KL, DellaPenna D, Buell CR, O'Connor SE. **2011**. A Stereoselective Hydroxylation Step of Alkaloid Biosynthesis by a Unique Cytochrome P450 in *Catharanthus roseus*. *Journal of Biological Chemistry* **286**: 16751–16757.

Grefen C, Donald N, Hashimoto K, Kudla J, Schumacher K, Blatt MR. **2010**. A ubiquitin-10 promoter-based vector set for fluorescent protein tagging facilitates temporal stability and native protein distribution in transient and stable expression studies. *The Plant Journal* **64**: 355–365.

Hansen CC, Nelson DR, Møller BL, Werck-Reichhart D. **2021**. Plant cytochrome P450 plasticity and evolution. *Molecular Plant* **14**: 1244–1265.

Han-ya Y, Tokuyama H, Fukuyama T. **2011**. Total Synthesis of (−)-Conophylline and (−)-Conophyllidine. *Angewandte Chemie International Edition* **50**: 4884–4887.

Hisiger S, Jolicoeur M. **2007**. Analysis of Catharanthus roseus alkaloids by HPLC. *Phytochemistry Reviews* **6**: 207–234.

Hong B, Grzech D, Caputi L, Sonawane P, López CER, Kamileen MO, Lozada NJH, Grabe V, O'Connor SE. **2022**. Biosynthesis of strychnine. *Nature* **607**: 617–622.

Jiang B, Gao L, Wang H, Sun Y, Zhang X, Ke H, Liu S, Ma P, Liao Q, Wang Y, *et al.* 2024. Characterization and heterologous reconstitution of Taxus biosynthetic enzymes leading to baccatin III. *Science* **383**: 622–629.

Kamileen MO, DeMars MD, Hong B, Nakamura Y, Paetz C, Lichman BR, Sonawane PD, Caputi L, O'Connor SE. **2022**. Recycling Upstream Redox Enzymes Expands the Regioselectivity of Cycloaddition in Pseudo-Aspidosperma Alkaloid Biosynthesis. *Journal of the American Chemical Society* **144**: 19673–19679.

Kellner F, Geu-Flores F, Sherden NH, Brown S, Foureau E, Courdavault V, O'Connor SE. **2015**. Discovery of a P450-catalyzed step in vindoline biosynthesis: a link between the aspidosperma and eburnamine alkaloids. *Chemical Communications* **51**: 7626–7628.

Kruse LH, Sunstrum FG, Garcia D, Pérez GL, Jancsik S, Bohlmann J, Irmisch S. **2024**. Improved production of the antidiabetic metabolite montbretin A in Nicotiana benthamiana: discovery, characterization, and use of Crocosmia shikimate shunt genes. *The Plant Journal* **117**: 766–785.

Kumar M, Ayzenshtat D, Marko A, Bocobza S. **2022**. Optimization of T-DNA configuration with UBIQUITIN10 promoters and tRNA–sgRNA complexes promotes highly efficient genome editing in allotetraploid tobacco. *Plant Cell Reports* **41**: 175–194.

Martin LBB, Kikuchi S, Rejzek M, Owen C, Reed J, Orme A, Misra RC, El-Demerdash A, Hill L, Hodgson H, *et al.* 2024. Complete biosynthesis of the potent vaccine adjuvant QS-21. *Nature Chemical Biology* **20**: 493–502.

Mehri H, Plat M. **1992**. The Structure of Scandomelidine, Bisindole Alkaloid from Melodinus scandens. *Journal of Natural Products* **55**: 241–244.

Nett RS, Dho Y, Tsai C, Passow D, Grundman JM, Low Y-Y, Sattely ES. **2023**. Plant carbonic anhydrase-like enzymes in neuroactive alkaloid biosynthesis. *Nature* **624**: 182–191.

Nguyen T-D, Dang T-TT. **2021**. Cytochrome P450 Enzymes as Key Drivers of Alkaloid Chemical Diversification in Plants. *Frontiers in Plant Science* **12**: 682181.

Pompon D, Louerat B, Bronine A, Urban P. **1996**. [6] Yeast expression of animal and plant P450s in optimized redox environments. *Methods in Enzymology* **272**: 51–64.

Sarrion-Perdigones A, Vazquez-Vilar M, Palací J, Castelijns B, Forment J, Ziarsolo P, Blanca J, Granell A, Orzaez D. **2013**. GoldenBraid 2.0: A

Comprehensive DNA Assembly Framework for Plant Synthetic Biology . *Plant Physiology* **162**: 1618–1631.

Schweizer F, Colinas M, Pollier J, Moerkercke AV, Bossche RV, Clercq R de, Goossens A. **2018**. An engineered combinatorial module of transcription factors boosts production of monoterpenoid indole alkaloids in Catharanthus roseus. *Metabolic Engineering* **48**: 150–162.

Sim DS-Y, Navanesan S, Sim K-S, Gurusamy S, Lim S-H, Low Y-Y, Kam T-S. **2019**. Conolodinines A–D, Aspidosperma–Aspidosperma Bisindole Alkaloids with Antiproliferative Activity from Tabernaemontana corymbosa. *Journal of Natural Products* **82**: 850–858.

Tatsis EC, Carqueijeiro I, Bernonville TD de, Franke J, Dang T-TT, Oudin A, Lanoue A, Lafontaine F, Stavrinides AK, Clastre M, *et al.* 2017. A three enzyme system to generate the Strychnos alkaloid scaffold from a central biosynthetic intermediate. *Nature Communications* **8**: 316.

Urban P, Mignotte C, Kazmaier M, Delorme F, Pompon D. **1997**. Cloning, Yeast Expression, and Characterization of the Coupling of Two Distantly Related Arabidopsis thalianaNADPH-Cytochrome P450 Reductases with P450 CYP73A5*. *Journal of Biological Chemistry* **272**: 19176–19186.

Walia M, Teijaro CN, Gardner A, Tran T, Kang J, Zhao S, O'Connor SE, Courdavault V, Andrade RB. **2020**. Synthesis of (−)-Melodinine K: A Case Study of Efficiency in Natural Product Synthesis. *Journal of Natural Products* **83**: 2425–2433.

Wang Z, Xiao Y, Wu S, Chen J, Li A, Tatsis EC. **2022**. Deciphering and reprogramming the cyclization regioselectivity in bifurcation of indole alkaloid biosynthesis. *Chemical Science* **13**: 12389–12395.

Williams D, Qu Y, Simionescu R, Luca VD. **2019**. The assembly of (+)-vincadifformine- and (−)-tabersonine-derived monoterpenoid indole alkaloids in Catharanthus roseus involves separate branch pathways. *The Plant Journal* **99**: 626–636.

Supporting Information

Fig. S1 Design of multi-transcriptional unit constructs

Fig. S2 *N. benthamiana* leaf disk assay workflow

Fig. S3 Testing multi-gene constructs in *N. benthamiana.*

Fig. S4 Chiral LC-MS analysis of pseudo-tabersonine.

Fig. S5 Phylogenetic tree of *Tabernanthe iboga* (Ti) cytochrome P450s.

Fig. S6 Iboga CYP71s assayed with (+)-pseudo-tabersonine in *N. benthamiana*.

Fig. S7 HPLC isolation of hydroxylated tabersonine products from yeast workup.

Fig. S8 Structure elucidation of (–)-16-OH-tabersonine by NMR.

Fig. S9 MS^2 spectral comparison of lochnericine and CL9160.contig1 product.

Fig. S10 Structure elucidation of (–)-pachysiphine by NMR.

Fig. S11 Electronic circular dichroism (ECD) spectra of (–)-pachysiphine.

Fig. S12 Structure elucidation of (–)-16-OH-pachysiphine by NMR.

Fig. S13 LC-MS metabolite profiles of *T. iboga* tissues.

Fig. S14 MIA precursors present in *C. roseus* var. LBE flowers.

Fig. S15 Derivatization of tabersonine by endogenous enzymes present in *C. roseus* flowers.

Fig. S16 Structure confirmation of (–)-[^{13}C]-tabersonine.

Fig. S17 Incubation of *C. roseus* flowers with ^{13}C-labelled tabersonine.

Fig. S18 Overexpression of TiPS and TiT16H in *C. roseus* flowers.

Fig. S19 Overexpression of TiPS and TiT16H in *C. roseus* flowers with ^{13}C-labeled tabersonine.

Fig. S20 Percentage of identity shared by TiPS and TiT16H with *C. roseus* P450s.

Fig. S21 Sequence alignment of TiPS and TiT16H.

Fig. S22 Molecular docking of tabersonine into AlphaFold models of TiPS and TiT16H.

Fig. S23 Transcriptomics and metabolomics related to 16-OH-pachysiphine biosynthesis in *T. iboga*.

Methods S1 Materials and methods.

Table S1 Nucleotide sequences of genes described in this study.

Table S2 Primers used in this study.

3.5 Supporting Information

***New Phytologist* Supporting Information**

Article title: **Streamlined screening platforms lead to the discovery of pachysiphine synthase from *Tabernanthe iboga***

Authors: Mohamed O. Kamileen, Yoko Nakamura, Katrin Luck, Sarah Heinicke, Benke Hong, Maite Colinas, Benjamin R. Lichman, Sarah E. O'Connor

Article acceptance date: 25 August 2024

The following Supporting Information is available for this article:

Fig. S1 Design of multi-transcriptional unit constructs

Fig. S2 *N. benthamiana* leaf disk assay workflow

Fig. S3 Testing multi-gene constructs in *N. benthamiana.*

Fig. S4 Chiral LC-MS analysis of pseudo-tabersonine.

Fig. S5 Phylogenetic tree of *Tabernanthe iboga* (Ti) cytochrome P450s.

Fig. S6 Iboga CYP71s assayed with (+)-pseudo-tabersonine in *N. benthamiana*.

Fig. S7 HPLC isolation of hydroxylated tabersonine products from yeast workup.

Fig. S8 Structure elucidation of (–)-16-OH-tabersonine by NMR.

Fig. S9 MS^2 spectral comparison of lochnericine and CL9160.contig1 product.

Fig. S10 Structure elucidation of (–)-pachysiphine by NMR.

Fig. S11 Electronic circular dichroism (ECD) spectra of (–)-pachysiphine.

Fig. S12 Structure elucidation of (–)-16-OH-pachysiphine by NMR.

Fig. S13 LC-MS metabolite profiles of *T. iboga* tissues.

Fig. S14 MIA precursors present in *C. roseus* var. LBE flowers.

Fig. S15 Derivatization of tabersonine by endogenous enzymes present in *C. roseus* flowers.

Fig. S16 Structure confirmation of (–)-[^{13}C]-tabersonine.

Fig. S17 Incubation of *C. roseus* flowers with ^{13}C-labelled tabersonine.

Fig. S18 Overexpression of TiPS and TiT16H in *C. roseus* flowers.

Fig. S19 Overexpression of TiPS and TiT16H in *C. roseus* flowers with ^{13}C-labeled tabersonine.

Fig. S20 Percentage of identity shared by TiPS and TiT16H with *C. roseus* P450s.

Fig. S21 Sequence alignment of TiPS and TiT16H.

Fig. S22 Molecular docking of tabersonine into AlphaFold models of TiPS and TiT16H.

Fig. S23 Transcriptomics and metabolomics related to 16-OH-pachysiphine biosynthesis in *T. iboga*.

Fig. S24 LC-MS profiles and MS^2 spectra of authentic standards.

Table S1 Nucleotide sequences of genes described in this study.

Table S2 Primers used in this study.

Methods S1 Materials and methods.

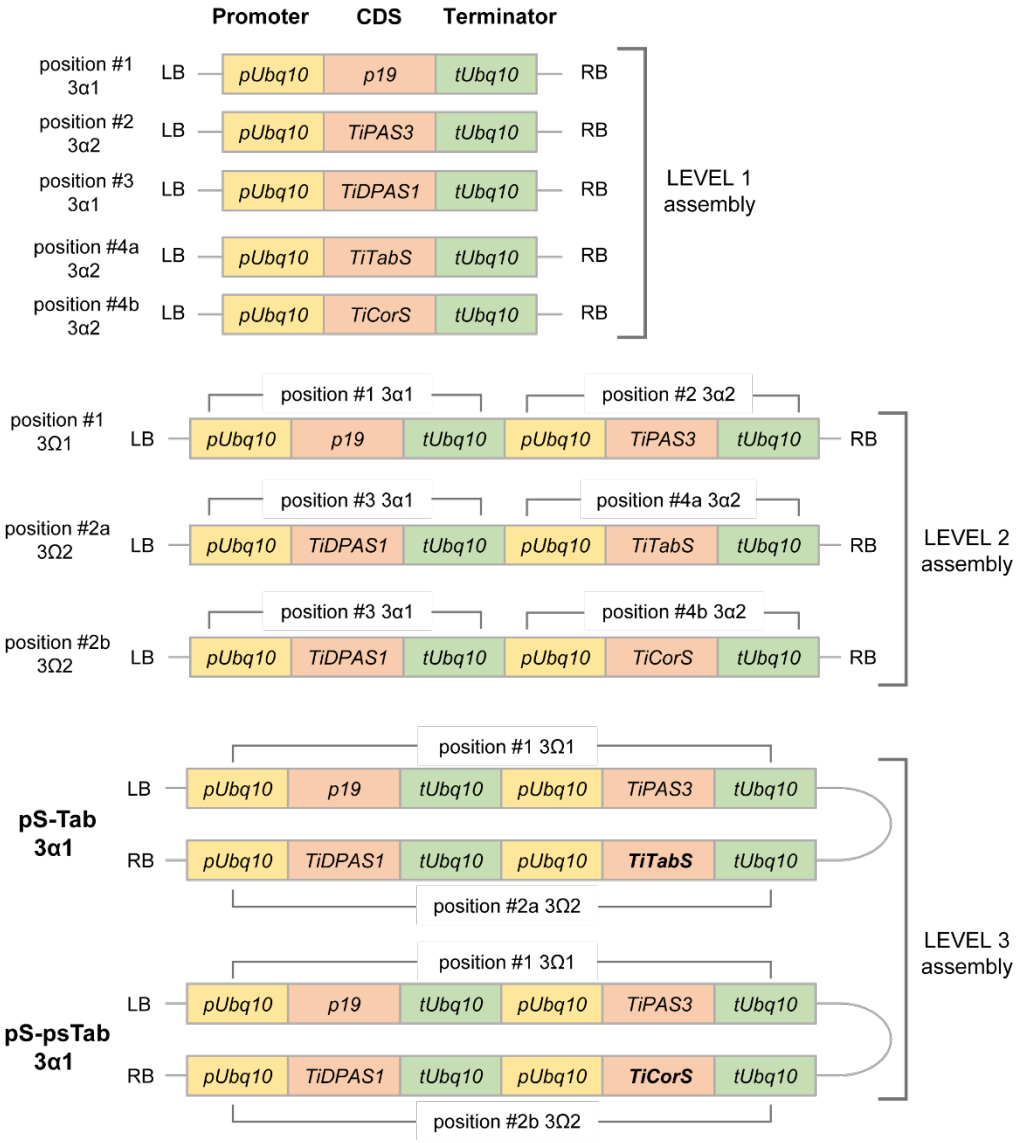


Fig. S1 Design of multi-transcriptional unit constructs.

Overview of the design of Level 1 constructs, and the assembly of Level 2 and Level 3 multi-transcription unit constructs encoding for tabersonine and pseudo-tabersonine biosynthesis for transient expression in *Nicotiana benthamiana*. Transcriptional units were assembled and constructed using the GoldenBraid 2.0 kit. Biosynthetic genes and P19 suppressor are assembled into 3α1 and 3α2 vectors as a transcriptional unit with a Ubiquitin10 promoter (pUbq10) and Ubiquitin10 terminator (tUbq10) at Level 1. Level 1 assemblies are paired into 3Ω1 and 3Ω2 vectors as Level 2 multi-transcriptional unit (multigene) constructs. Level 2 constructs are combined into the 3α1 vector to generate the final multi-gene (4 gene) pS-Tab and pS-psTab, encoding for transient gene expression of tabersonine and pseudo-tabersonine biosynthesis respectively, in *N. benthamiana*. LB and RB indicate the left and right border of the binary plasmid.

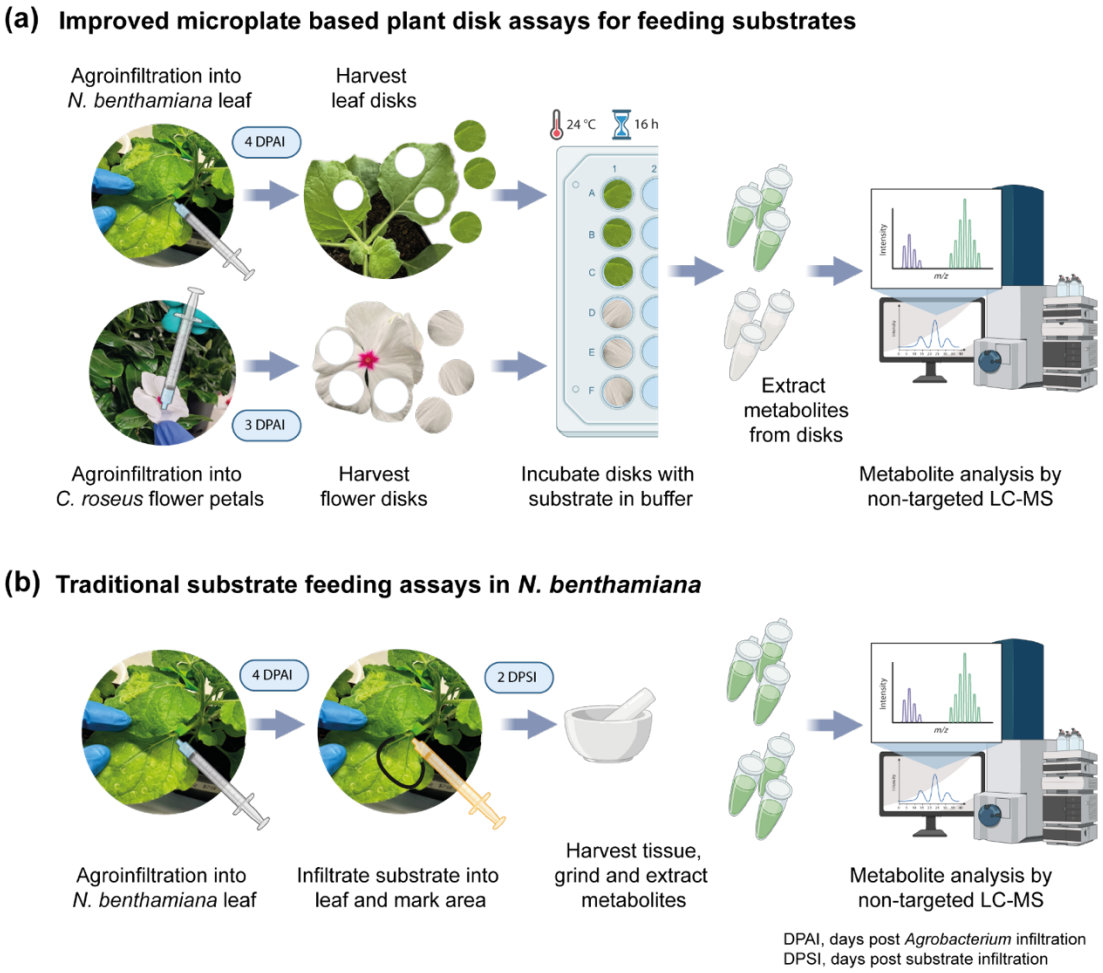


Fig. S2 *N. benthamiana* leaf disk assay workflow.

(a) Schematic of the plant disk-based screening system designed to test for enzyme activity of transiently expressed genes in *N. benthamiana* leaves or *Catharanthus roseus* flowers with exogenous substrate(s). Plant disks are harvested four days post *Agrobacterium* infiltration (DPAI) and incubated in a microplate containing buffer and substrate of known volume and concentration. After overnight incubation, the disks are collected, pulverized, and extracted for LC-MS analysis. (b) Workflow of conventional enzyme activity screening involving syringe-based substrate feeding in *N. benthamiana*. Drawbacks of this workflow include the requirement for larger quantities of substrate, wastage during syringe infiltration, and the lack of precise control over substrate delivery into the plant tissue.

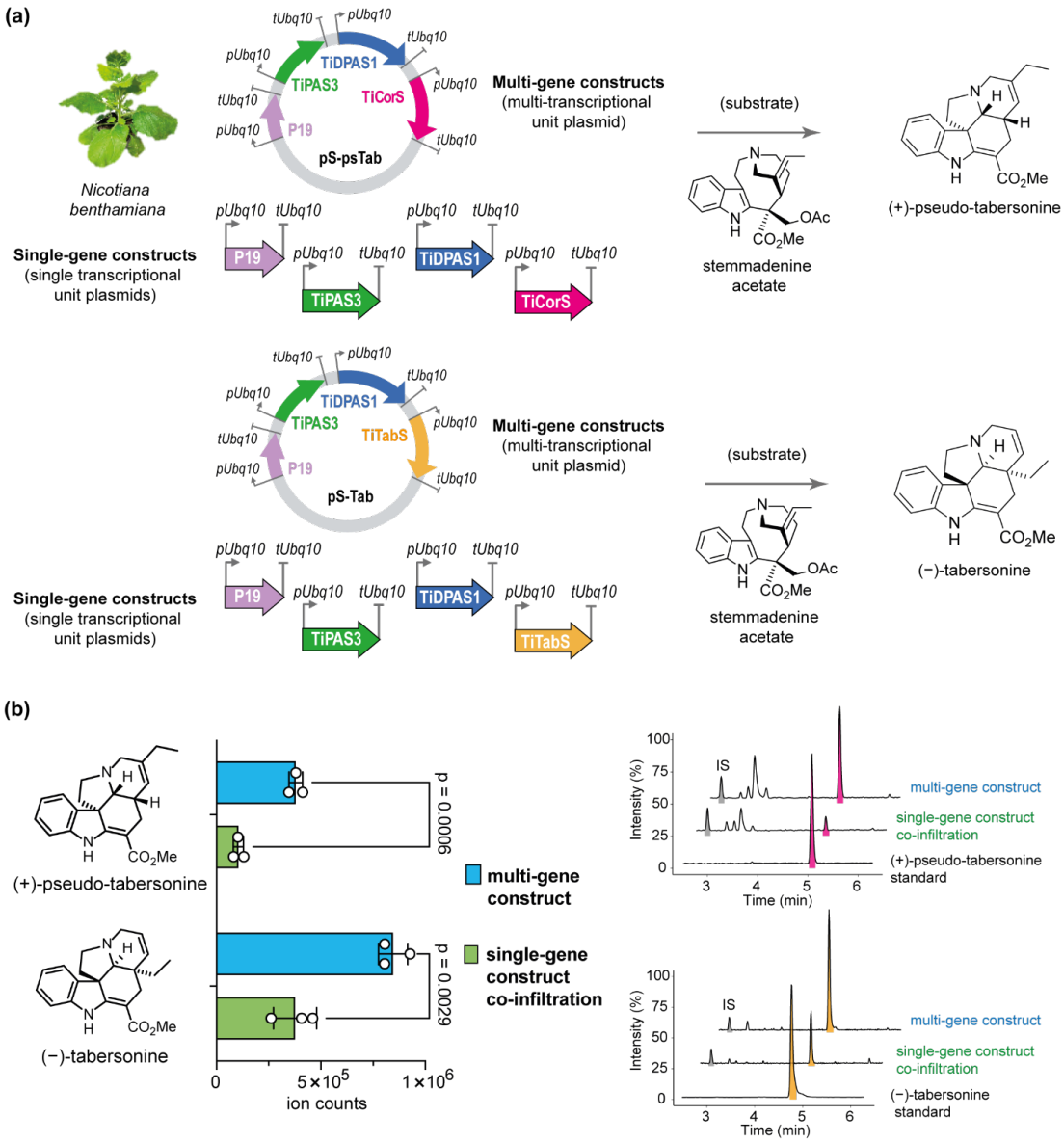


Fig. S3 Testing multi-gene constructs in *N. benthamiana*.

(a) Design of multi-gene constructs pS-Tab and pS-psTab to produce tabersonine and pseudo-tabersonine, respectively, through transient expression in *N. benthamiana* and substrate feeding with stemmadenine acetate. (b) Comparison of the qualitative biosynthetic yields of tabersonine and pseudo-tabersonine produced by the multi-gene constructs (blue bars) versus the equivalent single-gene co-infiltrated constructs (green bars). Representative LC-MS profiles (total ion chromatograms) show the production of tabersonine and pseudo-tabersonine qualitatively, with ajmaline as the internal standard (IS). The values represent mean ± SD (n = 3), two-tailed Student's t-test.

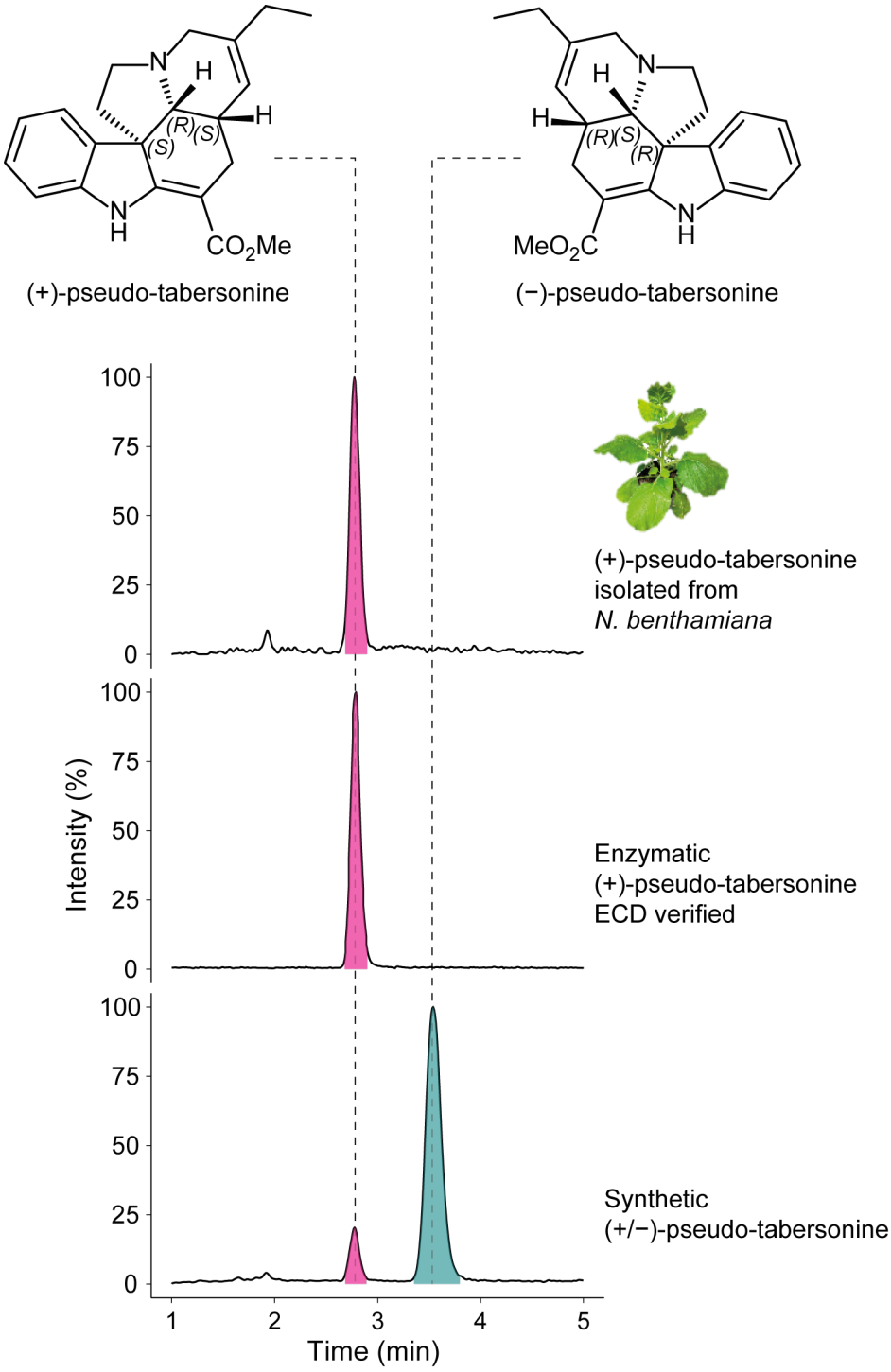


Fig. S4 Chiral LC-MS analysis of pseudo-tabersonine.

The biosynthetic product of pseudo-tabersonine generated in *N. benthamiana* is enantiomerically pure (+)-pseudo-tabersonine. LC-MS traces are presented as total ion chromatograms (solid lines).



Fig. S5 Phylogenetic tree of *Tabernanthe iboga* (Ti) cytochrome P450s. Full-length P450s were extracted from de novo assembled transcriptome. Selected *Arabidopsis thaliana* (At) CYPs were included in the analysis to define CYP clans and CYP71 based on (Hansen *et al.*, 2021). The maximum-likelihood phylogenetic tree was constructed using iQtree (Trifinopoulos *et al.*, 2016) with default parameters and 1000 bootstraps (shown out of 100). The CYP71 family and major P450 clans are highlighted and labelled. P450s functionally characterised to be involved in monoterpene indole alkaloid (MIA) biosynthesis are coloured in red. Clan 86 was used to root the tree. The phylogenetic tree was visualized and inferred using iToL (Letunic & Bork, 2024).

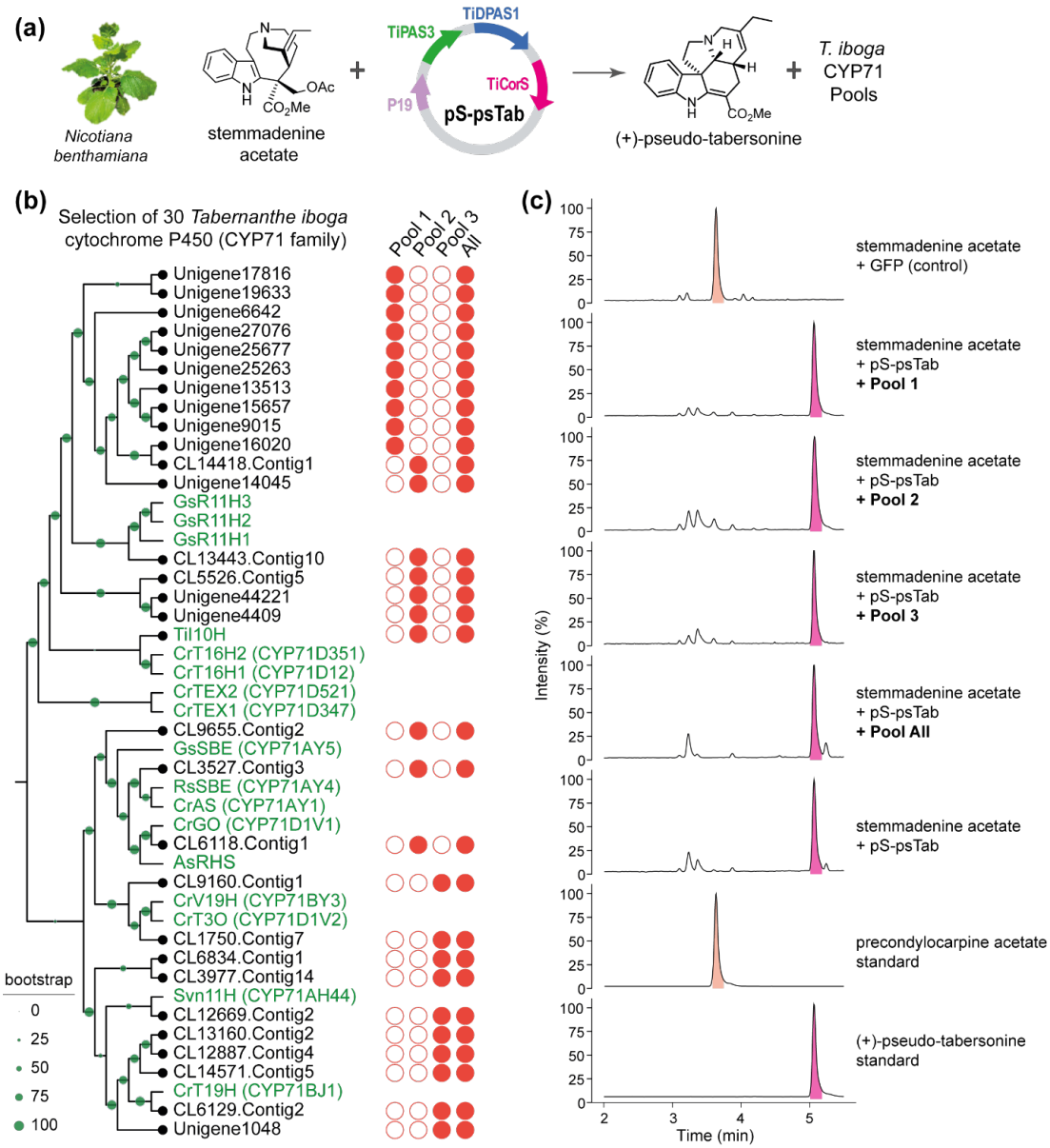


Fig. S6 Iboga CYP71s assayed with (+)-pseudo-tabersonine in *N. benthamiana*. (a) Assay plan for screening CYP71 gene candidate pools with the (+)-pseudo-tabersonine producing multigene construct pS-psTa. (b) Phylogenetic tree of the iboga CYP71s and the candidate pools selected for screening in *N. benthamiana*. (c) LC-MS analysis of the iboga CYP71 candidate pools tested for activity in *N. benthamiana* with the multigene construct pS-psTab. LC-MS traces are presented as total ion chromatograms (solid lines). Stemmadenine acetate is oxidized to precondylocarpine acetate by an endogenous *N. benthamiana* enzyme.

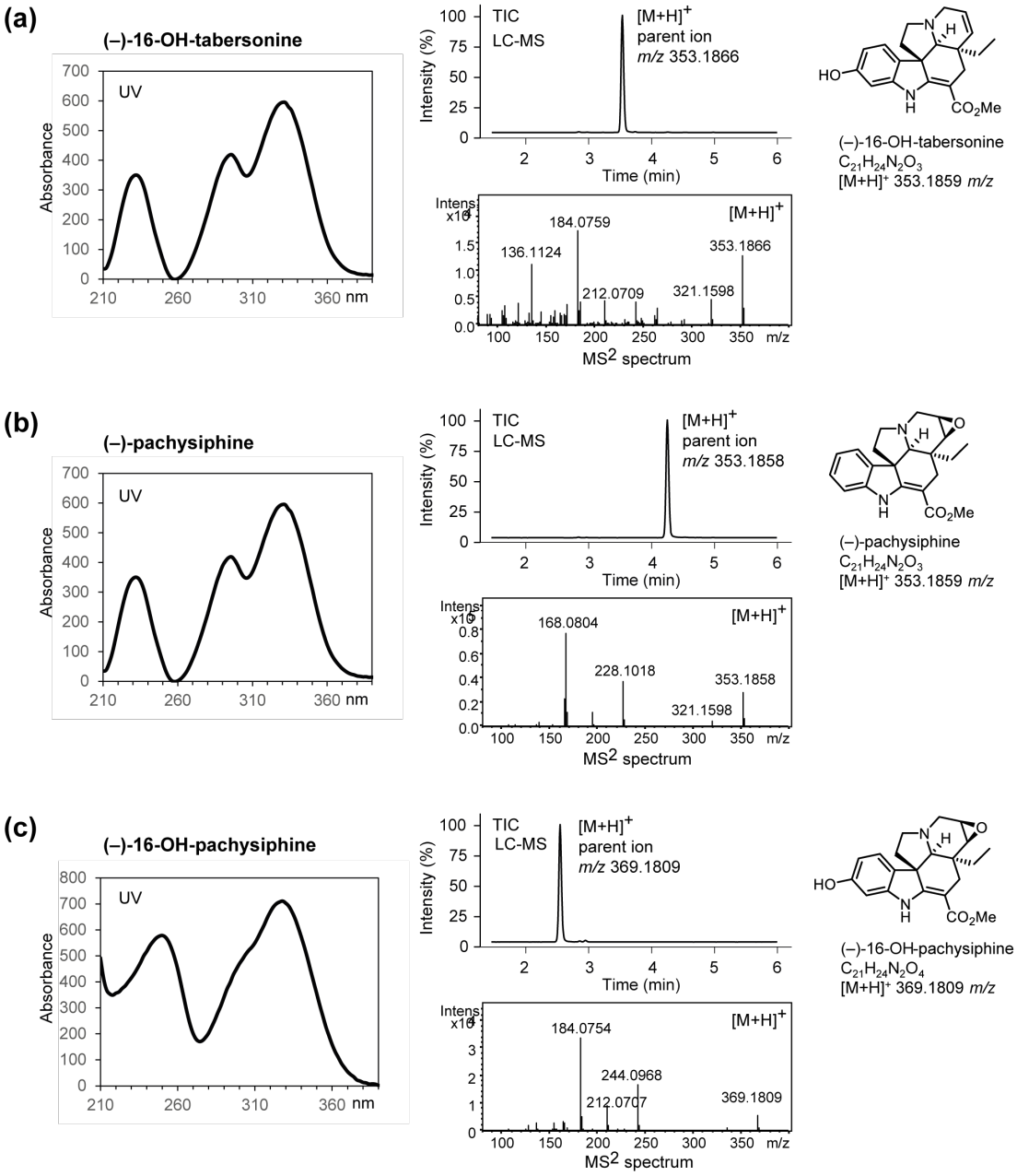
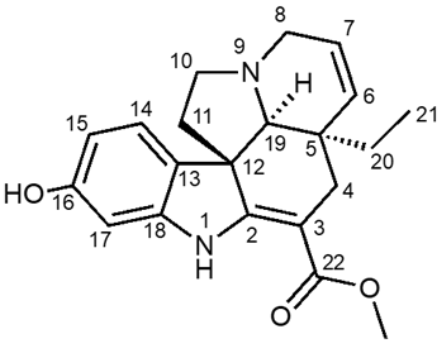


Fig. S7 HPLC isolation of hydroxylated tabersonine products from yeast workup.

HPLC isolation of hydroxylated tabersonine products from yeast workup. (a) Isolated product (–)-16-OH-tabersonine. (b) Isolated product (–)-pachysiphine. (c) Isolated product (–)-16-OH-pachysiphine. Traces indicate UV spectrum, LC-MS chromatography profile, and MS^2 spectrum of parent ions of the isolated compounds. LC-MS traces are presented as total ion chromatograms.



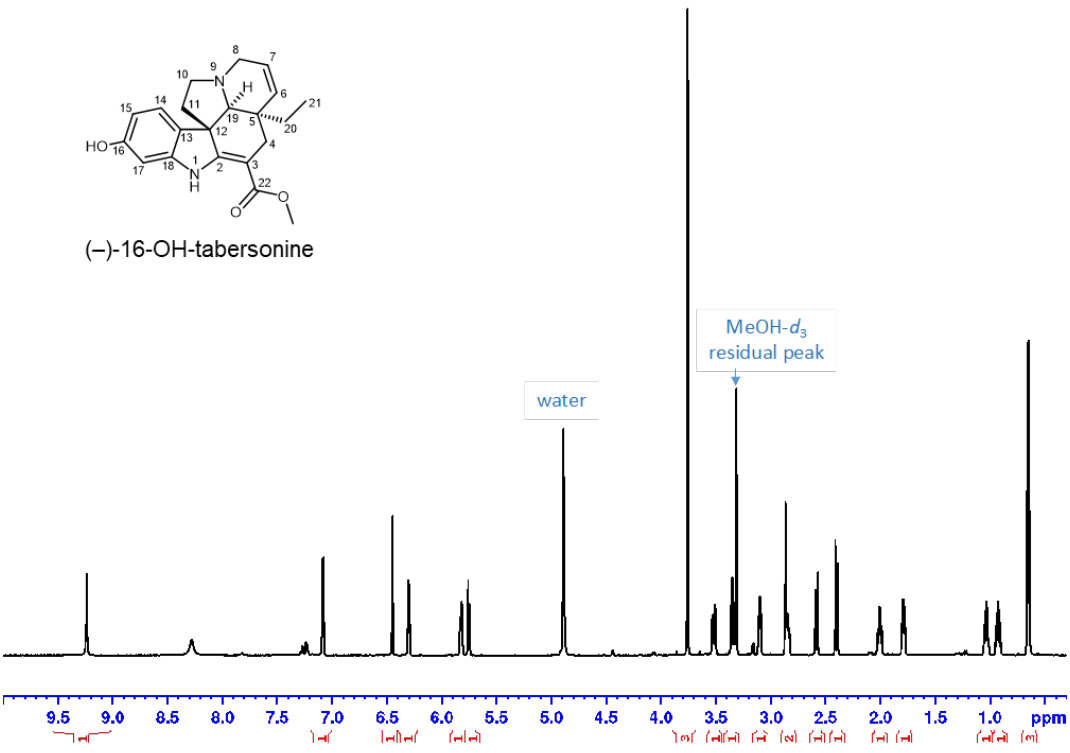
(–)-16-OH-tabersonine
^{1}H-NMR, MeOH-d_3
700 MHz, 25 °C

pos.	δ_H	mult.	J_{HH}	δ_C
1	9.23	*bs*	-	-
2	-	-	-	168.1
3	-	-	-	91.5
4α	2.58	*bd*	15.4	29.7
4β	2.40	*d*	15.4	29.7
5	-	-	-	42.5
6α	5.75	*bd*	10.0	134.4
7α	5.82	*bdd*	10.0/4.5	125.4
8α	3.34	*bd*	16.0	51.5
8β	3.52	*dd*	16.0/4.5	51.5
10α	2.85	*m***	-	51.9
10β	3.10	*dd*	7.5/6.4	51.9
11α	1.78	*dd*	11.8/4.4	45.8
11β	2.00	*ddd*	11.8/11.6/6.4	45.8
12	-	-	-	55.8
13	-	-	-	129.6
14	7.08	*d*	8.0	122.8
15	6.30	*dd*	8.0/1.8	108.2
16	-	-	-	159.3
17	6.45	*d*	1.8	99.2
18	-	-	-	146.1
19α	2.86	*bs*	-	71.6
20a	0.92	*dq*	14.5/7.4	28.0
20b	1.03	*dq*	14.5/7.4	28.0
21	0.65	*t*	7.4	7.9
22	-	-	-	170.0
OMe	3.75	*s*	-	51.6

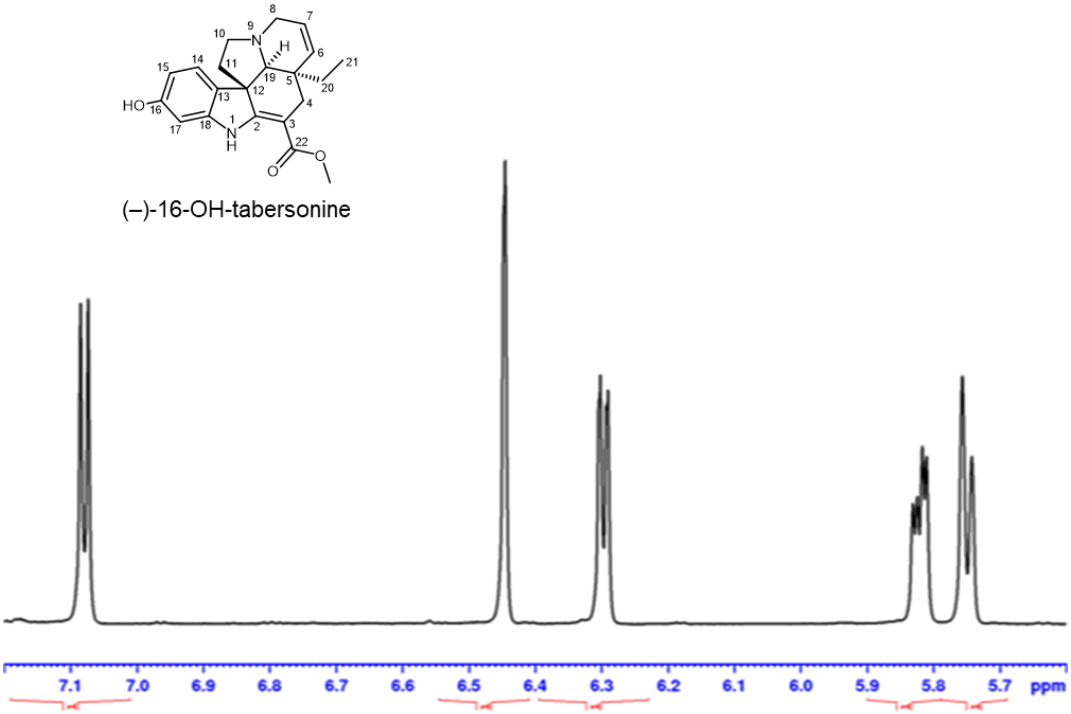
** overlapped signals J unresolved

Fig. S8 Structure elucidation of (–)-16-OH-tabersonine by NMR.

Structure elucidation of (–)-16-OH-tabersonine by NMR. (Continued to next page)

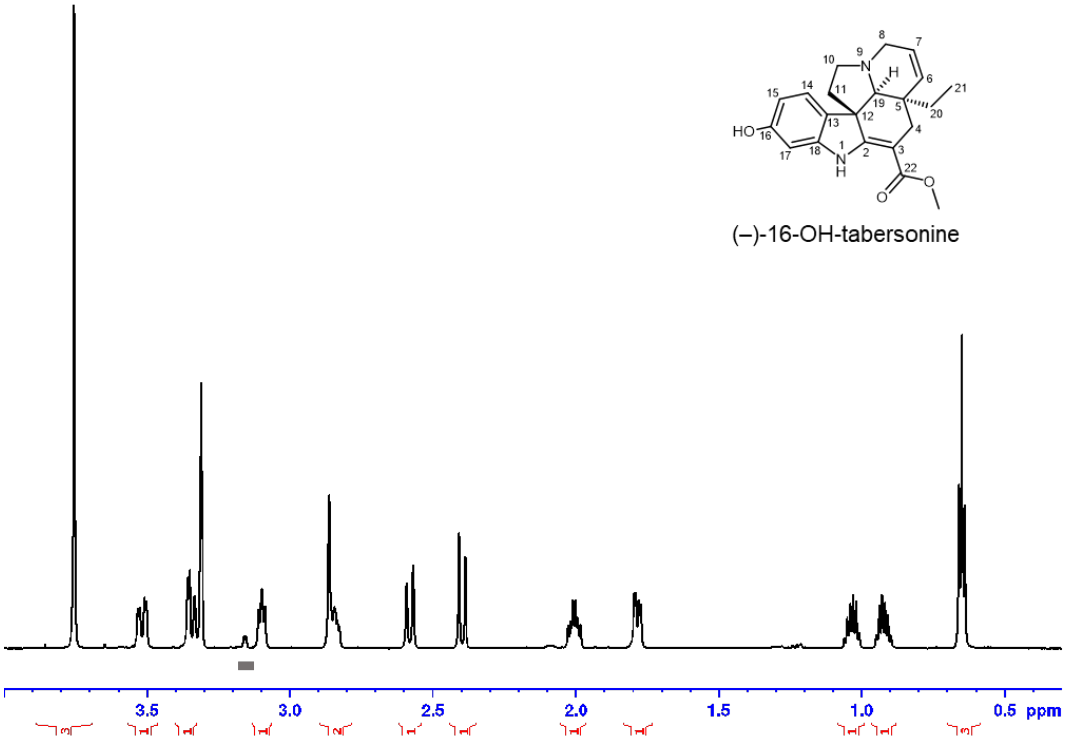


^{1}H NMR with water suppression (zgpr) full range in MeOH-d_3

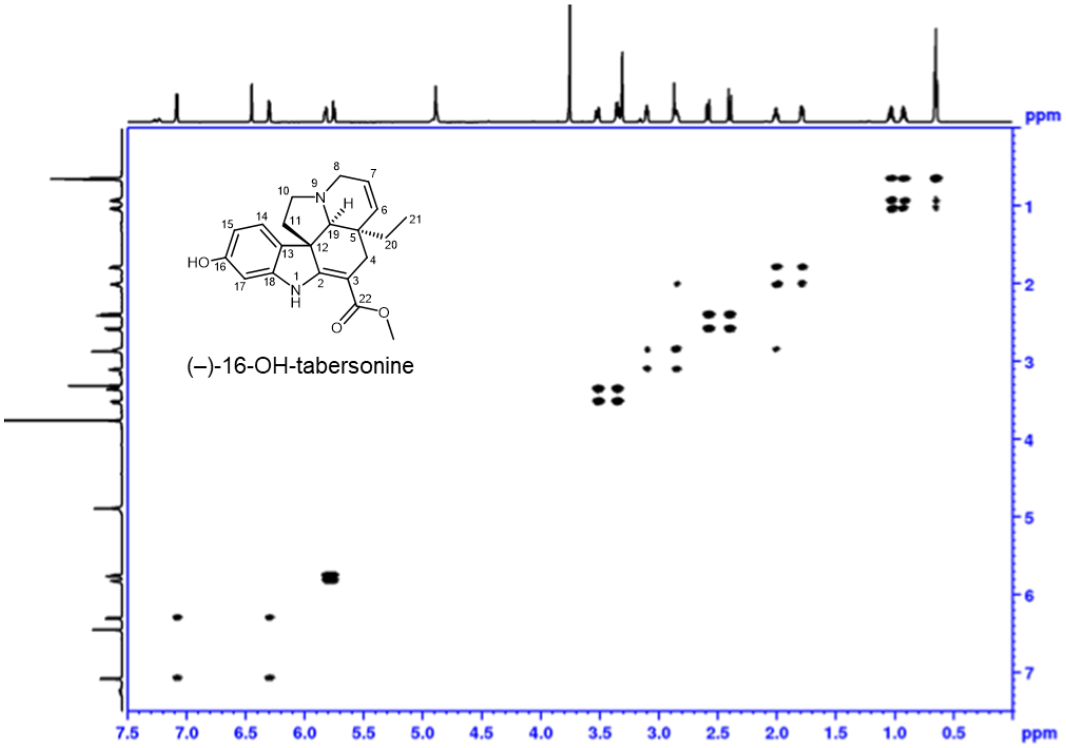


^{1}H NMR with water suppression (zgpr)
5.6-7.2 ppm in MeOH-d_3

Fig. S8 Structure elucidation of (–)-16-OH-tabersonine by NMR. (Continued to next page).

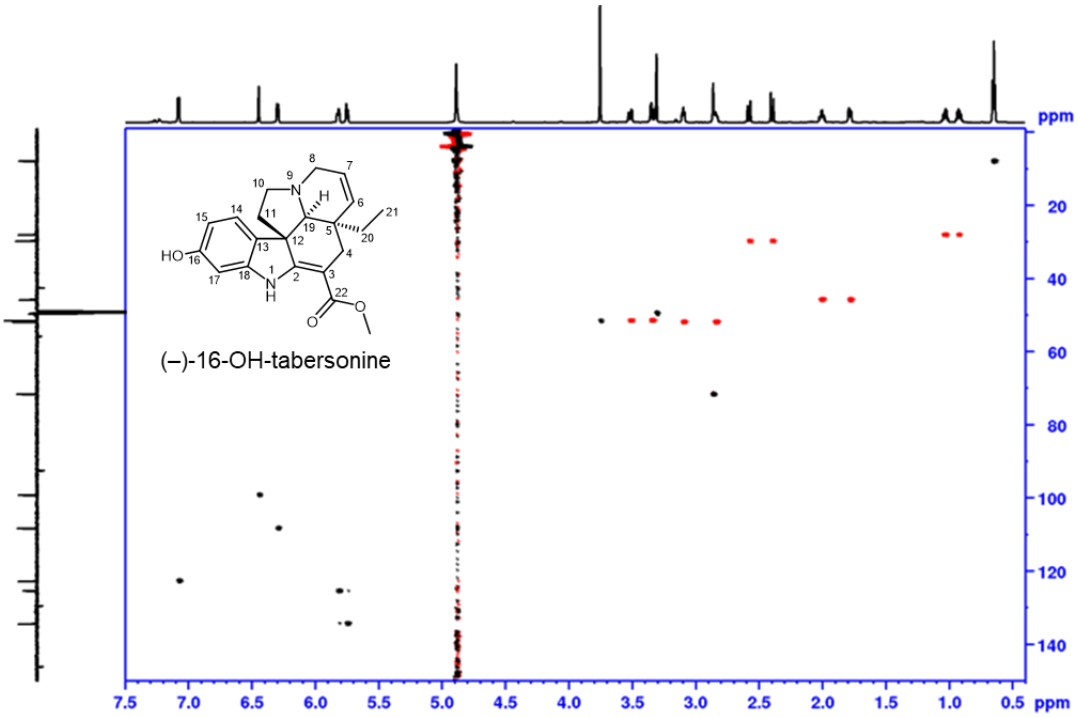


^{1}H NMR with water suppression (zgpr)
aliphatic range in MeOH-d_3. Shaded areas mark impurity

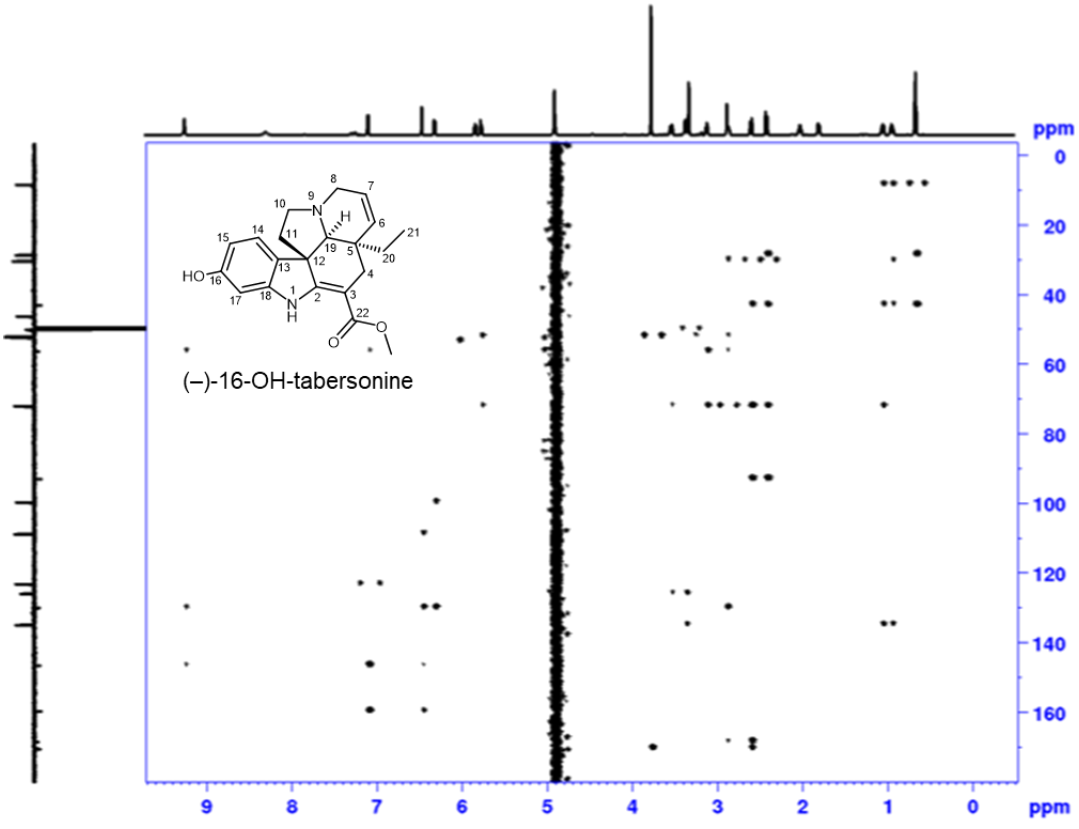


^{1}H-^{1}H DQF COSY with water suppression
full range in MeOH-d_3

Fig. S8 Structure elucidation of (–)-16-OH-tabersonine by NMR. (Continued to next page).

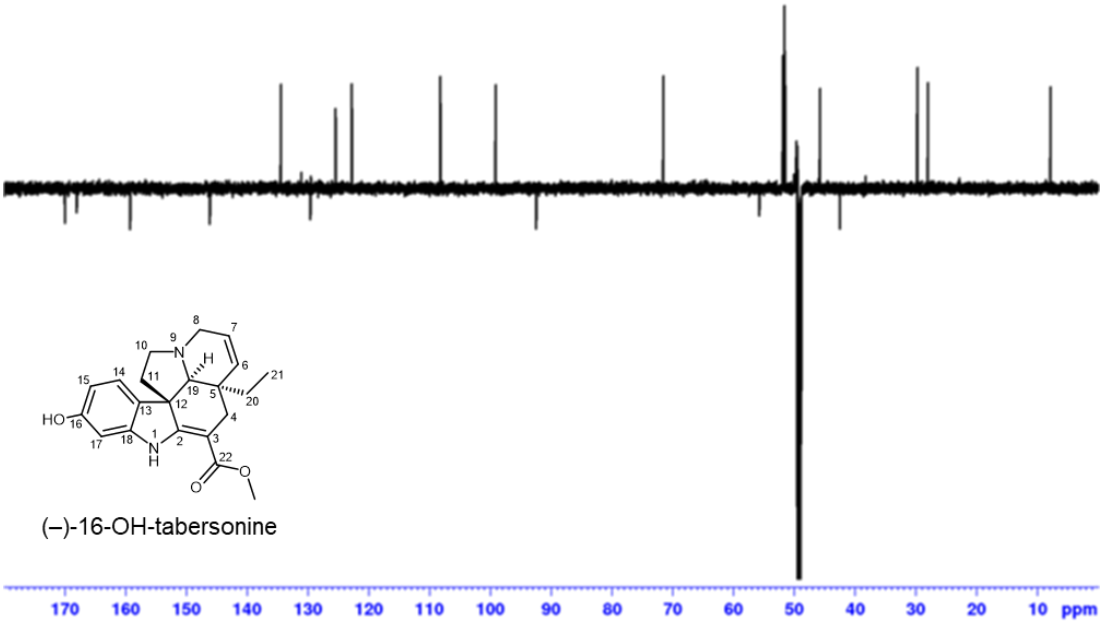


phase sensitive HSQC, full range in MeOH-d_3
red: CH_2, black: CH, CH_3

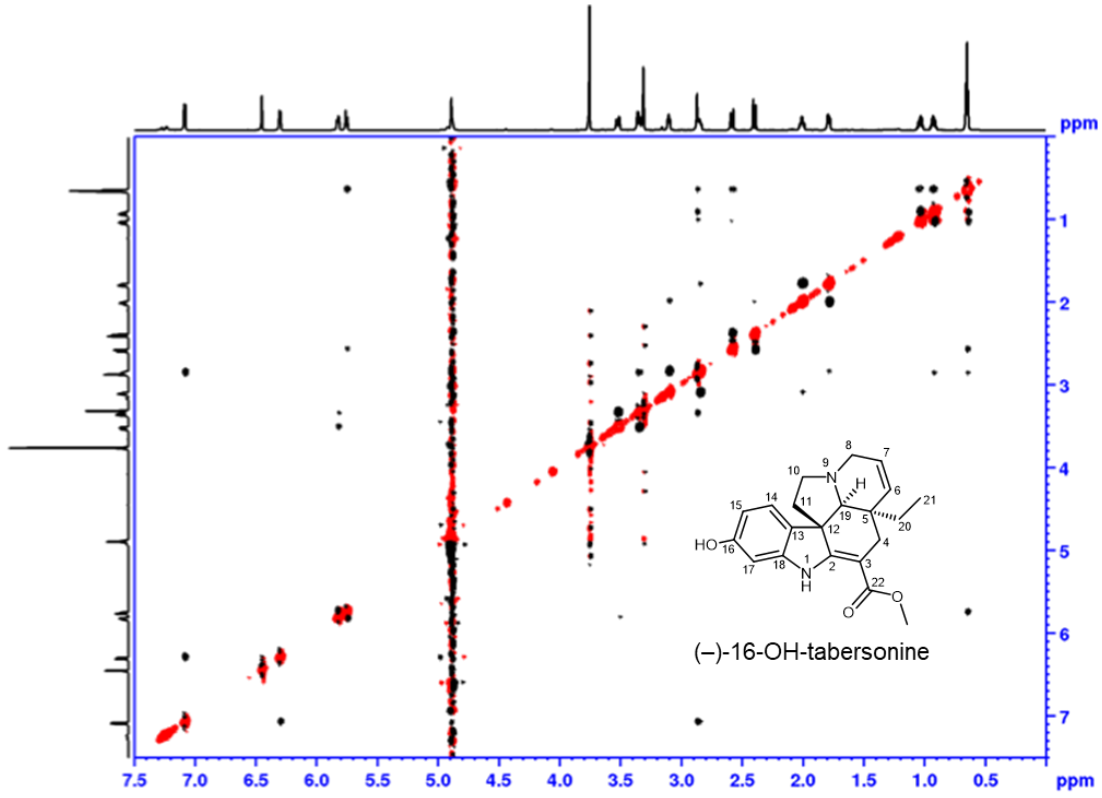


HMBC, full range in MeOH-d_3

Fig. S8 Structure elucidation of (–)-16-OH-tabersonine by NMR. (Continued to next page).



DEPTQ, full range in MeOH-d_3



^{1}H-^{1}H ROESY with water suppression
full range in MeOH-d_3

Fig. S8 Structure elucidation of (–)-16-OH-tabersonine by NMR. (End).

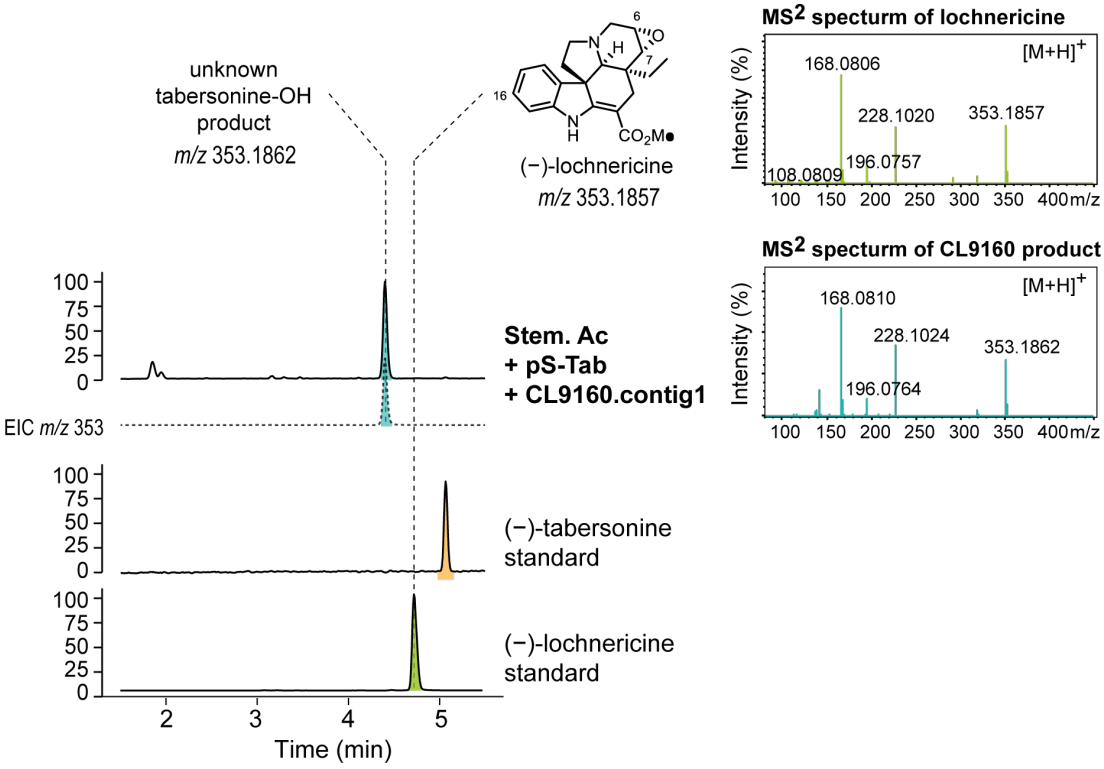
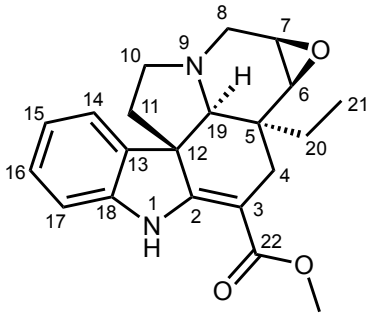


Fig. S9 MS^2 spectral comparison of lochnericine and CL9160.contig1 product.

LC-MS profiles and MS^2 spectra of lochnericine standard and the hydroxylated tabersonine product of CL9160.contig1. Comparison of MS^2 spectra of the parent ions *m/z* 353.18 shows similar fragmentation patterns between the two compounds, suggesting structural similarities.

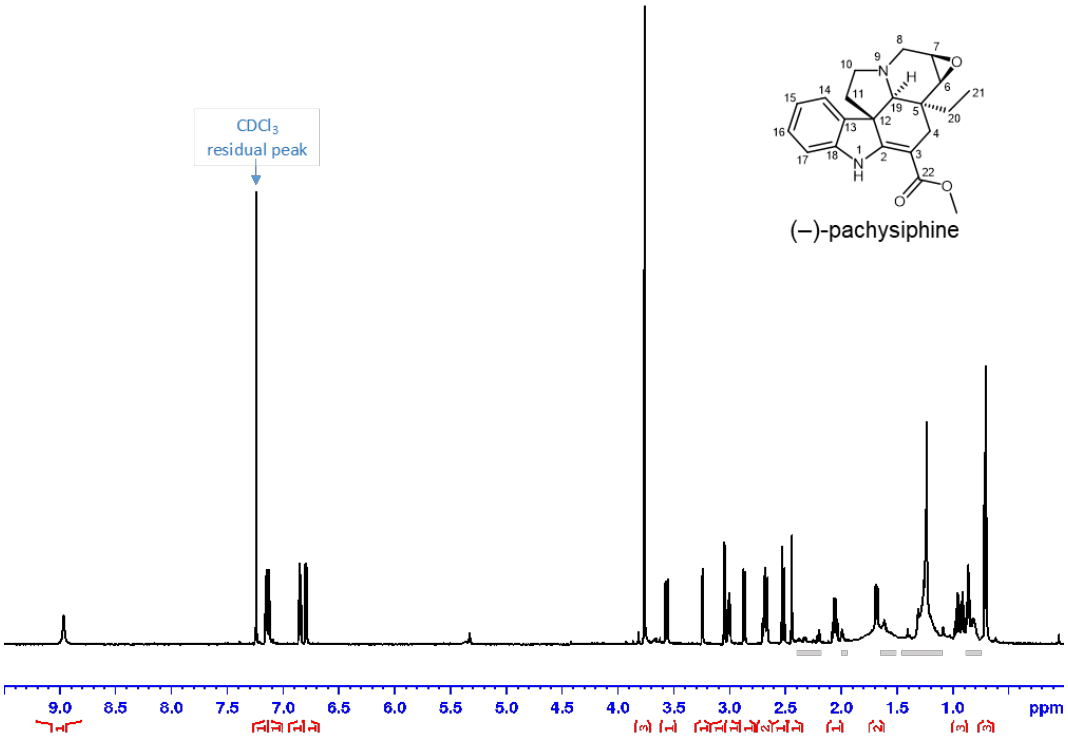


(–)-pachysiphine
^{1}H-NMR, $CDCl_3$
700 MHz, 25 °C

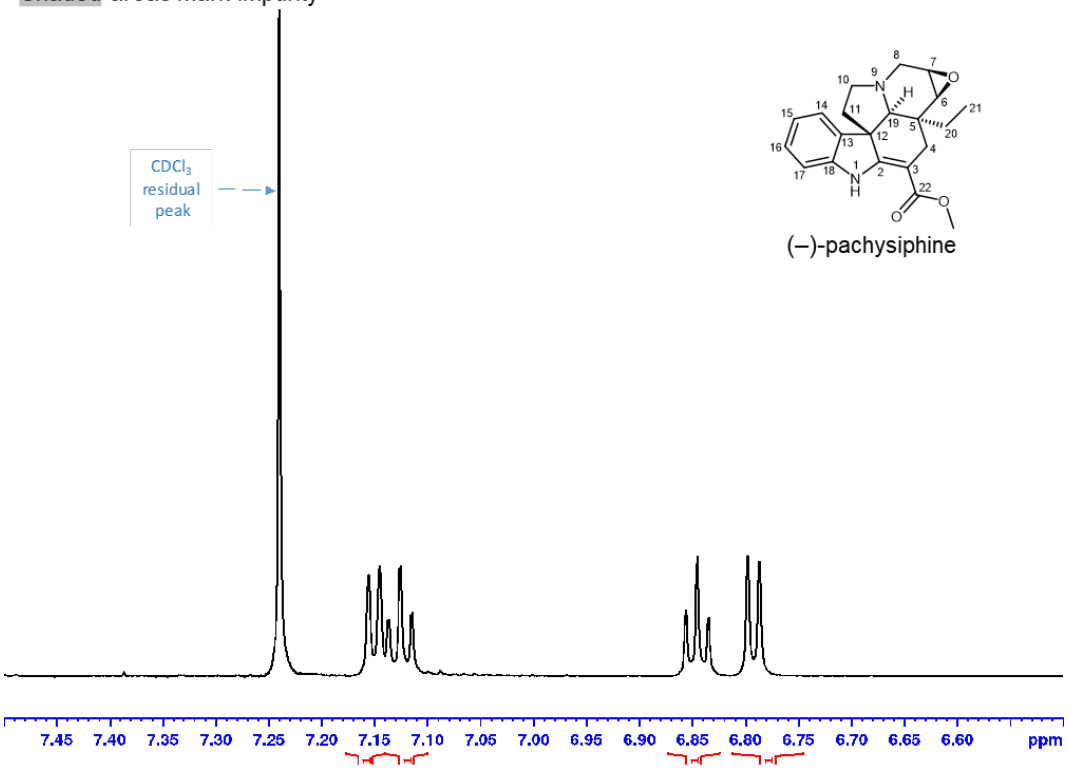
pos.	δ_H	mult.	J_{HH}	δ_C
1	8.97	*bs*	-	-
2	-	-	-	165.5
3	-	-	-	91.4
4α	2.67	*dd*	15.4/1.6	23.6
4β	2.52	*d*	15.4	23.6
5	-	-	-	37.4
6α	3.05	*d*	3.9	56.6
7α	3.24	*ddd*	3.9/1.1/0.4	52.4
8α	2.87	*bd*	12.9	49.9
8β	3.56	*dd*	12.9/1.1	49.9
10α	2.69	*ddd*	11.5/8.2/4.4	51.4
10β	3.01	*dd*	8.2/6.5	51.4
11α	1.68	*dd*	11.6/4.4	44.3
11β	2.06	*ddd*	11.6/11.5/6.5	44.3
12	-	-	-	54.9
13	-	-	-	137.9
14	7.15	*bd*	7.4	121.7
15	6.85	*ddd*	7.4/7.4/0.9	120.8
16	7.13	*ddd*	7.7/7.4/1.0	128.1
17	6.79	*bd*	7.7	109.6
18	-	-	-	143.3
19α	2.44	*bd*	1.6	71.4
20a	0.91	*dq*	14.7/7.4	26.7
20b	0.96	*dq*	14.7/7.4	26.7
21	0.71	*t*	7.4	7.4
22	-	-	-	169.2
OMe	3.76	*s*	-	51.3

Fig. S10 Structure elucidation of (–)-pachysiphine by NMR.

Structure elucidation of (–)-pachysiphine by NMR. (Continued to next page)

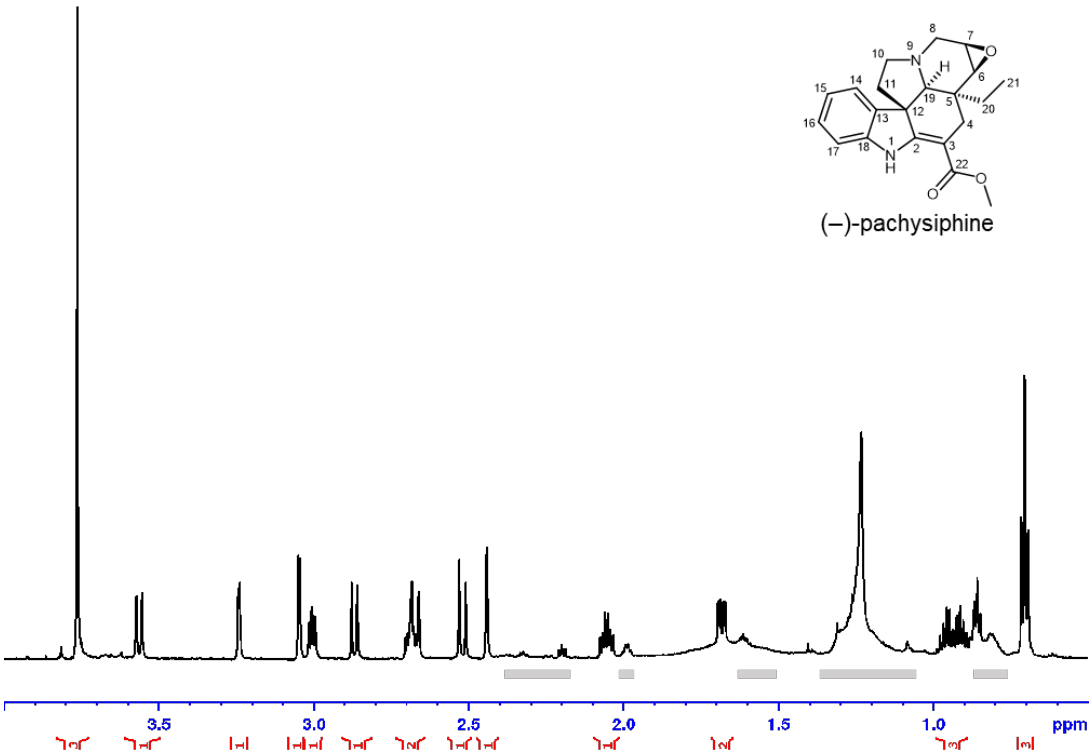


^{1}H NMR with water suppression (zgpr) full range in $CDCl_3$
Shaded areas mark impurity

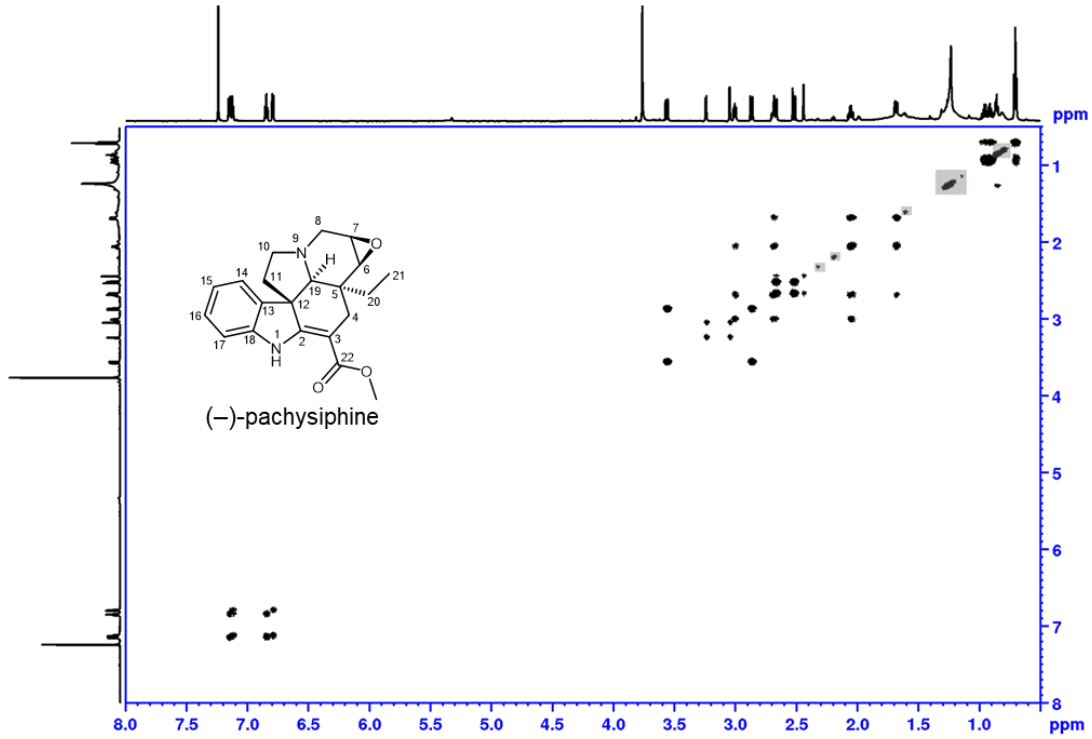


^{1}H NMR with water suppression (zgpr)
aromatic range in CDCl3

Fig. S10 Structure elucidation of (–)-pachysiphine by NMR. (Continued to next page).

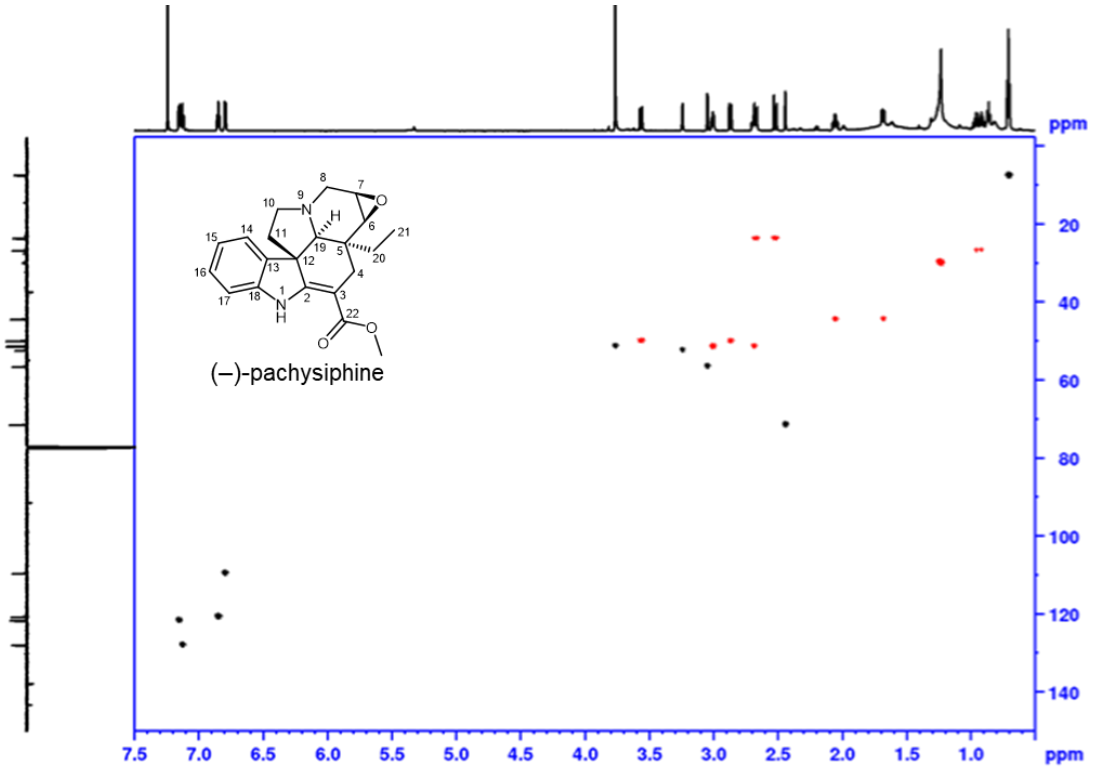


^{1}H NMR with water suppression (zgpr)
aliphatic range in $CDCl_3$. Shaded areas mark impurity.

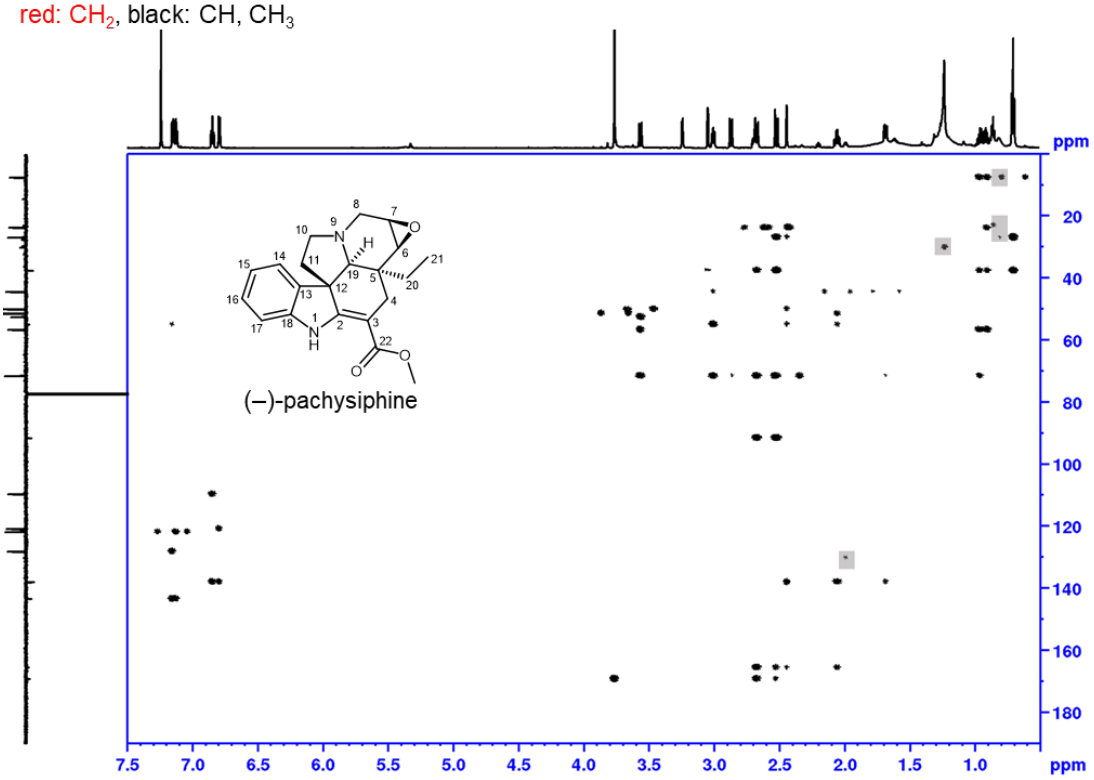


^{1}H-^{1}H DQF COSY, full range in $CDCl_3$
Shaded areas mark impurity

Fig. S10 Structure elucidation of (–)-pachysiphine by NMR. (Continued to next page).

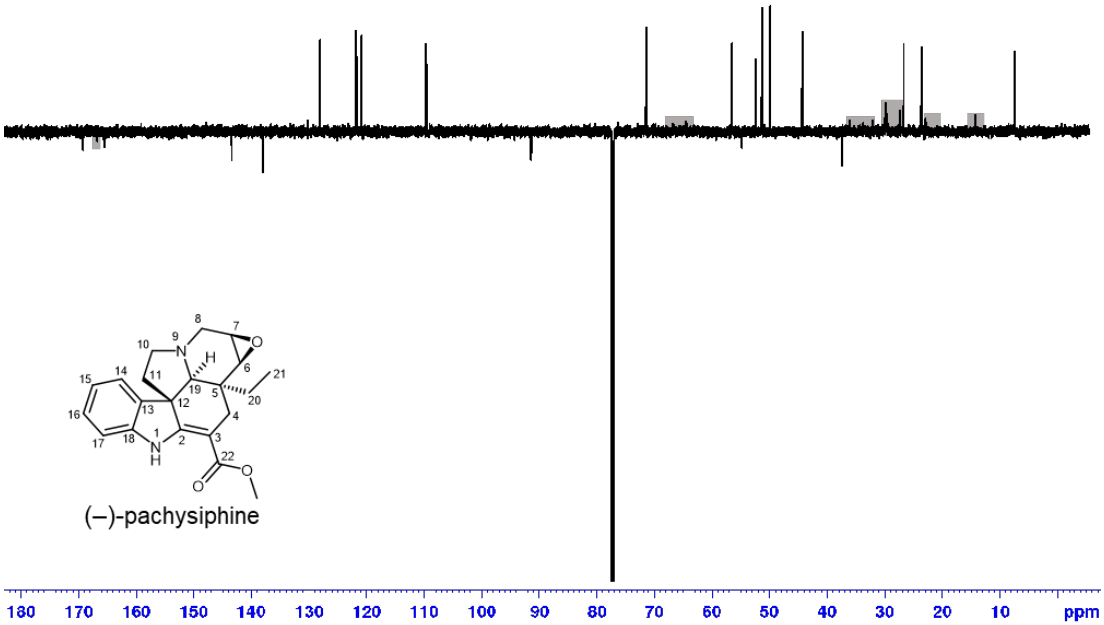


phase sensitive HSQC, full range in $CDCl_3$
red: CH_2, black: CH, CH_3

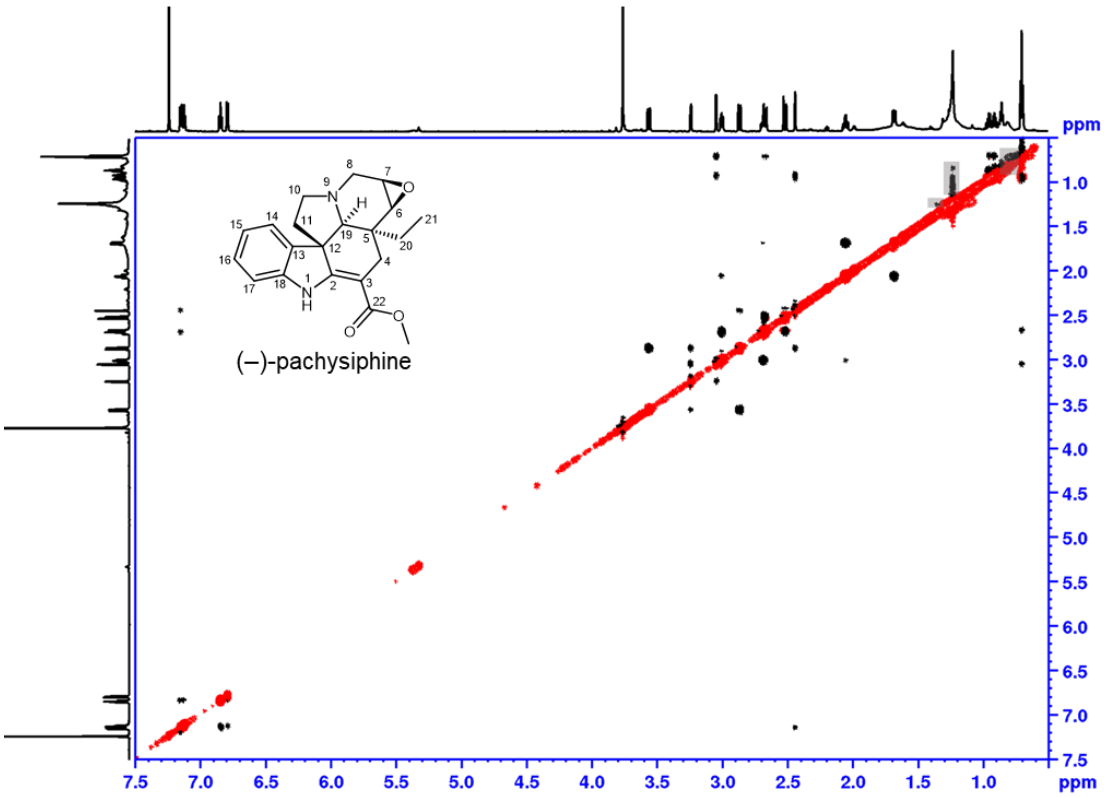


HMBC, full range in $CDCl_3$
Shaded areas mark impurity

Fig. S10 Structure elucidation of (–)-pachysiphine by NMR. (Continued to next page).

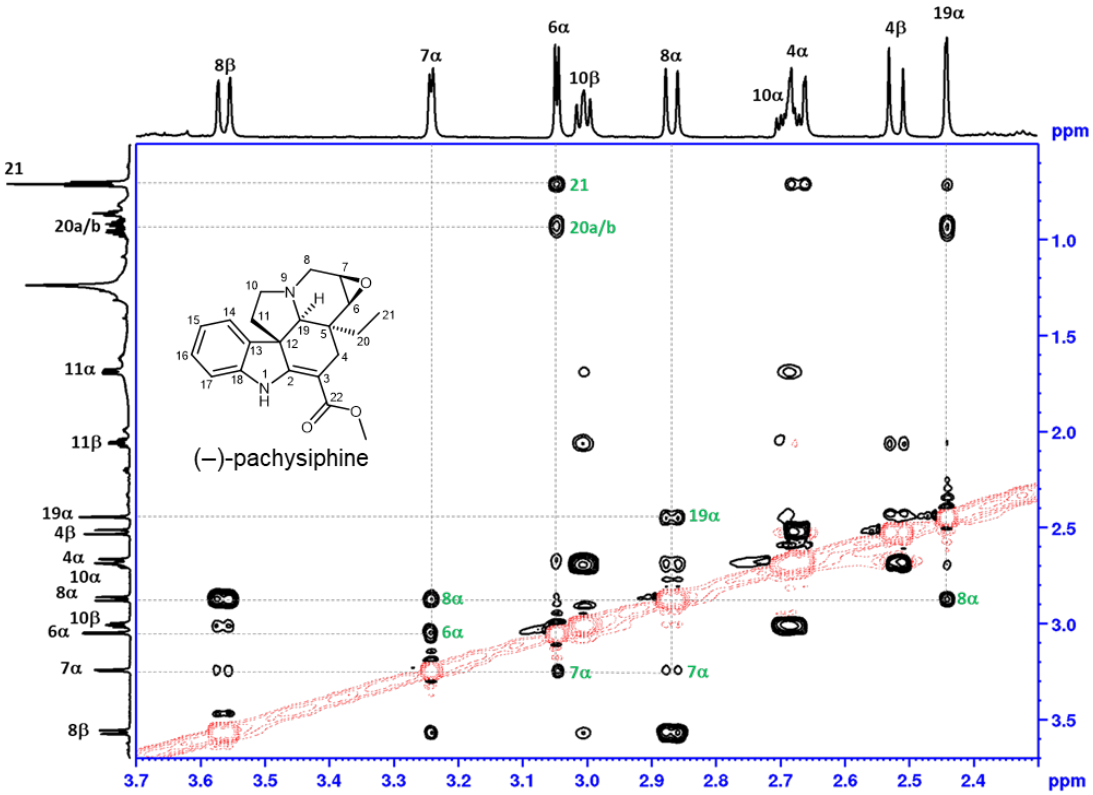


DEPTQ, full range in $CDCl_3$
Shaded areas mark impurity

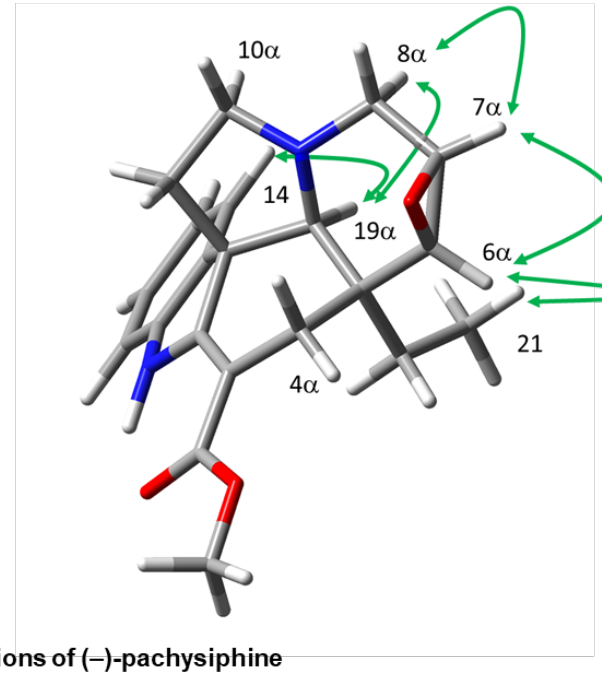


^{1}H-^{1}H ROESY with water suppression
full range in $CDCl_3$. Shaded areas mark impurity

Fig. S10 Structure elucidation of (–)-pachysiphine by NMR. (Continued to next page).



^{1}H-^{1}H ROESY with water suppression
aliphatic range in $CDCl_3$. Important ROESY correlations are depicted in green



ROESY correlations of (–)-pachysiphine

Optimized using Gaussian 16W (DFT, APFD/6-311G+(2d,p), solvent MeOH). Important ROESY correlations are depicted in green.

Fig. S10 Structure elucidation of (–)-pachysiphine by NMR. (End).

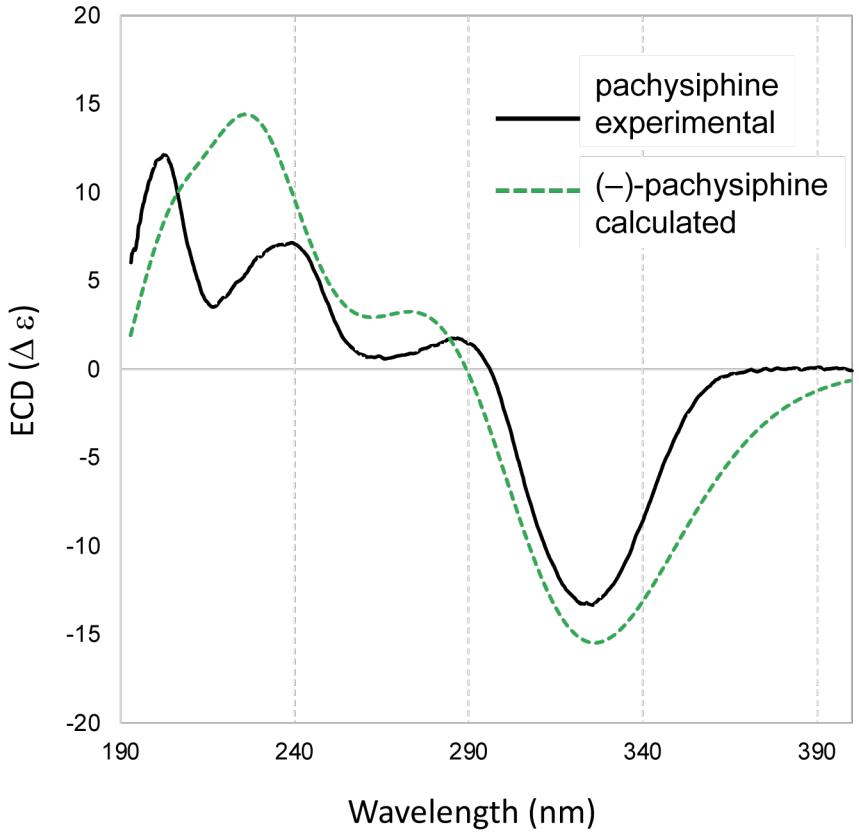
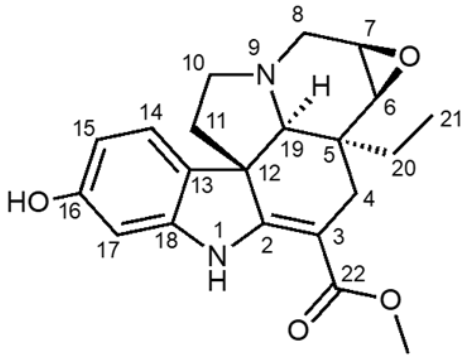


Fig. S11 Electronic circular dichroism (ECD) spectra of (–)-pachysiphine.

Comparison of simulated ECD spectrum (dashed green) and experimental ECD spectrum (solid black) of (–)-pachysiphine.

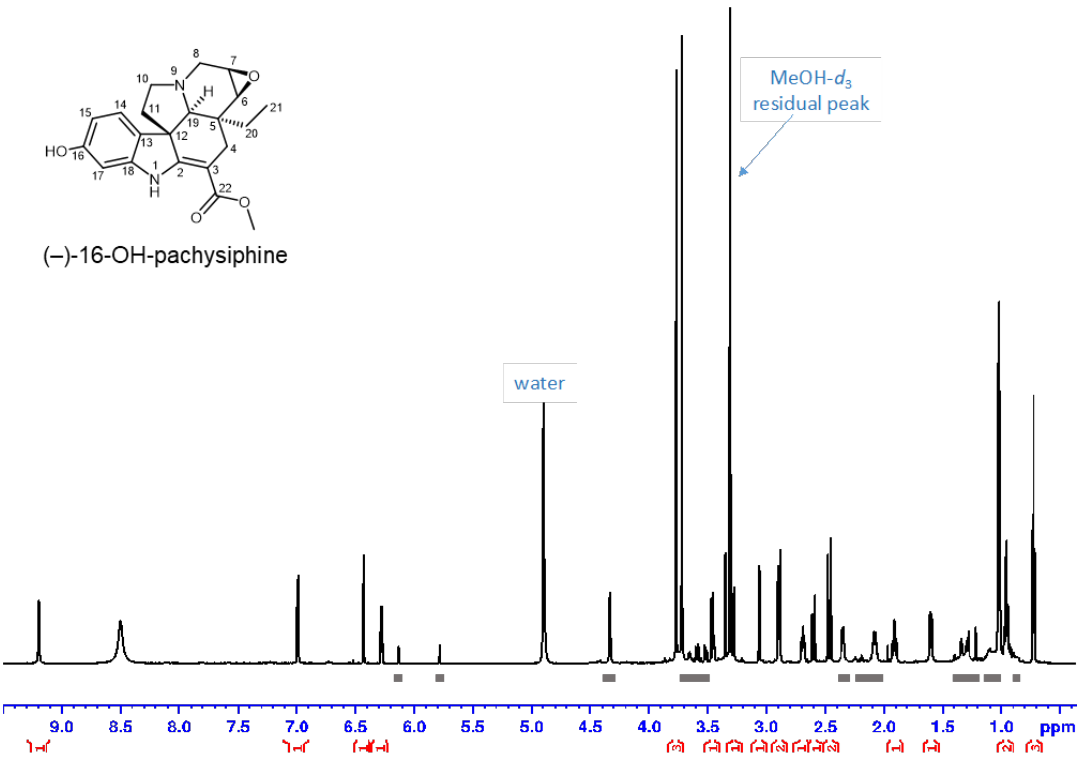


(–)-16-OH-pachysiphine
^{1}H-NMR, MeOH-d_3
700 MHz, 25 °C

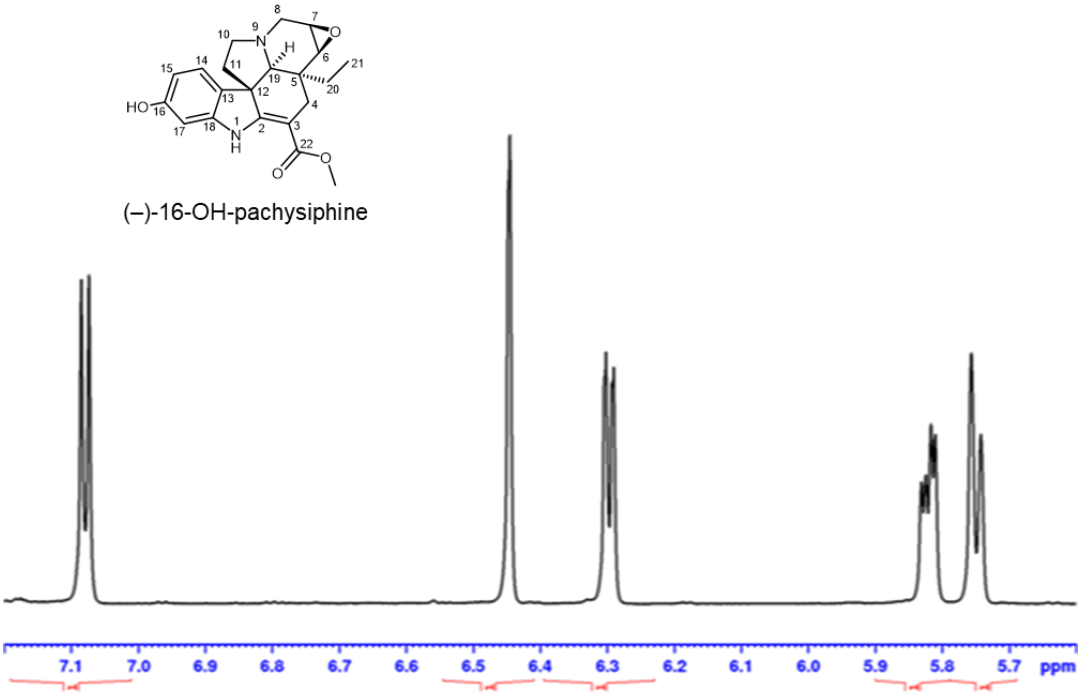
pos.	δ_H	mult.	J_{HH}	δ_C
1	9.19	*bs*	-	-
2	-	-	-	167.6
3	-	-	-	91.3
4α	2.60	*dd*	15.4/1.6	24.6
4β	2.46	*d*	15.4	24.6
5	-	-	-	38.5
6α	3.06	*d*	3.7	57.6
7α	3.28	*bd*	3.7	53.6
8α	2.88	*d*	12.8	50.7
8β	3.46	*bd*	12.8	50.7
10α	2.68	*ddd*	11.4/8.4/4.3	51.8
10β	2.88	*dd*	8.4/6.3	51.8
11α	1.60	*dd*	11.4/4.3	45.8
11β	1.91	*ddd*	11.4/11.4/6.3	45.8
12	-	-	-	55.7
13	-	-	-	130.0
14	6.99	*d*	8.1	122.8
15	6.28	*dd*	8.1/2.0	108.1
16	-	-	-	159.1
17	6.43	*d*	2.0	99.1
18	-	-	-	146.0
19α	2.45	*bd*	1.6	72.5
20a	0.96	*q*	7.3	27.3
20b	0.96	*q*	7.3	27.3
21	0.72	*t*	7.3	7.5
22	-	-	-	170.1
OMe	3.77	*s*	-	51.5

Fig. S12 Structure elucidation of (–)-16-OH-pachysiphine by NMR.

Structure elucidation of (–)-16-OH-pachysiphine by NMR. (Continued to next page)

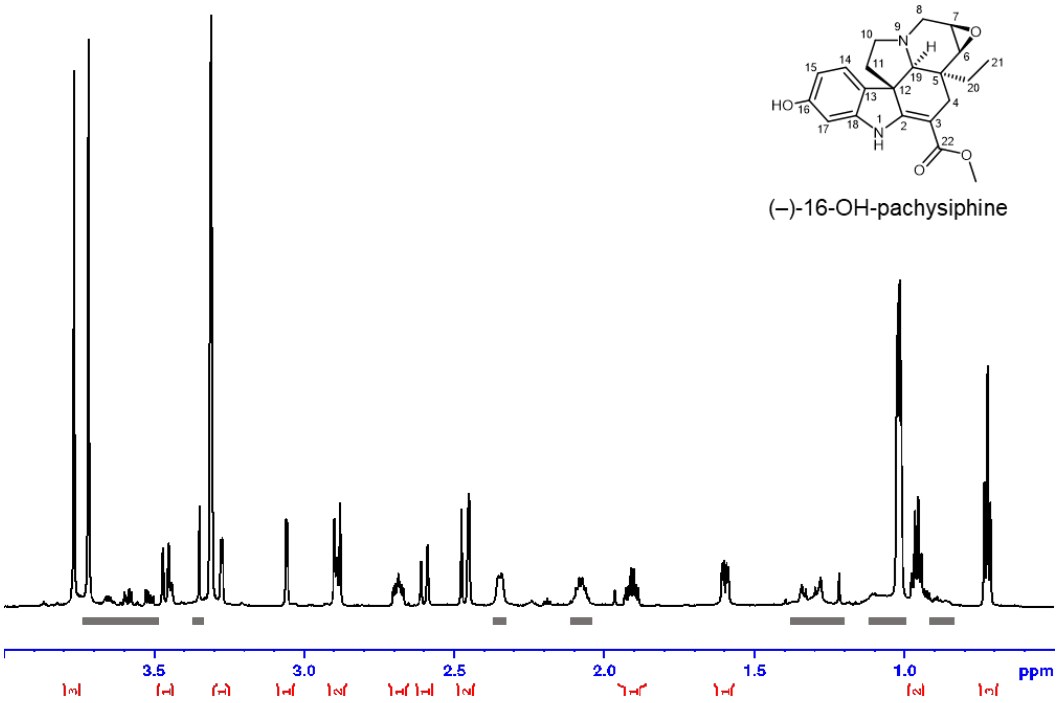


^{1}H NMR with water suppression (zgpr) full range in MeOH-d_3

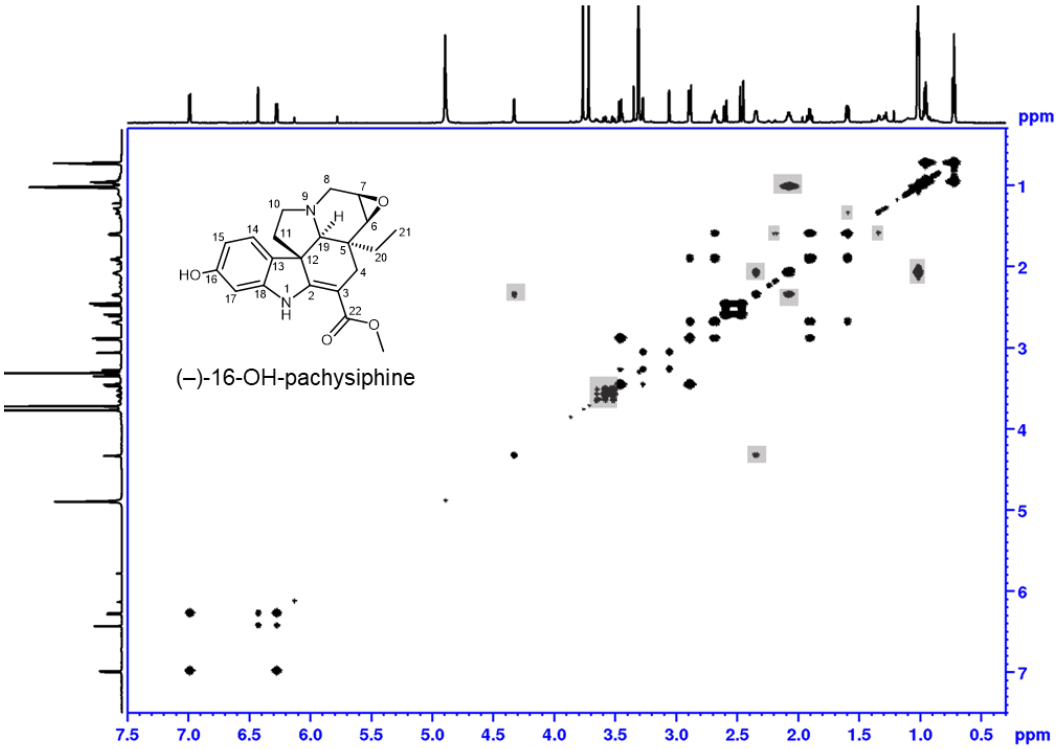


^{1}H NMR with water suppression (zgpr)
5.6-7.2 ppm in MeOH-d_3

Fig. S12 Structure elucidation of (–)-16-OH-pachysiphine by NMR. (Continued to next page).

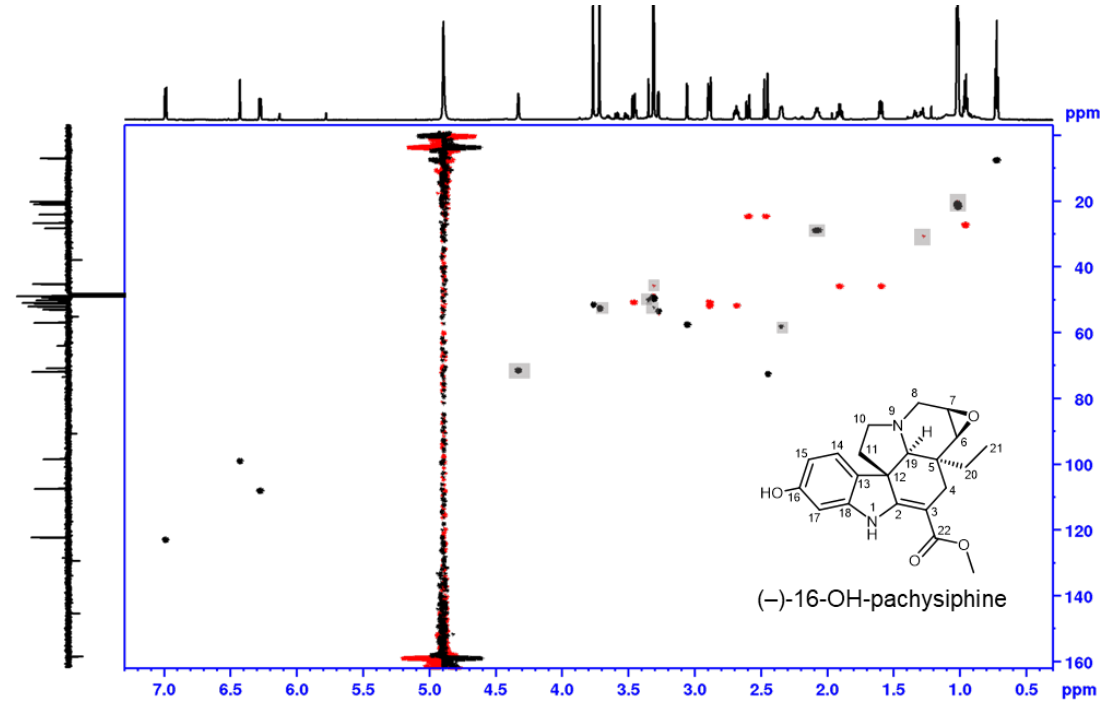


^{1}H NMR with water suppression (zgpr)
aliphatic range in MeOH-d_3. Shaded areas mark impurity

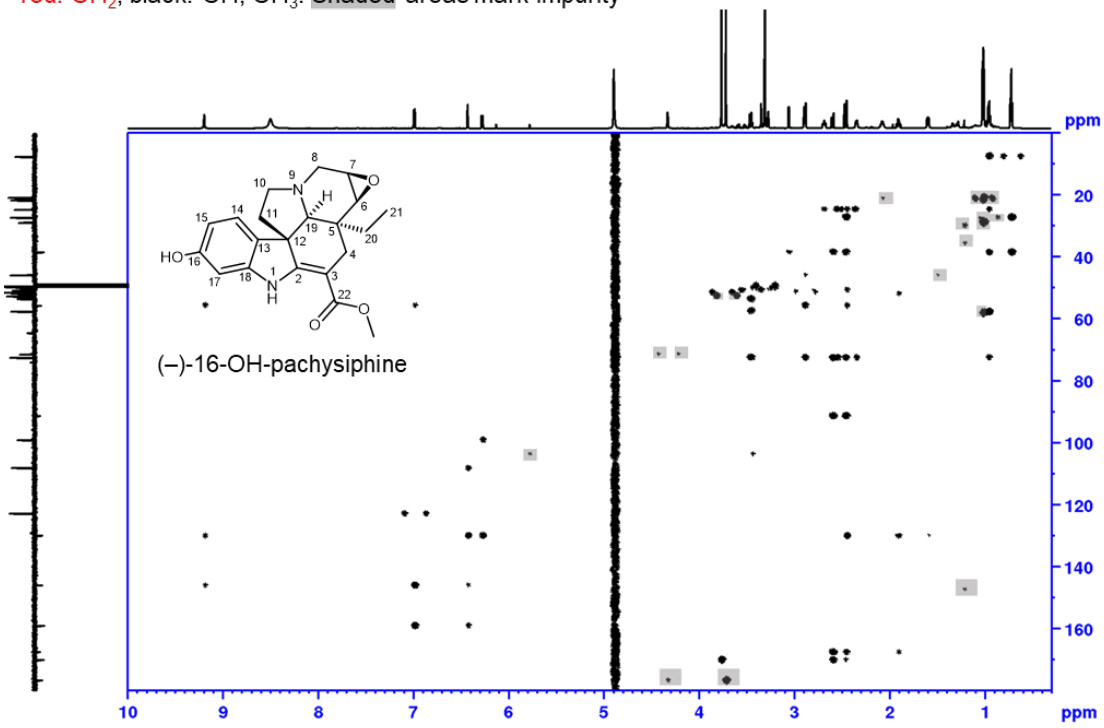


^{1}H-^{1}H DQF COSY with water suppression
full range in MeOH-d_3. Shaded areas mark impurity

Fig. S12 Structure elucidation of (–)-16-OH-pachysiphine by NMR. (Continued to next page).

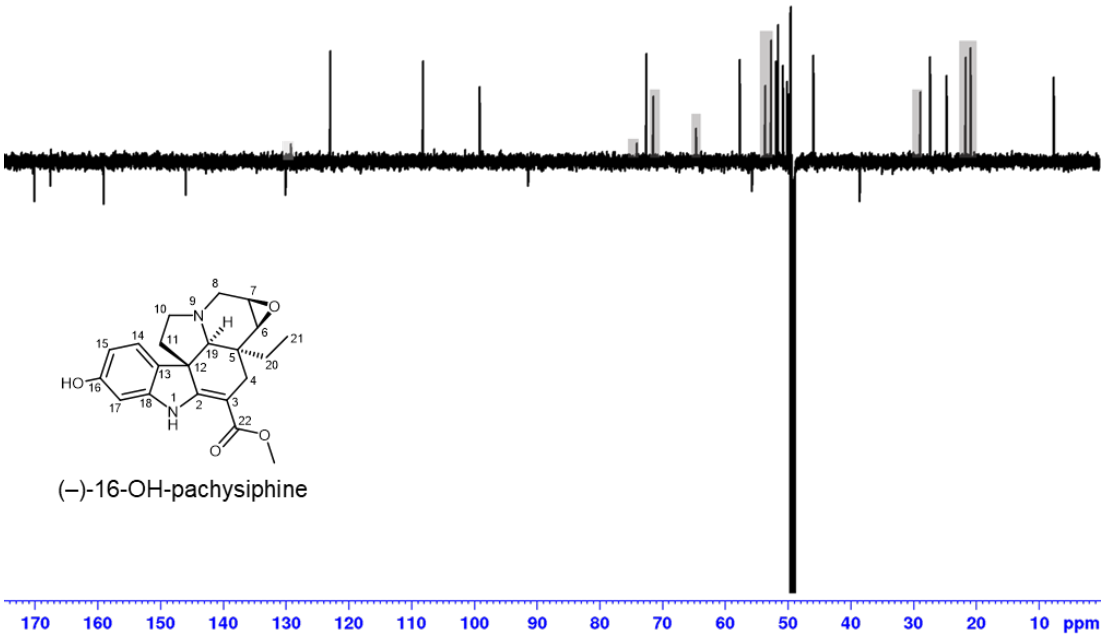


phase sensitive HSQC, full range in MeOH-d_3
red: CH_2, black: CH, CH_3. Shaded areas mark impurity

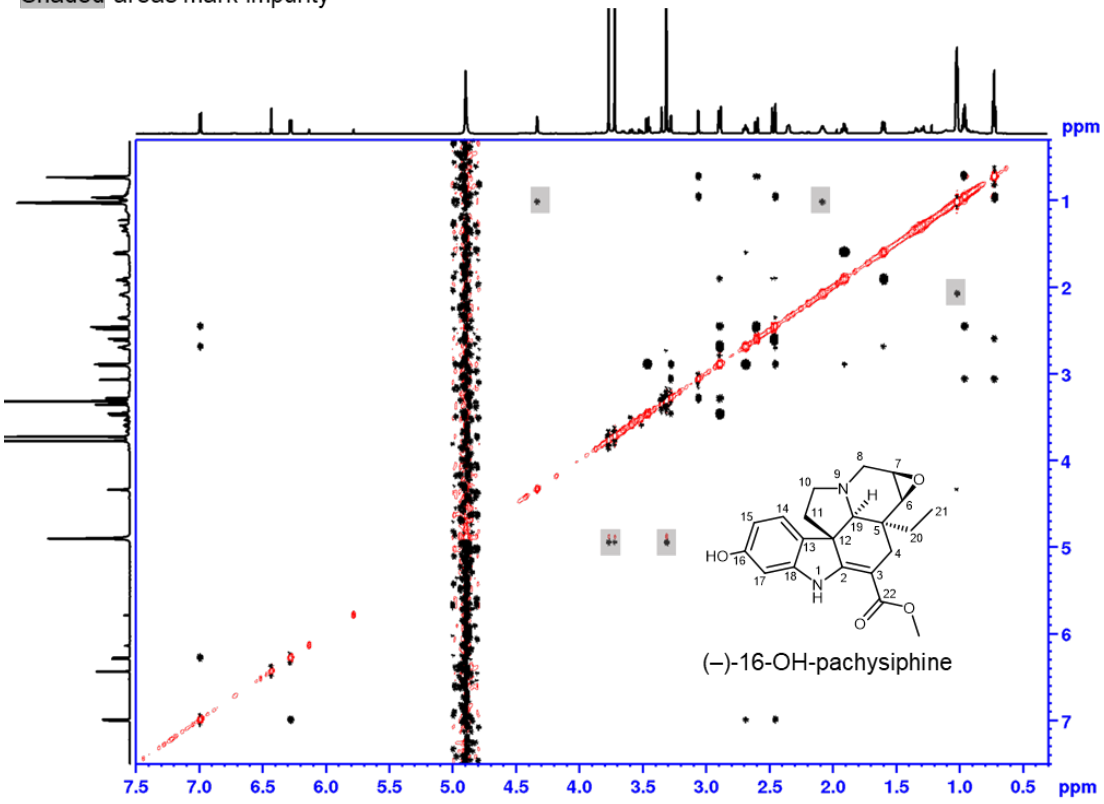


HMBC, full range in MeOH-d_3
Shaded areas mark impurity

Fig. S12 Structure elucidation of (–)-16-OH-pachysiphine by NMR. (Continued to next page).

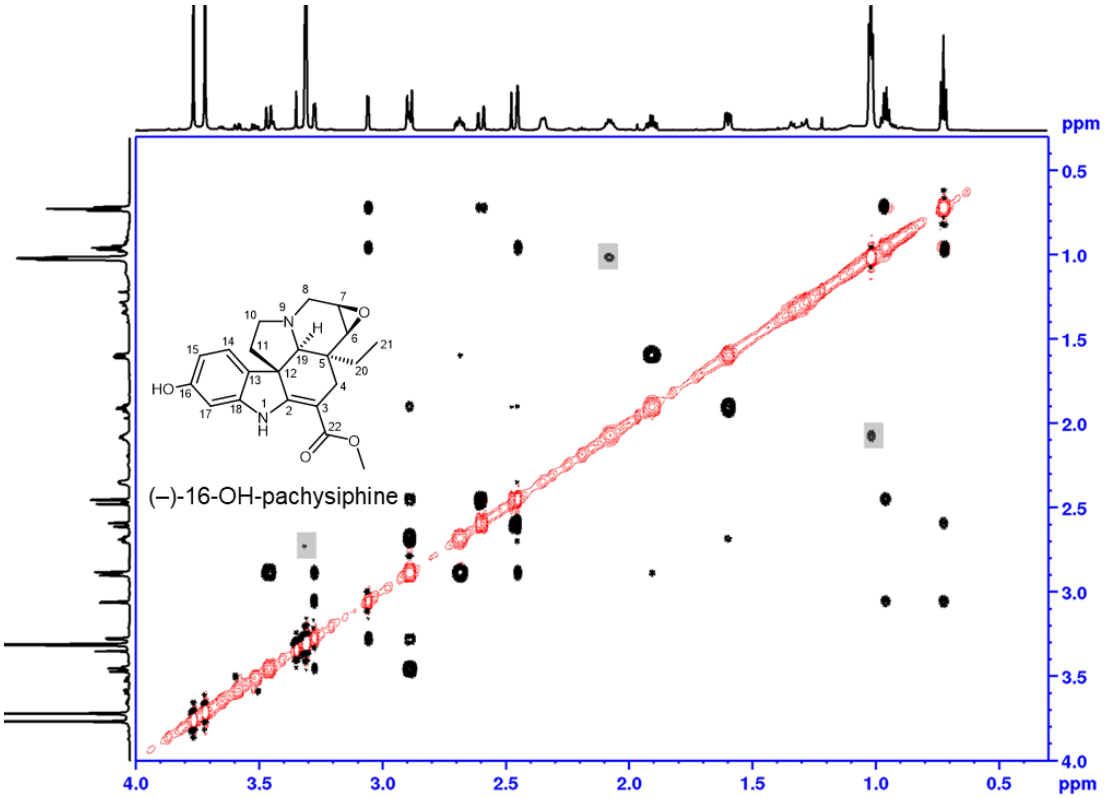


DEPTQ, full range in MeOH-d_3
Shaded areas mark impurity



^{1}H-^{1}H ROESY with water suppression
full range in MeOH-d_3. Shaded areas mark impurity

Fig. S12 Structure elucidation of (–)-16-OH-pachysiphine by NMR. (Continued to next page).



^{1}H-^{1}H ROESY with water suppression.
aliphatic range in MeOH-d_3. Shaded areas mark impurity

Fig. S12 Structure elucidation of (–)-16-OH-pachysiphine by NMR. (End).

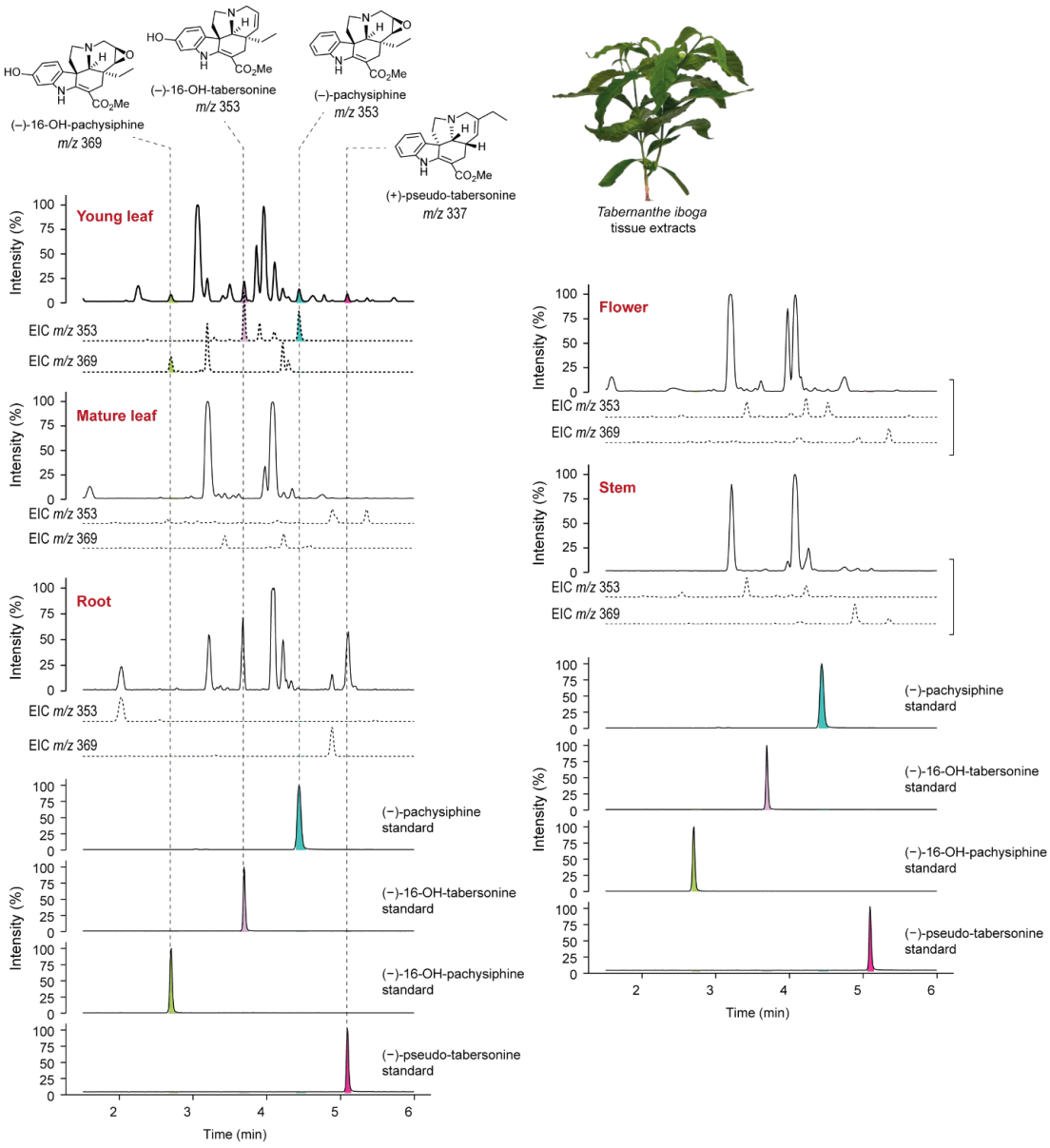


Fig. S13 LC-MS metabolite profiles of *T. iboga* tissues.

Untargeted LC-MS profiles of young leaves, mature leaves, stems, roots, and flowers of *T. iboga* methanolic extracts. The young leaf tissue shows an accumulation of pachysiphine, (–)-16-OH-tabersonine, and (–)-16-OH-pachysiphine as confirmed by authentic standards and MS^2 spectra. Total ion chromatograms are shown in solid lines, and extracted ion chromatograms are shown in dashed lines.

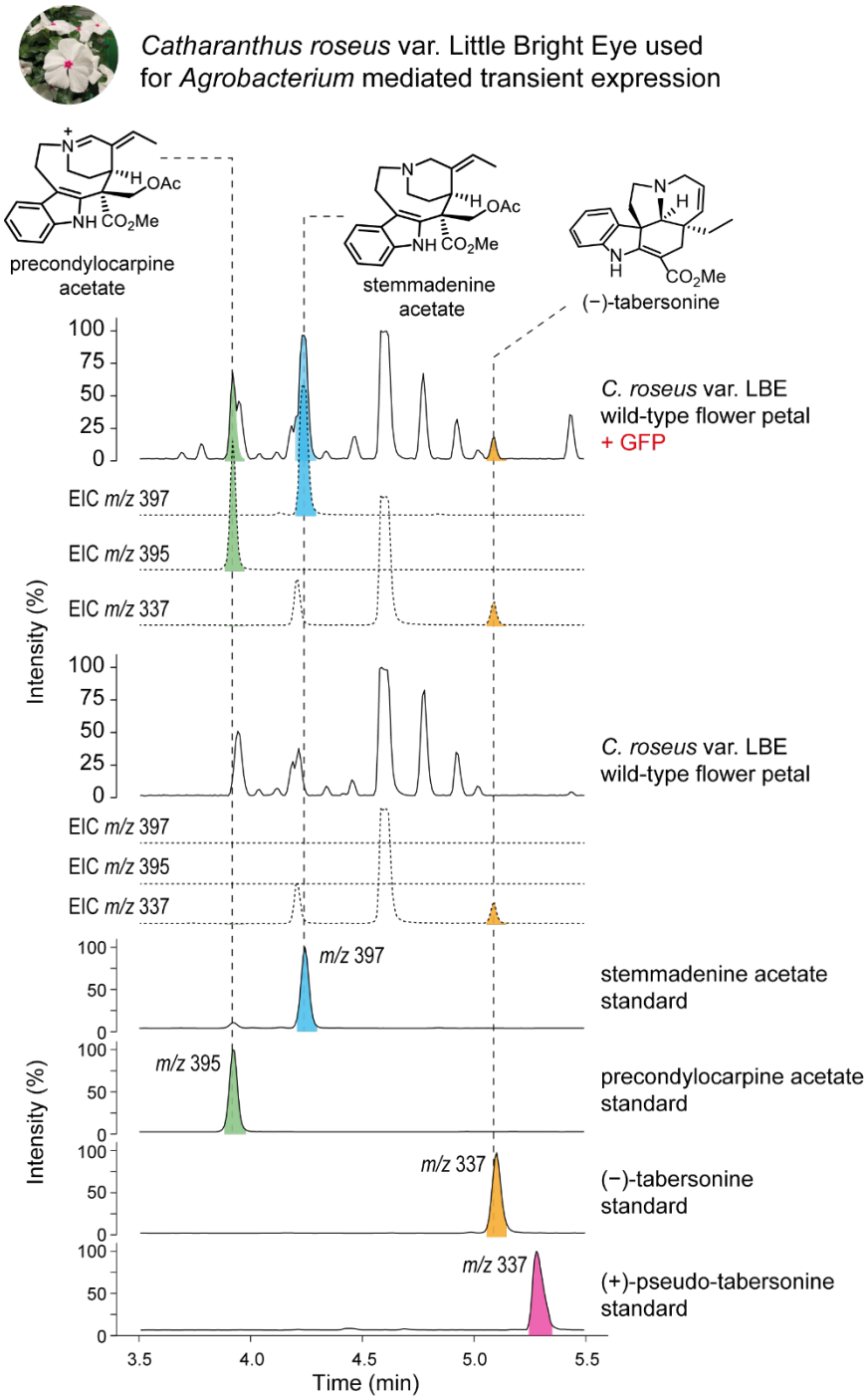


Fig. S14 MIA precursors present in *C. roseus* var. LBE flower petals.
Metabolic changes analyzed by LC-MS when *C. roseus* var. LBE flower petals are subjected to *Agrobacterium* infiltration (GFP control). Upon agroinfiltration, the flowers accumulate MIA alkaloids stemmadenine acetate, precondylocarpine acetate, and tabersonine as confirmed by authentic standards. These alkaloids are important precursors for MIA biosynthesis. LC-MS traces are presented as total ion chromatograms (solid lines) and extracted ion chromatograms are presented as dotted lines.

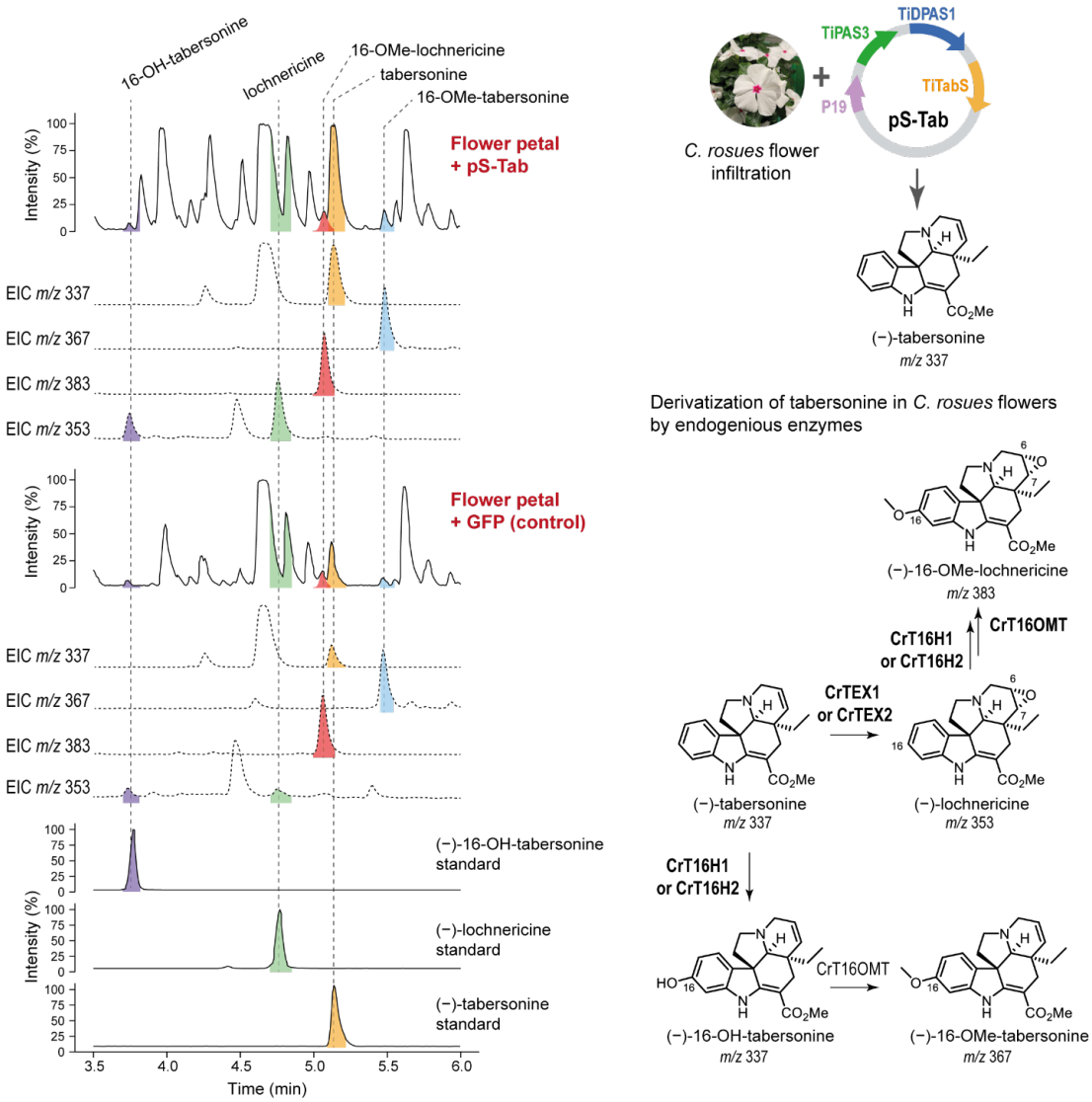
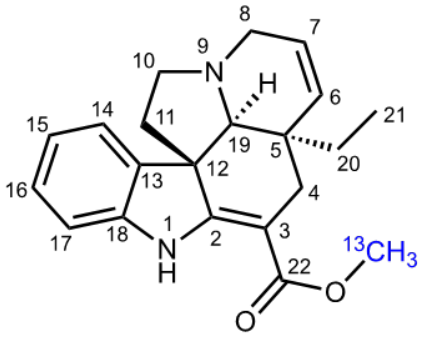


Fig. S15 Derivatization of tabersonine by endogenous enzymes present in *C. roseus* flowers.

LC-MS profiles of tabersonine derivatives observed when *C. roseus* flower petals are transfected with pS-Tab construct. In comparison to the GFP transfected control, the multigene construct pS-Tab substantially increases its product, tabersonine using endogenous substrate stemmadenine acetate. As confirmed by authentic standards, tabersonine is derivatized to lochnericine and 16-hydroxy-tabersonine by endogenous P450 enzymes CrTEX1/2 (Carqueijeiro *et al.*, 2018) and CrT16H1/2 (Besseau *et al.*, 2013) in the flowers. These compounds are further derivatized to 16-methoxy-tabersonine and 16-methoxy pachysiphine by CrT16OMTs in the flower (Sun *et al.*, 2018; Colinas *et al.*, 2021).



(–)-^{13}C-tabersonine
^{1}H-NMR, MeOH-d_3
500 MHz, 25 °C

pos.	δ_H	mult.	J_{HH}	δ_C
1	9.29	*bs*	-	-
2	-	-	-	168.0
3	-	-	-	92.6
4a	2.55	*dd*	15.2/1.7	29.9
4b	2.44	*d*	15.2	29.9
5	-	-	-	42.5
6a	5.71	*ddd*	10.0/1.8/1.8	134.2
7a	5.81	*ddd*	10.0/4.8/1.5	126.8
8a	3.22	*ddd*	15.9/1.8/1.5	51.6
8b	3.45	*ddd*	15.9/4.8/1.8	51.6
10a	2.76	*ddd*	11.2/8.5/4.7	51.8
10b	3.03	*dd*	8.5/6.4	51.8
11a	1.74	*bdd*	11.6/4.7	46.1
11b	2.01	*ddd*	11.6/11.2/6.4	46.1
12	-	-	-	56.7
13	-	-	-	139.1
14	7.26	*bd*	7.5	122.4
15	6.86	*ddd*	7.5/7.5/0.7	121.8
16	7.13	*ddd*	7.9/7.5/1.1	129.0
17	6.94	*bd*	7.9	110.8
18	-	-	-	145.0
19a	2.75	*m***	-	71.4
20a	0.87	*dq*	14.3/7.5	26.7
20b	0.99	*dq*	14.3/7.5	26.7
21	0.63	*t*	7.5	7.8
22	-	-	-	170.1***
OMe	3.76	*d**	146.4*	51.5

** overlapped signals J unresolved

*as ^{13}C-H coupling

*** with ^{13}C-^{13}C coupling (2.6 Hz)

Fig. S16 Structure confirmation of (–)-[^{13}C]-tabersonine by NMR

Structure confirmation of (–)-[^{13}C]-tabersonine by NMR. (Continued to next page).

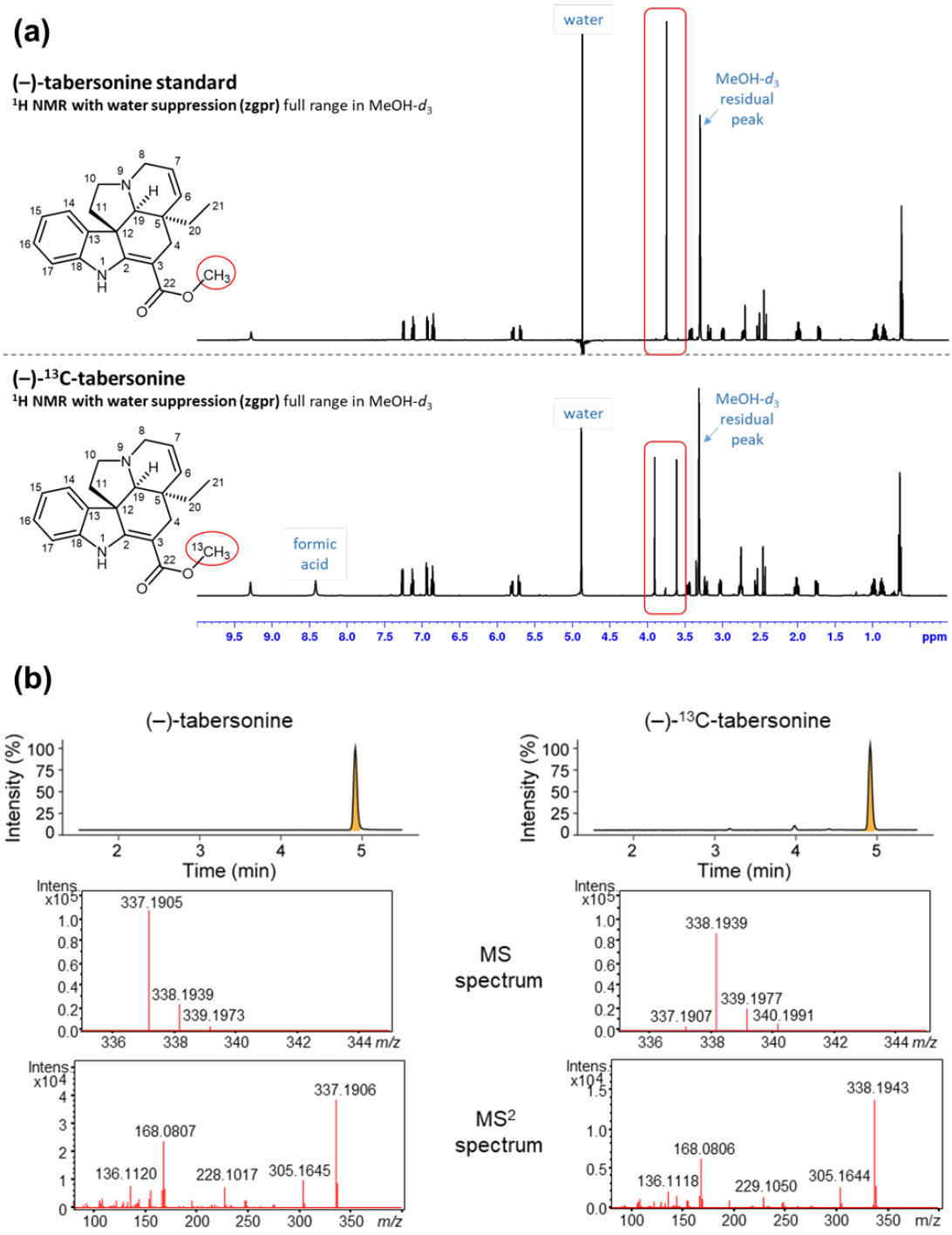


Fig. S16 Structure confirmation of (–)-[^{13}C]-tabersonine.

(a) NMR characterization of (–)-[^{13}C]-tabersonine. (b) LC-MS characterization of labeled, (–)-[13C]-tabersonine and un-labeled (–)-tabersonine. LC-MS traces are presented as total ion chromatograms.

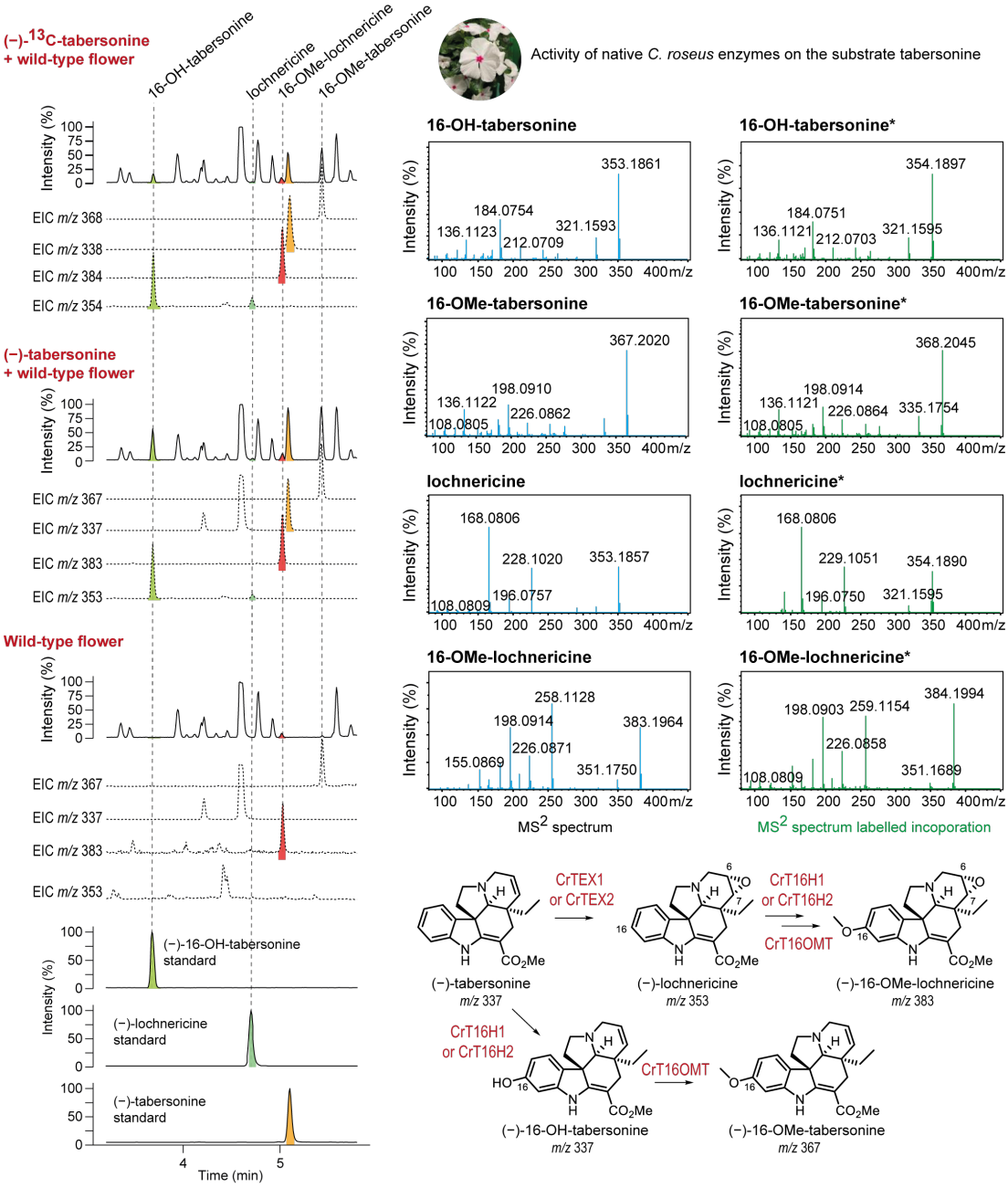


Fig. S17 Incubation of *C. roseus* flowers with ^{13}C-labelled tabersonine.

LC-MS profiles of labeled tabersonine derivatives observed when *C. roseus* flowers were incubated with ^{13}C-labeled tabersonine. MS^2 spectral comparison of standards and 13C-labeled tabersonine derivatives observed in the flowers reveals a biosynthetic network of tabersonine catalyzed by active endogenous enzymes present in the flowers. LC-MS traces with solid lines are presented as total ion chromatograms and dashed lines are extracted ion chromatograms.

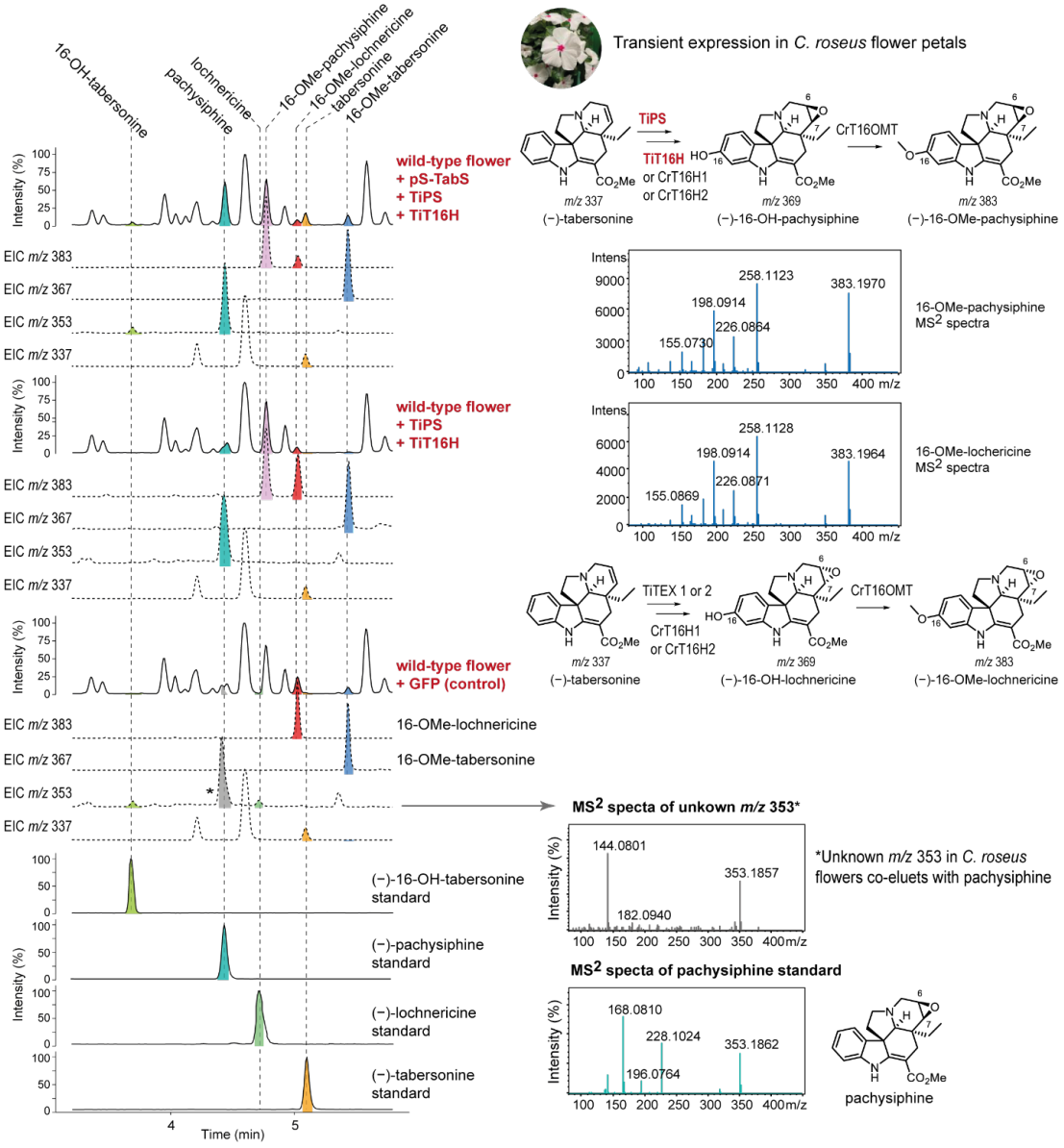


Fig. S18 Overexpression of TiPS and TiT16H in *C. roseus* flowers.

LC-MS analysis of *C. rosues* flowers simultaneously overexpressed with pS-Tab, TiPS and TiT16H indicate the formation of pachysiphine as confirmed by authentic standard and a derivative of pachysiphine with *m/z* 383 indicative of 16-methoxy-pachysiphine produced by endogenous flower enzymes. Both pachysiphine and 16-methoxy-pachysiphine are compounds not naturally present in *C. roseus.* Pachysiphine co-elutes with an unknown compound of *m/z* 353 (*) natively present in *C. roseus* flowers at low abundance but does not share MS^2 fragmentation pattern. LC-MS traces with solid lines are presented as total ion chromatograms and dashed lines are extracted ion chromatograms.

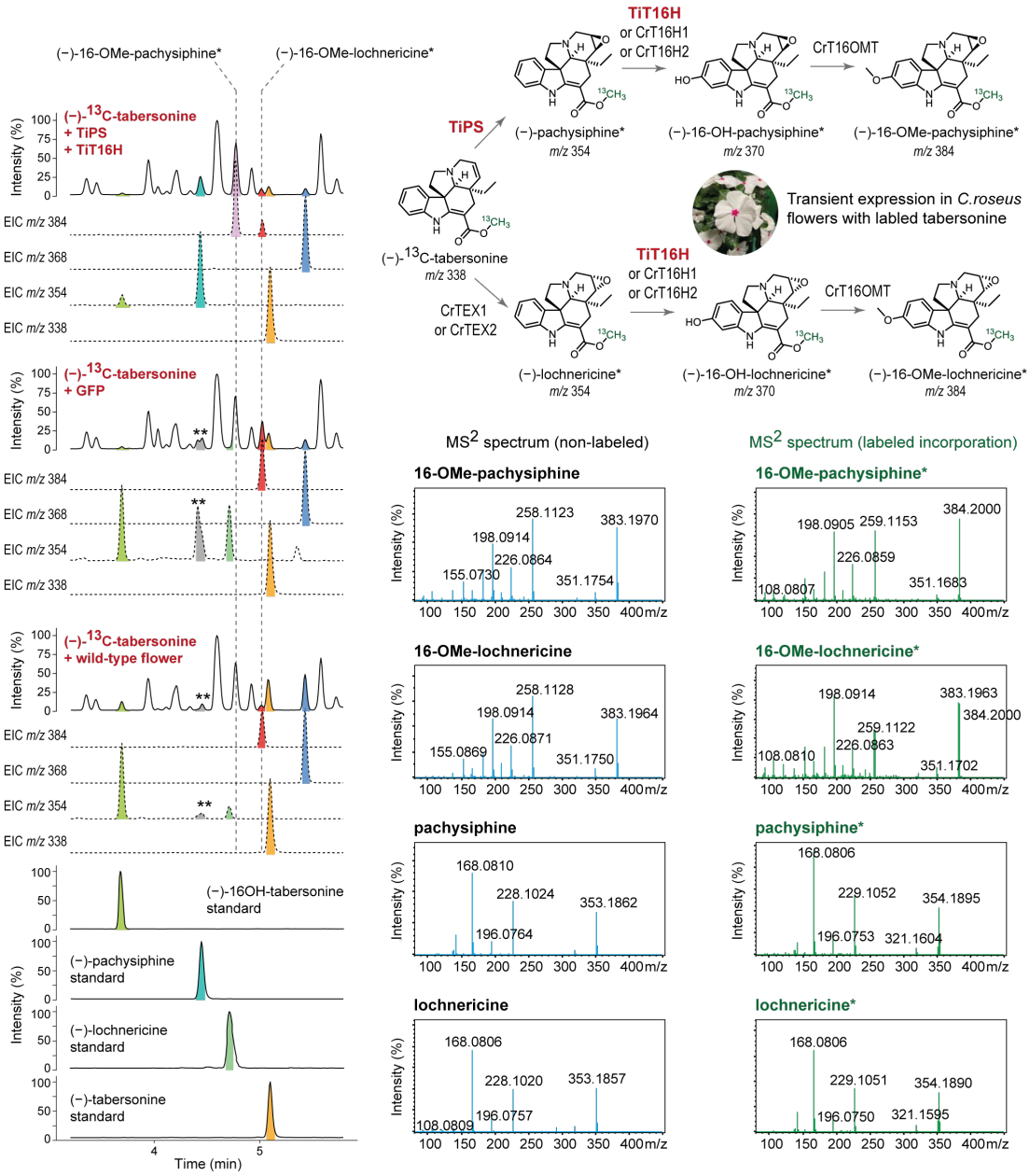


Fig. S19 Overexpression of TiPS and TiT16H in *C. roseus* flowers with ^{13}C-labeled tabersonine

LC-MS analysis and MS^2 spectral comparison confirm the formation of ^{13}C-labeled pachysiphine catalyzed by TiPS and labeled pachysiphine derivative,16-metoxy-^{13}C-tabersonine catalyzed by TiT16H and flower endogenous enzymes. *MS^2 profiles of ^{13}C-incorporated compounds. LC-MS traces with solid lines are presented as total ion chromatograms and dashed lines are extracted ion chromatograms. ** Unknown compound of *m/z* 353, which shares a similar retention time to pachysiphine (see Fig. S18).

	TiPS	TiT16H	CrGO	CrT3O	CrT16H1	CrT16H2	CrT19H	CrTEX1	CrTEX2
TiPS		45.63	36.75	53.62	45.84	46.05	34.23	46.32	45.38
TiT16H	45.63		32.94	42.35	56.34	56.89	35.4	53.42	53.1
CrGO	36.75	32.94		36.4	33.53	32.5	33.33	36.72	36.03
CrT3O	53.62	42.35	36.4		45.4	45.14	38.25	46.58	46.8
CrT16H1	45.84	56.34	33.53	45.4		80.85	35.27	57.62	56.65
CrT16H2	46.05	56.89	32.5	45.14	80.85		35.07	57.95	57.53
CrT19H	34.23	35.4	33.33	38.25	35.27	35.07		36.17	36.21
CrTEX1	46.32	53.42	36.72	46.58	57.62	57.95	36.17		87.21
CrTEX2	45.38	53.1	36.03	46.8	56.65	57.53	36.21	87.21	

Fig. S20 Percentage of identity shared by TiPS and TiT16H with *C. roseus* P450s.

Percentage identity of *T. iboga* pachysiphine synthase (TiPS) and tabersonine-16-hydroxylase (TiT16H) with known *C. roseus* P450s involved in aspidosperma (tabersonine) alkaloid hydroxylations.

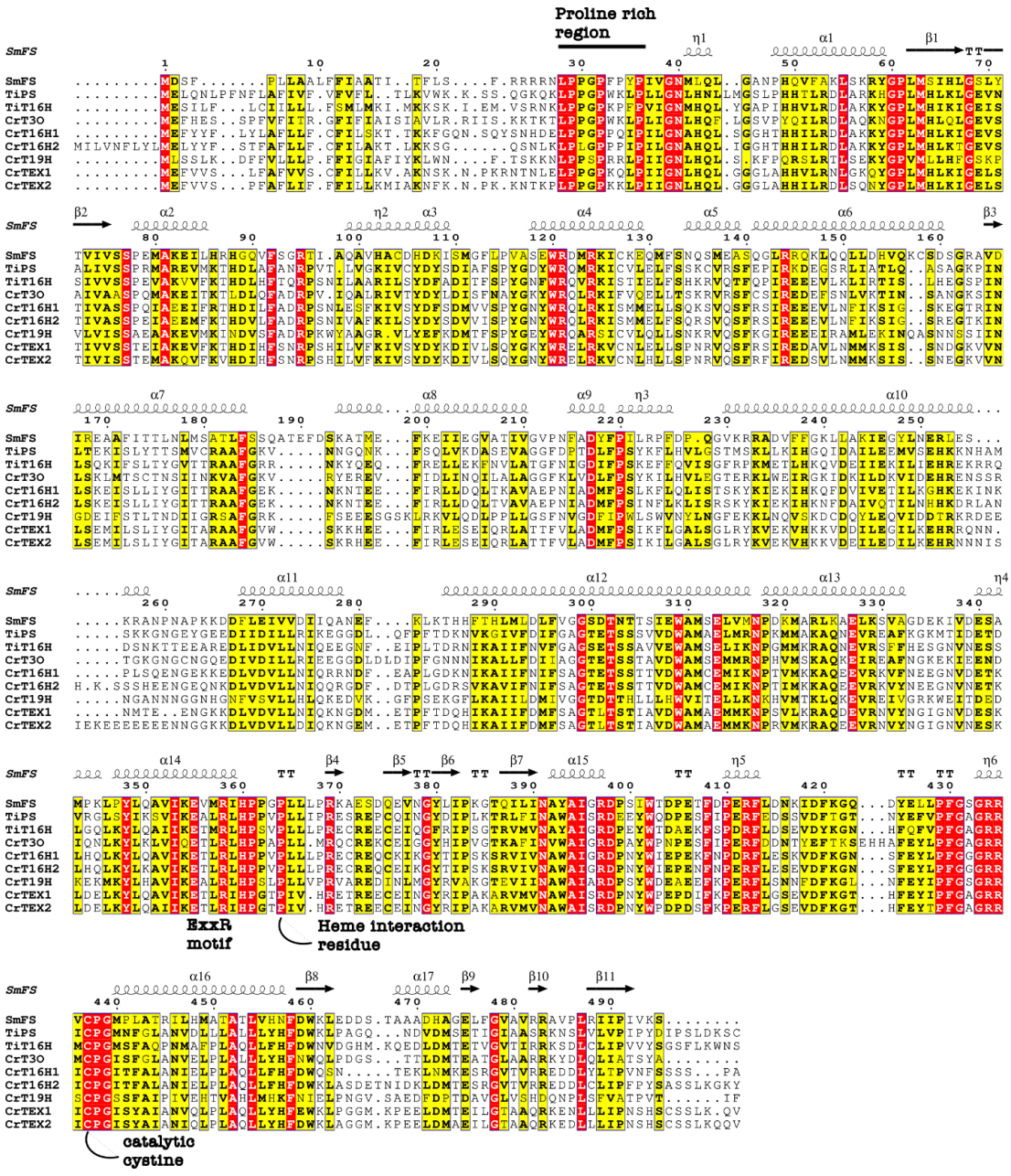


Fig. S21 Sequence alignment of TiPS and TiT16H.

Amino acid sequence alignment of *Tabernanthe iboga* pachysiphine synthase (TiPS) and tabersonine-16-hydroxylase (TiT16H) alongside known P450s from *Catharanthus roseus*. Structural features of the P450 enzyme are extracted from the crystal structure of *Salvia miltiorrhiza* Ferruginol synthase CYP76AH1 (PDB 7CB9).

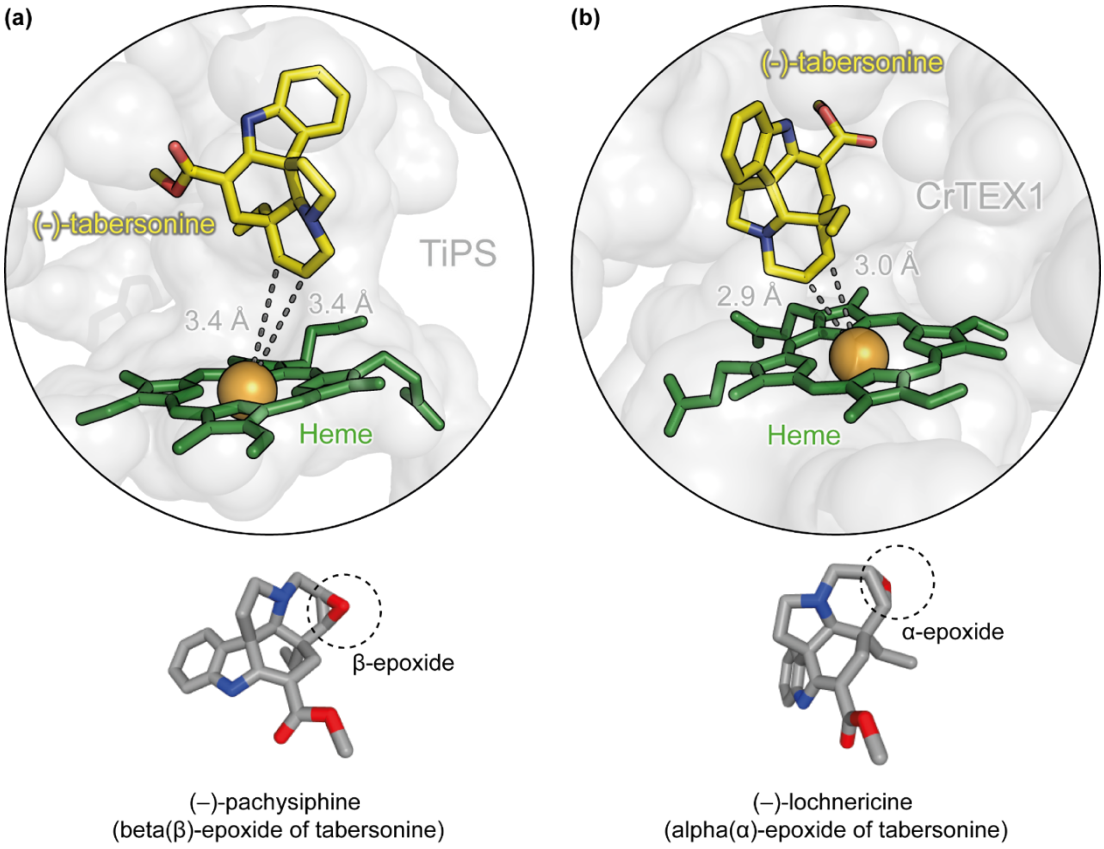


Fig. S22 Molecular docking of (–)-tabersonine into AlphaFold models of TiPS and TiT16H.

(a) AlphaFold model of TiPS docked with the substrate (–)-tabersonine. The predicted binding pocket (grey transparent surface) of TiPS orients (–)-tabersonine to the stereospecific beta (β) epoxide product. (b) AlphaFold model of TiT16H docked with the substrate tabersonine. The predicted binding pocket (grey transparent surface) of TiT16H orients (–)-tabersonine to the stereospecific alpha (α) epoxide product. Dashes represent the distance between the carbon and heme (orange) coordinated by the thiolate ligand (green) to the substrate (–)-tabersonine (yellow sticks) in Angstrom. TiPS and TiT16H protein models with the catalytic heme were generated using AlphaFold3 (Abramson *et al.*, 2024) and the (–)-tabersonine (PubChem CID 20485) ligand was docked into the active site using Webina (AutoDock Vina) (Kochnev *et al.*, 2020). Protein models were visualized and data interpreted using PyMol (Version 2.5.5, Schrödinger, LLC).

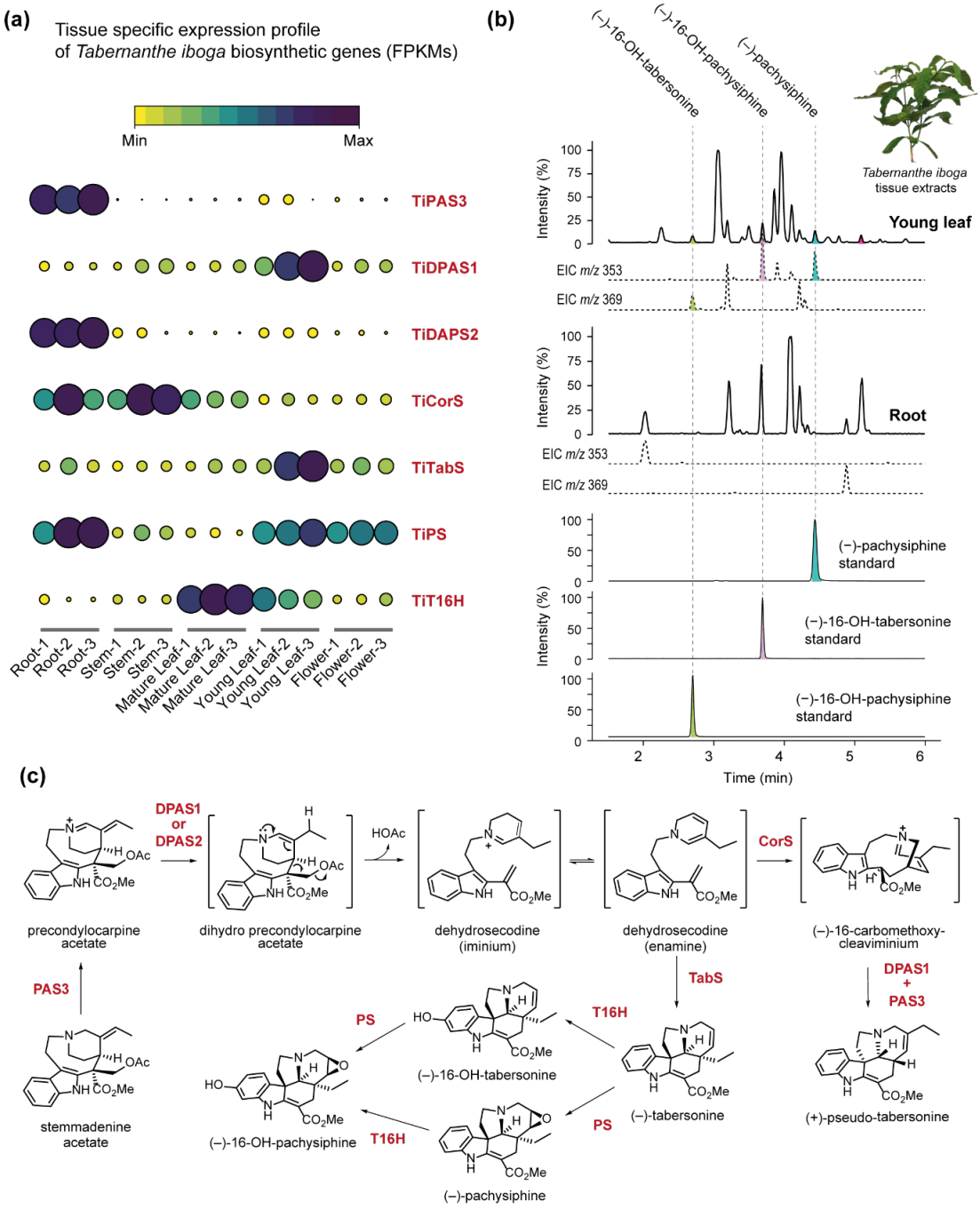


Fig. S23 Transcriptomics and metabolomics related to (–)-16-OH-pachysiphine biosynthesis in *T. iboga*.

(a) Tissue-specific transcriptomic profile of the genes involved in 16-OH-pachysiphine biosynthesis from stemmadenine acetate in *T. iboga*. (b) Representative metabolomic profile of *T. iboga* young leaf and root with authentic standards. (c) Biosynthesis of (–)-16-OH-pachysiphine from stemmadenine acetate in *T. iboga*.

Table S1 Nucleotide sequences of genes transcriptional elements described in this study.

Gene Name (Genbank ID)	**Nucleotide sequence**
P19 Goldenbraid 2.0 part ID (GB0038)	ATGGAACGAGCTATACAAGGAAACGACGCTAGGGAACAAGCTAACAGTGA ACGTTGGGATGGAGGATCAGGAGGTACCACTTCTCCCTTCAAACTTCCTG ACGAAAGTCCGAGTTGGACTGAGTGGCGGCTACATAACGATGAGACTAAT TCGAATCAAGATAATCCCCTTGGTTTCAAGGAAAGCTGGGGTTTCGGGAA AGTTGTATTTAAGAGATATCTCAGATACGACAGGACGGAAGCTTCACTGCA CAGAGTCCTTGGATCTTGGACGGGAGATTCGGTTAACTATGCAGCATCTC GATTTTTCGGTTTCGACCAGATCGGATGTACCTATAGTATTCGGTTTCGAG GAGTTAGTATCACCGTTTCTGGAGGCTCTCGAACTCTTCAGCATCTCTGTG AGATGGCAATTCGGTCTAAGCAAGAACTGCTACAGCTTGCCCCAATCGAA GTGGAAAGTAATGTATCAAGAGGATGCCCTGAAGGTACTGAAACCTTCGAA AAAGAAAGCGAGTGA
GFP	ATGGTGAGCAAGGGCGAGGAGCTGTTCACCGGGGTGGTGCCCATCCTGG TCGAGCTGGACGGCGACGTAAACGGCCACAAGTTCAGCGTGTCCGGCGA GGGCGAGGGCGACGCCACCTACGGCAAGCTGACCCTGAAGTTCATCTGC ACCACCGGCAAGCTGCCCGTGCCCTGGCCCACCCTCGTGACCACCTTCA GCTACGGCGTGCAGTGCTTCAGCCGCTACCCCGACCACATGAAGCAGCA CGACTTCTTCAAGTCCGCCATGCCCGAAGGCTACGTCCAGGAGCGCACC ATCTTCTTCAAGGACGACGGCAACTACAAGACCCGCGCCGAGGTGAAGTT CGAGGGCGACACCCTGGTGAACCGCATCGAGCTGAAGGGCATCGACTTC AAGGAGGACGGCAACATCCTGGGGCACAAGCTGGAGTACAACTACAACA GCCACAACGTCTATATCATGGCCGACAAGCAGAAGAACGGCATCAAGGTG AACTTCAAGATCCGCCACAACATCGAGGACGGCAGCGTGCAGCTCGCCG ACCACTACCAGCAGAACACCCCCATCGGCGACGGCCCCGTGCTGCTGCC CGACAACCACTACCTGAGCACCCAGTCCGCCCTGAGCAAAGACCCCAAC GAGAAGCGCGATCACATGGTCCTGCTGGAGTTCGTGACCGCCGCCGGGA TCACTCACGGCATGGACGAGCTGTACAAGTGA
pUbq10 *Solanum lycopersicum* Ubiquitin 10 promoter	GGAGGTCAACTACCCCAATTTAAATTTTATTTGATTAAGATATTTTTATGGAC CTACTTTATAATTAAAAATATTTTCTATTTGAAAAGGAAGGACAAAAATCATAC AATTTTGGTCCAACTACTCCTCTCTTTTTTTTTTTGGCTTTATAAAAAAGGAA AGTGATTAGTAATAAATAATTAAATAATGAAAAAAGGAGGAAATAAAATTTTC GAATTAAAATGTAAAAGAGAAAAAGGAGAGGGAGTAATCATTGTTTAACTTT ATCTAAAGTACCCCAATTCGATTTTACATGTATATCAAATTATACAAATATTTTA TTAAAATATAGATATTGAATAATTTTATTATTCTTGAACATGTAAATAAAAATTAT CTATTATTTCAATTTTTATATAAACTATTATTTGAAATCTCAATTATGATTTTTTA ATATCACTTTCTATCCATGATAATTTCAGCTTAAAAAGTTTTGTCAATAATTAC ATTAATTTTGTTGATGAGGATGACAAGATTTCGGTCATCAATTACATATACAC

	AAATTGAAATAGTAAGCAACTTGATTTTTTTTCTCATAATGATAATGACAAAG ACACGAAAAGACAATTCAATATTCACATTGATTTATTTTTATATGATAATAATTA CAATAATAATATTCTTATAAAGAAAGAGATCAATTTTGACTGATCCAAAAATTT ATTTATTTTTACTATACCAACGTCACTAATTATATCTAATAATGTAAAACAATTC AATCTTACTTAAATATTAATTTGAAATAAACTATTTTTATAACGAAATTACTAAA TTTATCCAATAACAAAAAGGTCTTAAGAAGACATAAATTCTTTTTTTGTAATG CTCAAATAAATTTGAGTAAAAAAGAATGAAATTGAGTGATTTTTTTTTAATCA TAAGAAAATAAATAATTAATTTCAATATAATAAAACAGTAATATAATTTCATAAAT GGAATTCAATACTTACCTCTTAGATATAAAAAATAAATATAAAAATAAAGTGTT TCTAATAAACCCGCAATTTAAATAAAATATTTAATATTTTCAATCAAATTTAAAT AATTATATTAAAATATCGTAGAAAAAGAGCAATATATAATACAAGAAAGAAGAT TTAAGTACAATTATCAACTATTATTATACTCTAATTTTGTTATATTTAATTTCTTA CGGTTAAGGTCATGTTCACGATAAACTCAAAATACGCTGTATGAGGACATAT TTTAAATTTTAACCAATAATAAAACTAAGTTATTTTTAGTATATTTTTTTGTTTA ACGTGACTTAATTTTTCTTTTCTAGAGGAGCGTGTAAGTGTCAACCTCATTC TCCTAATTTTCCCAACCACATAAAAAAAAAATAAAGGTAGCTTTTGCGTGTT GATTTGGTACACTACACGTCATTATTACACGTGTTTTCGTATGATTGGTTAAT CCATGAGGCGGTTTCCTCTAGAGTCGGCCATACCATCTATAAAATAAAGCTT TCTGCAGCTCATTTTTTCATCTTCTATCTGATTTCTATTATAATTTCTCTGAAT TGCCTTCAAATTTCTCTTTCAAGGTTAGAATTTTTCTCTATTTTTTGGTTTTT GTTTGTTTAGATTCTGAGTTTAGTTAATCAGGTGCTGTTAAAGCCCTAAATT TTGAGTTTTTTTCGGTTGTTTTGATGGAAAATACCTAACAATTGAGTTTTTTC ATGTTGTTTTGTCGGAGAATGCCTACAATTGGAGTTCCTTTCGTTGTTTTGA TGAGAAAGCCCCTAATTTGAGTGTTTTTCCGTCGATTTGATTTTAAAGGTTT ATATTCGAGTTTTTTTCGTCGGTTTAATGAGAAGGCCTAAAATAGGAGTTTT TCTGGTTGATTTGACTAAAAAAGCCATGGAATTTTGTGTTTTTGATGTCGCT TTGGTTCTCAAGGCCTAAGATCTGAGTTTCTCCGGTTGTTTTGATGAAAAA GCCCTAAAATTGGAGTTTTTATCTTGTGTTTTAGGTTGTTTTAATCCTTATAA TTTGAGTTTTTTTCGTTGTTCTGATTGTTGTTTTTATGAATTTTGCAG
tUbq10 *Solanum lycopersicum* Ubiquitin 10 terminator	GCTTGTTGTGGTTGTCTGGTTGCGTCTGTTGCCCGTTGTCTGTTGCCCAT TGTGGTGGTTGTGTTTGTATGATGGTCGTTAAGGATCATCAATGTGTTTTCG CTTTTTGTTCCATTCTGTTTCTCATTTGTGAATAATAATGGTATCTTTATGAAT ATGCAGTTTGTGGTTTCTTTTCTGATTGCAGTTCTGAGCATTTTGTTTTTGC TTCCGTTTACTATACCACTTACAGTTTGCACTAATTTAGTTGATATGCGAGCC ATCTGATGTTTGATGATTCAAATGGCGTTTATGTAACTCGTACCCGAGTGGA TGGAGAAGAGCTCCATTGCCGGTTTGTTTCATGGGTGGCGGAGGGCAAC TCCTGGGAAGGAACAAAAGAAAAACCGTGATACGAGTTCATGGGTGAGAG CTCCAGCTTGATCCCTTCTCTGTCGATCAAATTTGAATTTTTGGATCACGG CAGGCTCACAAGATAATCCAAAGTAAAACATAATGAATAGTACTTCTCAATG ATCACTTATTTTTAGCAAATCAGCAATTGTGCATGTCAAATGATTTCGGTGTA AGAGAAAGAGTTGATGAATCAAAATATCTGTAGCTGGATCAAGAATCTGAG GCAGTTGTATGTATCAATGATCTTTCCGCTACAATGATGTTAGCTATCCGAG TCAAATTGTTGTAGAATTGCATACTTCGGCATCACATTCTGGATGACATAATA AATAGGAAGTCTTCAGATCCCTAAAAAATTGAGAGCTAATAACATTAGTCCT

	AGATGTAACTGGGTGACAACCAAGAAAGAGACATGCAAATACTACTTTTGT TTGAAGGAGCATCCCTGGTTTGACATATTTTTTCTGAATATCAAACTTTGAA ACTCTACCTAGTCTAATGTCTAACGACAGATCTTACTGGTTTAACTGCAGTG ATATCTACTATCTTTTGGAATGTTTTCTCCTTCAGTTATACATCAAGTTCCAA GATGCAGGTGTGCTTGATTGATGTACATGGCTGTGAGAAGTGCATCCTGAT GTTCAGATGATGGTTCATTCTAATGTCTTTTCCTTCAATCAGTTTTCTCAGT CTGACTTAGCTTGTTTCATCTGCATGTTTGAATGTTCGTTTACTCATAGTAAT TGCATTTTTGTAGCAGAACATATCATTGGTCATGGTTTCAACTGTGCGCGA GTCTTATGCTTATTCAAACTAGGAAAGCCTCCGTCTAGAGGGTACACGAGT TGTTGCTCTGTGTGCGTCAGTCCATAGTATTAATCTTGCTAGTTGTAGTATAT TGTTTATGTGGACTCGGAATTCATCATATGCTCCTTCTTTGCATCAAGTAAG GCAAGGTAATGTATAGAAGCTTTTTAACTCTTTCATGGAAGCTGGCCTTTGC CAGCATACCATCCAGAAGATATCAACCCTGCATCTTGGCTGCCG
TiPAS3 (*Tabernanthe iboga* BBL-like) (MK840852.1)	ATGATAAAAAAAGTCCCAATAGTTCTTTCAATTTTCTGCTTTCTTCTTCTACT CTCATCATCCCATGGCTCAATTCCTGAAGCTTTTCTCAATTGTATTTCCAATA AATTTTCATTAGATGTATCCATTTTAAACATTCTTCATGTTCCCAGCAATTCTT CCTATGATTCTGTTCTCAAATCTACTATCCAAAATCCAAGATTCCTCAAATCA CCCAAGCCCTTAGCTATAATCACCCCAGTACTTCACTCCCATGTCCAATCT GCTGTTATCTGTACCAAACAAGCCGGTTTACAAATTAGAATCCGAAGCGGA GGAGCTGATTACGAGGGCTTATCCTATCGTTCTGAGGTTCCCTTTATTCTG CTAGATCTCCAGAATCTTCGATCAATTTCCGTTGATATTGAAGACAACAGCG CTTGGGTCGAATCAGGAGCAACAATTGGTGAATTCTATCATGAGATAGCTC AGAACAGCCCTGTTCATGCGTTTCCAGCTGGGGTCTCTTCCTCTGTTGGA ATTGGCGGCCATTTGAGTAGCGGCGGTTTTGGTACATTGCTTCGGAAATAT GGATTAGCAGCCGATAATATAATCGATGCAAAAATTGTTGATGCCAGAGGC AGAATTCTTGATAGGGAATCAATGGGAGAAGATCTATTTTGGGCTATTAGAG GAGGAGGAGGAGCTAGTTTTGGTGTTATAGTTTCTTGGAAGGTTAAACTTG TAAAAGTCCCTCCGATGGTAACTGTTTTCATCTTGTCCAAGACTTATGAAGA AGGAGGTTTAGATCTTCTACACAAATGGCAATATATAGAACACAAACTCCCT GAAGATTTATTCCTTGCTGTAAGCATCATGGATGATTCATCTAGTGGAAATA AAACACTTATGGCAGGTTTTATGTCTCTGTTTCTTGGAAAAACAGAGGACC TTCTGAAAGTAATGGCGGAAAATTTCCCACAACTTGGATTGAAAAAGGAAG ATTGCTTAGAAATGAATTGGATTGATGCAGCAATGTATTTTTCAGGACACCC AATTGGAGAATCCCGATCTGTGCTTAAAAACCGAGAATCTCATCTTCCAAA GACATGCGTTTCGATCAAATCAGACTTTATTCAAGAACCACAATCCATGGAT GCATTGGAAAAGTTATGGAAGTTTTGTAGGGAAGAAGAAAATAGTCCCATA ATACTGATGCTTCCACTGGGGGGAATGATGAGTAAAATATCAGAATCAGAA ATCCCATTTCCTTACAGAAAAGATGTGATTTACAGTATGATATACGAAATAGT TTGGAATTGTGAAGACGATGAATCATCGGAAGAATATATCGATGGATTGGG AAGGCTTGAGGAATTAATGACTCCATATGTGAAACAACCAAGAGGTTCTTG GTTCAGCACCAGAAACCTTTATACCGGTAAAAATAAAGGTCCAGGAACAAC TTATTCCAAAGCTAAAGAATGGGGATTTCGGTATTTTAATAATAATTTCAAAA AGTTGGCCCTTATCAAAGGACAAGTTGATCCAGAAAACTTCTTCTACTATG AACAAAGCATTCCCCCTCTCCATTTACAAGTCGAACTTTAA

TiDPAS1 (*Tabernanthe iboga* ADH) (MK840855.1)	ATGGCTGTAAAATCACCTGAAGCAGAGCACCCAGTGAAGGCTGTAAAATC ACCTGAAGAAGAGCACCCAGTGAAGGCATACGGATGGGCTATCAAAGACA GAACATCTGGCATTCTTTCCCCCTTCAAGTTTTCCAGAAGGGCAACAGGA GATGAAGACGTTCGAATAAAGATCCTCTGTTGCGGAGTTTGTCACACGGAT CTCACGTCTACCAAGAATGAATACGAGTTTCTTTCATATCCGCTAGTGCCTG GGTTAGAGACTGTCGGAATAGCGACAGAGGTCGGAAGCAAAGTCACAAAA GTAAAAGTTGGTGAAAAAGTAGCAGTGGCAGCCTATTTGGGCACTTGTGG AAAATGCCACAATTGTCTAAATGACCAAGAGAATTACTGTCCCGAAGTGAT CATTAGCTACGGCACACCATATCACGACGGAACAATCAACTACGGAGGCTT CTCGAATGAGACAGTCGTAAATGAGCGCTTCGTTCTTCATTTTCCTGAAAA GCTTTCACTTTCTGGTGTTGCACCGCTAGTCAGCGCAGGAAGCACCGCTT ACAGTGCAATAAGAAATCAAGGCCTTGACAAACCCGGTATCCACTTGGGA GTCGTCGGCCTTGGTGGACTTGGTCATCTGGCTGTGAAGTTTGCAAAGGC TTTTGGTGTCAAGGTGACAGTGATTAGTTCCACTCCCAGCAAGAAGGATG AAGCCATCAAGAGCCTTGGTGCCGATGCGTTCTTGTTCAGTCGTGATGAT GAACAAATGAAGGCCGCTATTGGAACTTTCGATGCAATCATAGATACTATTG CAGTCGCTCATCCTCTTGCGCCATTACTTGATCTACTAAGGAGTCATGGAA AAATTATTTTGGTCGGGGCACCGACCACCCCACTTGAGGTGCCAGTTATTC CTTTAGTAGCAGGAGGGAAATCAATTACTGGATGCGTAGTTGGAAATTTGA AGCAAACTCAAGAAATGCTTGAATTTGCTGCAGAACACAACATCACTGCAA ACGTTGAGGTTATTTCAATGGATTACATAAACACTGCAATGGAACGTTTAGA AAAAGGTGATGTTAGATATAGATTTGTAATTGATATTGGAAACACACTAACTC CACCGGAATAG
TiTabS (*Tabernanthe iboga* Hydrolase) (MK840853.1)	ATGGCTTCTTCAACTGAAAGCTCTGATGAGATTATTTTTGATCTTCCTCCAT ACATTAGAGTCTTTAAGGATGGAAGAGTAGAGAGACTCCACTCCTCACCAT ATGTTCCACCATCACTAGATGATCCCGCAACCGGCGTATCCTGGAAAGAC GTCCCAATTTCATCAGAGGTTTCGGCTAGAATCTACCTCCCAAAGATAAGC CAAAAGGAAAAGGAAAAGCTTCCCATTGTGGTCTATTTCCATGGTGCAGG CTTCTGTCTGGAATCCGCCTACAAGTCATTTTTCCACACTTATGTCAAGCA CTTTGCAGCCGAGGCCAAAGCAATTGCAGTTTCGGTTGAGTTCAGGCTCT CCCCAGAGCACCACCTGCCTGCAGCTTATGAAGATTGCTGGACTGCCCTT CAGTGGGTGGCTTCACATGTAGATGTTGACAACTCCAGCCTCAAGAATGC TATAGATAAAGAGCCTTGGATAATCAACCATGGAGACTTTGACAAGGTCTAC TTGTGGGGTGATAGTACGGGTGCCAATATTGTGCACAACGTACTCATCAGA GCTGGTAATGAGAGCTTGCATGGCGGAGTGAAAATCGTGGGTGCAATTCT TTATTACCCATATTTCTTGATCAGGACAAGCTCCAGACAGAGCGATTATATG GAGAACGAGTACAGAGCATACTGGAAGCTGGCTTATCCATCTGCTCCAGG TGGGAACGACAACCCGATGATAAACCCCGTGGCTGAGAACGCTCCTGATT TGGCCGGATATGGATGTTCGAGGCTGCTGGTATCCATGGTGGCAGACGAG GCCAGAGACATAACCCTTCTCTACATCGAGGCGGTGAAGAAGAGTGGGTG GAAAGGTGAATTGGAGGTGGCTGATTTCGAAGGAGATTACTTTGAAATATT CAGCCCAGAAACTGAGACAGGCAAGAACAAGGTCAAACGTTTAACGTCTT TCATCAACAAGGACTAA

TiCorS (*Tabernanthe iboga* Hydrolase) (MK840854.1)	ATGGCTAATTCAACTGCGAACTCTGATGAGATTGTTTTCGATCTTCATCCAT ACATCAGAGTCTTTAAAAACGGCAAGGTAGAAAGACTTCACGACACCCCAT ATGTTCCGCCATCACTTGAAGATCCAGCTACCGGTGTATCCTGGAAAGAC GTCCCAATTTCATCCGACGTTTCAGCTAGAGTCTACCTCCCGAAGATCAGC GAAGCGGAAAAGAAAAAGCTCCCCATTTTCGTCTATTTCCATGGTGCAGG CTTCTGTCTGGAATCAGCCTTCAAATCATTTTTCCATACTTATGTTAAGCAC GTTGTTGCCGAAACCAAAGCTGTCGGAGTTTCGGTTGAGTACAGACTCGC CCCCGAGCACCCTTTACCTGCGGCTTATGAAGATTGCTGGACTGCCCTTC AGTGGGTGGCTTCCCATGTTGGTCTTGACAACTCCAGCCTCAAGAATGCT ATTGATAAAGAGCCTTGGATAATCAACCATGGCGACCTCAATAAGCTTTACT TGGGGGGTGATAGTCCTGGTGGAAATATTGTGCACAACGTACTCATTAGG GCTGGTAAGGAGAGCTTGCATAACGGAGTGAAAATCCGGGGTGCAATTCT TTATTACCCATATTTCTTGATCAGGACAAGCAACAGACAGAGTGATTATATG GAGATTGACTATAGAGGCTACTGGAAGTTGGCTTATCCATCTGCTCCTGGC GGCACTGACAACCCAATGATAAACCCTGTAGCTAAGAATGCTCCTGATTTG GCCGGATATGGATGTTCGAGGCTGCTTGTTTCCATGGTTTCGGACGAGAC CAGAGATATAACCCTTCTCTACCTTGAGGCATTGAAGAAGAGTGGGTGGAA AGGTGAATTGGAAGTGGGTGACTACGAAGCACATTTCTTTGACTTGTTCAG CCCTGAAAATGAAGTTGGCAAGACTTGGATCAAACGTTCAAGCGATTTCAT CAACAAGGAGTAA
TiPS (P450) (*Tabernanthe iboga* This study, PQ178877)	ATGGAGCTTCAGAACTTACCCTTTAACTTCTTAGCTTTCATCGTCTTCGTAT TCGTTTTCCTAACTCTTAAAGTCTGGAAAAAGTCCAGCCAGGGAAAGCAAA AGCTCCCACCAGGGCCATGGAAGCTACCTTTGTTAGGAAACCTTCATAATT TGCTGATGGGTTCTCTTCCACATCATACACTCAGGGATCTAGCTCGAAAAC ATGGACCTCTGATGCACCTAAAGCTCGGAGAAGTTAACGCTCTCATCGTAT CATCACCTCGTATGGCTAGGGAGGTGATGAAAACCCATGATCTTGCATTTG CAAACAGGCCTGTTACTCTGGTTGGGAAGATAGTATGTTATGACTATTCCG ATATTGCTTTTAGTCCTTACGGTGATTACTGGCGACAAATGCGCAAAATATG TGTATTGGAGCTTTTTAGCTCCAAGTGTGTTCGATCGTTTGAGCCTATCAG GAAGGATGAAGGCTCTCGTCTGATTGCCACTCTTCAAGCGTCAGCTGGGA AACCGATAAATCTGACGGAGAAAATCAGCTTGTATACAACTTCCATGGTCT GCAGAGCAGCATTTGGTAAGGTAAACAACGGGCAAAACAAATTCTCCCAG TTAGTGAAGGATGCATCAGAGGTAGCAGGAGGCTTTGACCCTACTGATCTA TTTCCATCCTACAAATTTCTTCACGTTCTTGGCAGTACGATGTCTAAATTGC TGAAGATTCATGGCCAAATAGACGCCATTTTGGAGGAAATGGTTAGTGAGC ACAAAAAGAATCATGCCATGTCAAAGAAAGGCAACGGTGAGTATGGTGAA GAAGACATTATTGATATCCTACTCAGAATCAAAGAAGGTGGTGACTTGCAAT TTCCATTCACGGACAAGAATGTCAAAGGCATCGTATTTGATATTTTTGGTGC TGGAACCGAAACTTCATCCTCAGTTGTTGACTGGGCTATGGCAGAATTGAT GAGAAATCCAAAAATGATGGCCAAGGCACAAAACGAAGTGCGAGAAGCAT TTAAGGGAAAGATGACAATTGATGAAACTGATGTTCGAGGATTGAGTTACA TCAAGTCAGTAATCAAAGAAGCTCTGAGGCTACATCCTCCTGTCCCTTTGT TGATTCCCAGAGAATCCAGAGAGCCTTGTCAAATTAATGGCTACGATATACC CCTCAAGACAAGGCTTTTCATCAATGCGTGGGCGATTTCAAGAGACGAAG

	AATACTGGCAGGATCCAGAGAGTTTTATTCCTGAGAGATTTGAAGACAGCT CCGTTGATTTTACAGGAACTAACTATGAGTTTGTACCCTTTGGTGCCGGAA GGAGGATATGCCCAGGAATGAATTTTGGTCTGGCAAATGTTGATCTTCTTC TAGCTCTGCTACTCTACCATTTTGACTGGAAACTCCCAGCTGGTCAGAATG ATGTAGACATGTCGGAGACCATTGGTATAGCAGCCAGCAGAAAAAATAGCC TCGTTTTGGTTCCCATTCCTTACGACATTCCATCTCTTGATAAATCATGCTG A
TiT16H (P450) (*Tabernanthe iboga* This study, PQ178876)	ATGGAGTCCATTCTTTTCCTTTGCATCATCCTCCTCCTTTTCTCTATGTTAAT GAAAATTATGAAGAAATCAAAGATCGAGATGGTCTCAAGAAACAAATTGCC CCCAGGGCCGAAACCATTTCCAGTTATAGGAAACATGCATCAGCTCTATGG AGCTCCAATCCACCATGTCCTCAGAGATTTAGCCAAGAAATATGGTCCTCT TATGCACATCAAGATTGGTGAAATTTCTAGCATTGTTGTCTCCTCGCCAGAA GTTGCCAAAGTGGTTTTCAAGACACATGATCTCCACTTCACTCAAAGACCC TCCAACATTCTAGCAGCGAGGATACTCTCATATGATTTCGCTGACATTACCT TCTCTCCTTATGGAAATTTCTGGAGACAAGTACGGAAAATCAGCACGATTG AACTTTTTAGTCACAAACGTGTTCAGACATTCCAACCAATTAGGGAAGAGG AGGTGCTGAAACTGATTAGAACCATTTCGTTGCATGAGGGATCACCGATCA ATCTCAGCCAAAAAATTTTTTCATTGACTTATGGAGTCACTACTCGTGCTGC CTTTGGTAGAAGAAACAAATATCAAGAACAATTCCGGGAACTTTTGGAAAA ATTCAATGTGCTAGCAACAGGATTTAACATAGGAGACATCTTCCCTTCAAAG GAATTCTTTCAAGTGATCAGTGGATTTCGTCCAAAGATGGAAACCCTACAC AAGCAGGTTGATGAAATAATTGAAAAAATCCTGATTGAGCACAGGGAGAAA CGCAGACAAGACTCCAATAAGACAACAGAAGAAGCAAGGGAGGATTTAAT TGACGTTCTTCTGAATATTCAAGAAGAAGGGAACTTTGAAATTCCTCTTACT GACCGCAACATCAAAGCAATCATCTTTAATGTATTCGGTGCAGGAAGTGAG ACATCTTCAGCAGTTGTAGAATGGGCGATGTCGGAACTAATAAAAAATCCA GGTATGATGAAAAGGGCACAAAACGAAGTTAGAAGTTTCTTCCATGAAAGT GGAAATGTTAATGAATCGAGCCTTGGACAACTTAAATACTTGCAAGCAATCA TTAAAGAAACCATGAGATTACACCCTAGTGTTCCATTGCTACTCCCCAGGG AATGCAGGGAAGAATGTGAAATCCAAGGATTTCGGATACCTTCCGGGACC AGAGTCATGGTAAATGCATATGCAATTGGCAGAGATCCTGAATACTGGACT GATGCTGAGAAATTCAGCCCCGACAGATTTCTTGATTCTGAAGTTGATTATA AGGGAAATCATTTCCAGTTTGTACCATTTGGTGCTGGAAGAAGGATGTGTC CAGGGATGTCGTTTGCTCAACCGAATATGGCATTCCCTCTCGCACAATTAT TGTTTCATTTTGACTGGAACGTTGATGGCCATATGAAGCAAGAAGATCTAG ACATGACCGAGACAGTTGGGGTGACCATTAGAAGGAAAAGTGACTTGTGC CTTATTCCAGTTGTCTATTCAGGTTCTTTTCTTAAATGGAATTCCTAG
CrT16H1 (*Catharanthus roseus* P450) (FJ647194.1)	ATGGAATTCTATTATTTTCTCTACTTGGCCTTCCTTCTTTTCTGCTTCATTTTA TCAAAAACCACAAAGAAATTTGGCCAAAACAGCCAATATTCAAACCATGAT GAGCTACCTCCGGGGCCTCCCCAAATTCCTATATTAGGAAATGCCCATCAA CTTAGCGGTGGCCATACTCATCACATTCTAAGAGATTTGGCCAAAAAATATG GGCCGTTGATGCACTTAAAGATTGGTGAAGTTTCAACTATTGTTGCATCTT CACCACAAATTGCTGAAGAGATTTTTAGAACGCATGATATTCTTTTTGCCGA TAGACCCTCAAATCTTGAGTCTTTTAAAATCGTGTCTTATGATTTTTCAGATA

	TGGTTGTTAGTCCATATGGTAATTATTGGAGACAACTTCGTAAAATTAGCAT GATGGAACTTCTAAGCCAAAAGAGTGTCCAATCTTTTAGATCAATTAGAGAA GAGGAAGTATTAAATTTTATTAAATCAATTGGTTCCAAAGAGGGTACAAGAA TTAATCTCAGCAAAGAGATATCGTTACTTATTTATGGAATTACTACGCGTGCT GCTTTTGGAGAGAAAAATAAGAATACAGAAGAATTTATTCGTCTACTTGATC AACTTACAAAGGCAGTAGCGGAACCTAACATTGCAGATATGTTCCCTTCTC TCAAATTTCTTCAATTGATTAGTACATCAAAATATAAGATTGAGAAAATACAC AAACAATTTGATGTTATAGTTGAAACTATTCTCAAAGGGCATAAGGAGAAAA TCAACAAGCCCTTAAGTCAAGAGAATGGAGAAAAAAAGGAGGACCTTGTT GATGTGCTACTCAATATTCAACGACGTAATGACTTTGAAGCCCCACTGGGG GATAAAAACATCAAAGCCATAATCTTCAACATATTCAGTGCCGGCACTGAGA CATCGTCAACAACAGTCGATTGGGCAATGTGCGAAATGATAAAAAATCCAA CGGTAATGAAAAAGGCACAAGAAGAGGTAAGAAAGGTATTTAATGAAGAAG GAAATGTTGATGAAACAAAACTTCATCAACTAAAATATTTACAAGCAGTGAT TAAAGAAACATTAAGGCTTCATCCACCAGTTCCATTACTACTTCCAAGAGAA TGTCGAGAACAATGTAAGATTAAAGGGTACACAATACCATCCAAATCTAGAG TTATAGTCAATGCATGGGCTATCGGAAGGGATCCAAATTACTGGATTGAAC CTGAGAAATTTAACCCGGATAGATTTCTTGAATCAAAAGTTGATTTTAAAGG AAATTCATTCGAGTATCTACCATTTGGTGGTGGAAGAAGGATATGTCCGGG CATAACATTTGCTTTGGCTAATATAGAATTGCCATTAGCACAACTTTTGTTCC ATTTTGATTGGCAATCAAATACTGAGAAATTAAATATGAAAGAGAGTAGAGG GGTAACAGTTAGGCGAGAAGATGATTTGTATTTGACTCCAGTTAATTTTTCT TCCTCTTCTCCTGCTTGA
CrT16H2 (*Catharanthus roseus* P450) (JF742645.1)	ATGGAGTTGTATTATTTTTCCACCTTTGCCTTCCTTGTTTTCTGCTTCATTTT AGCCAAAACTCTAAAGAAATCTGGCCAATCAAATCATAAGCTGCCTCCGGG GCCTCCCCCAATTCCTATATTAGGAAATGTCCATCAACTTATCGGTGGCCAT ACTCATCACGTTCTAAGAGATTTGGCCAAAAAATATGGACCGTTGATGCAC TTAAAGACTGGTGAAGTTTCAATCATTGTTGCATCCTCACCAGAAATTGCT GAAGAGATGTTTAAAACACATGATGTTCTCTTTGCGGACAGACCCTCAAAT ATTGTTGCCTTCAAAATCTTGTCTTATGATTATTCGGATATTGTCATTAGTCC ATATGGCAATTATTGGAGACAACTTCGTAAAATTAGCATGATGGAGCTTTTT AGCCAAAGGAGTGTCCAATCTTTCAGATCACTTAGAGAAGAGGAAGTCTT GAATTTTATTAAATCAATTGGTTCGAAAGAGGGTACAAAAATTAATCTTAGCA AGGAAATATCGTTACTTATTTATGGAATTACTACGCGTGCTGCTTTTGGAGA AAAAAATAAGAATACAGAAGAATTTATTCGTCTTCTTGATCAACTCACAGTG GCAGTAGCGGAACCTAACATTGCAGATATGTTCCCTTCTATCAATTTTCTTA AATTAATTAGTAGATCGAAATATAAGATTGAGAAAATACACAAAAATTTTGAT GCCATAGTTCAAACTATTCTCAACCATCATAAGGATAGATTAGCCAATTACAA GTCCTCAAGTCCTGAAGAGAATGGGGAACAAAACAAGGATCTTGTTGATG TGCTACTCAATATTCAACAACGTGGTGATTTTGATACACCACTAGGTGATCG CAACGTCAAAGCAGTAATTTTTAACATATTCAGTGCCGGAACTGAGACATC GTCAACGACAGTGGATTGGGCGATGTGTGAAATGATAGAAAATCCAACGAT GATGAAAAAGGCACAAGAAGAGGTAAGAAAGGTATATAACGAAGAAGGAA ATGTTAATGAAACAAAACTTCATCAGCTACAATATTTAAAAGCAGTGATTAAA

	GAAACATTAAGGCTTCATCCACCAGTTCCATTACTACTTCCAAGAGAATGTC GAGAACAATGTGAGATTAAAGGGTACACAATACCATCCAAATCTAGAGTTAT AGTCAATGCATGGGCTATCGGAAGGGATTCGAATTACTGGATTGAACCTGA AAATTTTAACCCGGAGAGATTTCTTGAATCAGAAGTTGATTTTAAAGGAAAC TCATTCGAGTATCTACCGTTTGGTGGTGGAAGAAGGATATGTCCGGGCATA ATATTTGCTTTGGCTAATATAGAACTGCCATTGGCACAACTTTTGTTCCATTT TGATTGGAAACTTGCCAGTGATGAAACAAATATTGATAAATTAGACATGACG GAGAGTAGAGGAGTAACAGTTAGAAGAGAAGATGATTTGTGTCTGATTCCA TTTCCTTATTCTGCTTCTTCTCTCAAAGGTAAATATTGA
CrTEX1 (*Catharanthus roseus* P450) (A0A343URW6.1)	ATGGAGTTTGTGGTTTCCCTCTTTGCCTTCGTCGTTTCCTGCTTCATTTTAC TTAAAGTAGCAAAGAATTCCAAGAACCCAAAGAGAAACACAAATCTTGAGC TTCCCCCGGGGCCAAAACAACTTCCTATAATTGGAAACCTTCATCAGCTTG GCGGCGGCTTAGCTCATCATGTACTTAGAAATTTGGGCAAACAATATGGAC CTTTGATGCACTTGAAAATTGGTGAACTTTCAACAATAGTAGTTTCCTCAAC AGAAATAGCAAAAGAAGTTTTCAAGACTCATGATATCCACTTTTCTAATAGA CCTTCTCATATTCTTGTTTTTAAAATCGTTAGTTACGATTATAAAGACATTGTT CTTTCTCAATATGGAAAGTATTGGAGAGAGCTTCGAAAAGTTTGTAATCTCG AACTTCTCAGTCCAAATCGTGTCCAATCCTTCAGATCCATAAGGGAAGATG CTGTCCTTAATATGATGAAATCAATTTCTTCAAATGATGGCAAAGTTGTCAAT TTAAGTGAAATGATCCTCTCTCTTATTTATGGAATCACTGCACGTGCAGCTT TTGGTGTTTGGAGTAAAAAGCATGAAGAGTTCATAAGACTTGAGAGTGAAA TTCAGAGGTTGGCAACAACGTTTGTTTTAGCAGATATGTTTCCTTCGATTAA ATTTCTTGGAGCTCTAAGTGGATTGAGATATAAGGTTGAGAAAGTACATAAA AAGGTTGATGACATACTTGAAGGCATTCTGAAGGAGCATAGACGACAGAAT AATAATATGACAGAAGAAAATGGAAAAAAGGATCTTGTTGATGTCCTTCTCA ACATCCAAAAGAATGGAGACATGGAAACCCCTTTTACTGATCAACACATCA AAGCCATAATTTTTGATATGTTCAGTGCCGGAACTCTAACATCAACAATAGC AGTGGATTGGGCAATGGCGGAAATGATGAAGAATCCGAGCGTGCTGAAAA GGGCTCAAGATGAAGTTAGAAATGTGTATAATGGAATTGGAAATGTTGATGA GTCTAAGCTTGATGAATTAAAATATTTACAAGCGGTTATAAAAGAGACATTGA GAATACATCCTGGCACTCCTATTGTTCACAGAGAAACTCGTGAAGAATGTG AAATTAATGGGTATAGGATTCCTGCAAAAGCTAGAGTTATGGTCAATGCATG GGCTATCAGTAGAGATCCGAATTACTGGCCGGAGCCGGATATTTTTAAACC TGAAAGATTTCTAGGGTCGGAAGTTGATTTTAAGGGAACCCATTTTGAATAC ATTCCATTTGGAGCAGGAAGGCGTATTTGTCCGGGAATATCATATGCTATTG CTAATGTTCAACTACCGTTGGCACAGCTTTTGTACCATTTTGAGTGGAAAC TTCCAGGCGGAATGAAGCCAGAAGAACTGGACATGACCGAGATTTTGGGT ACTGCCGCCCAGCGCAAAGAAAATTTGCTTCTGATACCAAATTCGCATTCT TGTTCTTCTTTGAAACAAGTGTGA
CrTEX2 (*Catharanthus roseus* P450) (A0A343URW7.1)	ATGGAGTTTGTGGTTTCCCCCTTTGCTTTCCTCATTTTCTTCTTCATTTTACT CAAAATGATAGCAAAGAATTTCAAGAACCCCAAGAAAAACACAAAGCCTCT TCCTCCAGGGCCAAAAAAGCTTCCTATAATAGGAAACCTTCATCAGCTAGG TGGTGGTTTAGCTCACCATATCCTTAGAGATTTATCCCAAAACTATGGACCT TTGATGCATTTGAAAATCGGTGAACTTTCAACAATAGTCATTTCCTCAACAG

	AAATGGCTAAACAAGTTTTCAAGGTTCATGATATCCATTTCTCAAACAGACC TTCTCATATTCTTGTTTTTAAAATCGTTAGCTATGATTATAAAGACATCGTACT TTCCCAATATGGAAACTACTGGCGAGAGCTTCGTAAAGTCTGTAATCTCCA TCTTTTAAGTCCAAATCGTGTCCAATCCTTTAGATTCATAAGGGAAGATTCT GTTCTTAATATGATGAAATCAATTTCTTCCAACGAGGGTAAAGTTGTCAATTT AAGTGAAATGATTTTATCTCTTATTTATGGAATTACTGCTCGTGCTGCATTTG GTGTTTGGAGTAAAAGACATGAAGAATTCATAAGACTTGAGAGTGAAATTC AAAGGTTGGCAACAACGTTTGTTTTAGCAGATATGTTTCCTTCGATTAAAAT TCTTGGAGCTTTAAGTGGATTGAGATATAAGGTTGAGAAAGTACATAAAAAA GTTGATGAAATTCTTGAAGATATTCTCAAAGAGCATAGAAATAATAATATTAG TATTGAGAAAGAAGAAGAAGAAGAAGAAGAAAATAATGGTGGAAAAAAGGA TCTTGTTGATGTCCTTCTTGATATCCAAAAGAATGGAGAAATGGAAACCCC ATTTACAGATCAACATATCAAAGCCATCATTTTTGATATGTTCAGTGCCGGA ACCCTAACGTCGACGATAGCAGTGGATTGGGCAATGGCCGAAATGATGAA GAATCCAAGAGTGATGAAAAGGGCTCAAGAAGAAGTTAGGAATGTATACAA CGGAATAGGAAACGTAAACGAATCAAAACTCGATGAATTAAAATATTTACAA GCAATTATAAAAGAGACACTAAGAATACATCCAGGAACTCCCATAGTTCATA GAGAAACTCGTGAAGAATGCGAGATTAATGGGTATAGAATACCTGCAAAAG CTAGAGTTATGGTTAATGCATGGGCAATCAGTAGAGATCCAAATTACTGGC CAGATCCGGATAGCTTTAAACCTGAGAGATTTTTGGGATCAGAAGTCGATT TTAAAGGTACCCATTTTGAATATACTCCATTTGGAGCAGGTAGGCGTATTTG TCCGGGGATATCATATGCCATTGCCAATATTCAGCTGCCGTTGGCGCAACT TTTGTACCATTTTGATTGGAAACTTGCCGGTGGAATGAAGCCTGAAGAATT GGACATGGCGGAGATTTTGGGTACTGCTGCCCAACGCAAAGAAGATTTGC TTCTCATACCAAATTCCCATTCTTGTTCTTCTTTGAAACAACAAGTGTGA
CrT19H (*Catharanthus roseus* P450) (HQ901597.1)	ATGTTGTCTTCATTGAAAGATTTCTTCGTTCTACTTCTGCCTTTCTTCATTG GCATTGCATTTATATATAAATTATGGAATTTTACATCCAAGAAAAATCTTCCGC CATCGCCAAGAAGGCTACCGATTATCGGAAACCTTCATCAGCTCAGTAAAT TTCCTCAACGTTCACTGAGAACATTATCAGAAAAATATGGGCCTGTCATGTT ACTTCATTTTGGTAGCAAGCCAGTTTTGGTTATATCCTCAGCAGAAGCAGC TAAAGAAGTAATGAAAATCAATGATGTTTCTTTCGCTGATAGGCCTAAATGG TATGCTGCTGGTAGGGTTCTTTATGAATTTAAGGATATGACATTTTCACCCTA TGGTGAGTATTGGAGACAAGCTAGAAGTATATGTGTTCTTCAGCTTCTAAGT AACAAAAGGGTTCAATCTTTTAAAGGTATTAGAGAAGAAGAGATAAGGGCA ATGTTGGAAAAAATAAATCAAGCTAGTAATAATTCAAGTATCATTAATGGTGA TGAGATTTTCTCGACACTTACAAATGACATAATTGGAAGATCTGCTTTTGGG AGGAAATTTTCTGAAGAAGAAAGTGGAAGTAAATTAAGAAAAGTTCTTCAA GATTTGCCACCTTTGTTAGGTTCTTTCAATGTTGGTGATTTTATTCCATGGC TTTCTTGGGTTAATTATTTAAATGGTTTTGAAAAAAAATTGAACCAAGTTTCA AAAGATTGTGATCAATATCTTGAGCAAGTTATTGATGATACGAGGAAGAGAG ATGAAGAAAATGGAGCTAATAACAATGGCGGAAATCATGGAAATTTTGTTAG TGTTCTACTTCATCTCCAGAAAGAAGATGTCAAGGGTTTTCCTTCAGAAAA AGATTTTCTTAAAGCTATCATTTTGGACATGATTGTTGGGGGAACAGACACA ACACATTTGCTTTTGCATTGGGTAATCACAGAGCTTCTCAAAAACAAACATG

	TAATGACTAAATTACAAAAAGAGGTGAGAGAAATAGTCGGAAGAAAATGGG AGATAACTGATGAAGACAAAGAAAAAATGAAATATTTACACGCAGTTATAAA AGAGGCACTCCGGTTACATCCTTCTCTTCCTTTACTCGTTCCCAGAGTAGC AAGAGAGGATATAAACCTAATGGGTTATCGCGTAGCGAAAGGCACAGAAGT GATTATTAATGCTTGGGCAATAGCGAGAGATCCATCGTACTGGGATGAAGC CGAGGAGTTTAAGCCGGAGAGATTCTTGAGTAATAATTTTGATTTTAAAGGA CTTAATTTTGAGTATATTCCATTTGGTTCTGGAAGAAGAAGTTGCCCTGGAT CTTCATTTGCAATCCCCATTGTAGAACACACAGTGGCACATTTGATGCATAA ATTCAATATTGAGTTGCCAAATGGAGTCAGTGCTGAAGATTTTGATCCCACA GATGCCGTTGGACTCGTATCTCATGACCAAAACCCTCTCTCGTTTGTGGCA ACTCCGGTTACCATTTTTTGA
CrT3O (*Catharanthus roseus* P450) (JN613015.1)	ATGGAGTTTCATGAATCTTCTCCCTTCGTGTTCATCACTCGTGGCTTTATAT TCATAGCAATTTCAATAGCCGTACTGAGAAGAATAATATCAAAGAAAACTAA AACATTGCCTCCAGGACCATGGAAGCTACCTTTGATTGGAAATCTTCATCA ATTTCTGGGTTCTGTTCCTTATCAAATTCTCAGAGATTTAGCTCAAAAAAAT GGGCCTTTGATGCACCTTCAATTAGGTGAAGTTTCTGCCATCGTGGCAGC ATCTCCTCAAATGGCTAAGGAGATTACAAAAACTTTGGATCTTCAATTTGCA GACAGGCCAGTTATTCAAGCATTAAGGATTGTGACCTATGATTATTTAGATAT ATCCTTTAATGCATACGGAAAATATTGGAGACAATTGCGTAAAATTTTTGTCC AAGAACTATTAACTTCAAAGAGAGTTCGATCATTTTGCTCTATAAGAGAAGA TGAATTTTCCAATCTGGTAAAAACAATCAATTCTGCGAATGGAAAATCAATC AATTTGAGCAAATTGATGACGTCATGCACAAATTCAATTATTAATAAAGTAGC TTTTGGTAAAGTACGTTATGAACGGGAGGTGTTTATTGATCTAATTAATCAAA TATTAGCATTAGCAGGCGGTTTTAAGCTGGTTGATCTGTTTCCGTCCTACAA GATACTTCATGTTCTTGAAGGTACAGAACGTAAGCTGTGGGAAATCCGCG GTAAGATTGACAAGATTTTGGATAAAGTCATAGACGAGCACAGAGAAAATT CGTCAAGAACTGGAAAGGGCAACGGTTGTAATGGCCAGGAAGATATAGTT GATATTTTACTTAGGATTGAAGAGGGTGGTGATCTTGACCTTGATATTCCCT TTGGCAACAACAATATCAAAGCTCTTTTATTCGATATAATTGCAGGCGGAAC TGAAACCTCATCAACAGCAGTTGACTGGGCAATGTCAGAGATGATGAGAA ATCCCCATGTGATGAGCAAAGCGCAAAAGGAAATTAGGGAAGCGTTCAAT GGAAAGGAGAAGATTGAGGAGAATGATATTCAAAATTTGAAGTACCTAAAG TTAGTGATCCAAGAAACCTTAAGGTTACACCCTCCTGCTCCATTGTTGATG AGACAATGCCGAGAGAAATGTGAAATTGGCGGATATCATATACCTGTTGGA ACAAAAGCGTTCATCAATGTCTGGGCAATCGGAAGGGATCCTGCGTATTG GCCTAATCCAGAGAGTTTTATTCCGGAAAGATTTGACGATAATACTTATGAA TTTACAAAATCTGAACATCATGCGTTTGAATATTTGCCATTTGGTGCCGGAA GAAGGATGTGTCCGGGCATTTCATTTGGTTTGGCCAACGTGGAGCTTCCT TTAGCTCTACTTCTTTACCATTTCAACTGGCAACTCCCAGATGGTTCTACTA CTCTGGATATGACAGAGGCTACTGGATTAGCAGCAAGAAGAAAATATGATC TTCAATTAATCGCTACGTCCTATGCATGA

Table S2 Primers used in this study.

Gene	Plasmid	Primer direction	Sequence (5'-3')
Yeast expression constructs (In-Fusion cloning)			
TiPS	pESC-HIS	Forward	**GAGAAAAAACCCCGGATCC**ATGGAGCTTCAGAACTTACC
		Reverse	**ACTTCTGTTCCATGTCGAC**GCATGATTTATCAAGAGATGGAA
TiT16H	pESC-HIS	Forward	**GAGAAAAAACCCCGGATCC**ATGGAGTCCATTCTTTTCCTTT
		Reverse	**ACTTCTGTTCCATGTCGAC**CTAGGAATTCCATTTAAGAAAAGAA
CrT16H1	pESC-HIS	Forward	**GAGAAAAAACCCCGGATCC**ATGGAATTCTATTATTTTCTCTACTTG
		Reverse	**ACTTCTGTTCCATGTCGAC**AGCAGGAGAAGAGGAAGAAA
CrT16H2	pESC-HIS	Forward	**GAGAAAAAACCCCGGATCC**ATGGAGTTGTATTATTTTTCCAC
		Reverse	**ACTTCTGTTCCATGTCGAC**ATATTTACCTTTGAGAGAAGAAG
CrTEX1	pESC-HIS	Forward	**GAGAAAAAACCCCGGATCC**ATGGAGTTTGTGGTTTCCCT
		Reverse	**ACTTCTGTTCCATGTCGAC**CACTTGTTTCAAAGAAGAACAAGAA
CrTEX2	pESC-HIS	Forward	**GAGAAAAAACCCCGGATCC**ATGGAGTTTGTGGTTTCCC
		Reverse	ACTTCTGTTCCATGTCGACCACTTGTTGTTTCAAAGAAGAAC
CrT19H	pESC-HIS	Forward	**GAGAAAAAACCCCGGATCC**ATGTTGTCTTCATTGAAAGATTTCTT
		Reverse	**ACTTCTGTTCCATGTCGAC**AAAAATGGTAACCGGAGTTGC
CrT3O	pESC-HIS	Forward	**GAGAAAAAACCCCGGATCC**ATGGAGTTTCATGAATCTTC

		Reverse	**ACTTCTGTTCCATGTCGAC**TGCATAGGACGTAGC GATTA
Sequence verification primers pESC-HIS		Forward	ATGATTTTTGATCTATTAACAGATA
		Reverse	GTATAATGTTACATGCGTACAC
Gene	**Plasmid**	**Primer direction**	**Sequence (5'-3')**
Nicotiana benthamiana single transcriptional unit constructs (In-Fusion cloning)			
P19 (TBSV)	3Ω1	Forward	**TTTATGAATTTTGCAGCTCG**ATGGAACGAGCTATA CAAGGAAA
		Reverse	**GACAACCACAACAAGCACCG**TCACTCGCTTTCTT TTTCGAAGG
GFP	3Ω1	Forward	**TTTATGAATTTTGCAGCTCG** ATGGTGAGCAAGGGCGAG
		Reverse	**GACAACCACAACAAGCACCG**TCACTTGTACAGC TCGTCCATGC
TiPAS3	3Ω1	Forward	**TTTATGAATTTTGCAGCTCG**ATGTTAGCAGAAGTC TCCAAAGTTC
		Reverse	**GACAACCACAACAAGCACCG**TTACAATTCATCAT GTAAAGTTAGAG
TiDPAS1	3Ω1	Forward	**TTTATGAATTTTGCAGCTCG**ATGGCTGTAAAATCA CCTGAAGC
		Reverse	**GACAACCACAACAAGCACCG**CTATTCCGGTGGA GTTAGTGTG
TiCorS	3Ω1	Forward	**TTTATGAATTTTGCAGCTCG**ATGGCTAATTCAACT GCGAACTCT
		Reverse	**GACAACCACAACAAGCACCG**TTACTCCTTGTTGA TGAAATCGCTTG
TiTabS	3Ω1	Forward	**TTTATGAATTTTGCAGCTCG**ATGGCTTCTTCAACT GAAAGCTCTG
		Reverse	**GACAACCACAACAAGCACCG**TTAGTCCTTGTTGA TGAAAGACGTTAG
TiPS	3Ω1	Forward	**TTTATGAATTTTGCAGCTCG**ATGGAGCTTCAGAAC TTACC
		Reverse	**GACAACCACAACAAGCACCG**TCAGCATGATTTAT CAAGAGATGGAA

TiT16H	3Ω1	Forward	**TTTATGAATTTTGCAGCTCG**ATGGAGTCCATTCTTTTCCTTT
		Reverse	**GACAACCACAACAAGCACCG**CTAGGAATTCCATTTAAGAAAAGAA
CrT16H1	3Ω1	Forward	**TTTATGAATTTTGCAGCTCG**ATGGAATTCTATTATTTTCTCTACTTG
		Reverse	**GACAACCACAACAAGCACCG**TCAAGCAGGAGAAGAGGAAGAAA
CrT16H2	3Ω1	Forward	**TTTATGAATTTTGCAGCTCG**ATGGAGTTGTATTATTTTTCCAC
		Reverse	**GACAACCACAACAAGCACCG**TCAATATTTACCTTTGAGAGAAGAAG
CrTEX1	3Ω1	Forward	**TTTATGAATTTTGCAGCTCG**ATGGAGTTTGTGGTTTCCCT
		Reverse	**GACAACCACAACAAGCACCG**TCACACTTGTTTCAAAGAAGAACAAGAA
CrTEX2	3Ω1	Forward	**TTTATGAATTTTGCAGCTCG**ATGGAGTTTGTGGTTTCCC
		Reverse	**GACAACCACAACAAGCACCG**TCACACTTGTTGTTTCAAAGAAGAAC
CrT19H	3Ω1	Forward	**TTTATGAATTTTGCAGCTCG**ATGTTGTCTTCATTGAAAGATTTCTT
		Reverse	**GACAACCACAACAAGCACCG**TCAAAAAATGGTAACCGGAGTTGC
CrT3O	3Ω1	Forward	**TTTATGAATTTTGCAGCTCG**ATGGAGTTTCATGAATCTTC
		Reverse	**GACAACCACAACAAGCACCG**TCATGCATAGGACGTAGCGATTA
Sequence verification primers 3Ω1 InFusion		Forward	GATGAAAAAGCCCTAAAATTGGAG
		Reverse	ATTATTCACAAATGAGAAACAGAATGG
Gene	**Level 1 CDS**	**Primer direction**	**Sequence (5'-3')**
Nicotiana benthamiana multi-transcriptional unit constructs			
Level 1 CDS fragment for 3α1 or 3α2 golden-braid assembly			
Domesticati	Frag. A	Forward	GCGCCGTCTCGCTCGAATGGCTGTAAAATCACCT

on of TiDPAS1			GAAG
		Reverse	GCGCCGTCTCGCAGTCTCATTCGAGAAGCCT
	Frag. B	Forward	GCGCCGTCTCGACTGTCGTAAATGAGCGCTTC
		Reverse	GCGCCGTCTCGCTCGAAGCCTATTCCGGTGGAGTTAGTG
	Full length	Forward	GCGCCGTCTCGCTCGAATGGCTGTAAAATCACCTGAAG
		Reverse	GCGCCGTCTCGCTCGAAGCCTATTCCGGTGGAGTTAGTG
Domestication of TiCorS	Frag. A	Forward	GCGCCGTCTCGCTCGAATGGCTAATTCAACTGCGAAC
		Reverse	GCGCCGTCTCGTAGTCTCGTCCGAAACCATG
	Frag. B	Forward	GCGCCGTCTCGACTAGAGATATAACCCTTCTCTAC
		Reverse	GCGCCGTCTCGCTCGAAGCTTACTCCTTGTTGATGAAATCGC
	Full length	Forward	GCGCCGTCTCGCTCGAATGGCTAATTCAACTGCGAAC
		Reverse	GCGCCGTCTCGCTCGAAGCTTACTCCTTGTTGATGAAATCGC
TiPAS3	Full length	Forward	**TTCAGAGGTCTCTA**ATGTTAGCAGAAGTCTCCAAAG
		Reverse	**AGCGTGGGTCTCGAAGC**TTACAATTCATCATGTAAAGTTAGAG
TiTabS	Full length	Forward	**TTCAGAGGTCTCTA**ATGGCTTCTTCAACTGAAAGCT
		Reverse	**AGCGTGGGTCTCGAAGC**TTAGTCCTTGTTGATGAAAGACG
P19	Full length	Forward	**TTCAGAGGTCTCTA**ATGGAACGAGCTATACAAGGAAA
		Reverse	**AGCGTGGGTCTCGAAGC**TCACTCGCTTTCTTTTTCGAAGG
Plasmid validation	P19	Forward	TATTTAAGAGATATCTCAGATACG
		Reverse	CTGGTCGAAACCGAAAAATC
	TiPAS3	Forward	GCACTTCAGTTGTGGTGG
		Reverse	TCTTCGTCCGATGAGAACT

	TiDPAS1	Forward	CGTAAATGAGCGCTTCGTT
		Reverse	TGGGAGTGGAACTAATCACT
	TiTabS	Forward	CCACCTGCCTGCAGCTTAT
		Reverse	GGGTAATAAAGAATTGCACCC
	TiCorS	Forward	CCTTCAGTGGGTGGCT
		Reverse	CAATCTCCATATAATCACTCTGT
Overhangs designed for non-domesticated sequences 3α1 or 3α2 golden-braid assembly			

Methods S1 Detailed Materials and Methods

Candidate selection and phylogenetic analysis

The candidate genes were selected from a previously generated *T. iboga* transcriptome (Farrow *et al.*, 2019). Full-length cytochromes P450 gene sequences were extracted from the transcriptome using annotations corresponding to cytochrome P450, CYP, and EC:1.14. Transcripts were filtered to remove duplicates and include CDS (coding sequence) between 400 and 550 amino acids. Multiple sequence alignment (amino acid) was constructed using MUSCLE (Edgar, 2004) using default parameters, including 245 *Arabidopsis thaliana* cytochromes P450s (Schuler *et al.*, 2006) and functionally characterised cytochromes P450 involved in monoterpene indole alkaloid biosynthesis (Nguyen & Dang, 2021; Williams & Luca, 2023). The alignment was used to construct a maximum-likelihood phylogenetic tree using the iQtree web server (Trifinopoulos *et al.*, 2016) under default parameters. Phylogenetic trees were visualized using iToL (Letunic & Bork, 2024) and Geneious Prime ver. 2023.1.2. Major clades in the tree were identified and annotated based on *Arabidopsis thaliana* sequences, including the CYP71 family and Clan 86, the former used to identify candidates and the latter used to root the tree (Hansen *et al.*, 2021).

Cloning methods

Cytochrome P450 enzymes characterised in this study were amplified by PCR from a cDNA library generated from *T. iboga* as previously described (Farrow *et al.*, 2019). Known *C. roseus* cytochromes P450 genes (Table S1) were amplified from a cDNA library generated from *C. roseus* var. LBE. RNA was isolated from *C. roseus* var. LBE using the RNeasy Plant Mini Kit (Qiagen) and gDNA digestion and cDNA synthesis were performed using SuperScript IV-VILO Master-Mix (ThermoFisher). Overhangs compatible with the appropriate vector for yeast expression or plant transient expression (*N. benthamiana* or *C. roseus*) were included on the 5’ and 3’ end of the primers used for PCR amplification (Table S2). HiFi Q5 Hot-Start 2X Master Mix (New England Biolabs) was used for gene amplification. PCR products were analyzed on 1% agarose gel and purified using the Zymoclean Gel DNA Recovery Kit (Zymo Research). In-Fusion HD cloning kit (Takara Bioscience) was used to assemble the amplified genes into target vectors.

For yeast expression, amplicons were cloned into the MCS2 of pESC-HIS (Kan^R) plasmid (GenBank: AF063850.1, Agilent). The plasmid was linearized using *SalI* and *BamHI* restriction enzymes (New England Biolabs). The In-Fusion assembly products were transformed into *E. coli* TOP10 cells (ThermoFisher) by heat-shock. Positive transformants were selected on LB agar (50 µg ml^{-1} kanamycin), and colonies were screened by colony PCR using Phire Hot Start II 2X Master Mix (ThermoFisher). Plasmid DNA was isolated from positive colonies using Wizard Plus SV Minipreps DNA Purification Kit (Promega) and verified by Sanger sequencing (pESC-HIS sequencing primers, Table S2). Sequence-verified constructs were then transformed into yeast strain *Saccharomyces cerevisiae* WAT11 (*ade2*; contains the *Arabidopsis thaliana* cytochrome P450 reductase I gene, *ATR1*) (Urban *et al.*, 1997) using the Frozen-EZ Yeast Transformation II Kit (Zymo Research). Transformed yeast cells were plated on SD-His medium (6.7 g l^{-1} yeast nitrogen base without amino acids, 2 g l^{-1} drop-out mix without histidine, 74 mg l^{-1} adenine hemisulfate) containing 2% glucose (w/v) and grown at 30 °C for 48 hours. Positive transformants were confirmed by colony PCR as described above and used to inoculate 10 ml of SD-His medium + 2% glucose (w/v), which were grown at 30 °C, 220 rpm for 48 hours. These cultures were then used to store 25% glycerol stocks at -80 °C for further use.

For transient expression in *N. benthamiana* or *C. roseus*, all single transcriptional unit plasmids were generated by cloning the amplicons (Table S2) directly into a modified 3Ω1 (Sarrion-Perdigones *et al.*, 2013) vector. The 3Ω1 binary vector modification includes a *CCDB* gene cassette between ubiquitin-10 promoter (pUbq10) and ubiquitin-10 terminator (tUbq10) instead of *LacZ* (present in classical 3Ω1 plasmid). The vector was linearized using *BsaI* restriction enzyme (New England Biolabs), and the amplicon assembly was carried out using an In-Fusion HD cloning kit (Takara Bioscience). The assembled product of In-Fusion was transformed into *E. coli* TOP10 (ThermoFisher) cells. Positive transformants were identified by colony PCR as described above (3Ω1 sequencing primers, Table S2) and then grown overnight in liquid LB medium (200 µg ml^{-1} spectinomycin) at 37 °C, 200 rpm. Plasmid DNA was isolated, and the sequence was verified as described above. Sequence-verified constructs were used to transform electrocompetent *Agrobacterium tumefaciens* GV3101 cells (Goldbio) by electroporation. Cells were

plated on LB medium (20 µg ml^{-1} rifampicin, 30 µg ml^{-1} gentamicin, 200 µg ml^{-1} spectinomycin) containing agar (20 g l^{-1}) and grown at 28 °C for 48 hours. Positive colonies were identified by colony PCR, and a single transformant was grown in 10 ml LB medium (20 µg ml^{-1} rifampicin, 30 µg ml^{-1} gentamicin, 200 µg ml^{-1} spectinomycin) at 28 °C, 250 pm overnight, after which 25% glycerol stocks were prepared and stored at -80 °C for further use.

Multi-transcriptional unit constructs for plant transient expression in *N. benthamiana* or *C. roseus* were assembled using the Goldenbraid 2.0 toolkit (Sarrion-Perdigones *et al.*, 2013). Geneious Prime ver. 2023.1.2 was used to construct in-silico assemblies before cloning. Domestication (removal of *BsaI* and *BsmbI* cut-sites) of TiDPAS1 and TiCorS was performed by PCR according to primers generated by the Goldenbraid domesticator web tool (Sarrion-Perdigones *et al.*, 2013) (Table S2). All CDS elements used for multi-transcriptional unit assemblies were cloned into a Level 1 transcriptional unit in 3α1 or 3α2 plasmid (kanamycin) using *BsaI* (New England Bioscience). Level 2 multi-gene constructs were assembled into 3Ω1 or 3Ω2 (spectinomycin) plasmid with *Esp3I* (New England Bioscience) using Level 1 plasmids. Level 3 multi-gene constructs were assembled into 3α1 plasmid with *BsaI* (New England Bioscience) using Level 2 plasmids (Fig. S1). All transcriptional units consisted of a *Solanum lycopersicum* Ubiquitin10 promoter (pUbq10) and Ubiquitin 10 terminator (tUbq10, Table S1). The assembly was carried out by incubating the reaction mix at 37 °C for 5 min, followed by 5 min at 16 °C for 50 cycles, and terminated at 65 °C for 10 min. Plasmids were transformed into *E. coli* TOP10 (ThermoFisher) cells by heat shock. Blue-white screening was used to identify positive transformants. Sequence verification was performed at each stage of the assembly by Sanger sequencing using gene-specific primers (Table S2), and the final multi-transcriptional unit (Level 3) construct was verified using whole plasmid sequencing (Plasmidsaurus). Sequence-verified constructs were transformed into *A. tumefaciens* GV3101 cells (Goldbio) by electroporation. Transformed cells were grown, verified, and maintained in glycerol stocks described above in LB medium (20 µg ml^{-1} rifampicin, 30 µg ml^{-1} gentamicin, 100 µg ml^{-1} kanamycin).

Heterologous expression in yeast and microsome preparation

Yeast cells (WAT11) transformed with expression constructs including empty vector control were streaked on bacteriological agar (20 g l^{-1}) plates of SD-His medium (6.7

g l^{-1} yeast nitrogen base without amino acids, 2 g l^{-1} drop-out mix without histidine, 74 mg l^{-1} adenine hemisulfate) containing 2% glucose (w/v) from glycerol stocks and incubated at 30 °C for 48 hours for colonies to appear. Colonies were inoculated in 10 ml SD-His + 2% glucose medium and grown overnight at 30 °C, 200 rpm. A cell density (OD_{600}) corresponding to 1.0 was sub-cultured into 100 ml of SD-His medium + 2% glucose and incubated for 28-34 hours at 30 °C, 200 rpm. Cells were harvested at 4000 × g, room temperature for 5 min. Harvested cells were resuspended in 100 ml of SD-His medium + 1.8% galactose (w/v) + 0.2 % glucose (w/v) and incubated for 18-24 hours at 30 °C, 200 rpm for protein induction. Yeast culturing and handling were performed while maintaining aseptic conditions to avoid contaminations.

After protein expression, cells were harvested by centrifugation (4000 × g, 4 °C, 10 min) for yeast microsome preparation (Pompon *et al.*, 1996). The cell pellet was resuspended in 10 ml (2 ml g^{-1}) of TEK buffer (50 mM Tris-HCl, 1 mM EDTA, 100 mM potassium chloride, pH 7.4) and incubated at room temperature for 5 min. Cells were then harvested by centrifugation as above, and the supernatant was discarded; the pellet was resuspended in 2 ml of ice-cold TES buffer (50 mM Tris-HCl, 1 mM EDTA, 600 mM sorbitol, 10 g l^{-1} bovine serum albumin, pH 7.4). Cells were disrupted by glass beads (0.5 mm diameter, equal volume 2 ml) in a cold room (4 °C) using a Bead Genie (Scientific Industries) by pulsation at six rounds of 5000 rpm for 1 min on, 1 min off intervals. Following cell lysis, 5 ml of ice-cold TES buffer was added to the lysate/glass bead suspension, mixed well, and the supernatant was collected into a pre-chilled tube. The glass beads were washed three times and pooled for centrifugation at 8000 × g, 4 °C, 10 min. The supernatant was collected and ultra-centrifuged at 100,000 × g, 4 °C, 90 min. The supernatant was discarded, and the translucent pellet was washed first with 1 ml ice-cold TES buffer, then with 1 ml of TEG buffer (50 mM Tris-HCl, 1 mM EDTA, 20% glycerol, pH 7.4), and resuspended in 1 ml TEG buffer using a Dounce homogeniser. Microsomal protein preparations were stored at –80 °C for in vitro assays.

SPE purification of products of enzymatic reactions

Solid-phase extraction (SPE) was performed to remove impurities and concentrate the sample before HPLC isolation. For yeast and *N. benthamiana* sample clean-up, a 3 ml Chromabond-HLB (60 µm, 3 ml, 60 mg Macherey-Nagel) and a 6 ml

Chromabond-HLB (60 µm, 6 mL, 200 mg, Macherey-Nagel) SPE cartridge was used, respectively. The sample, reconstituted in 10% methanol (aqueous), was applied to a conditioned SPE cartridge for processing. The SPE cartridge was first conditioned with three-column volumes of methanol and three-column volumes of 10% methanol (aqueous). The sample was then applied to the SPE cartridge, washed with three-column volumes of 20% methanol (aqueous), and dried under vacuum. Finally, the reaction product was eluted with one column volume of methanol, and the flow-through was evaporated to dryness for semi-preparative HPLC isolation.

Semi-preparative HPLC isolation of enzymatic products

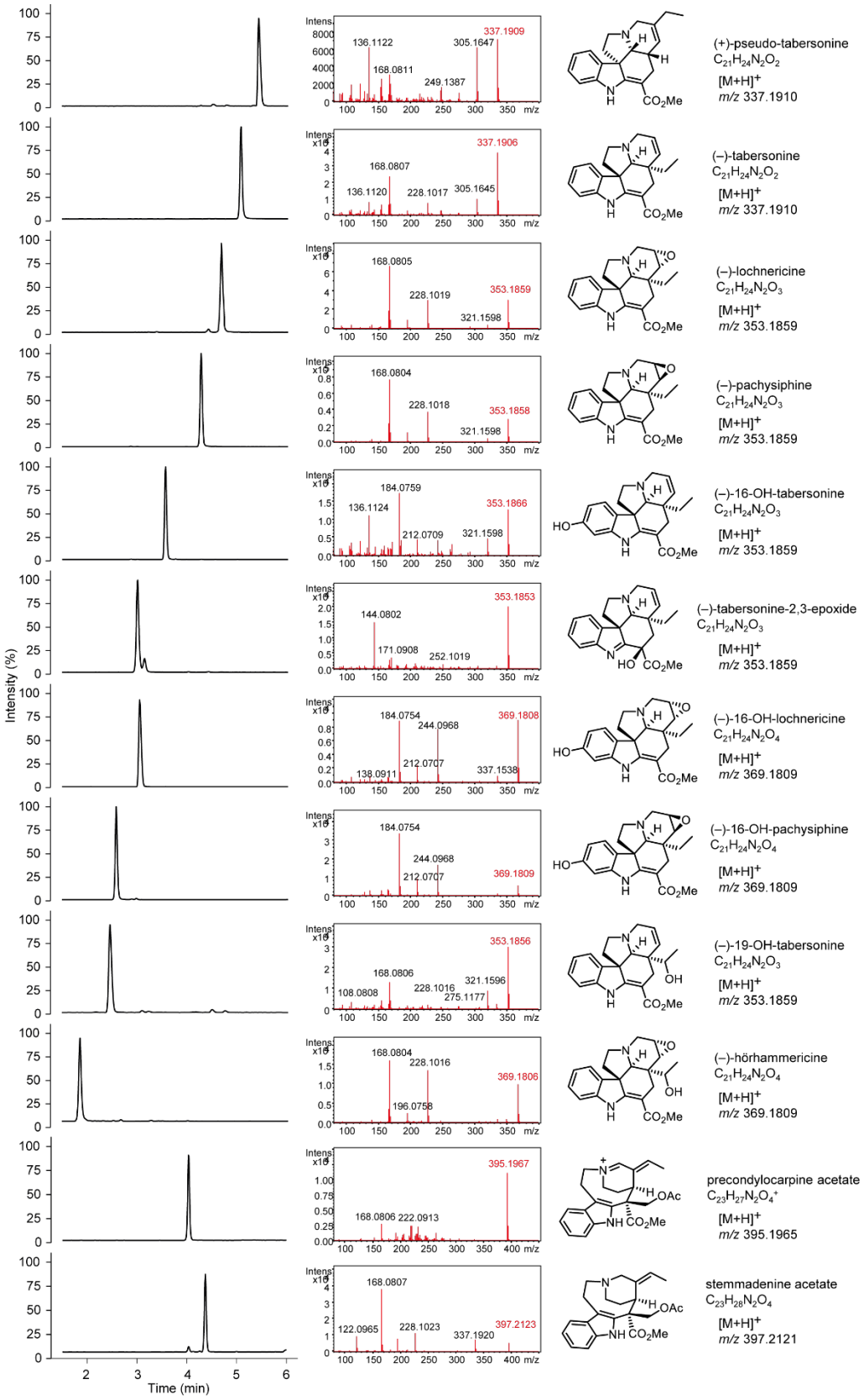
Semi-preparative-scale reaction workups of (–)-pachysiphine, (–)-16-OH-tabersonine, and (–)-16-OH-pachysiphine were subjected to high-performance liquid chromatography (HPLC) for compound isolation. The *N. benthamiana* extract containing pseudotabersonine was also subjected to HPLC isolation. An Agilent 1260 Infinity II HPLC instrument connected to an autosampler, diode array detector (DAD), and fraction collector for compound detection and isolation. Chromatographic separation was performed using a Phenomenex Kinetex XB-C18 (5.0 µm, 100 Å, 100 × 2.1 mm) column maintained at 40 °C under gradient elution using reversed phase conditions. The mobile phases used for separation were water with 0.1% formic acid (A) and acetonitrile (B). The flow rate was set at 1.2 ml min^{-1}, and chromatographic separation was performed at 10% B for 2 min, followed by a linear gradient from 10% to 30% B in 12 min, 90% B for 3 min, 10% B for 3 min (t_{total} 20 min). Prior to injection, the samples were diluted to 1 mg ml^{-1} with methanol and filtered using a 0.22 µm PTFE syringe filter. The diluted samples were placed in the autosampler, 50 ul injections were performed, and fractions were collected by monitoring the UV 254 nm and 328 nm corresponding to aspidosperma alkaloid absorbance (Hisiger & Jolicoeur, 2007). Fractions were analyzed by LC-MS to confirm identity and verified fractions were pooled and evaporated to dryness. The isolated compounds were then submitted for NMR analysis. In the case of pseudotabersonine, the isolated compound was analyzed further by chiral LC-MS.

LC-MS analysis.

All samples were analyzed using an UltiMate 3000 (Thermo Scientific) ultra-high performance liquid chromatography (UHPLC) system coupled to an Impact II UHR-Q-ToF (Ultra-High-Resolution Quadrupole-Time-of-Flight) mass spectrometer (Bruker Daltonics). Metabolites were separated by reversed-phase liquid chromatography using a Phenomenex Kinetex XB-C18 (100 x 2.1mm, 2.6 µm, 100 Å) column at 40 °C. The mobile phases for metabolite separation were water with 0.1% formic acid (A) and acetonitrile (B). A flow rate of 0.6 ml min^{-1} was used for the chromatography. The sample injection volume was 2 µl. The chromatographic separation started at 10% B for 1 min, and the linear gradient was from 10% to 30% B in 5 min, 90% B for 1.5 min, and 10% B for 2.5 min (t_{total} 10 min). Authentic standards were prepared as 20 µM solutions in methanol, and 2 µl were injected under the chromatographic conditions described above. Mass spectrometry acquisition was performed in positive electrospray ionization (+ ESI) mode with a capillary voltage of 3500 V and an end plate offset of 500 V; a nebulizer pressure of 2.5 bar was used, with nitrogen at 250 °C and a flow of 11 l min^{-1} as the drying gas. Acquisition was set at 12 Hz in the mass range from *m/z* 80 to 1000, with data-dependent MS^2 and an active exclusion after three spectra, released after 0.2 min. Fragmentation was triggered on an absolute threshold of 400 counts and limited to a total cycle time range of 0.5 seconds. The collision energies were applied dynamically and stepped from 20 to 50 eV. At the beginning of each sample run, a sodium formate-isopropanol calibration solution was directly infused into the source at 0.18 ml h^{-1} using an external syringe pump to calibrate the MS spectra recorded. To avoid injection peak and salt contamination of the MS, the initial 1 min of the active chromatographic gradient of each run was discarded to waste, and the calibration solution was directed to the MS during this time. At the end of the active LC gradient (6 min), the MS valve was switched to waste, and during re-equilibration time (2.5 min), the calibration solution was directed to the MS. Authentic standards (Methods S1 Fig. 1) were prepared at 25 µM concentration for confirmation of analytes by chromatographic retention time, high resolution mass spectrum, and MS^2 fragmentation spectrum. Data analysis was performed using Bruker Compass Data Analysis (Version 5.3) software.

Structure optimization and ECD spectral calculation for (–)-pachysiphine.

Electronic circular dichroism (ECD) spectra calculation was performed for (–)-pachysiphine. Based on the structure determined from NMR analysis, a molecular model was created in GaussView ver.6 (Semichem Inc., Shawnee, Kansas, USA) and optimized using the semi-empirical method PM6 in Gaussian (Gaussian Inc., Wallingford, Connecticut, USA). The resulting structure was used for conformer variation with the GMMX processor of the Gaussian program package. The resulting structures were DFT-optimized with Gaussian ver.16 (APFD/6-31G(d) level). A 4 kcal/mol cut-off level was used to select conformers subjected to another DFT optimization on a higher level (APFD/6-311G+(2d,p)). The lowest energy conformer from the high-level DFT calculation was used for the ROESY analysis. All structures up to a deviation of 2.5 kcal/mol from the lowest energy conformer were used to determine the ECD frequencies in a TD-SCF calculation on the same level as the former DFT optimization. The ECD curve was calculated from the Boltzmann-weighed contributions of all conformers with a cut-off level of two percent.



Methods S1 Fig. 1 LC-MS profiles and MS^2 spectra of authentic standards based on $[M+H]^+$ parent ion.

3.6 Supporting References

Abramson J, Adler J, Dunger J, Evans R, Green T, Pritzel A, Ronneberger O, Willmore L, Ballard AJ, Bambrick J, *et al.* 2024. Accurate structure prediction of biomolecular interactions with AlphaFold 3. *Nature* **630**: 493–500.

Besseau S, Kellner F, Lanoue A, Thamm AMK, Salim V, Schneider B, Geu-Flores F, Höfer R, Guirimand G, Guihur A, *et al.* 2013. A Pair of Tabersonine 16-Hydroxylases Initiates the Synthesis of Vindoline in an Organ-Dependent Manner in *Catharanthus roseus*. *Plant Physiology* **163**: 1792–1803.

Carqueijeiro I, Brown S, Chung K, Dang T-T, Walia M, Besseau S, Bernonville TD de, Oudin A, Lanoue A, Billet K, *et al.* 2018. Two Tabersonine 6,7-Epoxidases Initiate Lochnericine-Derived Alkaloid Biosynthesis in *Catharanthus roseus*. *Plant Physiology* **177**: 1473–1486.

Colinas M, Pollier J, Vaneechoutte D, Malat DG, Schweizer F, Milde LD, Clercq RD, Guedes JG, Martínez-Cortés T, Molina-Hidalgo FJ, *et al.* 2021. Subfunctionalization of Paralog Transcription Factors Contributes to Regulation of Alkaloid Pathway Branch Choice in *Catharanthus roseus*. *Frontiers in Plant Science* **12**: 687406.

Edgar RC. **2004**. MUSCLE: multiple sequence alignment with high accuracy and high throughput. *Nucleic Acids Research* **32**: 1792–1797.

Farrow SC, Kamileen MO, Caputi L, Bussey K, Mundy JEA, McAtee RC, Stephenson CRJ, O'Connor SE. **2019**. Biosynthesis of an Anti-Addiction Agent from the Iboga Plant. *Journal of the American Chemical Society* **141**: 12979–12983.

Hansen CC, Nelson DR, Møller BL, Werck-Reichhart D. **2021**. Plant cytochrome P450 plasticity and evolution. *Molecular Plant* **14**: 1244–1265.

Hisiger S, Jolicoeur M. **2007**. Analysis of *Catharanthus roseus* alkaloids by HPLC. *Phytochemistry Reviews* **6**: 207–234.

Kochnev Y, Hellemann E, Cassidy KC, Durrant JD. **2020**. Webina: an open-source library and web app that runs AutoDock Vina entirely in the web browser. *Bioinformatics* **36**: 4513–4515.

Letunic I, Bork P. **2024**. Interactive Tree of Life (iTOL) v6: recent updates to the phylogenetic tree display and annotation tool. *Nucleic Acids Research*: gkae268.

Nguyen T-D, Dang T-TT. **2021**. Cytochrome P450 Enzymes as Key Drivers of Alkaloid Chemical Diversification in Plants. *Frontiers in Plant Science* **12**: 682181.

Pompon D, Louerat B, Bronine A, Urban P. **1996**. [6] Yeast expression of animal and plant P450s in optimized redox environments. *Methods in Enzymology* **272**: 51–64.

Sarrion-Perdigones A, Vazquez-Vilar M, Palací J, Castelijns B, Forment J, Ziarsolo P, Blanca J, Granell A, Orzaez D. **2013**. GoldenBraid 2.0: A Comprehensive DNA Assembly Framework for Plant Synthetic Biology . *Plant Physiology* **162**: 1618–1631.

Schuler MA, Duan H, Bilgin M, Ali S. **2006**. Arabidopsis cytochrome P450s through the looking glass: a window on plant biochemistry. *Phytochemistry Reviews* **5**: 205–237.

Sun J, Zhao L, Shao Z, Shanks J, Peebles CAM. **2018**. Expression of tabersonine 16-hydroxylase and 16-hydroxytabersonine-O-methyltransferase in Catharanthus roseus hairy roots. *Biotechnology and Bioengineering* **115**: 673–683.

Trifinopoulos J, Nguyen L-T, von Haeseler A, Minh BQ. **2016**. W-IQ-TREE: a fast online phylogenetic tool for maximum likelihood analysis. *Nucleic Acids Research* **44**: W232–W235.

Urban P, Mignotte C, Kazmaier M, Delorme F, Pompon D. **1997**. Cloning, Yeast Expression, and Characterization of the Coupling of Two Distantly Related Arabidopsis thalianaNADPH-Cytochrome P450 Reductases with P450 CYP73A5*. *Journal of Biological Chemistry* **272**: 19176–19186.

Williams D, Luca VD. **2023**. Plant cytochrome P450s directing monoterpene indole alkaloid (MIA) and benzylisoquinoline alkaloid (BIA) biosynthesis. *Phytochemistry Reviews* **22**: 309–338.

Chapter 4

Divergent biosynthesis of monoterpene indole alkaloids from geissoschizine in *Catharanthus roseus.*

This Chapter of the thesis is written as a draft for publication with the intention of submission.

Divergent biosynthesis of monoterpene indole alkaloids from geissoschizine in *Catharanthus roseus*.

Mohamed O. Kamileen[1,2**], Benke Hong[1,3**], Klause Gasse[1], Maritta Kunert[1], Lorenzo Caputi[1], Benjamin R. Lichman[2], Sarah E. O'Connor[1*]

[1] Department of Natural Product Biosynthesis, Max Planck Institute for Chemical Ecology, D-07745 Jena, Germany.

[2] Centre for Novel Agricultural Products, Department of Biology, University of York, York YO10 5DD, UK.

[3] Department of Chemistry, Westlake University, 18 Shilongshan Road, 310024, Hangzhou, China.

**These authors contributed equally to this work

*Corresponding Author

4.1 Abstract

Plants generate structural diversity by rearranging bonds of a central intermediate through the action of biosynthetic enzymes. 19*E*-geisssochzine is a chemically versatile intermediate in monoterpene indole alkaloid biosynthesis (MIA) that can rearrange to generate core scaffolds of pharmacologically important alkaloids such as vinblastine. Here we report how 19*E*-geissoschizine undergoes oxidative rearrangements to generate four distinct alkaloid scaffolds by the action of three biosynthetic enzymes. Using in vitro enzymatic assays and gene silencing, we demonstrate how cytochrome P450 enzymes in the medicinal plant *Catharanthus roseus* are able to catalyze oxidative rearrangements of 19*E*-geisssochzine forging the crucial bonds that make the core scaffolds of *strychnos-type*, *sarpagine-type*, *akuammiline-type*, and *mavacurane-type* MIAs. The discovery of these P450 enzymes demonstrates how plants neo-functionalize cytochrome P450 enzymes to generate new chemical scaffolds.

4.2 Manuscript (draft)

The monoterpene indole alkaloids (MIAs) are a large family of ca. 3000 structurally diverse alkaloids originating from a single starting substrate, strictosidine[1]. In the Apocynaceae plants, strictosidine is deglucosylated by the enzyme strictosidine glucosidase (SGD) and then subsequently reduced to form geissoschizine by the medium-chain alcohol dehydrogenase enzyme geissoschizine synthase (GS)[2–4]. Geissoschizine, a *corynanthe-type* alkaloid, is densely functionalized, harbouring an alpha-beta unsaturated carbonyl, enol, indole and basic nitrogen, which allows, in principle, a wide range of downstream reactions[5]. In fact, geissoschizine is the precursor for *strychnos-type*, *sarpagine-type*, *akuammiline-type*, and *mavacurane-type* MIAs[5,6], though the mechanism by which these structurally divergent scaffolds are created from a single starting material is not completely clear (**Figure 1**). Here, we show how three cytochrome P450 enzymes oxidize geissoschizine to four distinct alkaloids scaffolds. This highlights how nature capitalizes on the inherent reactivity of a highly versatile starting substrate using highly similar enzyme homologs.

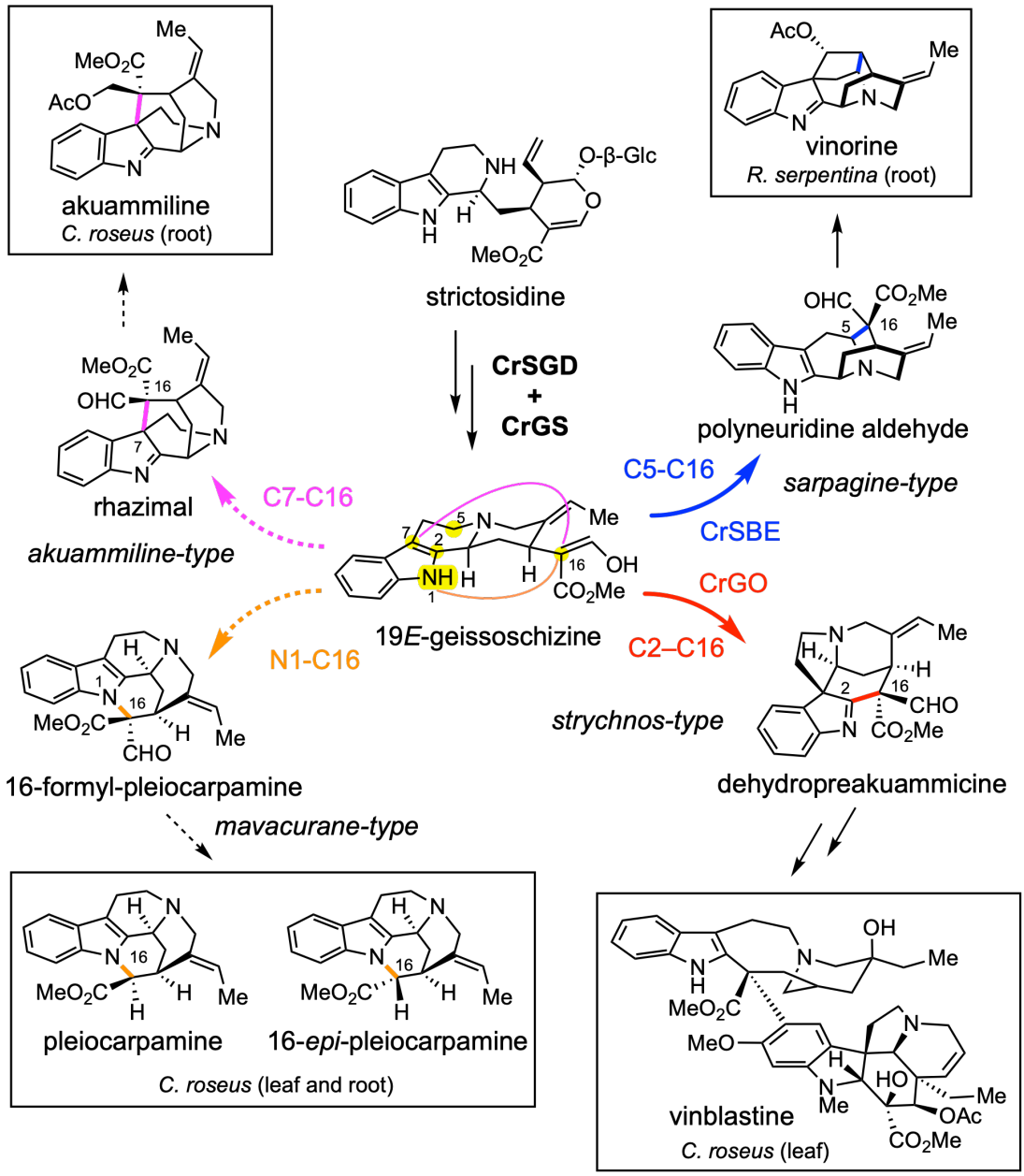


Figure 1. Divergent scaffold formations of 19*E*-geissoschizine.

Geissoschizine is a key intermediate in the formation of *strychnos-type*, *sarpagine-type*, *akuammiline-type*, and *mavacurane-type* MIAs. These structural scaffolds are distributed across plant families to produce chemically diverse alkaloids.

Previously reported enzymes that oxidize geissoschizine are all cytochromes P450, specifically from the CYP71 subfamily[2,7–10]. The C16-formyl ester moiety and, in turn, the C16 stereocenter of geissoschizine plays a crucial role in downstream biosynthesis, with the 16*R* configuration significantly influencing the enzymatic transformations catalyzed by subsequent enzymes[2,9,11]. Specifically,

dehydropreakuammicine is formed by oxidative coupling of C16 and C2 by the *Catharanthus roseus* CYP71 enzyme geissoschizine oxidase (GO)[2,9], while sarpagan bridge enzyme (SBE), isolated from the related plant *Rauvolfia serpentina*, catalyzes formation of the C16 and C5 bond to form polyneuridine aldehyde[7] (**Figure 1**). At least two other scaffolds can be, in principle, formed from the geissoschizine scaffold: the C16 carbon can react with C7 to form rhazimal, and the C16 carbon can react with the indole nitrogen (N1) to form the *mavacurane-type* alkaloids pleiocarpamine[5] (**Figure 1**). The vinblastine-producing medicinal plant *C. roseus* has been known to produce *strychnos-type*[2] and *heteroyohimbane-type*[7,12] alkaloids, with their biosynthetic pathways having been elucidated. However, the biosynthesis of *akuammiline-type*, *sarpagine-type,* and *mavacurane-type* alkaloids remains elusive in *C. roseus* despite a few records of isolation[13,14], indicating possible existence of these scaffolds in this plant.

To identify enzymes that may form these additional *akuammiline-type*, *sarpagine-type,* and *mavacurane-type* alkaloids scaffolds from geissoschizine in *C. roseus*, we mined the *C. roseus* transcriptome for cytochrome P450 enzymes, specifically members of the CYP71 family. We curated 16 uncharacterized CYP71 sequences and built a phylogeny consisting of these unknown CYP71 genes along with 7 functionally characterised *C. roseus* P450s (**Figure S1)**. With this phylogenetic tree in hand, we screened for the activity of the uncharacterized P450s using yeast microsomes with the substrate 19*E*-geissoschizine.

We observed oxidation of the substrate geissoschizine (*m/z* 353.1860) with the candidate *C. roseus* P450 candidate CRO_T014436, which was expressed in yeast and assayed as a microsomal preparation (**Figure 2a**). The major product (*m/z* 351.1703) observed co-eluted with the synthetic standard rhazimal. We therefore named this enzyme (CRO_T014436) rhazimal synthase (RS). Interestingly, we also observed two additional products at *m/z* 323.1754; one formed in only trace amounts and co-eluted with akuammicine (*m/z* 323.1754), and the other could not be identified. We scaled up these in vitro reactions and isolated the unknown product (*m/z* 323.1754). NMR analysis showed that this compound was the known natural product strictamine (*m/z* 323.1754) (**Supporting NMR**). RS activity was recently reported in *Alstonia scholaris*, catalyzed by the enzyme AsRS[9] (74 % amino acid identity to CrRS, **Figure S2, S3**) though simultaneous formation of strictamine was not reported for this orthologue.

Rhazimal was first isolated from *Rhazya stricta* along with strictamine[15], but to our knowledge, rhazimal or strictamine has never been isolated from in *C. roseus*. Therefore, we profiled the roots and leaves of *C. roseus* in search of strictamine or rhazimal derived alkaloids. Surprisingly, we found a rhazimal derived compound, akuammiline, in the roots of *C. roseus* (**Figure S4**). This suggests that rhazimal in *C. roseus* may be metabolized into akumallinine in the presence of downstream enzymes, while deformylation of rhazimal could lead to strictamine in the absence of these enzymes, as observed in the in vitro reactions. The in planta function of CrRS could not be definitively established by virus-induced gene silencing (VIGS), since CrRS is expressed in the roots and silencing is only possible in *C. roseus* leaf and stem tissue.

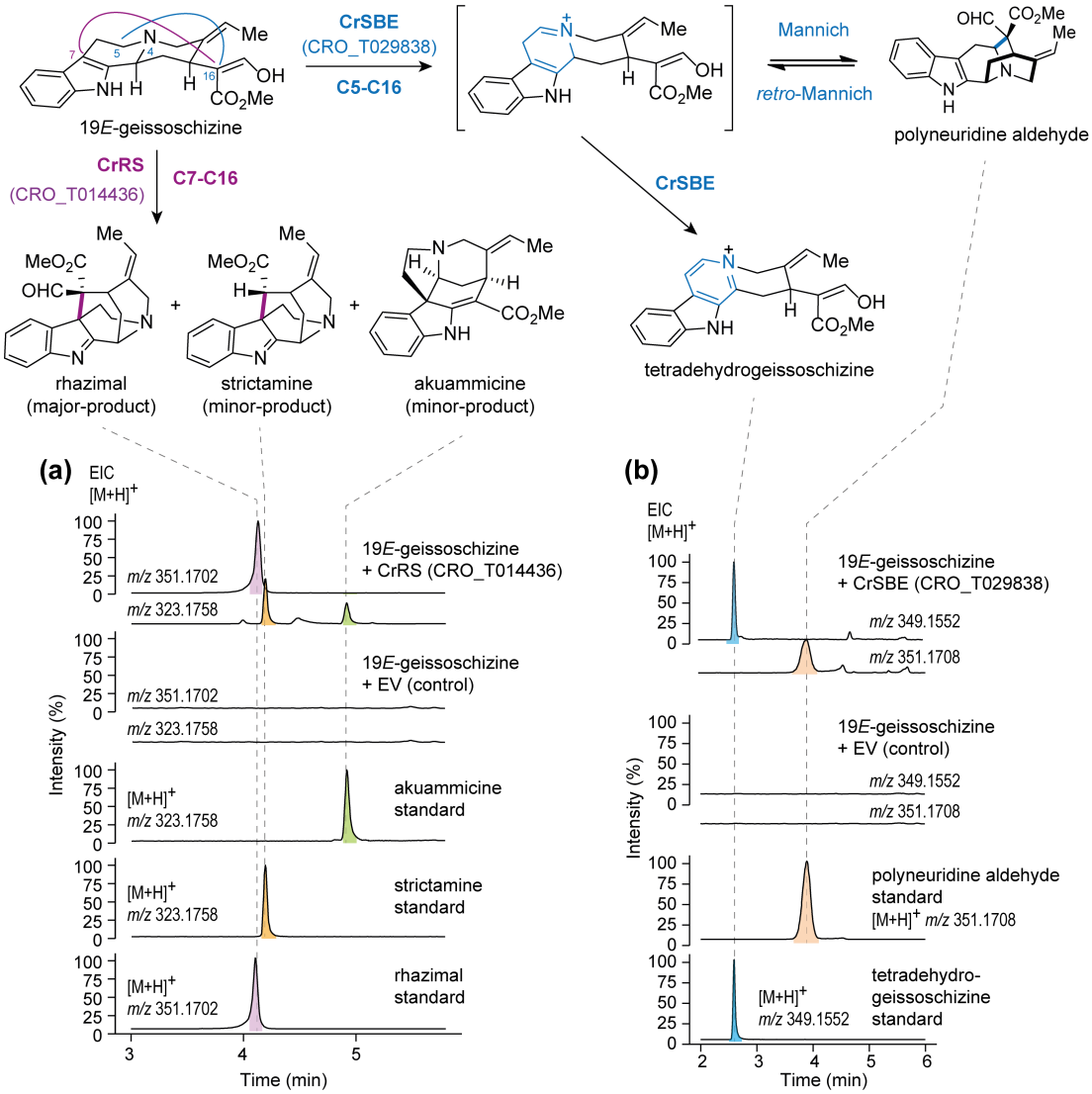


Figure 2. Oxidative rearrangements of geissoschizine in *C. roseus*.

Figure 2. Oxidative rearrangements of geissoschizine in *C. roseus*. (**a**) Biosynthesis of rhazimal from the *C. roseus* enzyme rhazimal synthase (RS) (CRO_T014436). RS catalyzes an oxidation to forge a bond between C7-C16 by oxidative rearrangement of the cis-configured 19*E*-geissoschizine substrate. Rhazimal is not highly stable and could deformylate to strictamine. Spontaneous oxidation of 19*E*-geissoschizine could lead to akuammicine. (**b**) Biosynthesis of polyneuridine aldehyde and tetradehydrogeissoschizine from the *C. roseus* enzyme named sarpagan bridge enzyme (SBE) (CRO_T014436). SBE catalyze an oxidation of geissoschizine leading to the bond formation between C5-C16, which then is rearranged to generate the kinetic product polyneuridine aldehyde and the thermodynamic product tetradehydrogeissoschizine via the unstable intermediate dehydrogeissoschizine.

When we assayed the *C. roseus* P450 candidate CRO_T029838 (from the CYP71AY family) with geissoschizine as described above, we observed a double oxidized product which co-eluted with synthetic dehydrogeissoschizine (*m/z* 349.1547) standard. We could detect also trace amounts of polyneuridine aldehyde (*m/z* 351.1703), which co-eluted with the standard (**Figure 2b**). We called this *C. roseus* enzyme sarpagan bridge enzyme (SBE). It is known that polyneuridine aldehyde is derived from this iminium ion intermediate[7] and can be further oxidized by the action of CrSBE described here to form dehydrogeissoschizine. CrSBE shares 78.9% and 49.6% amino acid sequence identity to previously characterised *C. roseus* SBE enzymes, alstonine synthase (AS)[7] and serpentine synthase (SS)[8] respectively (**Figure S2**).

Notably, in these CrSBE in vitro reactions, we observed the formation of polyneuridine aldehyde initially, but this product disappeared over time and appeared to be replaced with tetradehydrogeissoschizine (**Figure S5**). There is no obvious mechanism by which polyneuridine aldehyde can be converted into tetradehydrogeissoschizine. Therefore, we rationalized that formation of polyneuridine aldehyde is a reversible reaction, and that polyneuridine aldehyde can revert to the initial oxidation iminium ion product (dehydrogeissoschizine) by a retro-Mannich reaction (**Figure 2b**). In contrast, formation of tetradehydrogeissoschizine is likely to be irreversible, due to the formation of the aromatic moiety. The action of CrSBE forms the bonds between C5-C16 to generate the reactive iminium intermediate which is in equilibrium with polyneuridine aldehyde and also undergo

an additional oxidation to generate tetradehydrogeissoschizine (**Figure 2b**). However, if enzymes that convert polyneuridine aldehyde into downstream alkaloids are present, then polyneuridine aldehyde is effectively captured. In nature, products with a similar structure to dehydrogeissoschizine have been isolated from *Uncaria rhynchophylla* and *Rauvolfia serpentina* where the enol was methylated and glycosylated to prevent the Mannich reactions[16]. CrSBE exemplifies how a single enzyme can use kinetic control to create two entirely different scaffolds; the kinetic product is favoured when coupled with downstream enzymes, while the thermodynamic product predominates when the downstream enzymes are absent.

The previously reported SBE orthologs from *C. roseus*, CrAS[7] and CrSS[8], provide entry into the beta-carboline alkaloids, alstonine and serpentine by the aromatization of ajmalicine and tetrahydroalstonine, substrates that are structurally similar to geissoschizine. However, the closed “E” ring of ajmalicine and tetrahydroalstonine prevents the formation of the C16-C5 bond (**Figure S6**). Therefore, only the analogue of the aromatic product is observed with these substrates. However, when CrSBE (CRO_T029838) was silenced in *C. roseus* by VIGS, there was no significant reduction in the levels of alstonine compared to the control, indicating that CrSBE does not catalytically contribute to alstonine biosynthesis (**Figure S6**).

The last missing predicted enzyme would catalyze cyclization via N1-C16 bond formation to generate 16-formyl-pleiocarpamine, which would likely undergo spontaneous deformylation to produce pleiocarpamine and *epi*-pleiocarpamine[17] (**Figure 3a**). We could detect the presence of pleiocarpamine and 16-*epi*-pleiocarpamine in *C. roseus* leaves and root that matched authentic standards (**Figure 3b, Figure S7**). 16-*epi*-pleiocarpamine is less abundant than pleiocarpamine. Although 16-formyl-pleiocarpamine is considered to be the entry-point to all *mavacurane-type* alkaloids[5], this intermediate has not been detected or characterised from plant sources.

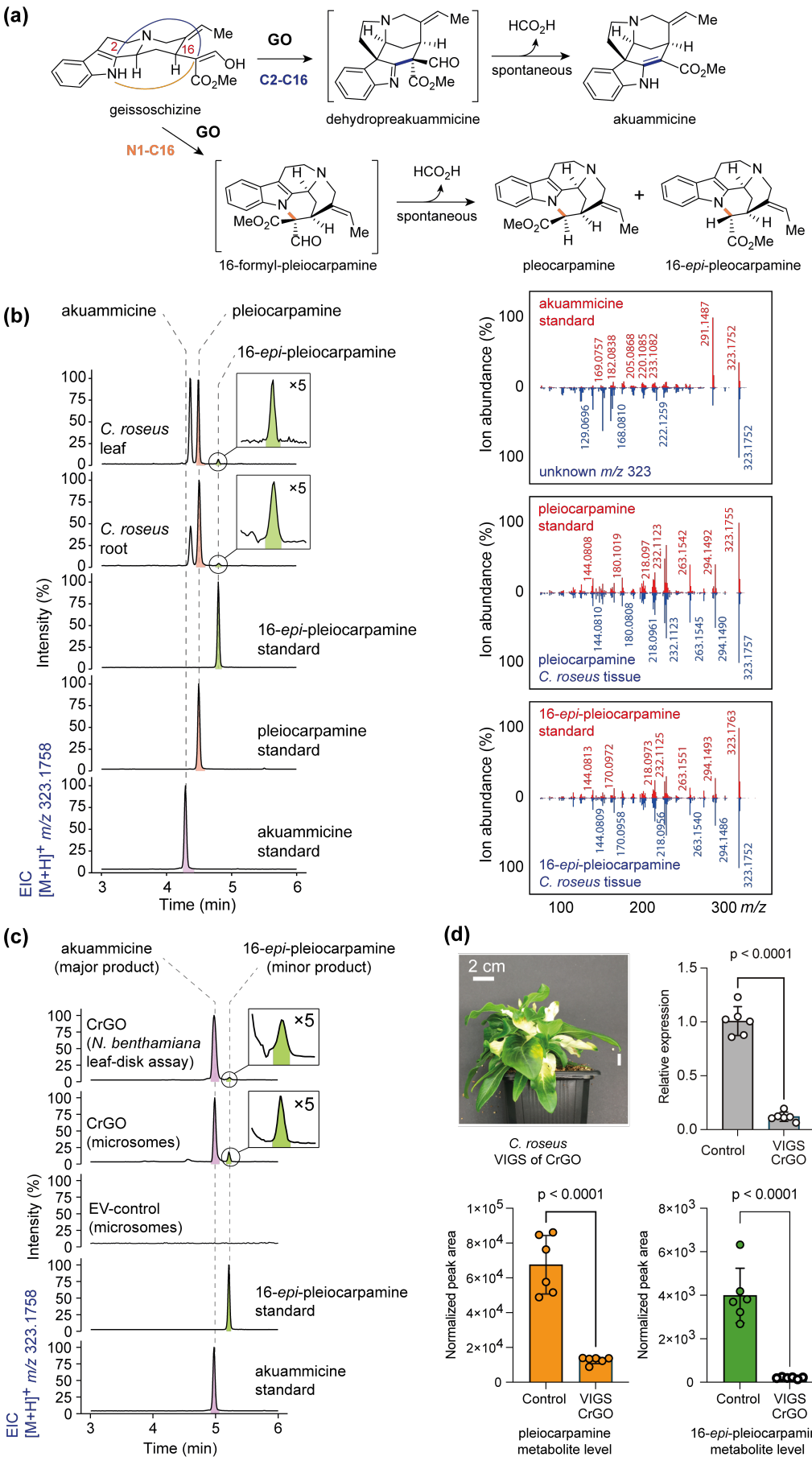


Figure 3. Biosynthesis of *Mavacurane-type* alkaloids.

Figure 3. Biosynthesis of *Mavacurane-type* alkaloids pleiocarpamine and 16-*epi*-pleiocarpamine in *C. roseus*. (**a**) Proposed biosynthesis of *Mavacurane-type* alkaloids pleiocarpamine and 16-*epi*-pleiocarpamine and *sarpagine-type* alkaloid, akuammicine. (**b**) Metabolite profiling of *Mavacurane-type* alkaloids in *C. roseus* roots and leaf alongside the MS^2 spectrum of authentic standards. An unknown analyte of *m/z* 323.1758, eluting very close to akuammicine is observed in *C. roseus* tissue, but no identical MS^2 spectral match is observed. (**c**) In vitro and in vivo activity of CrGO in producing 16-*epi*-pleiocarpamine. CrGO catalyze the canonical oxidation of 19*E*-gesissoschiznine forming C2-C16 bonds through oxidative rearrangement of the C16-formyl ester moiety. Additionally, a minor product 16-*epi*-pleiocarpamine is observed forging the mavacurane core (N1–C16 bond). (**d**) Silencing CrGO in *C. roseus* by VIGS leads to significant decrease of pleiocarpamine and 16-*epi*-pleiocarpamine. Bar graphs represent the values of the mean ± standard deviation (SD) of 6 independent biological replicates and statistical analysis of two-tailed Student's *t*-test. Extracted ion chromatograms (EIC) are presented with MS^2 spectra displaying the fragmentation of the parent $[M+H]^+$ ion.

None of the identified 16 CYP71 candidate genes from *C. roseus* (**Figure S1**) appeared to catalyze this N1-C16 bond formation. However, when we closely examined the product profile of CrGO in vitro reaction assay, which used yeast microsomes enriched with the GO enzymes, to our surprise, we observed low but detectable amounts of 16-*epi*-pleiocarpamine along with the major, previously reported product akuammicine product[2] (**Figure 3c**). This minor product shared identical MS^2 and retention time to an authentic standard of 16-*epi*-pleiocarpamine, which suggested deformylation from 16-formyl-pleiocarpamine, which would be the initially formed oxidation product. The same results were observed when the experiments were conducted in *Nicotiana benthamiana* leaf disk assays (**Figure 3c**).

To confirm whether GO is indeed involved in C-N bond formation in planta or if this is simply an artefact of an in vitro enzymatic reaction, we silenced CrGO in *C. roseus* using VIGS. Since the *mavacurane-type* alkaloids pleiocarpamine and 16-*epi*-pleiocarpamine could be detected in both the leaf and root of *C. roseus*, silencing CrGO should lead to a decrease in the levels of these metabolites. Silencing of CrGO using VIGS led to a significant reduction in the levels of pleiocarpamine and 16-*epi*-pleiocarpamine compared to the negative control (**Figure 3d, Figure S8**). Therefore, it appears that the minor product of this

enzymatic reaction plays a physiologically significant role. It has been reported in the total synthesis of *mavacurane-type* alkaloids, that 16-*epi*-pleiocarpamine is the thermostable epimer[11]. Hence, it can be inferred that in the plant, under conditions of active metabolism, the kinetic product pleiocarpamine is predominantly observed, with only trace amounts of 16-*epi*-pleiocarpamine (**Figure 3b**). In contrast, during in vitro enzymatic assays, the thermodynamic product 16-*epi*-pleiocarpamine is detected, with no pleiocarpamine present (**Figure 3c**).

Mavacurane-type alkaloids, such as pleiocarpamine and 16-*epi*-pleiocarpamine, have been isolated from plant species belonging to the Loganiaceae[18] and Apocynaceae[19] families. These alkaloids have received limited attention due to their low natural abundance and the lack of documented biological activities. Nevertheless, pleiocarpamine's enamine-type reactivity confers upon it the capacity to combine with various other MIAs, thereby generating chemically interesting complex bisindole alkaloids such as villastonine and bipleiophylline (dimeric *mavacurane-type* alkaloids)[5,20].

Here we report the discovery of two CYP71s, RS (rhazimal synthase) and SBE (sarpagan bridge enzyme), from *C. roseus*. Additionally, we also show that the enzyme GO (geissoschizine oxidase) can catalyze C-N bond formation required for the formation of the *mavacurane-type* alkaloids pleiocarpamine and 16-*epi*-pleiocarpamine in addition to C16-C2 bond formation required for *akuammiline-type* and *strychnos-type* alkaloids (**Figure 1**). Silencing of GO in *C. roseus* strongly suggests that, although pleiocarpamine and 16-*epi*-pleiocarpamine are only formed as minor products by GO, this enzyme nevertheless contributes to mavacurane biosynthesis in the *C. roseus* plant. Additionally, with SBE, we show how the reversible nature of an enzymatic reaction can tune the product profile. Specifically, we show how the ratio of the polyneuridine aldehyde and dehydrogeissoschizine are affected by the reversible nature of the retro-Mannich reaction that leads to polyneuridine aldehyde. Finally, we show that a trace amount of a product of an enzyme, namely the pleiocarpamine produced by GO, plays a physiologically relevant role in the alkaloid profile of the plant. This raises the intriguing possibility that the production of minor side products in enzyme reactions plays a significant role in shaping the evolution of metabolic diversity.

ASSOCIATED CONTENT

Supporting Information

Supplemental information: Additional experimental details, assays, materials, and methods, and NMR spectra described in this study.

Accession Codes

GenBank accession numbers: MH213134 (CrGO), pending (CrRS), pending (CrSBE).

Corresponding Author

*__Sarah E. O'Connor__ – Department of Natural Product Biosyn-thesis, Max Planck Institute for Chemical Ecology, Hans-Knöll-Straße 8, Jena 07745 Germany; Email: oconnor@ice.mpg.de

Notes: The authors declare no competing financial interests.

ACKNOWLEDGMENTS

We would like to thank Sarah Heinicke for assistance with mass spectrometry. We also thank the members of the Max Planck Institute for Chemical Ecology Research Greenhouse for their care and provision of *Nicotiana benthamiana* and *Catharanthus roseus* plants.

ABBREVIATIONS

AS, alstonine synthase; EIC, extracted ion chromatogram; GO, geissoschizine oxidase; GS, geissoschizine synthase; MIA, monoterpene indole alkaloid biosynthesis; RS, rhazimal synthase; SBE, sarpagan bridge enzyme; SS, serpentine synthase (SS); SD, standard deviation; SGD, strictosidine glucosidase; VIGS, virus-induced gene silencing

4.3 References

1. O'Connor SE, Maresh JJ. Chemistry and biology of monoterpene indole alkaloid biosynthesis. Nat Prod Rep. 2006;23(4):532–47.

2. Tatsis EC, Carqueijeiro I, Bernonville TD de, Franke J, Dang TTT, Oudin A, et al. A three enzyme system to generate the Strychnos alkaloid scaffold from a central biosynthetic intermediate. Nat Commun. 2017;8(1):316.

3. Qu Y, Easson MEAM, Simionescu R, Hajicek J, Thamm AMK, Salim V, et al. Solution of the multistep pathway for assembly of corynanthean, strychnos, iboga, and aspidosperma monoterpenoid indole alkaloids from 19E-geissoschizine. Proc Natl Acad Sci United States Am [Internet]. 2018;115(12):3180–5.

4. Qu Y, Thamm AMK, Czerwinski M, Masada S, Kim KH, Jones G, et al. Geissoschizine synthase controls flux in the formation of monoterpenoid indole alkaloids in a Catharanthus roseus mutant. Planta. 2018;247(3):625–34.

5. Mauger A, Jarret M, Kouklovsky C, Poupon E, Evanno L, Vincent G. The chemistry of mavacurane alkaloids: a rich source of bis-indole alkaloids. Nat Prod Rep. 2021;38(10):1852–86.

6. Sakamoto J, Kitajima M, Ishikawa H. Total Syntheses of (+)-Villocarine A, (−)-Apogeissoschizine, and (+)-Geissoschizine. Chem A Eur J. 2023;29(18):e202300179.

7. Dang TTT, Franke J, Carqueijeiro IST, Langley C, Courdavault V, O'Connor SE. Sarpagan bridge enzyme has substrate-controlled cyclization and aromatization modes. Nat Chem Biol. 2018;14(8):760–3.

8. Yamamoto K, Grzech D, Koudounas K, Stander EA, Caputi L, Mimura T, et al. Improved virus-induced gene silencing allows discovery of a serpentine synthase gene in Catharanthus roseus. Plant Physiol. 2021;187(2):846–57.

9. Wang Z, Xiao Y, Wu S, Chen J, Li A, Tatsis EC. Deciphering and reprogramming the cyclization regioselectivity in bifurcation of indole alkaloid biosynthesis. Chem Sci. 2022;13(42):12389–95.

10. Hong B, Grzech D, Caputi L, Sonawane P, López CER, Kamileen MO, et al. Biosynthesis of strychnine. Nature. 2022;607(7919):617–22.

11. Jarret M, Tap A, Turpin V, Denizot N, Kouklovsky C, Poupon E, et al. Bioinspired Divergent Oxidative Cyclizations of Geissoschizine: Total Synthesis of (–)-17-nor-Excelsinidine, (+)-16-epi-Pleiocarpamine, (+)-16-Hydroxymethyl-Pleiocarpamine and (+)-Taberdivarine H. Eur J Org Chem. 2020;2020(40):6340–51.

12. Stavrinides A, Tatsis EC, Caputi L, Foureau E, Stevenson CEM, Lawson DM, et al. Structural investigation of heteroyohimbine alkaloid synthesis reveals active site elements that control stereoselectivity. Nat Commun. 2016;7(1):12116.

13. Kohl W, Witte B, Höfle G. Alkaloide aus Catharanthus roseus-Zellkulturen, II [1] / Alkaloids from Catharanthus roseus Tissue Cultures, II [1]. Z für Naturforsch B. 1981;36(9):1153–62.

14. Deng ZT, Li WY, Wang L, Zhou ZP, Wu XD, Ding ZT, et al. Monoterpene Indole Alkaloids with Cav3.1 T-Type Calcium Channel Inhibitory Activity from Catharanthus roseus. Molecules. 2021;26(21):6516.

15. Atta-ur-Rahman, Habib-ur-Rehman. Isolation and NMR Studies on Rhazimal and Strictamine. Planta Med. 1986;52(03):230–1.

16. Kong F, Ma Q, Huang S, Yang S, Fu L, Zhou L, et al. Tetracyclic indole alkaloids with antinematode activity from Uncaria rhynchophylla. Nat Prod Res. 2017;31(12):1403–8.

17. Wenkert E, Wickberg B. General Methods of Synthesis of Indole Alkaloids. IV. A Synthesis of dl-Eburnamonine 1,2. J Am Chem Soc. 1965;87(7):1580–9.

18. Battersby AR, Hodson HF. Chapter 15 Alkaloids of Calabash Curare and Strychnos Species**The majority of Strychnos alkaloids which are based upon the strychnine skeleton are covered in Chapter 17. Alkaloids: Chem Physiol. 1965;8:515–79.

19. Jacquier MJ, Vercauteren J, Massiot G, Men-Olivier LL, Pussett J, Sevenet T. Alkaloids of Alstonia plumosa. Phytochemistry. 1980;21(12):2973–7.

20. Pandey KP, Rahman MT, Cook JM. Bisindole Alkaloids from the Alstonia Species: Recent Isolation, Bioactivity, Biosynthesis, and Synthesis †. Molecules. 2021;26(11):3459.

4.4 Supporting Information

Divergent biosynthesis of monoterpene indole alkaloids from geissoschizine in *Catharanthus roseus*.

Mohamed O. Kamileen[1,2**], Benke Hong[1,3**], Klause Gasse[1], Maritta Kunert[1], Lorenzo Caputi[1], Benjamin R. Lichman[2], Sarah E. O'Connor[1*]

[1] Department of Natural Product Biosynthesis, Max Planck Institute for Chemical Ecology, D-07745 Jena, Germany.

[2] Centre for Novel Agricultural Products, Department of Biology, University of York, York YO10 5DD, UK.

[3] Department of Chemistry, Westlake University, 18 Shilongshan Road, 310024, Hangzhou, China.

**These authors contributed equally to this work

*Corresponding Authors

Table of Contents

Materials and Methods	S02-S09
Supporting Tables	S10-S13
Supporting Figures	S14-S20
Supporting NMR	S21
Supporting References	S22-S23

Materials and Methods

Chemicals and Reagents.

Geissoschizine was synthesised as previously described by Hong[1]. Polyneuridine aldehyde was a kind gift from Dr. L. Evanno (Univ. Paris-Sud, CNRS, Université Paris-Saclay, France). 16-*epi*-pleiocarpamine was a kind gift from Dr. Guillaume Vincent (Univ. Paris-Sud, CNRS, Université Paris-Saclay, France). Pleiocarpamine was a kind gift from Prof. Dr. Hartmut Laatsch (Georg-August-Universität Göttingen, Germany). Rhazimal was synthesized according to Zhang[2]. Tetradehydrogeissoschizine was synthesized as described by Turpin[3]. Akuammicine was biosynthesized as previously described by Tatsis[4].

Plant Growth.

Catharanthus roseus (var. “Sunstorm Apricot”, SA) was germinated in a standard soil mix in a climate chamber under 16 h light/8 h dark photoperiod at 23-25°C, and 60% relative humidity. *C. roseus* var. SA plants, aged six months, were used to harvest young leaves for RNA isolation and cDNA synthesis for gene amplification. For the VIGS experiments, *C. roseus* var. SA 6-10 plants, 4 weeks old, were used. The *Nicotiana benthamiana* plants used for transient gene expression were grown in a greenhouse on a standard soil mix under a 16 h light/8 h dark photoperiod at 22 °C and 60% relative humidity. Plants were grown for 3-4 weeks before *Agrobacterium* infiltration. All plants were watered periodically before and after experiments.

Candidate selection.

Publicly available *C. roseus* var. SA (Medicinal Plant Genomics Resource) was used to mine for cytochrome P450s of the CYP71 family based on homology to known CYP71AY genes involved in MIA biosynthesis. CYP71AY genes, AsAS (*Alstonia scholaris* alstonine synthase, OM323327.1)[5], AsGO (*Alstonia scholaris* geissoschizine oxidase, OM323328.1)[5], AsRHS *(Alstonia scholaris* rhazimal synthase, OM323329.1)[5], CrAS (*Catharanthus roseus* alstonine synthase, W8JDE2.1)[6], CrGO (*Catharanthus roseus* geissoschizine oxidase, JN613015.1)[4,7,8], CrSS (*Catharanthus roseus* serpentine synthase, MT829151.1)[9,10], GsSBE (*Gelsemium sempervirens* sarpagan bridge enzyme, MF537712)[6], RsSBE

(*Rauvolfia serpentina* sarpagan bridge enzyme, MF537711)[6], SnvGO (*Strychnos nux-vomica* geissoschizine oxidase, OM304290.1)[1], SpGO (*Strychnos sp.* geissoschizine oxidase, OM304299.1)[1] were elected as bait to mine for uncharacterized CYP71AY genes from the *C. roseus* transcriptome. Full-length coding sequences (CDS) were curated, and MUSCLE[11] alignments were performed with *Arabidopsis thaliana* clan 86 genes as described in Kamileen[12]. A maximum-likelihood phylogenetic tree was created using IQ-TREE[13] under default parameters and visualized by iTOL[14]. Geneious Prime ver. 2023.1.2. was used for curation and analysis of transcriptomic data.

Cloning methods.

All genes described in this study (**Table S1**) were amplified by PCR from a cDNA library generated from *C. roseus* var. SA using the primers listed in **Table S2**. The cDNA library for *C. roseus var.* SA was prepared by RNA isolation of 50 mg of young leaf using the RNeasy plant Mini kit (Qiagen) and converted to cDNA using SuperScript IV VILO reverse transcriptase (Thermo Fisher Scientific). P19-TBSV was cloned as previously described by Kamileen[15].

High-Fidelity Q5 Hot-Start 2X Master Mix (New England Biolabs) was used for gene amplification according to the manufacturer's instructions. Following PCR amplification, DNA products were analyzed on 1% agarose gel, and the excised gel fragments were purified using Zymoclean Gel DNA Recovery Kit (Zymo Research). In-Fusion HD cloning kit (Takara Bioscience) was used to ligate all amplified genes into target vectors according to the manufacturer's instructions.

For heterologous protein expression in yeast (*Saccharomyces cerevisiae ,* WAT11), the purified PCR amplicons were cloned into pESC-HIS (GenBank: AF063850.1, Agilent) and chemically transformed into WAT11 cells as previously described by Kamileen[12]. For transient expression in *N. benthamiana*, the purified PCR amplicons were cloned into a modified 3Ω1[16] binary plasmid and transferred into *Agrobacterium tumefaciens* GV3101 cells by electroporation as previously described by Kamileen[12].

Transient expression of candidate genes in *N. benthamiana.*

The *Agrobacterium* strains transformed with the gene constructs of interest were grown overnight at 28°C with shaking at 220 rpm in volumes of 10 ml containing antibiotics 20 µg/ml rifampicin, 30 µg/ml gentamicin, 200 µg/ml spectinomycin. Cells were harvested by centrifugation at 4000 × *g* for 10 minutes, and the supernatant was discarded. The cell pellet was gently resuspended in infiltration buffer (10 mM MES, pH 5.6, 10 mM magnesium chloride, 200 µM acetosyringone). After a second centrifugation step, the supernatant was removed, and the pellet was resuspended in 10 ml of infiltration buffer, followed by incubation in the dark at room temperature with gentle rocking for 2 hours. Each *Agrobacterium* strain was adjusted to an OD600 of 0.3 and infiltrated into the abaxial side of a 3-week-old *N. benthamiana* leaf using a 1 ml needleless syringe. To account for batch variability, each experiment included at least three biological replicates, where individual leaves from three distinct plants were infiltrated. Wild-type and P19 controls were incorporated into the experimental design and tested both with and without substrate treatment. Leaves were harvested 4-days post-infiltration for subsequent plant disk assays..

Heterologous protein expression in yeast and microsome preparation

Yeast expression and microsomal preparation were performed as previously described by Kamileen[12]. Briefly, Yeast cells (WAT11) were cultured in 100 ml of SD-His medium containing 2% glucose (w/v) at 30°C, 200 rpm for 28–34 h. Cells were harvested and resuspended in 100 ml of SD-His medium + 1.8% galactose (w/v) + 0.2% glucose (w/v) for protein production at 30°C, 200 rpm for 18–24 h. Yeast cells were harvested, and microsomes were prepared as described by Pompon[17]. Prepared microsomes were stored at –80°C until assays were performed.

In vitro assays with *Agrobacterium* infiltrated *N. benthamiana* leaf disks.

The *N. benthamiana* leaf disk assays were performed as described by Kamileen[12]. Leaf disks were harvested from *N. benthamiana* three days post *Agrobacterium* infiltration. Each disk was incubated with 50 µM of substrate in a 250 µl volume of 50 mM HEPES buffer. The plates containing leaf disks were incubated in a growth chamber at 22 °C, 60% relative humidity and 16-h-light/8-h-dark photoperiod overnight (16-18h). After 16-h incubation, the disks were harvested for metabolite extraction. A 250 µl extraction solution (70% methanol in water acidified with 0.1%

formic acid) was added to the powdered tissue, mixed well by vortex and sonicated for 10 min at room temperature. The samples were then centrifuged at 20,000 × *g* for 10 min to pellet cell debris and the extract was diluted 1:2 with extraction solution. Samples were filtered through 0.22 µm PTFE syringe filters before metabolite analysis by LC-MS.

In vitro enzymatic assays.

In vitro, yeast microsomal assays were conducted in analytical-scale reactions, each with a total volume of 100 µl. The reactions were carried out in 50 mM HEPES buffer (pH 7.5) consisting of 50-60 µg of total microsomal protein (0.50 µg μl^{-1} microsomal protein), 1 mM NADPH, and 25 µM substrate. Negative control reactions were performed with empty vector (EV) yeast microsomes. Reactions were initiated by the addition of substrate, gently vortexed, and incubating at 30 °C for 1 hour unless specified otherwise. The reactions were quenched with extraction buffer, centrifuged at 20 000 × *g* at room temperature for 10 min and filtered through 0.22-µm PTFE filters before LC-MS analysis.

Semi-preparative scale isolation of strictamine.

Isolation of strictamine was performed using CrRS yeast microsomes and 19*E*-geissoschzine substrate following the protocol described by Kamileen[12]. Strictamine was a degradation product from rhazimal. Briefly, CrRS microsomes were prepared from 1 l of culture using the conditions described in Heterologous protein expression in yeast and microsome preparation. A 20 ml reaction was set up to generate rhazimal and strictamine from 13 mg of 19*E*-geissoschzine. The reaction consisted of 50 mM HEPES pH 7.5 buffer, NADPH generation system (1.0 mM NADP+, 2.0 U ml−1 glucose-6-phosphate dehydrogenase (G6PDH), 3.0 mM glucose-6-phosphate (G6P), 0.2 mM NADPH). Reactions were initiated by the addition of 8 mg of yeast microsomes and incubated at incubated at 30°C, 200 rpm for 16 h. The reactions were terminated by the addition of 10 ml ethyl acetate. The aqueous reaction mixture was extracted thrice with ethyl acetate and evaporated to dryness. Strictamine was then isolated by preparative TLC, as described previously by Zhang[2]. The resulting was then subjected to NMR analysis.

VIGS

The protocol for VIGS vector construction and VIGS generally followed the procedure described in Li. In brief, 300 bp fragments (**Table S3**) of the coding regions of CrRS, CrSBE, and CrGO from the genomic DNA (gDNA) from *C. roseus var*. SA, by PCR amplification with primers designed for InFusion cloning (Takara bioscience) (**Table S2**) using Phusion™ High-Fidelity DNA Polymerase (Thermo Fischer scientific). Genomic DNA was isolated from C. roseus leaves with the DNeasy Plant Mini Kit (Qiagen). To avoid off-target gene silencing, the target regions for VIGS were selected using the SGN VIGS tool[18]. The oligonucleotide sequences are given in supplemental material. The obtained PCR fragments were cloned in the BamHI and, XhoI digested VIGS vector pTRV2-MgChl [pTRV2-ChlH(F1R2)][19] with the In-Fusion Snap Assembly Master Mix (Takara bioscience), yielding pTRV2-MgChl-CrGO and pTRV2-MgChl-CrSBE constructs.

Agrobacterium tumefaciens GV3101 was transformed with the three constructed plasmids and used for the VIGS inoculations of *C. roseus* var. SA. For this, *A. tumefaciens* GV3101 with plasmid pTRV1[20] and *A. tumefaciens* GV3101 carrying pTRV2-MgChl-CrGO, pTRV2-MgChl-CrSBE, and pTRV2-MgChl-CrRS were grown overnight in a rotary shaker at 28 °C and 300 rpm in each 10 ml of LB medium supplemented with 50 µg ml^{-1} kanamycin, 25 µg ml^{-1} gentamicin and 100 µg $ml^{-}1$ rifampicin to an OD600 of 2. Cells were pelleted for 10 min at 4000 × *g* and resuspended in infiltration buffer (100 µM acetosyringone, 10 mM NaCl and 1.75 mM $CaCl_2$) to an OD600 of 2. After 2 h of incubation on a rotary shaker at room temperature and 60 rpm, 450 µl of each bacterial strain containing a pTRV2 plasmid were mixed with the same volume of the bacterial strain with pTRV1. VIGS inoculation was performed by pipetting 10 µl of the mixed bacterial suspension between plant stem and petiole of one leaf first grown after the cotyledons of a 30 days old *C. roseus* var. SA plant. The stem was pierced with a ø 0,40 x 25 mm Sterican® needle twice through the bacterial suspension drop. Per pTRV2 construct 8 plants were inoculated; the plants inoculated with pTRV2-MgChl strain served as controls. After VIGS inoculation, plants were grown under *C. roseus* standard greenhouse conditions. First VIGS symptoms (yellowing of the leaves due to magnesium chelatase subunit H gene silencing) could be observed after 12 days. The leaf tissue with complete target gene silencing indicated by yellow colour was harvested three weeks after inoculation.

qPCR analysis

Leaves with VIGS symptoms were carefully harvested from each experimental condition and the control plants from 6 independent biological replicates. The tissue was snap-frozen in liquid nitrogen and was ground to fine powder using tungsten beads. Total RNA extraction was performed using the RNeasy mini kit (Qiagen) according to the manufacturer's instructions. The genomic DNA was digested, and the RNA was further purified using RNA Clean & Concentrator-25 with DNAse I (Zymo research). RNA (1000 ng) was reverse-transcribed using SuperScript-IV VILO master mix (Thermo Fisher Scientific) following manufacturer's instructions. transcription kit (Applied Biosystems). Gene-specific primers were designed to target 150-200 bp target of the gene of interest with the Primer BLAST software (NCBI). Primers designed for qPCR are listed in **Table S4**. The qPCR experiment was performed as previously described by Payne[21] using the delta delta cycle method using the 40S ribosomal protein 9 (Rps9) as a reference gene for normalization. The primer efficiency for the designed qPCR primers was between 95–102%. Measurements for qPCR analysis were performed using a QuantStudio 1 cycler (Applied Biosystems). Statistical analysis (two-tailed Student's *t*-test) was performed using Prism 10 (Version 10.2.2).

Metabolite analysis of *C. roseus* tissue

Nearly identical plants of *C. roseus* var. SA, 6 months of age, were selected for tissue profiling. The young leaves and roots of the plants were harvested and snap-frozen in liquid nitrogen. Tissue was pulverized to fine powder using a mortar and pestle, and 50 mg of tissue was extracted with 1 ml of the extraction solution (70% methanol in water acidified with 0.1% formic acid). Samples were then prepared for LC-MS analysis as described in the section, In vitro assays with *Agrobacterium* infiltrated *N. benthamiana* leaf disks.

LC-MS data acquisition and analysis of metabolites

LC-MS analysis was performed as described previously by Kamileen[15]. Samples were analyzed using a Thermo Scientific UltiMate 3000 ultra-high performance liquid chromatography (UHPLC) system coupled to an Impact II UHR-Q-ToF (Ultra-High Resolution Quadrupole-Time-of-Flight) mass spectrometer (Bruker Daltonics). Metabolites were separated by reversed-phase liquid chromatography using a

Phenomenex Kinetex XB-C18 (100 x 2.1mm, 2.6 µm; 100 Å) column at 40 °C. The mobile phases for metabolite separation were water with 0.1% formic acid (A) and acetonitrile (B). A flow rate of 0.6 ml/min was used for the chromatography. The injection volume was 2 µl. The chromatographic separation was performed starting at 10% B for 1 min, linear gradient from 10% to 30% B in 6 min, 90% B for 1.5 min, 10% B for 2.5 min. Authentic standards were prepared as 20 µM solutions in methanol, and 2 µL was injected under the chromatographic conditions described above. Mass spectrometry acquisition was performed in positive electrospray ionization mode with a capillary voltage of 3500 V and an end plate offset of 500 V; a nebulizer pressure of 2.5 bar was used, with nitrogen at 250 °C and a flow of 11 L/min as the drying gas. Acquisition was done at 12 Hz in the mass range from 80 to 1000 *m/z*, with data dependent MS^2 and an active exclusion window of 0.2 min. For tandem mass spectroscopy (MS^2) fragmentation was triggered on an absolute threshold of 400 and limited to a total cycle time range of 0.5 s. For collision energy, the stepping option model (from 20 to 50 eV) was used. At the beginning of each sample run, a sodium formate-isopropanol calibration solution was directly infused to the source at 0.18 ml/hour using a syringe pump to calibrate MS spectra recorded. To avoid injection peak and salt contamination of the MS, the initial 1 min of the active chromatographic gradient of each run was discarded to waste.

For the analysis of 19*E*-geissoschizine, the LC method was modified as described by Hong[1]. The mobile phase (A) was changed to 0.1% [v/v] NH_4OH in water (pH 9.0), and the mobile phase (B) remained acetonitrile. The flow rate was set to 0.5 ml/min, and the gradient linearly increased from 15% to 50% acetonitrile in 4 minutes (from minutes 1 to 5), and the column was washed and equilibrated within 10 min. A Waters Acquity UPLC BEH-C18 column (2.1 x 50 mm; 1.7 µm) was used and was temperature controlled at 60°C). 2 µL of samples were injected. The MS conditions were not modified.

Data was visualized and analyzed using Bruker Compass Data Analysis (Version 5.3) software. For relative quantification and metabolomics, data was analyzed using default pipelines embedded in Bruker Compass MetaboScape 2021b software (version 7.0.1). The non-targeted metabolomics workflow was used to generate an output containing a list of mass signatures with retention times, along with qualitative peak intensities by automated integration of extracted ion chromatograms with 5 ppm tolerance, molecular formula determined by accurate mass of precursors and fragments and statistical test outputs (*P* value and two-tailed Student's *t*-tests).

NMR analysis.

NMR spectra were measured on a 700 MHz Bruker Advance III HD spectrometer (Bruker Biospin GmbH, Rheinstetten, Germany). For spectrometer control and data processing Bruker TopSpin (version 3.6.1) was used. Deuterated chloroform ($CDCl_3$) was used as a solvent, and all NMR spectra were referenced to the residual solvent signals at δ_H 7.24 and δ_C 77.23.

Supplementary Tables

Table S1. Nucleotide sequences for genes cloned and described in this study.

Gene Name (GenBank Accession))	Nucleotide sequence
CrGO (JN613015.1)	**ATG**GAGTTTTCTTTCTCCTCACCAGCTCTCTACATAGTTTATTTCTTGCTTT TCTTTGTGGTAAGGCAATTATTGAAACCCAAAAGTAAGAAAAAATTGCCAC CAGGTCCAAGAACACTACCCTTAATTGGAAACCTTCATCAACTCTCGGGA CCTTTACCTCATCGTACCCTAAAAAATTTGTCCGATAAACATGGTCCTTTG ATGCACGTGAAAATGGGCGAACGTTCGGCAATTATAGTATCAGATGCAAG AATGGCAAAAATAGTTCTTCATAATAACGGTTTAGCCGTTGCAGATCGGTC AGTAAATACTGTCGCAAGTATTATGACTTATAATAGTTTGGGTGTTACCTTT GCTCAGTATGGAGATTACTTAACAAAATTACGTCAAATCTATACTTTGGAA CTTTTAAGTCAGAAAAAAGTTCGATCTTTCTACAGTTGTTTTGAAGATGAA CTCGATACTTTTGTTAAGTCAATTAAGTCTAACGTTGGACAACCTATGGTT TTGTACGAGAAAGCTTCTGCTTATTTGTATGCTACCATTTGTAGAACTATTT TTGGGAGTGTTTGCAAGGAAAAGGAGAAAATGATTAAGATAGTGAAGAAA ACGTCGTTACTGTCTGGAACACCACTTAGATTGGAGGATCTTTTTCCTTCT ATGAGCATTTTTTGTAGATTTAGTAAAACTTTGAATCAATTGAGAGGACTTT TGCAAGAAATGGATGATATTTTGGAAGAAATCATAGTTGAAAGGGAAAAG GCTTCTGAAGTCTCAAAAGAGGCAAAGGATGATGAAGATATGCTTAGTGT TCTGTTGAGGCATAAATGGTACAATCCAAGTGGTGCTAAATTCAGAATCAC TAATGCAGACATCAAAGCCATTATCTTTGAGTTGATCTTAGCAGCAACCCT AAGTGTAGCAGATGTTACAGAATGGGCTATGGTTGAAATTCTAAGGGATC CCAAAAGTTTGAAAAAAGTGTACGAAGAAGTACGAGGTATTTGTAAAGAAA AGAAAAGAGTGACAGGATACGACGTTGAAAAAATGGAATTTATGCGTCTT TGTGTGAAGGAATCAACAAGAATACATCCAGCTGCTCCTCTTTTAGTTCCT AGAGAATGCAGAGAAGATTTTGAAGTAGATGGATACACAGTTCCAAAAGG GGCTTGGGTTATAACAAATTGCTGGGCTGTTCAAATGGATCCTACAGTAT GGCCCGAACCAGAGAAGTTTGATCCAGAAAGATATATTCGTAACCCAATG GATTTCTATGGAAGTAACTTTGAATTGATACCATTTGGGACAGGTAGAAGA GGATGTCCTGGTATTTTATATGGAGTGACAAATGCTGAGTTTATGTTGGCT GCTATGTTTTATCATTTTGATTGGGAAATAGCAGATGGTAAAAAACCAGAA GAAATTGATTTGACTGAGGACTTTGGTGCTGGTTGCATTATGAAGTATCCT TTGAAATTGGTTCCTCATCTTGTTAACGAT**TAG**
CrRS (Genbank ID pending)	**ATG**GAAACTATCAACTTCTTCTCCTTCTCCTTTCCACCAGTGGTCTACTTT CTCACCTTCATTGCCTTCCTTTTAGTAGCAAAAAGACTAATAAGTCCCAAA ACCCACAAAAAATTATTACCACCAGGTCCATGGACCTTACCCTTCATTGGA AATTTACATCAGCTCCTAGCCGGATCATTACCACATAGAATCCTCAAAAAT CTGTCCGATAAACACGGACCGCTGATGACAATAATGATGGGTGAAAGAAC AACAATAATAGTGTCCTCCGCAAGAATGGCAAAATTGGTGCTTCACACTAA TGGTCTAGCAGTTGCCAATAGACCAATTAATAGTGTGGCAGAAATTATTTG TTACAATAATTTAGGCACAACTTTTGCAAAATATGGTGAATATTTAAAACAA TTACGCCAACTTTACATGTCGGAACTTTTGAGCCCCAAAAGAGTAAAATCA TTTTCGGGCATTTTTGAAGATGAACTTGAGAAATTCGTTGGTTCAATTAGA TCTCAAGTTGGTAAAGAAATGGTAATTTATTGGAAATCAACTGAATATTTAT ATTCAGCAATTTGTAGGGTCATGTTTGGAAGTGTTTGTAGTGAAAGGGAA AAATTAATTAAAGTGTGTAAAAAAGTGTCGAAATTATCAGCAGCACCAATC AGGTTTGAAGATCTTTTTCCATCAATTAAAGGGCTTTCATTTTTAACAGGAA GAGATAATGTTTTAAAAGGTTTGGTTAAAGATCTTGATGATGTTCTTGATAT ATTAATAGCTCAGCGTGAAAATGGTACTACTTTTGATGAAGGAGATATGCT TGGACTTCTATTGAAGATTAAGAGTGGTGAAATCTATAATGCCAAACTCCA GATCACAAATGATGATATCAAAGCCATCATTTTCGAGCTGATGTTAGCTGC AACTCTAAGCGTAGCAGACGTAGTAGAATGGGCCATGGTTGAAATAATAA GATATCCACAAGTTTTGAAACAGGTGAAAGAAGAATTGAATAAAGTATTAA ATGGAAAACAAGAAATAAGAGGATCTGATCTAGAGAAAATGGAATATCTTC ATATGTGTGTTAAAGAATCGACCCGACTCCACCCAGCTGCCCCTCTTCTA TTCCCAAGAGAAGCCCGTGAAGAATTTCAAATTGATAACTACACAATTCCA AAAGGTTCATGGATCATGACTAATTATTGGGCAATTGGGCGTGACCCTGA AATTTGGCCTAAACCCGATGAATTTGATCCGGAAAGATTCAGAAATAGTAA

	TATTGATTTTTATGGAAACCATTTTGAATTAATTCCATTTGGTAGTGGAAGG AGAGGATGTCCAGGGATATTATTTGGAATTACTGAAGCTGAATTTATATTG GCTGCTTTATTTTATCATTTTGATTGGAAACTACCAGGTGGAATGGACCCG GATCAGATTGATATGACTGAAGTATTCGGTGCGGGATGTATTTTGAAAAAT CCATTGACTGTGATACCGGTTGTTGCACAAGAT**TGA**
CrSBE (Genbank ID pending)	ATGGATGAGATGATGAACTTCTCCCTCACCTCTCCCATTTCCTTTCTCCTC TCCTTACTTCTTATCCTATTTCTTATCCTATTTATGATGAAAGGAAACCAAA CCCACAATGGCAAAAAATTACCACCGGGTCCCAAAAAACTTCCTATTATAG GAAACCTCCATCAAATGATAGGTTCACATCCTCATCGTGTTCTAAAAAAAT TGGCCGATAAATATGGACCTATTATGCACTTGCAAATGGGCCAACGATCA GCCGTTGTTATATCATCAGCGGAAAAAGCAAAAGAAATATTGAACATTTAT GGTGTTCAAGTTGCTGATAGACCTCAACTCATCGTATCTAAAATTATGTTG TACAATAGTTTGGGTGTCACTTTTGCTCCTTATGGTGACTACTTAAAGCAA TTGCGTCAAATTTATGCCGTAGAACTTCTTAGCCCTAAAACAGTTAGGTCC TTTTGGACAATTATGGAAGATGAAGTTTCCACAATGGTTAACTCAATTAAA TCTGAAATTGGTCAACCAATAATTTTGCATGATAAAATGATGACTTATTTGT ATACTATGCTTTGTAGAGTTACATTTGGTGGCGTATGTAATGGACGCGAG ACACTAATAATGGCAGCTAAAGAAACGTCAGCGCTTTCTGCTGCTATTAG GATTGAGGATTTGTTTCCTTCAGTGAAAATACTTCCTTTAATTAGTGGATTA AAGTCAAGATTAAACAATTTGTTGAAAACACTTGATACCATTCTTGAGGAT ATTATCAGTGTTCGTGAGAAGAAATTATTAACTCAGCCATTGTTGGATGAT GAAGATATGTTGGGAGTTCTCCTCAAGTACAAAAATGGAAAGGGAAAAGA TACTAAATTTAGAGTCACCAACAACGACATCAAGGCAGTCATTTTTGAAAT TATCTTAGCTGGCACCCTAAGTTCATCAGCTATAGTAGAATGGTGTATGTC TGAAATGATAAAAAACTCTGAAAAGTTTAAAAAGGCACAAGATGAAGTTAG GAAAGTTTTAAAGGGTAAAAAAACAATTAGTGGAAGTGATGTTGGTAAAAT GGAATATGTTAAAATGGTGGTTAAGGAATCTTTGAGATTACACCCTCCTGC TCCCATATTGTTTCCAAGAGAATGTAGGGAAGAATTTGAGATAGATGGAAT GACTATACCTAAAAAAACTTGGTTGATTGTAAACTACTGGCCAATAGGAAG AGATCCCAGACTTTGGGACGACGCCGACAAGTTTGAGCCGGAGAGGTTC AGTAATAGCAGCATTGATTTCAATGGAAGCCATTTTGAGTTGATACCATTT GGTGCTGGAAGAAGGATTTGTCCTGGAATATTACTTGGAACAACAAATGT TGAGCTTTTACTTGCTACATTTCTCTATTATTTTGATTGGAAACTTCCTCAA GGTATGAAACCCGAAGAATTAGATATGAATGAGGTATTTGGTGCTGGTTG CATAAGGGAAAGTCCATTGTGTCTCATTCCTAGCATCTCATCAGCAGTTGA AGGAAAT**TAA**

Notes

1. Start codon is highlighted in **bold**.

2. Stop codon is <u>underlined</u>.

Table S2. Primers used in this study. Primer sequences. Primer sequences with homology to the destination plasmid for DNA assembly are in bold.

Gene	Plasmid	Primer direction	Sequence (5‘-3‘)
Nicotiana benthamiana transient expression			
CrGO	3Ω1	Forward	**TTTATGAATTTTGCAGCTCG**ATGGAGTTTTCTTTCTCCTCA
		Reverse	**GACAACCACAACAAGCACCG**CTAATCGTTAACAAGATGAGGAA
p19-TBSV	3Ω1	Forward	**TTTATGAATTTTGCAGCTCG**ATGGAACGAGCTATACAAGGAAA
		Reverse	**GACAACCACAACAAGCACCG**TTACTCGCTTTCTTCTTCGAAGG
Gene	**Plasmid**	**Primer direction**	**Sequence (5‘-3‘)**
Saccharomyces cerevisiae (WAT11) expression			
CrGO	pESC-HIS	Forward	**GAGAAAAAACCCCGGATCC**ATGGAGTTTTCTTTCTCCTCA
		Reverse	**ACTTCTGTTCCATGTCGAC**CTAATCGTTAACAAGATGAGGAA
CrSBE	pESC-HIS	Forward	**GAGAAAAAACCCCGGATCC**ATGGATGAGATGATGAACTTCTC
		Reverse	**ACTTCTGTTCCATGTCGAC**TTAATTTCCTTCAACTGCTGATGA
CrRS	pESC-HIS	Forward	**GAGAAAAAACCCCGGATCC**ATGGAAACTATCAACTTCTTCTC
		Reverse	**ACTTCTGTTCCATGTCGAC**TCAATCTTGTGCAACAACCG
pTRV2 constructs for VIGS			
CrGO	pTRV2-MgChl	Forward	**ATATTGCTGCGGATC**CCTTTGATGCACGTGAAAATGGG
		Reverse	**ATGCCCGGGCCTCGAG**GTCCAACGTTAGACTTAATTGACT
CrSBE	pTRV2-MgChl	Forward	**ATATTGCTGCGGATCC**GGCAAAAAATTACCACCGGG
		Reverse	**ATGCCCGGGCCTCGAG**CAATTGCTTTAAGTAGTCACCA
Gene	**Plasmid**	**Primer direction**	**Sequence (5‘-3‘)**
Primers used for sequencing plasmid constructs			
	3Ω1	Forward	GATGAAAAAGCCCTAAAATTGGAG
		Reverse	ATTATTCACAAATGAGAAACAGAATGG
	pESC-HIS	Forward	ATGATTTTTGATCTATTAACAGATA
		Reverse	GTATAATGTTACATGCGTACAC
	pTRV2-MgChl	Forward	GATGGACATTGTTACTCAAGGAAGC
		Reverse	CAGTCGAGAATGTCAATCTCGTAGG

Table S3. VIGS fragment (300 bp) used for silencing.

Gene	Nucleotide sequence
CrGO	CCTTTGATGCACGTGAAAATGGGCGAACGTTCGGCAATTATAGTATCAGA TGCAAGAATGGCAAAAATAGTTCTTCATAATAACGGTTTAGCCGTTGCAGA TCGGTCAGTAAATACTGTCGCAAGTATTATGACTTATAATAGTTTGGGTGT TACCTTTGCTCAGTATGGAGATTACTTAACAAAATTACGTCAAATCTATACT TTGGAACTTTTAAGTCAGAAAAAAGTTCGATCTTTCTACAGTTGTTTTGAA GATGAACTCGATACTTTTGTTAAGTCAATTAAGTCTAACGTTGGAC
CrSBE	GGCAAAAAATTACCACCGGGTCCCAAAAAACTTCCTATTATAGGAAACCT CCATCAAATGATAGGTTCACATCCTCATCGTGTTCTAAAAAAATTGGCCGA TAAATATGGACCTATTATGCACTTGCAAATGGGCCAACGATCAGCCGTTG TTATATCATCAGCGGAAAAAGCAAAAGAAATATTGAACATTTATGGTGTTC AAGTTGCTGATAGACCTCAACTCATCGTATCTAAAATTATGTTGTACAATA GTTTGGGTGTCACTTTTGCTCCTTATGGTGACTACTTAAAGCAATTGC

Table S4. Primers used for qPCR analysis.

Target	Primer direction	Sequence (5‘-3‘)
CrGO	Forward	TGGCCCGAACCAGAGAAGTT
	Reverse	AGCAGCCAACATAAACTCAGCA
CrSBE	Forward	CACCCTCCTGCTCCCATATTGT
	Reverse	ACTGAACCTCTCCGGCTCAA
q-Rps9 (reference gene)	Forward	TTGAGCCGTATCAGAAATGC
	Reverse	CCCTCATCAAGCAGACCATA

Reference gene was used as described by Payne[22] and Li[22].

Supplementary Figures

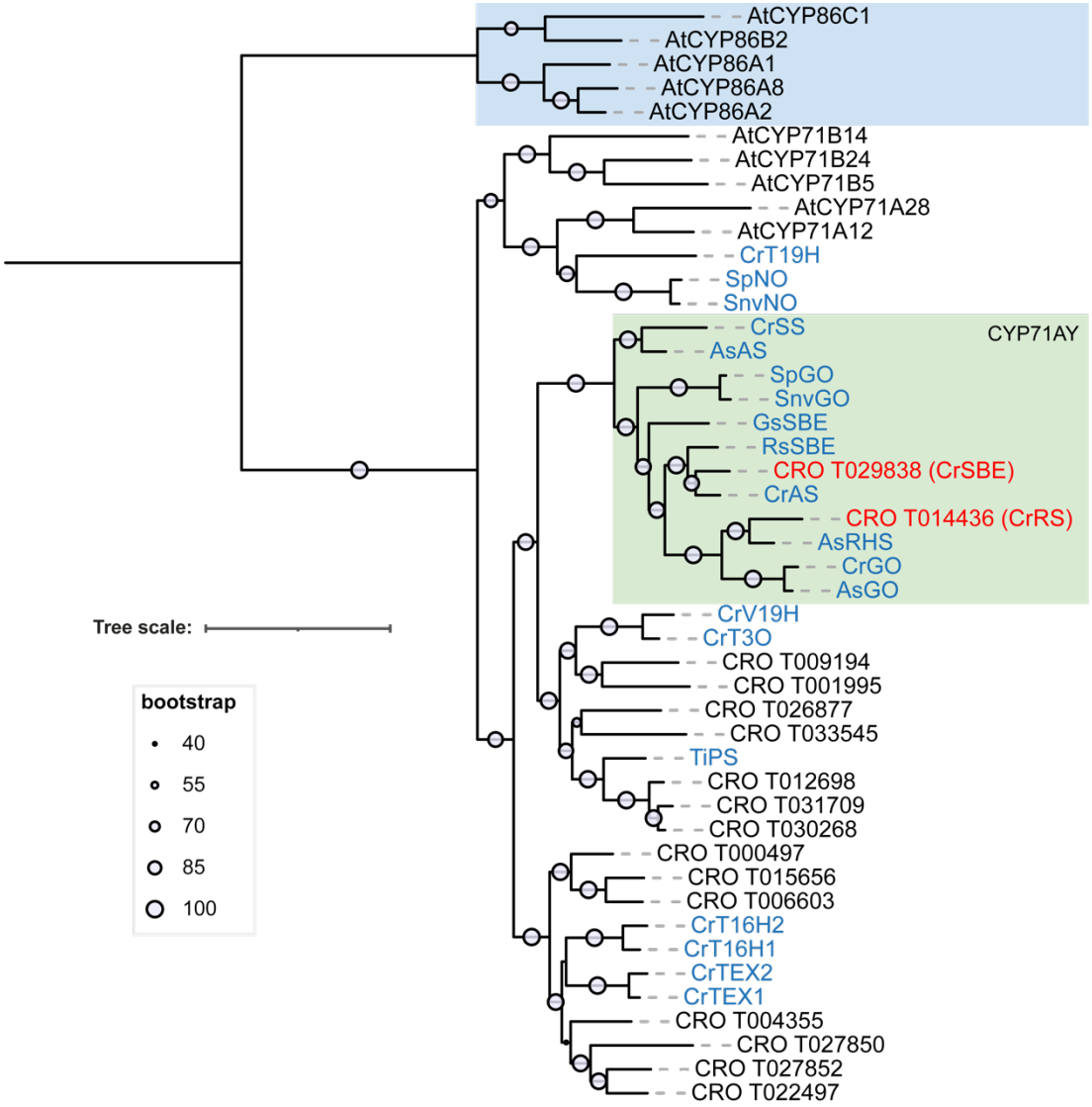


Figure S1. Phylogenetic tree of *Catharanthus roseus* (CRO) cytochrome P450s of the family CYP71.

Phylogenetic relationship of the cytochrome P450 (P450) enzymes identified from the CYP71 clan with known CYP71AY involved in MIA biosynthesis. The maximum-likelihood phylogenetic tree was constructed using iQtree[13] with default parameters and 1000 bootstraps (shown out of 100). The CYP71AY family investigated in this work is highlighted in green. P450s functionally characterised to be involved in monoterpene indole alkaloid (MIA) biosynthesis are coloured in blue. *Arabidopsis thaliana* (At) CYP86 clan 86 shaded in blue was used to root the tree. The phylogenetic tree was visualized and inferred using iToL[14].

	CRO_T014436 (CrRS)	CRO_T029838 (CrSBE)	AsRHS	GsSBE	RsSBE	CrAS	AsAS	CrGO	SnvGO	AsGO	SpGO	CrSS
CRO_T014436 (CrRS)		51.3	73.5	50.5	51.6	51.2	48.9	58.3	47.7	59.3	49.1	44.0
CRO_T029838 (CrSBE)	51.3		53.9	58.7	73.6	78.9	58.1	50.9	55.7	52.3	56.6	49.6
AsRHS	73.5	53.9		53.1	55.3	55.0	49.4	61.6	49.5	62.4	50.4	44.9
GsSBE	50.5	58.7	53.1		59.4	59.2	55.5	50.9	54.5	51.3	54.6	52.0
RsSBE	51.6	73.6	55.3	59.4		74.1	58.0	52.0	53.7	52.6	55.5	51.2
CrAS	51.2	78.9	55.0	59.2	74.1		58.7	51.5	53.6	52.6	54.7	50.8
AsAS	48.9	58.1	49.4	55.5	58.0	58.7		47.7	54.9	48.8	55.8	67.8
CrGO	58.3	50.9	61.6	50.9	52.0	51.5	47.7		46.8	90.2	47.8	44.6
SnvGO	47.7	55.7	49.5	54.5	53.7	53.6	54.9	46.8		47.6	92.1	50.0
AsGO	59.3	52.3	62.4	51.3	52.6	52.6	48.8	90.2	47.6		48.8	45.6
SpGO	49.1	56.6	50.4	54.6	55.5	54.7	55.8	47.8	92.1	48.8		49.9
CrSS	44.0	49.6	44.9	52.0	51.2	50.8	67.8	44.6	50.0	45.6	49.9	

Figure S2. Sequence similarity of CrRS and CrSBE to known CYP71AY proteins.

The percentage of amino acid sequence similarity of CrRS (CRO_T014436) and CrSBE (CRO_T029838) to that of functionally characterised CYP71AY cytochrome P450 enzymes involved in MIA biosynthesis.

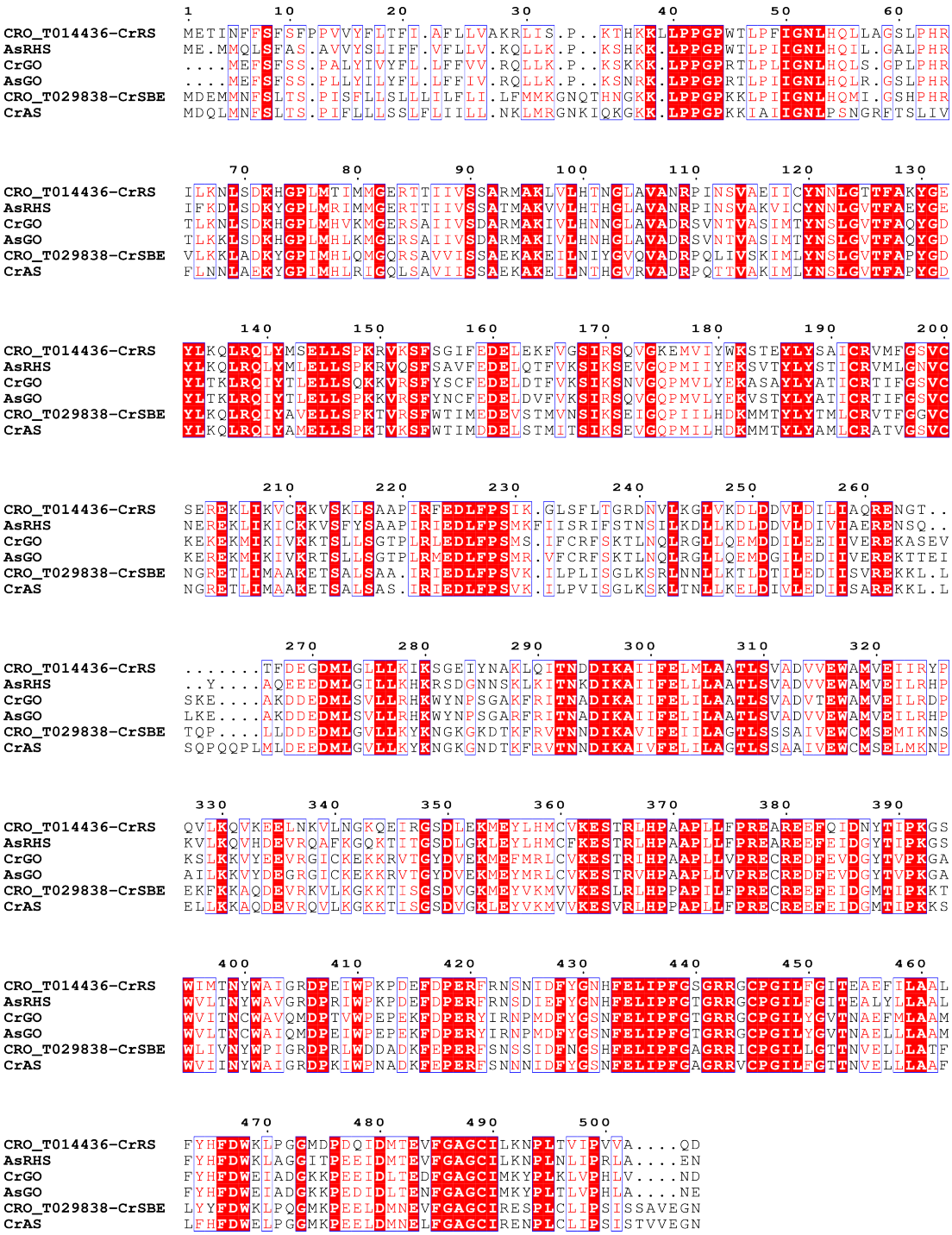


Figure S3. Multiple sequence alignments of CrRS and CrSBE.

MUSCLE[11] amino acid alignments of CrGO, CrRS (CRO_T014436), CrSBE (CRO_T029838), *Alstonia scholaris* geissoschizine oxidase (AsGO), *Alstonia scholaris* rhazimal synthase (As RHS), and *Catharanthus roseus* Alstonine synthase (CrAS). Sequences in Figure S2 with the highest amino acid identity to CrGO, CrRS and CrSBE were selected for alignment. Alignment was visualised using ESPript[23] webserver.

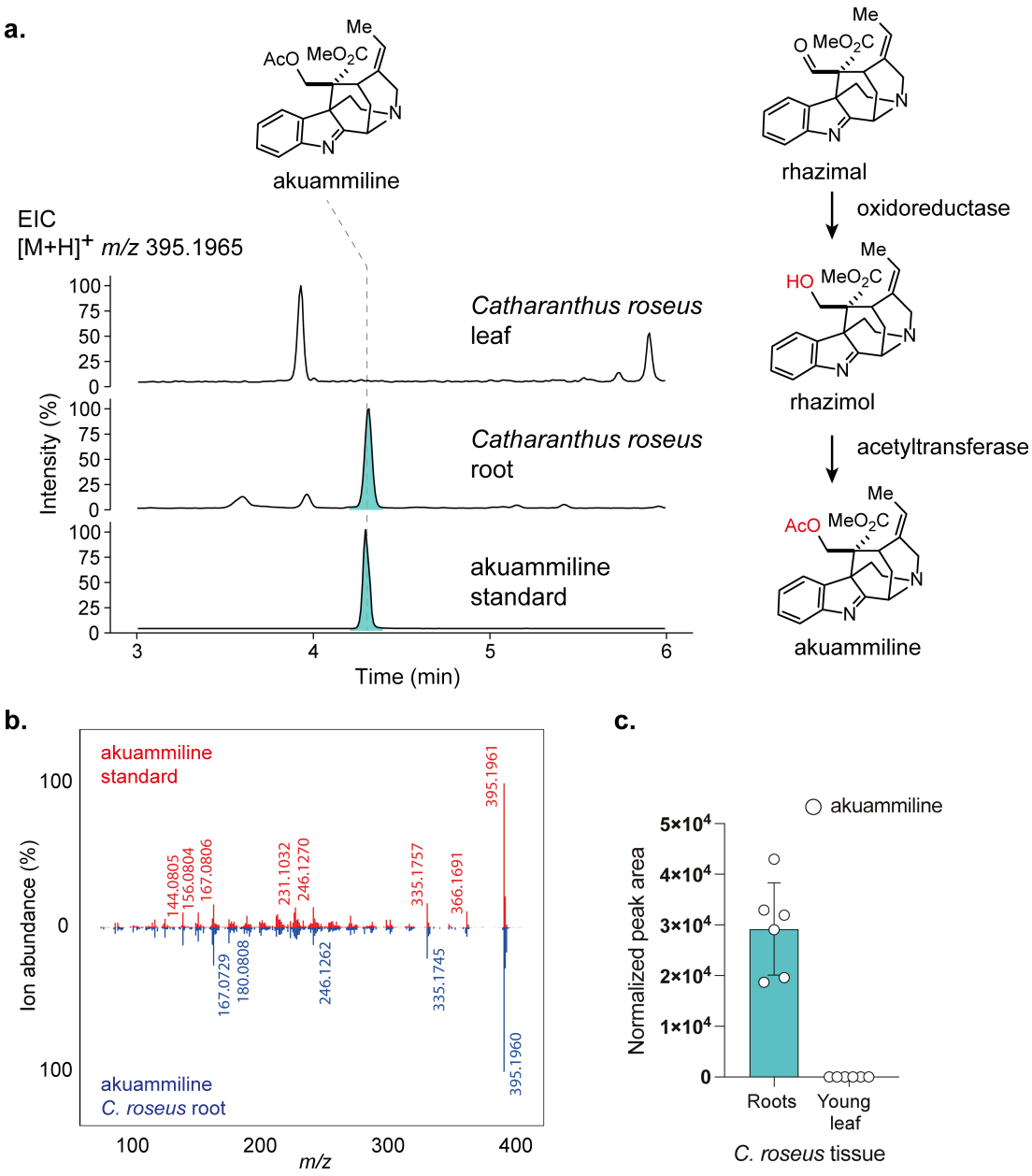


Figure S4. Metabolite analysis of akuammiline in *C. roseus* tissues.

(**a**) LC-MS profiles of *C. roseus* root and young leaf tissue showing the detection and accumulation of akuammiline. Akuammiline is present in the roots of *C. roseus* and is not detected in the young leaves. Akuammiline shares its biosynthetic origins with rhazimal, where an oxidoreductase could reduce the aldehyde to form rhazhimol, and subsequent acetylation could lead to the formation of akuammiline. While akuammiline biosynthesis has been reported in the MIA-producing plant *Alstonia scholaris*[5], it is yet to be elucidated in *C. roseus*. (**b**) MS^2 spectra of akuammiline authentic standard (red) compared to analyte detected in *C. roseus* roots (blue) show identical spectral match. (**c**) Normalized peak area of akuammiline detected in the roots of 6 independent *C. roseus* plants. Peak areas were normalized to internal standard tabersonine.

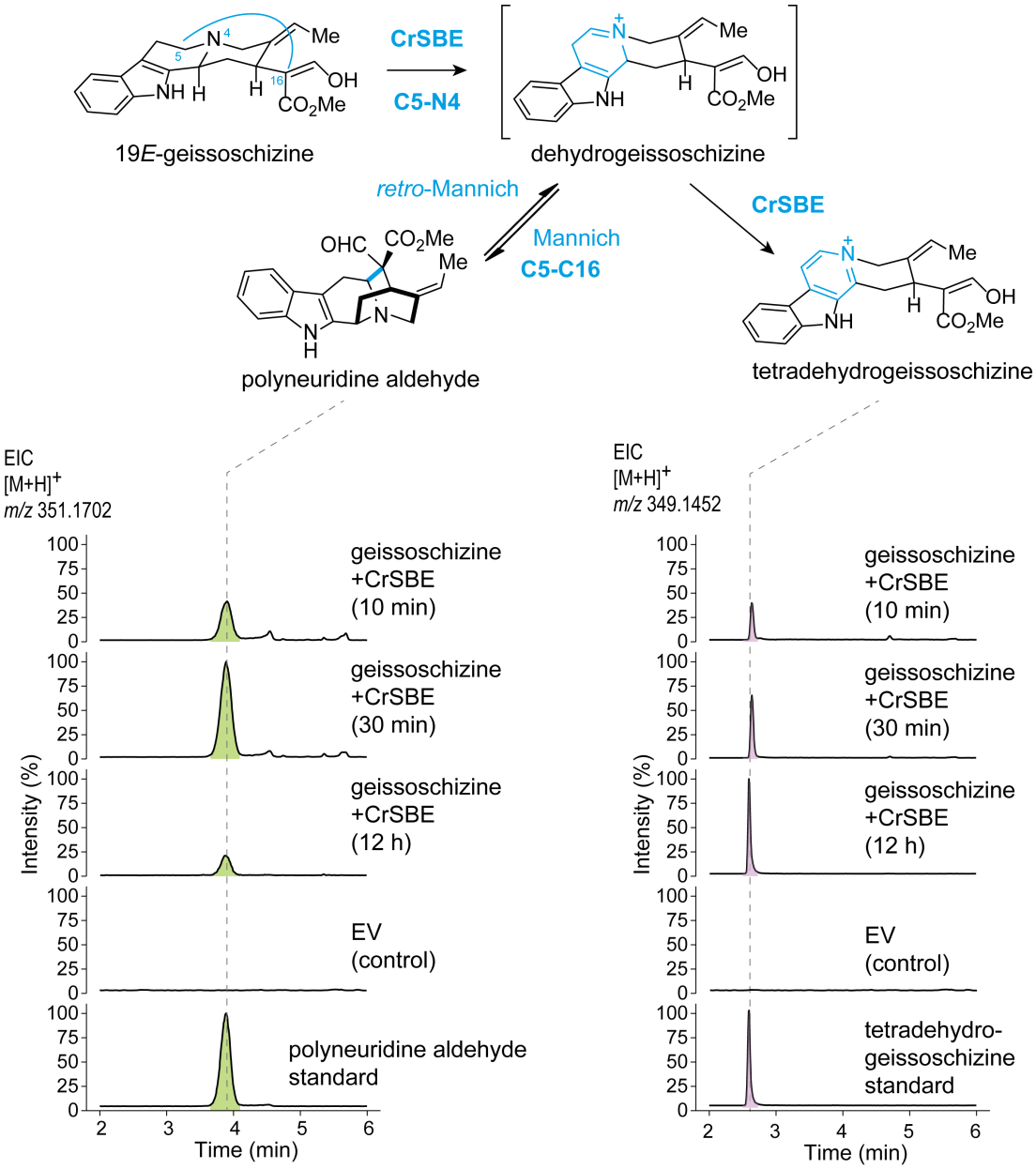


Figure S5. In vitro reactions of CrSBE (CRO_T029838).

In vitro yeast microsomal assays in which 19*E*-geissoschizine is incubated with CrSBE and quenched at 10 min, 30 min, and 12 h time course. The dehydrogeissoschizine iminium intermediate appears to be in an equilibrium with polyneuridine aldehyde via a Mannich-type rearrangement over the short-time course experiment. In prolonged incubation, polyneuridine aldehyde could revert to the dehydrogeissoschizine iminium and generate the thermodynamic product, tetra-dehydro-geissoschizine.

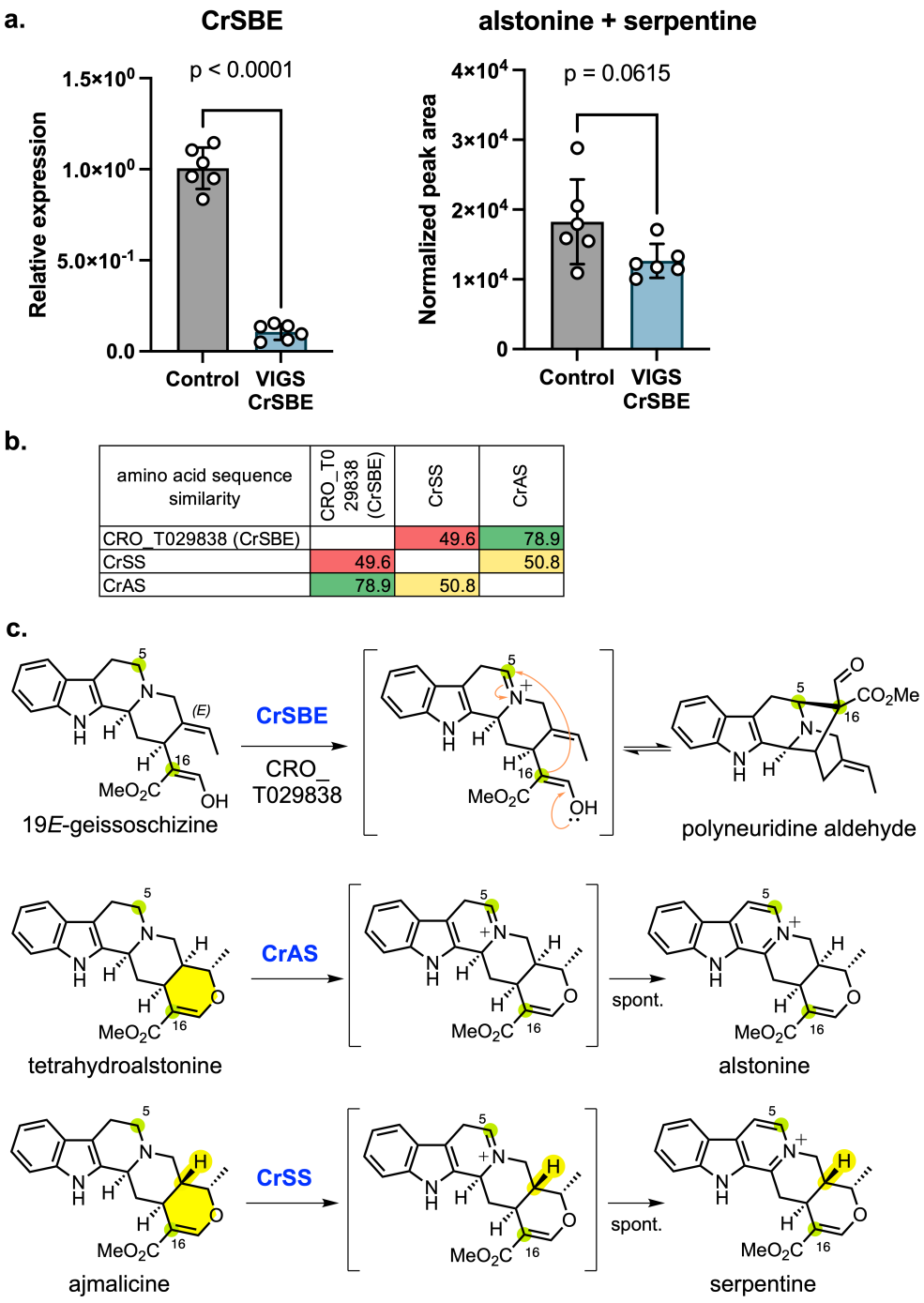


Figure S6. In planta VIGS of CrSBE (CRO_T029838) in *C. roseus*.

(a) Effective silencing of CrSBE in *C. roseus* va. SA leaves. Despite significant silencing of CrSBE, no statistically significant changes in alstonine metabolite levels were observed. The values represent mean ± standard deviation (SD) (n = 6), two-tailed Student's *t*-test. (**b**) Amino acid similarity of the CrSBE **(**CRO_T029838) against previously characterised *C. roseus* SBE enzymes, AS (alstonine synthase), and SS (serpentine synthase). (**c**) Reactions catalyzed by the CrSBE **(**CRO_T029838) reported in this study and CrAS. The substrates of CrSBE and CrAS share structural similarities, but the aromatization of the E ring (yellow) generates different oxidative rearrangements.

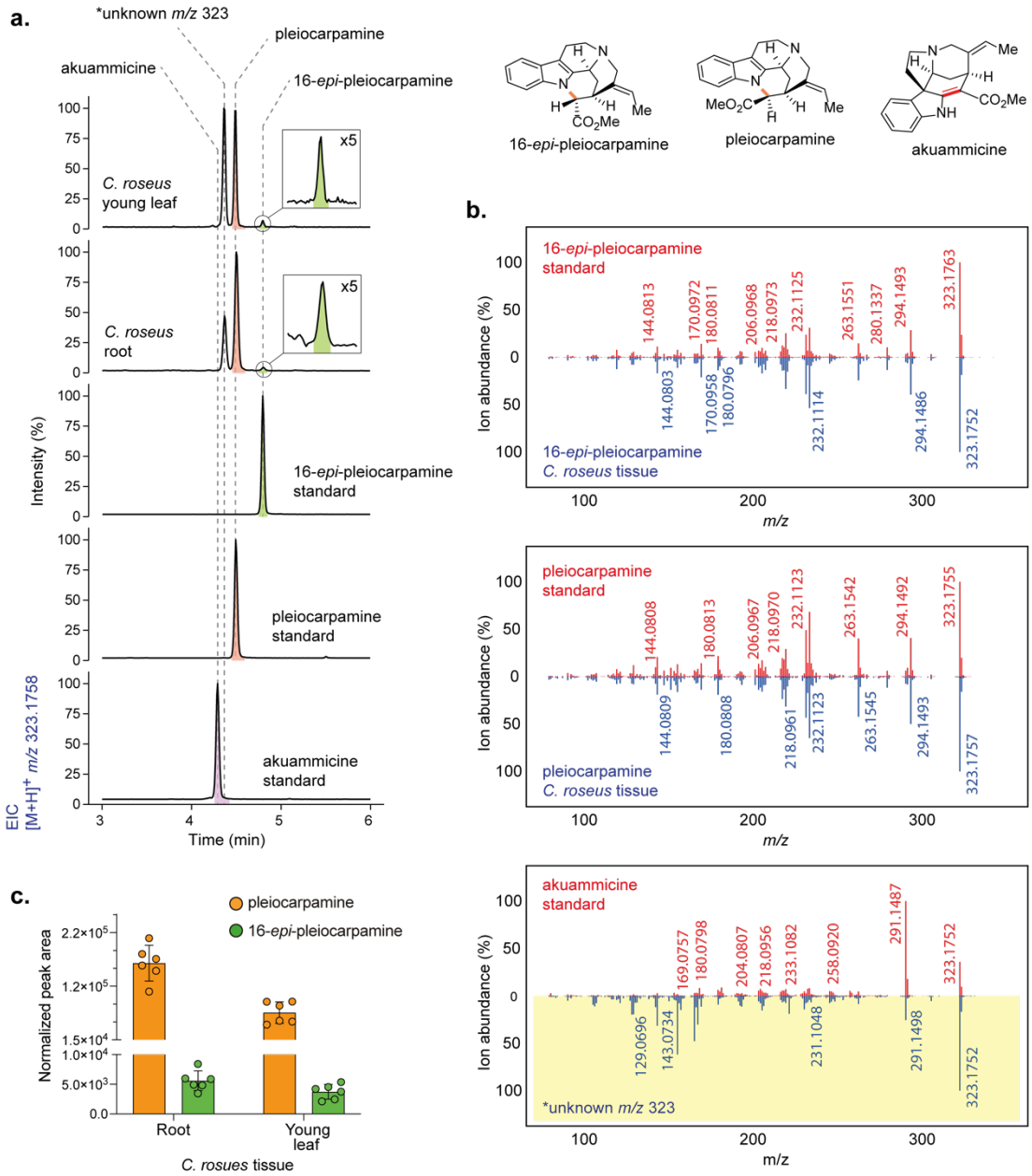


Figure S7. Metabolite analysis of pleiocarpamine and 16-*epi*-pleiocarpamine in *C. roseus* tissues.

(**a**) LC-MS profiles of *C. roseus* root and young leaf tissue showing the accumulation of pleiocarpamine and 16-*epi*-pleiocarpamine. Pleiocarpamine is present at considerable levels, compared to 16-*epi*-pleiocarpamine, which could be detected by LCMS. An unknown *m/z* 323 was recorded with elution times similar to akuammicine. (**b**) MS^2 spectra of pleiocarpamine, 16-*epi*-pleiocarpamine, and akuammicine authentic standards (red) compared to compounds detected in *C. roseus* tissue (blue). Pleiocarpamine and 16-*epi*-pleiocarpamine showed identical spectral match. The m/z 323 observed in the young leaf did not show MS^2 spectra similarity to the authentic standard. (**c**) Normalized peak areas of pleiocarpamine and 16-*epi*-pleiocarpamine detected in the roots and young leaves of 6 independent *C. roseus* plants. Peak areas were normalized to internal standard tabersonine. Error bars represent ± standard deviation (SD) of the mean.

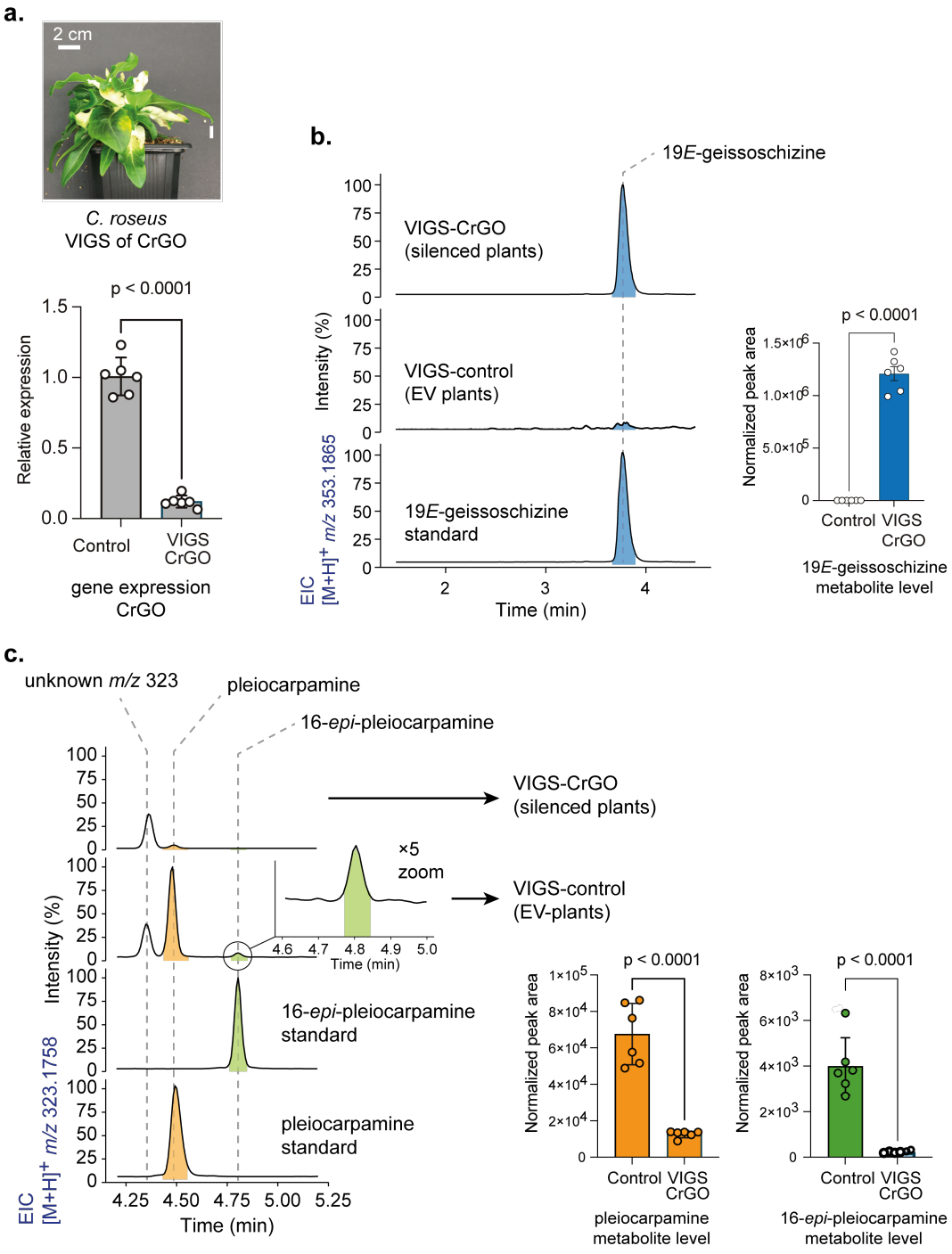
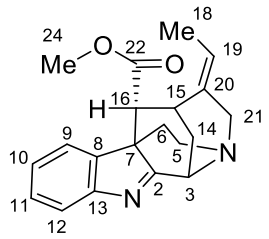


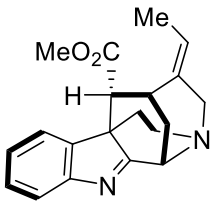
Figure S8. In planta VIGS of CrGO in *C. roseus*.

(**a**) GO is significantly silenced compared to the empty vector (EV) control, indicating successful VIGS of the target. (**b**) Silencing GO in the leaves, lead to the accumulation of the canonical GO substrate 19*E*-geissoschizine further demonstrate the effective transient knock down of the gene. Representative LCMS extracted ion chromatogram (EIC) is shown alongside the bar graph for metabolite accumulation. (**c**) Metabolite levels of the GO knockdown tissue in comparison to controls. Representative LCMS extracted ion chromatogram (EIC) is shown alongside the bar graph for metabolite accumulation The values represent mean ± standard deviation (SD) (n = 6), two-tailed Student's *t*-test.

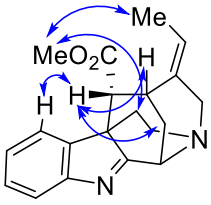
Supporting NMR

NMR analysis of strictamine

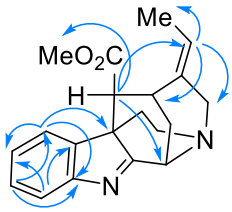




^{1}H-^{1}H COSY
bold line



NEOSY



HMBC
(H to C)

^{1}H NMR (700 MHz, $CDCl_3$) δ 7.71 (d, *J* = 7.8 Hz, 1H, H-12), 7.47 – 7.41 (m, 1H, H-9), 7.41 (d, *J* = 7.5 Hz, 1H, H-11), 7.29 – 7.24 (m, 1H H-10), 5.84 (d, *J* = 7.5 Hz, 1H, H-19), 5.29 (s, 1H, H-3), 4.43 (d, *J* = 15.2 Hz, 1H, H-21), 3.75 (s, 3H, H-24), 3.78-3.73 (m, 1H, H-6), 3.68 (s, 1H, H-15), 3.65 (d, *J* = 13.8 Hz, 1H, H-21), 3.26 – 3.19 (m, 1H, H-5), 2.90 (d, *J* = 15.6 Hz, 1H, H-5), 2.82 (d, *J* = 14.4 Hz, 1H, H-14), 2.20 (dd, *J* = 15.8, 5.1 Hz, 1H, H-6), 2.15 (d, *J* = 3.4 Hz, 1H, H-16), 2.01 (d, *J* = 13.3 Hz, 1H, H-14), 1.65 (d, *J* = 6.6 Hz, 3H, H-18).

^{13}C NMR (176 MHz, $CDCl_3$) δ 192.3 (C-2), 170.5 (C-22), 154.7 (C-13), 144.3 (C-8), 129.2 (C-11), 127.3 (C-19), 127.2 (C-10), 127.0 (C-20), 123.5 (C-9), 122.4 (C-12), 55.1 (C-3), 54.9 (C-7), 54.1 (C-16), 52.7 (C-21), 52.1 (C-24), 51.3 (C-5), 33.7 (C-14), 31.0 (C-15), 25.5 (C-6), 13.4 (C-18).

4.5 Supporting references

1. Hong B, Grzech D, Caputi L, Sonawane P, López CER, Kamileen MO, et al. Biosynthesis of strychnine. Nature. 2022;607(7919):617–22.

2. Zhang X, Kakde BN, Guo R, Yadav S, Gu Y, Li A. Total Syntheses of Echitamine, Akuammiline, Rhazicine, and Pseudoakuammigine. Angew Chem Int Ed. 2019;58(18):6053–8.

3. Turpin V, Poupon E, Jullian J, Evanno L. Biosynthetically Relevant Reactivity of Polyneuridine Aldehyde. Eur J Org Chem. 2020;2020(45):6989–91.

4. Tatsis EC, Carqueijeiro I, Bernonville TD de, Franke J, Dang TTT, Oudin A, et al. A three enzyme system to generate the Strychnos alkaloid scaffold from a central biosynthetic intermediate. Nat Commun. 2017;8(1):316.

5. Wang Z, Xiao Y, Wu S, Chen J, Li A, Tatsis EC. Deciphering and reprogramming the cyclization regioselectivity in bifurcation of indole alkaloid biosynthesis. Chem Sci. 2022;13(42):12389–95.

6. Dang TTT, Franke J, Carqueijeiro IST, Langley C, Courdavault V, O'Connor SE. Sarpagan bridge enzyme has substrate-controlled cyclization and aromatization modes. Nat Chem Biol. 2018;14(8):760–3.

7. Huang L, Li J, Ye H, Li C, Wang H, Liu B, et al. Molecular characterization of the pentacyclic triterpenoid biosynthetic pathway in Catharanthus roseus. Planta. 2012;236(5):1571–81.

8. Qu Y, Easson MEAM, Simionescu R, Hajicek J, Thamm AMK, Salim V, et al. Solution of the multistep pathway for assembly of corynanthean, strychnos, iboga, and aspidosperma monoterpenoid indole alkaloids from 19E-geissoschizine. Proc Natl Acad Sci United States Am [Internet]. 2018;115(12):3180–5.

9. Yamamoto K, Grzech D, Koudounas K, Stander EA, Caputi L, Mimura T, et al. Improved virus-induced gene silencing allows discovery of a serpentine synthase gene in Catharanthus roseus. Plant Physiol. 2021;187(2):846–57.

10. Miettinen K, Dong L, Navrot N, Schneider T, Burlat V, Pollier J, et al. The seco-iridoid pathway from Catharanthus roseus. Nat Commun. 2014;5(1):3606.

11. Edgar RC. MUSCLE: multiple sequence alignment with high accuracy and high throughput. Nucleic Acids Res. 2004;32(5):1792–7.

12. Kamileen MO, Nakamura Y, Luck K, Heinicke S, Hong B, Colinas M, et al. Streamlined screening platforms lead to the discovery of pachysiphine synthase from Tabernanthe iboga. N Phytol. 2024;

13. Nguyen LT, Schmidt HA, Haeseler A von, Minh BQ. IQ-TREE: A Fast and Effective Stochastic Algorithm for Estimating Maximum-Likelihood Phylogenies. Mol Biol Evol. 2015;32(1):268–74.

14. Letunic I, Bork P. Interactive Tree of Life (iTOL) v6: recent updates to the phylogenetic tree display and annotation tool. Nucleic Acids Res. 2024;gkae268.

15. Kamileen MO, DeMars MD, Hong B, Nakamura Y, Paetz C, Lichman BR, et al. Recycling Upstream Redox Enzymes Expands the Regioselectivity of Cycloaddition in Pseudo-Aspidosperma Alkaloid Biosynthesis. J Am Chem Soc. 2022;144(43):19673–9.

16. Sarrion-Perdigones A, Vazquez-Vilar M, Palací J, Castelijns B, Forment J, Ziarsolo P, et al. GoldenBraid 2.0: A Comprehensive DNA Assembly Framework for Plant Synthetic Biology. Plant Physiol. 2013;162(3):1618–31.

17. Pompon D, Louerat B, Bronine A, Urban P. [6] Yeast expression of animal and plant P450s in optimized redox environments. Methods Enzymol. 1996;272:51–64.

18. Fernandez-Pozo N, Rosli HG, Martin GB, Mueller LA. The SGN VIGS Tool: User-Friendly Software to Design Virus-Induced Gene Silencing (VIGS) Constructs for Functional Genomics. Mol Plant. 2015;8(3):486–8.

19. Liscombe DK, O'Connor SE. A virus-induced gene silencing approach to understanding alkaloid metabolism in Catharanthus roseus. Phytochemistry. 2011;72(16):1969–77.

20. Liu Y, Schiff M, Marathe R, Dinesh-Kumar SP. Tobacco Rar1, EDS1 and NPR1/NIM1 like genes are required for N-mediated resistance to tobacco mosaic virus. Plant J. 2002;30(4):415–29.

21. Payne RME, Xu D, Foureau E, Carqueijeiro MIST, Oudin A, Bernonville TD de, et al. An NPF transporter exports a central monoterpene indole alkaloid intermediate from the vacuole. Nat Plants. 2017;3(2):16208.

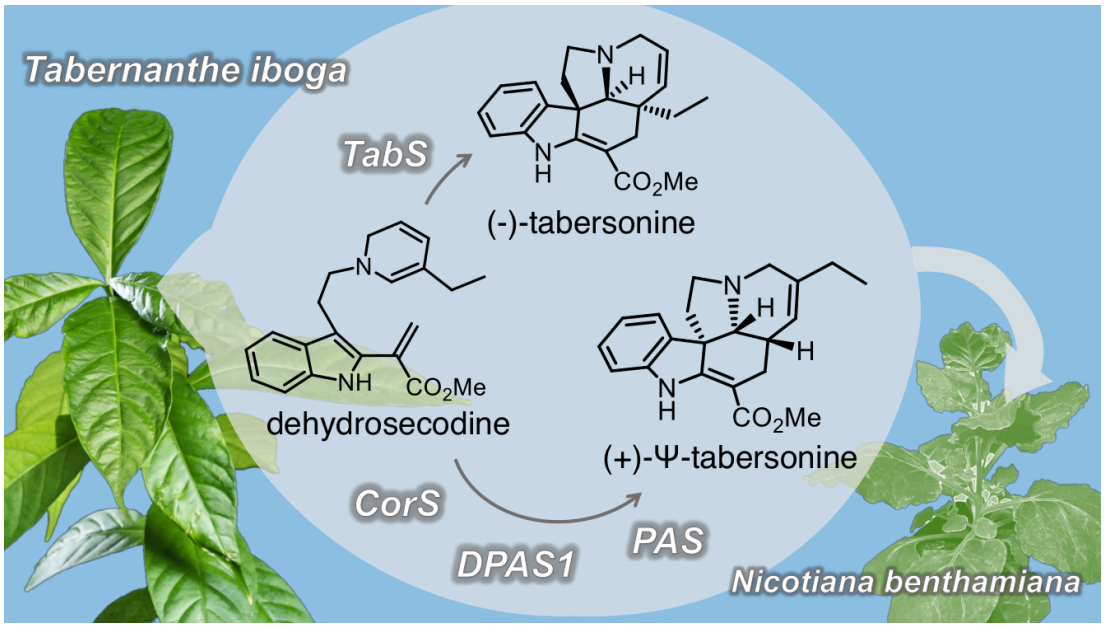
22. Li C, Wood JC, Vu AH, Hamilton JP, Lopez CER, Payne RME, et al. Single-cell multi-omics in the medicinal plant Catharanthus roseus. Nat Chem Biol. 2023;19(8):1031–41.

23. Gouet P, Robert X, Courcelle E. ESPript/ENDscript: extracting and rendering sequence and 3D information from atomic structures of proteins. Nucleic Acids Res. 2003;31(13):3320–3.

Chapter 5
Conclusions, Future Perspective and Outlook

5.1 Conclusions

5.1.1 Pseudo-aspidosperma Alkaloid Biosynthesis



Chapter 2 of this thesis presents the discovery of the pathway responsible for the biosynthesis of chemically rare *pseudo-aspidosperma-type* alkaloids in *T. iboga*[1], resolving their mechanism of biogenesis, studies first initiated by Scott more than 50 years ago[2]. This work provides biochemical and mechanistic insights into the formation of these alkaloids. The cyclase enzyme TiCorS produces (–)-16-carbomethoxy-cleaviminium (16-cmc-iminium), a versatile intermediate not only for the biosynthesis of *iboga-type* alkaloid (–)-coronaridine but also for (+)-pseudo-tabersonine and (+)-pseudo-vincadifformine. This intermediate demonstrates unexpected biochemical versatility for 1,2-iminium and 1,4-iminium reductions enabling pathway divergence for *iboga-type* and *pseudo-aspidosperma-type* alkaloids. Mechanistic studies revealed that upstream redox enzymes PAS and DPAS intercept and modify the reactive (–)-16-cmc-iminium intermediate after it is

released from the TiCorS active site. These redox modifications of (–)-16-cmc-iminium allow two new regioselective cyclization modes. Deuterium labelling experiments further supported the proposed stepwise mechanism, which involves multiple reduction and oxidation events. In conclusion, the research findings of Chapter 2 emphasize that plant pathways are dynamic and nonlinear. Rather than being strictly sequential, pathway enzymes can be recruited and reused in varying orders to build chemical complexity in plants.

5.1.2 Pachysiphine Synthase Discovery

Chapter 3 of this thesis highlights the development of streamlined screening platforms for plant enzyme discovery and the identification of two cytochrome P450 enzymes involved in MIA biosynthesis in *T. iboga*[3]. The pachysiphine synthase (TiPS) and tabersonine 16-hydroxylase (TiT16H) enzymes catalyze key oxidative modifications of the aspidosperma scaffold, (+)-tabersonine, generating precursors for pharmacologically relevant dimeric alkaloids[4,5]. Using *N. benthamiana* leaf disks and *C. roseus* flower petals as expression systems, this work demonstrates efficient approaches for characterizing plant biosynthetic enzymes with minimal substrate requirements and sets the stage for further elucidation of complex natural product pathways. The discovery of these *T. iboga* enzymes provides insight into how plants use oxidative tailoring to expand their chemical diversity by modifying of core scaffolds derived from common intermediates. Specifically, the structural MIA scaffolds described in Chapter 2 are derivatized with the potential for further modifications through the action of cytochrome P450 enzymes identified in Chapter 3, illustrating how plants employ site specific, stereocontrolled oxidations to expand their chemical repertoire.

5.1.3 Divergent Biosynthesis of MIAs from Geissoschizine

Chapter 4 of this thesis explores the oxidative rearrangement of 19*E*-geissoschizine into four distinct MIA structural scaffolds catalysed by three cytochrome P450 enzymes in *Catharanthus roseus*, a medicinal plant closely related to *T. iboga*. By using a phylogeny-assisted approach to elucidate genes and

conducting in vitro enzyme assays, the discovery of two specific cytochrome P450 enzymes, SBE (sarpagan bridge enzyme) and RS (rhazimal synthase) highlights the oxidative rearrangement of geissoschizine to form the core *sarpagan-type and akuammiline-type* alkaloid scaffold in *C. roseus*. Additionally, with SBE, a retro-Mannich reaction exemplifies how nature leverages concerted enzymatic reactions to fine-tune product profiles and expand scaffold diversity. Gene silencing experiments led to a surprising discovery, suggesting that geissoschizine oxidase (GO) is involved in catalysing an essential C-N bond formation for the *mavacurane-type* alkaloid scaffold. In addition to GO's canonical role in forming the C2-C16 bond for *strychnos-type* alkaloid scaffolds, GO likely contributes to forging the C-N bond, unlocking a biosynthetic route to the underexplored *mavacurane-type* alkaloid scaffolds. Building on the findings from Chapters 2 and 3, this chapter demonstrates the versatility of MIA precursors, like 19*E*-geissoschizine, in the divergent formation of core *sarpagan-, akuammiline-, strychnos-,* and *mavacurane- type* MIA alkaloid scaffolds through oxidative rearrangements by cytochrome P450 monooxygenase enzymes. This discovery highlights how plants generate novel chemical scaffolds by rearranging bonds in central precursors through oxidative rearrangements catalysed by neo-functionalized enzymes.

5.2 Future perspective

Advances in technology for plant pathway elucidation are increasingly merging the boundaries between scientific disciplines, improving detection, resolution, and accuracy in delivering meaningful measurements in addressing long-standing, fundamental questions in plant biosynthesis that were previously elusive. It is an exciting time for plant biosynthesis research, particularly regarding *Tabernanthe iboga,* given its ethnobotanical and scientific significance. The plant has gained considerable attention with the revival of ibogaine research, particularly for its potential in treating neurological disorders and addiction. Although the biosynthesis of ibogaine has been partially elucidated, several cryptic steps remain unresolved. There is great momentum in the scientific community to fully decipher the biosynthetic pathways to access these valuable bioactive molecules. By leveraging state-of-the-art technologies, the research outcomes from *T. iboga* can potentially address longstanding questions in plant natural product biosynthesis.

This section aims to provide a brief discussion and perspective on the future of iboga MIA biosynthesis research, highlighting several themes that could inform and benefit future studies by incorporating lessons learned from this thesis.

5.2.1 Integrative Omics Technologies

Plant single-cell technologies have reached a critical stage of development[6–12] expanding beyond model systems. Notably, the research groups of O'Connor and Buell have made landmark contributions by developing singe-cell omics technologies, including metabolomics[13,14] and transcriptomics[13,15], to unveil mechanistic insights into the MIA biosynthetic pathway leading to vinblastine in *C. roseus*.

Single-cell RNA sequencing (scRNA-seq) has advanced to routine laboratory use, with Particle-templated Instant Partition sequencing (PIP-seq)[16] being one example. Applying scRNA-seq has revolutionized candidate selection for pathway elucidation, offering greater accuracy than conventional bulk sequencing. Additionally, these datasets can reveal non-catalytic genes and transporters that support biosynthesis, streamlining the design, build, and test phases of plant pathway studies by reducing labor, time, and cost.

In iboga, scRNA-seq can be leveraged to uncover the biosynthesis of unknown MIAs and the regulation of known MIAs produced across various tissues in a cell-type-specific manner. However, physiological challenges, such as the latex production, complicate the isolation of intact protoplasts or nuclei, which is critical for generating high-quality scRNA-seq data. Surveying plant tissues at different developmental stages and using alternative platforms, such as iboga cell suspension cultures[17,18], could provide a technical advantage in obtaining high-quality protoplasts. Despite these challenges, the progress made with scRNA-seq in *C. roseus* offers valuable insights for the design, application, and interpretation of scRNA-seq in *T. iboga*.

Single-cell metabolomics (scMet) has proven valuable in MIA research, particularly for the vinblastine biosynthesis pathway of *C. roseus*[14]. Adopting scMet methods from *C. roseus* to *T. iboga* can provide cell-specific quantitative and qualitative data on metabolites, aiding in identifying plausible intermediates and building a single-cell metabolite network. When interpreted in combination with

scRNA-seq data, a comprehensive picture of the localization of biosynthesis can be inferred. Co-localization of metabolites with biosynthetically characterised intermediates can indicate in which cell type new biosynthetic genes may be found.

Genome sequencing technologies and assembly pipelines have advanced into the third generation, enabling the assembly of highly accurate, well-resolved plant genomes at the chromosome level with low cost and turnaround times[19,20]. A high-quality iboga genome could offer numerous benefits[21]. Beyond serving as a resource for scRNA-seq, it could provide valuable insights into gene organization[13], comparative analysis[22,23], pathway regulation[24], and evolutionary studies[25,26]. Genomic data provides a crucial resource for efficient assembly and interpretation of bulk and scRNA-seq datasets. Although gene clustering is not widely observed in MIA biosynthesis, there are numerous examples of co-located genes that have arisen from gene duplication and neo-functionalization[27]. Therefore, carefully examining adjacent genes can lead to new enzyme discoveries. Comparative synteny analysis between species could help identify genes exclusive to specific biosynthetic pathways; analyzing the synteny among evolutionarily related plants, each with a specific MIA profile can provide clues as to which genes are shared or unique to the observed MIA pathways. Broader genomic studies could shed light on the evolution of ibogaine biosynthesis and related MIA alkaloid pathways. Additionally, the genome could facilitate the identification of transcription factors and gene- or cell-specific promoters, enhancing our understanding of how MIA biosynthetic pathways are regulated within cells and how these proteins function in their native context.

Significant progress has been made in applying spatial transcriptomics[28] and imaging mass spectrometry[29,30] techniques. However, caution is required when applying these methods to *T. iboga*, as the presence of latex can hinder sample preparation. Moreover, these approaches often demand specialized training and protocol optimization depending on tissue type, with limited potential for automation. In contrast, single-cell technologies offer higher throughput, are more suited to automation, and provide a clear advantage in building reproducible pipelines with integrated quality controls.

In summary, combining genomic information with single-cell omics data, such as scRNA-seq and scMet, could offer unprecedented insights and address fundamental questions regarding MIA biosynthesis and evolution in *T. iboga*.

5.2.2 Protein-Protein Interactions

Protein-protein interactions (PPI) are an emerging field in plant natural product biosynthesis[31,32]. Biophysical techniques for studying PPIs in both model and non-model plants are advancing[32–34], making *T. iboga* a prime case study to explore how the same enzymes selectively catalyze different alkaloid formations. Surveying the *T. iboga* genome for gene-specific promoters could help design better constructs to study PPIs, particularly in replicating physiological contexts, as key genes are often expressed poorly in presumably rare cell types yet have significant biochemical impacts. Testing these enzymes pairwise, or in combination with a third enzyme, along with intermediates of interest, could facilitate building a protein network model for dehydrosecodine-mediated MIA scaffold formations. Dynamic PPIs, if discovered, could explain the biosynthesis of *aspidosperma-type*, *iboga-type*, and *pseudo-aspidosperma-type* alkaloids, and how plants like *T. iboga* orchestrate such complex biosynthetic pathways from common intermediates. Furthermore, determining the subcellular localization of the key enzymes such as PAS, DPAS, and the cyclase in *T. iboga* warrants more attention. Subcellular localization studies can complement PPI research, and the combined knowledge can be leveraged to optimize biosynthetic pathways for metabolic engineering in heterologous hosts.

5.2.3 Biosynthesis, Chemical Logic and Alternative Routes

Understanding the biosynthesis of a molecule is the first step to allow more complex questions to be addressed. Identifying key intermediates is crucial to uncovering how the pathways are directed. Inspired by the seminal experiments of incorporation studies using labelled precursors by Scott[35–37] on MIA-producing *Vinca* species, the same could be attempted with *T. iboga*. Although, Leete[38] and Yamasaki[39] described incorporation of labelled tryptophan into ibogaine in *T. iboga* in 1964, no similar studies have been conducted since. An excellent review[40] highlights state-of-the-art isotope labelling experiments that could aid in deciphering the chemical logic and pathway hypotheses for biosynthetic elucidation including the use of plant cell culture systems. Additionally, a single cell-based approach could be envisioned, bypassing the need to feed valuable labelled precursors into live iboga plants with latex-filled tissues. Instead, the iboga protoplast could be incubated with

labelled substrates, and the incorporation monitored via scMet. This approach could provide in vivo evidence linking tissue-specific MIA scaffold formation to specific cell types (presumably rare), addressing questions related to shoot and root-specific biosynthesis and metabolite transport.

Iboga shoots predominantly accumulate *pseudo-aspidosperma-type* alkaloids, including (+)-ibophyllidine, (+)-iboxyphylline, and (+)-20-*epi*-iboxyphylline, for which the biosynthesis remains unexplored (Chapter 1, section 1.5.3, **Figure 1.15**). Biomimetic synthesis and proposed mechanisms of biosynthesis of these alkaloids have been reported by Kuehne[41,42]. It is proposed these alkaloids are synthesised via the intermediate pandoline (**Figure 5.1a**). A plausible enzyme mechanism could involve N-oxidation of the D ring of pandoline, resulting in the molecular cleavage and Polonovski–Potier fragmentation, generating an iminium ion. This iminium could undergo intramolecular cyclization (aldol reaction), leading to D-ring expansion and the formation of ketone intermediates, which could be reduced to produce iboxyphylline. Alternatively, the iminium could undergo hydrolysis and cyclization to form a D-ring contracted enamine, with subsequent reduction leading to ibophyllidine (**Figure 5.1b**). Enzymes that could catalyze these steps include cytochrome P450s (CYP450s), FAD-dependent oxidases, and 2-Oxoglutarate/Fe(II)-Dependent Dioxygenases (2-ODD) for oxidation, oxidoreductases such as aldo-keto reductases (AKRs) for aldehyde reduction, and alcohol dehydrogenases (ADH) for iminium reduction.

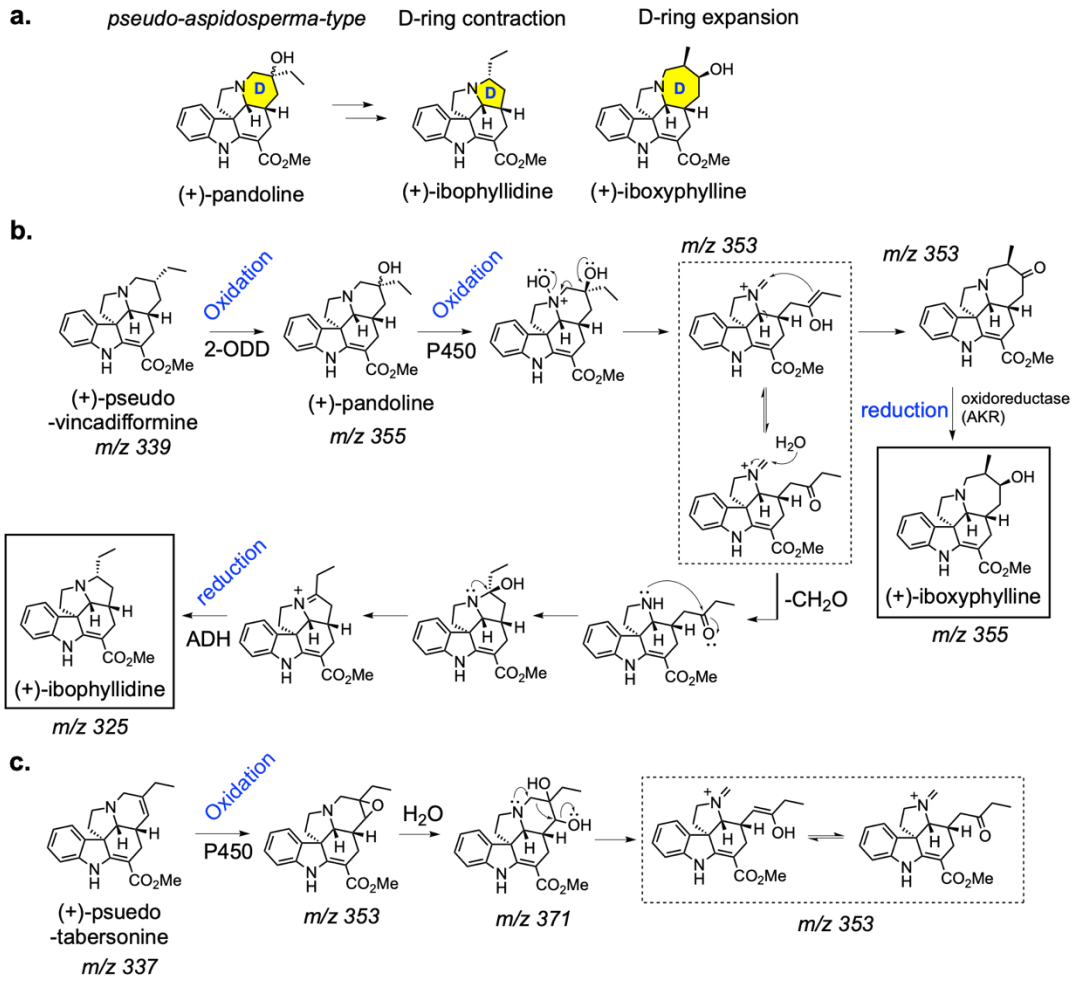


Figure 5.1. Proposed biosynthesis of (+)-ibophyllidine and (+)-iboxyphylline. (**a**) D-ring contraction and D-ring expansion of the *pseudo-aspidosperma-type* alkaloid scaffold result in the formation of (+)-ibophyllidine and (+)-iboxyphylline, respectively. (**b**) Proposed biosynthesis of (+)-ibophyllidine and (+)-iboxyphylline from (+)-pseudo-vincadifformine via the intermediate pandoline. Reaction steps are highlighted in blue with plausible enzyme classes. The crucial intermediate is highlighted in a dashed box and exists in equilibrium as a keto-enol tautomer. (**c**) Plausible epoxidation of (+)-pseudo-tabersonine to generate biosynthetic intermediate for (+)-ibophyllidine and (+)-iboxyphylline biosynthesis. This route provides access to the proposed biosynthetic intermediate highlighted in a dashed box for (+)-ibophyllidine and (+)-iboxyphylline biosynthesis without the need for (+)-pandoline as a pathway intermediate.

The biosynthesis of pandoline remains unknown, though its biogenetic precursors are proposed to be (+)-pseudo-vincadifformine[41]. Pandoline could be biosynthesized from pseudo-vincadifformine via direct oxidation, presumably

catalyzed by a 2-Oxoglutarate/Fe(II)-Dependent Dioxygenase (2-ODD) or CYPP450 enzyme. The existence of pseudo-vincadifformine epimers and the corresponding pandoline epimers may provide clues to the substrate of pandoline. The presence of epimers would suggest that the predicted oxidase enzyme may not hydroxylate C20 stereoselectively.

An alternative mechanism starting from (+)-pseudo-tabersonine is also possible (**Figure 5.1c**). An epoxidation catalyzed by a P450 could facilitate the diol intermediate by transferring a proton from the weakly acidic solvent (H_2O). This approach provides access to the proposed *m/z* 353 iminium intermediate required for the biosynthesis of (+)-ibophyllidine and (+)-iboxyphylline, bypassing the need for (+)-pandoline as an on-pathway intermediate (**Figure 5.1c**).

The biosynthesis of ibophyllidine, iboxyphylline and their pathway intermediates could be investigated by testing the proposed gene candidates using the *N. benthamiana* screening platform described in Chapter 3[3]. By employing the multigene construct and co-infiltration strategy described in Chapter 3, the pathway could be tested from the precursor stemmadenine acetate. As part of this thesis, *T. iboga* MIAs (+)-20-*epi*-pandoline, ibophyllidine, and iboxyphylline were isolated from the plant leaves as authentic standards.

T. iboga produces an array of *iboga-type* alkaloids tailored with hydroxylations and methylations in the roots and stems (Chapter 1, section 1.5.1, **Figure 1.13**). However, the biosynthetic enzymes responsible for these modifications remain unknown. A plausible biosynthetic pathway could be envisioned, starting from the iboga alkaloids (–)-ibogamine (Figure 5.2a) and (–)-coronaridine (Figure 5.2b), involving oxidations catalyzed by cytochrome P450 enzymes (CYP71[3,43] and/or CYP81[44–46] family) and methylations by *O*-methyltransferases (N10OMT[43] or T16OMT[47]-like) (**Figure 5.2a,b**). Gene candidates could be identified based on tissue-specific expression and correlation to upstream scaffold-forming enzymes. Gene candidates could be identified based on tissue-specific expression and correlation with upstream scaffold-forming enzymes. The screening system described in Chapter 3 could then be applied to test the activity of these candidates, potentially uncovering the biosynthetic enzymes responsible for iboga-scaffold oxidations.

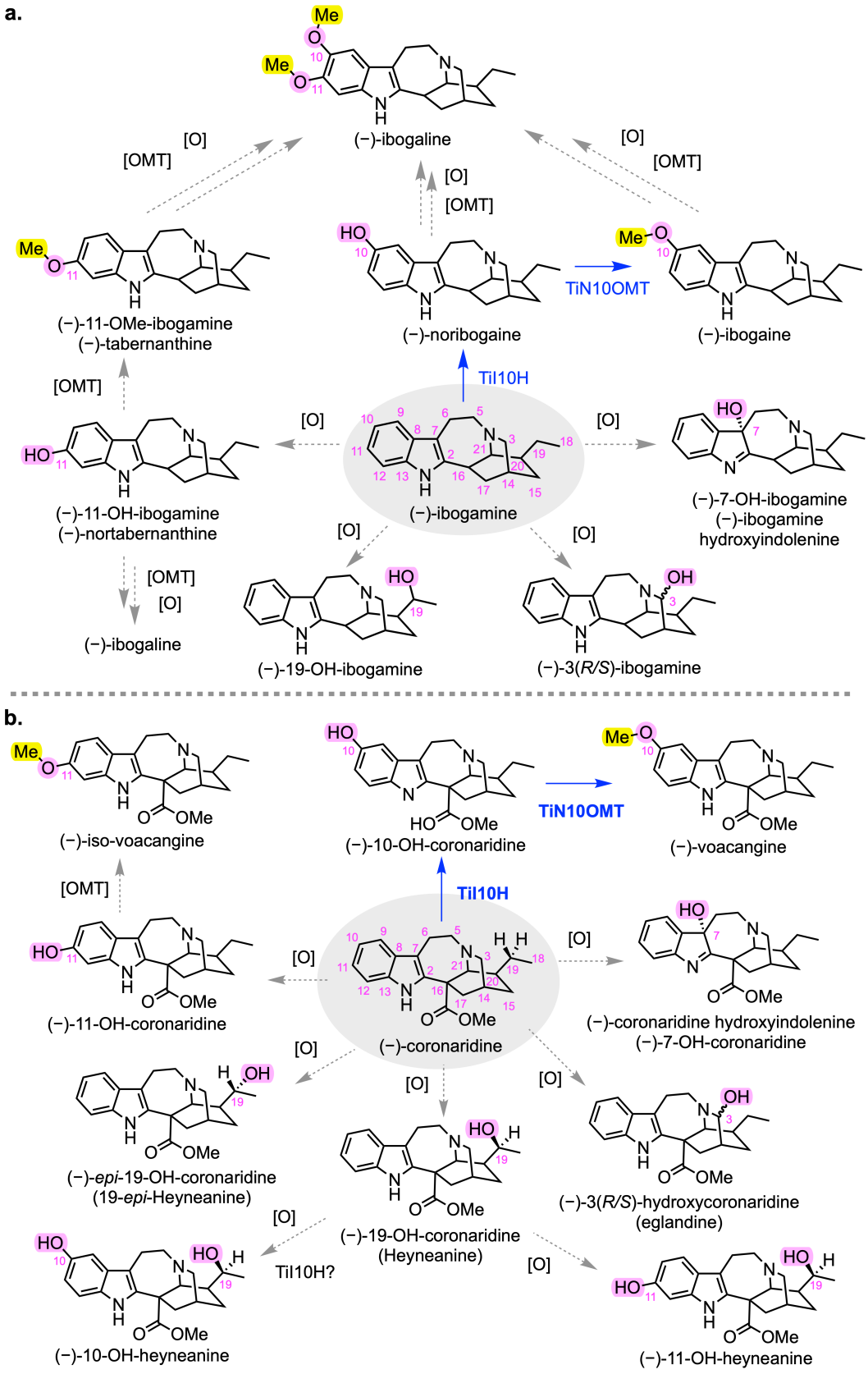


Figure 5.2. Hydroxylations of the *iboga-type* alkaloid scaffold observed in *T. iboga*.

(**a**) Proposed biosynthesis of (–)-ibogamine oxidative tailoring. (**b**) Proposed biosynthesis of (–)-coronaridine oxidative tailoring.

The biosynthesis of (–)-coronaridine has been experimentally deduced in previous studies[48] and as part of Chapter 2[1] of this thesis. However, the biosynthesis of this compound was only favorable in vitro at an elevated pH of 9.5, under non-physiological conditions, making reconstitution in *N. benthamiana* impossible. This represents a bottleneck in bioproduction of (–)-ibogaine, since (–)-coronaridine is the reported precursor for (–)-ibogaine pathway. There are several possible reasons why (–)-coronaridine biosynthesis has not been attained under physiological conditions (pH 7.5). One possibility is that an unidentified ADH enzyme to be responsible for the selective 1,4-iminium reduction of the 16-carbomethoxy-cleavamiminium intermediate[1]. A survey of iminium reducing ADH enzymes[49] of *T. iboga*, *C. roseus*, and related *T. divericata* and *V. africana* species could help identify the missing enzyme for combinatorial screening. The oxidase enzyme precondylocarpine acetate synthase (PAS) plays a key role in (–)-coronaridine formation. Three PAS homologs are known[1,48], but roles of the individual homologs in the biosynthesis remains unclear other than oxidation of stemmadenine acetate at various amounts. PAS enzymes are challenging to assay due to difficulties in expressing active proteins in heterologous hosts and the limitations of the *N. benthamiana* platform, which can catalyze endogenous reactions of the PAS substrate, stemmadenine acetate. We speculate that PAS may serve a scaffolding role in a PAS-CorS-DPAS metabolon, assisting in a concerted reaction system and help form substrate channeling to facilitate DPAS or an equivalent ADH enzyme with the 1,4-iminium reduction of the CorS product. Therefore, any enzyme testing would be best coupled with multigene constructs described in Chapter 3[3] together with the PAS homologs and the substrate stemmadenine acetate. The involvement of a helper protein, which could serve DPAS 2 to facilitate a 1,4-minium reduction at physiological pH also cannot be ruled out. Such helper proteins are known to assist in cyclization, ensuring correct stereochemistry in plant iridoid biosynthesis[25]. Interestingly, (–)-coronaridine is highly abundant in *C. roseus* “Little Bright Eye” flowers and was recently detected using scMet[14]. However, scRNA-seq of petals suggest that mature flowers are not biosynthetically active. The presence of alkaloids in flower tissue may be due to active biosynthesis at an earlier stage of flower development, or alternatively, it is possible that (–)-coronaridine is synthesized in the roots of *C. roseus* roots, where a CorS gene is expressed, and

exported to the flowers for storage. Notably, unlike other MIAs, (–)-coronaridine is stable and is not derivatized or decomposed by *N. benthamiana* host metabolism.

5.2.4 Pathway Reconstitution and Metabolic Engineering

De novo pathway reconstitution of strictosidine has been successfully realized in *N. benthamiana*[50] and yeast[51,52]. Additionally, reconstitution of vinblastine precursors in yeast has been recently reported[53]. Leveraging these established platforms, the biosynthetic genes of *pseudo-aspidosperma-type* and *iboga-type* alkaloids could be deployed for the overproduction of these and related compounds of interest. Moreover, production platforms can also be used to generate new to nature analogues[54,55] via combinatorial biosynthesis and could also facilitate gene candidate testing for pathway discovery. CRISPR-based stable transformation of *N. benthamiana* has seen significant improvements[56–58], offering faster turnaround times for plant generation with the development of Cas-integrated transgenic lines[59]. The rapidly expanding synthetic biology toolbox[60–64] and well-documented genomic resources [65–68] provide clear advantages when selecting *N. benthamiana* as a host platform. Using these tools, improved *N. benthamiana* lines could be generated, tailored for MIA overproduction and pathway elucidation, with minimized host metabolic crosstalk. For example, the *N. benthamiana* oxidase that competes with the *T. iboga* PAS enzyme for the stemmadenine acetate substrate could be identified and deleted.

5.2.5 Functional Characterization

Once the biosynthetic pathway is known, it becomes possible to investigate the physiological relevance and mechanisms by which these MIAs are produced within specialized cells. However, reverse genetics approaches such as virus-induced gene silencing (VIGS) are not established in *T. iboga* because of the physiological limitations imposed by latex and the long generation times of this woody shrub. Alternatively, cell culture platforms derived from *T. iboga* tissues could potentially provide a system for gene knockdown and overexpression, enabling gene function studies that provide in planta evidence within a biosynthetic context.

These platforms could be utilized not only for understanding the biosynthesis but also for exploring the ecological relevance of MIAs. Feeding assays with both generalist and specialist insects could help determine the role these MIAs play in plant defense to establish ecological fitness.

5.3 Outlook

The MIA biosynthesis genes, enzymes and pathways described in Chapters 2, 3, and 4 reveal the intricate mechanisms by which redox enzymes generate complex alkaloids from highly reactive intermediates. This complexity is likely facilitated not only by the inherent reactivity of the molecules but also by the spatial arrangement and interaction of enzymes within the cell. The emergence of new technologies to elucidate biosynthetic genes and enzymes has greatly accelerated the rate at which new pathways are discovered. The development of synthetic biology as a discipline has allowed the reconstitution of long and complex pathways in heterologous hosts. Historically, plant-derived natural products have been considered expensive and difficult to obtain. These developments suggest that these valuable molecules will be far more accessible in the near future.

5.4 References

1. Kamileen MO, DeMars MD, Hong B, Nakamura Y, Paetz C, Lichman BR, et al. Recycling Upstream Redox Enzymes Expands the Regioselectivity of Cycloaddition in Pseudo-Aspidosperma Alkaloid Biosynthesis. J Am Chem Soc. 2022;144(43):19673–9.

2. Scott AI, Wei CC. Regio- and stereospecific models for the biosynthesis of the indole alkaloids—II: Biogenetic type synthesis of Aspidosperma and Iboga alkaloids from a corynanthe precursor. Tetrahedron. 1974;30(17):3003–11.

3. Kamileen MO, Nakamura Y, Luck K, Heinicke S, Hong B, Colinas M, et al. Streamlined screening platforms lead to the discovery of pachysiphine synthase from Tabernanthe iboga. N Phytol. 2024;

4. Han-ya Y, Tokuyama H, Fukuyama T. Total Synthesis of (−)-Conophylline and (−)-Conophyllidine. Angew Chem. 2011;123(21):4986–9.

5. Walia M, Teijaro CN, Gardner A, Tran T, Kang J, Zhao S, et al. Synthesis of (−)-Melodinine K: A Case Study of Efficiency in Natural Product Synthesis. J Nat Prod. 2020;83(8):2425–33.

6. Souza LP de, Borghi M, Fernie A. Plant Single-Cell Metabolomics—Challenges and Perspectives. Int J Mol Sci. 2020;21(23):8987.

7. Seyfferth C, Renema J, Wendrich JR, Eekhout T, Seurinck R, Vandamme N, et al. Advances and Opportunities of Single-Cell Transcriptomics for Plant Research. Annu Rev Plant Biol. 2021;72(1):1–20.

8. Ryu KH, Zhu Y, Schiefelbein J. Plant Cell Identity in the Era of Single-Cell Transcriptomics. Annu Rev Genet. 2021;55(1):1–18.

9. Shaw R, Tian X, Xu J. Single-Cell Transcriptome Analysis in Plants: Advances and Challenges. Mol Plant. 2021;14(1):115–26.

10. Zhu M, Taylor IW, Benfey PN. Single-cell genomics revolutionizes plant development studies across scales. Development. 2022;149(6).

11. Hu R, Li Y, Yang Y, Liu M. Mass spectrometry-based strategies for single-cell metabolomics. Mass Spectrom Rev. 2023;42(1):67–94.

12. Pandian K, Matsui M, Hankemeier T, Ali A, Okubo-Kurihara E. Advances in single-cell metabolomics to unravel cellular heterogeneity in plant biology. Plant Physiol. 2023;193(2):949–65.

13. Li C, Wood JC, Vu AH, Hamilton JP, Lopez CER, Payne RME, et al. Single-cell multi-omics in the medicinal plant Catharanthus roseus. Nat Chem Biol. 2023;19(8):1031–41.

14. Vu AH, Kang M, Wurlitzer J, Heinicke S, Li C, Wood JC, et al. Quantitative Single-Cell Mass Spectrometry Provides a Highly Resolved Analysis of Natural Product Biosynthesis Partitioning in Plants. J Am Chem Soc. 2024;146(34):23891–900.

15. Sun S, Shen X, Li Y, Li Y, Wang S, Li R, et al. Single-cell RNA sequencing provides a high-resolution roadmap for understanding the multicellular compartmentation of specialized metabolism. Nat Plants. 2023;9(1):179–90.

16. Clark IC, Fontanez KM, Meltzer RH, Xue Y, Hayford C, May-Zhang A, et al. Microfluidics-free single-cell genomics with templated emulsification. Nat Biotechnol. 2023;41(11):1557–66.

17. Pawelka KH, Stöckigt J. Indole alkaloids from cell suspension cultures of Tabernaemontana divaricata and Tabernanthe iboga. Plant Cell Rep. 1983;2(2):105–7.

18. Basile DV, Punch MS, Pablo J, Brenner B, Hearn WL, Mash DC. Indole Alkaloids From Tissue-Cultured Tabernanthe Iboga H. Bn. Nat Prod Lett. 1999;13(3):233–8.

19. Marks RA, Hotaling S, Frandsen PB, VanBuren R. Representation and participation across 20 years of plant genome sequencing. Nat Plants. 2021;7(12):1571–8.

20. Sun Y, Shang L, Zhu QH, Fan L, Guo L. Twenty years of plant genome sequencing: achievements and challenges. Trends Plant Sci. 2022;27(4):391–401.

21. Zhou X, Liu Z. Unlocking plant metabolic diversity: A (pan)-genomic view. Plant Commun. 2022;3(2):100300.

22. Liu Z, Cheema J, Vigouroux M, Hill L, Reed J, Paajanen P, et al. Formation and diversification of a paradigm biosynthetic gene cluster in plants. Nat Commun. 2020;11(1):5354.

23. Conde D, Kirst M. Decoding exceptional plant traits by comparative single-cell genomics. Trends Plant Sci. 2022;27(11):1095–8.

24. Gao L, Gonda I, Sun H, Ma Q, Bao K, Tieman DM, et al. The tomato pan-genome uncovers new genes and a rare allele regulating fruit flavor. Nat Genet. 2019;51(6):1044–51.

25. Lichman BR, Godden GT, Hamilton JP, Palmer L, Kamileen MO, Zhao D, et al. The evolutionary origins of the cat attractant nepetalactone in catnip. Sci Adv. 2020;6(20):eaba0721.

26. Lichman BR, Godden GT, Buell CR. Gene and genome duplications in the evolution of chemodiversity: perspectives from studies of Lamiaceae. Curr Opin Plant Biol. 2020;55:74–83.

27. Smit SJ, Lichman BR. Plant biosynthetic gene clusters in the context of metabolic evolution. Nat Prod Rep. 2022;39(7):1465–82.

28. Serrano K, Tedeschi F, Andersen SU, Scheller HV. Unraveling plant–microbe symbioses using single-cell and spatial transcriptomics. Trends Plant Sci. 2024;

29. Yin Z, Huang W, Fernie AR, Yan S. Mass spectrometry imaging techniques: a versatile toolbox for plant metabolomics. Trends Plant Sci. 2022;28(Trends Plant Sci. 21 2016):250–1.

30. Eljounaidi K, Radzikowska BA, Whitehead CB, Taylor DJ, Conde S, Davis W, et al. Variation of terpene alkaloids in Daphniphyllum macropodum across plants and tissues. N Phytol. 2024;243(1):299–313.

31. Zhang Y, Fernie AR. Metabolons, Enzyme-Enzyme Assemblies that Mediate Substrate Channeling, and Their Roles in Plant Metabolism. Plant Commun. 2020;2(1):100081.

32. Cuadrado AF, Damme DV. Unlocking protein–protein interactions in plants: a comprehensive review of established and emerging techniques. J Exp Bot. 2024;75(17):5220–36.

33. Strotmann VI, Stahl Y. Visualization of in vivo protein–protein interactions in plants. J Exp Bot. 2022;73(12):3866–80.

34. Zhang Y, Chen M, Liu T, Qin K, Fernie AR. Investigating the dynamics of protein–protein interactions in plants. Plant J. 2023;114(4):965–83.

35. Scott AI. Biosynthesis of the indole alkaloids. Acc Chem Res. 1970;3(5):151–7.

36. Scott AI, Reichardt PB, Slaytor MB, Sweeny JG. Mechanisms of indole alkaloid biosynthesis. Recognition of intermediacy and sequence by short-term incubation. Bioorg Chem. 1971;1(1–2):157–73.

37. SCOTT AI, REICHARDT PB, SLAYTOR MB, SWEENY JG. Mechanisms of Indole Alkaloid Biosynthesis. Recognition of Intermediacy and Sequence by Short-Term Incubation. Recent Adv Phytochem. 1973;6:117–45.

38. Leete E. Biosynthesis of Alkaloids. Science. 1965;147(3661):1000–6.

39. Yamasaki M, Leete E. Biosynthesis of the Iboga alkaloids : The incorporation of tryptophan-3-C14 into Ibogaine. Tetrahedron Lett. 1964;5(23):1499–501.

40. Seligmann B, Liu S, Franke J. Chemical tools for unpicking plant specialised metabolic pathways. Curr Opin Plant Biol. 2024;80:102554.

41. Kuehne ME, Kirkemo CL, Matsko TH, Bohnert JC. Studies in biomimetic alkaloid syntheses. 5. Studies syntheses of .psi.-vincadifformine, 20-epi-.psi.-vincadifformine, pandoline, 20-epipandoline, and the C-16 epimeric(carbomethoxy)velbanamines. J Org Chem. 1980;45(16):3259–65.

42. Kuehne ME, Bohnert JC. Studies in biomimetic alkaloid syntheses. 7. Stereospecific total syntheses of ibophyllidine and 20-epiibophyllidine. J Org Chem. 1981;46(17):3443–7.

43. Farrow SC, Kamileen MO, Meades J, Ameyaw B, Xiao Y, O'Connor SE. Cytochrome P450 and O-methyltransferase catalyze the final steps in the biosynthesis of the anti-addictive alkaloid ibogaine from Tabernanthe iboga. J Biol Chem [Internet]. 2018;293(36):13821–33.

44. Nguyen TAM, Nguyen TD, Leung YY, McConnachie M, Sannikov O, Xia Z, et al. Discovering and harnessing oxidative enzymes for chemoenzymatic synthesis and diversification of anticancer camptothecin analogues. Commun Chem. 2021;4(1):177.

45. Hong B, Grzech D, Caputi L, Sonawane P, López CER, Kamileen MO, et al. Biosynthesis of strychnine. Nature. 2022;607(7919):617–22.

46. Chen Y, Huang J, Wang Y, Tu M, Li J, Xu B, et al. Identification and characterization of camptothecin tailoring enzymes in Nothapodytes tomentosa. J Integr Plant Biol. 2024;66(6):1158–69.

47. Levac D, Murata J, Kim WS, Luca VD. Application of carborundum abrasion for investigating the leaf epidermis: molecular cloning of Catharanthus roseus 16-hydroxytabersonine-16-O-methyltransferase. Plant J. 2008;53(2):225–36.

48. Farrow SC, Kamileen MO, Caputi L, Bussey K, Mundy JEA, McAtee RC, et al. Biosynthesis of an Anti-Addiction Agent from the Iboga Plant. J Am Chem Soc. 2019;141(33):12979–83.

49. Langley C, Tatsis E, Hong B, Nakamura Y, Paetz C, Stevenson CEM, et al. Expansion of the Catalytic Repertoire of Alcohol Dehydrogenases in Plant Metabolism**. Angew Chem Int Ed. 2022;61(48):e202210934.

50. Dudley QM, Jo S, Guerrero DAS, Chhetry M, Smedley MA, Harwood WA, et al. Reconstitution of monoterpene indole alkaloid biosynthesis in genome engineered Nicotiana benthamiana. Commun Biol. 2022;5(1):949.

51. Brown S, Clastre M, Courdavault V, O'Connor SE. De novo production of the plant-derived alkaloid strictosidine in yeast. Proc National Acad Sci [Internet]. 2015;112(11):3205–10.

52. Shahsavarani M, Utomo JC, Kumar R, Paz-Galeano M, Garza-García JJO, Mai Z, et al. Improved protein glycosylation enabled heterologous biosynthesis of monoterpenoid indole alkaloids and their unnatural derivatives in yeast. Metab Eng Commun. 2023;16:e00215.

53. Zhang J, Hansen LG, Gudich O, Viehrig K, Lassen LMM, Schrübbers L, et al. A microbial supply chain for production of the anti-cancer drug vinblastine. Nature. 2022;609(7926):341–7.

54. Boccia M, Grzech D, Lopes AA, O'Connor SE, Caputi L. Directed Biosynthesis of New to Nature Alkaloids in a Heterologous Nicotiana benthamiana Expression Host. Front Plant Sci. 2022;13:919443.

55. Bradley SA, Lehka BJ, Hansson FG, Adhikari KB, Rago D, Rubaszka P, et al. Biosynthesis of natural and halogenated plant monoterpene indole alkaloids in yeast. Nat Chem Biol. 2023;19(12):1551–60.

56. Ellison EE, Nagalakshmi U, Gamo ME, Huang P jui, Dinesh-Kumar S, Voytas DF. Multiplexed heritable gene editing using RNA viruses and mobile single guide RNAs. Nat Plants. 2020;6(6):620–4.

57. Stuttmann J, Barthel K, Martin P, Ordon J, Erickson JL, Herr R, et al. Highly efficient multiplex editing: one-shot generation of 8× Nicotiana benthamiana and 12× Arabidopsis mutants. Plant J. 2021;106(1):8–22.

58. Cody JP, Maher MF, Nasti RA, Starker CG, Chamness JC, Voytas DF. Direct delivery and fast-treated Agrobacterium co-culture (Fast-TrACC) plant transformation methods for Nicotiana benthamiana. Nat Protoc. 2023;18(1):81–107.

59. Uranga M, Aragonés V, Daròs JA, Pasin F. Heritable CRISPR-Cas9 editing of plant genomes using RNA virus vectors. STAR Protoc. 2023;4(1):102091.

60. Vazquez-Vilar M, Orzaez D, Patron N. DNA assembly standards: Setting the low-level programming code for plant biotechnology. Plant Sci. 2018;273:33–41.

61. Molina-Hidalgo FJ, Vazquez-Vilar M, D'Andrea L, Demurtas OC, Fraser P, Giuliano G, et al. Engineering Metabolism in Nicotiana Species: A Promising Future. Trends Biotechnol. 2020;

62. Park J, Demirer GS, Cheung LS. Toolboxes for plant systems biology research. Curr Opin Biotechnol. 2022;75:102692.

63. Rizzo P, Chavez BG, Dias SL, D'Auria JC. Plant synthetic biology: from inspiration to augmentation. Curr Opin Biotechnol. 2023;79:102857.

64. Golubova D, Tansley C, Su H, Patron NJ. Engineering Nicotiana benthamiana as a platform for natural product biosynthesis. Curr Opin Plant Biol. 2024;81:102611.

65. Ranawaka B, An J, Lorenc MT, Jung H, Sulli M, Aprea G, et al. A multi-omic Nicotiana benthamiana resource for fundamental research and biotechnology. Nat Plants. 2023;9(9):1558–71.

66. Kurotani K ichi, Hirakawa H, Shirasawa K, Tanizawa Y, Nakamura Y, Isobe S, et al. Genome Sequence and Analysis of Nicotiana benthamiana, the Model Plant for Interactions between Organisms. Plant Cell Physiol. 2023;64(2):248–57.

67. Ko SR, Lee S, Koo H, Seo H, Yu J, Kim YM, et al. High-quality chromosome-level genome assembly of Nicotiana benthamiana. Sci Data. 2024;11(1):386.

68. Wang J, Zhang Q, Tung J, Zhang X, Liu D, Deng Y, et al. High-quality assembled and annotated genomes of Nicotiana tabacum and Nicotiana benthamiana reveal chromosome evolution and changes in defense arsenals. Mol Plant. 2024;17(3):423–37.